RECEPTOR MODELLING OF INDUSTRIAL AIR POLLUTANTS

BY

ADEWALE MATTHEW TAIWO

(B Sc., M Sc.)

A thesis submitted to the
University of Birmingham
For the Degree of
Doctor of Philosophy

Division of Environmental Health
Risk Management
School of Geography, Earth, and
Environmental Sciences
University of Birmingham
November 2013

ABSTRACT

The presence of particulate and gaseous pollutants at elevated concentrations in the atmospheric environment is detrimental to public health. The present study has investigated the impacts of a steelworks complex on the air quality in Port Talbot, South Wales, United Kingdom.

Different offline and online air monitoring instruments were deployed to four sites around the perimeter of the steelworks (at one coastal site (Little Warren LW) and 3 inland sites placed along the length of the steelworks (Fire Station FS, Prince Street PS and Dyffryn School DS) in the study area for a four-week campaign (April 16 to May 16, 2012). Prior to Port Talbot campaign, a separate two week sampling (March 30 to April 12, 2012) was conducted at Elms Road Observatory Site (EROS) for a representation of an urban background.

Gaseous and meteorological data logged during the period of sampling were also collected from the Automatic Urban and Rural Network (AURN) site at Port Talbot Margam (FS site). Hourly and daily data collected were prepared for receptor modelling using Positive Matrix Factorization (PMF) and with the use of Open Air and Lakes Environmental WRPLOT View software, windrose and polar plots were produced to show the directional emissions of particulate and gaseous pollutants. The online sampling instrument of Aerosol Time of Flight Mass Spectrometer (ATOFMS) as well as PMF solutions for Streaker and Partisol were able to identify different processing units of the steelworks responsible for pollutant emissions. The polar plots for most air pollutants revealed the steel industry as the major contributor to air pollution in the study area.

DEDICATION

This is Thesis is dedicated to the One who stood by me during my study at the University Birmingham, The Trinity; and also to my wife, Seyi and my children: Anointed-Matthew and Beloved-Jane

ACKNOWLEDGEMENTS

My ‘big thanks’ goes to my lead supervisor, Professor Roy Harrison for his guidance and counsel during the course of my study. I really appreciate all the research tutorials given to me through my study. I have really gained from your vast knowledge in Environmental Science

I also appreciate the efforts of my second supervisor, Zongbo Shi who was there for me anytime I need his assistance.

My appreciation is extended to David Beddows who has been of tremendous help during the study, most especially during the sampling campaign.

It would be unfair to forget the assistance rendered by Jianxin Yin and our Laboratory Managers-Gillian Kingston and Eimear Orgill during Laboratory analysis.

My thanks also go to my work colleagues-Lami Abdullahi, Palavi Pant, Barbara Macias Hernandez, Massimiliano Mascelloni, Adaobi Okam, Eun-Hwa Jang, Suad Alkindi, Bunthoon Laongsri and all occupants of room 412. You have all contributed meaningfully to the success of this Thesis. I appreciated you guys: Paul, James, Alan, Salim and Eden who have helped read through this thesis.

Lastly, my gratitude goes to the Tertiary Education Trust Fund of the Federal University of Agriculture, Abeokuta who sponsored my PhD programme.

TABLE OF CONTENTS

List of Tables.....xiii

List of Figures.....xv

List of Definitions and/Or Abbreviations.....xx

CHAPTER 1- INTRODUCTION.....1

1.1 Abstract. 1

1.2 General Overview of Airborne Particulate Matter.....2

1.3 Health Effects of Particulate Matter.....6

1.4 Effects of PM on the Environment.....9

1.5 Particulate Matter Measurements.....10

1.6 Single Particle Analysis.....11

1.6.1 Literature review on ATOFMS.....12

1.7 Receptor Models.....15

1.7.1 Principal component analysis (PCA).....17

1.7.2 Positive matrix factorization (PMF).....17

1.7.3 Enrichment factor (EF).....18

1.8 Integrated Iron and Steel Production.....18

1.8.1 Cokemaking (Coking).....20

1.8.2 Sintering production.....20

1.8.3 Ironmaking.....20

1.8.4 Steelmaking.....20

1.8.5 Literature review on industrial emission, in particular from steelworks.....21

1.9 Objectives of the Study.....25

CHAPTER 2 – GENERAL METHODOLOGY.....27

2.1 Abstract.....27

2.2 Offline Instruments for PM measurement.....28

2.2.1 Micro-orifice uniform deposit impactor (MOUDI) sampler.....28

2.2.2 Partisol dichotomous sequential air sampler ($PM_{2.5}$ and $PM_{2.5-10}$).....30

2.2.3 Filter dynamic measuring system instrument (FDMS).....32

2.2.4 Streaker sampler.....33

2.2.5 Digitel high volume aerosol sampler.....35

2.3 Online Instruments.....36

2.3.1 Portable aerosol spectrometer.....36

2.3.2 Aerosol time of flight mass spectrometer (ATOFMS).....37

2.4 Determination of Black Carbon (BC).....40

2.5 Laboratory Analysis of Offline PM Filters.....41

2.5.1 Filter weighing.....41

2.5.2. Sample digestion for metals determination.....41

2.5.3 Water soluble ions analysis.....42

2.5.4 Thermal optical reflectance analysis of organic and elemental carbon (OC/EC).....44

2.5.5 Inductively coupled plasma mass spectrometer (ICP-MS).....45

2.5.6 Particle induced X-ray emission (PIXE) analysis.....46

2.6 Meteorological and Gaseous Parameters.....47

2.7 Data Processing.....47

2.7. 1 Offline data processing.....47

2.7. 2 Online data processing with ENCHILADA software.....47

2.7.3 Receptor models.....50

2.7.3.1 Principal matrix factorization (PMF).....50

2.7.3.2 Principal component analysis (PCA).....52

2.7.3.3 Enrichment factor (EF).....53

2.7.4 Windrose and Polar Plots.....54

2.8 Summary of Port Talbot Sampling Campaign.....54

CHAPTER 3- EROS AND BROS CAMPAIGN.....55

3.1 Abstract.....55

3.2 Introduction.....56

3.3. Materials and Methods.....56

3.3.1 Particulate matter sampling.....57

3.3.2 Sample digestion and analysis.....58

3.4 Results.....58

3.4.1 Partisol PM compositions at EROS and BROS.....58

3.4.2 Partisol versus MOUDI data at EROS.....64

3.4.3 Pearson's correlation coefficients of $PM_{2.5}$ and $PM_{2.5-10}$ data at EROS and BROS.....66

3.5 Discussion.....68

3.6 Conclusion.....71

CHAPTER 4 - COMPARISON OF SIZE DISTRIBUTION OF PM AT EROS AND PORT TALBOT.....72

4.1 Abstract.....72

4.2 Introduction.....74

4.3 Materials and Methods.....75

4.3.1 The study areas.....75

4.3.1.1 Port Talbot (PT).....75

4.3.1.2 Elms Road Observatory Site (EROS).....76

4.3.2 Particulate matter sampling.....76

4.3.3 Sample digestion and analysis.....77

4.3.4 Number size distributions.....77

4.4 Results and Discussion.....77

4.4.1 MOUDI particle size distributions at EROS.....77

4.4.1.1 Port Talbot.....77

4.3.1.2 Elms Road Observatory Site (EROS).....80

4.4.2 Comparison of average MOUDI size distributions from EROS and PT.....82

4.3.3 Data from specific sampling periods.....92

4.3.3.1 Influence of wind conditions upon size distributions.....92

4.3.3.1.1 Port Talbot.....94

4.3.3.1.2 EROS site.....96

4.3.4 Coarse particle increment at Port Talbot.....98

4.3.5 Analysis of particle size spectra collected with the Grimm Optical Spectrometer.....98

4.4 Conclusions.....100

CHAPTER 5 - PORT TALBOT PARTICULATE AND GASEOUS POLLUTANT CONCENTRATIONS.....104

5.1 Abstract.....104

5.2 Introduction.....105

5.3 Materials and Methods.....106

5.3.1 Particulate matter sampling 106

5.3.2 Sample digestion and analysis.....106

5.3.3 Gaseous Pollutants.....107

5.4 Results and Discussion.....107

5.4.1 FDMS versus Partisol PM mass concentration data 107

5.4.2 Inter-comparison between FDMS and Partisol PM at the monitoring sites.110

5.4.3 $PM_{2.5}$ to PM_{10} ratios.....113

5.4.4 Gaseous pollutant data during Port Talbot campaign 113

5.4.5 Relationships between FDMS and Partisol PM versus gaseous pollutants.115

5.4.6 Meteorological conditions during the sampling campaign.....116

5.4.7 Black carbon concentrations during the campaign.....118

5.4.8 Polar plots of particulate and gaseous pollutants.....119

5.4.9 Grimm vs. Partisol, FDMS and MOUDI mass concentrations.....121

5.4.10 Diurnal variations of PM, PNC and gaseous pollutants 123

5.5 Conclusion.....125

CHAPTER 6- CHEMICAL COMPOSITIONS OF PARTISOL AND STREAKER SAMPLES.....126

6.1 Abstract.....126

6.2 Introduction.....127

6.3 Results.....128

6.3.1 Partisol PM data.....128

6.3.1.1 The Average elemental concentrations at the monitoring sites.....128

6.3.1.2 Time series plots for water soluble ion and metal concentrations of Partisol fine and coarse PM.....131

6.3.1.3 Aerosol chemistry at the monitoring sites.....133

6.3.1.4 Mass ratios of NO_3/nss-SO_4.....135

6.3.1.5 Enrichment factors 136

6.3.1.6 Concentration ratios of PM chemical compositions.....138

6.3.1.7 Correlations among Partisol PM constituents and other pollutants at FS..140

6.3.1.8 Analysis of variance (ANOVA) of Partisol PM components at the monitoring sites.....147

6.3.2. Streaker PM components.....147

6.3.2.1 Comparison of hourly Streaker and FDMS mass components.....147

6.3.2.2 Average elemental concentrations for Streaker (PIXE) PM Data.....150

6.3.2.3 Temporal variations of Streaker PM elemental concentrations.....152

6.3.2.4 Enrichment factor analysis of Streaker data.....156

6.3.2.5 Correlational analysis among Streaker elemental components.....158

6.3.2.6 Streaker elemental ratios.....162

6.3.2.7 Polar plots of elements.....162

6.3.3 Organic Carbon (OC) and Elemental Carbon (EC) Concentrations of $PM_{2.5}$ at FS.....169

6.4 Partisol and Streaker Data Discussion.....170

6.5 Conclusion.....175

CHAPTER 7 - RECEPTOR MODELLING OF PARTISOL AND STREAKER SAMPLES.....176

7.1 Abstract.....176

7.2 Introduction.....177

7.3 Results and Discussion.....179

7.3.1 Positive matrix factorization (PMF).....179

7.3.1.1 PMF for Partisol PM data.....179

7.3.1.2 PMF for Streaker (PIXE) data.....188

7.3.2 Principal component analysis (PCA).....198

7.3.2.1 PCA for Partisol fine and coarse data.....198

7.3.2.2 Rotated PCA for Streaker data.....202

7.4 Conclusions.....206

CHAPTER 8 - SINGLE PARTICLE ANALYSIS DURING THE PORT TALBOT CAMPAIGN.....207

8.1 Abstract.....207

8.2 Introduction.....208

8.3 Materials and Methods.....208

8.4 Results and Discussion.....209

8.4.1 ATOFMS chemical compositions.....209

8.4.1.1 K-rich particle class.....211

8.4.1.1.1 K-CN particle.....211

8.4.1.1.2 K-NO_3 particle.....214

8.4.1.1.3 K-EC particle type.....214

8.4.1.1.4 K-Cl-PO_3 particle type.....215

8.4.1.2 Sea salt class.....215

8.4.1.2.1 Na-NO_3 particle.....215

8.4.1.3 Silica dust particle.....217

8.4.1.3.1 Na-$HSiO_2$ particle.....218

8.4.1.4 Sulphate (K-HSO_4) particle class.....219

8.4.1.5 Nitrate (AlO-NO_3) particle class.....219

8.4.1.6 Ca rich particle class.....220

8.4.1.7 Carbon class particles.....222

8.4.1.7.1 Mn-OC particle type.....224

8.4.1.7.2 Metallic-EC particle type.....225

8.4.1.7.3 EC particle type.....225

8.4.1.7.4 OC particle type.....225

8.4.1.7.5 OC-EC particle type.....226

8.4.1.7.6 EC-NO_3 particle type.....226

8.4.1.8 Aromatic hydrocarbon (Arom) and PAH particle class.....227

8.4.1.8.1 Aromatic-CN particle type.....228

8.4.1.8.2 Fe-PAH-NO_3 particle type……..229

8.4.1.8.3 PAH-CN particle particle type…….229

8.4.2 Source contributions by ATOFMS particles.....230

8.4.3 Size Distribution of particle classes 232

8.3.4 Temporal variations and polar plot of total particle number concentrations239

8.4.5 Comparison of the daily ATOFMS mass and other PM measuring instruments.....241

8.5 Conclusion.....243

CHAPTER 9- SUMMARY AND FURTHER WORKS.....245

9.1 Offline Partisol, MOUDI and Streaker Data.....245

9.1.1 Mass and chemical composition.....245

9.1.2 Average steelworks increments associated with wind sectors.....251

9.1.3 The annual PM steelworks increments.....263

9.2 Online Instruments Data 266

9.3 Conclusion.....273

9.4 Further Work.....276

REFERENCES.....278

APPENDICES.....304

LIST OF TABLES

Table 1.1: Guidelines for average ambient particulate and gaseous concentrations.8

Table 1.2: Contribution of each trace metal from industrial processes to total emissions and their major sources in the UK based on 1999 NAEI.....22

Table 3.1: Inter-site correlations between EROS and BROS PM.....68

Table 5.1: Summary of mean concentrations of FDMS and Partisol PM_{10}.....112

Table 6.1: Mean, standard deviation and percentage composition of water soluble ions and metal concentrations of Partisol $PM_{2.5}$ and $PM_{2.5\text{-}10}$ in Port Talbot.....129

Table 6.2: Reduced Major Axis (RMA) equations for ionic balance.....132

Table 6.3: Pearson's correlation coefficient $PM_{2.5}$ metal compositions, water-soluble ions and gaseous pollutants at FS site.....143

Table 6.4: Pearson's correlation coefficient $PM_{2.5\text{-}10}$ metal compositions, water-soluble ions and gaseous pollutants at FS site.....145

Table 6.5: Mean, standard deviation of Streaker elemental concentrations of $PM_{2.5}$ and $PM_{2.5\text{-}10}$ in Port Talbot.....151

Table 6.6: The EF values of elemental concentrations of PM at FS and LW stations.....157

Table 6.7: Pearson correlations coefficients at FS for (a) $PM_{2.5}$.....160

Table 6.8: Pearson correlation coefficients at LW for (a) $PM_{2.5}$.....161

Table 7.1: Summary of emissions from the steelworks components.....178

Table 7.2: Rotated Component Matrix for Partisol.....200

Table 7.3: Rotated components for FS Streaker.....204

Table 7.4: Rotated Component Matrix of LW Streaker.....205

Table 8.1: Summary of ATOFMS particles' clusters information.....210

Table 8.2: Locations of the steelwork sectors from the Fire Station sampling site...211

Table 8.3: Summary of the particle cluster emission sources.....231

Table 8.4: Table showing the hit rate of particle diameters 233

Table 9.1: General observation at the FS site during the period when high PM_{10} concentrations were recorded.....248

Table 9.2: The wind sector locations of the steelworks facilities.....252

Table 9.3: Annual PM steelworks increment calculated from the wind-determined and PMF analyses at (a) FS.....265

LIST OF FIGURES

Figure 1.1: The arrangement of particles by their typical mass/size distribution in the atmosphere.....5

Figure 1.2: Materials flowchart in integrated steelworks.....19

Figure 2.1: A pictorial representation of MOUDI and Schematic diagram of a stage in MOUDI.....29

Figure 2.2: A picture and schematic diagram of dichotomous sampler.....31

Figure 2.3: FDMS unit and the schematic of operation.....33

Figure 2.4: A unit and sampling diagram of a Streaker.....34

Figure 2.5: A filter loaded and schematic unit of a digitel high-volume sampler....36

Figure 2.6: A unit of a potable GRIMM aerosol spectrometer.....37

Figure 2.7: A pictorial and schematic diagram of TSI ATOFMS.....38

Figure 2.8: The Mobile Laboratory showing sampling inlets of ATOFMS and other instruments during Port Talbot sampling campaign.....40

Figure 2.9: The Magee Scientific Aethalometer during Port Talbot sampling campaign.....41

Figure 2.10: Schematic diagram showing ion analysis process.....44

Figure 2.11: Plot of clustering error against numbers of K.....48

Figure 2.12: *m/z* calibration plots for positive and negation spectra 49

Figure 2.13: Size calibration curve.....49

Figure 2.14: Summary of PT sampling methodology.....54

Figure 3.1: Map showing EROS and BROS monitoring sites.....57

Figure 3.2: Compositions of PM at EROS and BROS.....62

Figure 3.3: Linear regression analysis of $PM_{2.5}$ and $PM_{2.5\text{-}10}$ at EROS and BROS...63

Figure 3.4: PM elemental difference between background (EROS) and roadside (BROS) indicating roadside increments.....64

Figure 3.5: Comparison between average Partisol and MOUDI data at EROS.....66

Figure 3.6: Relationship between Partisol and MOUDI data at EROS.....66

Figure 4.1: Port Talbot sampling station and the steelworks processing units.....76

Figure 4.2: Variations of 72-hour MOUDI PM mass size distributions at the PT site.....78

Figure 4.3: Variations of 72-hour MOUDI PM size distributions of Fe at the PT site.....79

Figure 4.4: Variations of 72-hour MOUDI PM mass size distributions at the EROS site.....80

Figure 4.5: Variations of 72-hour MOUDI PM size distributions of Fe at the EROS site.....81

Figure 4.6: Average MOUDI size distributions at the EROS and PT sites.....84

Figure 4.7: Wind roses for the individual sampling periods (a) Port Talbot (b) EROS.....92

Figure 4.8: Polar plots of particle number concentrations from the Grimm analyser in 14 size bins as a function of wind direction and speed.....98

Figure 5.1: Daily plots of Partisol and FDMS PM_{10} and $PM_{2.5}$ at the four sampling stations.....108

Figure 5.2: Time series plot comparing FDMS and Partisol PM all the monitoring site.....111

Figure 5.3: $PM_{2.5}/PM_{10}$ ratio for FDMS and Partisol in all the monitoring sites.....113

Figure 5.4: Daily variations of gaseous pollutants during

the sampling at Port Talbot.....114

Figure 5.5: Meteorological data variations at Port Talbot during the monitoring period.....117

Figure 5.6: Windrose plots at Port Talbot during the PM_{10} pollution episodes on (a) April 26 (b) May 8 and (c) May 11.....118

Figure 5.7: Daily and diurnal concentrations of Black Carbon.....119

Figure 5.8: Polar Plots of air pollutants during Port Talbot campaign.....121

Figure 5.9: Temporal variations between GRIMM, FDMS, Partisol and MOUDI PM size distribution.....122

Figure 5.10: Diurnal variations of PM and gaseous pollutants.....125

Figure 6.1: NO_3/nss-SO_4 mass ratios for $PM_{2.5}$ and $PM_{2.5-10}$.....136

Figure 6.2: Enrichment factors for $PM_{2.5}$ and $PM_{2.5-10}$ metals.....138

Figure 6.3: Variations in hourly FDMS and Streaker constructed mass concentration at (a) FS and (b) LW.....148

Figure 6.4: Diurnal variations of Streaker elemental concentrations.....155

Figure 6.5: Scatter plots of coarse PM showing relationships among Al, Si and Ti at FS and LW.....157

Figure 6.6: Polar Plots of elemental concentrations of Streaker $PM_{2.5}$ at FS.....165

Figure 6.7: Polar Plots of elemental concentrations of Streaker $PM_{2.5-10}$ at FS.....166

Figure 6.8: Polar Plots of elemental concentrations of Streaker $PM_{2.5}$ at LW.....168

Figure 6.9: Polar Plots of elemental concentrations of Streaker $PM_{2.5-10}$ at LW.....169

Figure 6.10: Daily variations of OC-EC during Port Talbot campaign.....170

Figure 7.1: PMF profiles for daily Partisol PM at Port Talbot.....182

Figure 7.2: Percent contributions to sources identified by PMF.....187

Figure 7.3: Streaker PMF profiles for $PM_{2.5}$ and PM_{10} at FS and LW.....191

Figure 7.4: Source contributions by PMF at the two monitoring sites for $PM_{2.5}$ and PM_{10} (Streaker samplers).....195

Figure 7.5: Polar Plots for Streaker PMF profiles at FS and LW.....198

Figure 7.6: PCA source contributions for $PM_{2.5}$ and $PM_{2.5-10}$.....201

Figure 8.1: Mass spectra plots of K particle class.....213

Figure 8.2: Polar plots of K-rich particle class.....213

Figure 8.3: Sea salt particle spectra and polar plots.....216

Figure 8.4: Silica particle mass spectra and polar plots.....218

Figure 8.5: Mass spectra and polar plots of $K\text{-}HSO_4$ particle.....219

Figure 8.6: Mass spectra, polar and diurnal plots of $AlO\text{-}NO_3$ particle.....220

Figure 8:7: Mass spectra, polar and diurnal plots of Ca particle.....221

Figure 8:8: Mass spectra trends of carbonaceuos particles.....223

Figure 8:9: Polar plots of carbonaceuos particles.....224

Figure 8.10:Mass spectra plots of Arom-PAH particles.....227

Figure 8.11: Polar plots of Arom-PAH particles.....228

Figure 8.12: Source contribution of particle classes.....232

Figure 8.13: Inverse transmission Efficiency versus D_a.....233

Figure 8.14: Size distribution of scaled particle class counts.....236

Figure 8.15: Mass distribution of particle classes.....239

Figure 8.16: ATOFMS total particle number concentration 240

Figure 8.17: Polar plot of ATOFMS total particle counts.....241

Figure 8.18: Daily mass distribution of ATOFMS and other mass-measuring instruments.....242

Figure 8.19: Wind direction plots during elevated ATOFMS mass concentrations.....243

Figure 9.1: Wind rose plots showing days where prevailing winds blow across the steelworks to the receptor location at FS for which the steelworks increments for Partisol data are calculated.....253

Figure 9.2: Map of Port Talbot showing the 16 wind sectors linking the steelworks productions units to the receptor site at FS 255

Figure 9.3: Wind-determined and PMF mass and chemical profiles for steelworks sinter plant at FS.....258

Figure 9.4: Wind-determined and PMF mass and chemical profiles for BF steelworks at FS.....259

Figure 9.5: Wind-determined and PMF mass and chemical profiles for steelworks BOS/Coking at FS.....260

Figure 9.6: Wind-determined and PMF mass and chemical profiles of steelworks factors at LW.....262

Figure 9.7: The annual wind rose plot at Port Talbot from January 1 to December 31, 2012.....264

.

LIST OF DEFINITIONS AND/OR ABBREVIATIONS

ANOVA	Analysis of Variance
AQEG	Air Quality Expert Group
ART	Adaptive Resonance Theory
AURN	Automatic Urban Rural Network
ATOFMS	Aerosol Time of Flight Mass Spectrometry
BC	Black Carbon
BF	Blast Furnace
BOS	Basic Oxygen Furnace Steelmaking
BROS	Bristol Road Observatory Site
CCA	Copper chromate arsenate
CMB	Chemical Mass Balance
CO	Carbon monoxide
CO_2	Carbon dioxide
COPD	Obstructive Pulmonary Disease
CPC	Condensation Particle Counter
DEFRA	Department for Environment, Food and Rural Affairs
DfT	Department for Transport
DMRT	Duncan Multiple Range Test
DS	Dyffryn School site
EAF	Electric Arc Furnace
EC	Elemental Carbon
EC	European Commission
EF	Enrichment Factor

ENCHILADA	Environmental Chemistry through Intelligent Atmospheric Data Analysis
EROS	Elms Road Observatory Site
ESE	East south-westerly
EU	European Union
EUSAAR	European Supersites for Atmospheric Aerosol Research
FDMS	Filter Dynamic Measurement System
FID	Flame Ionization Detector
FS	Fire Station site
HDDV	Heavy Duty Diesel Vehicle
ICPMS	Inductively Coupled Plasma Mass Spectrometer
ICS	Ion Chromatography System
IPCC	Inter-governmental Panel on Climate Change
LDV	Light Duty Vehicle
LW	Little Warren site
MDL	Method Detection Limit
MLR	Multiple Linear Regression
MOUDI	Micro-Orifice Uniform Deposit Impactor
NAEI	National Atmospheric Emissions Inventory
NIST SRM	National Institute of Standards & Technology Standard Reference Material
NO	Nitrogen monoxide
NO_2	Nitrogen dioxide
NO_x	Nitrogen Oxides
NPTCBC	Neath Port Talbot County Borough Council
NRW	Natural Resources Wales

O_3	Ozone
OC	Organic Carbon
OHF	Open Hearth Furnace
OPC	Optical Particle Counter
PAH	Polycyclic Aromatic Hydrocarbon
PBDE	Polybrominated diphenyl Ether
PCA	Principal Component Analysis
PCB	Polychlorinated diphenyl
PCDD/F	Polychlorinated dibenzo-dioxin and dibenzofuran
PIXE	Particle Induced X-ray Emission
PM	Particulate Matter
$PM_{2.5}$	Particulate matter with aerodynamic diameter less than 2.5 μm
$PM_{2.5-10}$	Particulate matter with aerodynamic diameter greater than 2.5 μm but less than 10 μm
PM_{10}	Sum of $PM_{2.5}$ and $PM_{2.5-10}$
PMF	Positive Matrix Factorization
PNC	Particle Number Concentration
PS	Prince Street site
PT	Port Talbot
R & P	Rupprecht & Patashnick
S	Southerly
SE	South-easterly
SO_2	Sulphur dioxide
SPSS	Statistical Package for Social Sciences

SSW	South south-westerly
SW	South-westerly
TSP	Total Suspended Particulates
UF-ATOFMS	Ultra Fine Aerosol Time of Flight Mass Spectrometer
UK	United Kingdom
USA	United States of America
US EPA	United Stated Environmental Protection Agency
W	Westerly
WHO	World Health Organization
WSW	West South-westerly

CHAPTER 1- INTRODUCTION

1.1 Abstract

This section details the general overview of particulate matter, its sources and composition as well as its health effects. Receptor models often used for source apportionment of particulate matter are discussed within this chapter. The aims and objectives of the study are also highlighted in this section. Literature reporting work conducted around steel industrial sites is also reviewed. Part of this review has been prepared for publication.

1.2 General Overview of Airborne Particulate Matter

Particulate matter (PM) is a mixture of organic and inorganic substances suspended as liquid droplets or solid particles in the air. These suspended minute particles originate from diverse sources, and with sizes ranging from tens of micrometers to a few nanometers. These particulate pollutants are emitted from different sources and are transported into the atmosphere, where they are mixed, transformed, some are bio-accumulated and consequently cause ill-effects on both biotic and abiotic systems. Particle pollution is made up of a number of components such as ionic and carbonaceous species, organic constituents (including acids), metals, and soil or dust particles.

Rapid economic and industrial developments have led to increased energy consumption, emission of air pollutants and poor air quality in the major cities of the world (Chan and Yao, 2008). According to Celis *et al.* (2004), Penner *et al.* (2004), Hong *et al.* (2002), Khoder (2002), Kaufman *et al.* (2002) and Rajkumar and Chang (2000), PM is capable of influencing many atmospheric processes including cloud formation, visibility, solar radiation and precipitation. It also plays a major role in acidification of clouds, rain and fog. It may also carry some toxic or acidic substances like heavy metals and carcinogenic organic compounds and may initiate detrimental health effects on humans and ecosystems (Karthikeyan *et al.*, 2006; Lewtas, 2007).

Aerosols found in urban areas represent a mixture of primary particles from several sources such as vehicles, coal-fired power plants, oil refineries, forest fires, and steel, cement and paper plants (DoT, 2002; Braga *et al.*, 2002; Samara *et al.*, 2003) and secondary particles formed by chemical reactions. These urban particles are very diverse

in chemical composition and structure because of their sources (Johnson *et al.*, 2005). Although, measures have been put in place by the developed nations to abate air pollution, epidemiological studies still show that the current air pollution episodes are capable of causing harm to the public. The Natural Resources Defence Council reported that particulate air pollution causes 64,000 deaths annually in the United States (Mysliwiec and Kleeman, 2002). In Europe, Watkiss *et al.* (2005) has reported around 350,000 annual premature deaths, while at the global scale more than 1 million deaths per year are recorded due to exposure to ambient particulate matter (WHO, 2009; Anenberg *et al.*, 2010).

Two important airborne particulate matter metrics are fine (< 2.5μm aerodynamic diameter; $PM_{2.5}$) and coarse (> 2.5 μm <10 μm aerodynamic diameter; $PM_{2.5-10}$) particles. PM_{10} is the summation of the two fractions (i.e $PM_{10} = PM_{2.5} + PM_{2.5-10}$). Fine and coarse particles are defined primarily in terms of their formation mechanisms and sizes; and they also differ in sources, chemical composition, and removal processes (Harrison *et al.*, 2001).

Fine particles normally arise from anthropogenic sources (Pope and Dockery, 2006) and can be subjected to regulation by air pollution control technologies. The formation of coarse particles is a result of mechanical disruption and attrition processes, and these are largely re-suspended soils and street dusts, fugitive dusts from industrial sources, sea salts, pollen and fungi spores, plant and animal fragment and tyre-wear debris. These particles are mainly of natural origin (as well as from industries like construction, mining and quarrying) and therefore extremely difficult to develop control strategies for (Harrison *et*

al., 2001; Pope and Dockery, 2006). The processes such as condensation, evaporation and coagulation may change the size and composition of particulate matter (Braga *et al.*, 2005; Debry *et al.*, 2006).

Ultrafine particles are those with an aerodynamic diameter less than 0.1 μm ($PM_{0.1}$). These particles are released into the ambient atmosphere from combustion-related sources, such as vehicle exhaust, and atmospheric nucleation and reactions (Oberdorster, *et al.*, 2005). They are short-lived and rapidly grow to form larger particles. Particles are formed through gas-to-particle conversion processes which are condensation, nucleation and coagulation (Malm, 1999).

Condensation occurs when gaseous vapours condense or combine with existing small nuclei known as condensation nuclei. These small condensation nuclei may originate from marine or combustion activities. Particles may be formed when gases interact and combine with molecules of their own kind in a process called homogeneous nucleation (Malm, 1999). When gases nucleate on particles of a different kind than themselves, this is called heterogeneous nucleation. After aerosols are formed, they can grow in size by coagulation, in which particles essentially collide and stick together (Malm, 1999). These processes are summarized in Figure 1.1. Fine particles arise predominantly from high temperature sources or from gas to particle conversion processes within the atmosphere (Harrison *et al.*, 2001).

Fine particles contain substantial amounts of sulphate and nitrate in the form of their ammonium salts, plus organic and elemental carbon as well as varied trace metals

(Harrison and Yin, 2000; Mysliwiec and Kleeman, 2002). Carbonaceous species are a major component of PM and could account for up to 50% of the fine particulate mass concentration ($PM_{2.5}$) on an annual average (Baltensperger *et al.*, 2005). A study has also revealed ionic species to constitute up to 70% of the total aerosol mass (Hueglin *et al.*, 2005).

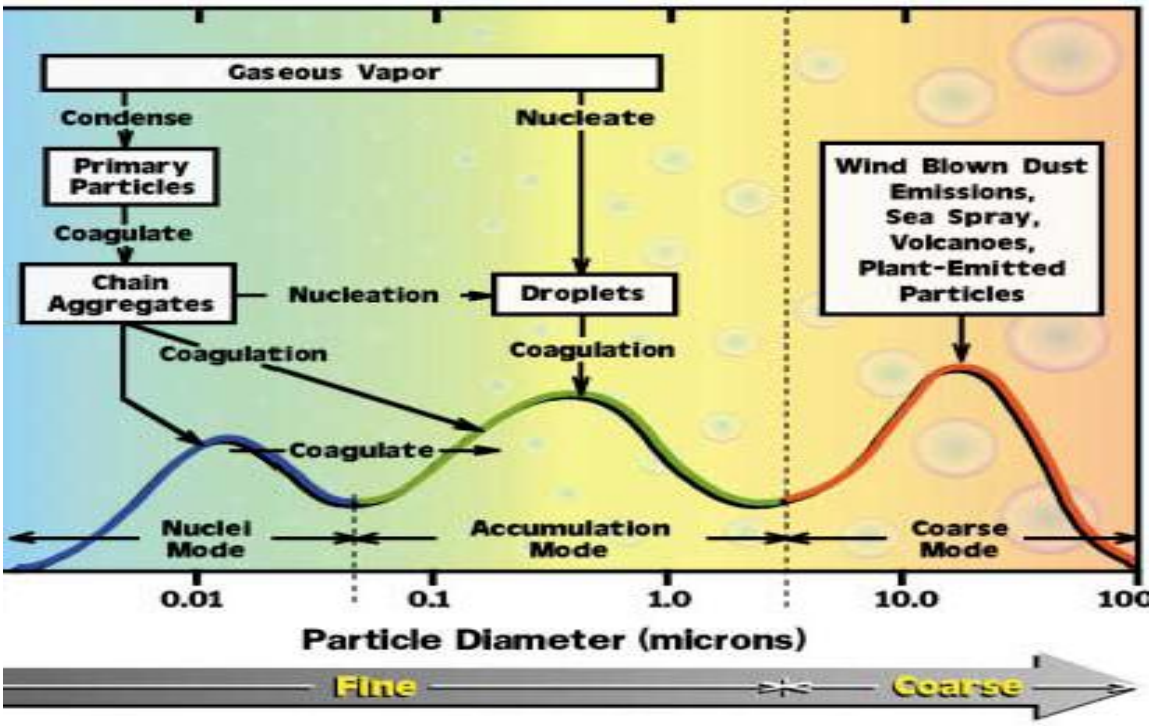

Figure 1.1: The arrangement of particles by their typical mass/size distribution in the atmosphere (Malm, 1999)

Fine particulate matter is the most dangerous component because it can travel over long distances and can penetrate into the respiratory tract carrying toxic substances (Pope and Dockery, 2006). Many studies have suggested that the fine particles rather than coarse particles (PM_{10}) are more damaging to health (Harrison and Yin 2000; Samet *et al.* 2000). Schwartz *et al.* (1996) disputed these theories that fine particles produce more health

effects than coarse particles. This is because during certain times, one size range of particles has been shown to produce a certain health effect, while at the other times this same size range of particles has shown no effect. The health effects may be irrespective of particle size but dependent upon source type. Particles from different sources have been shown to have quite different health effects (Laden *et al.*, 2000; Morawska and Zhang, 2002). However, the concentrations of fine and coarse particles are well correlated (Anderson *et al.*, 2001). An increase in daily mortality by approximately 1% per 10 μg m^{-3} increase in PM_{10} concentration has been reported by Harrison and Yin (2000). Similar evidence has been reported by Anderson *et al.* (2001), as they linked ambient particles of PM_{10} measured in the West-Midlands conurbation of the UK with daily mortality.

Determination of particulate matter size and identification of aerosol sources are important tools for strategizing abatement measures in air quality control and for policy making. Aside from the health consideration of PM_{10}, Hien *et al.* (2001) stated that it also provides information about dissimilarity between anthropogenic and natural crustal matter sources.

1.3 Health Effects of Particulate Matter

Continuous exposure to small-sized particle of atmospheric aerosols could pose negative effects on human health and the environment. The World Health Organization (WHO), European Union (EU), and the United States Environmental Protection Agency (US EPA) have highlighted guidelines for ambient particles concentration exposure (Table 1.1) for protection of human health. These guidelines are based on clinical, toxicological, and epidemiological evidence and were established by determining the concentrations with the lowest observed adverse effect (World Bank Group, 1998).

The health problems caused by particulate matter had been reviewed by many researchers (Harrison and Yin, 2000; Davidson *et al.*, 2005; Pope and Dockery, 2006). These particles may due to their relatively minute sizes be dangerous to both human health and the ecosystem. It has been proven that toxicity of a substance would increase as particle size decreases (Buzea *et al.*, 2007) due to greater surface area per unit mass.

Epidemiological studies from many researchers have indicated a strong correlation between elevated concentrations of PM_{10} and increased mortality and morbidity (Lin and Lee, 2004; Arditsoglou and Samara, 2005; Namdeo and Bell, 2005). Pope *et al.* (2002) have shown an association between PM pollution and the number of deaths from cancer and cardiovascular and respiratory diseases. US EPA (2004) also linked PM concentration to increased adverse cardiac and respiratory health effects. Schwartz *et al.* (2002) demonstrated a strong relationship between $PM_{2.5}$ and mortality in US six cities.

Special importance has also been attributed to ultrafine particles by Pope and Dockery (2006) due to their high toxicity and effect on public health. Particles of less than 0.1 μm have been reported to form 60% total lung deposition while particles of sizes 0.1-1.0 μm and 5.0 μm formed 20 and 80% deposit, respectively (WHO, 2000). Elemental carbon (EC) or black carbon (BC) is a component of PM that has been associated with respiratory diseases and adverse cardiac effects in children (Tolbert *et al.*, 2000; Gauderman *et al.*, 2004).

Table 1.1: Guidelines for average ambient particulate and gaseous concentrations

Pollutant	Averaging Time	AQG value		
		µg m^{-3}		
		WHO (2006)	EC (2006)	US EPA (2008)
$PM_{2.5}$	1 year	10	25	15
	24 h (99 Percentile)	25	50	35
PM_{10}	1 year	20	40	
	24 h (99 Percentile)	50		150
Ozone, O_3	8 h, daily maximum	100	120	75
Nitrogen dioxide, NO_2	1 year	40	40	
	1 h	200	200	
Sulphur dioxide, SO_2	24 h	20	125	14
	10 min	500		
Benzene	1 year		5	
Lead	1 year		0.5	0.15
		ng m^{-3}		
Arsenic			6	
Cadmium			5	
Nickel			20	
PAH			1	
		mg m^{-3}		
Carbon monoxide, CO	8 h daily Maximum		10	9

Accumulated data suggested that PM may lead to pulmonary inflammation, lung diseases such as asthma and chronic obstructive pulmonary disease (COPD) (Gong *et al.*, 2003; Gan *et al.*, 2004). A study conducted in Germany has also shown a consistent significant increase in blood pressure in adults in association with increased concentrations of total suspended particulates (TSP) at a central site (Ibald-Mulli *et al.*, 2001). Additionally, PM from combustion sources contains polycyclic aromatic hydrocarbon (PAH), which are anticipated to be carcinogenic (NTP, 2003). The potential carcinogenic effect of certain

dust compounds have been analyzed, and in some cases (for example, for silica dust), limited evidence of carcinogenic effects has been found (Soutar *et al.*, 2000). Epidemiologic evidences suggested that there may be no safe threshold for fine particulate matter and that the effects are linearly related to its concentration (DiBattista and Brown, 2003; Daniels *et al.*, 2004). WHO (2000) observed that about 30% of the respiratory diseases are related to personal exposure to high levels of outdoor PM concentration.

1.4 Effects of PM on the Environment

Atmospheric particles can alter the amount of solar radiation transmitted through the Earth's atmosphere (USEPA, 2004). Absorption of solar radiation by atmospheric particles, together with the trapping of infrared radiation emitted by the Earth's surface by certain gases, enhances the heating of the Earth's surface and lower atmosphere (Jacobson, 2002). Increases in the atmospheric concentration of these gases due to human activities may lead to climate change with subsequent effect on humans and ecological system (IPCC, 2001). Reflective particles can also cause cooling by reflecting incoming solar radiation back to space. Stanhill and Cohen (2001) has shown a correlation between significant reductions in solar radiation received globally over 50 years on the earth surface due to increase in atmospheric aerosol. Hence, particulate matter plays a significant role in defining climate on both global and regional scales.

Effects of air pollution on materials are related to both loss of aesthetic value and physical damage (US EPA, 2005). Studies have demonstrated that particle pollutants, primarily carbonaceous compounds caused soiling of commonly used building materials and culturally important items, such as statutes and artistic works (Ghedini *et al.*, 2006; Nava

et al., 2010). This may lead to an increase in cleaning and maintenance costs and a loss of utility. Physical damage from the dry deposition of air pollutants, especially sulphates and nitrates, and the absorption or adsorption of corrosive agents on deposited particles also can result in the acceleration of naturally occurring weathering processes of man-made building and cultural materials (US EPA, 2004).

1.5 Particulate Matter Measurements

Aerosols are complex in nature, and the understanding of them depends on the instrumentation available to study them. Over time, different instruments have evolved ranging from offline to online. These instruments enable measurement of particles at different size ranges. Generally, offline PM measurement involves collection of aerosol onto filter substrates over a specified collection time. Offline air samplers such as micro-orifice uniform deposit impactor, Partisol dichotomous and Streaker have been used for airborne particle sampling (Nava *et al*, 2002; Gietl *et al.*, 2010; Yin *et al.*, 2010; Gupta *et al.*, 2012). The exposed filters are transported to laboratory for chemical analysis. Major disadvantages of offline measurement include bulky sampling, poor temporal resolution, problems of internal and external mixing, aerosol volatility during sampling, loss of materials during transportation of samples, filter weighing or cutting, and general laboratory errors (Rodriguez *et al.*, 2012). Most of these shortcomings could be circumvented by practising good sampling and laboratory procedures. The use of online instruments for aerosol measurement provides solutions to all the problems arising from offline sampling methods of PM. Online instruments entail measuring PM in a real time. This gives a high time resolution measurement and can be used to complement offline instruments.

1.6 Single Particle Analysis

Aerosol time of flight mass spectrometry (ATOFMS) provides continuous, real-time detection and characterization of single particles from poly-disperse samples, supplying information on particle size and composition (see details in the methodology chapter). Single particle analysis involving airborne particulate matter has been traced back to the 1970s (Gross *et al.*, 2000). The breakthrough of simultaneous analyses of both negative and positive spectra of a single particle in a real time came when Prather and co-workers developed ATOFMS in 1994 at the Department of Chemistry, University of California, Riverside, California, United States. The instrument was used for calibration and optimization of organic-based particles containing small amounts of various salts including NaCl, KCl, and Na_2SO_4. Three clear distinct mass spectra were created indicating that the instrument was capable of sizing and ionising particles typical of the atmospheric environment.

Single particle mass spectrometry is a documented technique well suited to determine the size and composition of large numbers of particles (Sullivan and Prather, 2005). The advantage of ATOFMS over other methods of source apportionment is its ability to identify association among species within individual particles. This association can be related to direct source apportionments (Kelly *et al.,* 2003). ATOFMS is also capable of avoiding incorrect mass assignment due to interferences (multiple ions detected at the same nominal mass) (Noble and Prather, 2000). However, the key disadvantage is its cost of purchase and interpretation of the spectra which requires a steep learning curve (Kelly *et al.,* 2003).

1.6.1 Literature review on ATOFMS

The single particle mass spectrometry technique with ATOFMS has been used extensively for online source apportionment of ambient aerosols as well as indoor air quality monitoring (Dall'Osto *et al.*, 2004; Dall'Osto *et al.*, 2007; Toner *et al.*, 2008; Smyth *et al.*, 2013).

In 1997, during the South California Ozone Study-North American Research Strategy for Tropospheric Ozone (SCOS97-NARSTO), an ATOFMS instrument was used by Pastor and co-workers for single particle measurements. The data were published in 2003. ART-2a (Adaptive Resonance Theory) software applied for the analysis of particles identified classes such as organic carbon with amines, elemental carbon, organic carbon, ammonium nitrate, sea salt, soil dust and various metal-rich types.

In 2008, Toner *et al.* deployed Ultra Fine Aerosol Time of Flight Mass Spectrometer (UF-ATOFMS) to a freeway site in San-Diego, California, USA for a single particle analysis. With the aid of ART-2a, UF-ATOFMS revealed clusters categorized as emissions from diesel powered heavy duty diesel vehicles (HDDV) and gasoline powered light duty vehicles (LDV). The study showed that 83% of the UF-ATOFMS detected particles were emitted from vehicles of which 51% and 32% were apportioned to HDDV and LDV, respectively. The single particle analysis revealed HDDV as the major emitter of ultrafine particles of diameter 50-100 nm while LDV was a major contributor to fine particles (100-300 nm). The study was consistent with many studies which linked HDDV to ultrafine particle emissions (Hallquist *et al.*, 2012). The ATOFMS instrument has proven its ability to resolve different particles associated with different fuel-types.

In Northern Mexico City, Moffet *et al.* (2008) was able to measure ambient aerosol in the industrial and residential areas of the city using ATOFMS. Their findings indicated that biomass burning and industrial emissions made significant contributions to primary particle loadings in Mexico City, depicting strong correlations with local meteorology. Results also showed that the majority of particles in the submicron mode were emitted from biomass/bio fuel burning (40%) and aged organic carbon (31%), internally mixed with oxidized OC marker (C_2H_3O, *m/z* = 43), nitrate, sulphate and ammonium. This study showed the relevance of ATOFMS instrument in the identification of biomass markers; and also for the apportionment of particulate matter.

Dall'Osto and Harrison have employed the ATOFMS instrument for single particle analysis of PM in Athens (Greece) in 2006. A unique 'car particle' due to signals at *m/z* 54 ($^{54}[Fe]^+$), 56 ($^{56}[Fe]^+$), 88 $[FeO_2]^+$, 138 $[Ba]^+$ and 154 $[BaO]^+$ was identified as a traffic fingerprint. Five broad classes of PM identified during the study were sea salt, dust, carbon, inorganic and K-rich particles. Secondary carbonaceous particles which could have been difficult to detect by ion chromatography analysis were also revealed in the study.

Sullivan *et al.* (2007) also adopted ATOFMS for online characterization and composition of 731,309 particles from the marine environment. The ART-2a software used for classification of particles showed that nitrate and sulphate made up of 60-80% of PM in the super-micrometer size range. The observed nitrate and sulphate were associated with mineral dust particles formed during dust events. Information about the chemical mixing

state, which could have been difficult to obtain with filter-based measurement, was highlighted by the ATOFMS instrument.

In 2008, Dall'Osto *et al.* published the work done in the vicinity of an integrated steelworks in Port Talbot using ATOFMS. The single particle analysis linked with wind sectors has attributed Fe and Mn particles to basic oxygen furnace steelmaking (BOS), cokemaking, and/or coal stockyards emissions at the integrated steel units. The study further attributed Ni, Pb and Zn to hot and cold mills; Fe-rich particles were linked to the sinter plant/blast furnace and ore stockyard demonstrating that ATOFMS is a formidable tool for characterizing chemical fingerprints of steelworks emissions.

Recently, Giorio *et al.* (2012) applied three different techniques to analyse ATOFMS data collected in London, UK. The data analysis techniques used were PMF, ART 2a and Environmental Chemistry through Intelligent Atmospheric Data Analysis (ENCHILADA) (K mean cluster). Among the components revealed by ATOFMS were fresh and aged EC, organics, sodium chloride, sulphate, nitrogen and potassium. This showed that ATOFMS is capable of identifying aged and freshly emitted particles.

With an ATOFMS instrument, Smyth *et al.* (2013) in their recent study at a sampling site in Milwaukee, USA attributed emissions of Se, Cd, Sb and Mo to coal-fired plant. Bromine containing compounds that could have been difficult to determine with offline instrumentation was revealed by ATOFMS.

1.7 Receptor Models

The fundamental principle of receptor models is that mass conservation can be assumed and a mass balance analysis can be used to identify and apportion sources of airborne particulate matter in the atmosphere (Viana *et al.,* 2008a). They infer contributions from different source types using multivariate measurements taken at one or more receptor locations, which could be indoor or outdoor (Watson *et al.*, 2002). They are a complementary air quality assessment to the source models (dispersion model) that estimate receptor concentrations from source emissions and meteorological measurements. Receptor models use mathematical approach to quantify sources contribution using the analytical results obtained from chemical markers (Watson *et al.*, 2002). The receptor model attributes primary particles to their source types and determines the chemical form of secondary aerosol when appropriate chemical components have been measured (Guttikunda, 2009).

The two main types of receptor models are the Chemical Mass Balance (CMB) (Watson *et al.*, 2002) and multivariate statistical methods (Hopke, 2003). Multivariate models include Principal Component Analysis (PCA) (Garcia *et al.*, 2006), Positive Matrix Factorization (PMF) (Paatero and Tapper, 1994) and Unmix (Henry, 1997; 2002).

The CMB model reconstructs the chemical compositions of ambient samples through co-linearity between the emission source and compositional profiles (Watson *et al.*, 2002). The model assumes that the chemical species to be included in source profiles do not undergo chemical transformation between the sources of emission and receptor sites (Held *et al*., 2005), which implies that CMB model is not suitable for apportionment of secondary aerosols. This assumption is one of the major drawbacks of the model.

However, CMB has been applied extensively for source apportionment of PM; the model has been able to identify and apportion PM to vehicular, industrial, coal combustion, vegetative and wood burning, sea salt, crustal materials, fly ash, paved road dust, gasoline engines, meat cooking (Vega *et al*., 2000; Watson *et al*., 2001; Held *et al*., 2005, Yin *et al*., 2010).

Generally, the major advantage of multivariate statistical analysis over CMB is that no prior knowledge of emission source profiles is required (Watson *et al.*, 2002). However, large numbers of samples are needed to be fed into the models for optimal results to be achieved. Difficulty in selection of the numbers and types factors in the multivariate receptor model stands as another limitation. It is obvious that none of these models is without its own limitation. To overcome this problem, combinations of two or more models have been found feasible and plausible for source apportionment of environmental data.

Receptor models of principal component analysis (PCA), principal matrix factorization (PMF) and enrichment factor (EF) were used in this study.

1.7.1 Principal component analysis (PCA)

PCA is a technique which attempts to explain the statistical variance in a number of original variances by a minimum number of significant components. It is a multi-element statistical measurement that has been widely applied to source apportionment of particulate pollutants such as inorganic (metals and water soluble ions) (Jeon *et al.*, 2001; Venkataraman, *et al.*, 2002; Marcazzan *et al.*, 2003; Almeida *et al.*, 2005; Ayrault *et al.*,

2010), and organic (polycyclic aromatic hydrocarbons) (Singh *et al.*, 2008; Liu *et al.*, 2009; Yang *et al.*, 2013).

1.7.2 Positive matrix factorization (PMF)

Positive matrix factorization (PMF) is a source apportionment model based on the measurement of ambient data with the knowledge of the specific study for interpreting the resolved factors into meaningful sources (Johnson *et al.*, 2006). It allows for the determination of source composition profile and source contribution simultaneously. PMF is an advanced algorithm in receptor modelling developed by Paatero and Tapper (1994). Details of the PMF model have been extensively discussed in Hopke (2000) and Paatero (2000). It has been used to identify sources of bulk wet deposition concentration of strong acids in Finland (Anttila *et al.*, 1995), urban aerosol (Ramadan *et al.*, 2000; Harrison *et al.*, 2011), exposure to volatile organic compounds (VOCs) in New Jersey and California (Anderson, Miller and Milfor, 2001), and hydrocarbon emissions in Houston, Texas (Xie and Berkowitz, 2006). PMF has been used for a variety of source apportionment and spatial analysis (Hopke *et al.*, 2003; Paatero *et al.*, 2003; Kim *et al.*, 2004; Kim *et al.*, 2005; Harrison *et al.*, 2011; Gupta *et al.*, 2012). One major advantage of PMF is that it does not require source profiles to determine source contribution. However, it could be difficult to identify potential sources without some sort of profiles to which to compare the final results (Rizzo and Scheff, 2007).

1.7.3 Enrichment factor (EF)

Enrichment factor model has to do with the comparing the ratios of atmospheric concentrations of elements to a reference element and same ratios in geological or marine

material. Reference ratios vary substantially between bulk soil and suspendable particles, and among different regions. Heavy metal enrichments are commonly attributed to industries: sulphur to secondary sulphate as potassium to biomass burning; vanadium and nickel to oil combustion, selenium to coal-fired plants, iron and manganese to steel and calcium to construction or cement (Watson and Chow, 2007). Many researchers have applied this technique in particulate matter analysis (Choi *et al.*, 2001; Braga *et al.*, 2005; Reimann and de Caritat, 2005; Ayrault *et al.*, 2010).

1.8 Integrated Iron and Steel Production

Steel production is globally significant in the aspect of construction, machinery, equipment, household materials, agriculture, power generation and distribution, and medicine. However, it has been linked to emission of major air pollutants especially PM and heavy metals (Remus *et al.*, 2013). In the UK, emission data in 2006 attributed 36% of Pb, 32% Zn, 40 % Mn and 12% Cd to steel emissions (Dore *et al.*, 2008). Air pollutants emitted from the integrated steelworks could be attributed to the diverse operation units involved in steel production (Figure 1.2). Amongst the production processes involved in the integrated steel works are coke production, blast furnace (BF) and basic oxygen furnace steelmaking (BOS). These processes entail primary production of steel from the iron ore. Secondarily, steel scraps can be processed into steel at the electric arc furnace. Presently, about 70% of the world steel is produced from BOS while 29% in EAF (World Coal Association, 2013). Each of these steelmaking processes from the materials handling to steelmaking contributes significantly to emissions of metals into the atmospheric environment (Tsai *et al.*, 2007). Researchers around the world have assigned certain

chemical fingerprints to the individual processing units in the steel industry to attribute their PM sources.

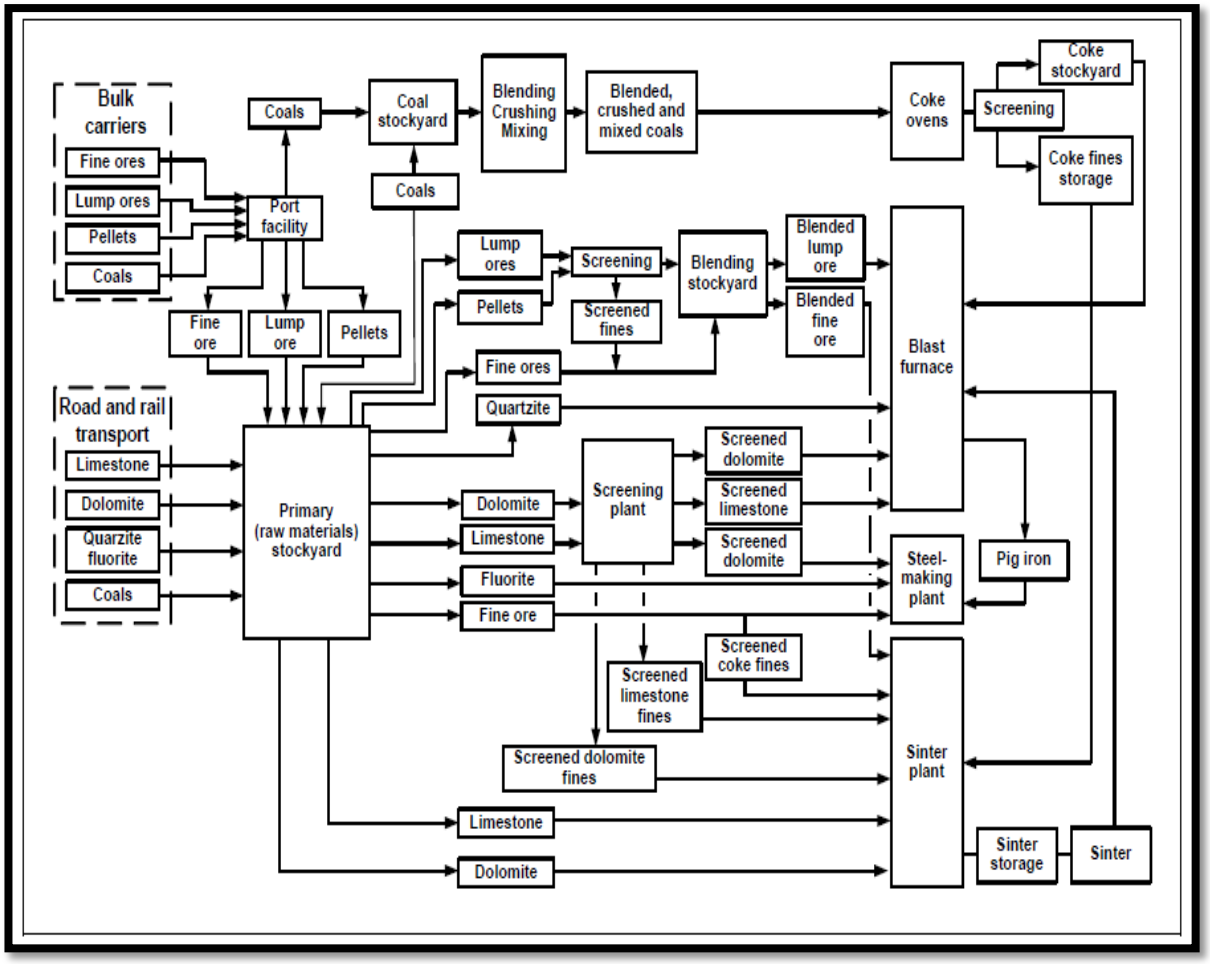

Figure 1.2: Materials flowchart in an integrated steelworks (Remus *et al.*, 2013)

1.8.1 Cokemaking (Coking)

This involves coal (pulverized, bituminous coal) cooking that is subsequently used as fuel to reduce the iron ores and also drive off volatile impurities that would interfere with iron reduction step. The process is associated with release of particulate matter, carbon

monoxide, nitrogen dioxide, sulphur dioxide, toluene, naphthalene, phenol and other aromatics, cyanide compounds, hydrogen sulphide, and ammonia (Liberti *et al.*, 2006).

1.8.2 Sintering production

This involves mixing materials such as iron ores, filter dusts and mill scale, together to prepare an appropriate feedstock for the blast furnace (Brigden *et al.*, 2000). The sinter plant is associated with the emission of dust, polychlorinated dibenzodioxin and dibenzofuran (PCDD/F), heavy metals, SO_2 and NO_x in waste gases (Anderson and Fisher, 2002).

1.8.3 Ironmaking

This is a high temperature process where metallic iron reduction from the oxide form takes place by burning with coke produced in the coking process. The process takes place in a blast furnace with copious release of carbon monoxide, nitrogen oxides and sulphur oxides as major air pollutants.

1.8.4 Steelmaking

This is the final stage in iron and steel production, which involves the addition of various alloying elements to give the finished material the combination of properties desired. Steel making takes place in three ways viz: Basic Oxygen Furnace Steelmaking (BOS) used for processing pig iron; Electric Arc Furnace (EAF) used for recycled materials; and Open Hearth Furnace (OHF) where excess carbon and other impurities are burnt out of the pig iron to produce steel.

1.8.5 Literature review on industrial emission, in particular from steelworks

In this section, the major types of PM-related pollutants will be briefly introduced with a particular focus on those from iron and steel industries. Particulate phase pollutants from industries include metals (Passant *et al.*, 2002; Querol *et al*., 2007; Tsai *et al.*, 2007), OC/EC (organic carbon, elemental carbon), PAHs (Rehwagen *et al.*, 2005; Querol *et al*., 2007), and water soluble ions (Querol *et al.*, 2002).

The iron and steel industry seems to contribute significantly to the emission of several key trace elements, such as Cd, Cr, Cu, Hg, Ni, Se, V, and Zn (Table 1.2). Analysis of airborne PM close to steel plants also showed that Fe, Mn, Zn, Pb, Cd and K are associated with emissions from the steel and iron plants. Microscopic analysis of individual particles also identified individual Fe-rich particles close to steel plants. For example, Moreno *et al.* (2004) identified iron spherules in both fine and coarse PM fractions at a steelworks in Port Talbot, South Wales, UK; Ebert *et al.* (2012) observed a significant fraction of individual iron oxides and iron mixtures in airborne PM near a steel industry in Duisburg, Rhine-Ruhr area, Germany. Elevated concentrations of these elements at the steel industry sites derive from the raw materials being used for steel production.

A study by Tsai *et al.* (2007) also suggested that K and Pb, which contribute a significant percentage (15 and 2%) to the total observed particle mass, are associated with the sintering process. Similarly, Oravisjarvi *et al.* (2003) found that the sinter plant contributes 96% and 95% of the total measured concentrations of Pb and Cd at Rahee, Finland. At the coke making process, major elements observed by Tsai *et al.* (2007) were S, Fe and Na. In the cold forming aspect of the iron and steel industry, major elements observed in the

particles were S, Fe, Na, K and Ni. The hot forming process showed high abundance of S, Fe, Na and Ca (Tsai *et al*., 2007).

Table 1.2: Contribution of each trace metal from industrial processes to total emissions and their major sources in the UK based on 1999 NAEI (adapted from Passant *et al*., 2002)

	Industrial contribution, %	Major sources
As	16	blast furnaces; basic oxygen furnaces; electric arc furnaces; primary lead/zinc production; secondary copper production; cement production; glass production
Cd	60	sinter plant; basic oxygen furnaces; primary lead/zinc production; secondary lead production; glass production; other processes (cadmium pigment manufacture)
Cr	60	coke ovens; sinter plants; basic oxygen furnaces; electric arc furnaces; primary lead/zinc production; cement production; glass production; chromium chemicals
Cu	53	sinter plants; blast furnaces; electric arc furnaces; secondary copper production; copper alloys and semis; chemicals
Pb	28	sinter plants; basic oxygen furnaces; electric arc furnaces; primary lead/zinc production; secondary lead production; glass production; alkyl lead processes
Hg	32	electric arc furnaces; iron and steel foundries; primary lead/zinc production; cement production; chloralkali processes
Ni	14	sinter plants; blast furnaces; electric arc furnaces; primary aluminium production; glass production; nickel production
Se	49	sinter plants; blast furnaces; secondary lead production; cement production; glass production
V	10	sinter plants; blast furnaces; glass production
Zn	71	blast furnaces; basic oxygen furnaces; electric arc furnaces; primary lead/zinc production; secondary copper production; glass production; other processes (zinc alloys, chemicals)

The study of Machemer (2004) showed elevated concentration of Fe, Al, Si, S and Zn at sections close to both BOS and BF. Raw materials including iron ores (FeO, Fe_2O_3,

Fe_3O_4), limestone ($CaCO_3$) and dolomite ($CaMg(CO_3)_2$) are used in a BF while, lime (CaO) and fluorspar (CaF_2) are used in a BOS plant (Machemer, 2004).

Integrated steel plants are also known for high emissions of mercury (Pacyna and Pacyna, 2002; Themelis and Gregory, 2002; Borderieux *et al.*, 2004). Asia and Europe are the regions where steel industries contribute most to the global mercury budget (Pirrone *et al.*, 2001; Pacyna *et al.*, 2006). Mukherjee *et al.* (2008) reported that annual mercury emissions from iron and steel industries in India increased by a factor of 1.25 between 2000 and 2004.

Querol *et al.* (2007) observed higher mean concentrations of metals in the PM sampled at the industrial sites in Spain between 1995 and 2006 compared to rural background values. Metals observed showed some concentrations peculiar to corresponding industries: steel industry (Cr, Mn, Zn, Se, Mo, Cd, Sn and Pb); stainless steel industry (V, Cr, Mo); copper metallurgy industry (Cu, As); zinc metallurgy industry (Zn); petrochemical estates (V, Ni); glaze and ceramic estates (Zn, As, Se, Zr, Pr, Tl, Pb and Bi); and brick manufacturing industry (Li, Ti, V, Ni, Ge, Se, Rb, Ce and Tl).

Steel industry is an important emitter of PAHs into the atmosphere (Yang *et al.*, 2002; Manoli *et al.*, 2004). PAHs are usually released from coke manufacturing, sintering, iron making, casting, mould pouring and cooling and steelmaking (Yang *et al.*, 2002). Bjorseth and Ramdahl (1985) estimated PAH emissions from the iron and steel industries as 12% of yearly total PAH emission in Norway and therefore, represented the second major emitter of PAH in the country. Choi *et al.* (2007) suggested that the steel complex was the

major PAH emitter in the South Eastern city of Korea. PAH emission profiles from iron and steel industries have also been measured by Yang and co-workers (2002) in southern Taiwan. According to Liberti *et al.* (2006), the level of benzo[a]pyrene around a coke oven battery may range from 100 to 200 μg m^{-3}. High concentrations of PAH have been documented by Rehwagen *et al.* (2005) at the industrial site of La Plata in Argentina. The study showed a wide difference in the concentration of benzo (a) anthracene and chrysene between the industrial locations compared to a control site. The sum of PAH at the industrial study site was found to be five times higher than at the control site, and almost two times higher than at a La Plata city centre monitoring location.

In addition, steel smelters have been reported to be amongst the largest source of dioxins to the atmosphere of Europe (Lexen *et al.*, 1993; HMIP, 1995; EC, 1999). The study by Choi *et al.* (2008) assessed the atmospheric levels and distribution of dioxin-like polychlorinated biphenyls (PCBs) and polybrominated diphenyl ethers (PBDEs) around an iron and steel industry. High concentrations of dioxin-like PCBs and PBDEs were observed near the steel plants compared to those at residential and semi-rural areas, and the source was attributed to the steel complex. The study concluded that the unexpectedly high levels of PBDEs in the steel complex might be caused by the emissions of PM from the mini mills where scrap metals and flame-retardant materials are used in the plant.

Highly time-resolved ambient measurement made at a fence line site adjacent to a large coke production facility have also revealed periodic spikes of high pollutant concentrations associated with the emissions from the coke plant (Weitkamp *et al.*, 2005). Major emissions from the coke plant were OC, EC and trace metals. PM emissions from

the coke facility were dominated by $PM_{2.5}$, which were estimated to contribute 84% of the PM_{10} mass.

Apart from the primary particulate pollutants discussed above, industries are also known for emission of gaseous pollutants such as carbon dioxide (CO_2), carbon monoxide (CO), sulphur dioxide (SO_2), nitrogen oxides (NO_x) and hydrogen gas (H_2), and volatile organic carbon (Tsai *et al.*, 2008; Johansson and Soderstrom, 2011). Some of these gaseous pollutants can be transformed into secondary aerosols which are commonly detected in urban aerosols. It is challenging to estimate how much of the secondary aerosols are from the primary pollutants emitted from different industries based on receptor modelling.

1.9 Objectives of the Study

The main aim of this study is to quantity the contribution of a steelwork complex to airborne particulate matter concentrations.

Specific objectives are:

- To quantify the mass and chemical concentrations of PM in the vicinity of the Port Talbot steelworks,
- Understanding the composition and sources of individual particles at Port Talbot steelworks,
- Determination of the size distribution of PM mass, number and chemical concentrations in the vicinity of steel industry and at an urban background site,
- Source apportionment of particle compositional concentrations using PMF and PCA,

- Understanding the contribution of different pollutants from the specific steelwork processes using pollution rose plots of air pollutants during Port Talbot sampling campaign,
- Quantification of the steelworks increment by wind sector linking source to receptor locations.

This work will identify different emission components of an integrated iron and steel industry responsible for particle and gaseous pollution in Port Talbot. This will provide pollution control and mitigating strategies for relevant agencies and policy makers in the study area.

CHAPTER 2 - GENERAL METHODOLOGY

2.1 Abstract

This chapter describes the general instrumentations for aerosol sampling and online monitoring and for the analysis of offline samples. Details of the sampling sites and the individual campaigns will be described in the following chapters. Aerosol sampling was achieved using two approaches: offline and online sampling methods. Part of this thesis methodology has been published in AWE International. The offline aerosol samplers used include Dichotomous Partisol 2025, Micro-Orifice Uniform Deposit Impactor (MOUDI), PCR TECTORA Streaker and High Volume Sampler (Digitel). The online instruments include Aerosol Time of Flight Mass Spectrometer (ATOFMS), Aethalometer, Grimm Optical Particle Counter (OPC) (model #1.108) and Filter Dynamic Measurement System (FDMS).

Particulate matter (PM) mass analysis involves both online (FDMS) and gravimetric analyses. PM chemical components measured include metals (Al, V, Cr, Fe, Mn, Cu, Ba, Sb, Pb, Zn, Ni, Cd) and water soluble ions (Cl^-, NO_3^-, SO_4^{2-}, Na^+, NH_4^+, K^+, Mg^{2+}, Ca^{2+}). Metal concentrations were measured by Inductively Coupled Plasma Mass Spectrometry (ICP-MS) while water soluble ions were measured by Ion Chromatography (IC). Streaker filters were analysed by Particle Induced X-ray Emissions (PIXE) analysis for elemental concentrations (Na, Mg, Al, Cl, S, K, Ca, Ti, V, Cr, Ni, Mn, Fe, Cu, Zn, As, Se, Rb, Sr, Si,Br, Pb). Black carbon (BC) mass concentrations were monitored online using an athalometer.

Gaseous pollutants including NO, NO_2, NO_x, SO_2, CO and ozone and meteorological parameters were monitored during the campaign.

2.2 Offline Instruments for PM Measurement

2.2.1 Micro-orifice uniform deposit impactor (MOUDI) sampler

Size resolved particles were sampled with a MOUDI sampler. The MOUDI (MSP Corporation, Shoreview, MN, USA) sampler is a general-purpose impactor that has been adopted for sampling indoor and outdoor particles. It has been employed for many studies such as visibility, underground mine and environmental pollution (e.g., Marple *et al.*, 1991). The MOUDI sampler used for this study was an 8-stage version (Model 100) with the cut points 10, 5.6, 3.2, 1.8, 1.0, 0.56, 0.32 and 0.18 µm; and a nominal flow rate of 30 L min^{-1}. However, the flow rate of 30 L min^{-1} could not be attained during the sampling, thus a correction factor was adopted using the formula:

$$\mathbf{D_p} * \sqrt{\frac{F1}{F2}} \qquad (2.1)$$

where D_p is the MOUDI stage nominal cut-point, F1 is the design flow rate of the MOUDI sampler (30 L min^{-1}) while F2 was the achieved flow rate during the campaign (21.5 L min^{-1}).

Polytetrafluoroethylene (PTFE) filters (Whatman, diameter 47 mm and pore size 1.0 µm) were used for particle collection on all the impaction stages while quartz filters (Whatman, diameter 37 mm) were used as backups (after-filters).

The operational principle of the instrument follows the same steps as any other inertial cascade impactor with multiple nozzles (MSP Corporation, 1998). However, unlike other conventional cascade impactors, MOUDI uses a large number of micro-orifice nozzles to reduce jet velocity and pressure drop. It minimizes particle bounce and re-entrainment thereby encouraging collection efficiency.

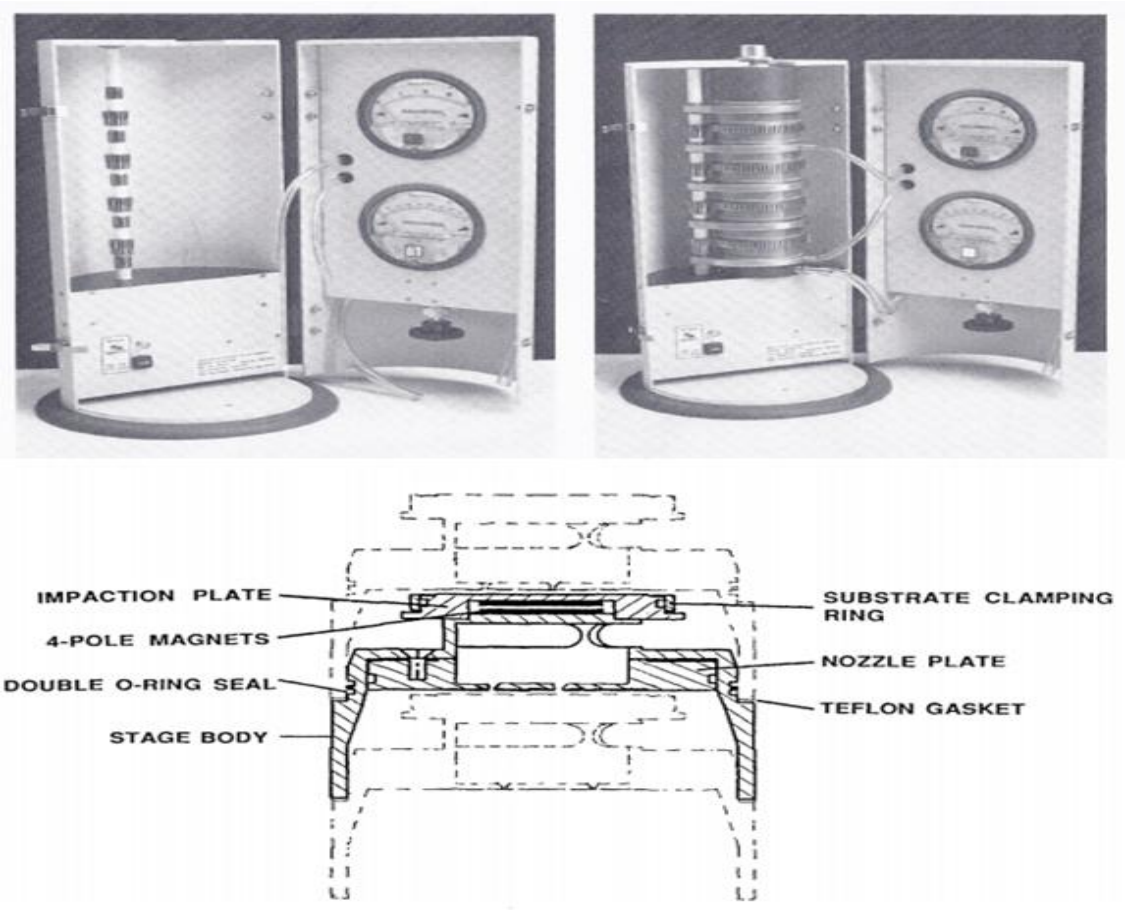

Figure 2.1: A pictorial representation of MOUDI and schematic diagram of a stage in MOUDI (MSP Corporation, 1998)

The particle laden air impinges upon an impaction plate at each stage where particles larger than cut-size cross the air streamlines and are collected on the impaction plate. Particles of smaller sizes with less inertia move to the next stage with smaller nozzles

(higher velocity) and are collected. This process continues through the cascade impactor until the after-filter stage (back-up) where the smallest particles are collected. Details of particle collection by MOUDI have been discussed explicitly in Marple *et al.* (1991). Figure 2.1 shows a picture of a fully assembled MOUDI and a stage in a MOUDI instrument.

2.2.2 Partisol dichotomous sequential air sampler ($PM_{2.5}$ and $PM_{2.5-10}$)

A Partisol-Plus dichotomous sequential sampler (Model 2025) was employed for 24-hour (noon to noon) sampling of $PM_{2.5}$ and $PM_{2.5-10}$ on PTFE filters of diameter 47 mm. This is a sequential air sampler that splits a PM_{10} sample stream into $PM_{2.5}$ and $PM_{2.5-10}$ fractions with a virtual impactor (Rupprecht & Patashnick Inc., 2001). In the system there are four cartridges each with a capacity of 16 cassettes containing the 47 mm filters. The two cartridges automatically supply the loaded 47mm filters for sampling while the remaining two cartridges store the exposed filters. One of the unique features of the dichotomous Partisol is its configuration for a range of programming, data input and storage. The schematic diagram of the Partisol-plus Model displaying the flow configuration of the sampler is displayed in Figure 2.2. The volumetric flowrate of the Partisol is 15 L min^{-1} for fine PM, and 1.7 L min^{-1} for coarse PM.

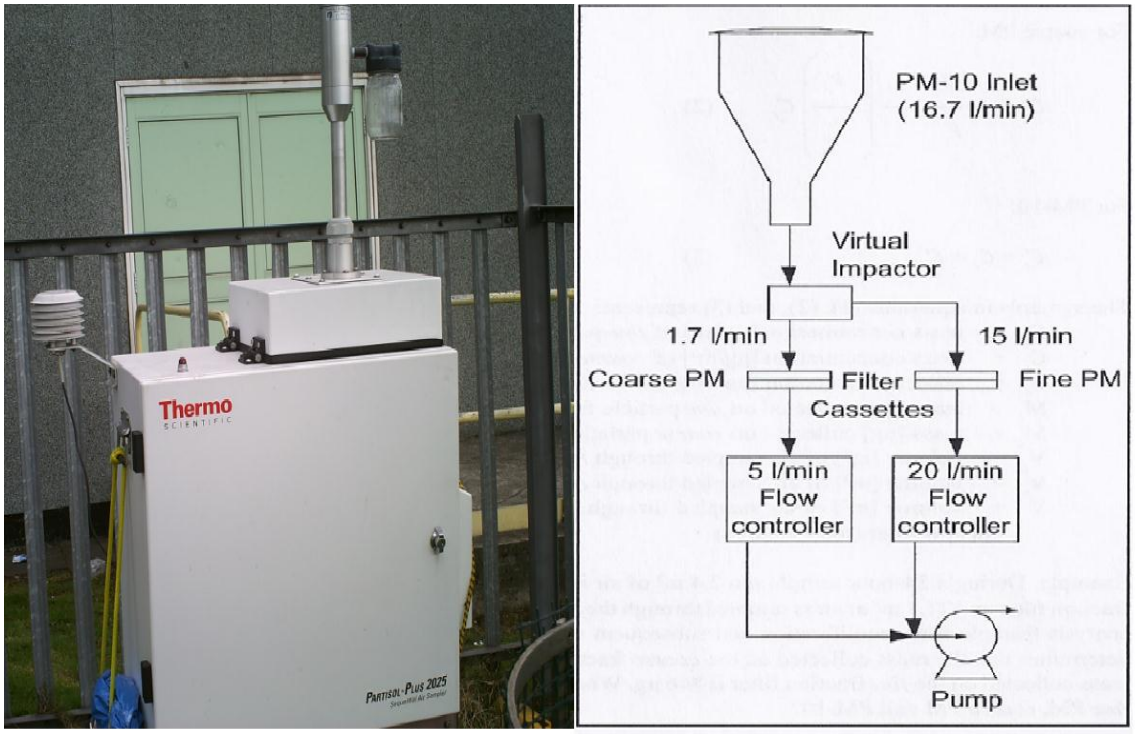

Figure 2.2: A picture and schematic diagram of dichotomous sampler (Rupprecht & Patashnick Inc., 2001)

The formulas required for calculation of fine and coarse PM are presented in equation 2.2 and 2.3.

For fine PM:

$$C_f = \frac{Mf}{Vf} \qquad (2.2)$$

For Coarse PM:

$$C_c = \frac{Mc}{Vt} - \frac{Vc}{Vt} * C_f \qquad (2.3)$$

C_f = concentration of fine PM

C_c = concentration of coarse PM

M_f = mass of fine filter

M_c = mass of coarse filter

V_f = volume of air sampled by fine (Flowrate (15.0 L min^{-1}) * time (60*24 min)

V_t = volume of total air sampled (Flowrate (16.7 L min^{-1}) * time (60*24 min)

V_c = volume of air sampled by coarse component (Flowrate (1.7 L min^{-1}) * time (60*24 min)

2.2.3 Filter dynamic measurement system instrument (FDMS)

The Filter Dynamic Measurement System (FDMS, Model 8500, Rupprecht & Patashnick Inc., Albany, NY) instrument belonging to the Automatic Urban Rural Network (AURN), Port Talbot is an online PM measuring instrument based on Tapered Element Oscillating Microbalance (TEOM) technology. The evolution of FDMS was a result of TEOM shortcomings in which semi-volatile compounds such as ammonium-nitrate and organic aerosols are lost during measurement (Charron *et al.*, 2004). The FDMS instrument measures PM mass concentration and also quantifies the change in filter mass from evaporative and condensation processes (Green, 2004). Like TEOM (principles detailed in Green (2004), airflow of 16.7 L min^{-1} enters through the Rupprecht & Patashnick PM_{10} inlet. By the principle of isokinetism, the airflow is split into two (main, 3.0 L min^{-1} and auxiliary, 13.7 L min^{-1}) with the main flow going through a microbalance. Instead of heating to 50 ^{o}C as in TEOM, air stream is passed over a dryer and mass is measured at 30 ^{o}C. Air sample is then alternated between base and purge mode where changes in the mass

of filter is measured. The FDMS instrument is depicted in Figure 2.3. FDMS PM data were downloaded from the Department for Environment, Food and Rural Affair (DEFRA) Air Quality Data Achieve at (http: //uk-air.defra.gov.uk/data/.), and Welsh Air Quality website (http://www.welshairquality.co.uk/data_and _statistics.php).

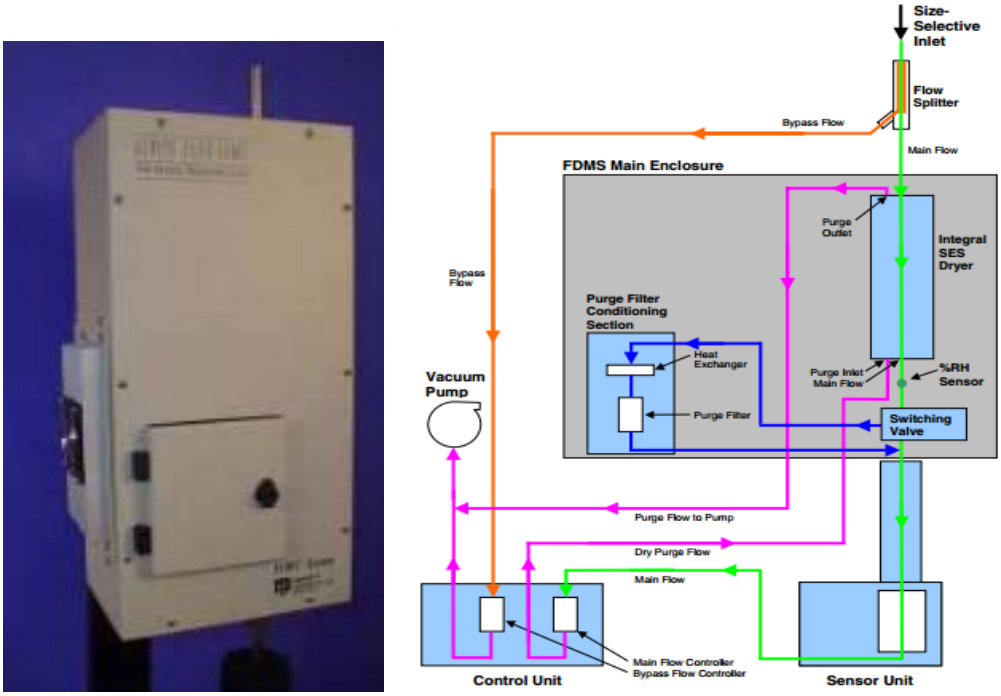

Figure 2.3: FDMS unit and the schematic of operation (Rupprecht & Patashnick Inc., 2003)

2.2.4 Streaker sampler

In this study, two Streaker samplers (TCR TECTORA) were employed. The first Streaker was placed at the background site (Little Warren) while the second Streaker was placed at the Fire Station site (which is about 250 m away from the steelworks). Figure 2.4 shows a unit of a Streaker instrument as well as its sampling component.

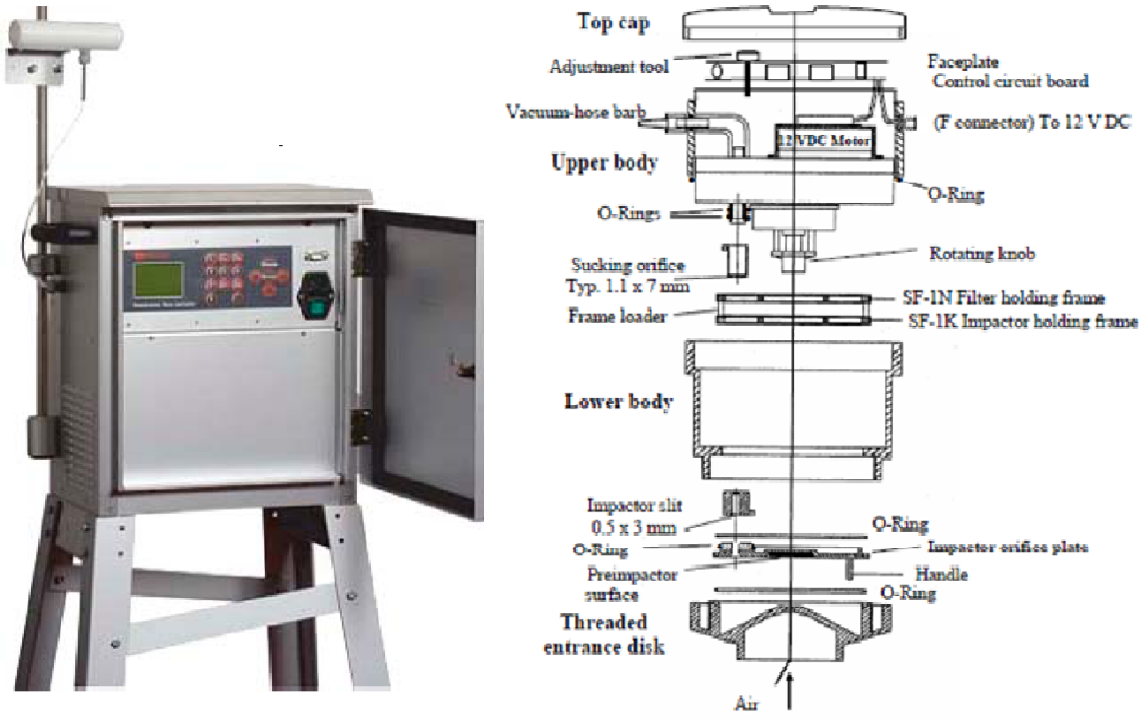

Figure 2.4: A unit and sampling diagram of a Streaker (PIXE International Corporation, 2003-2008)

Generally, the Streaker sampler is a two-stage continuous sampler that separates PM_{10} into two fractions: fine by filtration and coarse by impaction. An air flow of one litre per minute enters through the sampler's inlet into the non-rotation impactions stage (PM_{10}), followed by a rotating impaction stage ($PM_{2.5\text{-}10}$) which exits through a rotating filter stage where smaller particles ($PM_{2.5}$) are retained (Figure 2.4). It should be noted that the Streaker sampler employed in this study is not the PIXE Streaker. However, in operations and principles, there are no differences between these Streakers (PIXE International Corporation, 2003-2008). Therefore, readers are directed to PIXE international manual for further reading. An interesting aspect of a Streaker sampler is its selectiveness in operational time and sizes that is switch controlled. Particle samplings are collected on a special 82 mm filter (kapton (yellow colour) for $PM_{2.5\text{-}10}$ and nucleophore (white) for

$PM_{2.5}$). Although, the Streaker filter size is 82 mm in diameter, only a 7 mm circular portion of the filter collects the particles. The sampled filters are analysed using ion beam analysis of Particle Induced X-ray Emission (PIXE).

2.2.5 Digitel high volume aerosol sampler

The Digitel high-volume sampler (model DHA-80 Digitel Elektronik GA, Hagnau, Switzerland) employed in this study is an automatic air sampler for the collection of aerosol samples ($PM_{2.5}$). The exposed Digitel filter samples were subsequently analysed for organic and elemental carbon. Unlike a conventional high volume sampler, the Digitel high volume sampler is equipped with an integrated microprocessor unit for collecting necessary sampling data as well as for filter exchange at a preset time. Airflow is also controlled, even though the instrument was designed for air flowrate of 100-1000 L min^{-1}, the flowrate set for this study was 506 L min^{-1}. The filters (150 mm) are held in holders and are loaded in a cartridge that could contain 15 filter holders. Prior to sampling, the quartz filters (Whatman) were pre-treated by heating in an oven set at 500 ^{o}C for 4 hours. The meteorological measurements can be integrated with the sampler if their sensors are available. The pictorial and schematic diagram of a Digitel sampler showing its mode of operation is presented in Figure 2.5.

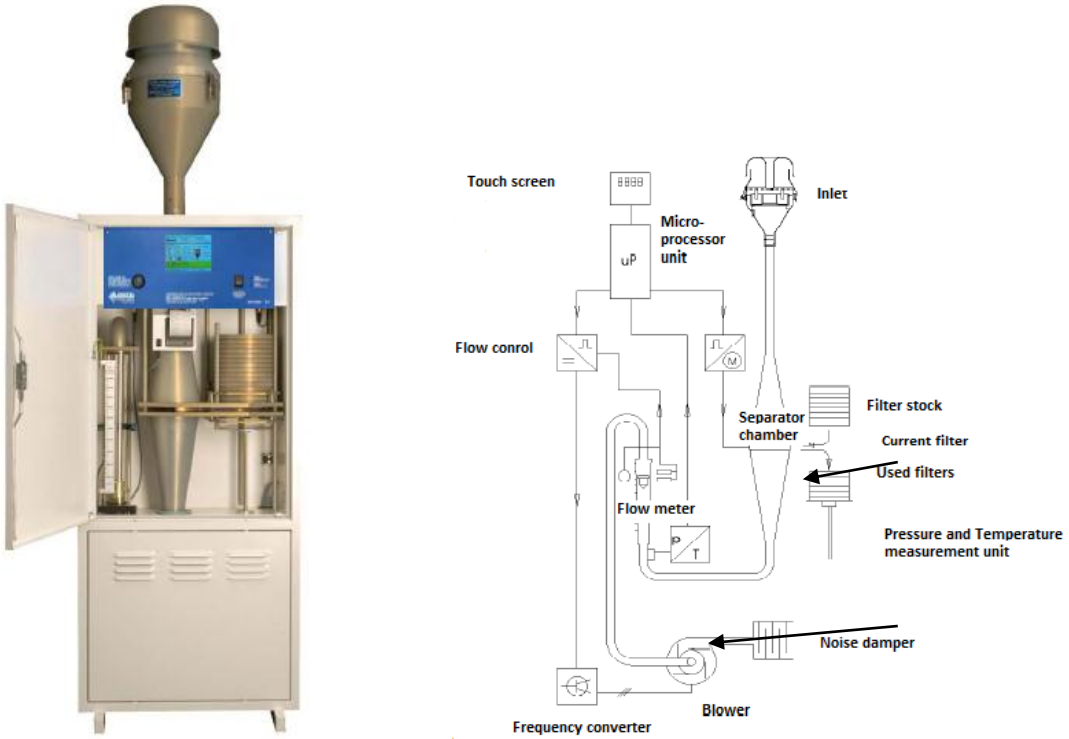

Figure 2.5: A filter loaded and schematic unit of a Digitel high-volume sampler (Digitel Elektronik, 2010)

2.3 Online Instruments

2.3.1 Portable aerosol spectrometer

Particle number concentration was determined with a Grimm optical particle counter (OPC) (Figure 2.6). The Grimm instrument (model #1.108) developed by Grimm aerosol Technik GmbH, Ainring, Germany, is a real time particle counter with 15 particle size bins (from 0.3 to 20 µm). Particles of different sizes enter into the system through an inlet placed on top of the mobile laboratory roof deployed to the sampling site. The particles sizes are scattered by a flat light beam produced by a laser diode. The scattered light signal produced by each particle is detected by a high speed diode. This particle signal is then counted into 15 size fractions by a pulse height analyser incorporated into the spectrometer. The response time was set at 6 seconds for the counts to be displayed on the

computer system. The Grimm instrument could measure particle number concentrations up to 2000 # cm^{-3}.

Figure 2.6: A unit of a potable Grimm aerosol spectrometer

2.3.2 Aerosol time of flight mass spectrometer (ATOFMS)

Single particle analysis was achieved using ATOFMS (TSI model 3800) instrument. ATOFMS was developed by Professor Kimberly Prather and her research group in 1994. The instrument provides a real time measurement for aerosol sizes, concentration, and compositions. The ATOFMS model used for this study is TS1 3800 model (Figure 2.7). The entire system includes three notable compartments: (1) sampling or an aerosol introduction interface (2) particle sizing; and (3) mass spectrometry region for analysis of single particle composition (Figure 2.7; Huang *et al.*, 2006).

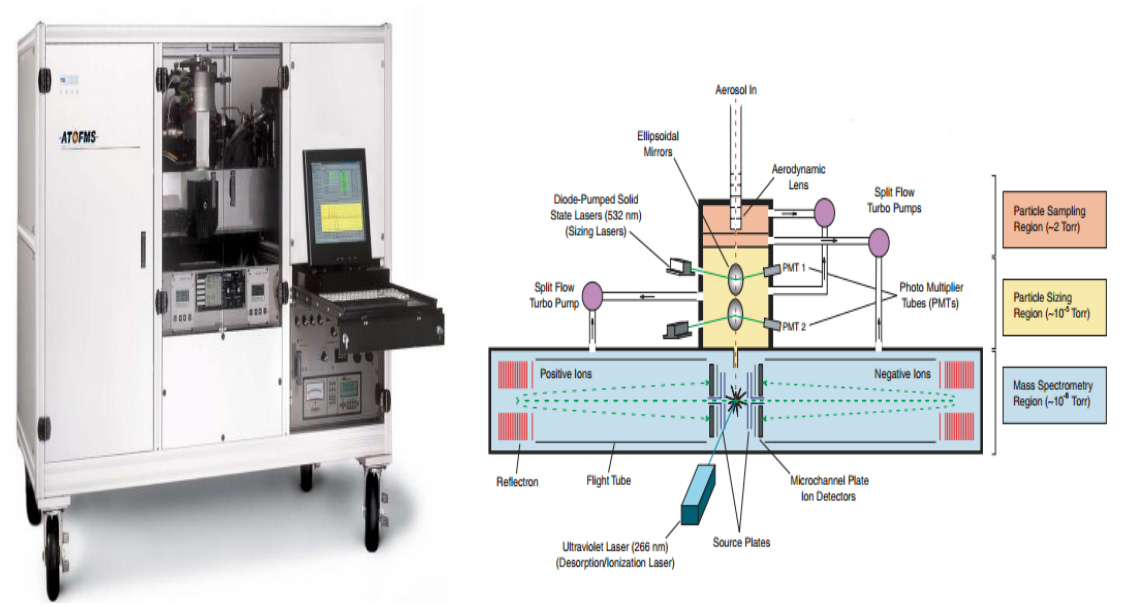

Figure 2.7: A pictorial and schematic diagram of TSI ATOFMS (TSI Inc., 2004)

The instrumentation of ATOFMS has been discussed by Gard *et al.* (1997). Aerosol particles from ambient atmospheric conditions are drawn through an inlet nozzle at a certain atmospheric pressure (760 torr) where the gas undergoes expansion. The small particles are accelerated to a higher velocity. The aerosol beam then passes through two stages of differential pumping before getting into the particle sizing region (Prather, 1998). The aerodynamic diameter of the particle size is determined here based on the velocity distribution within the particle beam.

The inlet in this study is made up of a copper pipe placed on top of the deployed mobile laboratory (Figure 2.8); and was fitted to an aerodynamic focusing lens (AFL). The inlet is protected with a rain cap. Air flow of 0.1 L min^{-1} is drawn into the AFL at a pressure of 2 torr (Giorio *et al.*, 2012). The particles then pass through a continuous-wave argon laser beam and generate a pulse of scattered light which is collected by a photomultiplier tube (PMT) (Gard *et al.*, 1997). The particles then encounter a second laser beam (after

travelling 6.0 cm) placed orthogonally to the first and another scatter pulse is generated and detected with the second PMT (Gard *et al.*, 1997). The distance between the scattering lasers and the measured time are used to calculate the particle velocity, which equates the particle's aerodynamic diameter (Gard *et al.*, 1997). Transforming the transit time into size is done by calibrating the instrument with a number of particles of known size to create a calibration curve from which the unknown sample particle's size is determined.

The particle after sizing enters the region of the laser desorption/ionization time-of-flight mass spectrometer where both the positive and negative ions generated by the desorption/ionization laser (Nd:YAG; 266 nm) are measured (Gard *et al.*, 1997; Dall'Osto and Harrison, 2006; Giorio *et al.*, 2012).

From the calibration of this instrument, the measured ion transit times can be converted to the corresponding mass-to-charge ratios, which are related to the chemical components in the original particle.

Size calibration was achieved by ranges of polystyrene latex spheres (PSL) in the diameter range 0.1-1.3 μm. These were introduced with TSI atomizer. Mass-to-charge (*m/z*) calibration was done with NaCl and graphite powder. A solution containing Li, Na, K and Pb was also introduced for mass calibration. Upon calibration, the data is loaded to MS Analyse programme to obtain a better fit curve for both size and mass. The files are saved and latter used in Environmental Chemistry through Intelligent Atmospheric Data Analysis (ENCHILADA) programme for K-mean clustering analysis.

Figure 2.8: The Mobile Laboratory showing sampling inlets of ATOFMS and other instruments during Port Talbot sampling campaign

2.4 Determination of Black Carbon (BC)

The aethalometer (model AE-31) developed by Magee Scientific Company, Berkeley, CA, USA was adopted for determination of black carbon. It provides a real time measurement for black carbon (BC) in aerosol through optical absorption analysis. An air stream of 4 L min^{-1} flow rate is drawn continuously through the inlet placed on the roof of the mobile laboratory housing the instrument, onto the quartz fiber filter tape. The attenuation of a light beam at wavelengths 880 nm, 370 nm and others passed through the filter tape (where aerosol particles are collected) is measured, and BC is calculated (Hansen, 2005). The time base of the instrument in this study was set at five minutes. Figure 2.9 shows the pictorial plate of the aethalometer used for online measurement of BC in this study.

Figure 2.9: The Magee Scientific Aethalometer during Port Talbot sampling campaign

2.5 Laboratory Analysis of Offline PM Filters

2.5.1 Filter weighing

Prior to sampling and after sampling, all filters were weighed with a Sartorius microbalance (Model MC 5; 1 µg sensitivity) equipped with a Polonium-210 anti-static source having been subjected to at least 24 hours pre-conditioning (25 ± 5ºC and 30 ± 10% R.H.) in our clean weighing room.

2.5.2. Sample digestion for metals determination

All exposed Teflon filters for Partisol and MOUDI samplers were cut into two equal portions. One-half portion was digested for metal analysis by reverse *aqua regia* procedures described in Harrison *et al.* (2003). Filters were digested in a solution of mixed concentrated acids (2.23 M HCl and 1.03 M HNO_3) prepared by mixing concentrated nitric acid (65 mL) and concentrated hydrochloric acid (185 mL) in a 1000 cm^3 volumetric flask and making up to 1 L with distilled deionised water. The mixed acid extractant (2

mL) was introduced into filters placed inside 4 mL narrow neck bottles and heated at 100^{o}C for 30 minutes in a water bath and then placed in an ultrasonic bath at 50 ^{o}C for another 30 minutes. This cycle was repeated and the ready digests transferred into 15 mL narrow neck bottles and made up to 10 mL with distilled deionised water. The ready extracts of filter samples were then analysed using an inductively coupled plasma mass spectrometer **(**ICPMS). The instrument was calibrated with appropriate standards to obtain calibration curves. The detection limits were calculated as three times standard deviations of the blank concentration.

2.5.3 Water soluble ions analysis

The second half of the exposed filter samples were analysed for water soluble ions (cations-Na^{+}, K^{+}, Mg^{2+}, Ca^{2+}, NH_4^{+}, anions-Cl^{-}, NO_3^{-}, SO_4^{2-}, $C_2O_2^{2-}$, PO_4^{3-}). The filter samples were leached with 7.5 mL distilled de-ionized water in a Sonicator for 30 minutes. The leachates were measured with Dionex ICS 2000 and DX 500 for anions and cations, respectively.

An Ion Chromatography System (ICS) was employed for the analysis of water soluble anions. Generally, ion analysis processes involve eluent delivery, sample injection, separation, suppression, detection and data analysis (Figure 2.10). The samples were loaded into an autosampler in 0.5 mL vials. The sample was injected into the eluent stream of the instrument. For anionic component (Dionex ICS 2000), the eluent used was potassium hydroxide (KOH). The eluent and the sample are pumped through an analytical (separator) column, AS 11 HC (2x250 mm) and a guard column, AG 11 HC (2x50 mm) for separation or ion exchange and contaminants removal respectively (Thermo Fischer

Scientific Inc., 2012). For water soluble cations, the IC employed was Dionex DX 500 equipped with CS 12A analytical column (4x250 mm) and CG12A guard column (4x50 mm) (Thermo Fischer Scientific Inc., 2012). The eluent solution used was 1N methane sulphonic acid. On leaving the column, sample ions and eluent enter into a suppressor compartment. Here, sample ion detection is enhanced, while the eluent conductivity is suppressed. The next step is detection where the electrical conductance of sample ions are detected by conductivity cell based on the chemical and physical properties of the analyte (Thermo Fischer Scientific Inc., 2012). The signal is sent to a Chromeleon data collection system for further processing. Normally, the results in the Chromeleon are displayed as an ion chromatogram of the analytes.

Calibration curves (for anions and cations) were obtained with series of mixed standard solutions prepared in the range concentration between 0.5 and 10 ppm. Ten blank filters were run for all the elemental concentrations to cancel the matrix effect of background levels.

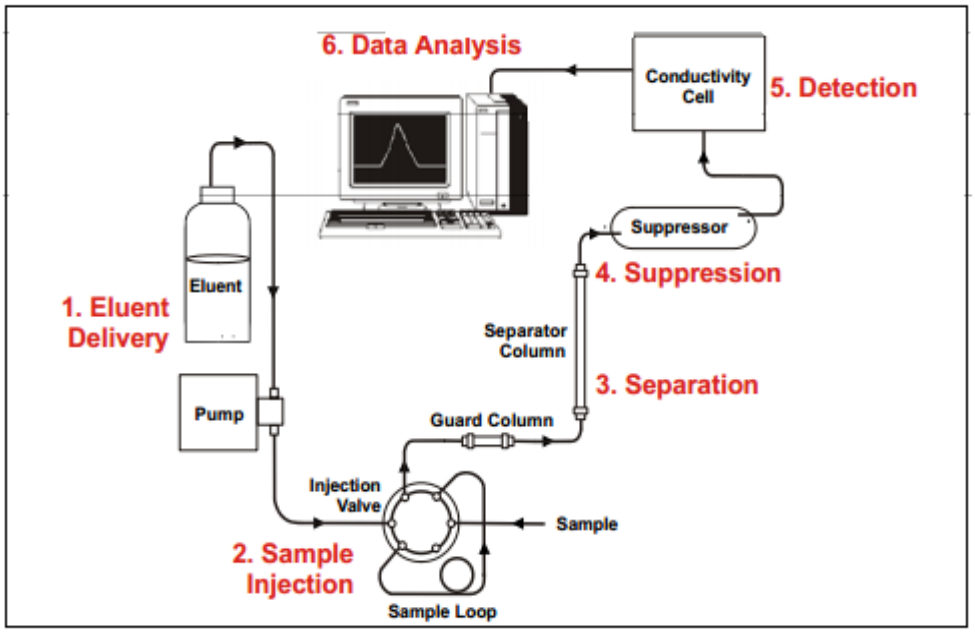

Figure 2.10: Schematic diagram showing ion analysis process (Thermo Fischer Scientific Inc., 2012)

2.5.4 Thermal optical reflectance analysis of organic and elemental carbon (OC/EC)

OC/EC analysis was determined using a Sunset Laboratory thermal-optical carbon aerosol analyzer after the EUSAAR (European Supersites for Atmospheric Aerosol Research) protocol. Prior to determination, the quartz filters used for OC/EC analyses have been pre-heated in an oven set at a temperature of 500^{o}C for 4 hours. The essence of this is to remove any OC present in the blank filters. A punch of the exposed quartz filters (1.0 cm^2) was placed into the manganese dioxide (MnO_2) oven of the OC/EC measurement for analysis.

The thermal-Optical Carbon Aerosol Analyzer uses thermal desorption in combination with optical transmission of laser light through the sample to speciate carbon collected on a quartz fibre filter (Sunset Laboratory Inc., 2000). OC is the optically transparent carbon

removed during an initial non-oxidizing temperature ramp from ambient temperature to 870 ^{o}C under a helium atmosphere. The pyrolysed carbon fragment then passes through a MnO_2 oxidizing oven where it is converted to carbon dioxide, which is mixed with hydrogen gas and quantitatively converted to methane over a heated nickel catalyst (Yin *et al.*, 2010). The methane is subsequently measured by a flame ionization detector (FID). The oven then cools down to 600^{o}C after completion of first temperature ramp.

EC, an optically absorbing carbon removed at a high second temperature ramp from 550 to 850^{o}C is then initialized with the carrier gas switched to a helium/oxygen mixture, under which elemental carbon and pyrolysis products are oxidized and carried through the system and measured in the same manner as the organic carbon (Sunset Laboratory Inc., 2000, Yin *et al.*, 2010). The OC/EC instrument was calibrated with a sucrose solution standard.

2.5.5 Inductively coupled plasma mass spectrometer (ICPMS)

The extracts of filter samples for metals were analysed with an ICPMS (Agilent 7500 Ce) at the University of Birmingham. The version of this ICPMS is a quadrupole equipped with octopole reaction system that removes interfering species. Metals of interest were Al, Mn, Cr, V, Fe, Zn, Cu, Ni, Cd, Sb, Ba and Pb. The mixed standards (from the stock 1000 mg L^{-1} VWR standard solution) were prepared in the series 0, 1, 5, 10, 20, 50 and 100 ppb. Internal standards used for ICPMS analysis were Sc, Ge, Y, In and Bi.

In earlier work, this procedure has been evaluated by analysis of NIST SRM 1648a (Allen *et al.*, 2001) and more recent trials have shown high efficiency (< 85%) for all elements

analysed except Al (*ca* 50% efficiency, also by comparision with XRF) and Cr (*ca* 50% efficiency).

2.5.6 Particle induced X-ray emission (PIXE) analysis

Streaker filters were sent to the University of Milan, Italy for particle induced x-ray emission (PIXE) analysis. PIXE is based on an ion beam analysis (IBA) technique involving hitting a target with a high energy ion beam to produce beam of accelerated particles. PIXE analysis could detect up to 20 elements from Na to Pb in less than ten minutes of bombardment (Lucarelli *et al.*, 2011). Being a non-destructive technique, it also gives room for further complementary sample analysis. The exposed Streaker filters (Nucleophore and Kapton) were analysed with PIXE instrument (KN3000 3 MV Van de Graaf accelerator) (D'Alessandro *et al.*, 2003). PIXE analysis of aerosol has been described in detail in Chiari *et al.* (2005). In brief, it involves air extraction of a proton beam of 3 MeV energy through a 7.5 µm Upilex Window. The Streaker filter samples were placed perpendicular to the beam at a distance 1 cm from the window and irradiated with a current beam of between 5 and 10 nA for around 10 minutes per sample. The collimated rectangular 'streak' (1 x 1.8 mm^2) to the beam is equivalent to one hour aerosol sampling where the emitted X-rays for each spot are collected for 5 minutes (Nava *et al.*, 2002). It takes about 15 hours to completely scan through a whole Streaker filter with a mean collection of 3 µC per step. Loss of volatiles during irradiation was handled using helium flow. The spectra produced by PIXE were analysed using GUPIX software package. The elemental concentrations were obtained with calibration curves constructed with known certified standards (Micromatter Inc., USA). The elements observed with PIXE were Na, Mg, Al, Si, S, Cl, K, Ca, Ti, V, Cr, Mn, Fe, Ni, Cu, Zn, As, Se, Br, Rb, Sr,

Ba and Pb. Detection limits in the low Z elements (Z≤20) for Nucleophore ranged 12-46 and 1-5 ng m^{-3} for medium to high Z elements (Z>20). In the Kapton, detection limits variations were 7-31 ng m^{-3} and 1-2 ng m^{-3} for low and medium-to-high Z elements, respectively. Si and Br were not detected in the Nucleophore filters while V was scarcely detected in both fine and coarse particles.

2.6 Meteorological and Gaseous Parameters

The meteorological and gaseous data were downloaded from the Department of Environment, Food and Rural Affairs (DEFRA) Air Quality Data Achieves at http://uk-air.defra.gov.uk/data/.

2.7 Data Processing

2.7. 1 Offline data processing

The daily and hourly data collected with offline instruments were processed with Statistical Package for Social Sciences (SPSS) for descriptive statistics, Analysis of Variance (ANOVA) and Duncan Multiple Range Test (DMRT). Time series and MOUDI size distribution curves were plotted using Microsoft Excel package.

2.7.2 Online ATOFMS data processing with ENCHILADA software

The ATOFMS detected 5,162,018 particles during sampling, out of which 580,798 particles were ionised. ATOFMS data was transferred to the ENCHILADA software package for K-mean clustering. ENCHILADA software was developed by Gross and her research group at the Department of Chemistry, Carleton College, Minnesota, USA. In K-mean clustering (non-hierarchical), the centres of clusters are picked to minimize the total

Euclidean distance (Gross *et al.* 2010). It involves sub-dividing single particles into a number of clusters defined at the operator's discretion (Giorio *et al.*, 2012). The numbers of clusters were determined in this study by analysing the particles with varying numbers of clusters from 5 to 35. The errors of clusters were plotted against numbers of clusters (K). The best fit for the K mean cluster was 20 (Figure 2.11).

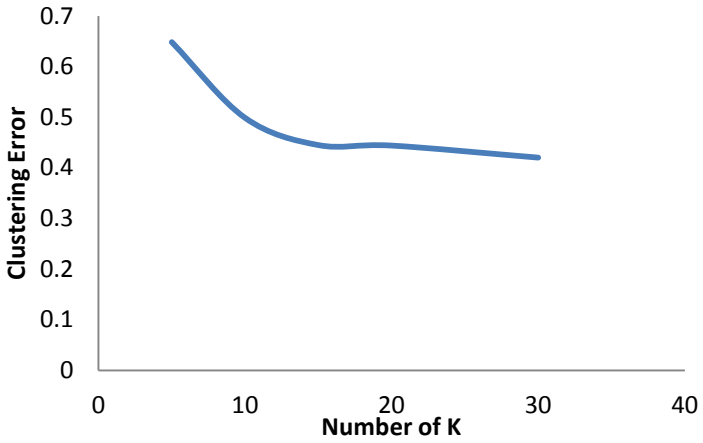

Figure 2.11: Plot of clustering error against numbers of K

ENCHILADA requires that calibration data of chemical (*m/z*) and size be fed into the programme along with the ATOFMS data before operation. These calibration data were generated by uploading the raw ATOFMS data to MS Analyse programme. The chemical (*m/z*) calbration curve is displayed in Figure 2.12 while that of size is shown in Figure 2.13 (r^2=0.9999).

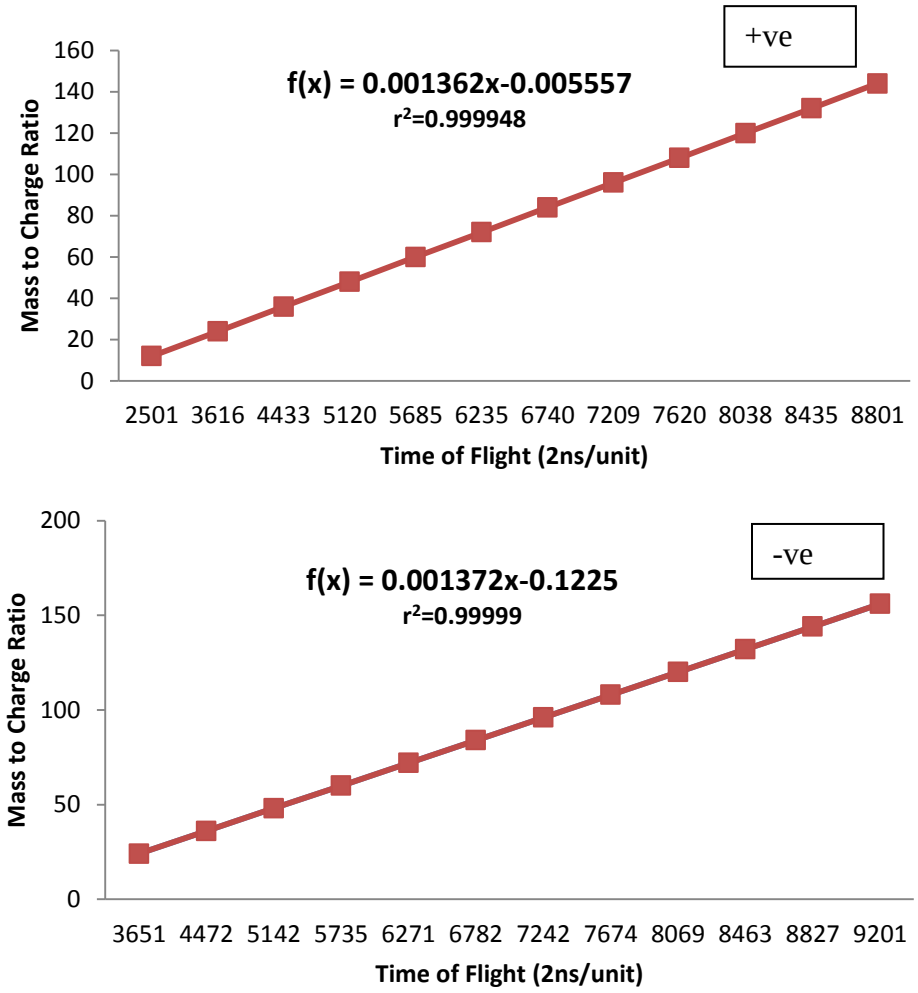

Figure 2.12: *m/z* calibration plots for positive and negation spectra

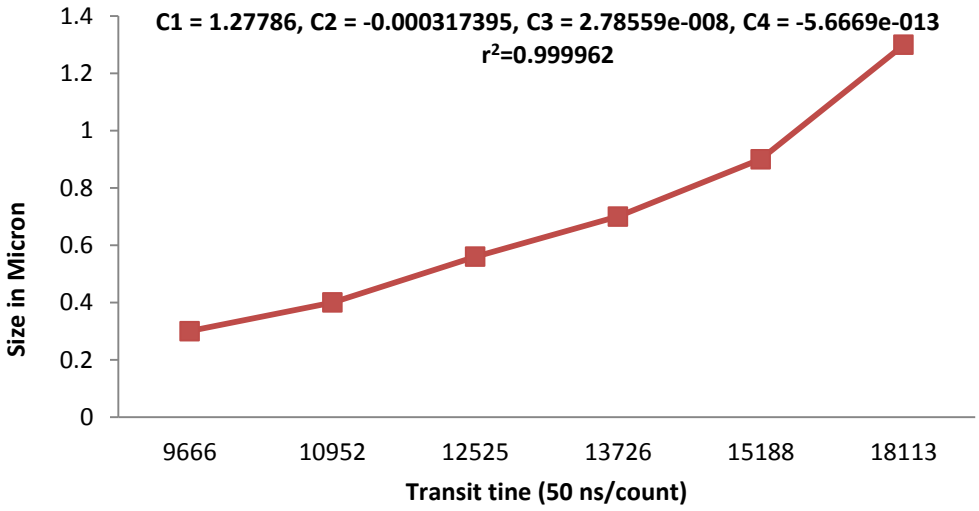

Figure 2.13: Size calibration curve

2.7.3 Receptor models

2.7.3.1 Principal matrix factorization (PMF)

Daily and hourly data of particulate matter chemical composition were used for the source apportionment of PMF (model 3.0). Generally, all multivariate statistical models including PMF aim at solving environmental problems using the equation that can be written as:

$$x_{ij} = g_{ik} * f_{kj} + e_{ij} \quad \textbf{(2.1)}$$

Where x_{ij} is the elemental concentration of j species measured on i^{th} sample, g_{ik} is the contributing factor of k to i^{th} sample; f is the fraction of j species in the profile factor k, while e_{ij} is the residual error of PMF. This equation could be written as X matrix with i and j dimensions and expressed as:

$$x_{ij} = \sum_{k=1}^{p} g_{ik} * f_{kj} + e_{ij} \quad \textbf{(2.2)}$$

The main goal of PMF solution is to find the best fit for x_{ij} by adjusting g_{ik} and f_{kj} until a minimum Q is obtained for a given contributing factor, p (Reff *et al.*, 2007). Q can be defined as:

$$Q = \sum_{i=1}^{n} \sum_{j=1}^{m} \left(\frac{e_{ij}}{\delta_{ij}} \right)^2 \quad \textbf{(2.3)}$$

Where n is the number of samples, m is the number of species and δ_{ij} is the uncertainty of *j* species concentration in the i^{th} sample.

It is required that the error estimates are determined in order to optimize the PMF model. This is usually achieved through proper handling of missing and below-detection-limit data as well as calculation of uncertainties. There were few below-detection-limit data in the Partisol daily samples compared to the Streaker hourly samples. In this regard, some chemical species were excluded from the PMF analysis.

Uncertainties for both Partisol and Streaker samples were calculated using the formula adopted by Viana *et al.* (2008b) as:

$$0.1*C+\frac{MDL}{3} \qquad (\textbf{\textit{2.4}})$$

where C is the concentration and MDL is the method detection limit. All below-detection-limit data as well as missing data were treated equally by replacing with 1/2*MDL and their corresponding uncertainties calculated as 5/6*MDL (Polissar *et al.*, 1998).

Signal to noise (S/N) ratios were also adopted to maximize PMF solution. S/N values less than 0.2 were assigned 'bad' while S/N values between 0.2 and 2 were assigned 'weak' as stated in the PMF manual. Additionally, the values of correlation coefficient, r^2 between the observed and predicted particulate constituents were also taken into consideration during PMF base model run. As a result of this, correlation coefficient (r^2) values less than 0.60 were marked 'weak' while $r^2>0.60$ were marked 'strong'. Relationship between Q

theory, Q robust and Q true values were taken into consideration in the PMF solutions. These Q values were indications of the goodness-of-fit of calculated parameters. The ratios of Q robust to Q true for all PM categories subjected PMF analysis in this study were less than 1.5. The Q theory was calculated as mn-p(m+n), where m, n and p are the number of species, samples and factors, respectively. The Q theory and Q robust values were close for Streaker and Partisol PM_{10} data. But for Partisol $PM_{2.5}$ and $PM_{2.5-10}$, PMF Q values were about 2 times higher than Q theory. Complementary to the base model, Bootstrap model runs were performed (minimum of r^2=0.6) as described in the PMF EPA guide. The Bootstrap summary of the PMF model was used either to accept or reject the base model runs. In a situation where two or more Bootstrap mapped values are less than 90, the base run model is rejected and re-run by varying the number of factors.

The Partisol dataset at each sampling site was not enough to satisfy PMF data adequacy requirements, and hence all the data were pooled together to make N=99. After the PMF runs, source contributions by each site were separated.

2.7.3.2 Principal component analysis (PCA)

The technique which is based on eigenvalues involves mathematical operations where sets of variables are orthogonally transformed into a set of values of uncorrelated principal components (Ali and Chahouki, 2011). The PCA analysis in this study was carried out with SPSS package version 19.0. All the Partisol data for each PM size fraction at the four sites were pooled together and varimax rotations were performed. The hourly Streaker data were also screened through the varimax PCA. Multiple Linear Regression (MLR) analysis was conducted on the principal scores obtained from the varimax PCA for the

calculation of percentage source contribution. Details of PCA analysis has been given in Guo *et al.* (2004).

2.7.3.3 Enrichment factor (EF)

Enrichment is applied to environmental measurements in order to identify the origins of measured elements in the atmosphere, seawater and rainfall (Reimann and de Caritat, 2000). EF is calculated as the double ratio of the concentration of a measured element to the reference element in the atmosphere and earth crust. Calculation of EF is expressed as:

$$\mathbf{EF} = \frac{[\mathbf{Ca}]}{[\mathbf{Xa}]}\ \mathbf{Sample} \div \frac{[\mathbf{Cb}]}{[\mathbf{Xb}]}\ \mathbf{Crust} \qquad (2.5)$$

Where C_a and X_a are the concentrations of desired and reference elements in the atmosphere while C_b and X_b are the concentrations of desired and reference elements in the earth crust. Reference elements are usually taken as Al, Li, Sc, Ti, Zr, Mn and Fe (Reimann and de Caritat, 2005). In this study, Al was selected as the reference material. The choice of Al was based on the fact that it is the most abundant terrestrial element. Apart from this, most of the elements adopted as reference materials are not considered in this study except Fe and Mn. This study was conducted at a steelworks complex and as Fe is one of the most concentrated elements measured at the steel industries (Oravisjarvi *et al.*, 2003; Moreno *et al.*, 2004 a, b, Tsai *et al.*, 2007), it would therefore be unsuitable to select Fe as a reference element. The $[C_b]/[X_b]$ crust ratio used in this study was adopted from Wedepohl's (1995) published work on the composition of the continental crust.

2.7.4 Windrose and Polar Plots

The Open Air (version 0.8-0) and Lakes Environmental WRPLOT View™ (version 7.0.0) softwares were employed for polar and windrose plots of particulate and gaseous pollutants. Open Air software is a statistical package based on R computer programming language. Operational details of Open Air software can be seen in Carslaw (2013) while that of Lakes Environmental WRPLOT View is at www.weblakes.com/products /wrplot/resources/ lakes_wrplot_view_release_notes_7.pdf).

2.8 The Summary of Port Talbot (PT) Sampling Campaign

Receptor models were used in this study to identify and apportion the emission sources of PM in Port Talbot. Different PM sampling instruments were deployed during a one month monitoring campaign. Figure 2.14 summarizes the methodology applied in this study.

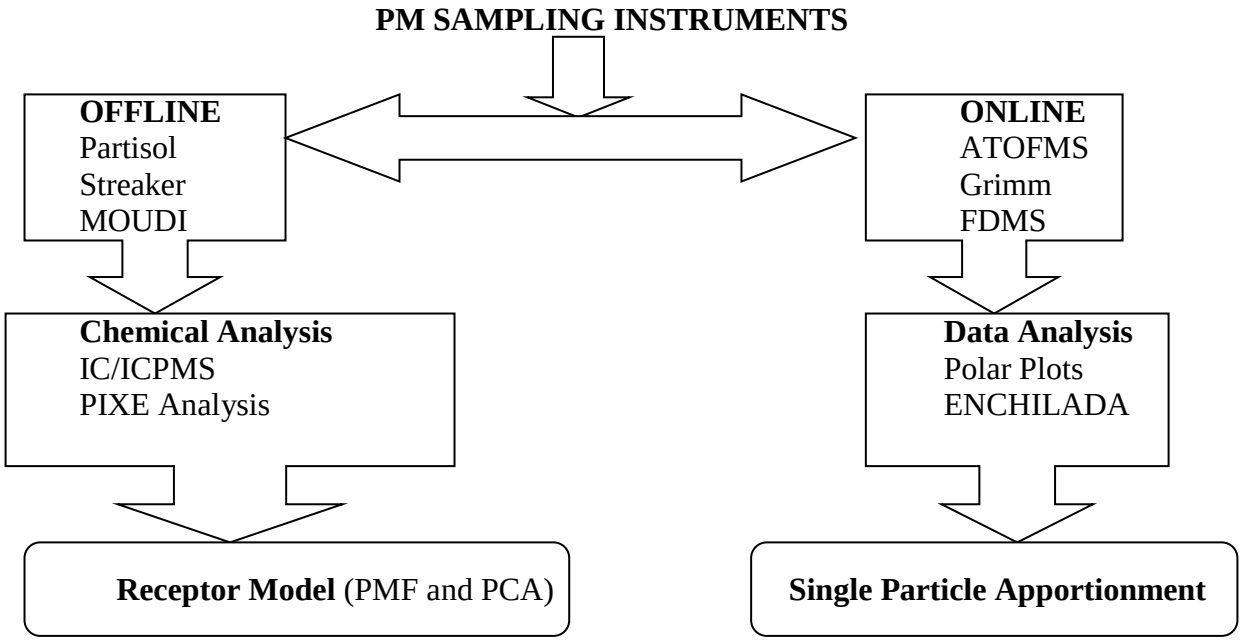

Figure 2.14: The flow chart showing the methodology applied in Port Talbot study

CHAPTER 3- EROS AND BROS CAMPAIGN

3.1 Abstract

This chapter details the study conducted at an urban background (EROS) and roadside (BROS) site in Birmingham for comparison with the Port Talbot campaign, which is a typical industrial location. At EROS, both MOUDI and Partisol samplers were used for measurement of mass and compositional size distributions. At BROS, only the Partisol sampler was used for a two-week sampling campaign between March 28 and April 11, 2012. Observed parameters include water soluble ions (Cl^-, NO_3^-, SO_4^{2-}, Na^+, NH_4^+, K^+, Mg^{2+}, Ca^{2+}) and trace metals (V, Al, Cr, Mn, Fe, Zn, Cu, Sb, Ba, Pb). Results showed higher concentrations of NO_3^-, NH_4^+, Al and Fe at BROS than EROS for fine particles, and Cl^-, NO_3^-, Na^+, K^+ and Fe for coarse PM indicating roadside increments. The ionic and trace metal components of $PM_{2.5}$ at EROS constituted 44 and 7% of the total measured mass, respectively. The proportion of these species were 46 and 8% at BROS. For coarse PM fraction, water soluble and trace metal components represented 42 and 12% at EROS, and 56 and 11% at BROS. Good agreement was also found between Partisol and MOUDI PM data at EROS.

3.2 Introduction

The presence of particulate matter at a high concentration could pose serious environmental and health concerns. Particles are emitted from numerous anthropogenic and natural activities. The prominent sources of PM in cities and urban areas include traffic, secondary, industrial, crustal, marine, combustion activities and power plants (Levy *et al.*, 2003; Charron and Harrison, 2005; Liu and Harrison, 2011).

The contribution of traffic to $PM_{2.5}$, $PM_{2.5-10}$ and PM_{10} was researched by Liu and Harrison (2011) in the UK. The results showed a significant increment at the roadside relative to urban background site. The study also indicated industrial and marine aerosol as major contributors to coarse PM in the UK. A related study by Harrison *et al.* (2012a) also showed an elevated mean concentration of $PM_{2.5}$ at roadside sites compared to background sites.

The aim of this section is to compare the PM compositional data collected at the urban background and traffic sites. The mass size distribution patterns of particles collected at the urban background site (EROS) will also be compared with that of the Port Talbot industrial site.

3.3. Materials and Methods

3.3.1 Description of the study area

Elms Road Observatory Site (EROS; 1.93^{o}W, 52.46^{o}N) is a typical urban background site which is located on an open field within the University of Birmingham campus. The nearest roads are lightly trafficked and the nearby railway line carries mainly electric

trains. Bristol Road Observatory Site (BROS; 1.93^{o}W, 52.45^{o}N) is a traffic polluted site also located within the University of Birmingham campus. These two sites are about 3.5 km southwest of the centre of Birmingham (population of over one million and is part of a conurbation of 2.5 million people (Yin *et al.*, 2010). EROS and BROS sites are shown in Figure 3.1.

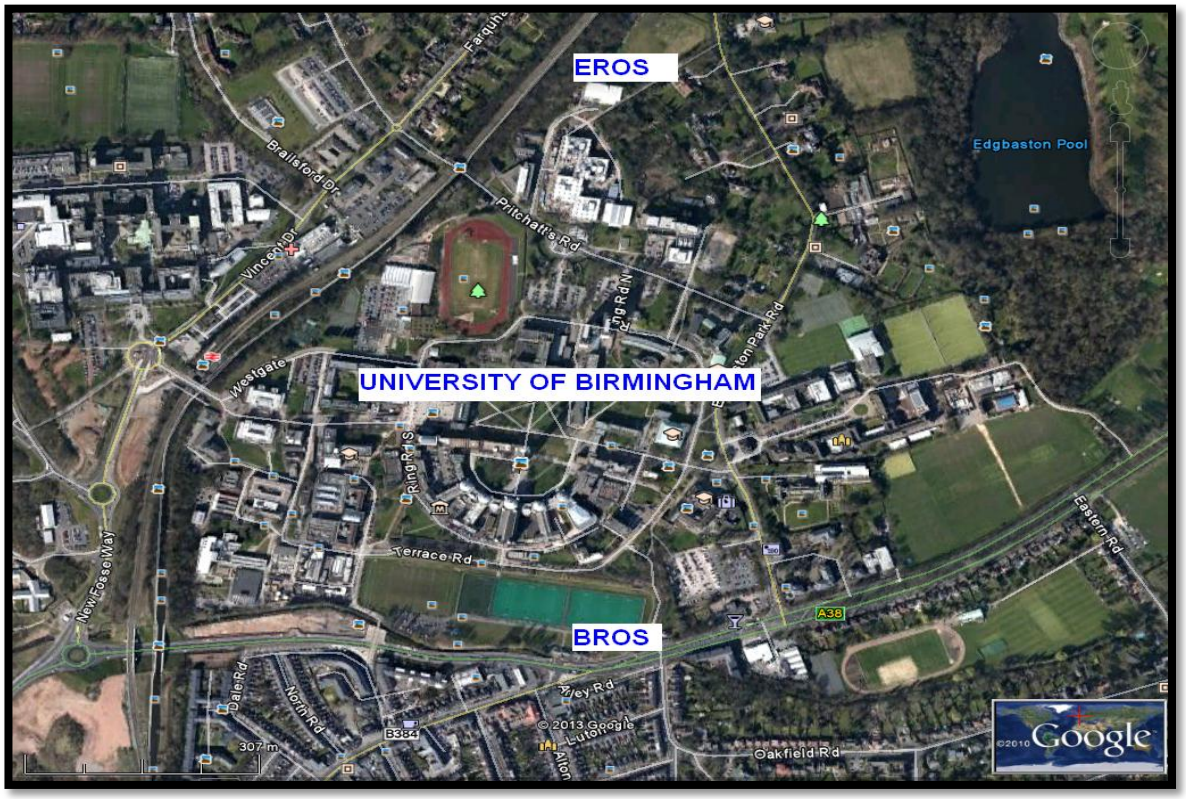

Figure 3.1: Map showing EROS and BROS monitoring sites

3.3.2 Particulate matter sampling

Particle sampling was carried out with Partisol samplers placed at the two monitoring sites within the University of Birmingham, UK for two weeks between March 28 and April 11. MOUDI 72 hour-samples were also collected at the EROS site only during the sampling period (March 30-April 11, 2012).

3.3.3 Sample digestion and analysis

Details of sample digestion and analysis have been described in chapter two (section 2.5).

3.4 Results

3.4.1 Partisol PM compositions at EROS and BROS

Figure 3.2 shows the mean mass and chemical compositions of $PM_{2.5}$ and $PM_{2.5-10}$ at EROS and BROS. The two sites show higher mass concentration of $PM_{2.5}$ than $PM_{2.5-10}$ signifying more influence by anthropogenic emissions. The two categories of PM were higher at BROS, probably due to traffic contribution. The water soluble components of PM showed domination of NO_3^- at BROS and SO_4^{2-} at EROS. The order of abundance of species in $PM_{2.5}$ at EROS is as follows: sulphate (17% of $PM_{2.5}$), nitrate (13%), ammonium (12%) and Al (6%). The water-soluble and trace metal species constituted 44 and 7% of measured $PM_{2.5}$ mass concentration, respectively. In the $PM_{2.5-10}$ fraction, the sequence of abundance of species followed: NO_3^- >Al>SO_4^{2-} >Cl^- >Ca^{2+} >Na^+ /Fe>Mg^{2+}. These components represented 42 and 12%, respectively for $PM_{2.5-10}$. The remaining components of PM could be attributable to carbonaceous species which were not measured during the study.

At BROS, NO_3^- constituted 20 and 24% of the total $PM_{2.5}$ and $PM_{2.5-10}$ mass concentration, respectively. The sequence followed 15 and 10% for SO_4^{2-}, 15 and 1% for NH_4^+, 1 and 7% for Cl^-, 1 and 4% for Na^+, 8 and 5% for Al, and 1 and 5% for Fe. Mg and Ca^{2+} occupied 1 and 4% of $PM_{2.5-10}$ mass, respectively. The measured components of $PM_{2.5}$ showed dominance by water soluble ions (46%) while trace metals only constituted 8% of $PM_{2.5}$ mass. A total fraction of 56% of measured coarse mass concentration was attributed to

ionic species and 11% to trace metals. The summary of mean and standard deviations of EROS and BROS PM data are shown in Appendix I.

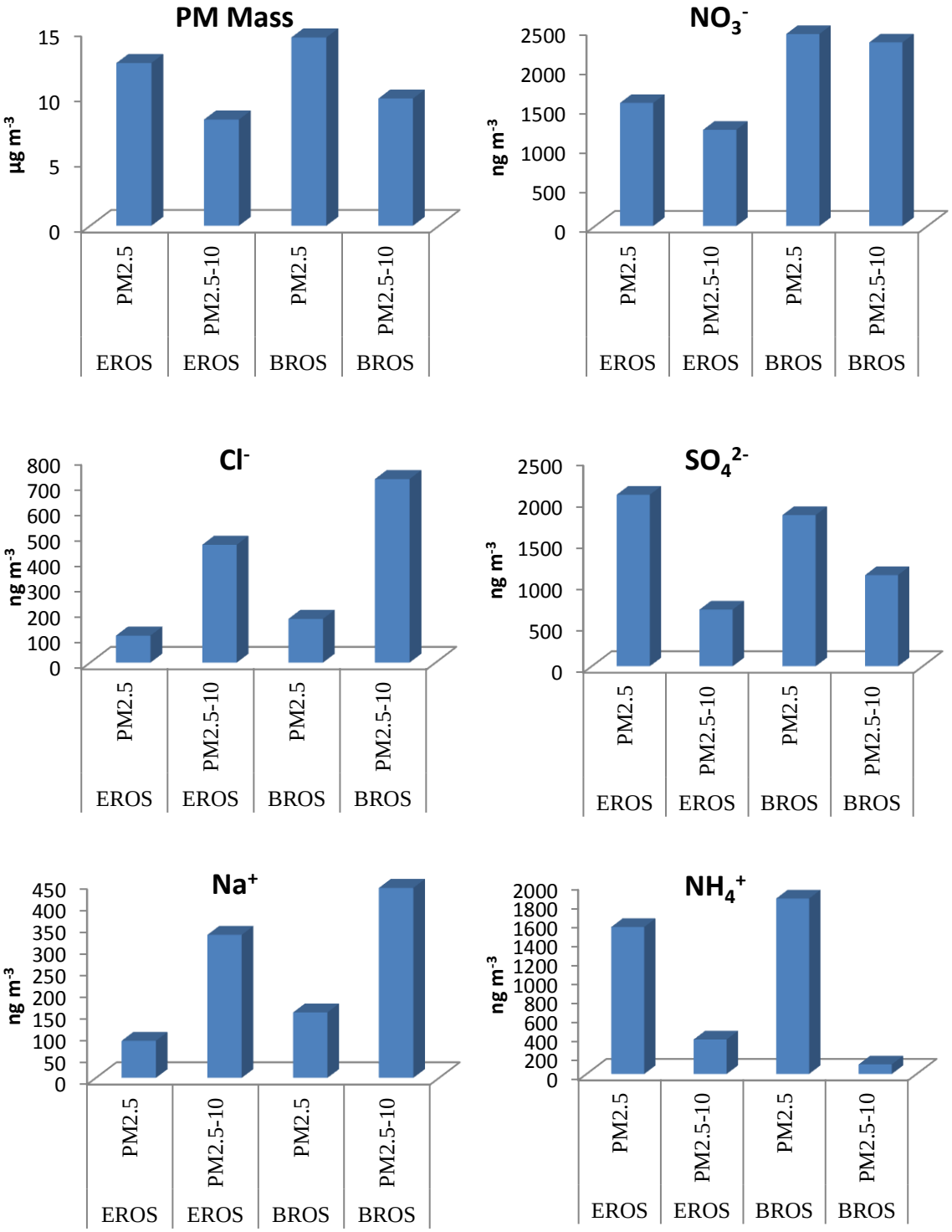

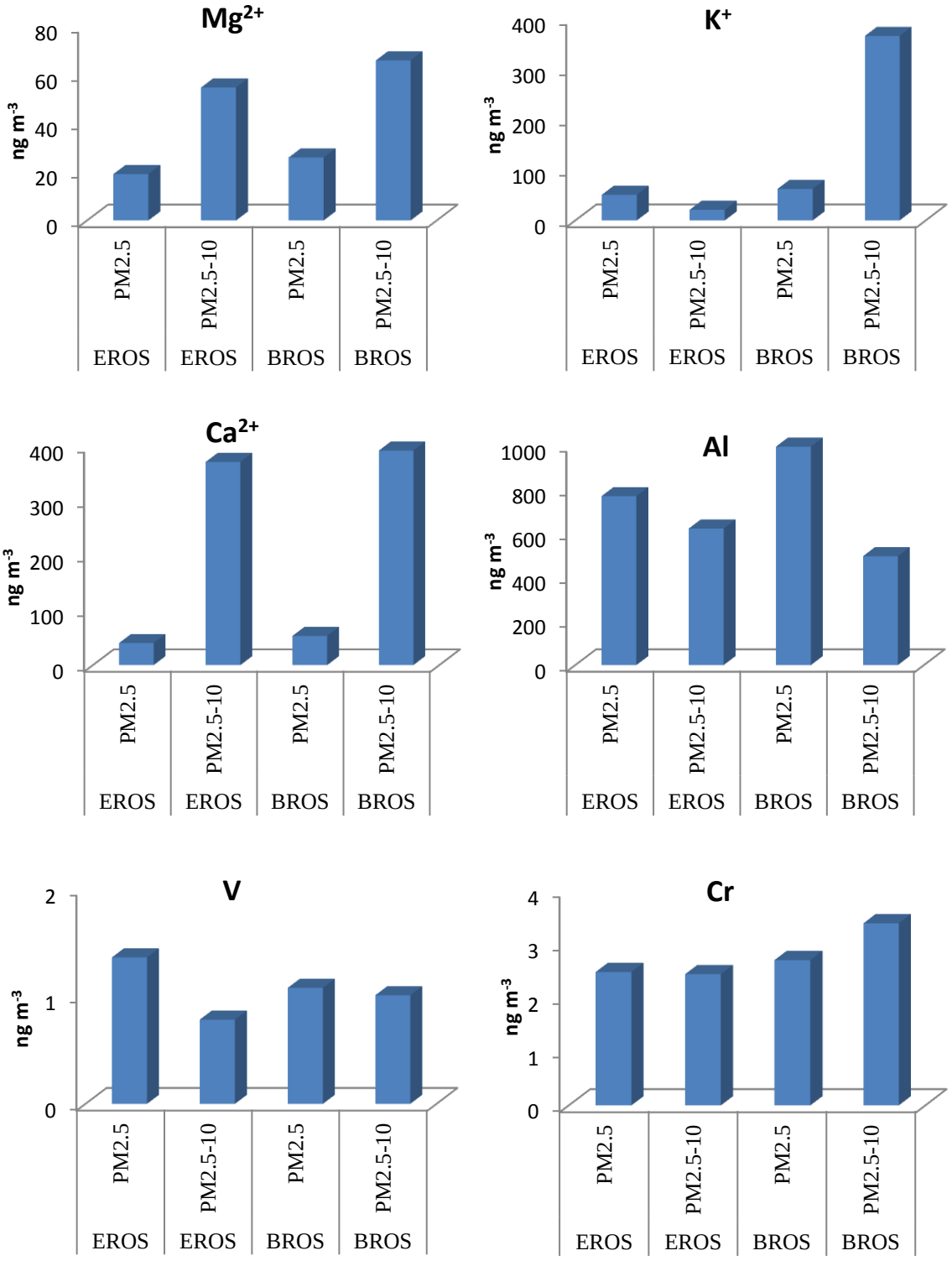
Mg2+
ng m-3
80
60
40
20
0
PM2.5
PM2.5-10
PM2.5
PM2.5-10
EROS
EROS
BROS
BROS
K+
ng m-3
400
300
200
100
0
PM2.5
PM2.5-10
PM2.5
PM2.5-10
EROS
EROS
BROS
BROS
Ca2+
ng m-3
400
300
200
100
0
PM2.5
PM2.5-10
PM2.5
PM2.5-10
EROS
EROS
BROS
BROS
Al
ng m-3
1000
800
600
400
200
0
PM2.5
PM2.5-10
PM2.5
PM2.5-10
EROS
EROS
BROS
BROS
V
ng m-3
2
1
0
PM2.5
PM2.5-10
PM2.5
PM2.5-10
EROS
EROS
BROS
BROS
Cr
ng m-3
4
3
2
1
0
PM2.5
PM2.5-10
PM2.5
PM2.5-10
EROS
EROS
BROS
BROS

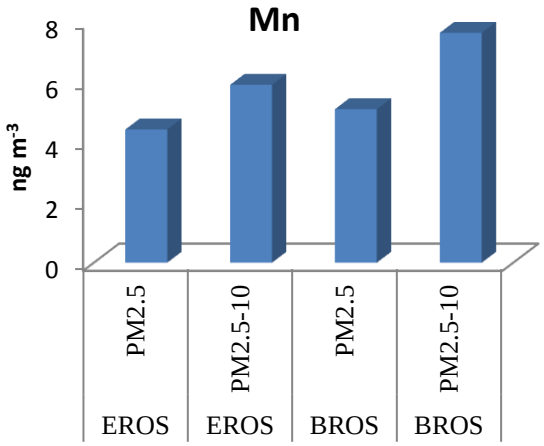
Mn
ng m-3
8
6
4
2
0
PM2.5
PM2.5-10
PM2.5
PM2.5-10
EROS
EROS
BROS
BROS

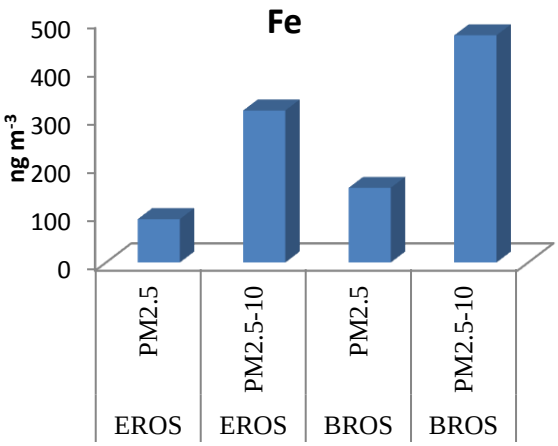
Fe
ng m-3
500
400
300
200
100
0
PM2.5
PM2.5-10
PM2.5
PM2.5-10
EROS
EROS
BROS
BROS

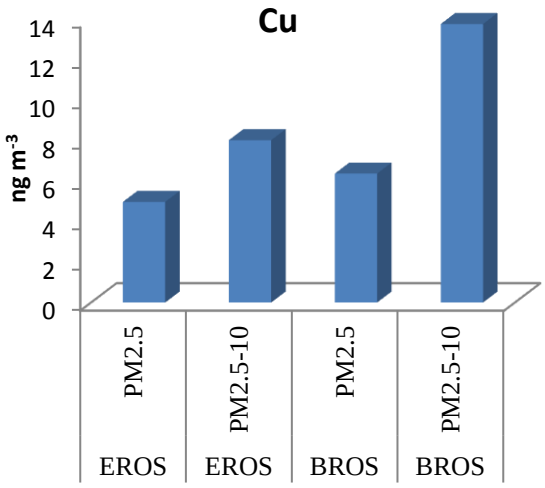
Cu
ng m-3
14
12
10
8
6
4
2
0
PM2.5
PM2.5-10
PM2.5
PM2.5-10
EROS
EROS
BROS
BROS

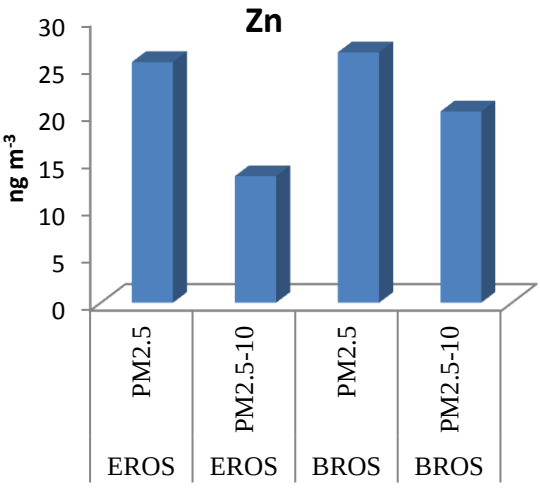
Zn
ng m-3
30
25
20
15
10
5
0
PM2.5
PM2.5-10
PM2.5
PM2.5-10
EROS
EROS
BROS
BROS

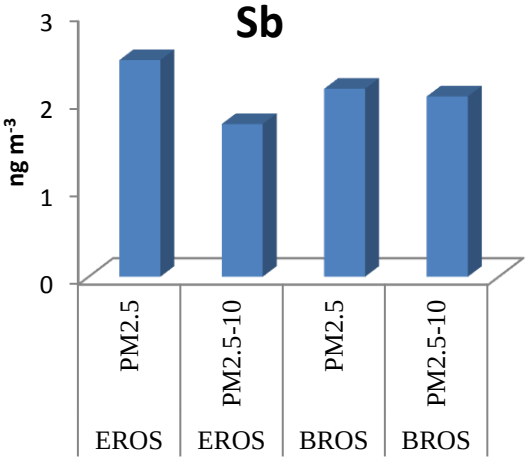
Sb
ng m-3
3
2
1
0
PM2.5
PM2.5-10
PM2.5
PM2.5-10
EROS
EROS
BROS
BROS

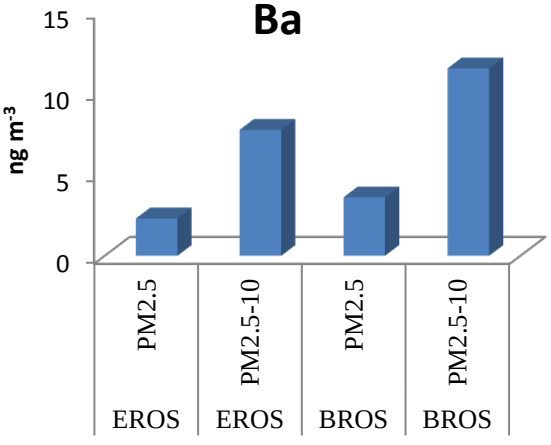
Ba
ng m-3
15
10
5
0
PM2.5
PM2.5-10
PM2.5
PM2.5-10
EROS
EROS
BROS
BROS

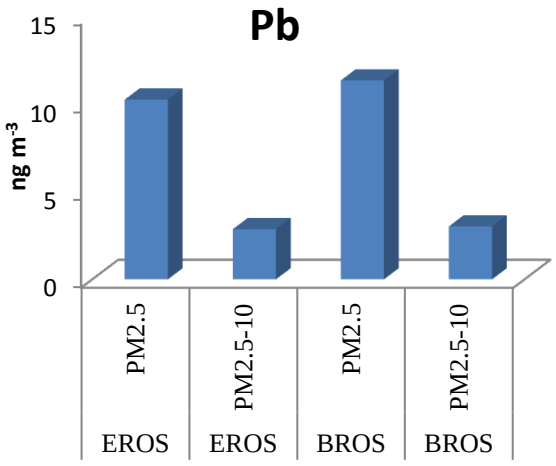

Figure 3.2: Compositions of PM mass and chemical components at EROS and BROS

The influence of ammonium, nitrate and aluminium were prominent in $PM_{2.5}$ at BROS while elevated SO_4^{2-}, V and Sb were observed at EROS. Cr, Mn, Zn and Cu exhibited similarities in their concentrations at the two sites. Higher values were clearly observed for coarse Cl^-, Na^+, Mg^{2+}, K^+, Cr, Mn, Fe, Cu and Ba at BROS. Reasons might be linked to more pronounced traffic emissions from exhaust and non-exhaust vehicular processes, and additionally, from the sea spray source (Mazzei *et al.*, 2008).

Figure 3.3 depicts the relationship between $PM_{2.5}$ and $PM_{2.5-10}$ mass concentrations measured at the EROS and BROS sites. $PM_{2.5}$ data at the two sites are well correlated with slope near 1.0. The strong relationship found between the $PM_{2.5}$ at the sites is a confirmation of common emission source. But the relationship between $PM_{2.5-10}$ data at both sites was poorly defined. Contribution of coarse fraction to PM load was slightly higher at BROS than EROS. This might be directly linked to re-suspension of road dust at BROS. $PM_{2.5}/PM_{10}$ ratio has been calculated for Partisol samples at both sites. $PM_{2.5}/PM_{10}$

ratio was 0.61 at EROS, and 0.60 at BROS indicating anthropogenic emissions at these sites.

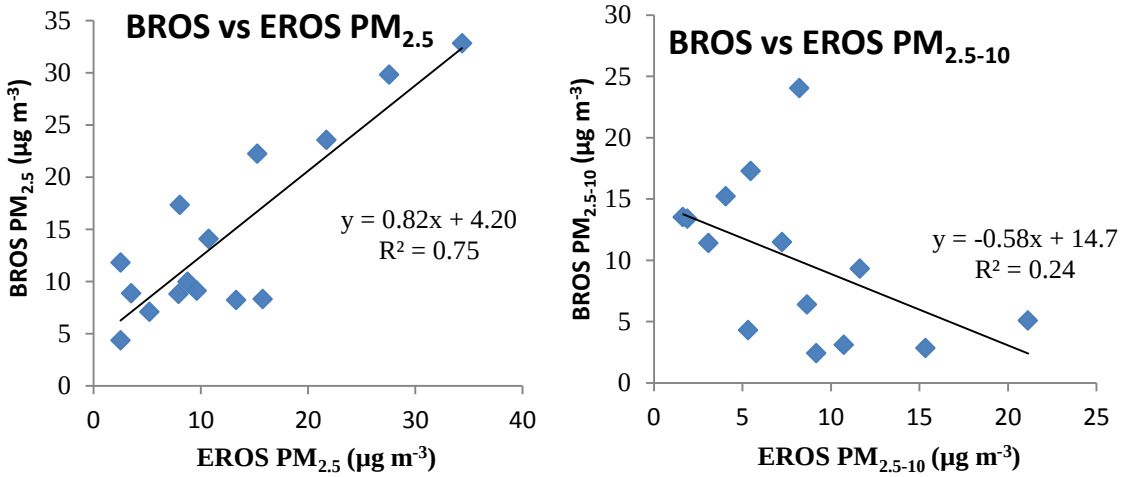

Figure 3.3: Linear regression analysis of $PM_{2.5}$ and $PM_{2.5-10}$ at EROS and BROS

PM elemental differences between background (EROS) and roadside (BROS) sites are plotted in Figure 3.4. There were convincing increments in the mean values of NO_3^-, NH_4^+, Al and Fe at the roadside for $PM_{2.5}$; and Cl^-, NO_3^-, SO_4^{2-}, Na^+, K^+ and Fe for $PM_{2.5-10}$. Incremental parameters of Fe, Cl^-, and Al have been reported as markers for traffic in many published studies (Kleeman *et al.*, 2002; Chung *et al.*, 2006; Lim *et al.*, 2010; Xia and Gao, 2010). The increment values observed for Na^+ and Cl^- at the roadside might be traced to de-icing salt (Harrison *et al.*, 2004). The observed higher concentrations of Fe at the roadside for $PM_{2.5}$ and PM_{10} agreed well with previous studies by Harrison *et al.* (2003).

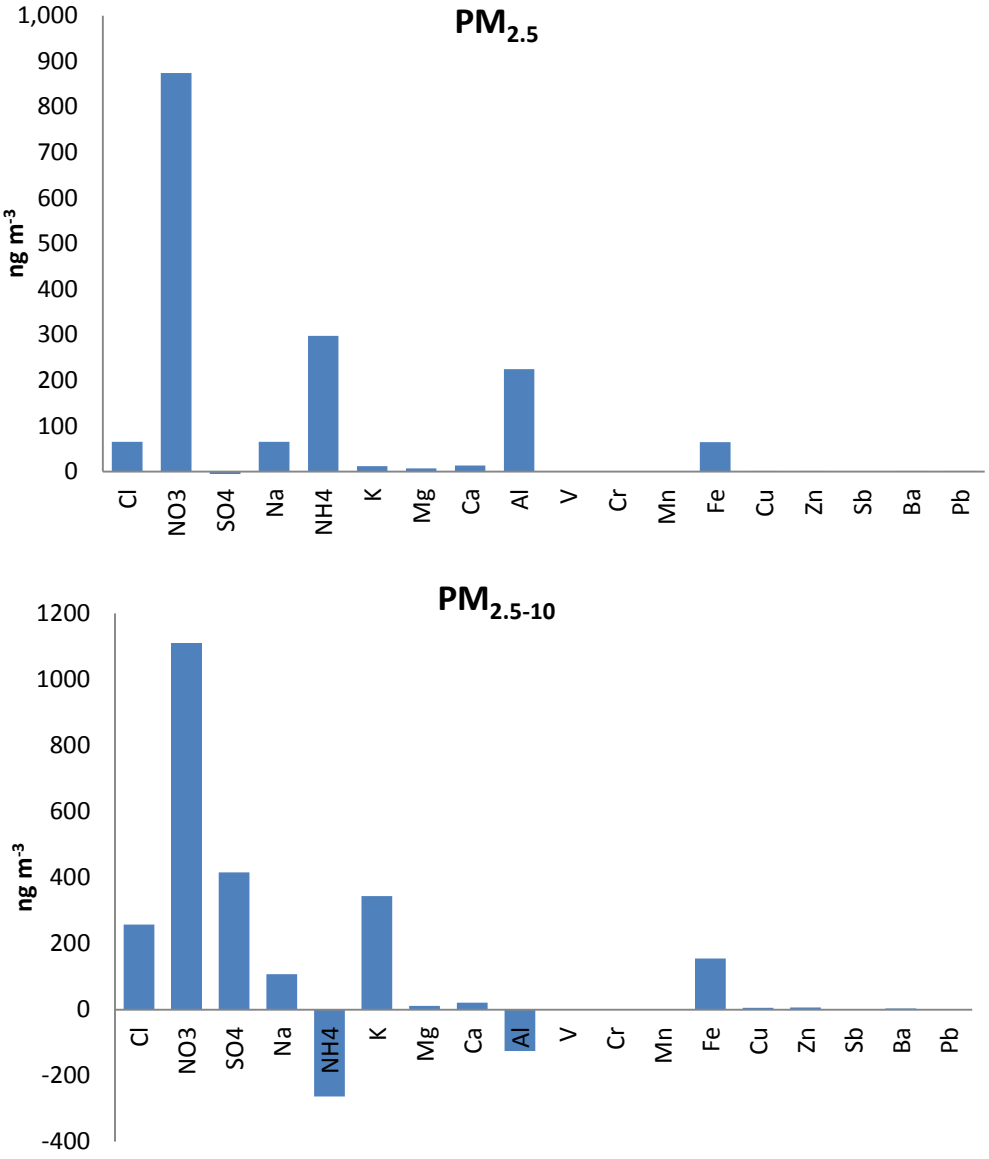

Figure 3.4: PM elemental differences between background (EROS) and roadside (BROS) sites indicating roadside increments

3.4.2 Partisol versus MOUDI data at EROS

Figure 3.5 shows comparison between the mean Partisol and MOUDI data for fine and coarse PM. The sum of MOUDI particle size less than 2.1 µm was adopted as fine PM ($PM_{2.5}$) while particles greater than 2.1 µm represent the coarse PM ($PM_{2.5-10}$). In $PM_{2.5}$ fraction, both instruments have depicted dominance by SO_4^{2-}. Notable distinctions were

clearly observed for Partisol mean values for NO_3^-, NH_4^+ and Al in $PM_{2.5}$. Elevated concentrations of NO_3^-, SO_4^{2-}, NH_4^+, Ca^{2+}, Al and Fe were observed for Partisol relative to MOUDI $PM_{2.5-10}$. However, Na^+ and Cl^- values were higher in MOUDI $PM_{2.5-10}$. PM data of MOUDI is shown in Appendix II.

The two measuring instruments have shown a well defined relationship for measured components at EROS. This is depicted in Figure 3.6 where all measured PM components for Partisol and MOUDI were correlated. Inclusion of mass concentrations in the regression analysis gave a better relationship. The $PM_{2.5}/PM_{10}$ mass concentration ratio calculated for MOUDI was 0.60, similar to the value of 0.61 obtained for Partisol at EROS. The absence of MOUDI data at BROS made its comparison with Partisol data impossible. The full detail of MOUDI size-resolved compositions will be discussed in the next chapter as it is compared with the Port Talbot campaign.

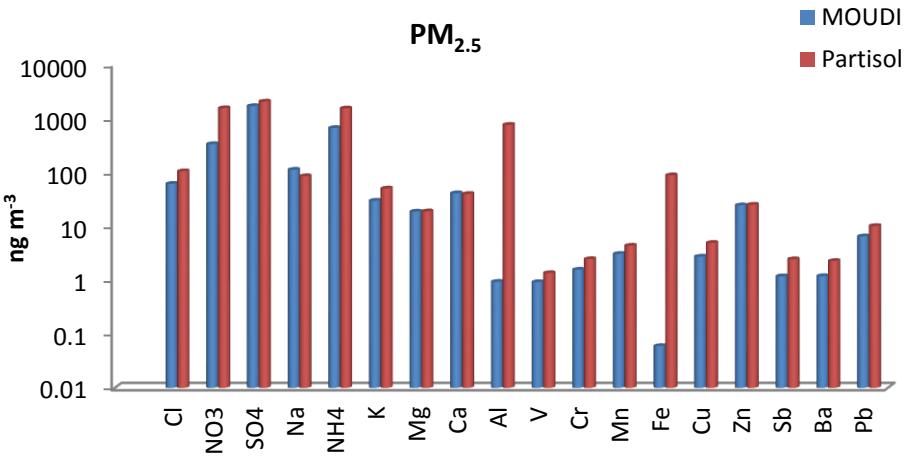

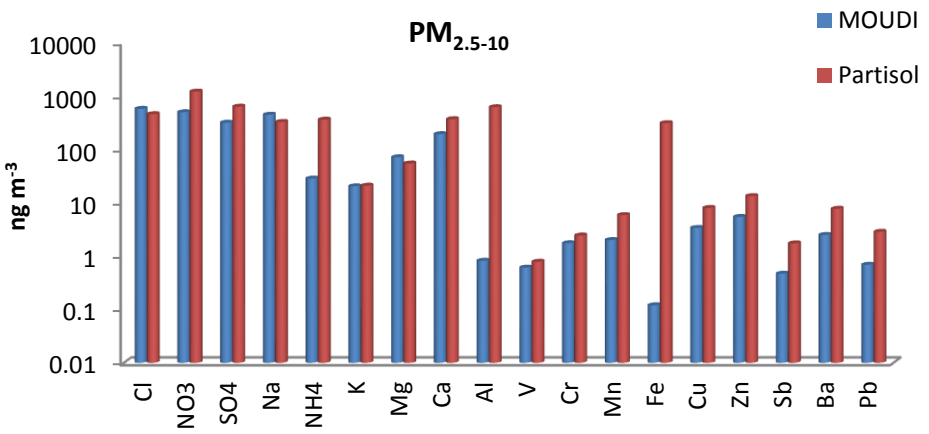

Figure 3.5: Comparison between average Partisol and MOUDI data at EROS

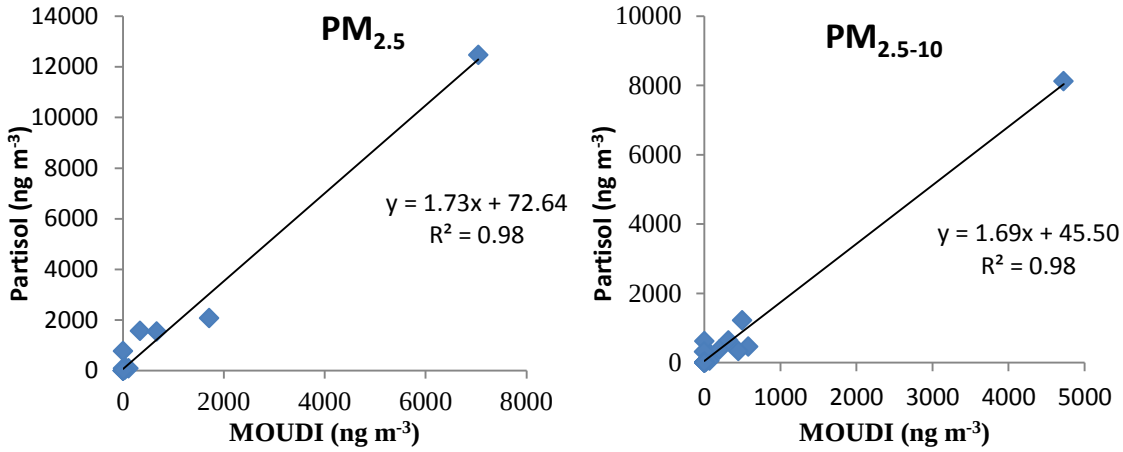

Figure 3.6: Relationship between Partisol and MOUDI data at EROS

3.4.3 Pearson's correlation coefficients of $PM_{2.5}$ and $PM_{2.5-10}$ data at EROS and BROS

Pearson's correlation coefficients (R^2) of $PM_{2.5}$ and $PM_{2.5-10}$ at EROS and BROS are presented in Appendix III. EROS $PM_{2.5}$ mass concentration exhibited good agreement with NH_4^+, K^+, Fe, Cr, Mn, Cu, Zn, Sb, Ba and Pb (R^2=0.56-0.86; $p<0.05$ and 0.01). This shows that EROS fine PM might largely be influenced by woodsmoke/biomass burning, crustal and traffic emissions. A better correlation between K^+ and NH_4^+ (R^2=0.74; $p<0.01$)

could indicate likely emissions from woodsmoke and incineration (Lim *et al.*, 2010). Most of the trace metals were highly associated with one another, especially Fe with Mn and Ba; and Sb with Ba, Zn, Fe and Pb. This could signify crustal and traffic emissions. The marine influence was prominent in EROS $PM_{2.5}$ with solid association that existed between Na^+ and Cl^- (R^2=0.78; $p<0.01$)

The $PM_{2.5-10}$ mass concentration at EROS showed strong correlations with NH_4^+, K^+, Ca^{2+}, Fe, Cr, Mn, Cu, Zn, Ba and Pb (R^2=0.68-0.86; $p<0.01$). A strong relationship was established for Na^- and Cl^- (R^2=0.95; $p<0.01$). Mn and Fe were significantly correlated indicating a similar emission source probably, from crustal or industry. Aluminium has not correlated well with Fe and Mn, suggesting their separate emission sources. Strong associations were established among the traffic signatures Sb, Fe, Cu, Zn and Ba in coarse PM.

Pearson's correlations for $PM_{2.5}$ mass with other constituents at BROS are similar to what was observed at EROS. Association of NH_4^+ with SO_4 and NO_3, though weak, was better defined in $PM_{2.5}$ at BROS than at EROS. Mg^{2+} and Ca^{2+} are also strongly correlated. Traffic signatures of Sb, Fe, Cu, Zn and Ba exhibit stronger correlations at BROS. The sea salt aerosols (Na^+, Cl^-) are weakly correlated at BROS. In $PM_{2.5-10}$ portion at BROS, mass concentration shows negative correlation with most observed constituents. Na, K and Mg are strongly associated (0.98-0.99; $p<0.01$) in the coarse PM component at BROS confirming probable influence from the road re-suspension dust. The traffic elements were also strongly associated at BROS for $PM_{2.5-10}$ as observed at EROS.

Table 3.1: Inter-site correlations between EROS and BROS PM

Components	Coefficient r^2	Components	r^2
$PM_{2.5}$ Mass	0.87**	Al	0.20
Cl^-	0.55	V	0.92**
NO_3^-	0.12	Cr	-0.17
SO_4^{2-}	0.36	Mn	0.87**
Na^+	0.29	Fe	0.81**
NH_4^+	0.86**	Cu	0.54*
K^+	0.62*	Zn	0.92**
Mg^{2+}	0.68*	Sb	0.85**
Ca^{2+}	0.44	Ba	0.89**
		Pb	0.71**
$PM_{2.5-10}$ Mass	-0.33	Al	-0.10
Cl^-	0.73**	V	0.87**
NO_3^-	0.18	Cr	0.07
SO_4^{2-}	-0.01	Mn	0.84**
Na^+	0.22	Fe	0.86**
NH_4^+	0.30	Cu	0.88*
K^+	-0.20	Zn	0.48
Mg^{2+}	0.05	Sb	0.91**
Ca^{2+}	0.90**	Ba	0.91**
		Pb	0.61*

Table 3.1 shows the inter-site relationship among the measured components of $PM_{2.5}$ and $PM_{2.5-10}$ at EROS and BROS. These sites are about 250 m apart and hence could be influenced by related a factor, of which traffic is the major suspect. Strong relationships were also observed at EROS and BROS for $PM_{2.5}$ and $PM_{2.5-10}$ components of V, Mn, Fe, Cu, Zn, Sb, Ba and Pb. The species such as NH_4^+, K^+, Mg^{2+} and Zn showed better associations at EROS and BROS for fine PM; while Cl^- and Ca^{2+} are better correlated in the coarse PM at the two sites.

3.5 Discussion

Most of the PM components (including mass concentrations) measured at the EROS background site are generally lower than those at BROS, a typical traffic-polluted site.

This is not surprising due to the roadside increment of pollutants. Elemental difference between fine SO_4^{2-} and coarse NH_4^+ at EROS and BROS were 245 and 262 ng m^{-3}. Conversely, coarse SO_4^{2-} and fine NH_4^+ were measured at higher concentrations at BROS with incremental difference of 415 and 298 ng m^{-3}, respectively. Since the two sites were within the University of Birmingham, insignificant regional transportation of these pollutants is expected (Harrison *et al.*, 2004). The discrepancies in NH_4^+ measured at the two sites might be related to emission sources like biomass burning or incineration (Lim *et al.*, 2010). Elevated coarse SO_4^{2-} at BROS might be attributable to road resuspended dust or soil (Harrison *et al.*, 1997). A large difference was found in the nitrate concentrations between the two sites for the fine (875 ng m^{-3}) and coarse (1108 ng m^{-3}) PM, which is evidence of a distinctive roadside emission. Higher $PM_{2.5}$ and $PM_{2.5-10}$ mass concentrations at BROS also indicate traffic contributions from vehicular emissions and road re-suspension. Harrison *et al.* (1997) found a very strong correlation between $PM_{2.5}$ and NO_x, suggesting that $PM_{2.5}$ mass concentration could be adopted as a better traffic signature.

This study shows elevated SO_4^{2-}, lower NO_3^- and Cl^- values in $PM_{2.5}$ component relative to the research recently published by Laongsri and Harrison (2013) at EROS. In $PM_{2.5-10}$ component, NO_3^- and SO_4^{2-} concentrations in this study are about 2 times higher than concentrations reported by Laongsri and Harrison (2013) but lower amount of Cl^-. At BROS, a previous study of Yin *et al.* (2010) for PM_{10} components Cl^-, SO_4^{2-}, NO_3^-, Ca^{2+} and Fe are calculated to represent approximately 3, 9, 6, 1 and 4% of the total measured mass, respectively. In this study, the corresponding values of these components in PM_{10} (computed by addition of $PM_{2.5}$ and $PM_{2.5-10}$) were 4, 12, 20, 2 and 5%, respectively. Except for NO_3^- where a relatively higher fraction was measured, it appeared that other

observed components are comparable to Yin *et al.* (2010) study. The wide difference observed in the percentages of these secondary aerosol (nitrate and sulphate) relative to previously reported values at these sites might still be linked with regional influence rather than local emissions (Abdalmogith *et al.,* 2006). Other probable reasons for the lack of agreement may be attributable to different sampling times and meteorological conditions.

Aluminium showed an increment of fine PM at BROS while the reverse was the case for coarse PM, which exhibited higher amounts at EROS. Fine Al can be attributed to vehicular emissions while coarse Al may take its source from soil. Traffic signatures such as Zn, Fe, Cu, Ba, Mn and Pb (Thorpe and Harrison, 2008) showed greater concentrations in fine and coarse PM at BROS agreeing with studies conducted at the roadsides (Gietl *et al.*, 2010; Amato *et al.*, 2009; Amato *et al.*, 2011). Pearson correlation coefficients depicted in Table 3.1 revealed strong significant correlations among these traffic signatures for $PM_{2.5}$ and $PM_{2.5\text{-}10}$ showing the pronounced contribution by traffic at both sites.

The $PM_{2.5}/PM_{10}$ ratios observed at EROS and BROS showed dominance of anthropogenic emissions at the two sites. This is comparable to most studies reported at urban sites. The earlier study of Yin and Harrison (2008) has observed $PM_{2.5}/PM_{10}$ ratio of 0.60 at BROS in perfect agreement with this present study. In the Harrison *et al.* (2004) study at an urban background site in London (High Holborn), the ratio of $PM_{2.5}/PM_{10}$ was calculated as 0.62 while the value was 0.64 at the roadsides. Across the UK, the mean ratio of $PM_{2.5\text{-}10}/PM_{10}$ has been reported as 0.31±0.13 (Liu and Harrison, 2011). This indicates dominance of $PM_{2.5}$ in agreement with observations at BROS and EROS.

3.6 Conclusion

The data of EROS and BROS presented above depicts higher concentrations of most PM parameters at the BROS site which reflects the road increment. The fine particles were dominated by sulphate at EROS (17% of $PM_{2.5}$ mass) while nitrate at BROS (20%). In the coarse fraction, nitrate was the highest chemical component at both sites, represented by 15% at EROS and 24% at BROS. The measured chemical components of PM (ionic and metal species) constituted only 51 and 54% of $PM_{2.5}$; and 54% and 67% of $PM_{2.5\text{-}10}$ at EROS and BROS, respectively. The remaining components can be attributed to the unmeasured carbonaceous species, mass-associated oxygen, particle-bound water and other chemical constituents.

CHAPTER 4 -COMPARISON OF SIZE DISTRIBUTION OF PM AT EROS AND PORT TALBOT

4.1 Abstract

The aim of this chapter is to compare the size-resolved composition of particulate matter (PM) sampled in the industrial town of Port Talbot (PT), UK and a typical urban background site in Birmingham (EROS). A Micro-Orifice Uniform Deposit Impactor (MOUDI) sampler was deployed for the two separate sampling campaigns with the addition of a Grimm optical spectrometer at the PT site. MOUDI samples were analysed for water soluble anions (Cl^-, NO_3^- and SO_4^{2-}) and cations (Na^+, NH_4^+, K^+, Mg^{2+} and Ca^{2+}) and trace metals (Al, V, Cr, Mn, Fe, Cu, Zn, Sb, Ba and Pb). Both 72-hour and campaign average data are discussed with comparison of PM composition highlighted for the two sites. The average MOUDI results showed a unimodal peak for Cl^-, Mg^{2+}, NH_4^+ and Ca^{2+} at EROS while other analytes exhibited at least two peaks occurring in the fine and coarse modes (except for Zn, Sb and Pb in which the two peaks occurred at fine modes of 0.5 and 1-2 μm). PT size-resolved mean data displayed bimodal distributions (with the exception of NH_4^+) with modes in the fine and coarse fractions, except Zn and Pb with two fine fraction modes as observed in the EROS data. The PM mass distribution showed a predominance of fine particle mass at EROS whereas the PT samples were dominated by the coarse fraction. SO_4^{2-}, Cl^-, NH_4^+, Na^+, NO_3^-, and Ca^{2+} were the predominant ionic species at both sites while Al and Fe were the metals with highest concentrations at both sites. Mean concentrations of Cl^-, Na^+, K^+, Ca^{2+}, Mg^{2+}, Cr, Mn, Fe and Zn were higher at PT than EROS due to industrial and marine influences. The contribution of regional pollution by sulphate, ammonium and nitrate was greater at EROS relative to PT. The

traffic signatures of Cu, Sb, Ba and Pb were particularly prominent at EROS. Overall, PM at EROS was dominated by secondary aerosol and traffic-related particles while PT was heavily influenced by industrial activities and marine aerosol. Profound influences of wind direction are seen in the 72-hour data, especially in relation to the PT local sources. Measurements of particle number in 14 separate size bins plotted as a function of wind direction and speed are highly indicative of contributing sources, with local traffic dominant below 0.5 µm, steelworks emissions from 0.5-15 µm, and marine aerosol above 15 µm. This chapter has been submitted for publication in a reputable journal-The Science of the Total Environment.

4.2 Introduction

The Micro-Orifice Uniform Deposit Impactor (MOUDI) has been widely used for particle size measurement in both indoor and outdoor pollution studies. These studies have reported PM size distributions for water soluble and trace metal components (Allen *et al.*, 2001; Cabada *et al.*, 2004; Harrison et al, 2003; Chang *et al.*, 2008; Dall'Osto *et al.*, 2008; Liu *et al.*, 2008; Zhao and Gao, 2008; Gietl *et al.*, 2010; Ny and Lee, 2011). Na, Cl, Ca and Al typically show modes in the coarse fraction while Cd, Zn, Mn, Ni and Cu have modes in the fine fraction (Ny and Lee, 2011). Allen *et al.* (2001) reported MOUDI data for trace metals from three urban background sites in the UK. Dall'Osto *et al.* (2008a) employed a MOUDI for particle size-resolved measurements at a steel industry site in the UK. Water soluble ions in particulate matter, from nanoparticles to the coarse mode, have been determined with a MOUDI and nano-MOUDI in Taiwan by Chang *et al.* (2008). In London, particle size-segregated aerosol has been measured at roadside and background sites by Gietl *et al.* (2010). PM size-segregation and associated metallic elements in an industrialized city in Korea have been reported (Ny and Lee, 2011). None of these studies have compared the size distribution of PM and its components collected at urban background and industrial (especially steelworks) locations for both water soluble ions and trace metals.

In this study, particle size distributions of both ionic species and trace metals at typical background (EROS) and industrial sites (Port Talbot) were studied, offering an opportunity for identifying source signatures of components contributing to PM in the atmosphere of the two study areas. Additionally, particle number spectra from 0.3 μm to > 15 μm are reported and analysed according to windspeed and direction.

4.3 Materials and Methods

4.3.1 The study areas

4.3.1.1 Port Talbot (PT)

PT is a coastal industrial town with roughly a population of 35,000 and located on the M4 corridor in South Wales (51° 34' N and 3° 46' W). The Tata steel complex located in Port Talbot town is the main industry in the study area and a major source of PM emissions (AQEG, 2011). The site covers approximately 28 km^2, comprises of ~50km of roads, 100 km of railway, and 25,000 vehicle movements per day. The production capacity is around 5 m tonnes per year with the main processes in the steelworks being iron-making (sintering, blast furnace and raw materials), steel-making (basic oxygen steel-making (BOS) and coking) and rolling mills (hot and cold mills) (Moreno *et al.*, 2004; Dall'Osto *et al.*, 2008). Figure 4.1 shows the sampling sites chosen in Port Talbot. These include Automatic Urban Rural Network (AURN) site located at Margam Fire Station (FS), Environmental Agency Wales monitoring sites at Prince Street (PS), NPTCBC stations at Dyffryn School (DS) and Little Warren (LW). FS, PS and DS were representative of upwind sites while LW as a downwind site.

Figure 4.1: Port Talbot sampling station and the steelworks processing units

4.3.1.2 Elms Road Observatory Site (EROS)

Detailed description of EROS site has been described in section 3.1 (Chapter 3).

4.3.2 Particulate matter sampling

Size-fractionated particle sampling was carried out with an 8-stage MOUDI ™ (Model 100, see section 2.2.1). At EROS, a total of four MOUDI 72 hour-samples were generated during the sampling period between March 30 and April 11. At the PT sampling site, ten MOUDI samples of 72 hours each were collected during a one-month sampling campaign that started on the April 17 and ended on May 16, 2012. The tenth sample was collected for just 36 hours.

4.3.3 Sample digestion and analysis

The procedures for sample digestion and analysis have been discussed in chapter 2.

4.3.4 Number size distributions

Particle number size spectra in the range 0.3 to 20 µm were measured at the Port Talbot site using a Grimm model #1.108 optical particle spectrometer which measures the intensity of light scattered at 90º to a beam produced by a laser diode. The full explanation of the Grimm instruments could be seen in chapter 2. Particles are classified into 14 size fractions between the smallest (0.3-0.4 µm) and largest (15-20 µm) bins.

4.4 Results and Discussion

4.4.1 MOUDI particle size distributions at EROS

4.4.1.1 Port Talbot

Figure 4.2 and Appendix IV detail the temporal variations of MOUDI data for mass and ionic components from the industrially influenced PT site. Bimodal peaks (0.5 and 2-6 µm) were observed for mass distribution for each MOUDI sample during the campaign with highest mass concentration observed on April 23-26 which coincided with the start of a PM_{10} episode on April 26th reaching hourly concentrations in excess of 100 µg m^{-3}. Most of the water soluble components displayed two distinct modal peaks in the fine mode except Cl^- (other than the May 11-14 sample which showed two modal peaks), NH_4^+ and Ca^{2+}. Common fine modal peaks of 0.5 µm and coarse modal peaks of 2-6 µm were observed for most of the ionic species except for K^+ which showed diverse modal peaks in various sampling periods, suggesting multiple sources of K^+ in Port Talbot. However, the common peak at 0.5 µm shown by K^+ in all the samples indicated a common emission

source for which biomass combustion or steelworks activities are the major suspects. An episode of Ca^{2+}, Cl^{-}, and NO_3^{-} was observed between May 2-5 all showing higher concentrations at 3.0 µm. This was also observed for ammonium and sulphate with a peak at 0.5 µm. Elevated Ca^{2+} observed during this episode might have sources either from construction activities or steelworks emissions. In the blast furnace of the steelworks, limestone ($CaCO_3$) and dolomite ($CaMg(CO_3)_2$) are used as fluxing agents while in the basic oxygen furnace (BOF) section, lime (CaO) and fluorspar (CaF_2) are fluxing raw materials (Machemer, 2004). The MOUDI sample of April 20-23 showed higher concentrations of Cl^{-}, Na^{+} and Mg^{2+} all peaking in the particle size range 3-5 µm. This typifies a sea spray episode.

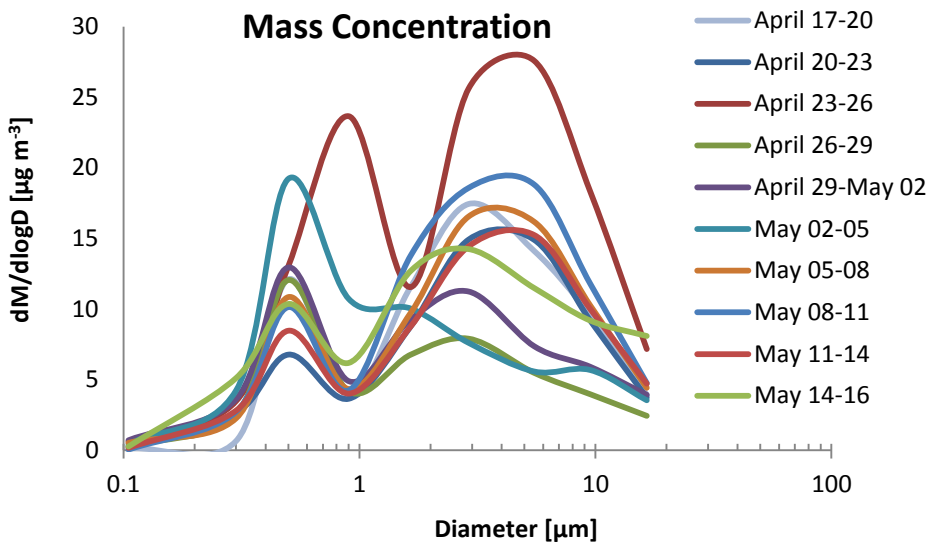

Figure 4.2: Variations of 72-hour MOUDI PM mass size distributions at the PT site

Figure 4.3 and Appendix V show the trace metal size distribution of MOUDI samples during the one-month campaign. The concentration of Fe was the highest (Figure 4.2), followed by Al and Zn. All the metal data show two or more modal peaks covering the fine and coarse particle ranges except Pb and Zn which have their modes in the fine

fraction only (0.5 and 1-2 µm). Mn and Fe showed similar modes throughout the sampling periods suggesting common emission sources. In the fine mode, most of the trace metals peak at 0.5 µm except for the April 26-29 sample which showed exceptional elevated peaks for Cr and Cu at 0.2-0.3 µm. Combustion of copper chrome arsenate (CCA) treated wood could explain the unusual peaks of these trace metals on these days. CCA was used as wood preservative before its ban in the UK in 2007 (Wood Protection Association, 2010). However, CCA treated woods may still remain in many structures. Despite the fact that Cu is often a good marker for traffic (brake dust), its appearance at 0.2-0.3 µm is not consistent with traffic as other traffic markers such as Sb and Ba were peaking at a different diameter (0.5 µm). Additionally, in the size range 1-2 µm significant amounts of Al and V appeared in the April 26-29 MOUDI sample. Apart from this date, V peaked at 0.5 µm throughout; but Al showed different fine modal peaks at 0.2-0.3, 0.5 and 1-2 µm.

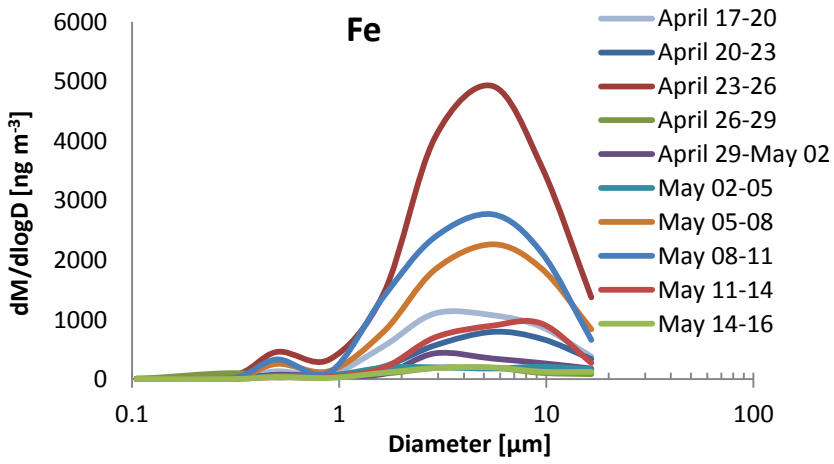

Figure 4.3: Variations of 72-hour MOUDI PM size distributions of Fe at the PT site

Al in the fine mode could arise from vehicular, coal combustion and metallurgical activities (Kleeman *et al.*, 2000; Xia and Gao, 2010) while fine V normally arises from fuel/oil combustion and shipping emissions (Figueroa *et al.*, 2006; Pandolfi *et al.*, 2011).

The appearance of irregular peaks on April 26-29 implies that Al and V could arise from the same sources that emitted Cu and Cr into the atmosphere. The wind rose for that sampling interval (see Figure 4.3) indicates that the source is unlikely to be associated with the steelworks.

4.4.1.2 EROS

Individual 72-h MOUDI size segregated mass and water soluble ion distributions from the EROS site are represented in Figure 4.4 and Appendix VI. The gravimetric mass showed modal peaks in the fine and coarse PM ranges at 0.5 µm and 2-4 µm. Among the water soluble ions, Cl^-, Na^+, Mg^{2+} and Ca^{2+} depicted a unimodal peak at 3-6 µm. Ammonium exhibited a single peak in the fine mode (0.5µm). Other ionic species showed bimodal behaviour generally peaking at 0.5 and 3 µm except in the April 8-11 sample where NO_3^- peaked at a single mode of 1-2 µm. A sulphate coarse mode occurred at around 5.0 µm. Among the ionic components of PM, sulphate constituted the highest concentration while $K^+ < Mg^{2+} < Ca^{2+}$ were the ionic species of lowest abundance.

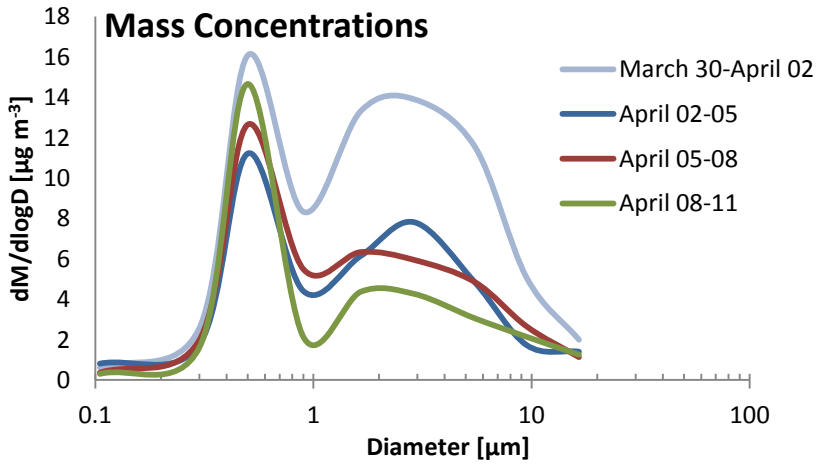

Figure 4.4: Variations of 72-hour MOUDI PM mass size distributions at the EROS site

MOUDI trace metal size distributions at the EROS sampling site are shown in Figure 4.5 and Appendix VII. Unlike water soluble ions where the highest concentrations were observed in the March 30-April 2 sample, metal concentrations were higher on April 5-8. All of the metals displayed at least two peaks covering fine and coarse PM fractions except Pb, Zn, Sb where the two modes were both in the fine fraction, other than in the sample collected on April 8-11 which displayed a coarse mode peak at 2-3 µm for Sb. Multiple modes were observed for Al, V and Cr (0.5, 1-2, 3 and 10 µm). On March 30-April 2, V, Cr, Cu, Zn, Sb and Pb all showed similar peaks at fine modes of 0.5 and 1-2 µm indicating possible emissions from traffic and industrial combustion processes (Zanobetti *et al.*, 2009). Zn measured on April 5-8 showed a coarse modal peak which might be linked with traffic emissions of brake or tyre dust (Harrison *et al.*, 2012b). Different peaks exhibited by the measured metals during different sampling periods suggested diverse emission sources.

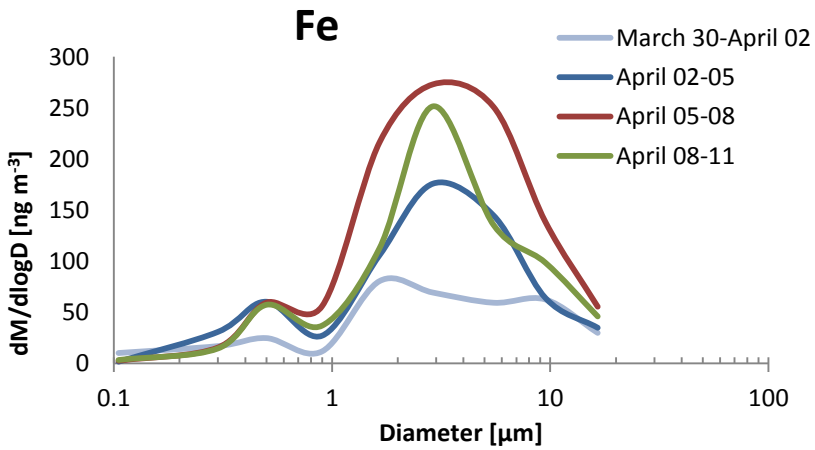

Figure 4.5: Variations of 72-hour MOUDI PM size distributions of Fe at the EROS site

4.4.2 Comparison of average MOUDI size distributions from EROS and PT

Figure 4.6 shows the average size distribution data for mass, water soluble ions and trace metal concentrations at EROS and PT sites. Different patterns were observed for these particle constituents. At both sites, mass concentrations, Na^+, K^+, Fe, Cu and Ba exhibited two modal peaks generally occurring at 0.5-0.6 µm and at 2-6 µm. Average mass concentrations showed a slight elevation of fine particle mass at EROS while an elevated concentration of coarse particles was evident at PT relative to the other sites. Meteorological conditions, especially windspeed and temperature are known to influence particle concentration and size distributions (Charron and Harrison, 2005; Jones *et al.*, 2010). During dry and windy conditions, elevated amounts of coarse particles could be favoured due to re-suspension of soil, road and industrial dusts. Average windspeed and temperature at the Birmingham (Tyburn) and Port Talbot (Fire Station) Automatic Urban Rural Network (AURN) sites were calculated (http://uk-air.defra.gov.uk/networks/aurn-site-info). The AURN station at Birmingham, Tyburn was used to represent the EROS site. During the period of sampling at EROS (March 30 – April 11), the average windspeed and temperature were 4.3±1.8 m s^{-1} and 6.7±1.4 ^oC respectively. At PT where the sampling campaign took place between April 17 and May 16, the values were 6.3±2.3 m s^{-1} and 8.6±1.4 ^oC. The higher average windspeed at PT would be expected to reduce concentrations of primary pollutants, other than those derived from the wind-driven processes such as resuspension.

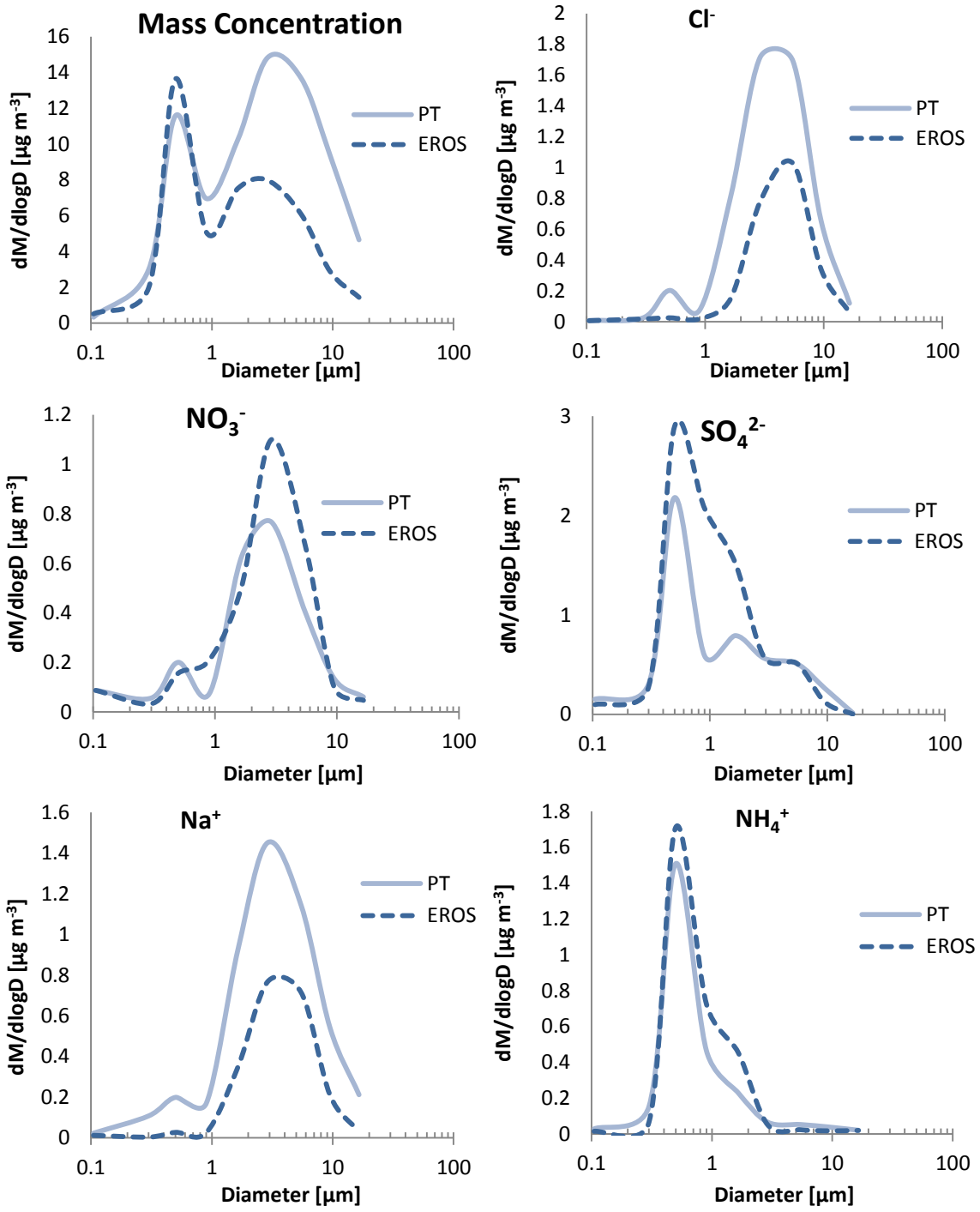
Mass Concentration
dM/dlogD [µg m-3]
Diameter [µm]
PT
EROS
Cl-
NO3-
SO4 2-
Na+
NH4+

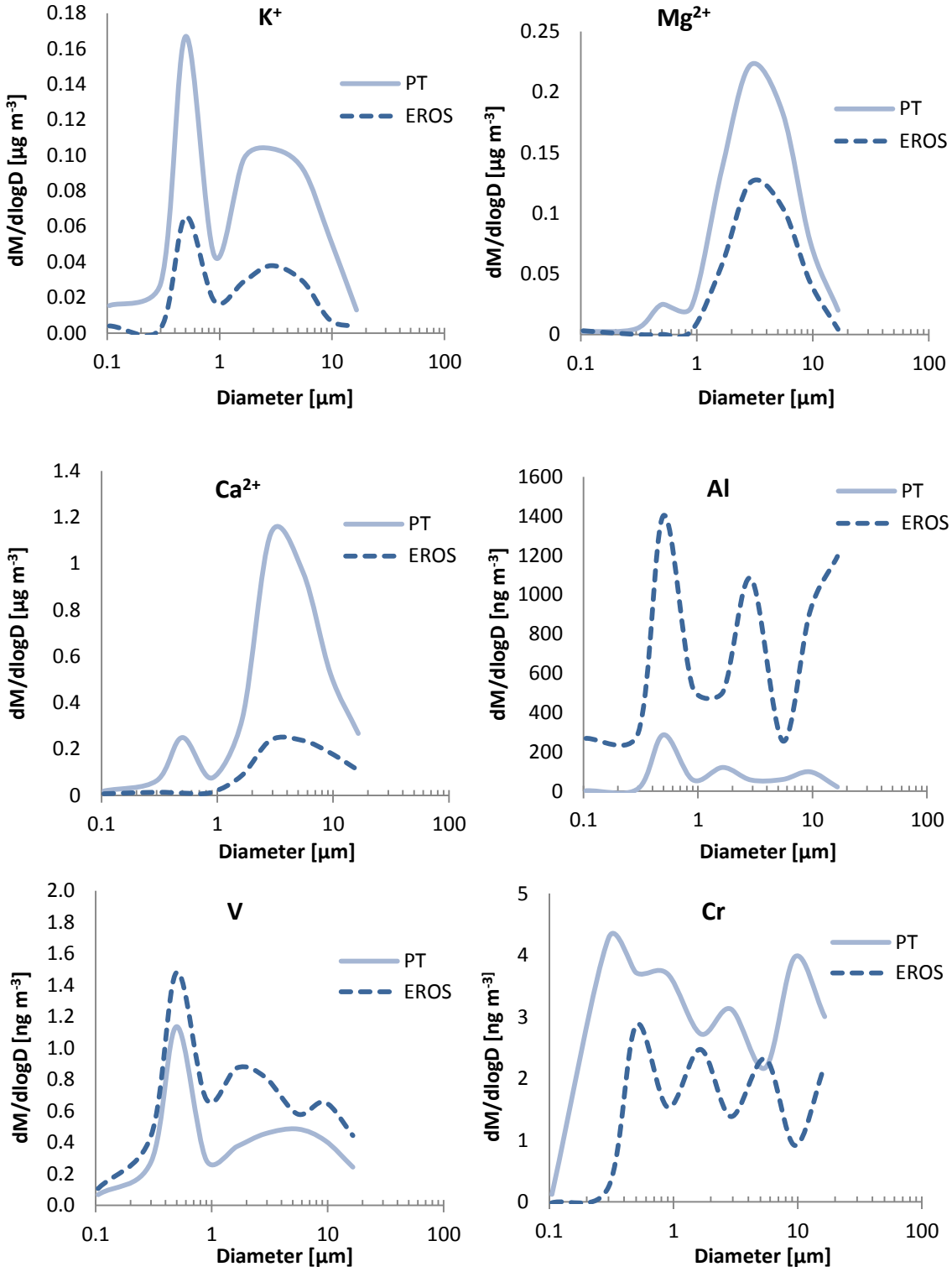
K+
Mg2+
Ca2+
Al
V
Cr
PT
EROS
dM/dlogD [µg m-3]
dM/dlogD [ng m-3]
Diameter [µm]
0.1
1
10
100

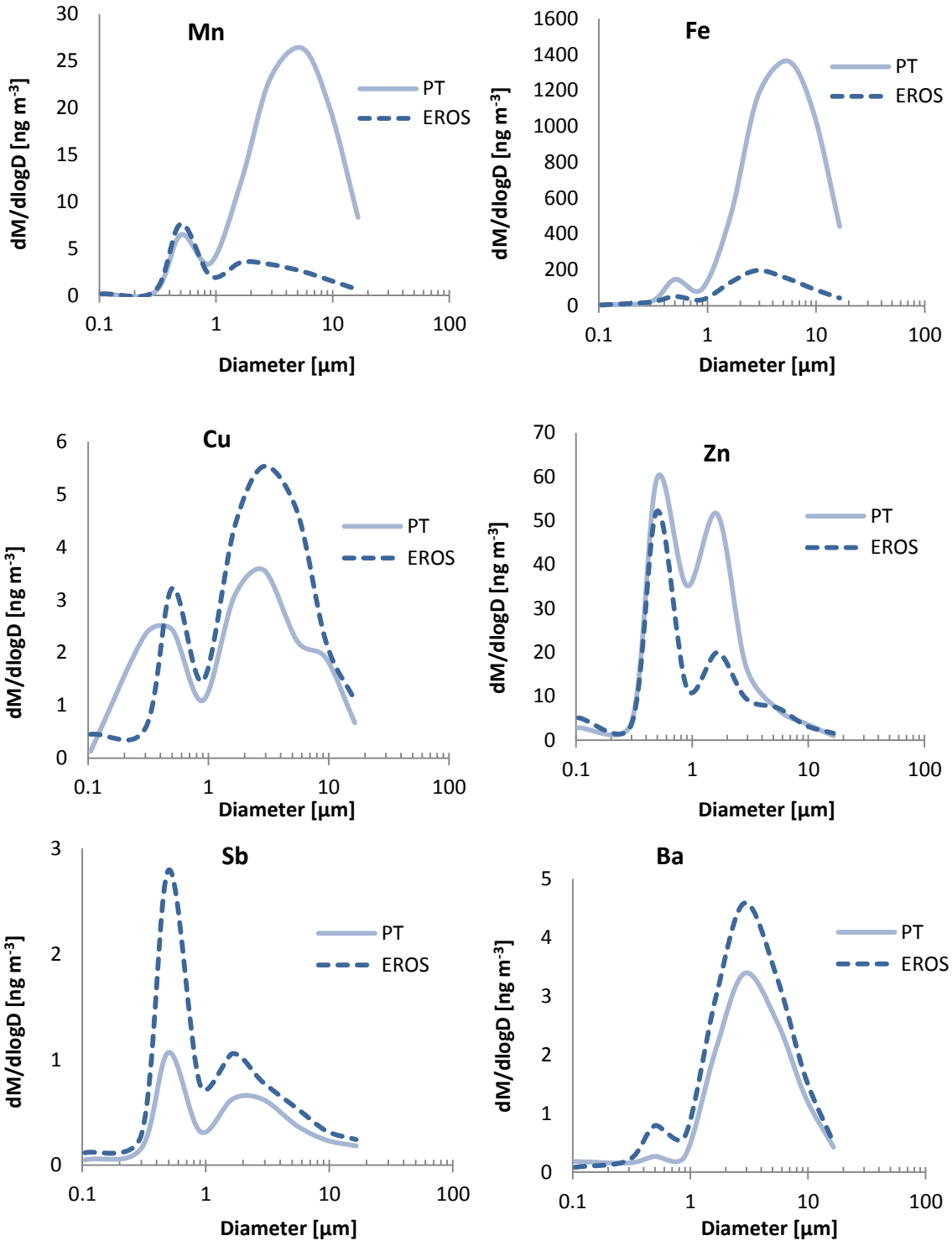
Mn
Fe
Cu
Zn
Sb
Ba
PT
EROS
dM/dlogD [ng m-3]
Diameter [µm]
0.1
1
10
100

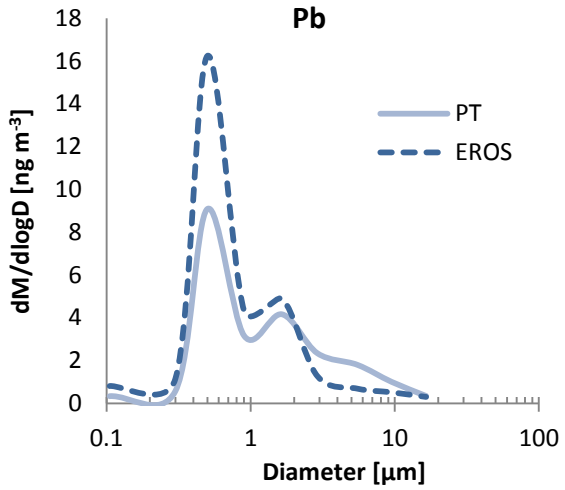

Figure 4.6: Average MOUDI mass size distributions of total PM and its components at the EROS and PT sites

Braga *et al.* (2005) working in south Brazil found high enrichment factor values for Zn, Mn, Fe and Cr; and attributed the origin to steelworks. Pandolfi *et al.* (2011) has applied Positive Matrix Factorization (PMF) to source apportionment of particle samples from Gibraltar (Iberian Peninsula) and adopted Zn, Mn, Fe, Cr as markers for the metallurgical industry. Mn, Fe and Zn emissions in Rahee (Finland) have been attributed to steel smelting by Oravisjarvi *et al.* (2003). Elevated coarse mode Ca^{2+} at PT could have been emitted from steel production activities (Oravisjarvi *et al.*, 2003). Ca can also emanate from construction processes especially in the large PM mode (Machemer, 2004; Ahn and Lee, 2006). The influence of soil dust and construction on the Ca emission has been assessed by Wang *et al.* (2005) using the Ca/Al ratio. A low value is indicative of soil dust while higher values indicate construction activities. The average Ca^{2+}/Al ratios of 0.2±0.3 and 8.1±6.8 were obtained across MOUDI data (PM_{10}) at EROS and PT respectively. In the fine mode the values were 0.1±0.1 (EROS) and 3.8±3.3 (PT); while in the coarse mode the ratios were 0.4±0.1 (EROS) and 13.5±7.2 (PT). The far higher ratios of Ca^{2+}/Al at PT

are most likely attributable to an emission from the steelworks (see previous section), as the only major local construction activity related to earthworks associated with road building, particularly the Port Talbot Peripheral Distribution Road, which would be expected to cause an elevation in both elements.

Seawater ratios of Cl/Na, K/Na, Ca/Na, Mg/Na and SO_4/Na are 1.8, 0.037, 0.038, 0.12 and 0.25 respectively (Parmar *et al.*, 2001). In the fine mode, these values in their respective order at EROS were 1.8±2.5, 0.93±0.95, 1.31±1.89, 0.11±0.11, 59.82±49.88 while their corresponding coarse particle ratios were 1.5±0.4, 0.06±0.04, 1.30±1.62, 0.16±0.03 and 0.53±0.32. Of these figures, Cl^-/Na^+ and Mg^{2+}/Na^+ at EROS were the closest ratios to seawater composition, and therefore portrayed marine aerosol as the major source of $Cl^-/Na^+/Mg^{2+}$ in fine and coarse PM. The observed ratios of Cl^-/Na^+, K^+/Na^+, Ca^{2+}/Na^+, Mg^{2+}/Na^+ and SO_4^{2-}/Na^+ at PT were 0.6±0.3, 0.43±0.32, 0.71±0.37, 0.11±0.04 and 2.81 for fine PM and 1.11±0.39, 0.08±0.02, 0.91±0.21, 0.13±0.03 and 0.35±0.19 for the coarse fraction. Comparing these ratios with seawater values revealed only Cl^-/Na^+ in the larger particles to be mainly influenced by marine aerosol, while the corresponding low value in the fine fraction is reflective of chloride loss. Mg^{2+}/Na^+ ratios in both modal peaks were also related to seawater composition at PT. Calculation of chloride depletion adopting the formula given by Zhao and Gao (2008) as % Cl = 1.81 x ([Na]-[Cl])/(1.81 x [Na]) x 100 for PM at EROS and PT gave 60 and 70% respectively. This Cl depletion value obtained at the PT site was similar to the study of Zhao and Gao (2008) who reported a Cl depletion value of 65% at a coastal site in the eastern US. The ratios again show a strong excess of coarse mode Ca^{2+} at the PT site. Reaction of sea salt with atmospheric strong acids (HNO_3 and H_2SO_4) is the likely cause.

SO_4^{2+} and NH_4^+ appearing in the fine mode at 0.5-0.6 µm suggests formation of $(NH_4)_2SO_4$ or NH_4HSO_4 in the droplet mode. The droplet phase reaction involving oxidation of SO_2 to sulphate is very important in the atmosphere (Khoder, 2002). The modal peaks of 0.5 µm and a small mode between 1-2 µm observed for SO_4^{2-} at PT coinciding with those of Zn and Pb suggested internal mixing between SO_4^{2-} and Pb, and Zn. Formation of $PbSO_4$ and $ZnSO_4$ from the reactions involving Pb, Zn and SO_4 at the two modal sizes might have evolved from separate emission sources, which might be linked to the steelworks units or other anthropogenic activities. Previous studies at the steelworks have identified Pb and Zn as major emissions from the sinter and basic oxygen steel making sectors (Oravisjarvi *et al.*, 2003; Dall'Osto *et al.*, 2008).

At the PT site, Dall'Osto *et al.* (2008a) found two peaks of Pb occurring at fine modes of 0.4-0.5 µm and 1-2 µm, which is similar to the modal peaks of Pb obtained in this study. Also, Dall'Osto *et al.* (2008a) reported Zn to have a lone peak occurring at 1-2 µm relating to that obtained in this present study. However, another larger mode was found for Zn at 0.5 µm in this study. A small peak of SO_4^{2-} concentration in the coarse mode at 5.0 µm is suggestive of a reaction with mineral dust forming $CaSO_4$. The coarse mode Ca^{2+} extended between 3 and 6 µm indicating internal mixing with coarse SO_4^{2-}. This may be an emission from the sinter process. Dall'Osto *et al.* (2008a) reported different coarse modes for Fe dependent on the emission source. Such behaviour is also reflected in the size distributions for Fe seen in Figure 4.6.

Generally, the modes in the size distributions were similar at the two sites (Figure 4.6). Notable differences in the modes were as follows:

- calcium showed a fine mode at PT which was not evident at EROS. This may be an emission from the steel industry.
- aluminium showed a pronounced mode > 10 µm at EROS which has no parallel at PT, and probably arises from resuspension of road dust (Harrison *et al.*, 2012b).
- chromium shows multi-modal behaviour at both sites, but the smallest mode at PT is at around 0.2 µm, whereas at EROS it is close to 0.5 µm. Either steelworks emissions or combustion of wood treated with copper chrome arsenate (CCA) preservative may be the source.
- manganese, for which PT shows a very pronounced coarse particle mode at *ca* 5 µm, while at EROS, the mode is much broader, peaking at 1-2 µm.
- iron, for which both sites show a bimodal distribution. The most obvious difference is the coarse mode, which centres on 5 µm at PT and 2 µm at EROS, and parallels the behaviour of manganese. The mode at 2 µm seems likely due to brake dust, as that for Cu and Ba at EROS are at a similar size, close to that reported by Gietl *et al.* (2010) from a site in central London. The large peak at Ca^{2+} 5µm for both Fe and Mn is most probably associated with emissions from the steelworks, based upon the much elevated concentrations observed at the PT site (see Figure 4.6).

Components showing similar size modes, but different relative abundances were:

- particle mass, for which the fine mode was very similar at both sites, but the coarse mode was much more prominent at PT due largely to increased marine aerosol (Cl^-, Na^+, Mg^{2+}) and metallic elements, most notably Fe and Mn.

- coarse Cl^- and Na^+ from marine aerosol reflecting the proximity of the PT site to the sea.
- SO_4^{2-} and NH_4^+ which showed a greater abundance at the EROS site and are primarily associated with regional transport of secondary ammonium sulphate.
- NO_3^- is markedly coarser than ammonium at both sites, and a little finer than Cl^- and Na^+, consistent with an association with aged marine aerosol (Ottley and Harrison, 1992). Concentrations are higher at EROS, probably reflecting the east to west gradient in secondary nitrate and sulphate observed across the UK (AQEG, 2012), although the relatively short duration of sampling is insufficient to establish this beyond doubt.
- K^+, which shows similar modes, but significantly higher concentrations at PT. Woodsmoke is usually the main source of fine K, while the coarse K may in part reflect marine aerosol, with also a likely contribution from steelworks emissions.
- coarse Ca^{2+} is also highly elevated at PT, probably reflecting emissions from steelworks processes and stockpiles.
- Al and V show elevated concentrations at EROS, probably reflective of soil/road dust as a source of Al (although the fine mode is hard to explain) and fuel oil combustion for V.
- Mn and Fe both show a much enhanced coarse mode at similar sizes at PT, consistent with a common steelworks source.
- Cu, Sb and Ba are all elements associated with brake wear emissions (Gietl *et al.*, 2010). All appear to show a brake dust component at both sites – the mode at 3 μm is characteristic (Gietl *et al.*, 2010). In all cases, the data from EROS show higher concentrations. Published studies have reported Cu/Sb values of 4.6 and 5.3

for brake wear emissions (Sternbeck *et al.*, 2002; Hjortenkrans *et al.*, 2007). Studies on major roads have measured higher Cu/Sb values of 8.7-12 for fine and 10.5-13 for coarse particles (Song and Gao, 2011); and 9.1 (Gietl *et al.*, 2010). In this study, these ratios were calculated to be 2.3, 7.2 and 3.7 (fine, coarse and PM_{10}) at EROS and 4.3, 5.4 and 4.9, respectively at PT. In the coarse mode the Cu/Sb ratio obtained at EROS was closer to Song and Gao (2011) and Gietl *et al.* (2010) consistent with a traffic influence. Cu, Sb, Pb and Zn all show a marked peak at 0.4-0.5 µm, probably associated with a higher temperature source, in the case of Cu, Sb and Pb most prominent at EROS.

- Zn shows modes at 0.4 µm and 2 µm which are more abundant at PT, especially the coarser mode. This is an element which has previously been associated with steelworks emissions (Dall'Osto *et al.*, 2008).

Comparing the results of this study with the past work on MOUDI size distributions at PT reported by Dall'Osto *et al.* (2008a), similarities were observed only for Fe, Pb and Zn, peaking at similar diameter. But unlike that study where Zn showed two peaks in the accumulation mode, only one peak was observed. Most of the elements reported in this study were not measured by Dall'Osto *et al.* (2008a) besides a dissimilar modal peak measured for Cl^-. As for the EROS site, MOUDI size distributions for ionic and trace metal species have not previously been published. However, the work in the urban background (Regents Park) in London by Gietl *et al.* (2010) could be expected to provide data comparable with EROS. Elements reported by Gietl *et al.* (2010) were Ba, Cu, Fe and Sb which are notable traffic markers. Except for Cu which exhibited two modal peaks, the EROS data were very similar to London for the other metals.

4.3.3 Data from specific sampling periods

4.3.3.1 Influence of wind conditions upon size distributions

Wind roses for the respective periods appear in Figures 4.7.

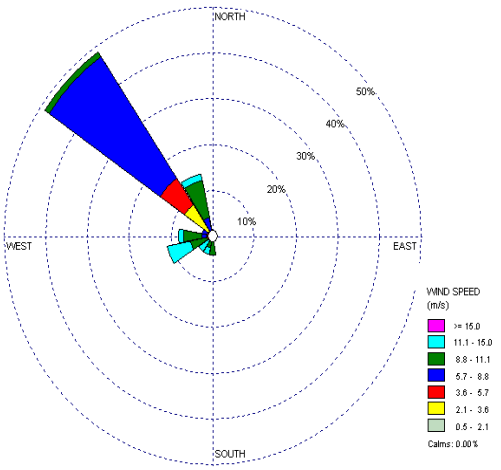

April 17-20

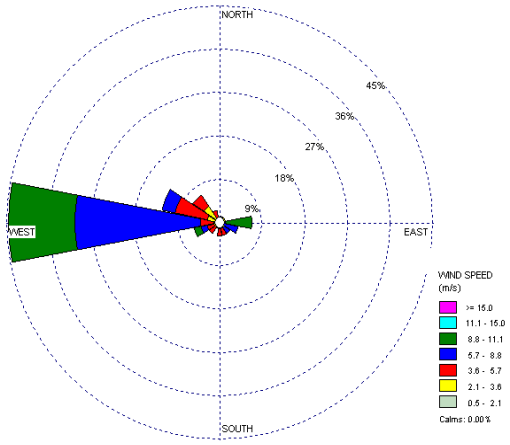

April 20-23

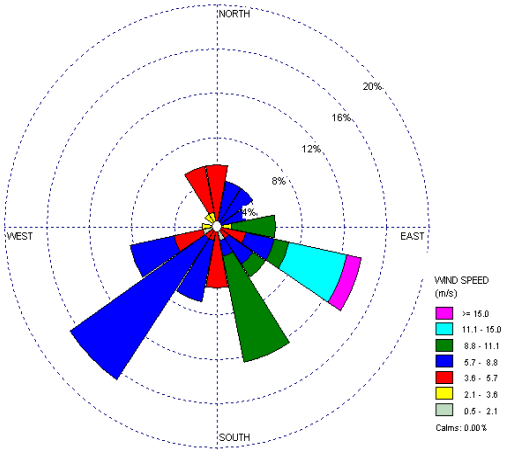

April 23-26

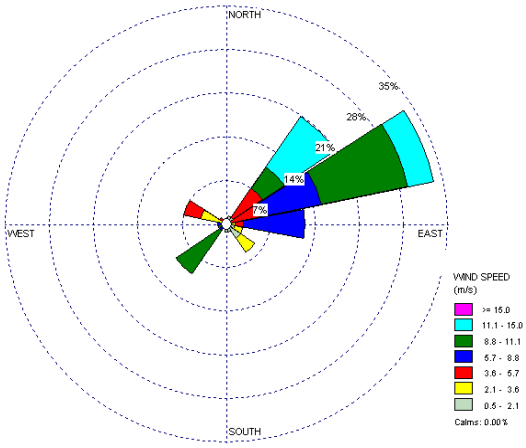

April 26-29

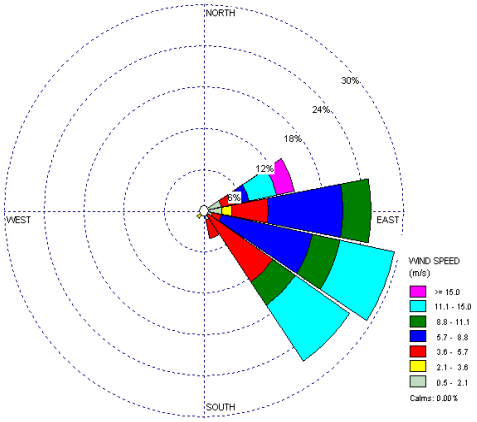

April 29-May 02

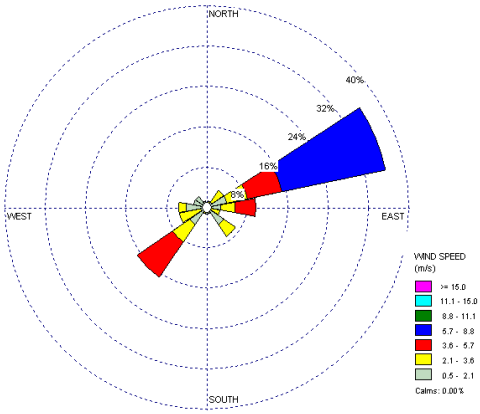

May 02-05

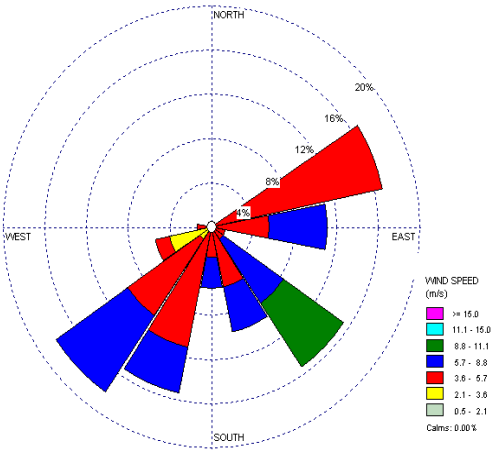

May 05-08

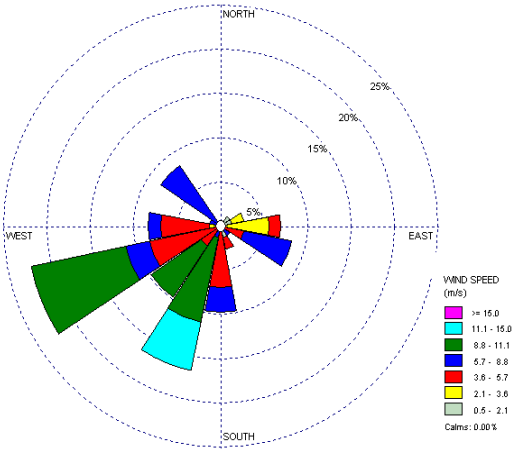

May 08-11

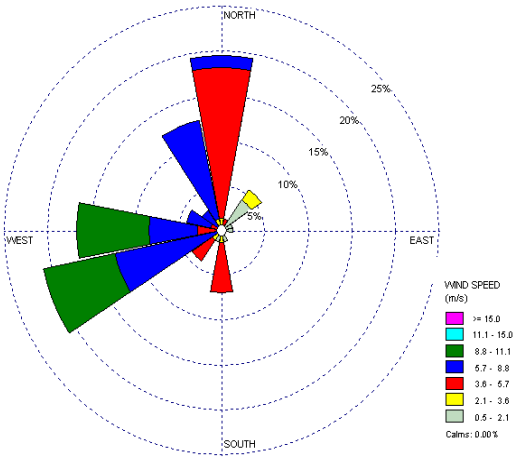

May 11-14

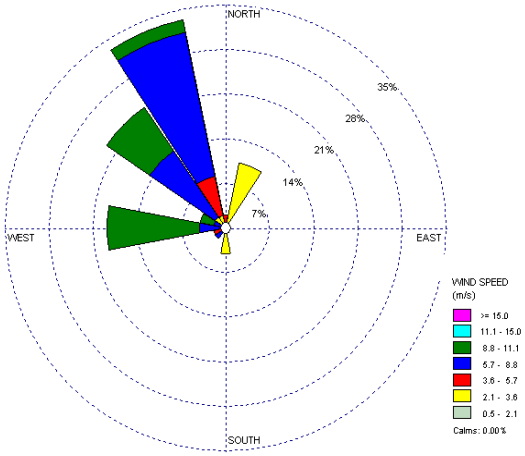

May 14-16

(a) Port Talbot

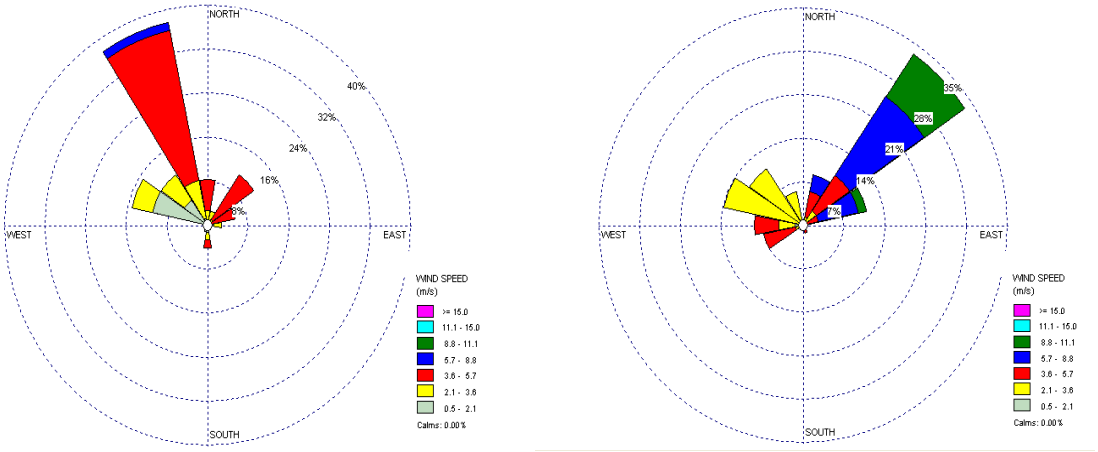

March 30-April 02 April 02-05

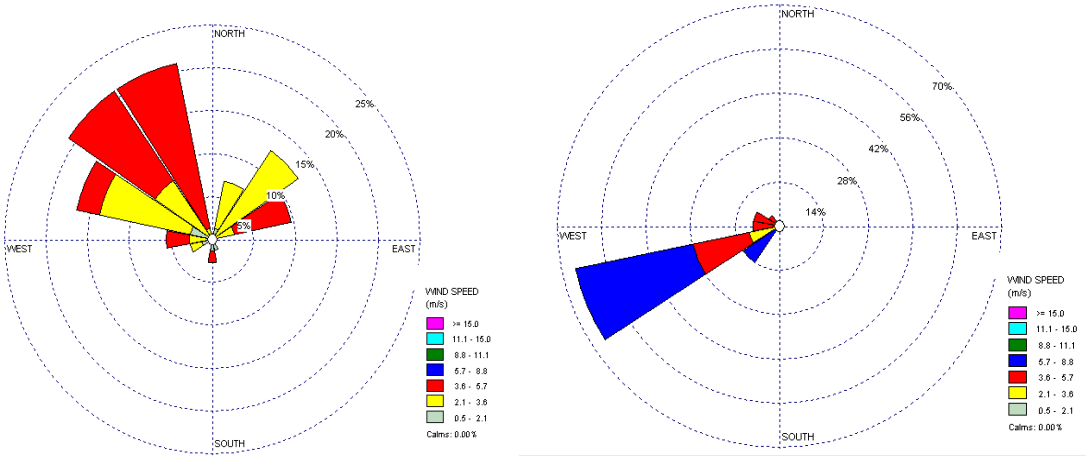

April 05-08 April 08-11

(b) EROS

Figure 4.7: Wind roses for the individual sampling periods (a) Port Talbot; (b) EROS

4.3.3.1.1 Port Talbot

The wind roses may be characterised as follows:

- April 17-20: Predominantly north-westerly with speeds of 5.7-8.8 m s^{-1}
- April 20-23: Predominantly westerly; speeds 5.7-11.1 m s^{-1}

- April 23-26: Predominantly a mix of south-westerly (5.7-11.1 m s^{-1}) and south-easterly (largely 5.7-15.0 m s^{-1})
- April 26-29: Predominantly north-easterly with strengths of 5.7-15 m s^{-1}
- April 29-May 2: From north-easterly to south-easterly; speeds ranging from 3.8-15 m s^{-1}
- May 2-5: Predominantly east-north-east; strength 3.8-8.8 m s^{-1}
- May 5-8: Covering a broad sector from east-north-east to west-south-west; speeds mostly in the range 3.6-11.1 m s^{-1}
- May 8-11: Predominantly in the sector between south and west with speeds of 3.6-16 m s^{-1} but minor contributions from other sectors
- May 11-14: Predominantly a mix of westerlies (5.7-11.1 m s^{-1}) and northerlies (3.6-8.8 m s^{-1})
- May 14-16: A predominance of west to north-north-west (5.7-11.1 m s^{-1})

The periods showing the greatest mass concentrations in the coarse fraction (Appendix IV) are April 23-26, May 8-11 and May 5-8. All of these show a significant component to the wind rose in the southerly to westerly sector consistent with atmospheric transport from the steelworks. These periods also correspond to a major elevation in the concentrations of iron and manganese (Appendix V). The period April 23-26 was also associated with high concentrations of zinc, barium, coarse vanadium, coarse calcium and coarse potassium, all of which have potential sources within the steelworks. The period with the highest concentrations of coarse sodium and chloride was April 20-23 consistent with strong winds in the westerly sector transporting marine aerosol. The period with the greatest association with the easterly wind sector were April 26-29, April 29-May 2 and

May 2-5. The latter period was associated with high concentrations of nitrate, sulphate and ammonium, the secondary constituents whose concentrations are typically elevated in easterly air masses in the UK. Also elevated in this sample were concentrations of calcium and chloride with a mode at around 3 μm consistent with that of nitrate. This would appear to be due to transport of crustal calcareous material from the land masses to the east of Port Talbot which had collected nitrate and chloride from the vapour phase during their transport. Concentrations of iron and manganese were very low in these easterly samples.

Coarse particle modes for barium, antimony and copper, all constituents associated with automotive brake wear, were notably elevated in the sample of April 17-20 consistent with a major automotive contribution on winds from the north-west. This sample was also elevated in fine potassium suggesting a possible wood burning source also within this sector.

4.3.3.1.2 EROS site

The predominant features of the wind roses displayed were as follows:

- March 30-April 2: Predominant concentrations were from the east-north-east (mainly 3.8-5.7 m s^{-1}) and north (3.8-8.8 m s^{-1})
- April 2-5: A major contribution from the north-east (3.8-11.1 m s^{-1}) but significant contributions from other compass points
- April 5-8: The vast majority of winds were in a sector between west-north-west and north-north-west with strength 2.1-5.7 m s^{-1}

- April 8-11: A single westerly sector predominated with speeds mostly in the range 3.6-8.8 m s^{-1}

The largest mass concentration in both the coarse and fine fractions was in the March 30-April 2nd sample (Appendix VI) which had the largest easterly wind component and intermediate windspeeds. The major ionic components exhibited their highest concentrations in this sample with ammonium and sulphate dominating the sub-micrometre fraction and chloride, nitrate and sodium, the coarse particle fraction. Concentrations of potassium, magnesium and calcium were also elevated in the coarse fraction in this sample. However, concentrations of the trace element constituents were in most cases relatively low in the sample of March 30-April 2 which is perhaps surprising given that the sample appears to contain a substantial continental component. The sample collected on April 5-8 stands out as having the highest concentrations of vanadium, manganese, copper, antimony and lead in the fine mode and of iron, manganese, barium and zinc in the coarse mode (Appendix VII). The wind directions associated with the sample were predominantly in the sector from north-west to north-east corresponding to the Birmingham city centre and these constituents appear to be associated largely with non-tailpipe emissions from road traffic. The sample collected on April 8-11 associated with a predominant westerly wind component showed the lowest concentrations of nitrate, sulphate, ammonium, potassium and calcium suggesting relatively clean marine air on this westerly sector, although concentrations of the marine indicator elements chloride and sodium were not particularly elevated. An interesting feature of the EROS dataset is that the ranking of concentrations between the samples for fine fraction potassium was the same as that for sulphate. Since the latter is well known as a pollutant subject to regional

transport, this suggests that fine potassium, whose main source is believed to be woodsmoke (Harrison *et al.*, 2012c), is also subject to long-range transport in a broadly similar manner. Other constituents which showed identical or similar rankings of concentration to one another (but not to sulphate and potassium) were vanadium, manganese, iron, antimony, barium and lead suggesting a common source for most elements, most probably in non-tailpipe emissions from road traffic.

4.3.4 Coarse particle increment at Port Talbot

The measured data are insufficient to conduct a mass closure on the aerosol composition, but it is nonetheless instructive to examine the differences in coarse particle mass and composition between PT and EROS (see Appendix II). The difference in coarse particle ($PM_{2.5-10}$) mass between the sites is 6.1 µg m^{-3}. Marine aerosol (taken as Na^{+}, Cl^{-} and Mg^{2+}) accounts for just 1.0 µg m^{-3} of this. Elements thought to be associated with steelworks (Fe and Ca^{2+}) together amount to 1.6 µg m^{-3}, which may approximately double to 3.2 µg m^{-3} when associated elements are added (e.g. Fe_2O_3 and $CaCO_3$). This suggests that under the conditions sampled, steelworks-related emissions account for at least half of the elevation in $PM_{2.5-10}$. The mass unaccounted for of *ca* 2 µg m^{-3} may be attributable to carbonaceous emissions, for example from the coke ovens, but data were not collected allowing this to be tested.

4.3.5 Analysis of particle size spectra collected with the Grimm Optical Spectrometer

The Grimm instrument has a response time of seconds, and in order to obtain statistically significant counts, the data were averaged over hourly periods and were then plotted as

polar plots as a function of wind direction and windspeed. The data are collected in 14 separate size bins and polar plots for each size bin appear in Figure 4.8.

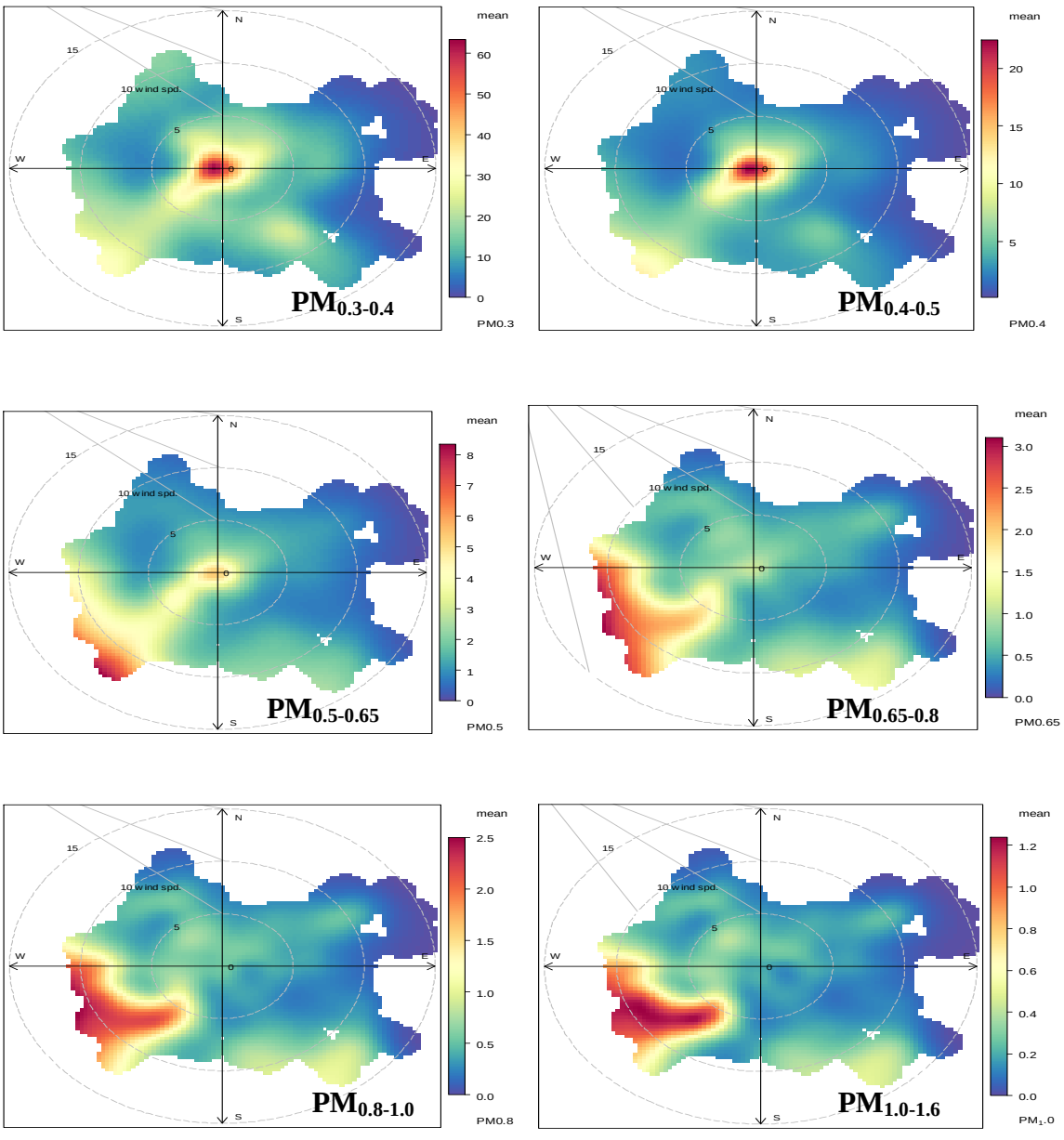

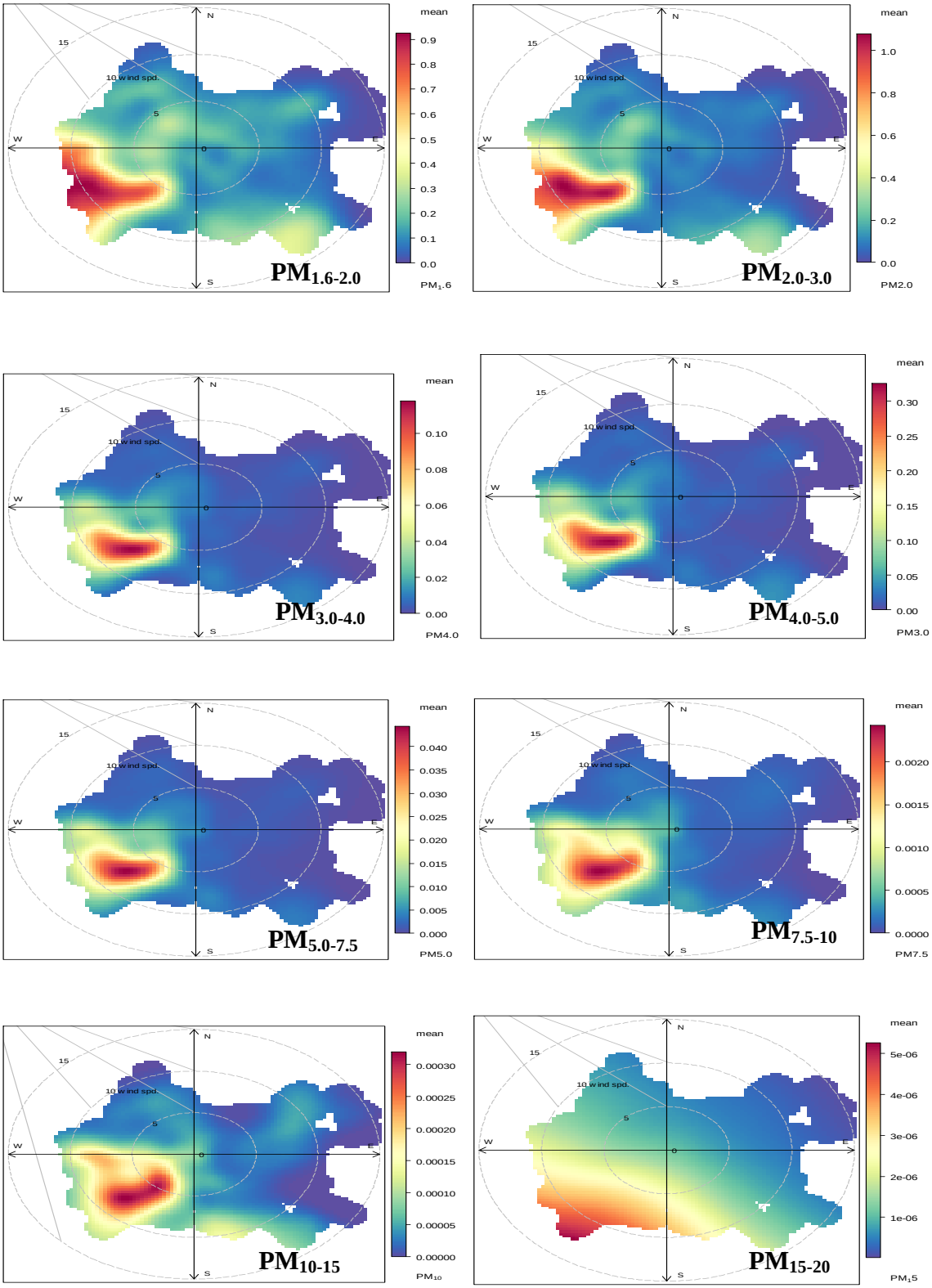

Figure 4.8: Polar plots of particle number concentrations from the Grimm analyser in 14 size bins as a function of wind direction and speed at Port Talbot

In the case of $PM_{0.4-0.5}$ (see Figure 4.8) the highest concentrations are associated with all wind sectors and very low windspeeds (the red area in the centre of the plot). This is indicative of a local ground-level source with maximum concentrations under low windspeed conditions. This was attributed to local road traffic. This behaviour is also seen for $PM_{0.3-0.4}$ and to a lesser extent for the $PM_{0.5-0.65}$ plot. For sizes between $PM_{0.5-0.65}$ and $PM_{5.0-7.5}$, the behaviour is very similar for each size fraction and is exemplified by the plot for $PM_{2.0-3.0}$ in Figure 4.8. This indicates a source area on a sector between 200º and 250º and intermediate windspeeds of 5-10 m s^{-1}, extending to the highest observed windspeeds of >10 m s^{-1} for particle sizes of $PM_{2.0-3.0}$ and below to $PM_{0.5-0.65}$. The association with the highest windspeeds becomes much less strong and the plot for $PM_{7.5-10}$ (Figure 4.8) shows a strong association with the intermediate windspeeds. The directional association of this peak clearly links it with sources within the steelworks and the association with intermediate windspeeds strongly suggests an elevated source. A ground-level emission source would most likely give peak concentrations at lower windspeeds (as for road traffic) and a resuspension source would be associated primarily with the highest windspeeds. Consequently, the data for particle sizes between the $PM_{0.5-0.65}$ and $PM_{2.0-3.0}$ plots appear to be a combination of both the elevated source and the ground-level resuspension source while the plots from $PM_{3.0-4.0}$ to PM_{10-15} are indicative of an influence predominantly from the elevated sources.

The plot for $PM_{7.5-10}$ gives a very clear indication of a predominant emission at intermediate windspeeds on the south-westerly sector (i.e. centred on 225º) which is the direction associated with the sinter plant and blast furnace within the steelworks. For the highest particle size bin (PM_{15-20}) the polar plot (Figure 4.8) has changed to one focussed

heavily on the strongest windspeeds and also covering a wider range of wind sectors strongly suggestive of a marine source (O'Dowd and Leeuw, 2007), possibly supplemented by resuspension from within the steelworks as indicated by the highest concentrations on the south-westerly sector.

It would be useful to look for associations between the modes in the MOUDI size distributions and the peaks in the polar plots for different particle sizes. This is, however, made difficult by the lack of a clear relationship between optical diameters measured by the Grimm spectrometer and aerodynamic diameters measured by the MOUDI. The elements showing far the greatest elevation at PT over EROS are Fe and Mn (Figure 4.6) with a mode at around 5 µm, extending from *ca* 2-10 µm aerodynamic diameter. This appears to be associated with the major peak in the polar plots at around 225º appearing for particles in size ranges from 0.3-3.0 µm to 10-15 µm (Figure 4.8). The two datasets therefore appear broadly consistent.

4.4 Conclusions

This study has revealed distribution patterns of size-segregated particles at a typical urban background (EROS) and an industrial setting (Port Talbot). Individual sample and average MOUDI data presented were diverse and varied between the two sites. EROS was dominated by fine particles while PT showed an elevated coarse particle concentration reflected in a higher ratio of $PM_{2.5}/PM_{10}$ obtained at EROS. The influence of secondary aerosol was more evident at the urban background than the industrial site. Port Talbot showed elevated concentrations of marine (Na^+, Mg^{2+} and Cl^-) and steelworks emissions (Fe, Mn and Ca^{2+}). Higher concentrations of trace metals such as V, Al and Pb were

observed at EROS. Strong similarities in mass size distributions were observed between Mn and Fe at PT (this was not so at EROS) suggesting a common emission source from the steel industry. Trace metals associated with brake wear (Cu, Sb, Ba) were clearly observed at both sites.

The analysis of size distributions from individual 72-hour sampling intervals confirmed the inferences derived from the average data, but allowed some appreciation of the episodicity of contributions both from the steelworks and secondary particles. Both showed the expected associations with, in the former case local winds from the direction of the steelworks, and easterly sector winds associated with regional transport in the latter. Although containing no chemical information, the polar plots of particle number size spectra revealed much source-related information. Local emissions, probably from road traffic dominated the smaller size bins (0.3-0.5 μm), while steelworks emissions dominated the range 0.5-15 μm, and for particles > 15 μm marine aerosol appeared dominant. Although there appeared to be contributions from more than a single source within the steelworks, the wind direction-dependence suggested the sinter plant and/or blast furnaces as the major contributor.

CHAPTER 5 - PORT TALBOT PARTICULATE AND GASEOUS POLLUTANT CONCENTRATIONS

5.1 Abstract

This chapter gives an overview of the PM mass concentration data collected at Port Talbot with different measuring instruments. Sample collections were achieved using Partisol Dichotomous, Filter Dynamic Measurement System (FDMS) and Grimm optical particle counter. Black carbon (BC) and gaseous pollutants were also measured. Time series and polar plots of gaseous and particulate constituents are shown in this section. FDMS and Partisol instruments at the Fire Station (FS) site have depicted similar days of PM_{10} episodes where the World Health Organization (WHO) limit of 24-hour mean value of 50 μg m^{-3} was exceeded. The Partisol $PM_{2.5}/PM_{10}$ ratios revealed elevated coarse particle concentrations while the FDMS $PM_{2.5}/PM_{10}$ ratios showed domination by $PM_{2.5}$ particles. The lack of agreement between the FDMS and Partisol instruments on $PM_{2.5}/PM_{10}$ ratios can be explained by greater losses of semi-volatiles in Partisol $PM_{2.5}$ than FDMS. This study has also established a good correlation between data from FDMS, Partisol, Grimm and MOUDI measuring instruments. The polar plots of PM_{10} (at FS, Prince Street (PS), Dyffryn School (DS) and Little Warren (LW)), $PM_{2.5}$ (FS and PS), NO, NO_2, NO_x, SO_2, CO and BC (FS) provide the directional emission patterns of particulate and gaseous pollutants indicating the steelworks as the major emission source.

5.2 Introduction

In 2001, the Neath Port Talbot County Borough Council (NPTCBC) who has been monitoring the exceedances of PM_{10} around the steel complex activities since 1997, declared the steel industry as the major source of PM_{10} in Port Talbot. Additionally, Air Quality Expert Group, AQEG (2011) has reported some years at Port Talbot when the daily PM_{10} average has exceeded 50 µg m^{-3} in 24 hours for more than 35 days per year. This is a breach of national air quality objective as well as WHO/EU limits for air quality standard. In the recent years however, the number of exceedances has reduced probably due to series of regulations put in place and constant monitoring by the concerned Environmental Authorities.

Undoutedbly, the steel complex activities remain the major contributor to the PM_{10} concentration in Port Talbot. The work done by Hayes and Chatterton (2009) has compared the PM_{10} collected in Port Talbot with that collected in Swansea and Narbeth. Elevated values were recorded in Port Talbot with PM_{10} mass concentration 20 µg m^{-3} higher than the neighboring rural background. The conclusion of the study was that the various industrial activities taking place at the steel complex in Port Talbot remained the leading emission source. Nevertheless, the principal contributor to PM from the steel industry is yet to be ascertained (AQEG, 2011), since many individual processes are engaged in the industrial complex.

This section will highlight the relationship between the gaseous and particulate data collected during the sampling campaign at Port Talbot.

5.3 Materials and Methods

5.3.1 Particulate matter sampling

Daily particle sampling was carried out with Partisol-Plus dichotomous sequential sampler (Model 2025) between April 17 and May 16, 2012 (12 pm to 12 pm). Four Partisol samplers were deployed to the four selected sites which were Fire Station (FS), Prince Street (PS), Dyffryn School (DS) and Little Warren (LW).

Hourly PM sampling was done with the Streaker samplers positioned at two monitoring sites (FS and LW) for upwind and downwind measurements. See details of the Streaker's instrumentation in chapter 2.

Filter Dynamic Measurement System (FDMS) mass concentration data ($PM_{2.5}$ and PM_{10}) for FS site were obtained from the data archive of the Department for Environment, Food and Rural Affairs (DEFRA) (available at http://uk-air.defra.gov.uk/networks/aurn-site-info). At the PS, DS and LW monitoring sites, FDMS PM_{10} data were downloaded from the Welsh Air Quality website (http://www.welshairquality.co.uk/data_and_ statistics.php?).

5.3.2 Sample digestion and analysis

The procedures for sample digestion and analysis of Partisol samples have been discussed in chapter 2. The Streaker samples were sent to the University of Milan, Italy for Particle Induced X-ray Emission (PIXE) analysis discussed explicitly in chapter 2.

5.3.3 Gaseous Pollutants

Gaseous pollutant data at the Fire Station monitoring site were also obtained at the AURN site (http://uk-air.defra.gov.uk/networks/aurn-site-info).

5.4 Results and Discussion

5.4.1 FDMS versus Partisol PM mass concentration data

Figure 5.1 shows the time series plot of daily PM mass data collected at the four sampling sites for both FDMS and Partisol instruments. Both the Partisol and FDMS PM_{10} data have shown similar variations in trend and pattern at all the monitoring sites. There seems to be small difference in the daily PM_{10} mass concentrations from the two PM measuring instruments. However, FDMS $PM_{2.5}$ values were higher than Partisol $PM_{2.5}$ daily concentrations.

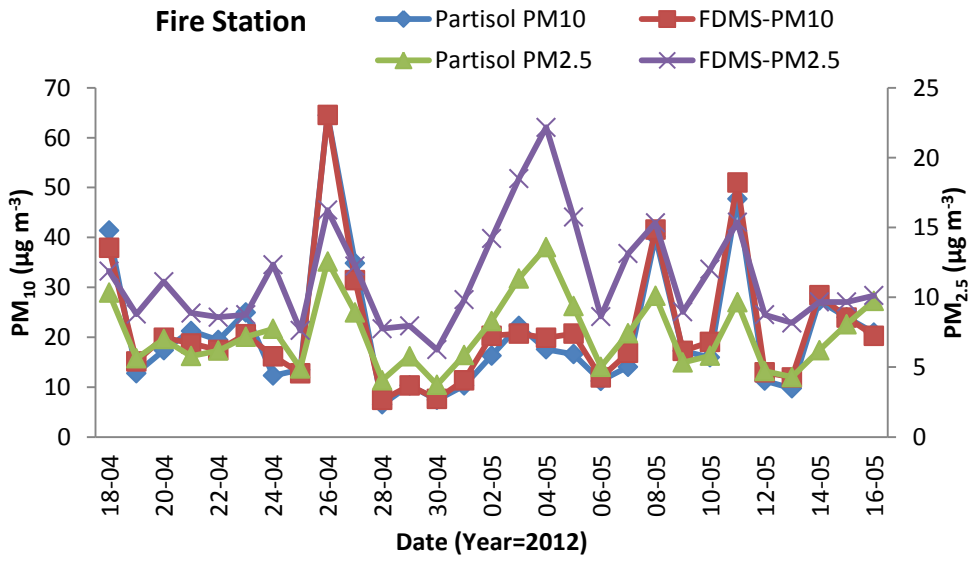

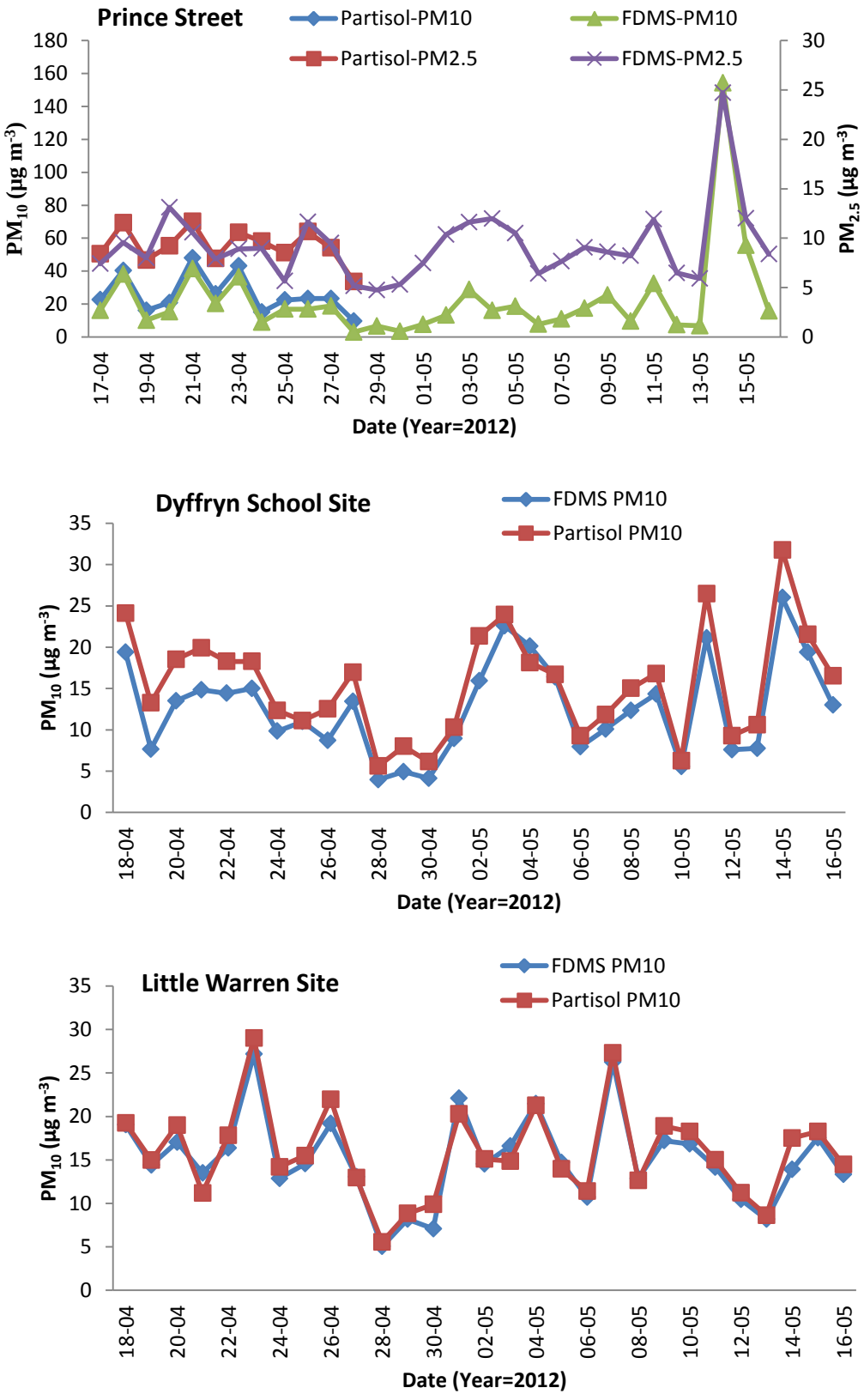

Figure 5.1: Daily plots of Partisol and FDMS PM_{10} and $PM_{2.5}$ at the four sampling stations

FDMS and Partisol instruments at FS have observed a common day of PM_{10} episode where the threshold of daily average value of 50 µg m^{-3} (WHO, 2006) was exceeded on April 26 (64.5 µg m^{-3} for both Partisol and FDMS). The activities of the steel industry may have contributed to the elevated PM_{10} mass concentration experienced on this day. Furthermore, FDMS data also demonstrated a PM_{10} exceedance on May 11 (51.0 µg m^{-3}). Some episodic days where PM_{10} concentrations were greater than 40 µg m^{-3} included May 8 for both Partisol and FDMS; and April 18 for Partisol only. $PM_{2.5}$ data have shown similar daily trends as observed for PM_{10} in Partisol and FDMS at FS monitoring site. The mean 24-hour threshold of 25 µg m^{-3} set for $PM_{2.5}$ (WHO, 2006) was not exceeded by either FDMS or Partisol PM throughout the sampling period.

At PS, there was a good agreement between FDMS and Partisol PM mass concentrations daily variations. Partisol measurement was discontinued on April 29 due to a faulty instrument. This made it difficult to compare the FDMS and Partisol data throughout the whole campaign. Nevertheless, during the period of active sampling, Partisol $PM_{2.5}$ and PM_{10} concentrations were slightly higher than FDMS PM. An extremely high value of FDMS PM_{10} (154.2 µg m^{-3}) with elevated FDMS $PM_{2.5}$ (24.7 µg m^{-3}) was observed on May 14. These FDMS PM values were the highest observed concentrations at all the sites during the whole campaign. The reason for this extreme PM_{10} value was unclear because on May 14, none of the remaining sampling sites measured PM_{10} concentrations > 35 µg m^{-3} by either of FDMS or Partisol sampler. It was unfortunate that there was no Partisol PM mass concentration on this day at PS to compare with the elevated FDMS PM_{10} concentration. By subtracting FDMS $PM_{2.5}$ from PM_{10}, it was clear that coarse PM formed the major constituent of PM_{10} on this episodic day representing 84% of the measured

PM_{10}. The coarse PM value calculated as 129.5 µg m^{-3}; the value was greater than the combined sum of all Partisol PM_{10} samples at FS, DS and LW stations on this episodic day.

At the DS and LW sites, there was no PM_{10} exceedance observed for FDMS and Partisol mass data on this day. Partisol PM_{10} was slightly higher than that of FDMS at DS while no significant temporal variations were observed for the two measuring instruments at LW.

5.4.2 Inter-comparison between FDMS and Partisol PM at the monitoring sites

FDMS and Partisol daily PM variations at FS, PS, DS and LW monitoring sites are shown in Figure 5.2. FDMS PM_{10} concentrations were generally high at Fire Station and Prince Street locations. Lowest concentrations of PM_{10} were recorded at DS and LW. A relatively higher Partisol $PM_{2.5}$ has been measured at FS monitoring station than PS site in contrast to FDMS measurement.

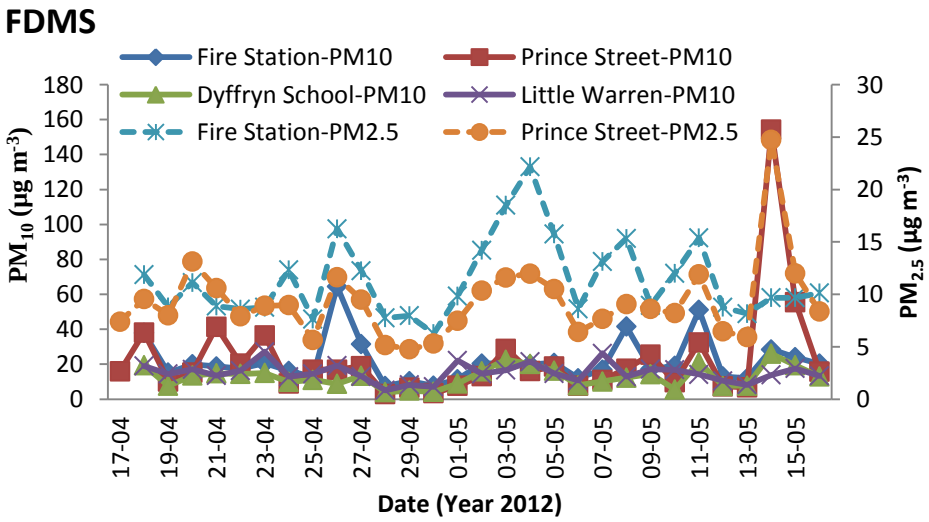

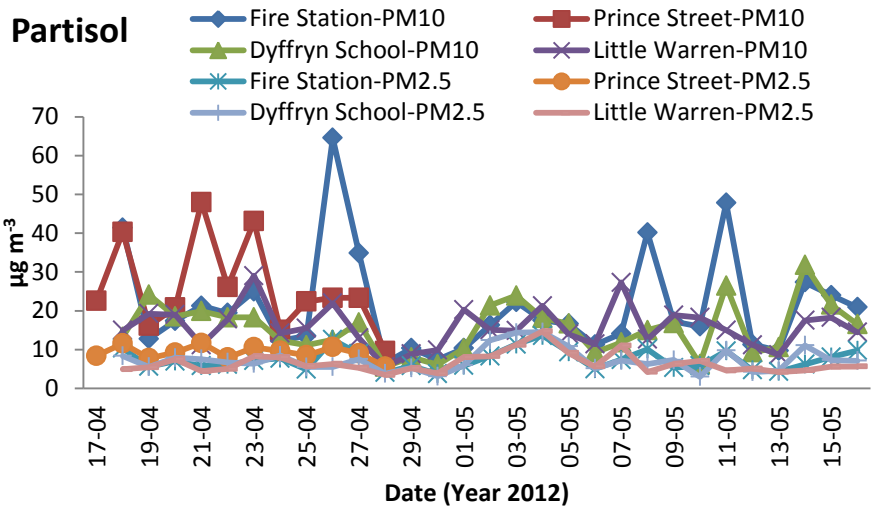

Figure 5.2: Time series plot comparing FDMS and Partisol PM all the monitoring site

The summary of FDMS and Partisol PM data are displayed in Table 5.1. At FS site, FDMS and Partisol mean concentrations were 21.7±12.9 and 21.0±13.3 µg m^{-3} for PM_{10} and 11.3±3.7 and 7.4±2.6 µg m^{-3} for $PM_{2.5}$ respectively. Highest average PM_{10} values were measured at PS for FDMS (22.7±27.7 µg m^{-3}) and Partisol (25.9±11.8 µg m^{-3}) relative to the other sites. PM_{10} mass concentrations at DS and LW were 12.8±5.8 and 15.1±5.1 µg m^{-3} for FDMS and 15.6±6.47 and 15.8±5.26 µg m^{-3} for Partisol, respectively. The lowest mean FDMS and Partisol PM_{10} value was recorded at DS against the LW site, which has been used as background site. For $PM_{2.5}$, there were no available data for FDMS PM at these two stations, while a slightly higher mean Partisol value was observed at DS than LW site. It is therefore apparent that the LW station was much influenced by coarse PM; this could have been responsible for its higher PM_{10} mean concentration compared to DS. LW is the nearest site to the Swansea Bay, therefore the impact of sea spray is likely to be more pronounced at this site than anthropogenic activities of the steel industry. Studies at the coastal sites have been reported to raise PM pollution due to sea salt aerosol (Pryor *et al.*, 2007; Athanasopoulou *et al.*, 2008).

Table 5.1: Summary of mean concentrations of FDMS and Partisol PM_{10}

Monitoring Sites	FDMS (µg m^{-3})		Partisol (µg m^{-3})	
	PM_{10}	$PM_{2.5}$	PM_{10}	$PM_{2.5}$
FS	21.7±12.9	11.3±3.7	21.0±13.3	7.4±2.6
PS	22.7±27.7	9.3 ±3.7	25.9±11.8	9.2±1.7
DS	12.8±5.8	-	15.6±6.5	7.3±3.0
LW	15.1±5.1	-	15.8±5.3	6.5±2.5

Note: FS- Fire Station, PS-Prince Street, DS-Dyffryn School, LW-Little Warren

The combined mean value of FDMS PM_{10} and $PM_{2.5}$ at all the sampling sites during the one-month sampling campaign in Port Talbot were 18.1±4.9 and 10.3±0.01 µg m^{-3} respectively. Fine PM formed a total 57% of PM_{10} while coarse PM fraction represented the remaining 43%. The pool mean of Partisol PM_{10} and $PM_{2.5}$ were 19.6±4.9 and 7.6±1.1 µg m^{-3} (39% $PM_{2.5}$ and 61 % $PM_{2.5-10}$).

Reduced major analysis (RMA) regression model (see Appendix VIII) showed strong relationships for PM data measured with FDMS and Partisol instruments at the four sites. FDMS and Partisol PM_{10} have shown exceptionally better correlation (r^2=0.92-0.99) with slope near unity than with $PM_{2.5}$ (r^2=0.79 at FS and 0.44 at PS, slope=0.62 and 0.76, respectively). The observations of Green (2004) with FDMS and Partisol PM_{10} data at Marylebone Road and North Kensington in London showed slopes of 0.80 and 0.93, with r^2 equal to 0.92.

FDMS and Partisol PM average concentration plots of the days of the week showed greatest peaks on Thursday and Friday while least peaks were observed on Sunday (see Appendix IX). Elevated PM values during the weekdays can be attributed to pronounced anthropogenic activities from industrial sources, traffic and railway.

5.4.3 $PM_{2.5}$ to PM_{10} ratios

Figure 5.3 represents the $PM_{2.5}$ to PM_{10} ratios calculated for FDMS and Partisol PM at the four air sampling sites. FDMS $PM_{2.5}/PM_{10}$ ratio showed higher value at PS than FS. High $PM_{2.5}/PM_{10}$ ratio is a confirmation of the domination by $PM_{2.5}$ particles. Owing to non-availability of FDMS $PM_{2.5}$ data at DS and LW, $PM_{2.5}/PM_{10}$ ratios at these sites could not be determined. Partisol $PM_{2.5}/PM_{10}$ ratios revealed contrary results showing the domination by $PM_{2.5-10}$ particles. Discrepancies between the FDMS and Partisol instruments on $PM_{2.5}/PM_{10}$ ratios at FS and PS can be explained by greater losses of semi-volatiles in Partisol $PM_{2.5}$ than FDMS (Charron and Harisson, 2005). The RMA equations between $PM_{2.5}$, $PM_{2.5-10}$ and PM_{10} also revealed coarse PM (Appendix X) as the major contributor to PM_{10} concentrations in Port Talbot.

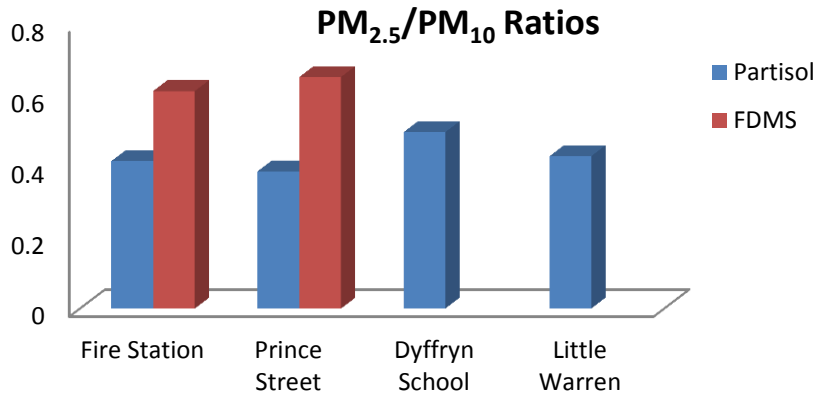

Figure 5.3: $PM_{2.5}/PM_{10}$ ratio for FDMS and Partisol in all the monitoring sites

5.4.4 Gaseous pollutant concentrations at FS site during Port Talbot campaign

Daily variations in gaseous pollutants are plotted in Figure 5.4. The average concentrations of gaseous pollutants during the one-month monitoring were NO_x (20.2±8.6 µg m^{-3}), O_3 (68.6±13.1 µg m^{-3}), SO_2 (4.6±5.6 µg m^{-3}) and CO (0.3±0.2 mg m^{-3}).

These gaseous concentrations were all within the standard limits set for them (WHO, 2006). The highest concentration of O_3 (90.4 µg m^{-3}) was observed on May 14 while the lowest value (30.3 µg m^{-3}) occurred on May 4. NO_x, NO_2 and NO have all peaked at the dates where the lowest O_3 concentration was measured. SO_2 has displayed a related pattern in variations with NO_x, NO_2 and NO with notable peaks on April 26 and May 8. Related elevated pollution peaks also occurred for CO on April 26 and May 8. The days of elevated concentrations observed for these gaseous pollutants coincided with PM_{10} pollution episodes measured at the FS site. $PM_{2.5}$ also showed the highest concentrations on these three days. It is possible that this is due to a common emission source from a distinctive process probably from the steelworks.

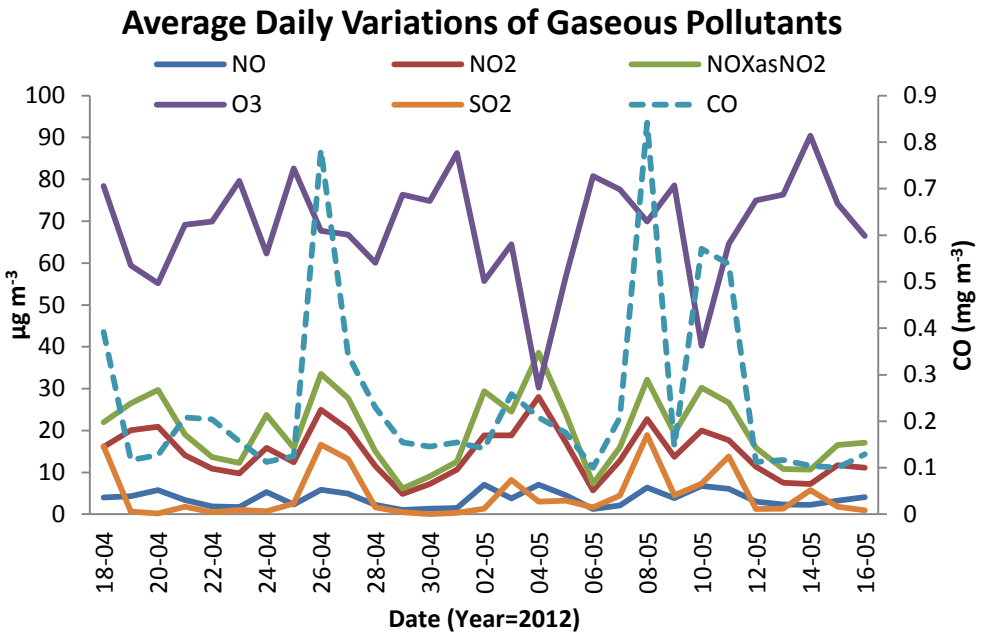

Figure 5.4: Daily variations of gaseous pollutants during the sampling at Port Talbot

The source strengths of gaseous pollutants could be determined to ascertain their specific emission source. The use of CO/NO_x and SO_2/NO_x ratios are important to identify mobile

and stationary sources (Aneja *et al.*, 2001). High CO/NO_x and low SO_2/NO_x ratios indicates mobile source while low CO/NO_x and high SO_2/NO_x could be linked to a point emission source. CO/NO_x ratio during the whole campaign has a range of 4.3 to 26.2 while SO_2/NO_x ratio varied from 0.01 to 0.47. The average ratios of CO/NO_x and SO_2/NO_x during the whole campaign were 12.1±6.3 and 0.21±0.21, suggesting that the impact of mobile source (especially from gasoline vehicles) appeared to be more important than point source. But, on the days where PM_{10} episodes were observed (April 26 and May 11), CO/NO_x ratios were 23.4 and 20.2, while SO_2/NO_x ratios were 0.50 and 0.52. This indicates that the impact of stationary source (steelworks emissions) was significant on these days. Aneja *et al.* (2001) has assigned SO_2/NO_x ratio of 0.6 to point source emission.

5.4.5 Relationships between FDMS and Partisol PM versus gaseous pollutants

As part of efforts to identify the possible emission sources of PM in Port Talbot, a linear relationship between FDMS and Partisol $PM_{2.5-10}$ and $PM_{2.5}$ against the gaseous pollutants has been examined (Appendix XI). Gaseous data are only available at the FS site. A better relationship was observed between FDMS/Partisol $PM_{2.5-10}$ and SO_2 (r^2=0.67 for FDMS and 0.73 for Partisol) than with NO_x (r^2=0.13 for FDMS and 0.15 for Partisol). However with $PM_{2.5}$, a well-defined positive correlation was established between FDMS/Partisol $PM_{2.5}$ and NO_x (r^2=0.60 and 0.49). It could be inferred that stationary emissions, probably from the steelworks, might influence coarse particle concentration while mobile emissions from traffic increased fine particle loads during the study.

FDMS $PM_{2.5}$ and $PM_{2.5-10}$ have moderately correlated with CO (r^2=0.38 and 0.28, respectively). The corresponding values of these coefficients for Partisol $PM_{2.5}$ and $PM_{2.5-10}$ are 0.28 and 0.27, respectively.

5.4.6 Meteorological conditions during the sampling campaign

Hourly variations of meteorological data at Port Talbot between April 18 and May 16 are shown in Figure 5.5a. PM_{10} episodes on April 26 and May 11 occurred when the windspeed >8 m s^{-1} and temperature > 8^{o}C. These conditions may be favourable to dust re-suspension leading to high concentrations of the coarse portion at the receptor site. Diurnal windspeed and temperature diagram (Figure 5.5b) showed similar trends with significant peaks observed between 10 am and 7 pm. This might be related to the active period of the steelworks activities, traffic and sea salt emissions. The windrose plots of April 26, May 8 and 11 when PM_{10} episodes were observed are shown in Figure 5.6 (a-c). The domination of south-easterly and mild north-westerly and north-easterly winds was observed. The prevailing south-westerly revealed the steel complex to be the main contributor to local emission source during these pollution events.

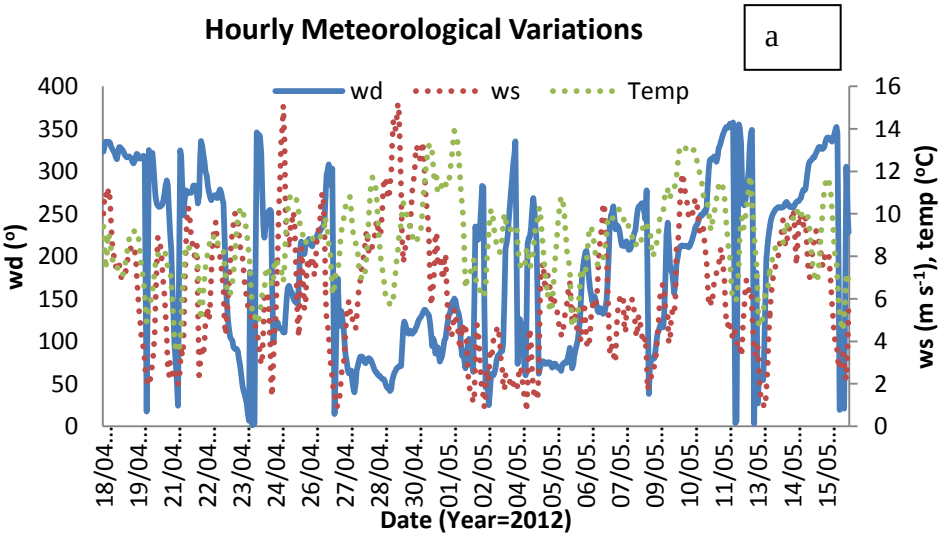

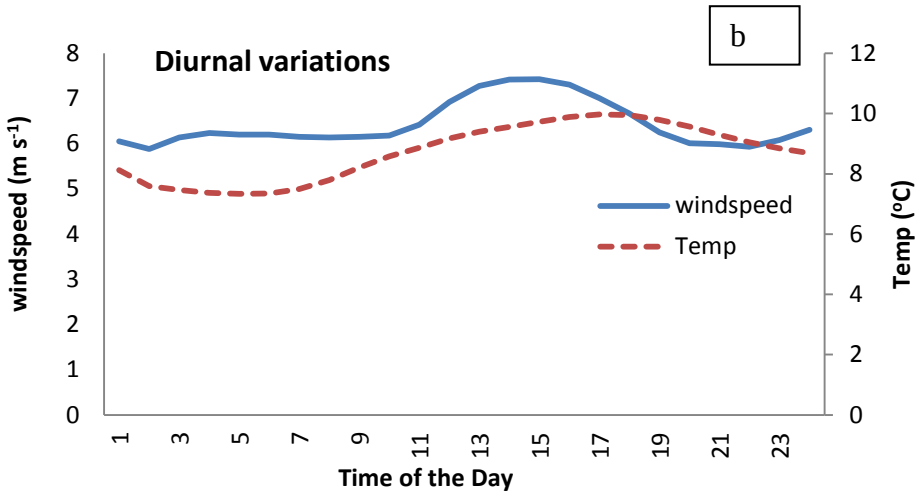

Figure 5.5: Meteorological data variations at Port Talbot during the monitoring period

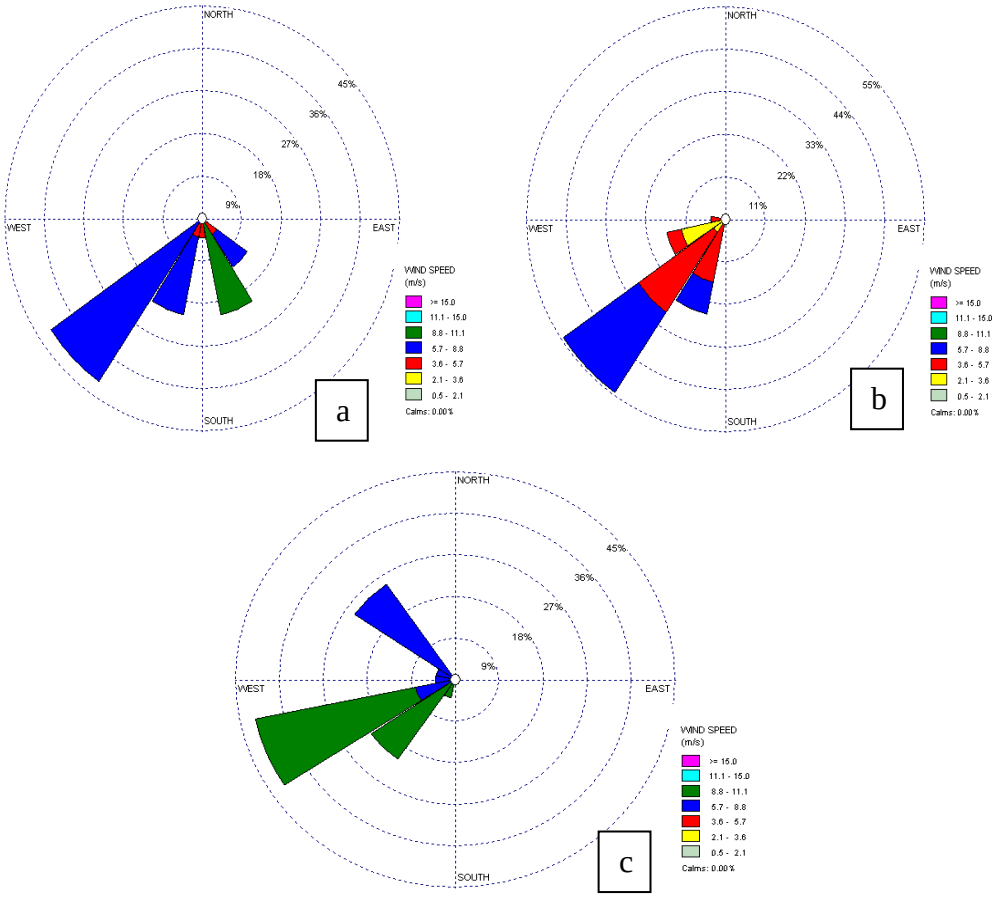

Figure 5.6: Windrose plots at Port Talbot during the PM_{10} pollution episodes on (a) April 26 (b) May 8 and (c) May 11

5.4.7 Black carbon concentrations during the campaign

Black Carbon (BC) daily concentration was presented in Figure 5.7a. On the average, BC concentration was 0.52±0.26 µg m^{-3}. The contribution of BC to PM episode of April 26 was significant while the highest elevated BC concentration was also observed on May 3. BC is usually emitted from industry, transport and residential sources (Qin and Xie, 2012; Zhang *et al.*, 2013). Since CO is also a product of incomplete combustion like BC, the relationship between BC and CO is important to identify their likely emission sources. A strong relationship has been established between BC and CO by Pan *et al.* (2011) with r^2>0.8. BC is poorly correlated with CO (r^2=0.13) in this study, but was well correlated with NO_x (r^2=0.59). BC also exhibited good correlation with $PM_{2.5}$ (r^2=0.62). These results suggest more of vehicular than industrial emissions. Diurnal variation of BC showed highest peak between 7-8 am (Figure 5.7b), which demonstrates the influence from traffic.

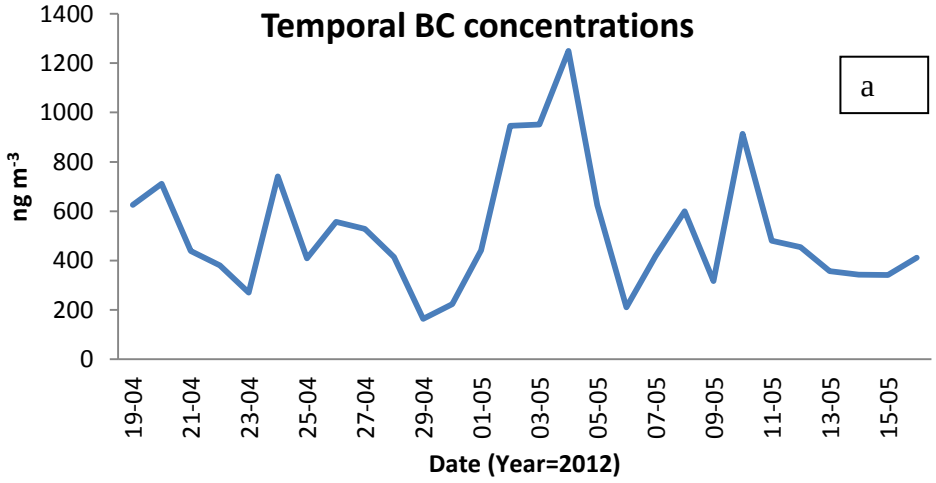

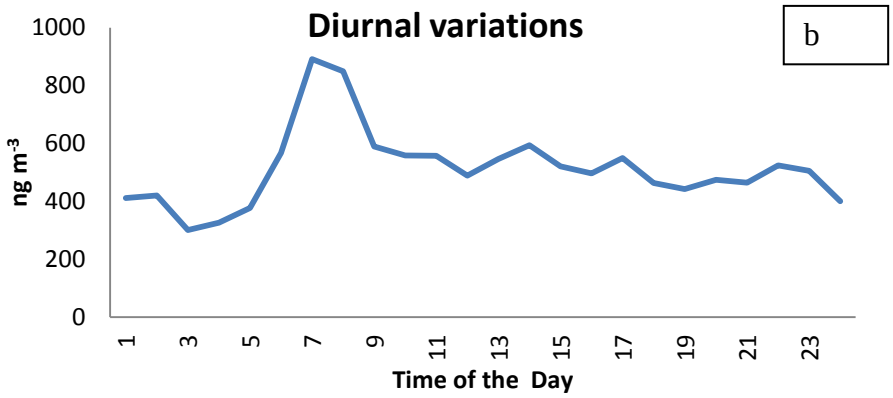

Figure 5.7: Daily and diurnal concentrations of Black Carbon

5.4.8 Polar plots of particulate and gaseous pollutants

The polar plots (Figure 5.8) of PM_{10} (at FS, PS, DS and LW), $PM_{2.5}$ (FS and PS), NO, NO_2, NO_x, SO_2, CO, O_3 and BC (FS) provide the directional emission patterns of particulate and gaseous pollutants during the sampling. Most of the air pollution parameters were concentrated towards the south-western region from the FS site where the steelworks complex is located. PM_{10} at the monitoring sites also showed a directional higher concentration towards the steelworks complex with additional significant contribution from marine aerosol. Ozone exhibited multi-dimensional higher concentrations explaining sources beyond the local impacts only. The impact of the industry could be indicated on PM_{10}, CO and SO_2 than the rest of the air pollutants. Other air pollutants might be more affected by regional long- range transport. NO, NO_2, NO_x and black carbon polar plots showed dual emission sources from both the local traffic and the steelworks. The polar plots have also revealed higher concentrations of most of these air pollutants at higher windspeed except PM_{10} at PS. However, BC and NO_x demonstrated elevated concentrations at low windspeed.

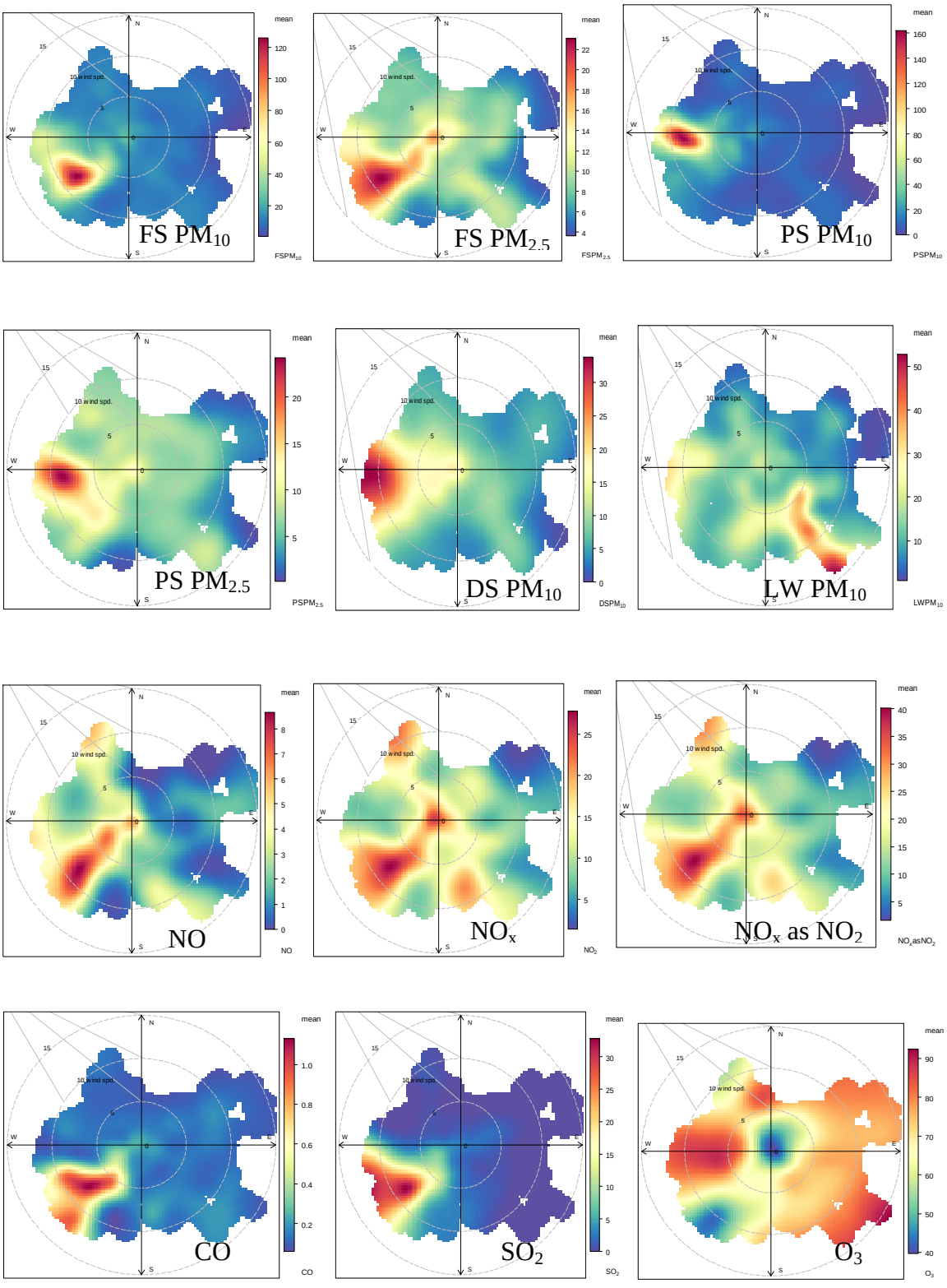
FS PM10
FS PM2.5
PS PM10
PS PM2.5
DS PM10
LW PM10
NO
NOx
NOx as NO2
CO
SO2
O3
10 w ind spd.
mean

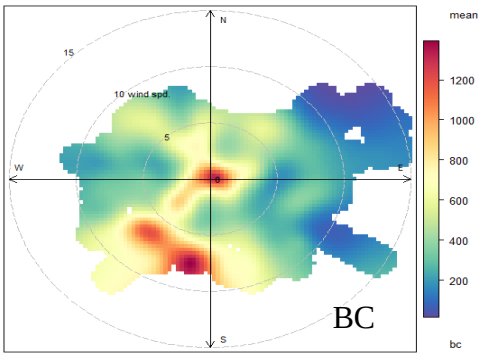

Figure 5.8: Polar Plots of air pollutants during Port Talbot campaign

5.4.9 Grimm vs. Partisol, FDMS and MOUDI mass concentrations

The polar plot data of Grimm particle number counts have been discussed in chapter 4. To compare the Grimm PM mass data with the other mass measuring instruments, particle number concentration (PNC) was converted to mass. Grimm fine ($PM_{2.0}$) and coarse ($PM_{2.0-10}$) mass concentrations were calculated from the volume distribution of Grimm particles. The mass concentration was calculated by multiplying the volume concentration with particle density which was assumed to be 1.7 g cm^{-3} (Pitz *et al.*, 2003). Results were plotted against daily FDMS, Partisol and MOUDI $PM_{2.5}$ and $PM_{2.5-10}$ mass concentrations (Figure 5.9). The time series plots of the four mass measuring instruments were consistent in patterns and variations for fine and coarse mass concentrations.

Reduced major axis (RMA) correlations of Grimm-calculated PM for fine and coarse fractions versus corresponding FDMS, Partisol and MOUDI PM data are outlined in Appendix XII. Grimm PM correlated well with all the PM mass-measuring devices with r^2 ranging between 0.49-0.91 for fine and 0.67 to 0.82 for coarse PM. The relationship was best defined between Grimm and FDMS and least defined with MOUDI.

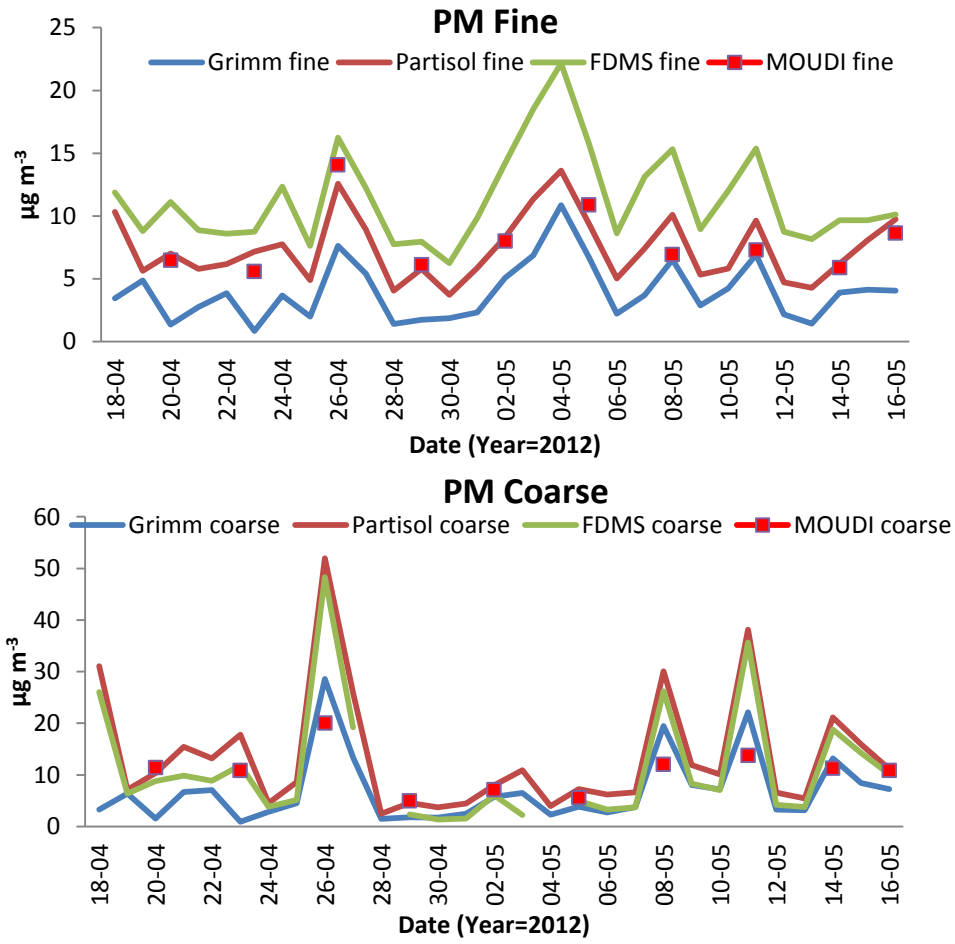

Figure 5.9: Temporal variations between Grimm, FDMS, Partisol and MOUDI PM size distribution

5.4.10 Diurnal variations of PM, PNC and gaseous pollutants

Diurnal variations of PM, PNC and gaseous pollutants are shown in Figure 5.10. Similar diurnal patterns were displayed by PM_{10} at FS and PS with common elevated peaks at 16 pm. A previous investigation by AQEG (2011) has also observed the highest peak of PS PM_{10} at 16 pm. At FS and PS, $PM_{2.5}$ showed a slight rise between 7 and 9 am. At DS and

LW, the diurnal patterns of PM_{10} showed no significant variations. Diurnal concentrations of $PM_{2.5}$ and PM_{10} suggested that they were linked with traffic and the steel industry. Pollution peaks of PM_{10} at 4 pm in Port Talbot (FS and PS) might be related to fugitive dust from the steelworks and road re-suspension favoured by high windspeed (Charron and Harrison, 2005). Particle number concentrations showed significant peaks for particles between diameter 0.3-0.65 μm at 7 am and 16 pm similar to peaks shown by mass concentrations of $PM_{2.5}$ and further re-affirming possible impact from rush hour traffic. For coarser particles greater than 2.0 μm, notable peaks were observed at 2 am, 14 and 19 pm indicating possible contributions by the steel industry or marine source.

A unimodal diurnal peak displayed by NO, NO_2, NO_x and SO_2 between 7 and 8 am might largely be due to high volume traffic and poor dispersion at this period (Bigi and Harrison, 2010). Ozone has shown only one peak extending between 7 am and 21 pm due to photochemical activity. The effect of NO titration on O_3 was observed between 7 and 8 am during the morning rush hour. Diurnal pattern of CO concentrations exhibited two notable peaks at 7 am and 12-19 pm probably due to both traffic and industrial emissions.

The diurnal variations of particle number concentration (Figure 5.10) showed significant peaks at 7 am and 16 pm which could be linked to morning and evening rush hour traffic, and also from the steelworks. The 7 am peak shown in this study was consistent with the study of Harrison and Jones (2005) who have used Condensation Particle Counter (CPC) instrument for their particle measurements. There were peaks also displayed by the particles at 2 am, 12, 1-2 pm and 8 pm.

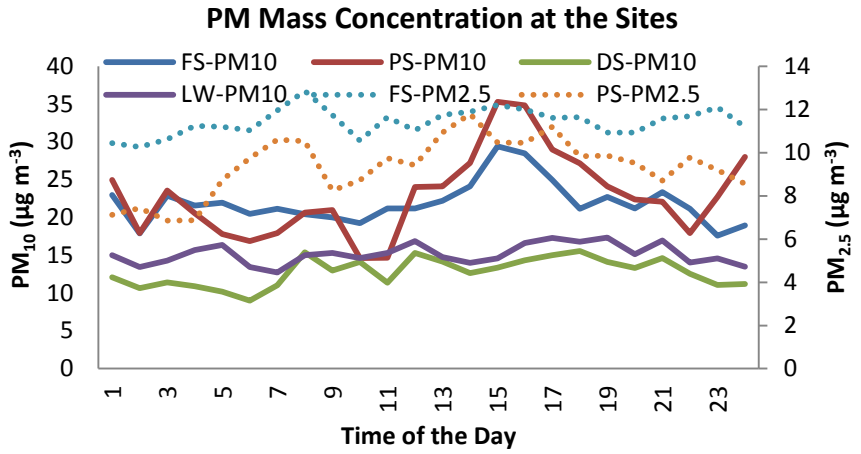
PM Mass Concentration at the Sites
FS-PM10
PS-PM10
DS-PM10
LW-PM10
FS-PM2.5
PS-PM2.5
PM10 (µg m-3)
PM2.5 (µg m-3)
Time of the Day

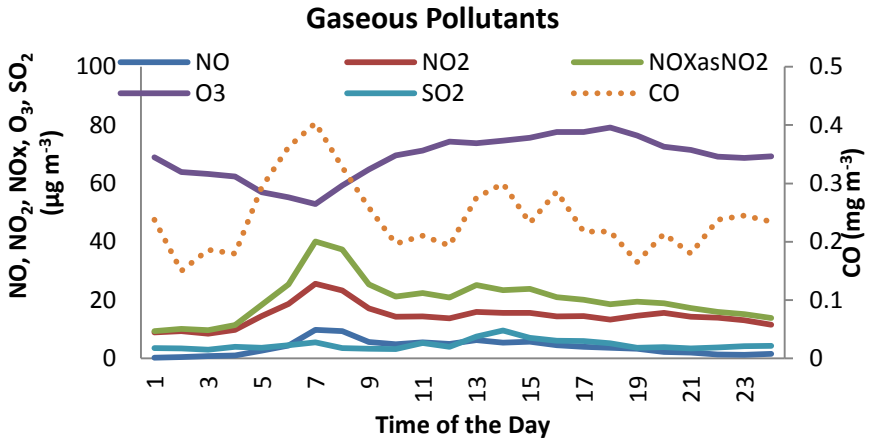
Gaseous Pollutants
NO
NO2
NOXasNO2
O3
SO2
CO
NO, NO2, NOx, O3, SO2 (µg m-3)
CO (mg m-3)
Time of the Day

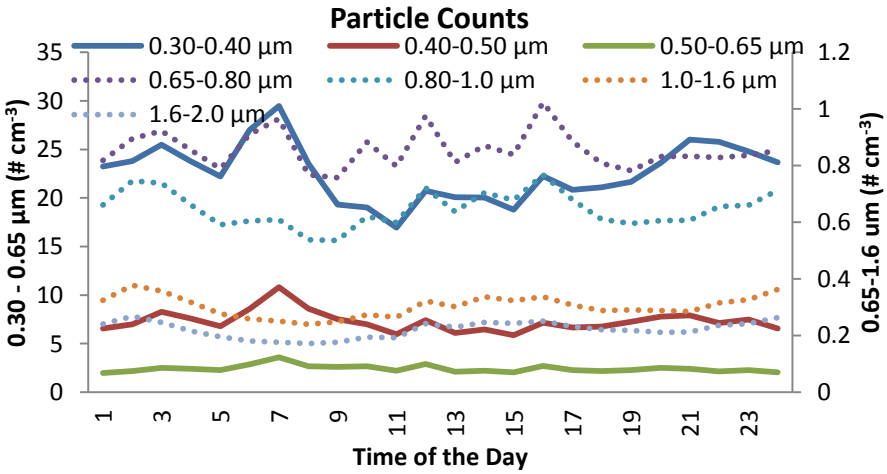
Particle Counts
0.30-0.40 µm
0.40-0.50 µm
0.50-0.65 µm
0.65-0.80 µm
0.80-1.0 µm
1.0-1.6 µm
1.6-2.0 µm
0.30 - 0.65 µm (# cm-3)
0.65-1.6 um (# cm-3)
Time of the Day

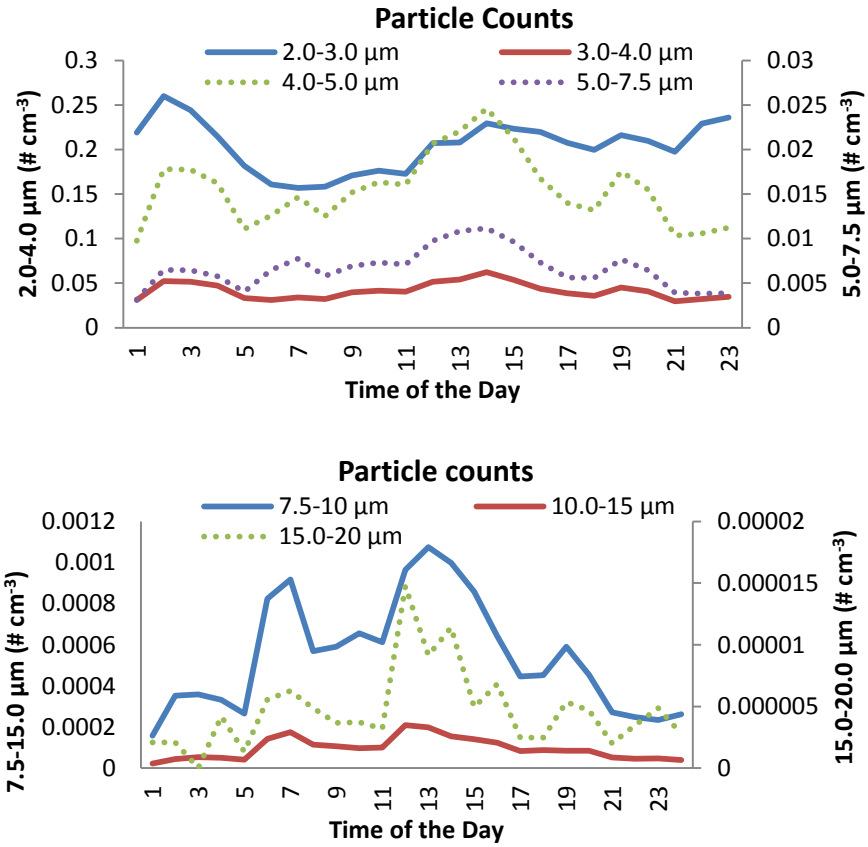

Figure 5.10: Diurnal variations of PM and gaseous pollutants

5.5 Conclusion

This study revealed the significant contributions by the steelworks complex activities in Port Talbot to particulate and gaseous pollutants. FDMS and Partisol PM data have shown days of exceedances when the 24 hour mean of 50 µg m^{-3} was breached. While coarse particles dominated the Partisol PM_{10}, fine particles dominated FDMS PM_{10}. The windrose plots indicted the steelworks as major contributor to PM episodes observed on April 26, May 8 and 11. This study has also established a good correlation between data from FDMS, Partisol, Grimm and MOUDI measuring instruments. The influence of meteorological conditions on particulate and gaseous pollutants has also been discussed. The activity of the steel industry on the PM, PNC and most gaseous pollutants became clearer with the polar plots.

CHAPTER 6- CHEMICAL COMPOSITIONS OF PARTISOL AND STREAKER SAMPLES

6.1 Abstract

This chapter documents the chemical components of particulate matter samples collected with Partisol and Streaker samplers at Port Talbot. For Partisol samples, metals analysed were Mn, Fe, Al, Cr, Zn, Ni, V, Cu, Sb, Ba, Pb, Cd; while ionic species include Cl^-, NO_3^-, SO_4^{2-}, Na^+, NH_4^+, K^+, Mg^{2+} and Ca^{2+}. For Streaker samples, 22 elements from Na to Pb were measured with PIXE. Results of PM chemical assays for Partisol PM showed domination of water soluble ions, which constituted the highest percentage varying between 42-87% for fine and 31-65% for coarse PM at the four stations. Non-sea-salt (nss) sulphate was the highest observed water-soluble ions for fine PM while chloride was observed highest in the coarse PM. The metal fractions represented between 4-5% for both PM categories. Fe was the most abundant metal and formed 38-52% of the total metals measured in $PM_{2.5}$ and 73-88% in $PM_{2.5-10}$.

Of all the measured PIXE elements, sulphur concentrations were highest constituting 31 and 29% of the summed up fine particles at Fire Station (FS) and Little Warren (LW). In the coarse portion, Fe (28% of the summed up $PM_{2.5-10}$ elemental concentration) was the most abundant element at FS while Cl^- (35%) was observed highest at LW. Furthermore, most observed elements have an enrichment factor greater than 10 indicating their anthropogenic origin. The polar plots of the hourly PIXE data suggested the steelworks to be major contributor to the local pollution in Port Talbot.

6.2 Introduction

Urban aerosol comprises organic and inorganic constituents originated from diverse natural and anthropogenic emission sources. The physical and chemical properties of particulate matter play important roles in atmospheric processes including visibility impairment, climate change, acidic precipitation and haze formation (Huang *et al.* 2003). Several adverse health effects associated with aerosol are also linked directly to their chemical compositions (Huang *et al.* 2003). Association between PM compositions, cardiovascular diseases, morbidity and mortality have been reported by many authors (Schwartz, 2000; Riediker *et al.*, 2004; Schwarze *et al.*, 2006; Pope and Dockery, 2006). Epidemiological evidence has demonstrated severe allergic respiratory disease in $PM_{2.5}$ exposed mice due to their metal toxicity (Gavett *et al.*, 2003). Deleterious effects of particulate matter on climate, environment and health are principally caused by their chemical and physical characteristics (Hueglin *et al.*, 2005; Aldabe *et al.*, 2011; Huang *et al.*, 2012).

There are still scanty published literature works on chemical compositions of particulate matter from the steel industry across the world, particularly in the UK. The aim of this chapter is to determine the elemental compositions of PM (fine and coarse portion) collected with Partisol and Streaker samplers during the Port Talbot sampling campaign.

6.3 Results

6.3.1 Partisol PM Data

6.3.1.1 The Average elemental concentrations at the monitoring sites

Table 6.1 shows the mean concentrations of ionic and metal components from 29 days of Partisol data collected at the four monitoring sites, with their percentages in the total PM mass. Most of the observed ionic components showed highest mean values at Little Warren while trace metal compositions at the Prince Street site was higher relative to the other three sites. In total, secondary aerosol components (nss-SO_4^{2-}, NO_3^- and NH_4^+) constituted 43% of measured $PM_{2.5}$ at FS, 30% at PS, 54% at DS and 67% at LW. Na^+ and Cl^- were also significant components of $PM_{2.5}$ at the monitoring sites. The combined component of Na and Cl represented 10, 7, 11 and 23% of the $PM_{2.5}$ fraction at FS, PS, DS and LW respectively. The LW site is the closest site to the Swansea Bay beach; therefore, the highest observed Na^+ and Cl^- concentrations at this site are expected. Average Ca^{2+} concentration of 0.15 μg m^{-3} was observed in $PM_{2.5}$ at FS and LW, and statistically higher than Ca^{2+} mean values at PS and DS. The average concentrations of fine particulate matter showed domination by Fe, Al and Zn. These 3 metals constituted over 90% all the measured metal components of $PM_{2.5}$ (apart from Na^+, K^+, Ca^{2+} and Mg^{2+}) and showed highest mean concentrations at PS except Al which was highest concentration at FS.

Table 6.1: Mean, standard deviation and percentage compositions of water soluble ion and Metal concentrations of Partisol $PM_{2.5}$ and $PM_{2.5-10}$ in Port Talbot

Site	Fire Station (N=29)				Prince Street (N=12)				Dyffryn School (N=29)				Little Warren (N=29)			
	$PM_{2.5}$ ($\mu g\ m^{-3}$)		$PM_{2.5-10}$ ($\mu g\ m^{-3}$)		$PM_{2.5}$ ($\mu g\ m^{-3}$)		$PM_{2.5-10}$ ($\mu g\ m^{-3}$)		$PM_{2.5}$ ($\mu g\ m^{-3}$)		$PM_{2.5-10}$ ($\mu g\ m^{-3}$)		$PM_{2.5}$ ($\mu g\ m^{-3}$)		$PM_{2.5-10}$ ($\mu g\ m^{-3}$)	
Parameters	Mean ±SD	%	Mean ±SD	%	Mean ±SD	%	Mean ±SD	%	Mean ±SD	%	Mean ±SD	%	Mean ±SD	%	Mean ±SD	%
Mass	7.4^{a} ±2.1	100	13.6^{bc} ±11.7	100	9.2^{b} ±1.7	100	16.7^{c} ±10.5	100	7.3^{a} ±3.0	10	8.3^{a} ±4.9	100	6.5^{a} ±2.5	100	9.3^{ab} ±4.36	100
Cl^-	0.34^{a} ±0.33	5	1.33^{a} ±1.06	10	0.41^{a} ±0.43	4	1.80^{a} ±1.34	11	0.44^{a} ±0.42	6	1.52^{a} ±1.54	20	0.40^{a} ±0.37	6	1.96^{a} ±1.47	21
NO_3^-	0.62^{a} ±0.49	8	0.45^{a} ±0.27	3	0.52^{a} ±0.41	6	0.47^{a} ±0.35	3	0.95^{a} ±0.81	13	1.03^{b} ±1.58	15	0.95^{a} ±0.74	15	0.81^{ab} ±0.79	9
nss-SO_4^{2-}	1.91^{ab} ±1.02	26	0.36^{a} ±0.38	3	1.66^{a} ±0.38	18	0.28^{ab} ±0.26	2	2.29^{ab} ± 1.31	31	0.70^{c} ±0.46	9	2.51^{b} ± 1.23	39	0.57^{bc} ±0.42	6
ss-SO_4^{2-}	0.09^{a} ±0.05	1	0.21^{a} ±0..13	2	0.08^{a} ±0.05	1	0.27^{ab} ±0.16	2	0.09^{a} ±0.05	1	0.21^{ab} ±0.15	3	0.12^{b} ±0.05	2	0.31^{b} ±0.19	3
Na^+	0.34^{a} ±0.20	5	0.82^{a} ±0.52	6	0.31^{a} ±0.19	3	1.06^{ab} ±0.62	6	0.34^{a} ±0.21	5	0.87^{ab} ±0.59	10	0.49^{b} ±0.22	8	1.23^{b} ±0.74	13
NH_4^+	0.68^{a} ±0.53	9	0.07^{a} ±0.06	0	0.58^{a} ±0.34	6	0.06^{a} ±0.04	0	0.75^{a} ±0.65	10	0.07^{a} ±0.09	2	0.82^{a} ±0.65	13	0.14^{b} ±0.11	2
K^+	0.11^{a} ±0.01	2	0.08^{a} ±0.07	1	0.14^{a} ±0.09	2	0.09^{a} ±0.08	1	0.10^{a} ±0.07	1	0.08^{a} ±0.06	1	0.15^{a} ±0.10	2	0.12^{a} ±0.07	1
Mg^{2+}	0.05^{a} ±0.04	1	0.13^{a} ±0.10	1	0.05^{a} ±0.02	1	0.16^{a} ±0.11	1	0.04^{a} ±0.03	1	0.12^{a} ±0.09	1	0.06^{a} ±0.03	1	0.15^{a} ±0.09	2
Ca^{2+}	0.15^{a} ±0.13	2	0.80^{b} ±0.77	6	0.11^{a} ±0.07	1	0.91^{b} ±0.77	5	0.10^{a} ±0.15	1	0.41^{a} ±0.45	5	0.15^{a} ±0.17	2	0.45^{a} ±0.37	5
Al*	128.9^{b} ±34.3	2	142.6^{b} ±58.5	1	109.6^{a} ±7.9	1	140.8^{ab} ±44.8	1	116.0^{ab} ±16.1	2	110.6^{a} ±34.1	1	117.9^{ab} ±24.7	2	123.6^{ab} ±48.3	1
V*	0.52^{a} ±0.23	0	0.53^{bc} ±0.42	0	0.50^{a} ±0.23	0	0.64^{c} ±0.34	0	0.49^{a} ±0.21	0	0.41^{a} ±0.32	0	0.59^{a} ±0.28	0	0.31^{ab} ±0.18	0
Cr*	3.48^{a} ±1.52	0	2.89^{a} ±1.52	0	4.76^{a} ±2.04	0	3.67^{a} ±1.16	0	2.78^{a} ±1.55	0	3.14^{a} ±1.49	0	4.52^{a} ±3.19	0	2.97^{a} ±1.49	0
Mn*	5.72^{a} ±7.6	0	26.47^{bc} ±35.1	0	12.76^{b} ±11.8	0	29.52^{c} ±27.0	0	7.03^{a} ±10.7	0	12.65^{ab} ±13.8	0	3.84^{a} ±4.8	0	10.0^{a} ±12.5	0

Note: * units in ng m^{-3}

Table 6.1 contd.

Site	Fire Station (N=29)				Prince Street (N=12)				Dyffryn School (N=29)				Little Warren (N=29)			
	$PM_{2.5}$ ($ng\ m^{-3}$)		$PM_{2.5-10}$ ($ng\ m^{-3}$)		$PM_{2.5}$ ($ng\ m^{-3}$)		$PM_{2.5-10}$ ($ng\ m^{-3}$)		$PM_{2.5}$ ($ng\ m^{-3}$)		$PM_{2.5-10}$ ($ng\ m^{-3}$)		$PM_{2.5}$ ($ng\ m^{-3}$)		$PM_{2.5-10}$ ($ng\ m^{-3}$)	
Parameters	Mean ±SD	%	Mean ±SD	%	Mean ±SD	%	Mean ±SD	%	Mean ±SD	%	Mean ±SD	%	Mean ±SD	%	Mean ±SD	%
Fe	173^{a} ±237	2	1196^{b} ±1642	9	290^{b} ±229	3	1439^{b} ±1485	9	142^{a} ± 147	2	421^{a} ±433	5	104^{a} ± 108	2	520^{a} ±669	6
Ni	0.20^{a} ±0.33	0	0.19^{ab} ±0.22	0	0.16^{a} ±0.27	0	0.24^{b} ±0.22	0	0.12^{a} ±0.17	0	0.11^{a} ±0.15	0	0.12^{a} ±0.20	0	0.14^{ab} ±0.22	0
Cu	1.89^{a} ±1.21	0	2.05^{b} ±0.87	0	2.90^{b} ±1.51	0	3.20^{c} ±1.69	0	1.42^{a} ±0.90	0	1.45^{ab} ±1.0	0	1.38^{a} ±1.26	0	1.12^{a} ±0.70	0
Zn	43.0^{a} ±85.55	1	7.30^{a} ±8.03	0	67.97^{a} ±165.8	1	16.26^{a} ±30.87	0	71.51^{a} ±117.2	1	20.31^{a} ±26.48	0	33.98^{a} ±86.7	1	8.30^{a} ±17.71	0
Cd	0.26^{a} ±0.55	0	0.02^{a} ±0.06	0	0.88^{a} ±2.11	0	0.06^{a} ±0.12	0	0.69^{a} ±1.34	0	0.08^{a} ±0.15	0	0.31^{a} ±0.52	0	0.03^{a} ±0.09	0
Sb	0.57^{a} ±0.52	0	0.36^{b} ±0.21	0	0.99^{b} ±1.14	0	0.66^{c} ±0.34	0	0.38^{a} ±0.32	0	0.13^{a} ±0.14	0	0.53^{a} ±0.71	0	0.11^{a} ±0.22	0
Ba	1.04^{b} ±0.5	0	3.03^{b} ±2.06	0	1.69^{c} ±0.75	0	4.04^{c} ±2.32	0	0.49^{a} ±0.25	0	1.41^{a} ±0.81	0	0.34^{a} ±0.26	0	1.15^{a} ±0.70	0
Pb	4.42^{a} ±3.88	0	2.04^{ab} ±2.40	0	7.65^{a} ±7.98	0	2.95^{b} ±4.20	0	8.12^{a} ±9.27	0	1.44^{a} ±1.51	0	7.02^{a} ±6.86	0	1.32^{a} ±1.43	0

Superscripts of the same alphabets on the rows are not significantly different at $p<0.05$

The marine aerosol component (Na^+ and Cl^-) constituted 16% of the total measured $PM_{2.5-10}$ at FS, 17% at PS, 30% at DS and 33% at LW. Ca^{2+} also formed a significant portion of $PM_{2.5-10}$ at the monitoring sites; with highest average concentrations observed at PS. The secondary aerosol components also contributed significantly to the total mass of coarse PM. The sea-sulphate formed 2% of $PM_{2.5-10}$ at FS and PS, and 3% at DS and LW. The crustal element, Al represents approximately 1% of coarse PM at each monitoring site.

6.3.1.2 Time series plots for water soluble ion and metal concentrations of Partisol fine and coarse PM

The daily variations of water soluble ion concentrations for $PM_{2.5}$ at the monitoring sites are plotted in Appendix XIII. The domination of nss-sulphate throughout the monitoring periods was clearly observed at the four sampling sites. At the FS, DS and LW sites, elevated concentrations of secondary aerosols occurred on May 4, and might explain the elevated concentrations of Partisol and FDMS $PM_{2.5}$ (see Figure 5.1 and 5.2) on this day. FDMS mass concentration data for fine PM are not available at the DS and LW sites. There are no distinctive patterns in temporal variations of other ionic species. However, at PS, peaks of K^+ and Ca^{2+} occurred together on April 21. The mass concentration data of $PM_{2.5}$ in chapter 5 showed a significant peak on April 21 at PS. Woodsmoke and blast furnace (BF) steelworks are notable emission sources of fine K^+ and Ca^{2+} (Machemer, 2004; Dall'Osto *et al.*, 2008a; Harrison *et al.*, 2011).

The daily patterns of water soluble components of coarse PM mode are presented also in Appendix XIII. The $PM_{2.5-10}$ ionic species was dominated by sea salt aerosols (Cl^-, Na^+, Mg^{2+}), sea salt-sulphate and Ca^{2+}. The common peaks of $PM_{2.5-10}$ water soluble ions were

shown at all the monitoring stations on April 22-23. Significantly elevated peaks were found for water soluble components at FS on April 26, May 8 and 11 which were days of PM_{10} episodes at the site. This shows the evidence of the steelworks contribution to coarse PM at the site.

In Appendix XIV are shown the time series plots of metal data for fine PM at the four sampling sites. At the Fire Station site, most of the metals have shown similar undulating pattern of daily concentrations. The notable peaks were observed on the April 18 and 26, May 2-4, 8 and 11. Elevated concentration of Fe (greater than 1,000 ng m^{-3}) observed on April 26 at FS is evidence of steelworks emissions (Connell *et al.*, 2006; Mazzei *et al.*, 2008; Hleis *et al.*, 2013). At the Prince Street sampling site, there were distinctive peaks of metal pollution on April 18, 23 and 26 similar to that of FS. It appeared that there was a factor responsible for the emission of Fe, Mn, Zn and Cd on these episodic days. The activities of the steelworks are likely to be the major suspect since these metals are best tracers for steel industry (Oravisjarvi *et al.*, 2003). A relatively small peak of Pb, Zn, Mn, and Fe was observed at the Dyffryn School (DS) on May 11 coinciding with the episode observed at FS.

Results of daily variations of metal concentrations in the $PM_{2.5-10}$ portion at the four sampling sites are displayed in Appendix XIV. Most of the peaks observed in the coarse PM are consistent with peaks displayed for $PM_{2.5}$ for Fe, Mn and Al on episodic days at FS. Except on April 21, daily variations of coarse metals have been inconsistent with fine metal values at PS. At DS site, significant peaks occurred on May 2, 11 and 14 similar to $PM_{2.5}$ metal variations. Interestingly, almost all the metals were peaked on May 2-3 and 11

indicating episodic events by the steelworks activities. The daily trends of metal concentrations at LW for coarse PM are related to what was observed for $PM_{2.5}$.

6.3.1.3 Aerosol chemistry at the monitoring sites

Ion balance equations of $PM_{2.5}$ and $PM_{2.5-10}$ using RMA regression is shown in Table 6.2. The aim of this is not only to show the reliability and accuracy of the measured data (Wang *et al.*, 2005), but also to study the chemistry of aerosol at each sampling site. The molar equivalent of NO_3^- + SO_4^{2-} versus NH_4^+ equation indicates acidity, alkalinity and neutrality of aerosol. In a situation where the slope is > 1.0, this indicates acidic aerosol; slope <1.0 depicts an alkaline aerosol, and slope=1.0 signify neutral aerosol formation. The molar equivalent of NO_3^- + SO_4^{2-} versus NH_4^+ in $PM_{2.5}$ showed a slope ranges from 0.62 at PS and 1.04 at DS. Correlation coefficient (r) varies between 0.55 at PS and 0.84 at FS. At DS and LW, where the slopes were approximately 1.0, a situation of complete neutralization of acidic aerosols by ammonium was observed. At FS where the slope was 0.94, the neutralization system was fair just like that of DS and LW. Complete formation of ammonium sulphate/ammonium bisulphate and ammonium nitrate were prominent. However, the condition at PS where the slope was 0.62 showed an incomplete system due to excess availability of ammonia and depletion of one of the acidic gases (Parmar *et al.*, 2001). In the coarse mode, the molar equivalent of NO_3^- + SO_4^{2-} versus NH_4^+ has slopes which vary from 3.01 to 4.57. Molar equivalent data for $PM_{2.5-10}$ are poorly correlated.

Table 6.2: Reduced Major Axis (RMA) equations for ionic balance

Sites	$[NO_3^-] + [SO_4^{2-}]$ vs. $[NH_4^+]$		$[Mg^{2+}] + [Na^+]$ vs. $[Cl^-]$		[Total Cations] vs. [Anions]	
	$PM_{2.5}$	$PM_{2.5-10}$	$PM_{2.5}$	$PM_{2.5-10}$	$PM_{2.5}$	$PM_{2.5-10}$
FS	y=0.94x r^2=0.84	y=3.16x r^2=0.01	y=1.12x r^2=0.66	y=1.01x r^2=0.96	y=0.98x r^2=0.69	y=1.76x r^2=0.81
PS	y=0.64x r^2=0.59	y=3.01x r^2=0.24	y=0.80x r^2=0.77	y=0.93x r^2=0.98	y=1.10x r^2=0.36	y=1.42x r^2=0.81
DS	y=1.05x r^2=0.63	y=4.57x r^2=0.01	y=1.16x r^2=0.72	y=1.03x r^2=0.95	y=0.93x r^2=0.56	y=1.29x r^2=0.79
LW	y= x r^2=0.76	y=3.49x r^2=0.04	y=1.04x r^2=0.60	y=0.94x r^2=0.96	y=x r^2=0.76	y=0.83x r^2=0.64

FS-Fire Station, PS-Prince Street, DS-Dyffryn School, LW-Little Warren

Titrations of $[Mg^{2+}] + [Na^+]$ against $[Cl^-]$ were defined well at all the monitoring sites for the two PM categories. The slopes (molar equivalent ratios) vary between 0.80 and 1.16 for $PM_{2.5}$ and 0.94 to 1.03 for $PM_{2.5-10}$. The associations of $[Mg^{2+}] + [Na^+]$ vs. $[Cl^-]$ have also been intimately defined (r^2=0.60-0.77 for fine, and 0.95-0.98 for coarse PM). A perfect formation of sea salt aerosol at both fine and coarse modes was prominent at all the monitoring sites. Sea salt aerosol in fine and coarse PM mode is mainly form of NaCl and $MgCl_2$. Marine influence on the atmospheric aerosol processes and formation is a significant factor to local emission source of particle pollutants in Port Talbot. However, the presence of NaCl and KCl in fine particles has also been attributed to emissions from waste incineration (Bourotte *et al.*, 2007). KCl is also a notable emission from the sinter plant (Oravisjarvi *et al.*, 2003; Dall'Osto *et al.*, 2008).

The molar equivalent of total cations and anions is also illustrated in Table 6.2. The ratio indicates slight domination of anions for $PM_{2.5}$ at FS and DS. At LW, it appears that there is a balance between cationic and anionic species in $PM_{2.5}$. For $PM_{2.5-10}$, domination of cationic species was obvious except at the LW site. More contribution from marine sources at LW (being the closest to the coast) might have resulted into higher concentrations of anionic species particularly chloride.

6.3.1.4 Mass ratios of NO_3/nss-SO_4

The mass ratio of NO_3/nss-SO_4 is used as indicator for mobile and stationary emission sources of nitrogen and sulphur to the atmospheric environment (Yao *et al.*, 2002). Sulphate and nitrogen are formed as a result of photochemical reactions of their precursor's gases (SO_2 and NO_x) with ammonia. When $NO_3/SO_4<1$, it signifies that emission is mainly from the stationary combustion source (industrial and power plants) and when the ratio is greater than 1, the mobile emission dominates (traffic). The NO_3/nss-SO_4 mass ratios for fine and coarse PM at the four monitoring stations are plotted in Figure 6.1. NO_3/nss-SO_4 mass ratios for fine PM were between 0.30-0.42 while for coarse PM it was 2.34-3.82. The results of NO_3/nss-SO_4 suggest that fine particles at Port Talbot are more influenced by traffic while coarse by the steelworks (AQEG, 2011).

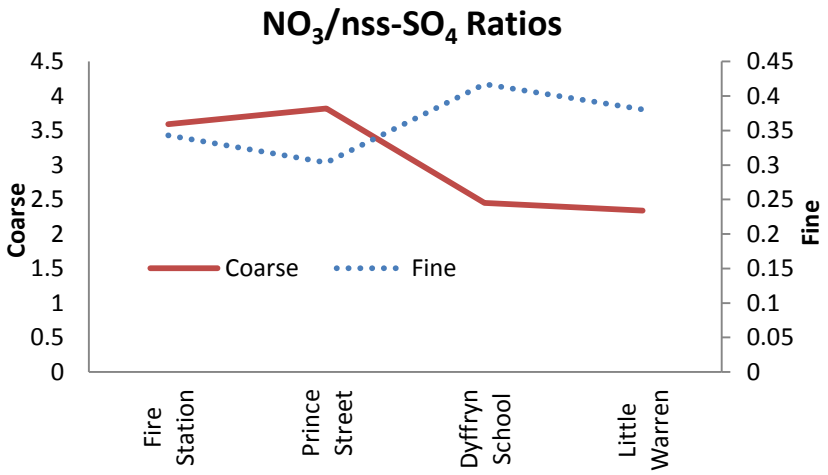

Figure 6.1: NO_3/nss-SO_4 mass ratios for $PM_{2.5}$ and $PM_{2.5-10}$

6.3.1.5 Enrichment factors

Results of enrichment factor analysis for $PM_{2.5}$ and $PM_{2.5-10}$ are displayed in Figure 6.2. In both PM fractions, EFs are classified into four groups based on their EF values. Aluminium was adopted as the reference element (see details in chapter 2). The groups are EF<10, EF>10, EF>100 and EF>1000. Elements with EF value less than 10 is usually taken as being from a crustal or natural origin while EF>10 is assigned to anthropogenic emission sources (Kothai *et al.*, 2011). EF values >100 and 1000 could be seen as highly and heavily enriched. EF value close to 1.0 has a strong crustal origin (Braga *et al.*, 2005). The EF results have shown mixed values at each sampling site. In the group of EF<10 for $PM_{2.5}$ are Al, Ba, K^+, Mg^{2+}, Fe, Ca^{2+}, V, Na (at FS and PS sites) and Mn (FS). These elements are typical crustal origin. However, higher EF data is expected of V and Fe in the fine PM due to the activities of the steel industry. It is not surprising as similar low EF value of V has been reported at a smelting industry in Northern Europe (Reinmann and de Caritat., 2005). In the category of EF>10 but less than 100 were Na^+ (DS and LW), Mn (PS), Cu and Cr. Elements with EF>100 were Pb, Cl^- and Zn. In the group with EF>1000

were found Sb and Cd. These metals are heavily enriched with emission sources likely from traffic and steelworks, respectively.

In the coarse PM fraction, Al, Ba, K^+, V, Mg^{2+}, Ni, Ca^{2+} (DS and LW), Fe (DS and LW), and Mn (LW) all have their enrichment factors less than 10 while Ca^{2+} (FS and PS), Cr (FS and DS), Mn (FS, PS and DS), Na^+, Pb (FS, DS, LW) and Zn (FS and LW) have EF>10. Elements in the highly enriched group with EF>100 are Pb (PS), Zn (PS and DS), Sb (FS, DS and LW) and Cd (FS). In the category of heavily enriched elements with EF above 1000 are Sb (PS) and Cd (PS, DS and LW) and Cl^-. The EF of Sb as heavily enriched element in Port Talbot aerosol is in accordance with reported studies of urban dusts (Ayrault *et al.*, 2010). The crustal elements (Fe, Mn, Ca) showed higher EF values in coarse than fine PM fraction. Elements of soil origin might be mobilized into the atmospheric environment from windblown dust or abrasion of rock-derived minerals, and road re-suspensions (Harrison and Yin, 2000). All the anthropogenic elements with high EF values might be generated via industrial activities including vehicular emissions, steelworks, shipping and residential emissions.

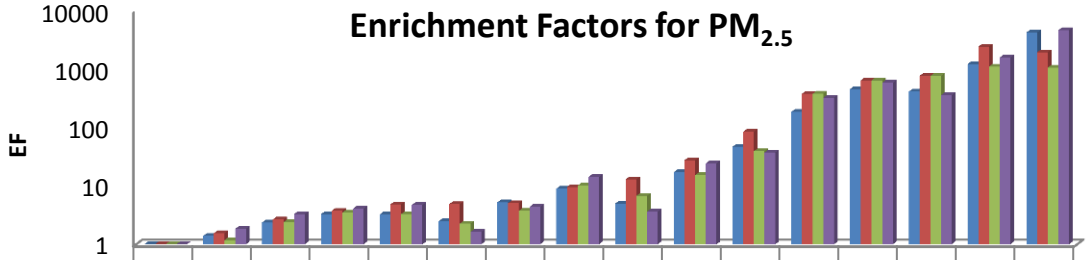

	Al	Mg	Ca	V	K	Fe	Ni	Na	Mn	Cr	Cu	Pb	Cl	Zn	Sb	Cd
FS	1	1.39	2.36	3.26	3.23	2.47	5.23	8.9	4.94	17.1	46.7	184	451	408	1208	4178
PS	1	1.55	2.65	3.72	4.81	4.86	5.04	9.52	12.9	27.4	84.2	375	635	759	2388	1914
DS	1	1.18	2.38	3.46	3.29	2.26	3.73	10.1	6.74	15.2	39.1	376	635	755	1088	1047
LW	1	1.84	3.28	4.06	4.7	1.63	4.36	14.1	3.62	24.2	37.2	320	576	353	1562	4588

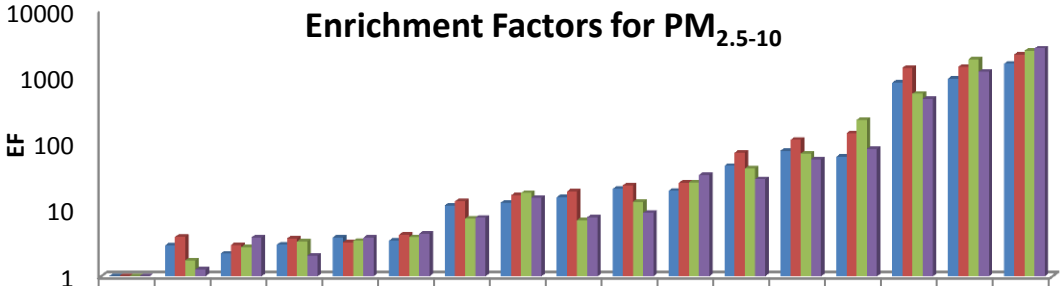

	Al	Ba	K	V	Ni	Mg	Ca	Cr	Fe	Mn	Na	Cu	Pb	Zn	Sb	Cd	Cl
FS	1	2.9	2.2	2.99	3.84	3.42	11.6	12.8	15.5	20.6	19.3	45.8	77.1	62.7	812	939	1568
PS	1	3.92	2.96	3.7	3.26	4.2	13.4	16.5	18.8	23.3	25.4	72.4	113	141	1358	1409	2160
DS	1	1.73	2.75	3.35	3.41	3.88	7.35	18	7.01	13.2	25.8	41.8	70	225	557	1832	2449
LW	1	1.26	3.83	2.05	3.81	4.39	7.58	15.2	7.75	8.99	33.5	28.8	57.4	82.2	467	1194	2667

Figure 6.2: Enrichment factors for Partisol $PM_{2.5}$ and $PM_{2.5\text{-}10}$ chemical components

6.3.1.6 Concentration ratios of PM chemical compositions

The ratios of metal concentrations provide useful information on the emission sources of particular metals or group of metals. Metal signatures for road traffic are Cu, Sb, Zn, Ba and Fe (Thorpe and Harrison, 2008, Amato *et al.*, 2011). Cu/Sb, Fe/Sb, Fe/Cu ratios are good indicators for road traffic signatures. The corresponding range ratios of these metals for $PM_{2.5}$ in this study are 12.6-3.7, 196-374 and 75-100 accordingly. Cu/Sb ratios at the sites and close to Sternbeck *et al.* (2002) value; this suggests traffic impact. At the LW where the Cu/Sb ratio is 2.6 gives indication of minimal emissions by traffic. Lowest Fe/Sb and Fe/Cu ratios are also documented at the LW site. In the $PM_{2.5\text{-}10}$ portion, ranges of Cu/Sb, Fe/Sb, Fe/Cu at the monitoring sites are 4.8-11.2, 2180-4427 and 290-583.

Ni/V ratio has been used to ascribe emissions to residual oil or gas/diesel burning or ship emissions (Figueroa *et al.*, 2006, Pandolfi *et al.*, 2011). Ni/V ratios in this study for $PM_{2.5}$

range between 0.20 at LW and 0.38 at FS. For coarse fraction, the ratios vary from 0.27 at DS and 0.45 at LW.

Mn/Zn ratio is a good indicator for identifying steel emissions (Connell *et al.*, 2006). These ratios in this study for $PM_{2.5}$ vary between 0.10 at DS to 0.19 at PS in line with 0.15 value reported by Connell *et al.* (2006) for $PM_{2.5}$ sampled at Steubenville, US. In the coarse PM, higher ratios of Mn/Zn are calculated with variation from 0.64 at DS to 3.63 at FS. The low Mn/Zn ratio (0.64) obtained at DS may suggest more pronounced influence of basic oxygen furnace steelmaking (BOS) section of the steelworks at the site.

Regarding the Pb/Cd ratios in this study; the values are 17 and 102 for $PM_{2.5}$ and $PM_{2.5\text{-}10}$, respectively at FS, 8.7 and 49.2 at PS; 11.8 and 18 at DS and 22.7and 44 at LW. These ratios are similar to calculated Pb/Cd ratios in emission profiles reported by Tsai *et al.* (2007) at a steel industry in Taiwan. In Tsai *et al.* (2007) study, Pb/Cd ratios at cokemaking, sintering, cold and hot forming processes are 3.0, 17.0, 0.69 and 20, respectively. Pb/Cd ratios calculated for USEPA speciates PM_{10} at the steel foundry, the BOS and sinter plants gave the values of 16, 11 and 22.2, respectively.

By calculating the corresponding mass ratios of Cl^-, K^+, Ca^{2+}, Mg^{2+} and SO_4^{2-} to Na^+, it is possible to infer the influence of marine and other emission sources on fine particles. Ratios of Cl^-/Na^+, K^+/Na^+, Ca^{2+}/Na^+, Mg^{2+}/Na^+ and SO_4^{2-}/Na^+ in seawater are 1.8, 0.037, 0.038, 0.12 and 0.25 respectively (Parmar *et al.*, 2001). In the $PM_{2.5}$ fraction, Cl^-/Na^+, K^+/Na^+, Ca^{2+}/Na^+, Mg^{2+}/Na^+ and SO_4^{2-}/Na^+ ratios are calculated for each site; the ratios are 1.01-1.33, 0.30-0.46, 0.30-0.43, 0.12-0.17 and 5.63-7.59. In the coarse PM portion, Cl^-

/Na^+, K^+/Na^+, Ca^{2+}/Na^+, Mg^{2+}/Na^+ and SO_4^{2-}/Na^+ ratios at the sites are 1.59-1.76, 0.09-0.10, 0.47-0.98, 0.12-0.17 and 0.50-1.08, respectively. Cl^-/Na^+, K^+/Na^+, Mg^{2+}/Na^+ as well as SO_4^{2-}/Na^+ ratios are close to seawater values indicating a marine influence.

The ratio of SO_4^{2-} to Ca^{2+} is important for identifying possible emission sources of SO_4^{2-} (Zhao *et al.*, 2011). Higher ratio value SO_4^{2-}/Ca^{2+} indicates anthropogenic influences and low ratio signifies emissions through natural processes (Ming *et al.*, 2007). The SO_4^{2-}/Ca^{2+} ratio was calculated for $PM_{2.5}$ and $PM_{2.5-10}$ in this study have range values of 13.57-22.68 and 0.51-2.31 (total-SO_4^{2+} value was used for calculation) at the four monitoring sites.

6.3.1.7 Correlations among Partisol PM constituents and other pollutants at FS

Tables 6.3 and 6.4 represent the Pearson's correlation coefficients (R^2) between Partisol $PM_{2.5}$ and $PM_{2.5-10}$ metal/water-soluble components, black carbon, meteorological parameters and gaseous pollutants at the FS monitoring sites. Pearson's correlation coefficients at the PS, DS and LW sites are presented in Appendices XV-XVII. Strong associations were found between $PM_{2.5}$ mass concentration and Cl^- (R^2=0.40; $p<0.05$), nss-SO_4^{2-} (R^2=0.48; $p<0.05$), NH_4^+ (R^2=0.55; $p<0.01$), Mn (R^2=0.56; $p<0.01$), Fe (R^2=0.57; $p<0.01$), Cu (R^2=0.42; $p<0.05$), Zn (R^2=0.50; $p<0.01$), Sb (R^2=0.39; $p<0.05$), Ba (R^2=0.68; $p<0.01$) and Pb (R^2=0.74; $p<0.01$). NH_4^+ is strongly related with NO_3^- (R^2=0.81; $p<0.01$), and nss-SO_4^{2-} (R^2=0.90; $p<0.01$) indicating secondary aerosol formation while Na^+ and Cl^- are well correlated (R^2=0.85; $p<0.01$) suggesting common emission sources.

V was significantly correlated with Sb (R^2=0.59; p<0.01) and Ba (R^2=0.52; p<0.01) with emissions probably from oil combustion (Lim *et al.*, 2010). Strong correlations were observed between Mn and, Fe (R^2=0.96, p<0.01), Zn (R^2=0.86, p<0.01), Cd (R^2=0.76, p<0.01), Ba (R^2=0.66, p<0.01), Pb (R^2=0.78, p<0.01). These elements are markers for steel industry (Oravisjarvi *et al.*, 2003, Yatkin and Bayram, 2007). Cu and Sb are highly related (R^2=0.75; p<0.01); the relationship was extended to Ba (R^2=0.72; p<0.01) and Pb (R^2=0.54; p<0.01). This suggests emissions from traffic.

The coarse FS PM mass concentration at FS site (Table 6.4) exhibited very strong relationships with Cl^- (R^2=0.67; p<0.01), nss-SO_4^{2-} (R^2=0.81; p<0.01), Na^+ (R^2=0.70; p<0.01), K^+ (R^2=0.42; p<0.05), Mg^{2+} (R^2=0.89; p<0.01), Ca^{2+} (R^2=0.95; p<0.01), Al (R^2=0.86, p<0.01), V (R^2=0.91; p<0.01), Mn (R^2=0.96; p<0.01), Fe (R^2=0.97; p<0.01), Cd (R^2=0.91; p<0.01), Ba (R^2=0.92; p<0.01) and Pb (R^2=0.87; p<0.01). The agreement of $PM_{2.5-10}$ with these metals gives possible contribution of soil, road dust, steelworks, brake wears and oil combustions to coarse PM load in the study area. Al and V have shown very strong relationship with each other (R^2=0.83; p<0.01) and with other metals except Cr. The natural crustal origin of Al and V in the coarse mode has been proved in their low EF values (Figure 6.2). Together with Ba, it could be established that Al and V could be of soil origin. The FS coarse metals have shown correlations between Sb and Ba with Cu suggesting traffic contributions. The strong relationship between Cl^-, Na^+ and Mg^{2+} showed domination of marine aerosol of NaCl and $MgCl_2$ in the coarse particles. Significant associations were found between Ca^{2+} and Cl^- (R^2=0.59; p<0.05), and Ca versus nss-SO_4^{2-} (R^2=0.77; p<0.01).

As regarding the gaseous pollutants, most of the observed metal species (in fine and coarse PM) formed strong correlations with the gaseous pollutants. Mn, Fe, Zn, Cd, Ba and Pb were all correlated significantly with NO, NO_2, NO_x, SO_2 and CO. The trios of NO, NO_2 and NO_x were all correlated with Cu, Sb and Ba indicating vehicular origin. V and Cd were found to be statistically correlated with CO and SO_2 to suggest oil combustion or shipping and steel emission sources. The influence of meteorology on particle formation was much observed between windspeed and Cl^- (R^2=0.40; $p<0.05$, for both fine and coarse) and Na (R^2=0.45; $p<0.05$). The relationship was extended to Ca^{2+} and Mg^{2+} for the coarse portion. Associations between the sea salt elements (Cl^-, Na^+, Mg^{2+}) in the fine and coarse PM, and windspeed were strongly defined. This shows the significant contribution of marine aerosol to particle pollution in Port Talbot.

Pearson's correlation has not shown significant agreement between the fine metal species and black carbon (BC) except with Sb (R^2=0.49, $p<0.01$). BC was strongly correlated with vehicular marker NO_3 (R^2=0.66; $p<0.01$). In the coarse fraction, BC defined good relationship with Cu (R^2=0.55; $p<0.01$). Cu, NO_3 and Sb are better tracers for vehicular emission; their close association with BC, which is a product of incomplete combustion of fuel (Reddington *et al.*, 2012) is a confirmation of influence by vehicular emission.

Table 6.3: Pearson's correlation coefficient $PM_{2.5}$ metal compositions, water soluble ions and gaseous pollutants at FS site

	$PM_{2.5}$	Cl^-	NO_3^-	nss-SO_4^{2-}	Na^+	NH_4^+	K^+	Mg^{2+}	Ca^{2+}	Al	V	Cr	Mn	Fe	Ni	Cu	Zn	Cd	Sb	Ba	Pb
$PM_{2.5}$	**1**	**.397***	**.489****	**.481***	**.153**	**.545****	**.251**	**.018**	**.163**	**.217**	**.282**	**.319**	**.562****	**.566****	**-.188**	**.421***	**.502****	**.488****	**.393***	**.677****	**.736****
Cl^-		**1**	**-.298**	**-.412***	**.853****	**-.325**	**-.151**	**.536****	**.431***	**.018**	**-0.19**	**-.023**	**.404***	**.365**	**.403**	**-.068**	**.447***	**.470***	**-.238**	**.257**	**.281**
NO_3^-			**1**	**747****	**-.381***	**.853****	**-.325**	**-0.151**	**.536****	**.431***	**.018**	**-0.19**	**-.023**	**.404***	**.365**	**.403**	**-.137**	**-.086**	**.629****	**.251**	**.253**
nss-SO_4^{2-}				**1**	**-.602****	**.895****	**.103**	**-.642****	**-.278**	**.134**	**.266**	**.063**	**-.003**	**-.034**	**-.278**	**.387***	**-.004**	**.053**	**.548****	**.233**	**.448***
Na^+					**1**	**-.546****	**-.111**	**.707****	**.242**	**.029**	**-.216**	**-.009**	**.259**	**.244**	**.315**	**-.124**	**.351**	**.381***	**-.230**	**.100**	**.061**
NH_4^+						**1**	**.078**	**-.479****	**-.281**	**.041**	**.150**	**.107**	**-.109**	**-.150**	**-.246**	**.296**	**-.128**	**-.062**	**.417***	**.190**	**.353**
K^+							**1**	**.271**	**.224**	**.051**	**.242**	**.316**	**.497****	**.525****	**-.406**	**.419***	**.418***	**.313**	**.164**	**.464***	**.334**
Mg^{2+}								**1**	**.309**	**-.136**	**-.251**	**-.012**	**.122**	**.155**	**.396**	**-.177**	**.149**	**.114**	**-.303**	**.087**	**-.156**
Ca^{2+}									**1**	**-.104**	**-.061**	**-.109**	**.413***	**.449***	**-.230**	**-.032**	**.330**	**.258**	**-.173**	**.285**	**.169**
Al										**1**	**.144**	**.064**	**.311**	**.249**	**-.114**	**-.013**	**.346**	**.404***	**-.045**	**.191**	**.394***
V											**1**	**-.070**	**.331**	**.321**	**-.161**	**.692****	**.136**	**.126**	**.593****	**.523****	**.279**
Cr												**1**	**.304**	**.360**	**-.126**	**.185**	**.404***	**.273**	**.076**	**.158**	**.279**
Mn													**1**	**.955****	**-.301**	**.416***	**.857****	**.758****	**.097**	**.664****	**.776****
Fe														**1**	**-.227**	**.358**	**.805****	**.666****	**.084**	**.624****	**.669****
Ni															**1**	**-.171**	**-.100**	**-.131**	**-.169**	**-.296**	**-.447**
Cu																**1**	**.343**	**.358**	**.749****	**.717****	**.541****
Zn																	**1**	**.942****	**.063**	**.517****	**.785****
Cd																		**1**	**.102**	**.502****	**.828****
Sb																			**1**	**.568****	**.359**
Ba																				**1**	**.705****
Pb																					**1**

*** p<0.05, ** p<0.01**

Table 6.3 contd.

	Dir	Speed	Temp	NO	NO_2	NO_x as NO_2	O_3	SO_2	CO	BC
$PM_{2.5}$	.167	-.240	.132	.608**	.712**	.697**	-.423*	.599**	.533**	.502**
Cl	.509**	.404*	.034	.072	.022	.035	.185	.406*	.207	-.176
NO_3	-.128	-.586**	-.077	.433*	.540**	.521**	-.548**	-.125	.088	.659**
nss-SO_4	-.395*	-.431*	.115	.394*	.495**	.479**	-.550**	.037	.169	.406*
Na	.552**	.453*	-.093	-.104	-.197	-.176	.379*	.266	.076	-.286
NH_4^+	-.278	-.539**	-.028	.387*	.482**	.468*	-.600**	-.046	.154	.452*
K	.200	-.286	.188	.423*	.543**	.517**	-.248	.446*	.404*	.035
Mg	.535**	.107	-.070	-.017	-.075	-.064	.260	.120	.071	-.255
Ca	.208	.142	.124	.140	.169	.161	.224	.421*	.220	-.187
Al	-.300	.182	.042	-.108	.029	-.014	.128	.349	-.097	-.122
V	.032	-.161	.389*	.288	.338	.334	-.003	.400*	.518**	.111
Cr	-.109	-.227	-.053	.234	.222	.231	-.298	.165	.318	.230
Mn	.195	.213	.450*	.557**	.591**	.595**	-.176	.938**	.684**	-.056
Fe	.180	.163	.375*	.493**	.555**	.549**	-.090	.911**	.657**	-.115
Ni	-.186	.273	-.313	-.512	-.574	-.574	.441	-.334	-.394	-.041
Cu	.232	-.185	.208	.562**	.629**	.625**	-.418*	.356	.468*	.358
Zn	.103	.306	.302	.388*	.469*	.454*	-.067	.782**	.481**	-.065
Cd	.131	.272	.166	.322	.427*	.403*	-.014	.751**	.393*	-.080
Sb	.047	-.412*	.054	.574**	.571**	.591**	-.443*	.118	.235	.486**
Ba	.410*	-.249	.123	.718**	.748**	.759**	-.363	.637**	.523**	.311
Pb	.051	-.068	.273	.619**	.726**	.710**	-.417*	.770**	.557**	.141
Dir	1	.048	-.096	.272	.243	.253	-.056	.148	.160	-.044
Speed		1	.219	-.327	-.348	-.350	.387*	.131	-.218	-.346
Temp			1	.356	.280	.312	-.217	.354	.490**	-.021
NO				1	.884**	.946**	-.745**	.469*	.565**	.534**
NO_2					1	.988**	-.718**	.533**	.487**	.408*
NO_x asNO_2						1	-.746**	.527**	.525**	.464*
O_3							1	-.025	-.238	-.548**
SO_2								1	.689**	-.172
CO									1	-.037
BC										1

Dir-wind direction, Temp-temperature, speed-windspeed, * p<0.05, ** p<0.01

Table 6.4: Pearson's correlation coefficient $PM_{2.5-10}$ metal compositions, water soluble ions and gaseous pollutants at FS site

	$PM_{2.5-10}$	Cl^-	NO_3^-	nss-SO_4^{2-}	Na^+	NH_4^+	K^+	Mg^{2+}	Ca^{2+}	Al	V	Cr	Mn	Fe	Ni	Cu	Zn	Cd	Sb	Ba	Pb
$PM_{2.5-10}$	1	.673**	.047	.813**	.696**	.099	.417*	.894**	.954**	.861**	.911**	-.394*	.963**	.973**	.332	.160	.366*	.919**	.454	.919**	.873**
Cl^-		1	-.181	.391*	.989**	.035	.313	.890**	.590**	.640**	.603**	-.460*	.521**	.533**	.248	.102	-0.041	.041	.081	.498**	.480**
NO_3^-			1	0.083	-.139	.064	-.123	-.056	.120	0.124	.212	.228	.082	.041	-.193	.446*	0.032	.179	.427*	.263	.187
nss-SO_4^{2-}				1	.377*	.136	.176	.625**	.767**	.715**	.789**	-.268	.896**	.878**	.362	-.063	0.314	.786**	.184	.748**	.890**
Na^+					1	-.012	.370*	.905**	.615**	.658**	.614**	-.454*	.538**	.552**	.268	.105	-0.024	.161	.123	.519**	.477**
NH_4^+						1	-.121	0.068	.090	0.039	.064	.082	.085	.104	.040	.194	0.03	.931	.180	.146	.087
K^+							1	.531**	.348	.394*	0267	-.484**	.344	.354	.264	-.074	0.292	.856	.432*	.400*	.232
Mg^{2+}								1	.817**	.795**	.783**	-.488**	.790**	.805**	.297	.106	0.206	.751	.306	.761**	.709**
Ca^{2+}									1	.800**	.945**	-.246	.948**	.940**	.194	.259	.474*	.883	.398	.916**	.871**
Al										1	.833**	-.331	.849**	.809**	.275	.205	.347*	.363	.403	.813**	.705**
V											1	-.240	.927**	.888**	.324	.251	.421*	.547	.302	.888**	.868**
Cr												1	-.306	-.340	-.459	.133	0.147	-.898	-.226	-.295	-.332
Mn													1	.985**	.308	.131	.466*	.885**	.334	.915**	.922**
Fe														1	.298	.104	.419*	.959*	.320	.904**	.915**
Ni															1	.395*	0.16	.873	-.060	.644**	.549**
Cu																1	0.284	-.516	.722**	.462*	.212
Zn																	1	-.59**	.268	.492**	.365
Cd																		1	.876	.970*	.515**
Sb																			1	.588**	.437*
Ba																				1	.884**
Pb																					1

*** p<0.05, ** p<0.01**

Table 6.3 Contd.

	Dir	Speed	Temp	NO	NO_2	NO_x as NO_2	O_3	SO_2	CO	BC
$PM_{2.5-10}$	.375*	.251	.214	.356	.396*	.392*	.121	.851**	.523**	-.115
Cl^-	.602**	.409*	-.043	-.041	-0.075	-.069	.360	.406*	.090	-.283
NO_3^-	-.013	-.285	-.136	.242	.409*	.369*	-.161	.143	.009	.252
nss-SO_4^{2-}	.099	.087	.311	.407*	.460*	.456*	-.097	.892**	.627**	-.086
Na^+	.617**	.446*	-.023	-.046	-.063	-.062	.387*	.411*	.094	-.279
NH_4^+	-.041	-.233	.131	.360	.290	.323	-.426*	.027	.050	.161
K^+	.238	.415*	.253	.043	.220	.164	-.025	.270	.093	-.181
Mg^{2+}	.513**	.427*	.179	.168	.191	.186	.218	.662**	.298	-.223
Ca^{2+}	.322	.225	.269	.409*	.413*	.423*	.118	.879**	.584**	-.016
Al	.442*	.193	.081	.387*	.447*	.438*	.072	.824**	.480**	-.075
V	.308	.211	.233	.434*	.453*	.458*	.074	.924**	.576**	.012
Cr	-.047	-.245	.029	.205	.097	.137	-.252	-.225	.153	.319
Mn	.248	.204	.348	.452*	.483**	.485**	.028	.943**	.642**	-.046
Fe	.248	.207	.298	.409*	.450*	.449*	.048	.890**	.567**	-.064
Ni	.399*	.067	.003	.389*	.386*	.397*	-.042	.259*	.388*	-.234
Cu	.469*	-.421*	-.078	.616**	.496**	.550**	-.312	.034	.156	.551**
Zn	.013	-.145	.408*	.552**	.497**	.529**	-.314	.499**	.711**	.296
Cd	.117	.250	.331	.428*	.487**	.479**	-.107	.494	.061	-.814
Sb	.612**	-.240	.038	.706**	.643**	.681**	-.329	.242	.146	.206
Ba	.404*	.050	.217	.584**	.610**	.618**	-.114	.819**	.571**	.114
Pb	.219	.131	.299	.420*	.448*	.451*	-.021	.857**	.536**	-.003
Dir	1	.048	-.096	.272	.243	.253	-.056	.115	.160	-.013
Speed		1	.219	-.327	-.348	-.350	.387*	.197	-.218	-.414*
Temp			1	.356	.280	.312	-.217	.386*	.490**	.026
NO				1	.884**	.946**	-.745**	.450*	.565**	.594**
NO_2					1	.988**	-.718**	.517**	.487**	.555*
NO_x as NO_2						1	-.746**	.510**	.525**	.621**
O_3							1	-0.011	-.238	-.575**
SO_2								1	.679**	.000
CO									1	.169
BC										1

Dir-wind direction, Temp-temperature, speed-windspeed, * p<0.05, ** p<0.01

6.3.1.8 Analysis of variance (ANOVA) of Partisol PM components at the monitoring sites

ANOVA results (Appendix XVIII) revealed significance ($p<0.05$) in concentrations of $PM_{2.5}$ mass, sodium and chromium. $PM_{2.5}$ mass and Cr concentrations at PS were significantly ($p<0.05$) higher relative to the other three sampling locations. Fine sodium was also significantly ($p<0.05$) higher at LW relative to the remaining stations. DS showed a significantly lower value of $PM_{2.5-10}$ mass concentration and highest nss-SO_4^{2-} concentrations. The coarse NO_3^- value was elevated at DS compared to PS. Ammonium was significantly higher at LW relative to the other sites. Significant elevated values of Ca^{2+} were observed at FS and PS than at DS and LW.

6.3.2 Streaker PM Components

6.3.2.1 Comparison of hourly Streaker and FDMS mass components

Figure 6.3 shows the hourly variations of FDMS and Streaker mass concentrations. The Streaker mass concentrations were determined by summing of all the measured elemental components. The emission patterns shown in Figure 6.3a depict similar variations between FDMS and Streaker mass concentrations for both $PM_{2.5}$ and PM_{10} at FS.

Episodic hours of PM_{10} pollution (> 50 µg m^{-3}) were observed for both PM measuring instruments on May 7th and 10th. On May 2nd and 14th, cases of hourly episodic peaks were observed for FDMS but not for Streaker. However, PM_{10} peak > 40 µg m^{-3} was observed for Streaker on May 14th.

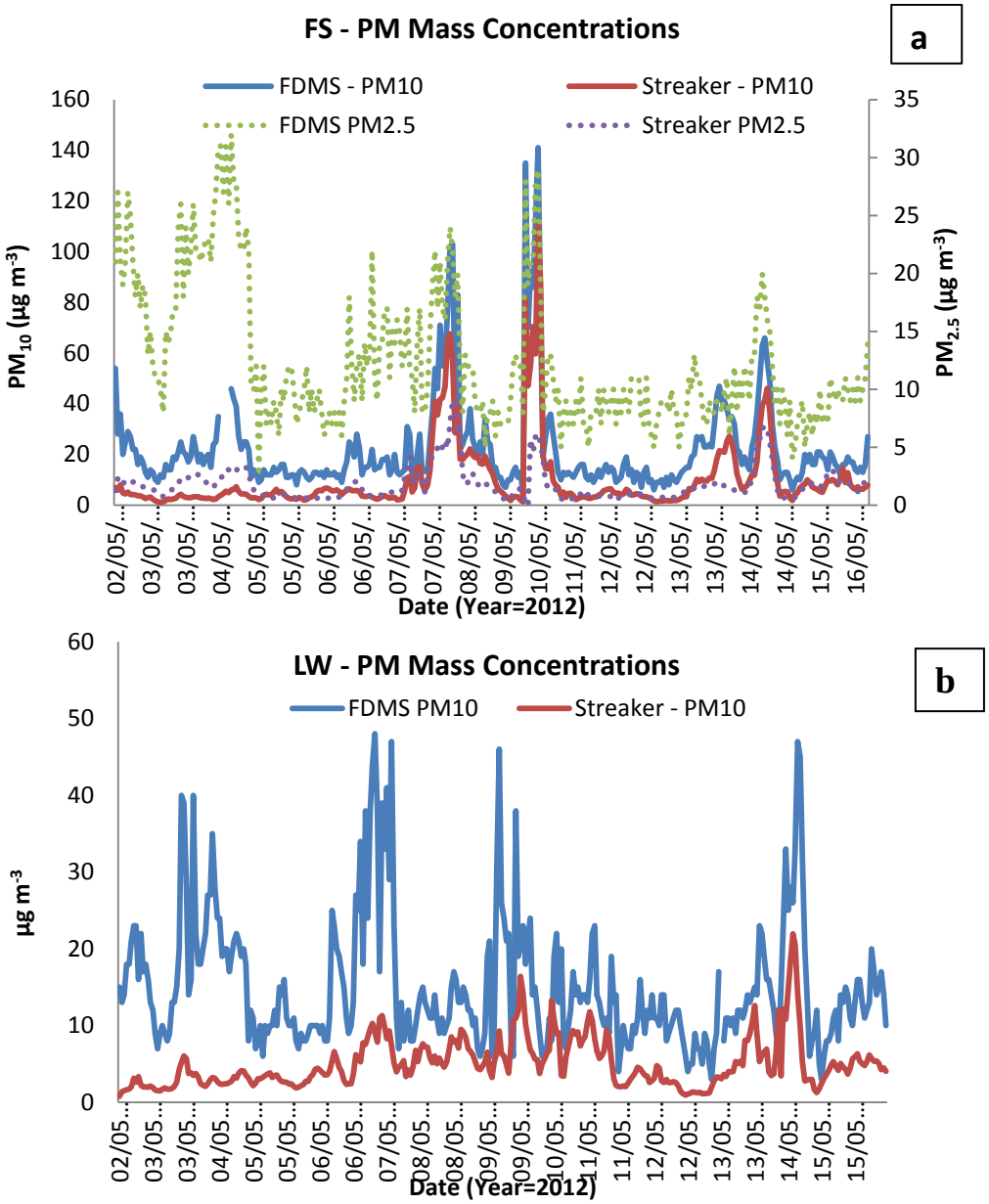

Figure 6.3: Variations in hourly FDMS and Streaker constructed mass concentration at (a) FS and (b) LW

At the LW site, related peaks patterns were observed for FDMS and Streaker PM_{10} constructed mass with no record of exceedances (Figure 6.3b). The hourly data of FDMS $PM_{2.5}$ was not available and hence their comparison with Streaker-summed $PM_{2.5}$ mass is impossible. Looking at the Figure 6.3a & b, the PM mass concentrations from the two

mass measuring instruments showed higher concentration at FS than LW. Hourly peak heights were seen on both May 7, 10 and 14. This suggests a related contributing factor at the two sites.

The hourly trend of each Streaker elemental concentration at FS site is presented in Appendix XIX. The dominating element on the May 10 episode was Fe with hourly concentration around 60 µg m^{-3}. Other elements with significant elevated concentration on this day were Cl, Ca, Na, S, Si, Mg, Al and Mn; these metals mostly concentrated at the coarse mode. These elements could be categorized into four clusters: marine (Cl, Na, Mg, Br), secondary (S), crustal (Ti, Ca, Al) and steel (Fe, Mn).

The hourly trend shown by Na, Mg and Cl in fine and coarse PM indicates a common emission source. These sea spray signatures have shown notable emission heights on May 5, 6, 7, 10, 13, 14 and 16. Elevated amounts of Al, Si, Ti, Mn, Fe, Ca and S were also observed on these days. The fine S exhibited additional huge hourly peaks on May 2-5 which can indicate plume emissions from the steelworks.

Appendix XX shows the Streaker hourly elemental trends of both fine and coarse particles at the LW monitoring station. Unlike at the FS site where highest peak of pollutants were observed on May 10; LW showed elevated components of elements on May 13-14. Al and Si showed a common episode at the two monitoring sites on May 7, 13 and 14. The hourly concentration of Fe, Mn and Ca on May 7 is an indication of a common emission source with the steel industry as the major suspect. Both Zn and Pb peaked on May 7 and 9. Br and Sr appeared to show related peaks on May 11 and 14 indicating similar emission

sources. On May 11, none of the marine aerosol showed peaks as observed for Br. Emission of Br on this day might be linked to a source other than marine origin. Ca displaying a peak on May 11 with Sr may suggest dual emission sources from the steelworks (blast furnace plant) and crustal matter from construction activities (Widory *et al.*, 2010).

6.3.2.2 Average elemental concentrations for Streaker (PIXE) PM data

The average Streaker (PIXE) elemental concentrations for $PM_{2.5}$ and $PM_{2.5-10}$ are displayed in Table 6.5. Like the Partisol nss-SO_4^{2-} which was the highest observed PM component in the fine PM, sulphur was the most abundant constituent at FS and LW. The order of abundance of elemental composition for $PM_{2.5}$ followed the sequence S>Fe>Na>Ca>Cl at FS and S>Na>Fe>Cl at LW. The wide gap between Fe concentrations at the two stations still depicted FS to be more affected by the steelworks probably due to its closeness to the blast furnace, basic oxygen furnace and sinter plants. The fine PIXE average concentrations for Al, Ti, V, Ni, Cu, As, Se and Sr were similar and imply equal contribution from the processes that emitted these particulate trace metals. The coarse fraction of PIXE elemental concentrations showed the order of concentration as: Fe>Cl>Na>Ca at FS and Na>Cl>Fe>Mg at LW.

Table 6.5: Mean, standard deviation of Streaker elemental concentrations of $PM_{2.5}$ and $PM_{2.5-10}$ in Port Talbot

	Fire Station				Little Warren			
Parameters		$PM_{2.5}$ (ng m^{-3})		$PM_{2.5-10}$ (ng m^{-3})		$PM_{2.5}$ (µg m^{-3})		$PM_{2.5-10}$ (µg m^{-3})
	N	Mean ±SD	N	Mean ±SD	N	Mean ±SD	N	Mean ±SD
Na	297	346.58 ±322.35	300	2085.83 ±1762.2	319	424.72 ±387.14	322	1309.38 ±1040.49
Mg	280	59.68 ±37.79	299	277.06 ±314.69	296	62.85 ±36.65	322	147.63 ±101.53
Al	294	48.38 ±22.64	298	116.81 ±180.03	289	42.35 ±24.32	294	42.70 ±54.17
Si	-	-	299	267.70 ±424.28	-	-	320	96.84 ±126.97
S	300	558.60 ±522.89	300	290.59 ±530.68	322	561.96 ±561.16	322	99.05 ±94.55
Cl	298	140.96 ±326.56	266	2185.52 ±2455.71	321	210.76 ±437.70	276	1235.81 ±1163.73
K	292	62.74 ±63.14	300	90.41 ±107.76	298	89.47 ±141.77	317	44.92 ±33.58
Ca	300	141.22 ±201.60	300	749.14 ±1755	312	95.91 ±124.17	322	117.70 ±168.61
Ti	130	8.58 ±3.33	214	16.14 ±28.20	108	8.05 ±3.86	133	5.82 ±4.86
V	23	4.30 ±1.09	16	4.94 ±4.37	30	4.05 ±0.91	15	1.91 ±0.80
Cr	298	3.67 ±1.77	278	3.04 ±3.58	256	2.65 ±1.08	309	1.91 ±0.62
Mn	264	10.35 ±17.27	259	39.29 ±105.01	166	11.15 ±16.15	187	6.44 ±9.41
Fe	299	377.79 ±688.03	300	2362.77 ±7431.10	321	231.24 ±452.03	322	306.63 ±725.40
Ni	271	1.37 ±0.62	227	0.67 ±0.26	294	1.29 ±0.63	294	0.60 ±0.24
Cu	297	3.34 ±3.86	296	3.03 ±2.76	237	2.63 ±4.74	231	0.74 ±0.71
Zn	300	32.51 ±82.27	298	9.30 ±20.34	321	80.64 ±383.57	316	9.24 ±42.30
As	32	1.36 ±0.62	29	0.76 ±0.77	28	1.31 ±0.80	15	0.45 ±0.31
Se	71	1.94 ±1.19	16	1.59 ±1.44	83	1.74 ±1.32	15	0.63 ±0.46
Br	-	-	94	1.03 ±0.84	-	-	140	1.73 ±1.87
Rb	24	9.33 ±5.95	85	44.01 ±88.49	27	7.29 ±3.09	55	5.39 ±5.79
Sr	13	2.11 ±0.50	126	1.62 ±0.98	20	2.34 ±0.86	127	1.51 ±1.0
Pb	230	7.40 ±7.37	106	9.53 ±23.93	200	14.44 ±19.64	69	3.58 ±3.41

SD- Standard Deviation

6.3.2.3 Temporal variations of Streaker PM elemental concentrations

The diurnal variations of Streaker fine and coarse PM at FS and LW are shown in Figure 6.4. Similar diurnal variations were highlighted for fine Fe and Mn at FS with notable peaks at 7-9 am, 2 pm and 6 pm. At LW, a common peak was observed at 1 pm and 10 pm while other peaks did not match. Different patterns of Fe and Mn peaks at FS and LW might be related to prevailing wind direction from the steelworks to the two sites. Additional contribution by traffic might probably explain the peaks observed at morning and evening rush hours at FS. The temporal trend of fine Zn and Pb is closely related to the pattern observed for Fe and Mn. Zn and Pb showed a common peak at 1 pm at the two sites. The Fe and Mn at the LW also showed a recognizable peak during this period. The fine Na, Cl and Mg displayed a stretched peak that started from 9 am till 8 pm at FS, and 9 am to 9 pm at LW.

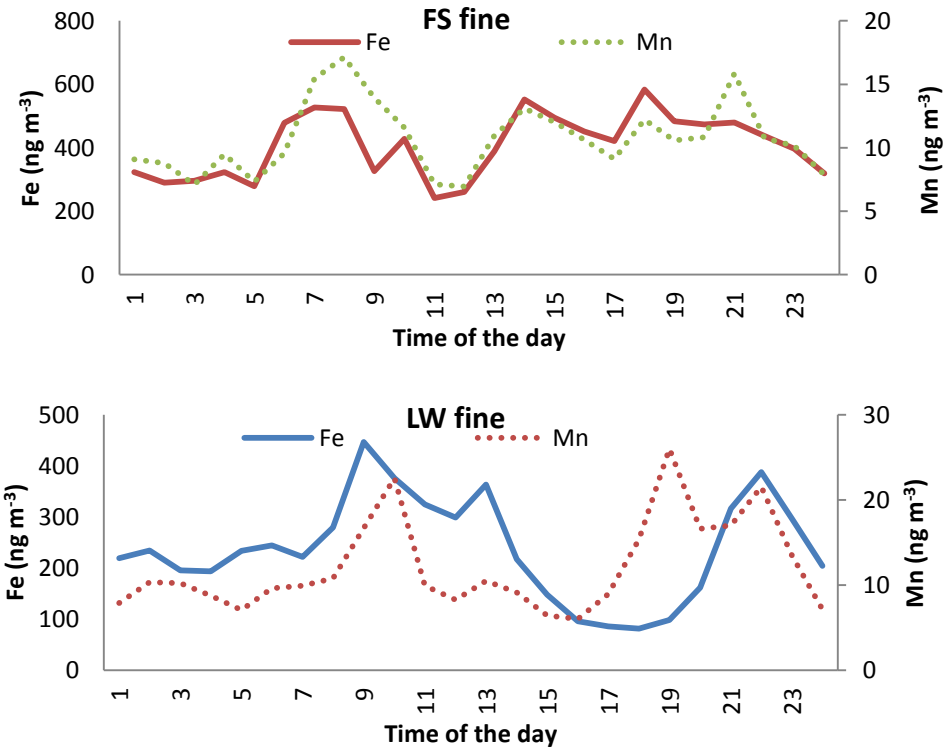

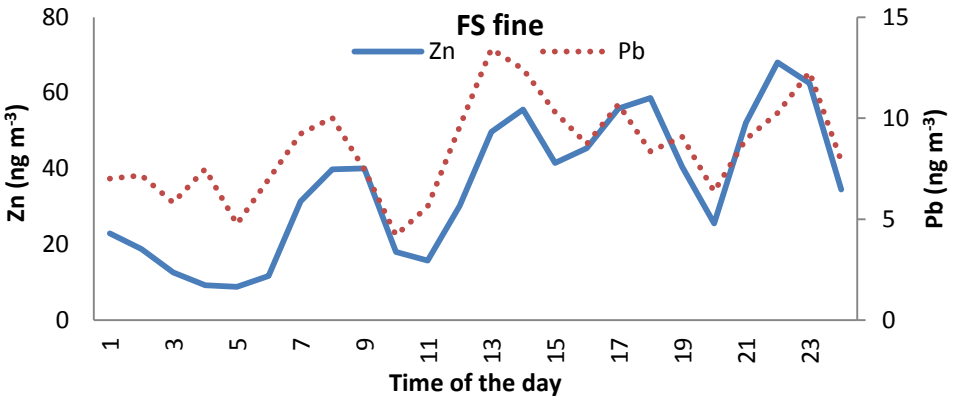
FS fine
Zn
Pb
Zn (ng m-3)
Pb (ng m-3)
Time of the day

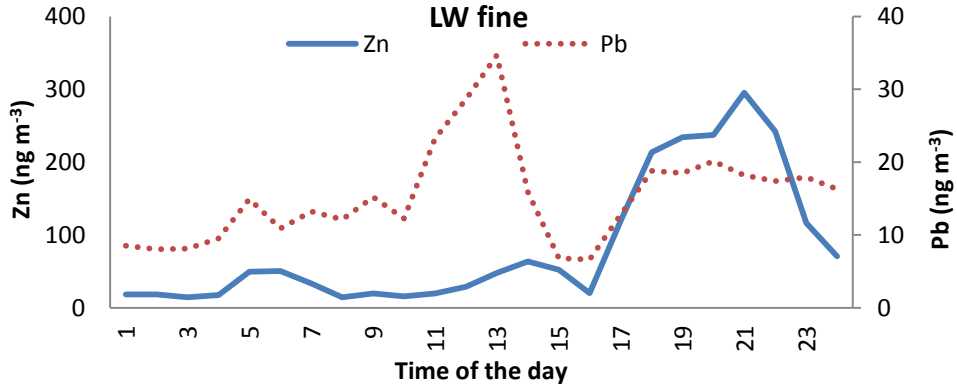
LW fine
Zn
Pb
Zn (ng m-3)
Pb (ng m-3)
Time of the day

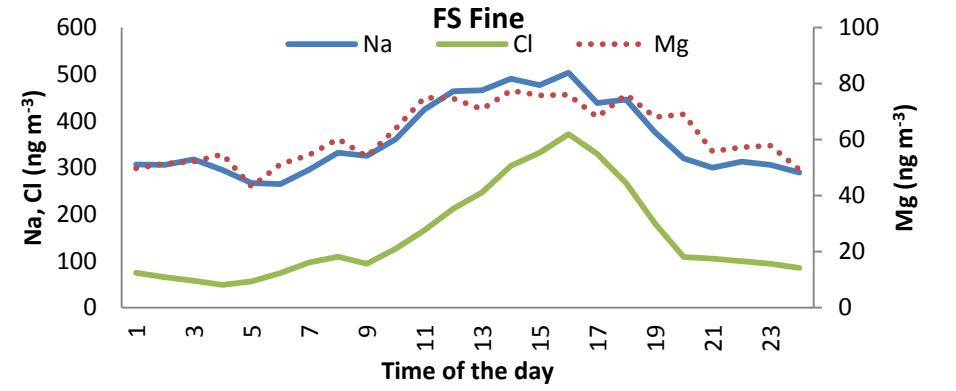
FS Fine
Na
Cl
Mg
Na, Cl (ng m-3)
Mg (ng m-3)
Time of the day

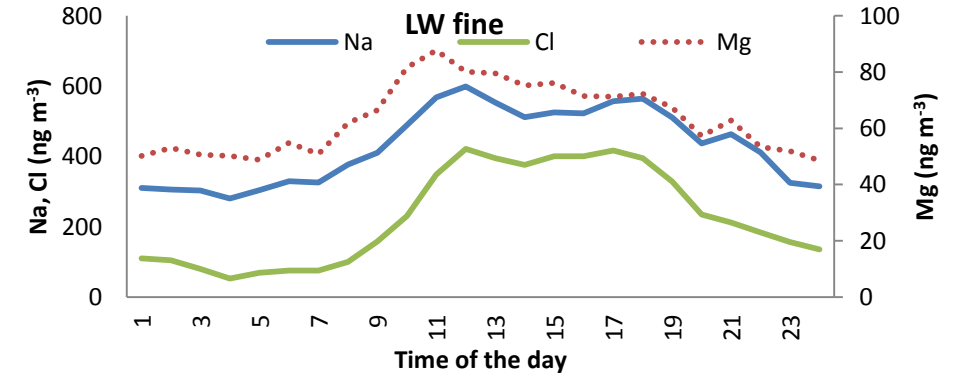
LW fine
Na
Cl
Mg
Na, Cl (ng m-3)
Mg (ng m-3)
Time of the day

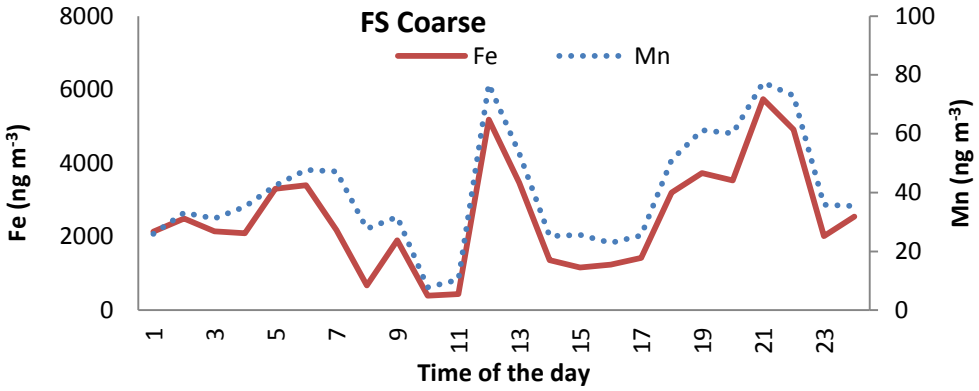
FS Coarse
Fe
Mn
Fe (ng m-3)
Mn (ng m-3)
Time of the day

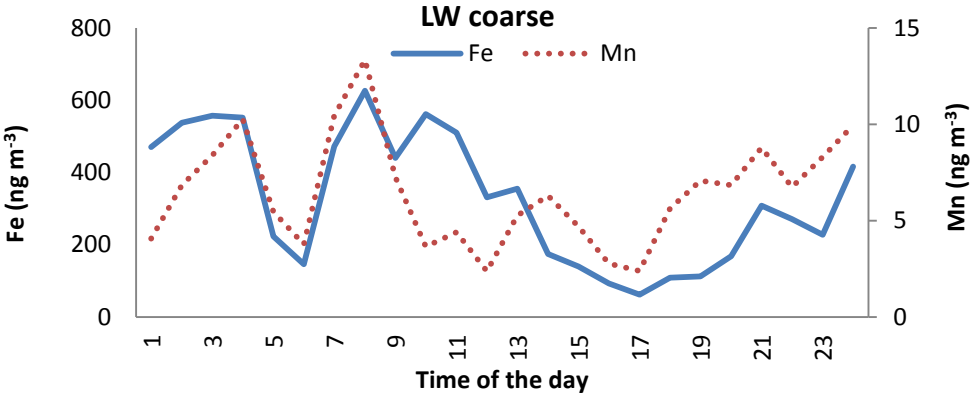
LW coarse
Fe
Mn
Fe (ng m-3)
Mn (ng m-3)
Time of the day

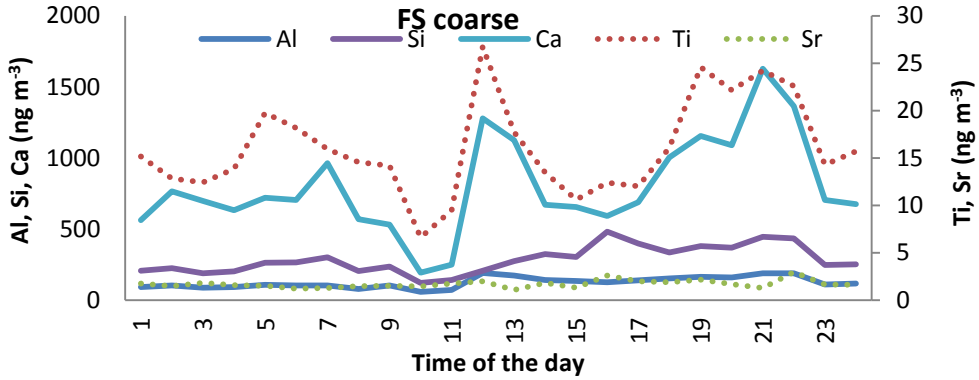
FS coarse
Al
Si
Ca
Ti
Sr
Al, Si, Ca (ng m-3)
Ti, Sr (ng m-3)
Time of the day

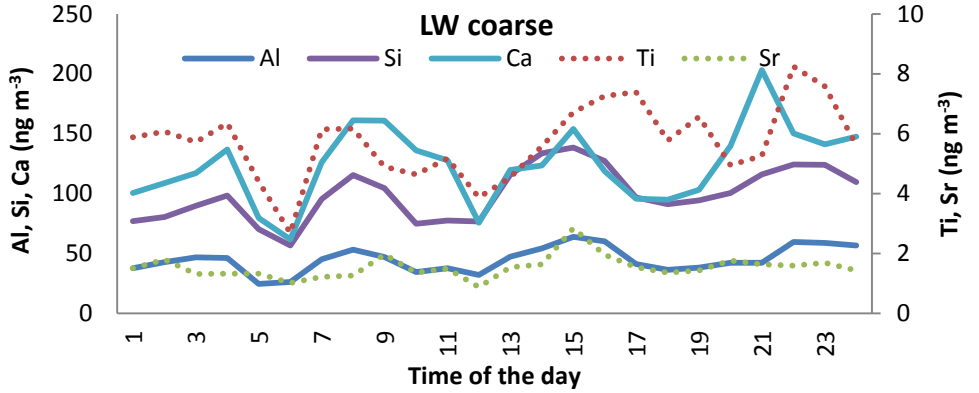
LW coarse
Al
Si
Ca
Ti
Sr
Al, Si, Ca (ng m-3)
Ti, Sr (ng m-3)
Time of the day

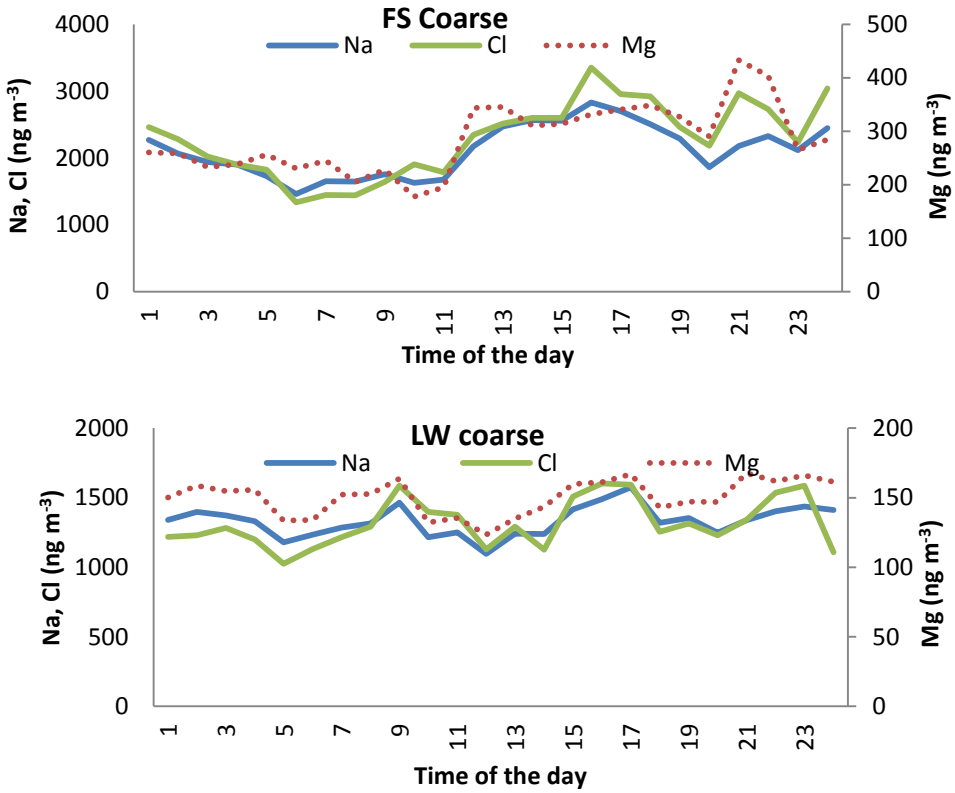

Figure 6.4: Diurnal variations of Streaker elemental concentrations

Diurnal peaks for coarse Fe and Mn at FS were 4-9 am, 11 am to 2 pm and 5-11 pm. At LW, there were times when Fe and Mn peak did not match, however, significant peaks were observed at 3-5 am and 6-9 am. The crustal elements (Al, Ti, Sr, Ca and Si) displayed different diurnal trends which suggested different emission sources at the two sites. The contributing factor from the road resuspension was more evident at LW than FS with peak heights observed around 6-11 am and 12 pm to 7 pm. Elevated concentrations of Ca and Ti between 9 and 10 pm could represent emissions from the steel production processes. The coarse marine aerosol (Na, Cl, Mg) showed similar temporal trends observed for fine PM at FS, and different diurnal variations with LW fine.

6.4.2.4 Enrichment factor analysis of Streaker data

Enrichment factors of Streaker elements for both fine and coarse PM at the two stations are presented in Table 6.6. $PM_{2.5}$ EF values for Mg, K, Ca and Ti at the two sites were <10 indicating their natural origins. The coarse fractions showed Si, K, Ti and Sr to be mainly of natural origin at FS and LW with their EF values less than 10. Additionally, Mg and Ni have EF<10 at FS while these elements showed some anthropogenic influence at LW.

EF ratios of Al, Si and Ti for coarse PM at the two stations have a strong link with crustal matter. The scatter plots of Al against Si and Ti at FS and LW shown in Figure 6.5 established also common origins of these metals. Si/Al ratios at FS and LW are 2.3 and 2.2, similar to the typical rock composition of 2.79 reported in D'Alessandro *et al.* (2003); and also similar to Si/Al ratio value of Wedepohl (1995) calculated as 3.6.

The fine particles at FS revealed S, As and Se as the most highly enriched elements with an EF value >1000. In the coarse fraction at this site, Cl and Se are highly enriched (EF>1,000). At LW, fine S, Zn, As, Se and Pb have EF values > 1000; while coarse Cl, Se and Br recorded EF>1000. The elevated EF amounts calculated for Na and Cl showed additional contributions from anthropogenic pathways especially the steelworks rather than from a wholly marine emission. Further confirmation could be established with relatively low Cl/Na ratios in $PM_{2.5}$ (0.41 and 0.50 at FS and LW, respectively) and $PM_{2.5-10}$ (1.1 and 0.9 at FS and LW) when compared with seawater value of 1.8.

Table 6.6: The EF values of elemental concentrations of PM at FS and LW stations

	Fire Station		Little Warren	
	$PM_{2.5}$	$PM_{2.5-10}$	$PM_{2.5}$	$PM_{2.5-10}$
Na	24	60	35	106
Mg	5	9	5	13
Al	1	1	1	1
Si	-	1	-	1
S	1331	284	1420	254
Cl	485.	3155	849	4785
K	5	3	8	4
Ca	6	13	5	6
Ti	3	3	4	3
V	73	34	78	36
Cr	48	16	359	28
Mn	24	37	31	17
Fe	14	37	10	14
Ni	41	8	42	20
Cu	219	83	201	53
Zn	831	97	2397	271
As	1311	307	1381	478
Se	26836	9037	27709	9559
Br	-	705	-	3131
Rb	198	384	171	122
Sr	10	3	13	8
Pb	895	439	1883	443

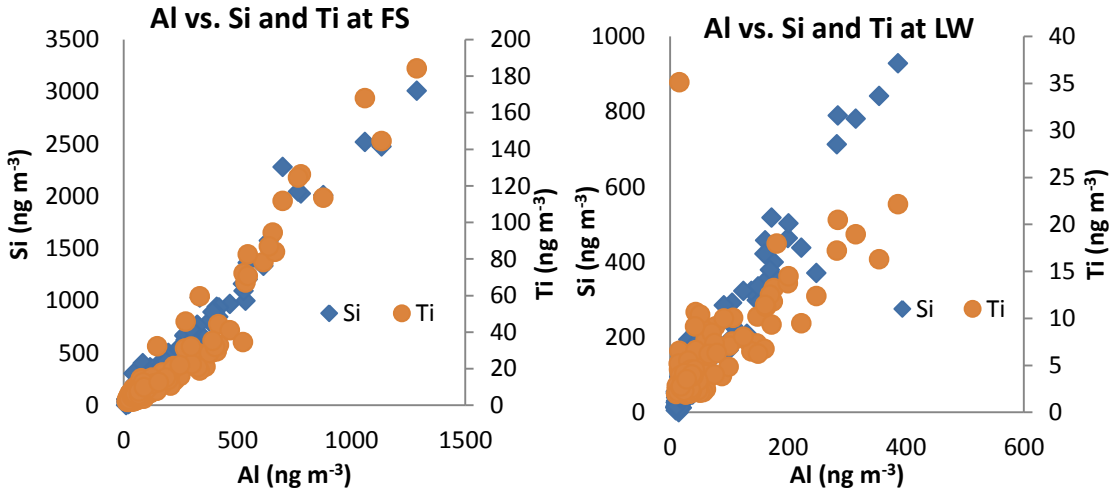

Figure 6.5: Scatter plots of coarse PM showing relationships among Al, Si and Ti at FS and LW

The significant influence of the steelworks could be established with higher EF values observed for the steel signatures of Fe, Mn, Zn, Pb and Cr. An elevated EF amount was observed for Br suggesting anthropogenic dominance which might be related to traffic influence. The ratio of Br/Pb has been adopted to establish traffic emission sources (D'Alessandro *et al.*, 2003). The values of Br/Pb for coarse PM in this study were 0.11 at FS and 0.48 at LW, close to 0.23-0.33 reported for traffic emissions in Italy (D'Alessandro *et al.*, 2003).

6.4.2.5 Correlational analysis among Streaker elemental components

Pearson correlation coefficients of PIXE data for fine and coarse PM at FS and LW sites are presented in Tables 6.7 and 6.8, respectively. In the Table 6.7a showed correlation coefficients for fine particles at FS. Strong correlations (R^2>0.70; p<0.01) were observed among Mg, Na and Cl depicting their related common origin. Al, Ca, Ti, Mn, Fe and Rb showed better correlations among themselves indicating possible emissions from the steelworks. Mn and Fe as well best markers for steelworks emissions showing a strong positive correlation (R^2=0.94; p<0.01) while K, As, Se and Zn also associated well with Mn and Fe. Pb is as well strongly associated with Zn (R^2=0.77; p<0.01) with the steel emission as the most suspected source.

A strong association existed between Cu and Sr (R^2=0.77; p<0.01) may signify contribution by the local traffic. Good relationship established between K and Se (R^2=0.77; p<0.01) suggested a woodsmoke emission. K and Se were reported to be emitted from combustion of plant tissues by Samsonov *et al.* (2005) during the fire episode of Siberian Scots pine forests. Ni and V are unusually anticorrelated at FS

showing their different emission sources. Instead, V has been correlated with Mn and Rb (R^2=>0.60) while Ni only strongly associated with Sr (R^2=0.68; p<0.01). A very strong correlation was also found betwen Se and Sr (R^2=1.0; p<0.01) similar to the relationship between Se and As (R^2=1.0; p<0.01). Se and As have been used as good marker elements for cokemaking emissions (Konieczynski *et al.*, 2012).

Pearson's correlations among the elemental components of coarse PIXE data is displayed in Table 6.7b. Most of the coarse elements showed better correlations than what was observed for fine Streaker data. A well defined correlation between coarse Br and Pb (R^2=0.81; p<0.01) may be related to a contribution from traffic emission (D'Alessandro *et al.*, 2003).

Table 6.8a shows the Pearson's correlation coefficients of fine Streaker data at LW. These elemental coefficients were not as strong at LW compared to the FS data. Notwithstanding, Mg, Na and Cl were strongly associated with R^2>0.80 (p<0.01). The notable crustal elements of Al, Ca, Sr and Ti were positively correlated. The high corelation coefficients between K, Mn, Fe, Zn, Sr and Pb might indicate emissions from the steel industry.

Table 6.7: Pearson correlations coefficients at FS for (a) $PM_{2.5}$

	Na	Mg	Al	S	Cl	K	Ca	Ti	V	Cr	Mn	Fe	Ni	Cu	Zn	As	Se	Rb	Sr	Pb
Na	1																			
Mg	.907**	1																		
Al	.370**	.598**	1																	
S	.223**	-.076	.141*	1																
Cl	.883**	.784**	.292**	.136*	1															
K	.285**	.456**	.577**	.269**	.151*	1														
Ca	.386**	.648**	.779**	.131*	.317**	.603**	1													
Ti	.323**	.525**	.720**	.112	.200*	.415**	.682**	1												
V	.500*	.624**	.482*	-.040	.422*	.272	.726**	.224	1											
Cr	.453**	.423**	.212**	.267**	.338**	.121*	.233**	.345**	.262	1										
Mn	.195**	.466**	.710**	.186**	.082	.727**	.891**	.639**	.692**	.076	1									
Fe	.223**	.501**	.722**	.183**	.096	.761**	.893**	.625**	.514*	.170**	.937**	1								
Ni	-.096	-.053	.008	.149*	-.084	.184**	.035	.025	-.264	-.009	.086	.058	1							
Cu	-.088	-.049	.100	.178**	-.042	.121*	.060	.213*	.144	-.096	.085	.048	.078	1						
Zn	.027	.099	.288**	.221**	-.015	.648**	.271**	.255**	.107	-.082	.462**	.375**	.144*	.167**	1					
As	-.292	-.329	.033	.747**	-.213	.386*	.352*	-.070	-.926	.394*	.467*	.342	.147	.698**	.486**	1				
Se	.379**	.619**	.572**	.117	.005	.766**	.668**	.504**	.537	.397**	.667**	.795**	.043	.034	.093	1.000**	1			
Rb	.157	.518**	.696**	.627**	.126	.440*	.678**	.572*	.731	.217	.789**	.879**	.388	-.367	-.176		.491*	1		
Sr	.137	.178	.466	.057	.289	.361	.748**	.809	-	.545	.460	.635*	.667*	.773**	.362		1.000**		1	
Pb	-.097	.026	.253**	.540**	-.098	.577**	.241**	.254*	-.020	.213**	.362**	.321**	.098	.255**	.772**	.551*	.105	.266	.135	1

(b) $PM_{2.5-10}$

	Na	Mg	Al	S	Cl	K	Ca	Ti	V	Cr	Mn	Fe	Ni	Cu	Zn	As	Se	Rb	Sr	Pb	Si	Br
Na	1																					
Mg	.774**	1																				
Al	.552**	.919**	1																			
S	.456**	.858**	.910**	1																		
Cl	.933**	.857**	.658**	.584**	1																	
K	.708**	.960**	.926**	.891**	.816**	1																
Ca	.475**	.894**	.947**	.927**	.613**	.896**	1															
Ti	.430**	.883**	.963**	.948**	.551**	.894**	.956**	1														
V	.662**	.860**	.896**	.873**	.728**	.836**	.935**	.906**	1													
Cr	.363**	.820**	.896**	.914**	.487**	.834**	.929**	.948**	.928**	1												
Mn	.380**	.859**	.947**	.950**	.512**	.869**	.967**	.988**	.917**	.951**	1											
Fe	.364**	.845**	.924**	.959**	.515**	.868**	.935**	.978**	.855**	.937**	.978**	1										
Ni	.346**	.443**	.533**	.534**	.319**	.456**	.509**	.560**	.243	.539**	.507**	.491**	1									
Cu	.355**	.618**	.693**	.610**	.440**	.599**	.621**	.640**	.812**	.630**	.619**	.604**	.416**	1	.							
Zn	.256**	.337**	.319**	.328**	.216**	.316**	.328**	.289**	.969**	.319**	.298**	.240**	.333**	.346**	1							
As	.613**	.743**	.843**	.918**	.619**	.715**	.913**	.955**	-	.795**	.965**	.966**	.518**	.242	.633**	1						
Se	.551*	.939**	.948**	.894**	.756**	.952**	.932**	.970**	-	.897**	.960**	.951**	.261	.544*	.808**	1.00**	1					
Rb	.205	.819**	.906**	.930**	.425**	.843**	.901**	.962**	.691	.916**	.956**	.988**	.547**	.619**	.045	.859*	.939**	1				
Sr	.695**	.829**	.771**	.788**	.732**	.732**	.783**	.791**	.988*	.638**	.733**	.797**	.438**	.374**	.308**	.993**	.904*	.911**	1			
Pb	.345**	.797**	.810**	.728**	.518**	.748**	.790**	.798**	.835*	.740**	.809**	.825**	.346**	.588**	.082	.921	.919**	.806**	.510**	1		
Si	.535**	.900**	.987**	.900**	.620**	.901**	.958**	.971**	.945**	.908**	.959**	.920**	.530**	.697**	.340**	.822**	.935**	.900**	.738**	.795**	1	
Br	.756**	.780**	.643**	.848**	.693**	.586**	.612**	.602**	.946	.582**	.705**	.747**	.464**	.477**	.590**	.863	-.716	.743*	.813**	.813**	.609**	1

*** P<0.05, ** p<0.01**

Table 6.8: Pearson correlation coefficients at LW for (a) $PM_{2.5}$

	Na	Mg	Al	S	Cl	K	Ca	Ti	V	Cr	Mn	Fe	Ni	Cu	Zn	As	Se	Rb	Sr	Pb
Na	1																			
Mg	.886**	1																		
Al	.211**	.402**	1																	
S	-.251**	-.238**	.238**	1																
Cl	.862**	.854**	.331**	-.127*	1															
K	.391**	.191**	.192**	.296**	.257**	1														
Ca	.230**	.352**	.701**	.298**	.293**	.539**	1													
Ti	.088	.184	.601**	-.009	.190*	.012	.386**	1												
V	-.230	-.226	.297	.091	-.325	.103	.029	-.430	1											
Cr	-.103	-.063	.098	.157*	-.057	.128	.159*	.007	.458*	1										
Mn	.390**	.201*	.145	.265**	.237**	.908**	.559**	.014	.308	.215*	1									
Fe	.028	.064	.370**	.444**	.005	.664**	.730**	.131	.215	.260**	.781**	1								
Ni	.133*	-.043	.032	.278**	.040	.626**	.245**	-.082	.078	.203**	.680**	.464**	1							
Cu	.021	.041	.001	.072	.014	.050	.047	.002	-.073	-.024	.069	.108	.214**	1						
Zn	.466**	.138*	-.048	.075	.263**	.822**	.259**	-.075	-.064	.050	.740**	.370**	.578**	.033	1					
As	-.304	-.280	-.005	.078	-.264	-.140	-.226	-.082	.380	.016	.490	.354	-.059	.094	.322	1				
Se	-.113	.047	.490**	.403**	-.147	.830**	.629**	.265	.569*	.406**	.818**	.889**	.441**	.338**	.270*	.836**	1			
Rb	.119	.330	.292	.173	.095	.331	.320	.102	.647	-.007	.272	.605**	.244	.011	.098		.661**	1		
Sr	-.090	-.028	.409	.463*	.039	.777**	.582**	.662*	-.049	.229	.783**	.741**	.423	-.226	.337	1.000**	.878		1	
Pb	.439**	.244**	.177*	.299**	.363**	.794**	.465**	-.001	.134	.174*	.761**	.621**	.590**	.424**	.671**	.114	.653**	.304	-.063	1

(b) $PM_{2.5-10}$

	Na	Mg	Al	S	Cl	K	Ca	Ti	V	Cr	Mn	Fe	Ni	Cu	Zn	As	Se	Rb	Sr	Pb	Si	Br
Na	1																					
Mg	.963**	1																				
Al	.345**	.447**	1																			
S	.644**	.767**	.623**	1																		
Cl	.960**	.932**	.335**	.605**	1																	
K	.792**	.863**	.699**	.840**	.810**	1																
Ca	.139*	.316**	.759**	.727**	.108	.583**	1															
Ti	.291**	.408**	.723**	.542**	.245**	.561**	.594**	1														
V	-.058	.148	.540*	.675**	-.146	.324	.720**	.266	1													
Cr	-.103	-.034	.245**	.210**	-.132*	.090	.363**	.315**	.780**	1												
Mn	-.171*	.044	.450**	.584**	-.336**	.218**	.806**	.330**	.677*	.415**	1											
Fe	-.084	.013	.369**	.420**	-.126*	.200**	.619**	.339**	.974**	.464**	.680**	1										
Ni	-.012	-.012	.035	.030	.055	.046	.059	.004	.485	.397**	.063	.096	1									
Cu	-.093	-.067	.063	.037	-.047	-.011	.117	.049	.328	.214**	.256**	.167*	.183**	1								
Zn	-.125*	.008	.096	.327**	-.149*	.216**	.545**	.094	.326	.167**	.522**	.293**	.104	.015	1							
As	-.389	-.301	.037	-.094	-.417	-.125	.331	.037	-	.490	.811**	.869**	-.557*	-.174	.807**	1						
Se	.154	.021	.671**	.440	.172	.260	.774**	.894**	-	.600*	.311	.978**	-.196	-.081	.270	.[a]	1	.963**				
Rb	.042	.092	.070	.354**	.051	.156	.341*	.111	.341	.481**	.227	.871**	.170	.450**	.143	.[a]	.963**	1				
Sr	.798**	.832**	.816**	.855**	.866**	.929**	.856**	.784**	.932*	.005	.430**	.384**	.057	-.080	.111	.130	-.361	.974**	1			
Pb	-.180	.090	.225	.551**	-.196	.341**	.677**	.306*	.087	.386**	.624**	.636**	.182	.080	.675**	-	.938	.474**	-.127	1		
Si	.345**	.440**	.969**	.618**	.351**	.722**	.752**	.723**	.597*	.215**	.393**	.360**	.043	.052	.129*	-.020	.759**	.080	.772**	.271*	1	
Br	.680**	.757**	.392**	.715**	.787**	.687**	.490**	.426**	.911*	-.108	.093	.005	-.048	.042	-.034	-.252	-.120	-.099	.658**	-.223	.340**	1

*** P<0.05, ** p<0.01**

The LW coarse particles correlation coefficients (Table 6.8b) showed significance among the sea salt (Na, Mg, Cl) and crustal elements (Al, Ca, Sr, Si and Ti). The steel metals (Mn, Fe, Ca, Pb, Zn) were also found to be strongly related. Association between Ni and V was better defined for coarse (R^2=0.49) than fine PM (R^2=0.09). Multi-emission sources of Br apart from traffic could be established with its strong correlation with Na, Mg, S, K, V and Sr. Notable emission sources of Br are marine, biomass burning, plant and biomass emission, gasoline fuel combustion, soil and salty marshes (Yvon-Lewis *et al.*, 2009).

6.4.2.6 Streaker elemental ratios

The ratios of the Streaker Ni/V for $PM_{2.5}$ was 0.32 at both FS and LW while for $PM_{2.5-10}$ the values were 0.14 and 0.31 at FS and LW, respectively. The Mn/Zn ratios for fine and coarse PM were 0.32 and 4.22 at FS, and 014 and 0.70 at LW. The observed ratios of Cl/Na, K/Na, Ca/Na, Mg/Na and SO_4/Na at FS were 0.40, 0.18, 0.41, 0.17 and 4.83 for fine PM and 1.05, 0.04, 0.36, 0.13 and 0.42 for the coarse fraction, respectively. At LW, the corresponding values of these elemental ratios were 0.50, 0.21, 0.23, 0.15 and 3.97 for $PM_{2.5}$ and 0.94, 0.03, 0.09, 0.11 and 0.23 for $PM_{2.5-10}$. The SO_4/Ca values at FS and LW were 11.9 and 17.6 for fine, and 1.16 and 2.52 for the coarse PM.

6.4.2.7 Polar plots of elements

Polar plots for each Streaker elemental concentration of fine and coarse PM at the FS monitoring site are presented in Figures 6.6 and 6.7. The marine significance of fine Na, Mg and Cl was predominant with the prevailing south-westerly wind blowing across the ore stockyard (ironmaking section) of the steelworks complex (see details of the steelworks locations in section 7, Table 7.1). Moderate concentrations of Mg were also

observed at the ironmaking section (BF/Sinter plants). Sulphur shows high values at the center of the polar plot, and also with the north-easterly wind direction probably due to residential emissions from fossil fuel combustion or traffic emissions. The steelworks' contribution to sulphur emissions was also identified at the south-westerly region of the wind sector polar plot.

High concentrations of Al, Ca, Fe, Mn, Cu, Zn and Pb were measured towards the south-westerly direction with probable emissions from the blast furnace (BF)/sinter /basic oxygen furnace steelmaking (BOS) sections of the steelworks. The mills unit of the steelworks shows elevated concentration of Cu. The wind sector plots of Cr and Ni suggest additional emission sources apart from the steelworks. Port Talbot shipping emissions from the docks may have contributed to fine Ni and Cr (Figueroa *et al.*, 2006). Elevated concentration of Cr towards the northerly and north-westerly wind sector may be attributed to emissions from a waste incineration plant located in Crymlyn Burrow, Swansea (Morawska and Zhang, 2002). Coarse Ni also exhibits similar wind plot pattern as observed for fine Cr.

The polar plots for Streaker coarse particulate matter at FS (Figure 6.7) revealed higher concentrations of most elemental concentrations towards the south-westerly axis of the steelworks. The wind sector plots of coarse metals are similar to those of fine PM except for Ni and Cr. The polar plot revealed emissions of coarse Cl from marine and steelworks sources. Silica and titanium were observed at elevated concentrations around the steelworks.

Figures 6.8 and 6.9 are polar plots for fine and coarse PIXE data at LW. The steelworks is located between the southern and south-western axis from the LW site. The polar plots of fine Na, Mg, Al, Ca and Cl at LW show high concentration towards the westerly prevailing wind due to marine and emissions from the dock. Cu showing a high concentration towards the northerly wind sector may suggest traffic emissions. The polar plots for Cr, Mn, Fe, Ni, Zn, Al, Ca and Pb showed the steelworks to be dominant emission source. Most of the coarse metals polar plots demonstrated emission trends similar to what was observed for fine plots with the exception of S, Ni and Cu. It appeared that shipping emissions contribute significantly to coarse Ni while the steelworks to fine Ni. This observation was also found for polar plots of Ni at the FS site.

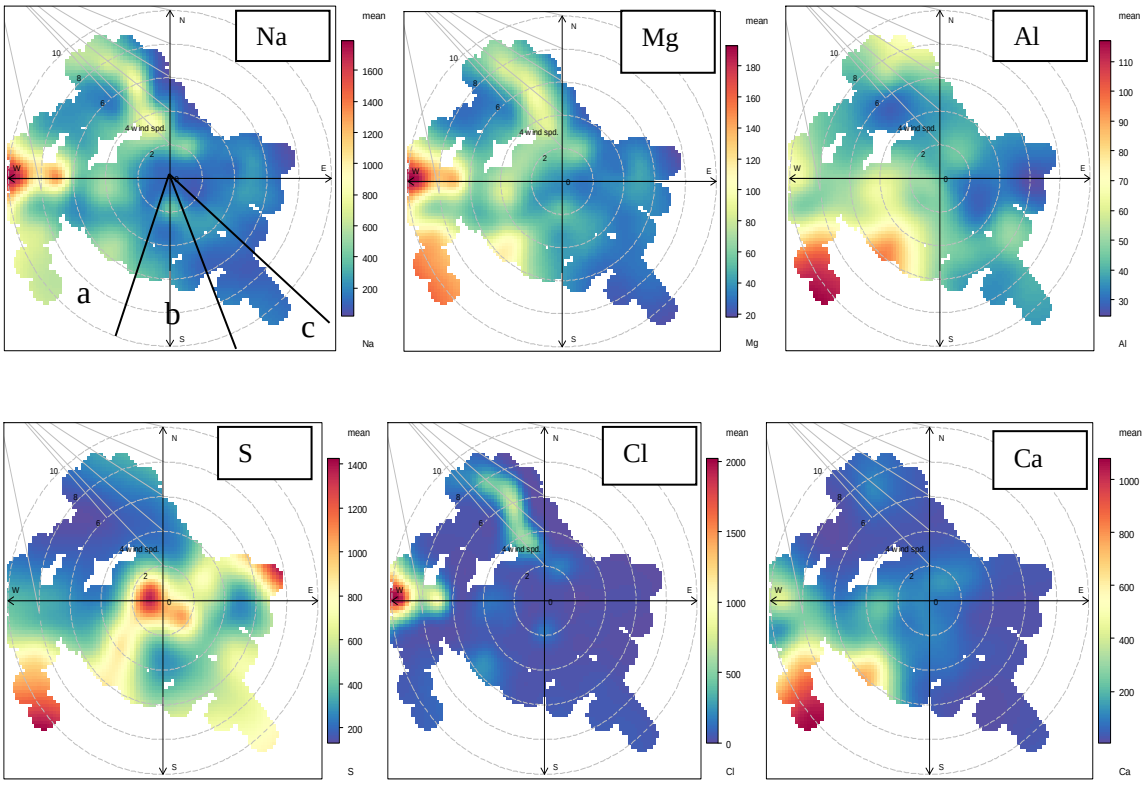

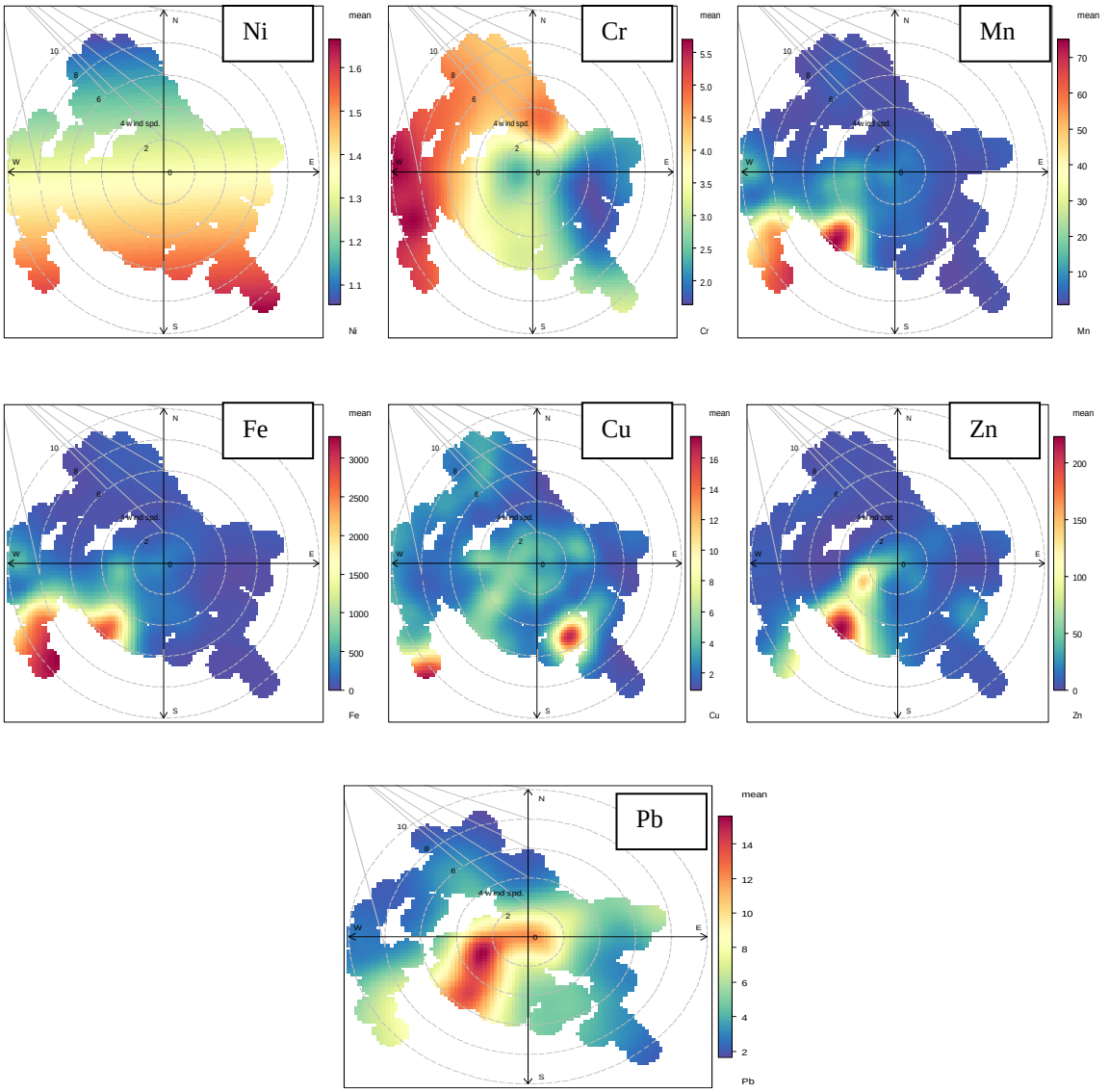

a-Ironmaking, b-Steelmaking, c-Mills

Figure 6.6: Polar Plots of elemental concentrations of Streaker $PM_{2.5}$ at FS

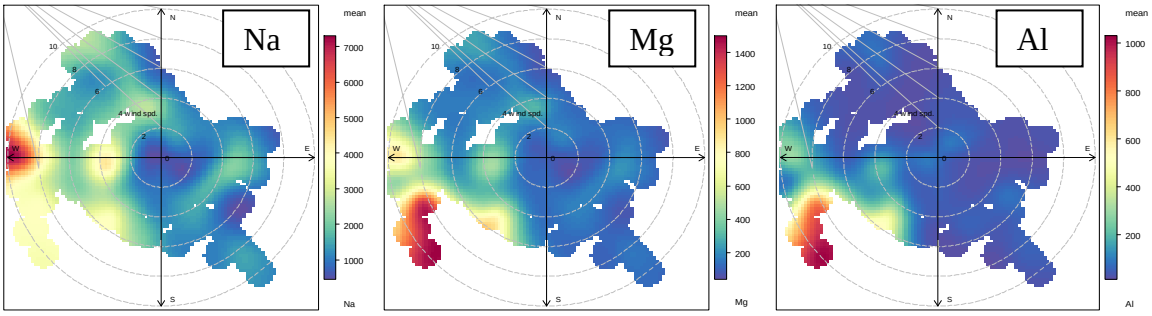

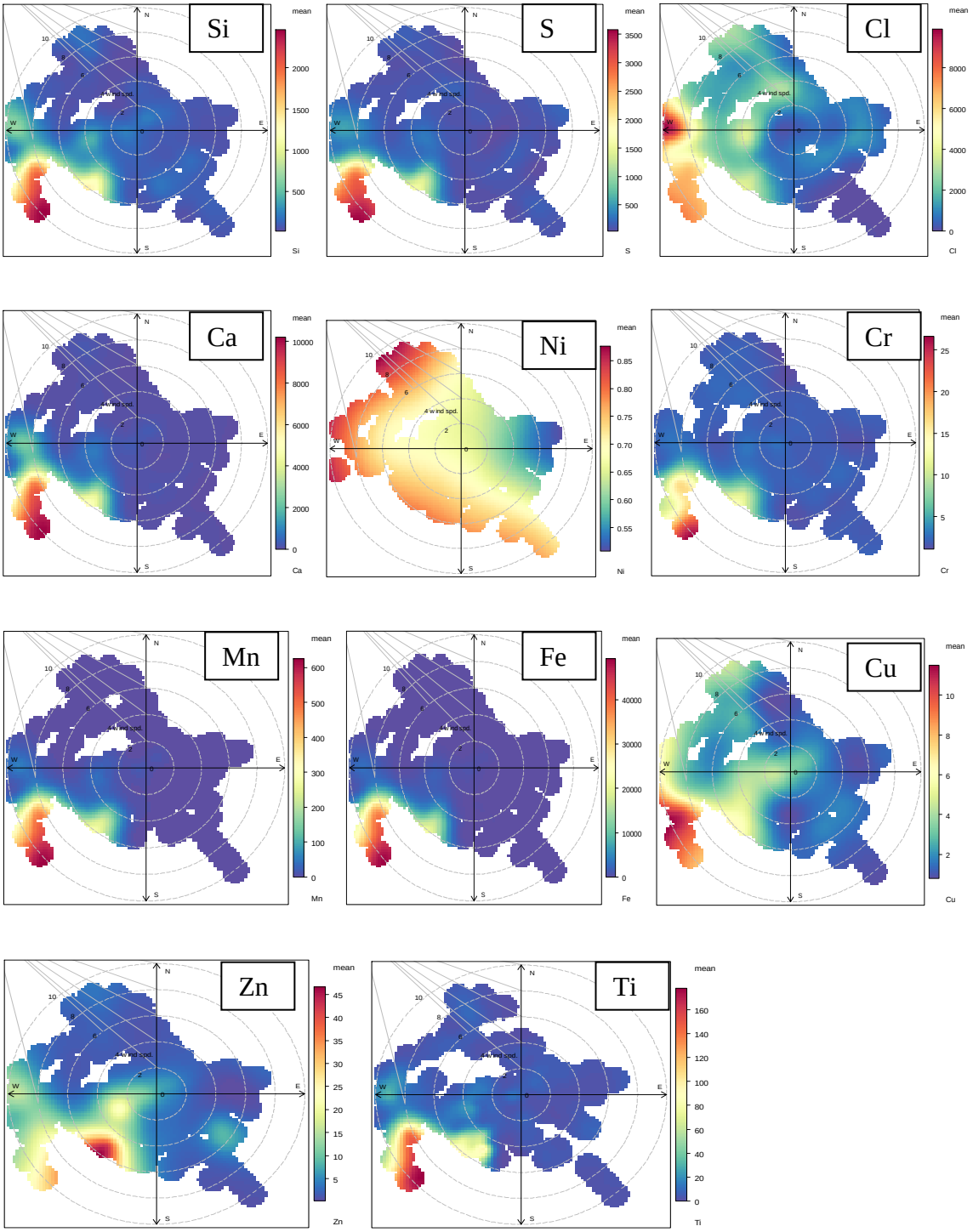

Figure 6.7: Polar Plots of elemental concentrations of Streaker $PM_{2.5-10}$ at FS

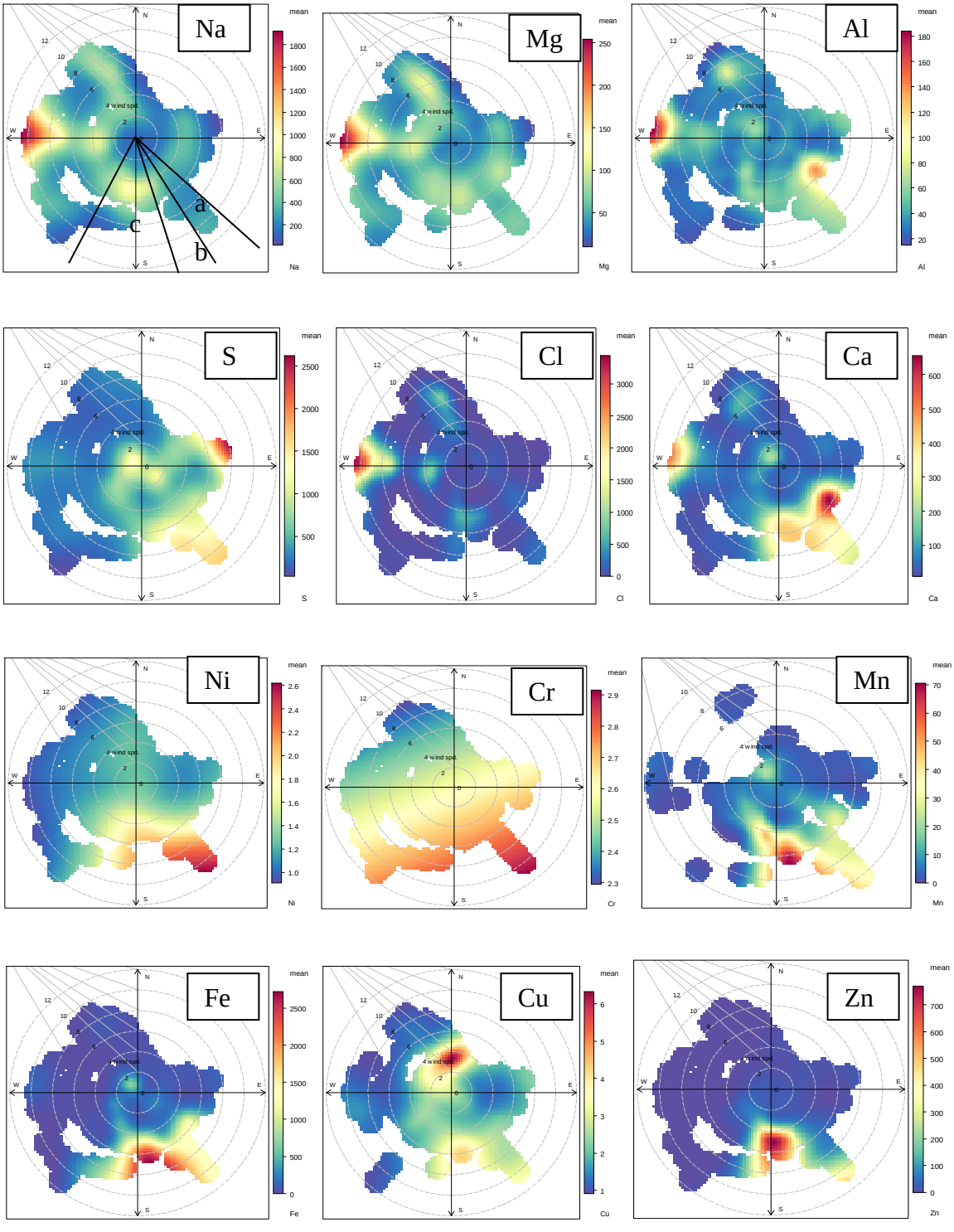
Na
Mg
Al
S
Cl
Ca
Ni
Cr
Mn
Fe
Cu
Zn
mean
a
b
c

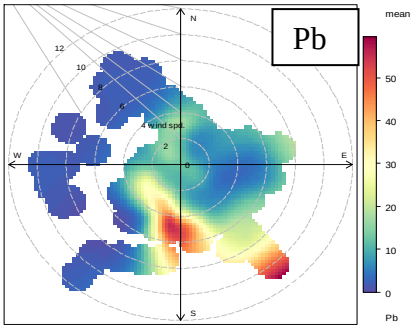

a-Ironmaking (BF/Sinter), b-Steelmaking & Mills, c-ore stockyard

Figure 6.8: Polar Plots of elemental concentrations of Streaker $PM_{2.5}$ at LW

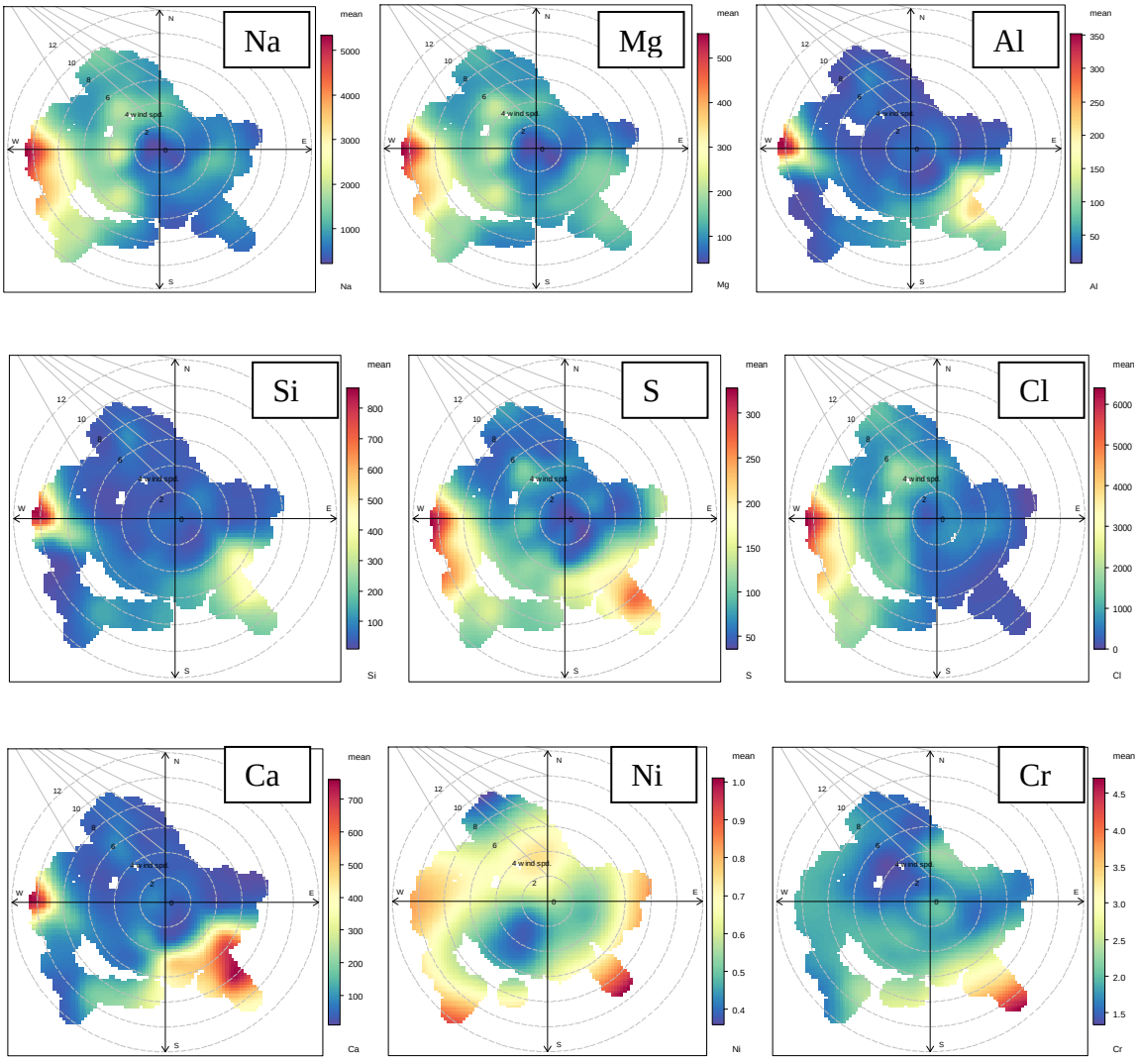

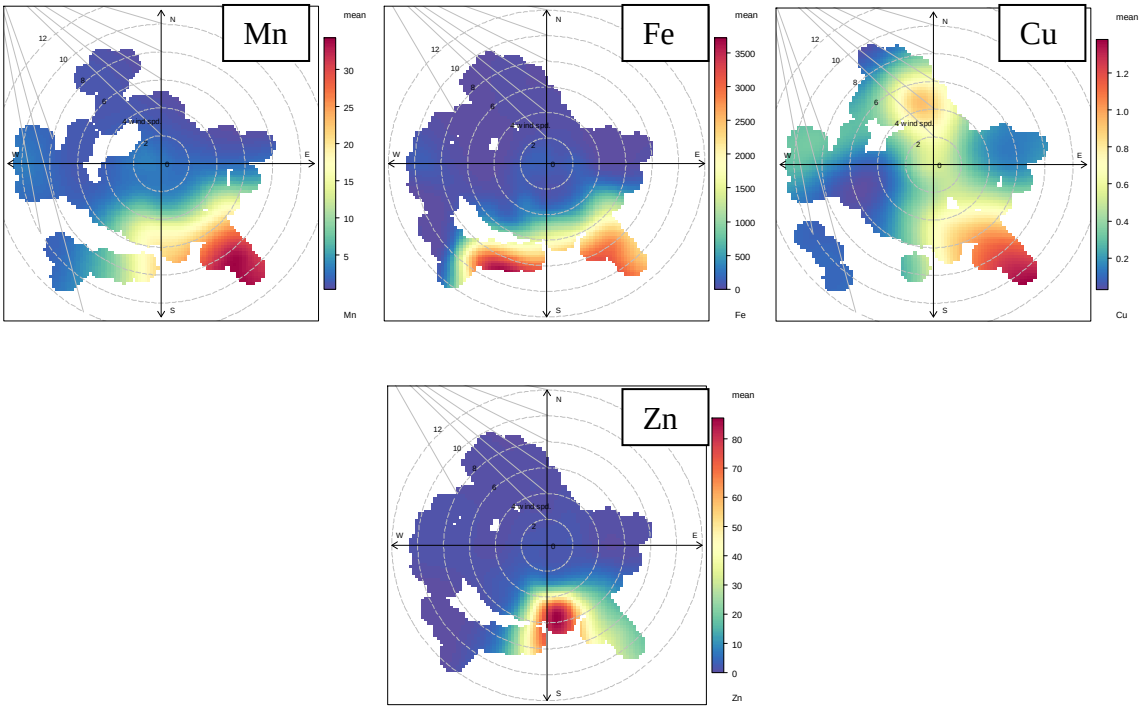

Figure 6.9: Polar Plots of elemental concentrations of Streaker $PM_{2.5-10}$ at LW

6.4.3 Organic carbon (OC) and elemental carbon (EC) concentrations of $PM_{2.5}$ at FS

OC and EC concentrations were measured on the $PM_{2.5}$ collected with the Digitel high volume sampler placed at FS monitoring site. Figure 6.10 shows the daily variations of OC and EC during Port Talbot campaign. A common elevated peak was observed for both PM chemical constituents on May 3. Higher concentrations of OC were also observed on April 26, May 4-5 and 13. The average concentrations of OC and EC were 1.0±0.36 and 0.68±0.29 µg m^{-3}, respectively. These carbonaceous species constituted 14 and 9% of the total $PM_{2.5}$ mass (Partisol), respectively. The mean OC/EC ratio calculated in this study was 1.6±0.6.

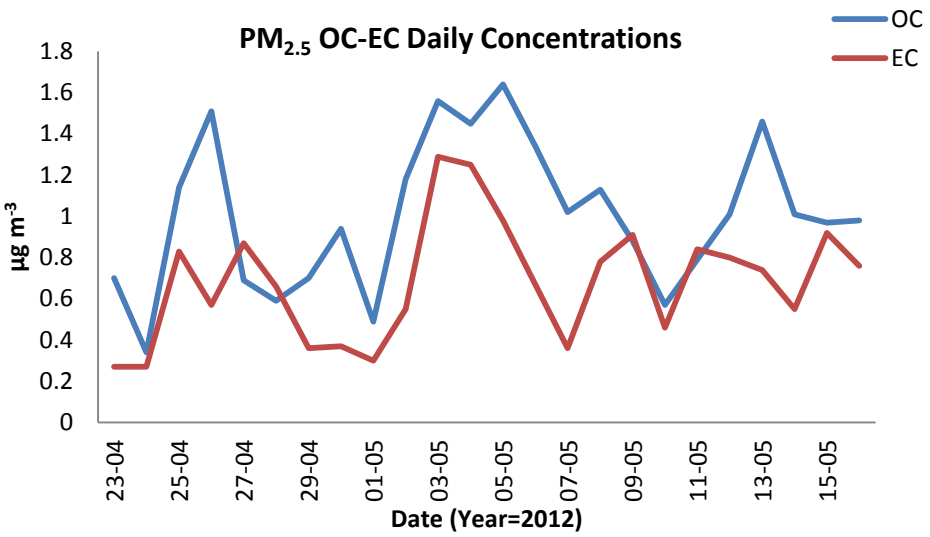

Figure 6.10: Daily variations of OC/EC during Port Talbot campaign

6.5 Partisol and Streaker Data Discussion

The daily plots of fine and coarse PM (May 4-16) for Partisol and Streaker data (Appendix XXI) has been consistent in trends and patterns for most observed chemical species at the FS and LW sites. The mean values of Partisol and Streaker data are comparable for Na, Mg, S, Ca and Cr for fine PM at FS, and Na, Mg, Cu and Pb for LW $PM_{2.5}$ (Appendix XXII). In the coarse fraction, the daily average of the two instruments are not far apart with close data for Al, Ca, Cr, Cu and Zn at FS, and Na, Mg, Cr, Cu and Zn at LW. The least squares regression plots shown in Appendix XXIII further confirm the strong relationships between Partisol and Streaker data for most measured chemical components.

The Partisol $PM_{2.5}$ was dominated by water soluble species at all the four sites in this study, which is in line with studies around the world. PIXE analysed Na, Mg, Cl, K, Ca and S are also the major components of Streaker $PM_{2.5}$. At the industrial and urban areas of Korea, Han *et al.* (2008) measured ionic constituents in $PM_{2.5}$ to form 35-60% of the total $PM_{2.5}$ mass. Related study in Taiwan found NH_4^+, SO_4^{2-}, and NO_3^- to constitute 70-

90% ionic components of PM<1.0 µm (Tsai *et al.*, 2012). It is obvious from the water-soluble species data that the activities of the steel industry spread across the monitoring sites probably due to local meteorology.

With Partisol instrument, Prince Street monitoring site recorded higher metal concentrations than the rest of the stations probably due to its closeness to the blast furnace (BF) plant. Both Streaker and Partisol demonstrated Fe and Al as the dominating metals at FS and LW. Mn and Zn are other trace metals measured at significant concentrations with Partisol and Streaker instruments. Fe, Al, Mn and Zn are typical emissions from the steelmaking industries (Hleis *et al.*, 2013). The previous work of Moreno *et al.* (2004b) based on scanning electron microscopy (SEM) has indicted steelworks as the major culprit to total load of metals (Fe, Zn, Mn and Ni) in Port Talbot. Unlike this study, where Fe and Al were the most abundant measured metals, Moreno *et al* (2004b) study has suggested Fe and Zn as the most elevated elements. Zinc is the third most abundant metal in this study. Al is a crustal element (Wang *et al.*, 2005) and hence the activities of the construction works during the period of this study might have responsible for the discrepancy against the Moreno *et al.* (2004b) work.

The values of Partisol NO_3^-/nss-SO_4^{2-} mass ratios which were generally < 0.45 at the four monitoring sites for fine and coarse PM indicates a greater impact of stationary emission sources (Figure 6.1). This could be directly linked to the activities of the steel industry (cokemaking) or alternately from domestic heating involving coal combustion. Studies at the industrial site of Castello, Spain showed low NO_3^-/SO_4^{2-} (0.30) value in PM_{10} (Viana *et al.*, 2008b). The low NO_3/SO_4 ratio for $PM_{2.5}$ in this study has shown good agreement

with the studies conducted in industrial/urban cities (Viana *et al.*, 2008b; Gupta *et al.*, 2012). In the UK, NO_3^-/SO_4^{2-} calculated at Birmingham roadside was 0.30-1.82 (Harrison *et al.*, 2003) while a higher ratio (1.28-1.47, for total suspended particles) has been reported in France (Ledoux *et al.*, 2006) and Italy (3.48 for $PM_{2.5}$, Lonati *et al.*, 2005).

The values of Cu/Sb, Fe/Sb and Fe/Cu ratios are important to identify traffic contributions. The corresponding values for these ratios in this study are 2.6-3.7, 196-374 and 75-100 for $PM_{2.5}$; 4.8-11.2, 2180-4427 and 290-583 for $PM_{2.5-10}$, respectively. At the roadside in Barcelona, Amato *et al.* (2011) has reported ratios of Cu/Sb, Fe/Sb, Fe/Cu in PM_{10} as 8.0, 137 and 17 against the values of 6.8, 158 and 29, respectively observed at an background site. Sternbeck *et al.* (2002) assigned Cu/Sb ratio of 4.6 to brake dust emissions. Cu/Sb ratio of 1.3 has been suggested by Adachi and Tainosho (2004) as the traffic signature precisely from the brake lining.

The Cu/Sb ratios obtained has agreed well with these reported values. The Cu/Sb ratio for $PM_{2.5-10}$ is closer to Sternbeck *et al.* (2002) value indicating traffic influence while the extreme ratio values of Fe/Cu and Fe/Sb could be linked to the activities of the steelworks. Comparing these ratios with Amato *et al.* (2011) study, Cu/Sb ratio is lower while Fe/Sb and Fe/Cu ratio values are extremely high. Suggestion for high Fe/Sb and Fe/Cu value could be explained by elevated concentration of Fe, which is a major steelworks (Mazzei *et al.*, 2008; Hleis *et al.*, 2013).

According to Figueroa *et al.* (2006), Ni/V value around 3.0 suggests oil burning while a range 0.3-0.5 indicates gas or diesel burning. The values of Ni/V (0.14-0.38) for Partisol

and Streaker $PM_{2.5}$ and $PM_{2.5-10}$ showed contribution from fuel combustions. The higher Ni/V ratio at LW (0.45 for Partisol $PM_{2.5-10}$ and 0.31 for Streaker $PM_{2.5-10}$) is similar to 0.32 value reported by Pandolfi *et al.* (2011) for shipping emissions at the Algeciras Bay in southern Spain. This might be expected at LW due to its closeness to the Docks. The Ni/V values are also in line with values assigned to traffic and boating by Figueroa *et al.* (2006). The PCA rotation in chapter 7 has identified oil combustion or shipping emissions at both LW and FS.

Pb and Cd are tracers for steelworks (Oravisjarvi *et al.*, 2003). Leaded gasoline could also be responsible for emission of Pb (Duan *et al.*, 2012). Leaded gasoline has been banned in most cities of the world with subsequent reduction in atmospheric lead. However, Pb is still present in road dusts in the cities (Amato *et al.*, 2009). Recent work of Razos and Christidies (2010) has reported Pb/Cd ratios of 88 and 99 in $PM_{2.5}$ and PM_{10} at an industrial site in Greece, which were attributed to heavy traffic emissions. The Pb/Cd values obtained in this study may be linked to the steel emissions comparable to the values obtained from the Tsai *et al.* (2007) and USEPA speciates steel profiles. Some studies conducted near steel industries have also recorded lofty ratios of Pb/Cd (Cetin *et al.*, 2007, Querol *et al.*, 2007).

The influence of marine contribution to aerosol pollution at Port Talbot has been calculated for Partisol and Streaker data with ratios of Cl/Na, K/Na, Ca/Na, SO_4/Na and Mg/Na. In Partisol $PM_{2.5}$, Cl^-/Na^+ mass ratio was less than 1.8 (Ooki *et al.*, 2002) at all the monitoring sites and could still be assigned to sea salt source. The corresponding Cl/Na ratio for Streaker $PM_{2.5}$ at FS was 0.41. Bourotte *et al.* (2007) reported a range of Cl/Na

ratios of 1.0-1.7 to be marine source. The Partisol Cl/Na ratios at FS and LW were higher than the values obtained for the Streaker. The values of Cl/Na for both instruments were lower than the sea water ratios suggesting additional contribution by the steelworks (Oravisjarvi *et al.,* 2003; Dall'Osto *et al.,* 2008). The mass distribution pattern for MOUDI Cl^- revealed bimodal peaks suggesting both natural and anthropogenic contributions. The Cl/Na values observed for coarse PM in this study is similar to what Dos Santos *et al.* (2012) reported at the coastal areas of Buenos Aires in Argentina suggesting marine influence. Mg/Na ratios for both Partisol and Streaker are perfectly aligned with marine incorporation while K/Na, Ca/Na and SO_4/Na ratios were greater than seawater ratios for Partisol and Streaker data. However, the corresponding values of K/Na, Ca/Na and SO_4/Na for Streaker $PM_{2.5\text{-}10}$ at the LW site depicted more of marine influence. The Mg/Na ratio observed in this work is similar to the observation of Hara *et al.* (2012) at the Antarctic coast. Ooki *et al.* (2002) has attributed K/Na ratio of 0.11-0.56 to coal combustion. K/Na ratio in this study (0.30-0.46 for Partisol and 0.18-0.21 for Streaker $PM_{2.5}$) fell within this range, and could therefore be traced to residential coal combustion or cokemaking steelworks. Globally, around 70% of the steel industries are absolutely dependent on the use of coking coal for production (World Coal Association, 2013).

The OC/EC ratio value of 1.6±0.6 obtained during the sampling period suggests contributions by the local traffic (Hildermann *et al.*, 1991; Watson *et al.*, 1994).

6.6 Conclusion

Chemical compositions of Partisol sampled-fine and coarse particles at the industrial and coastal town of Port Talbot have been presented. Variations and trends were observed in the data collected from element to element and site to site. High abundance of elements such as non sea salt-sulphate, ammonium, nitrate and iron were observed for fine PM while chloride and sodium were leading components of $PM_{2.5-10}$ at the monitoring sites. Water soluble constituents were the dominant constituents of both PM categories ranging between 42-87% for fine and 31-62% for coarse PM. Metal components represented between 4-5% of coarse and fine PM.

The hourly elemental concentration data of Streaker fine and coarse PM showed episodic pollution days common to the two selected sites. The sum of PIXE elemental data showed similar daily variations with that of FDMS mass concentrations. Most of the observed elements in the $PM_{2.5}$ and $PM_{2.5-10}$ fractions were higher at FS than LW site. High EF values observed for most measured components by Partisol and Streaker samplers indicated predominance of anthropogenic activities attributable to steelworks emissions. The interpretation of the EFs is dependent upon the assumption that there are no other sources of Al (used as the reference element) in the particles. The polar plots have also revealed the steelworks as a major contributor to elemental pollution in Port Talbot.

CHAPTER 7- RECEPTOR MODELLING OF PARTISOL AND STREAKER SAMPLES

7.1 Abstract

This section explains the source apportionment of hourly and daily PM data collected with Streaker and Partisol instruments. The two receptor models used are positive matrix factorization (PMF) and principal component analysis (PCA). Data analysis using PMF identified between 6 and 7 factors from the Partisol and Streaker data, respectively. PCA identified only 4-6 components. Both PMF and PCA solutions for datasets from the two measurement techniques were able to resolve different steel processing units including emissions from the sinter plant, blast furnace and basic oxygen furnace steelmaking plant. The PMF and PCA model showed secondary aerosol and steelworks emissions as the main contributors to $PM_{2.5}$ while marine aerosol and steelworks emissions dominated the PM_{10}. Among the steelworks factors, the blast furnace appeared to be the largest emitter of PM_{10} in the study area. The influence of steelworks sources on ambient particulate matter at Port Talbot was clearly distinguishable for several separate processing sections within the steelworks.

7.2 Introduction

Both acute and chronic exposures to airborne particulate matter (PM) have been associated with adverse effects upon health including premature mortality (Pope and Dockery, 2006). Consequently, the World Health Organisation (WHO, 2006) recommends strict guidelines for airborne particulate matter measured both as PM_{10} and $PM_{2.5}$. Governments around the world are developing and applying abatement strategies to reduce population exposures to particulate matter. The development of cost-effective strategies depends critically upon a quantitative knowledge of the contribution of different sources to airborne particulate matter concentrations. This is best determined by receptor modelling methods of which Positive Matrix Factorization (Paatero and Tapper, 1994) is probably the most commonly applied.

For many years the town of Port Talbot has suffered some of the worst air quality in the United Kingdom (AQEG, 2011) and earlier work (Moreno *et al.*, 2004a, b; Dall'Osto *et al.*, 2008; Hayes and Chatterton, 2009) has indicated the steelworks as a major contributor to local PM concentrations. However, knowledge has been lacking as to the size of the contribution of the steelworks to airborne PM concentrations as well as the identity of the predominant sources within the steelworks.

The basic operational steelworks units in Port Talbot are cokemaking, sintering, basic furnace, basic oxygen furnace and other steel processing units (Passant *et al.*, 2002). These units have been identified as major emission sources of important heavy metals such as chromium, copper, lead, cadmium, arsenic, zinc, manganese, iron, nickel, vanadium and selenium (Passant 2002; Moreno *et al.*, 2004a; Dall'Osto *et al.*, 2008; Table 7.1).

Table 7.1: Summary of emissions from the steelworks components (adapted from Dall'Osto *et al.*, 2008)

Sector/plant	Plant/operation	Emission type	Components	Wind Sectors			
				FS	PS	DS	LW
	Ironmaking			*190–270°*	*220-280°*	*270-310°*	*110-140°*
Sinter plant	Iron ore sintering	Stationary source – continuous	KCl, Fe, Pb, Zn, Mn				
	Sinter plant de-dusting	Stationary source – continuous	Fe, Mn				
Blast furnace	Tapping	Fugitive – intermittent	Fe, Mn				
	Slag processing	Stationary source – intermittent	Ca, Al, Si, S				
	Stove heating	Stationary source – continuous	CO_2, SO_2, NO_x				
Raw materials	Unloading, stocking, blending wind entrainment	Fugitive – intermittent	Fe, Ca, Mg, Mn				
	Steelmaking/cokemaking			*170–190°*	*180-220°*	*230-270°*	*140-170°*
BOS plant	Steelmaking	Stationary source – batch	Fe, Zn, Pb,Mn				
	Charging, blowing, tapping	Fugitive – intermittent	Fe, Zn, Pb, Mn				
Cokemaking	Battery underfiring	Stationary source - continuous	CO_2, SO_2, NO_x, soot (C)				
	Charging	Fugitive – intermittent	Organics, particulates				
	Door and top leakages	Fugitive – intermittent	Organics, particulates				
	Pushing	Fugitive – intermittent	Particulates				
	Quenching	Fugitive – intermittent	Particulates, soluble salts				
	Mills			*150–170°*	*150-180°*	*180-230°*	*130-150°*
Rolling mills	Hot mill	Fugitive – intermittent	Fe, coolants				
	Cold mill	Fugitive – intermittent	Lubricants, coolants				

FS-Fire Station, PS-Prince Street, DS-Dyffryn School, LW-Little Warren

As a complement to the reported studies at Port Talbot steelworks, the present study has applied Positive Matrix Factorization to identify and apportion emission sources of particle pollutants in the study area. The aim was not only to identify the steel emission

profiles, but also to attribute emissions to specific production units in the integrated steel complex.

7.3 Results and Discussion

7.3.1 Positive matrix factorization (PMF)

7.3.1.1 PMF for Partisol PM data

Figure 7.1 (a-c) presents the PMF profiles for Partisol $PM_{2.5}$, $PM_{2.5-10}$ and PM_{10} data. The optimal PMF solution showed six factors for $PM_{2.5}$ (Figure 7.1a). The first factor is significant for Cl^-, Na^+ and Mg^{2+} and accounted for 79, 67 and 61% of their modelled concentrations, respectively. This component accounted for 19% of $PM_{2.5}$ mass determined with a Filter Dynamic Measurement System (FDMS) instrument. This factor represents marine aerosol. The second factor describes secondary aerosol with significant percent contributions to NO_3^- (89%), NH_4^+ (79%) and non-sea sulphate (nss-SO_4^{2-}) (70%). This source makes the largest contribution to $PM_{2.5}$ of 36%. Moderate contributions to Pb (27%) and K^+ (13%) also occurred in this factor, suggesting likely regional transport of Pb and K^+ alongside the local emissions. Factor 3 is the largest contributor to K^+ with 61% of the modelled concentration loading for this factor. This represents a biomass burning emission source, most probably woodsmoke (Naeher *et al.*, 2007; Harrison *et al.*, 2012c). Mg^{2+}, Na^+ and nss-SO_4^{2-} also occurred in this factor with moderate percent contributions of 29, 15 and 12% respectively. Factor 4 is characterised by large contributions to Fe (67%), Mn (63%) with moderate amounts of Ba (28%), Pb (17%), K^+ (17%) and Cu (13%). This component may derive from the blast furnace (BF) plant of the steelworks. Fe has been generally observed at all the processing units of integrated steel production (Oravisjarvi *et al.*, 2003; Machemer, 2004; Moreno *et al.*, 2004a; Connell *et al.*, 2006;

Tsai *et al.*, 2007; Dall'Osto *et al.*, 2008; Hleis *et al.*, 2013). However, the recent source profile study of integrated steel facilities by Hleis *et al.* (2013) showed an elevated Fe concentration from the BF relative to the other steelworks units. The study of Mazzei *et al.* (2008) adopted Fe and Mn as marker elements for BF emissions. The fifth factor shows large contributions to Sb, Cu and Ba constituting 92, 68 and 59% of their modelled concentrations, respectively. Other elements that formed an appreciable fraction of this source include Pb (14%), Fe (12%) and Mn (10%). These trace metals are a signature of road traffic especially from brake wear (Sternbeck *et al.*, 2002; Thorpe and Harrison, 2008). About one-fifth of the measured $PM_{2.5}$ mass concentration is attributed to the traffic factor. The sixth factor in the $PM_{2.5}$ PMF profile is significant for Cd (90%), Zn (77%), Pb (46%), Mn (22%), Cl^- (14%) and Fe (13%). This factor is a mixed steelworks source from the basic oxygen furnace steelmaking (BOS) and sinter plants. The use of galvanised scrap in the BOS has been stated to increase Zn concentrations in the steelworks processing section (Oravisjarvi *et al.*, 2003; Hleis *et al.* 2013). The study of Hleis *et al.* (2013) has reported KCl has a major constituent of sinter plant emissions. Particle dust analysis from the industrial steelworks monitoring site in Rahee, Finland attributed 98 and 96% of measured Cd and Pb concentrations in $PM_{2.5}$ to sinter plant emissions (Oravisjarvi *et al.*, 2003).

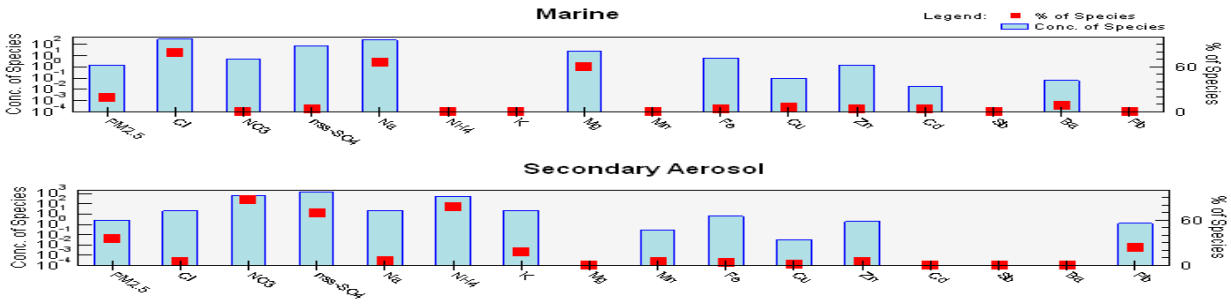

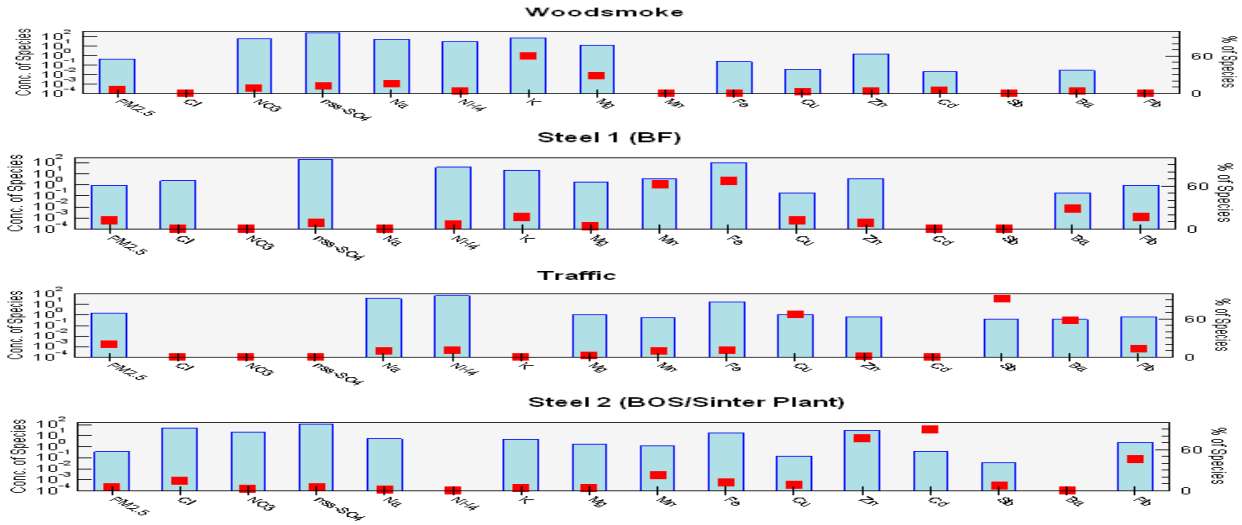

(a) Partisol $PM_{2.5}$

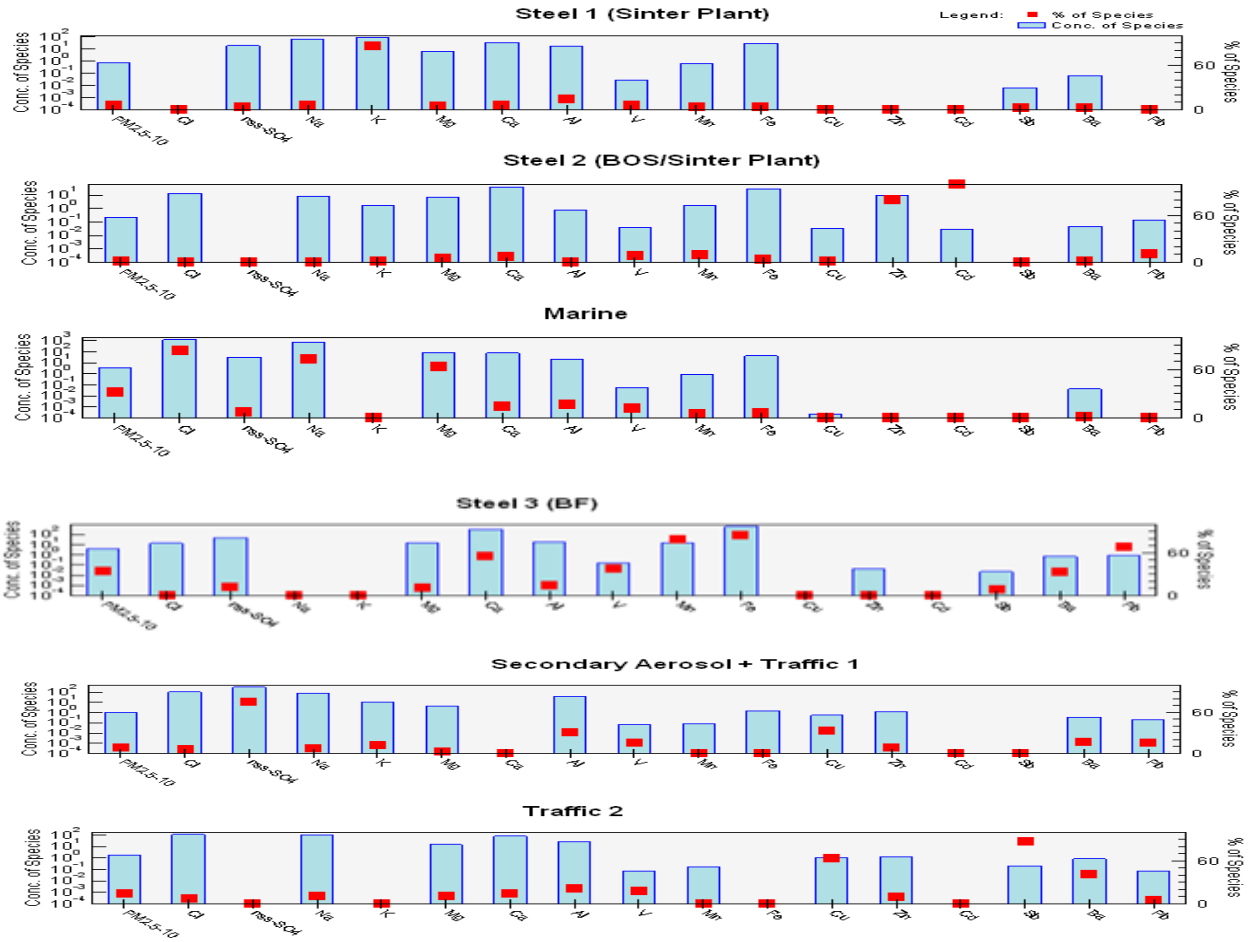

(b) Partisol $PM_{2.5\text{-}10}$

(c) Partisol PM_{10}

Figure 7.1: PMF source profiles for combined daily Partisol PM fractions at the four sites in Port Talbot

Figure 7.1 (b) shows the PMF profiles for Partisol coarse PM ($PM_{2.5\text{-}10}$) data where six factors were resolved by the PMF. In Factor 1 there is an elevated contributions to K^+ (86%) and a moderate contribution to Al (14%). This factor suggests steel emissions from the sinter plant. Coarse K^+ has been measured at elevated concentration at the vicinity of a

steel industry in France (Hleis *et al.*, 2013). A strong loading for Cd (100%) and Zn (80%) with 11% of modelled Pb characterizes the PMF profile in Factor 2 representing combined steelworks emissions from the BOS and sinter plants. In the third factor are found large amounts of Cl^- (85%), Na^+ (73%) and Mg^{2+} (64%) indicating a marine aerosol. About one-third of $PM_{2.5-10}$ mass is contributed by this factor. The fourth factor represents a source deriving from the steelworks (BF). Elements showing highly significant loadings in this factor include Fe (85%), Mn (80%), Pb (69%), Ca^{2+} (56%), V (38%) and Ba (34%). The crustal element, Al also appeared in this factor with its 14% profile concentration given to the factor, and nss-SO_4^{2-} and Mg^{2+} show moderate contributions from this factor. However, the occurrence of V in this source is suggestive of heavy oil burning or even shipping emissions (Figueroa *et al.*, 2006; Mazzei *et al.*, 2008; Amato *et al.*, 2009; Pandolfi *et al.*, 2011) consistent with sources in the harbour area. Factor 5 was unable to be separated by the PMF solution and mixed emission sources were identified. The factor is dominated by secondary aerosol having a contribution of 75% to the nss-SO_4^{2-} modelled concentration. Cu (34%), Al (32%), Ba (17%), V (16%) and K^+ (12%) are included in this factor suggesting traffic emissions may be accompanying the secondary particles. The sixth PMF factor of $PM_{2.5-10}$ demonstrates a highly significant contribution to Sb (88%), Cu (64%) and Ba (41%) representing a non-exhaust traffic source (Sternbeck *et al.*, 2002; Thorpe and Harrison, 2008). Moderate loadings of Al (22%) and Ca^{2+} (15%) are also found in this component also suggesting traffic.

PMF results for PM_{10} gave an optimal 7 distinctive factors (Figure 7.1 (c)). The first PMF component for PM_{10} is significant for Fe, Mn and Ca^{2+} with their 70, 65 and 41% of profile mass contributed. Ba (23%) and Pb (22%) also showed moderate loadings for this

factor. A steelworks (BF) factor is indicated. Factor 2 is dominated by the mixed steel sources of BOS and sinter plant with strong loadings for Zn (84%) and Cd (73%). Other elements that contributed moderately to this factor include Pb (40%) and Mn (13%). This factor is similar to Factor 6 and Factor 2 in $PM_{2.5}$ and $PM_{2.5-10}$, respectively. Marine aerosols contributing to Cl^- (82%), Na^+ (72%) and Mg^{2+} (58%) are highly significant for Factor 3. Elevated contributions to the traffic signature elements Cu (60%) and Ba (56%) characterize Factor 4. Ca^{2+} and V are contributed 32 and 28% respectively by this source. The PMF solution separated the PM_{10} secondary aerosol into two in contrast to the observations for $PM_{2.5}$ and $PM_{2.5-10}$. NH_4^+, nss-SO_4^{2-} and NO_3^- are dominating species in Factor 5 contributing 68, 43 and 21% to their profile masses respectively from this factor. This factor represents a secondary sulphate source. Factor 6 is also a secondary aerosol source dominated by NO_3^- (67%) and nss-SO_4^{2-} (28%) as a lesser component. The factor describes a secondary nitrate source. The abundance of K^+ (65%) with a significant contribution to Mg^{2+} (21%) in Factor 7 suggests another steelworks emission from the sinter plant.

Relationships between the measured and predicted concentrations for the 3 categories of PM are shown in equation 5.1:

$PM_{2.5} = 0.99x-0.21$, $r^2=0.78$

$PM_{2.5-10} = 0.94x+0.35$ $r^2=0.96$

$PM_{10} = 0.93x+0.81$ $r^2=0.95$ ***(5.1)***

The equations showed well-defined associations. The values of the slopes (0.93-0.99) and correlation coefficients, r^2 (0.78-0.96) showed the good performance of the PMF for the Partisol data. For individual chemical species, r^2 ranged from 0.71-0.95 for those within $PM_{2.5}$, 0.65-0.99 for $PM_{2.5-10}$ and 0.68-0.97 for PM_{10}.

Appendix XXIV represents the daily contributions by each identified factor to particulate fractions at each site. The fine $PM_{2.5}$ showed the greatest peak on May 4 at FS, DS and LW the large contribution by secondary aerosol. Distinguishable peaks of pollution episodes were observed for $PM_{2.5-10}$ at FS on April 18 and 26, and May 8 and 11 with none of these peaks coinciding with episode observed at DS on April 19 and May 15, and LW on April 22. The episodes of marine aerosol were prominent at each site contributing to coarse particle concentrations. The contribution from the steelworks is also observed on these episodic days. The daily contribution of profile factors to particle pollution for PM_{10} is similar to that of $PM_{2.5-10}$. This suggests that PM_{10} episodes are influenced by $PM_{2.5-10}$ concentrations in Port Talbot. Hayes and Chatterton (2009) reported that PM_{10} at Port Talbot is more impacted by the coarse than fine PM fraction.

Figure 7.2 illustrates the source contribution percentages of each factor for $PM_{2.5}$, $PM_{2.5-10}$ and PM_{10} at the four monitoring sites. The fine PM portion is dominated by secondary aerosol at the sites in the percentages of 52, 36, 57 and 58% at FS, PS, DS and LW respectively. The combined steelworks source formed the second largest contributor to $PM_{2.5}$ at the four sites except at LW. The steelworks has most impact at PS and least at LW during this sampling period. Marine, woodsmoke and traffic are other sources contributing to $PM_{2.5}$ across the four sites. Marine aerosol clearly dominated the coarse

PM fractions (38-60%). As expected, LW showed marine aerosol to represent more than half of the total observed coarse PM fraction. The combined steelworks source is another major contributor to $PM_{2.5-10}$ at FS and PS while secondary aerosol and traffic is next to marine at DS and LW. The secondary aerosols (secondary sulphate and nitrate) dominated PM_{10} pollution at all the stations followed by the marine source. The traffic contribution to PM_{10} is more pronounced at the PS and FS monitoring sites.

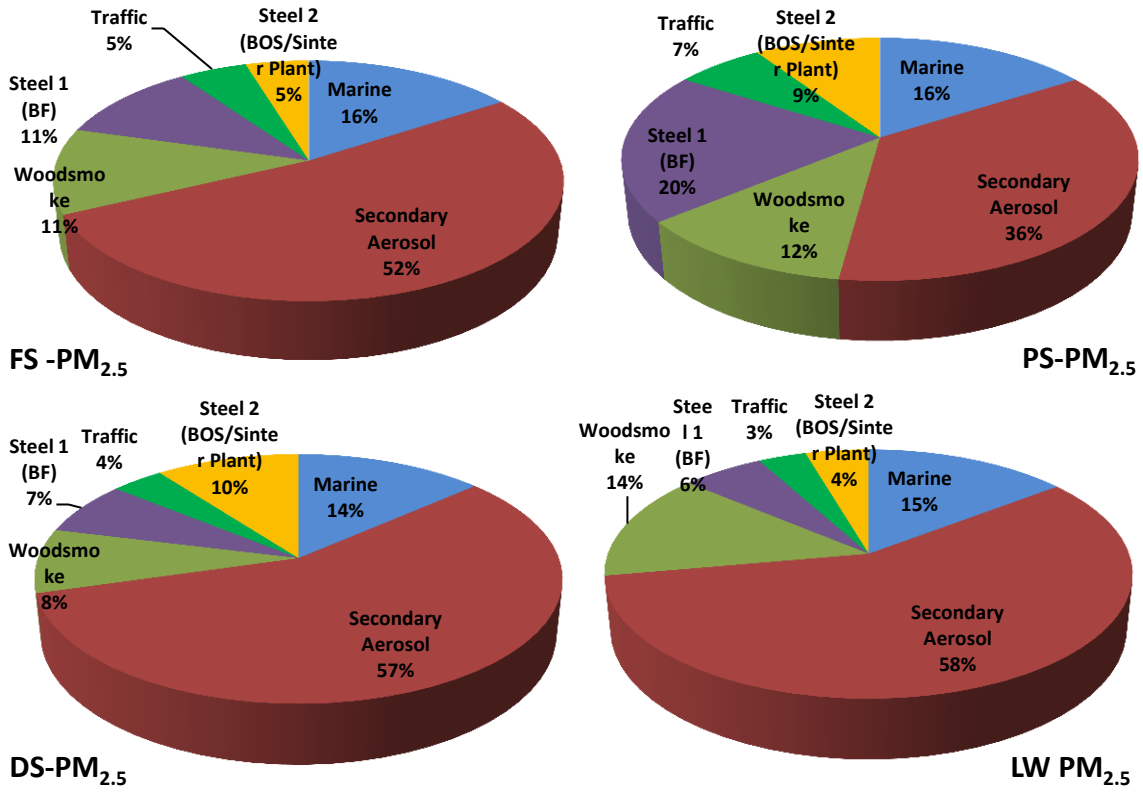

(a) Partisol $PM_{2.5}$

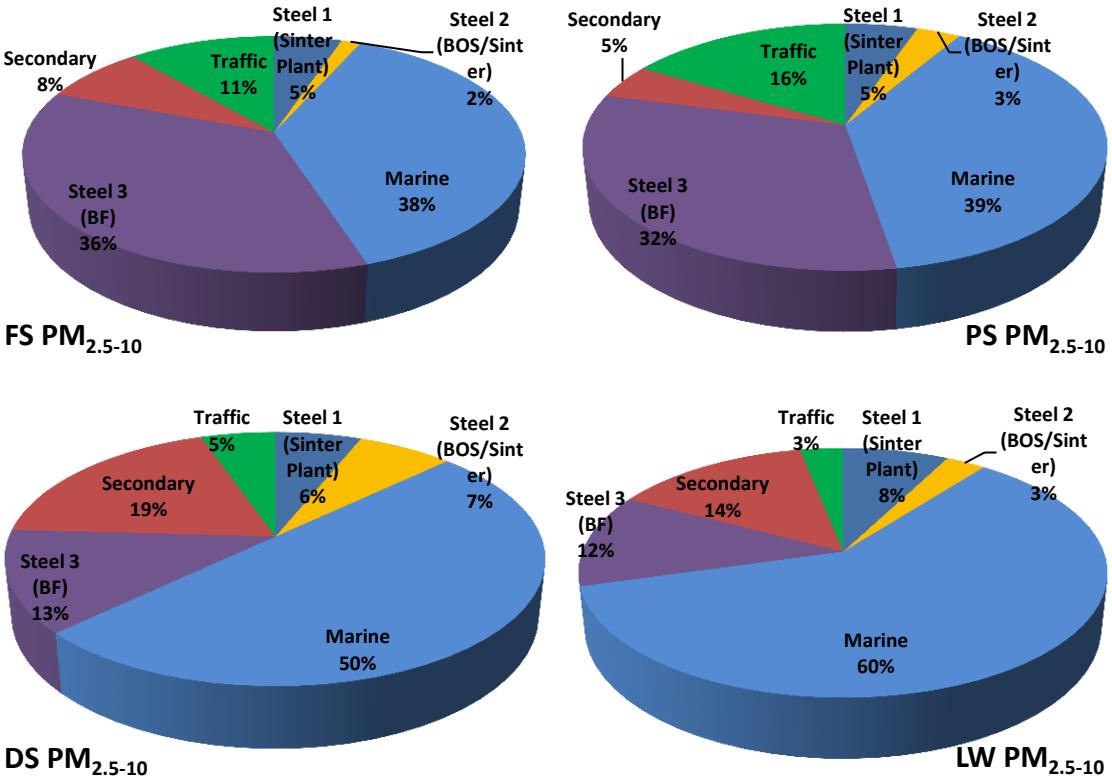

(b) Partisol $PM_{2.5-10}$

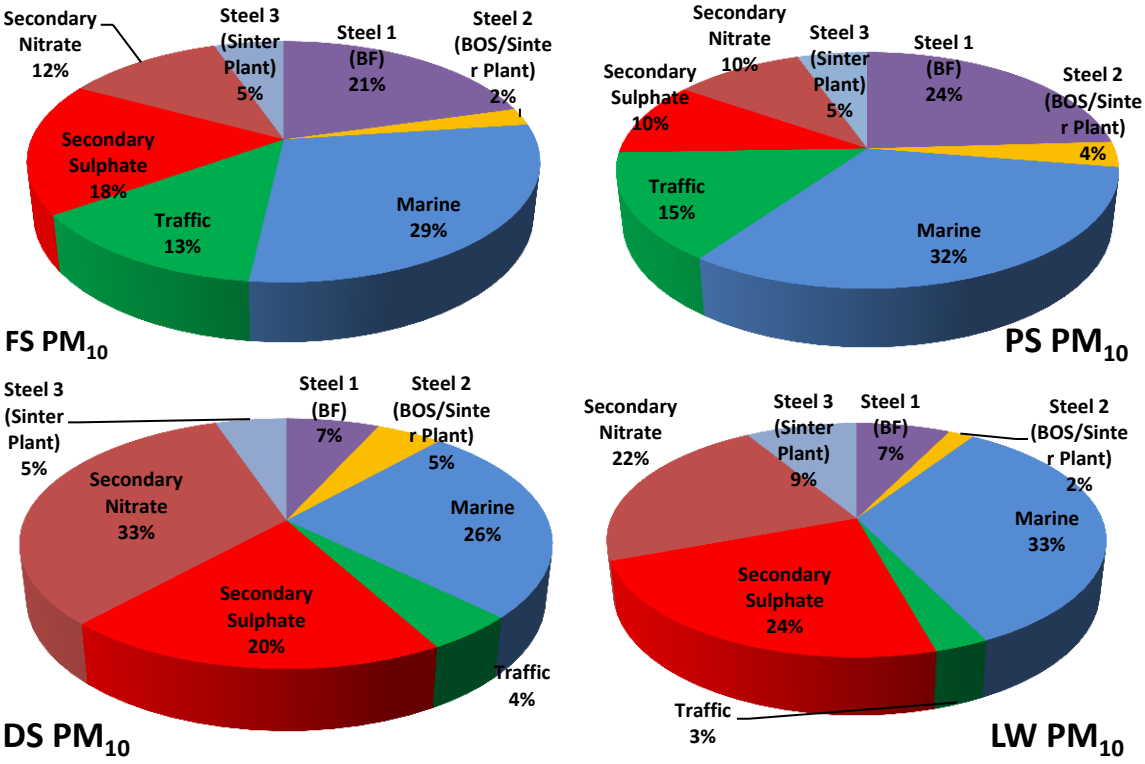

(c) Partisol PM_{10}

Figure 7.2: Percent contributions to sources identified by PMF

7.3.1.2 PMF for Streaker (PIXE) data

The PMF profiles of PIXE $PM_{2.5}$ and PM_{10} data at FS and LW sites are presented in Figure 7.3(a-d). PMF solution for $PM_{2.5-10}$ data did not yield good results and hence could not be presented. However, the model worked well with $PM_{2.5}$ and PM_{10} data. The PMF profiles for fine particles at FS and LW exhibit correlation coefficients (r^2) varying between 0.60-0.99 except for BC (0.46) and Al (0.33). For PM_{10}, components have r^2 >0.91 except for Pb (0.74). At LW, the correlations between observed and predicted components are also generally strong ($PM_{2.5}$ species show r^2 =0.65-0.99 while PM_{10} species exhibit r^2=0.81-0.99 except for PM_{10} mass (0.63) and Ti (0.53).

At FS, the PMF solution identified 6 prominent source components. Factor 1 is highly associated with 65% CO, 65% SO_2, 37% Se and 30% K. This suggests steelworks emissions from the coke ovens. Se and SO_2 have been attributed to coking emissions (Konieczynski *et al.*, 2012; Pancras *et al.*, 2013). SO_2 is a well-known stack emission from coal fired plants and the steel industry (Remus *et al.*, 2013). Factor 2 explains a large proportion of S (68%), Pb (42%) and BC (34%). 39% of the modelled $PM_{2.5}$ is associated with this factor, which we attribute to the sinter plant. Factor 3 provides an elevated contribution to Zn (76%) and a moderate contribution to Pb (28%). The factor is a steelworks emission source from the BOS plant. The fourth factor accounts for 77% NO_x, 49% BC, 31% Ti, 23% CO and 21% Al, and is attributed to road traffic. NO_x and CO are prominent emissions from traffic (Ogulei *et al.*, 2006; Wallington *et al.*, 2008). Factor 5 shows contributions to Fe (74%), Ca (71%), Mn (59%), Ti (17%), Se (18%), Al (15%) and SO_2 (14%) and thus represents a steelworks (BF). The last sixth factor is attributed marine aerosol due to a high association with 86% Mg, 80% Cl and 66% Mg. Other

elevated elements were Al (36%), Ti (34%), K (28%), 20% Se and Ca (19%) in this factor. This suggests a mixture of crustal elements with marine aerosol.

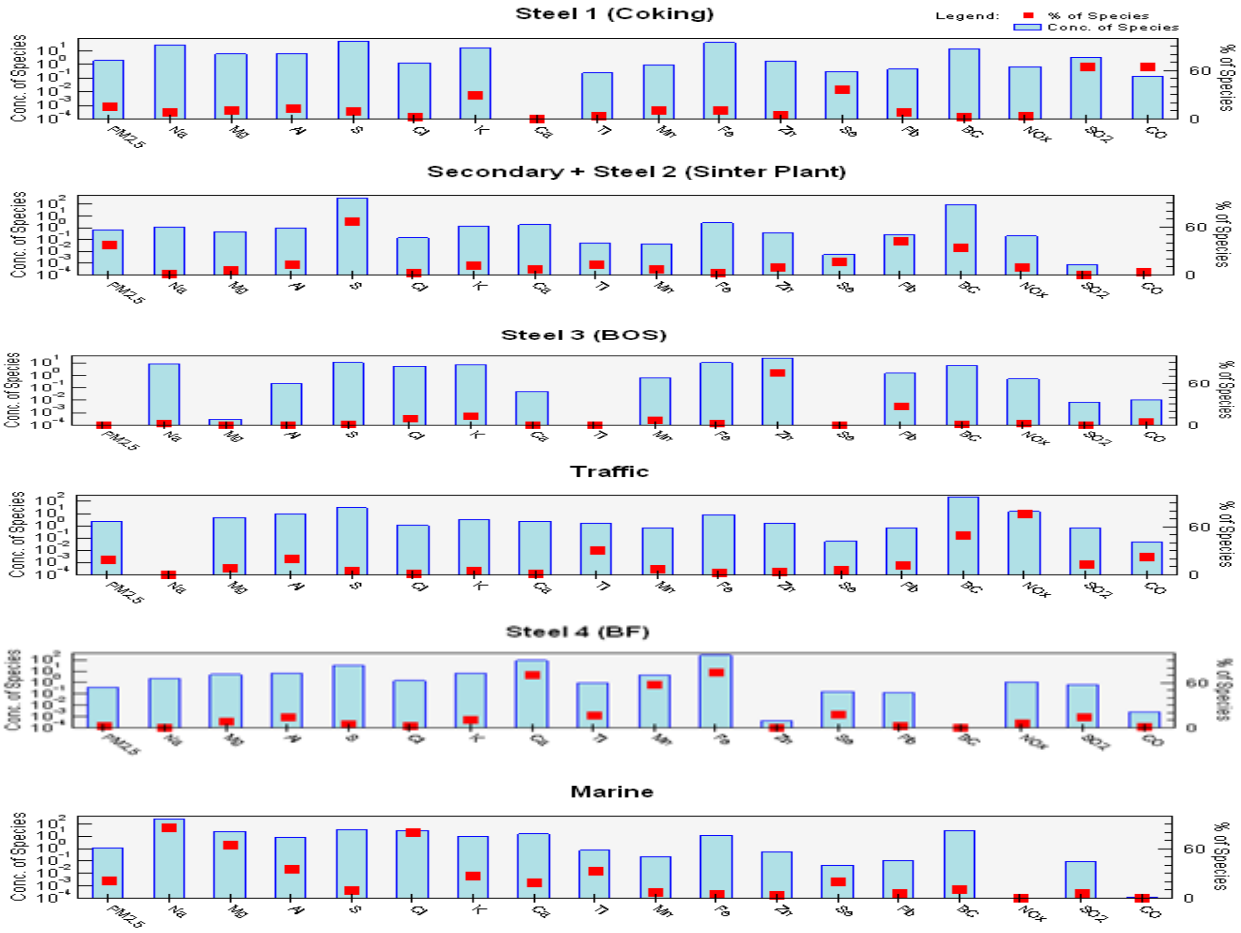

(a) FS $PM_{2.5}$

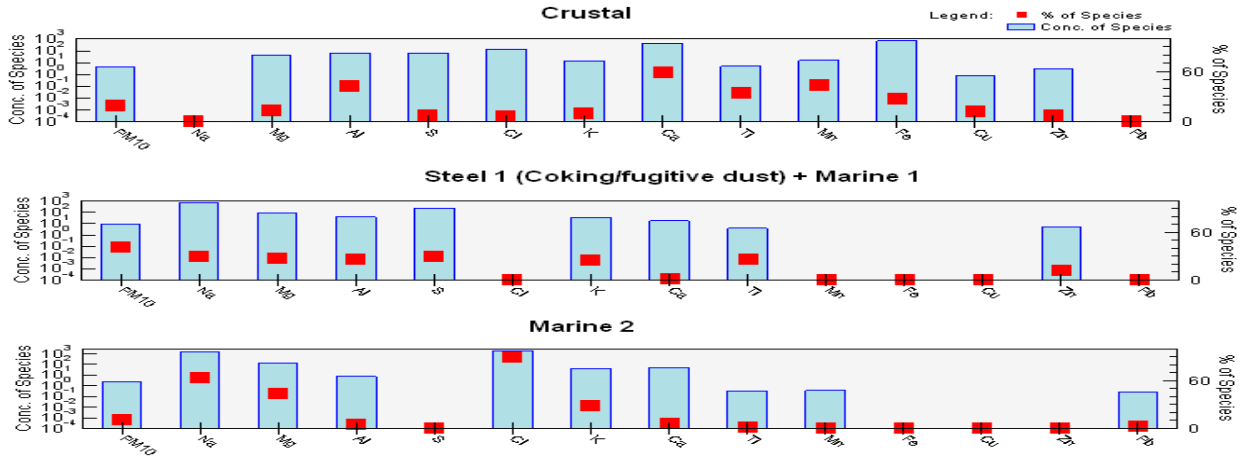

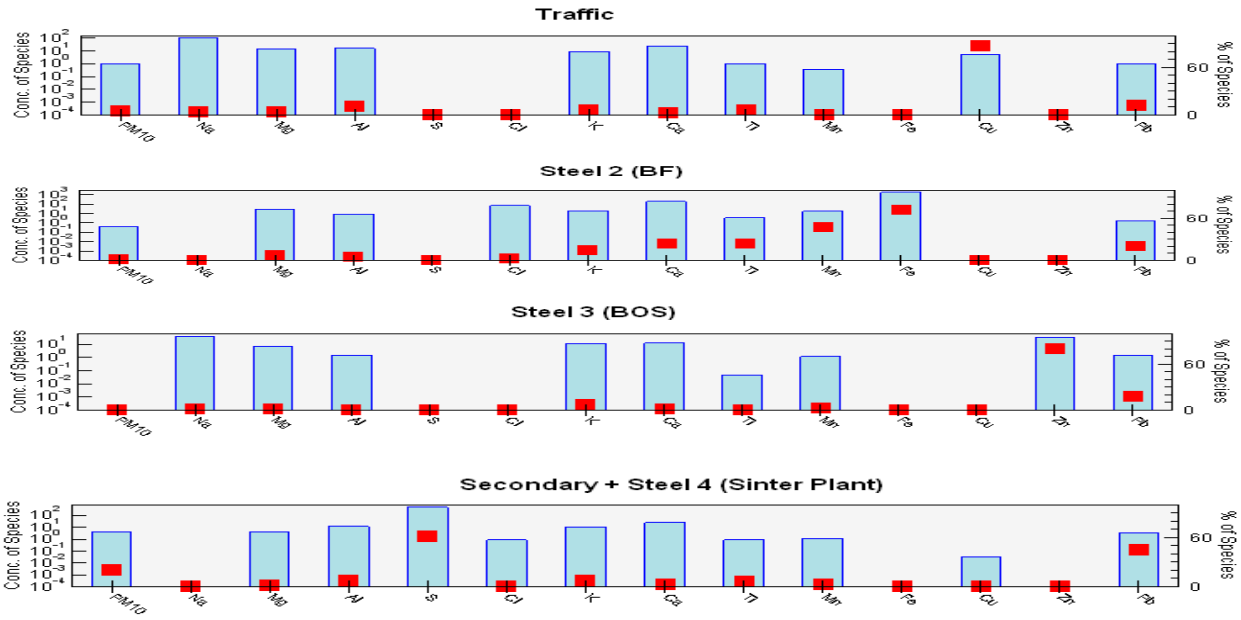

(b) FS PM_{10}

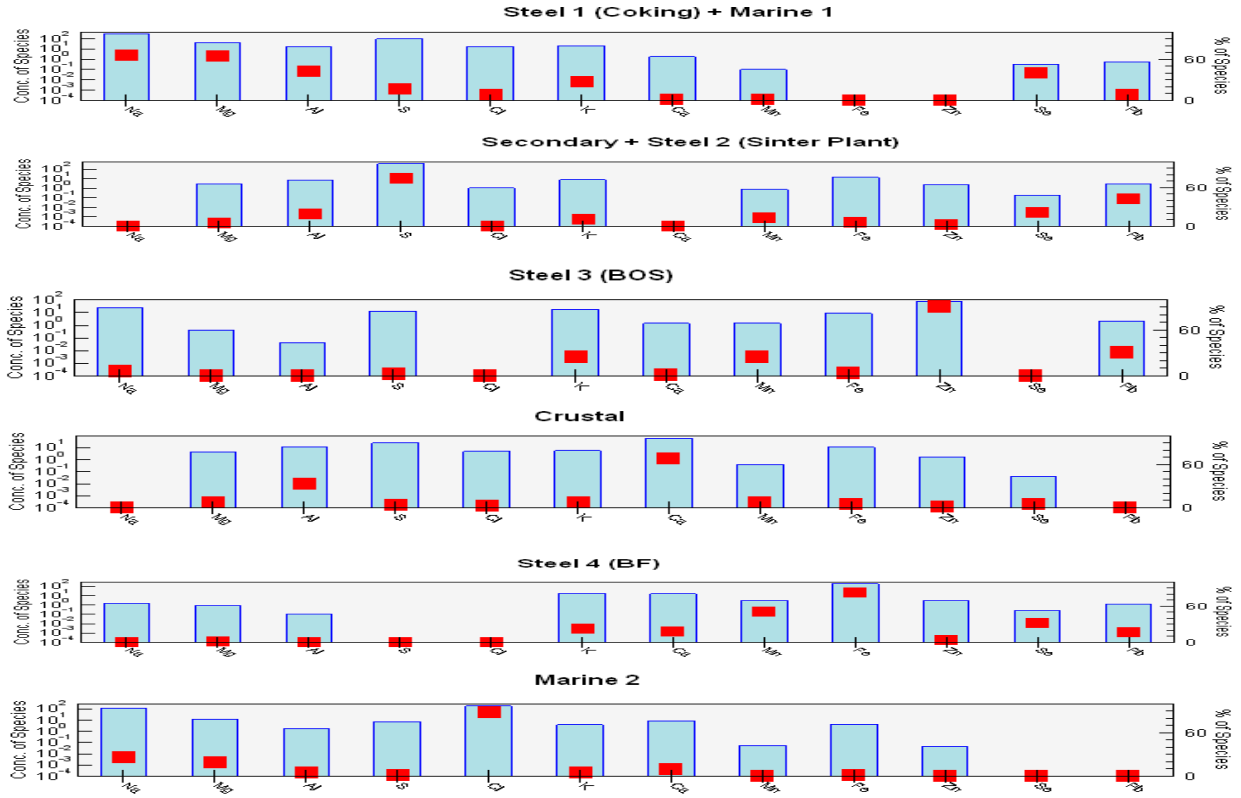

(c) LW $PM_{2.5}$

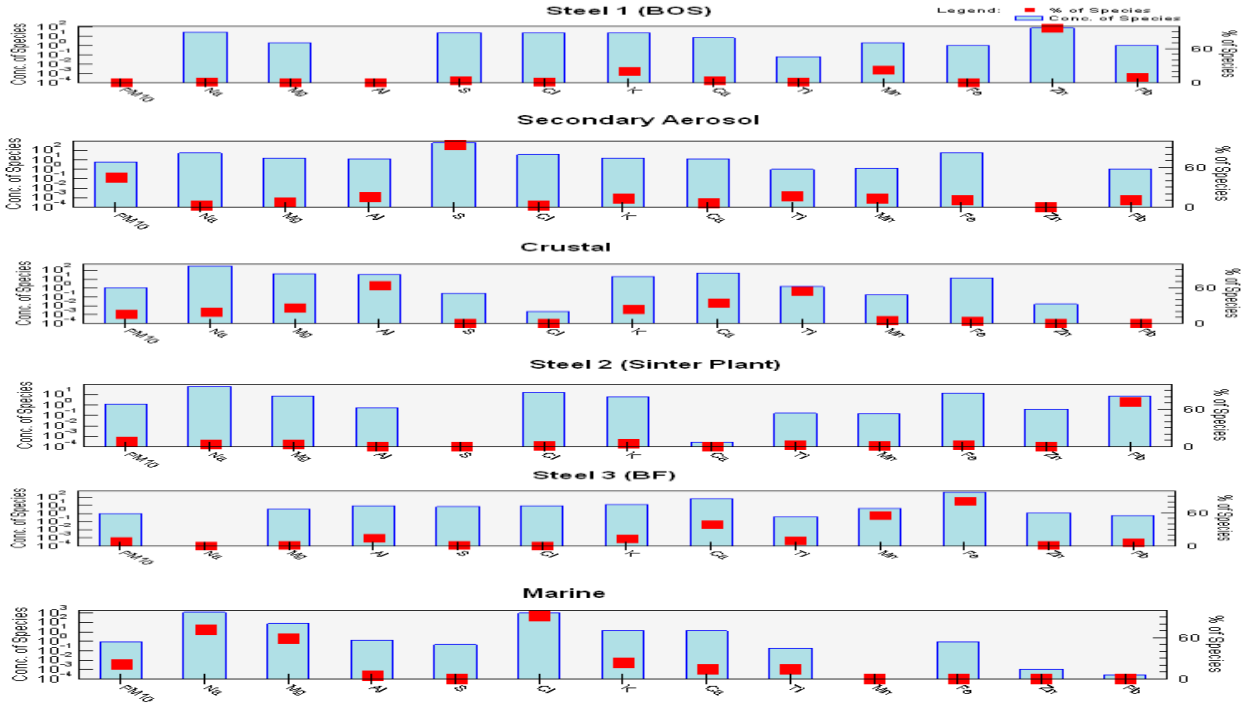

(d) LW PM_{10}

Figure 7.3: Streaker PMF profiles for $PM_{2.5}$ and PM_{10} at FS and LW

Seven factors are resolved by PMF for PM_{10} at FS. Four factors are attributed to the steelworks while two factors are linked to marine aerosol. Factor 1 shows major contributions of Ca, Mn, Al, Ti and Fe (59, 44, 43, 34 and 28%, respectively). This component represents a crustal matter source. A significant fraction of FDMS PM_{10} occurred in this factor representing 20% of the modelled PM. Factor 2 is a combined steel and marine aerosol with loadings for S (30%), Na (30%), Mg (27%), Ti (27%), Al (27), K (25%) and Zn (13%). Although there is not a clear steelworks contribution to this factor, steelworks fugitive dust may be a contributor. With 90% of Cl, 65% Na, 44% Mg and 30% K explained by Factor 3, marine aerosol is clearly the source (Harrison *et al.*, 2003). Factor 4 shows importance of Cu (87%), with Al the only other element associated. Both Cu and Al are characteristic of vehicular emissions arising from brake wear and resuspension respectively (Kleeman *et al.*, 2000; Harrison *et al.*, 2012b). Factor 5 is

dominated by Fe (72%), Mn (48%), Ca (25%), Ti (24%) and Pb (20%) suggesting BF emissions from the steelworks. Zn (80%) is highly loaded for Factor 6 indicating a source from the steelworks BOS plant. 19% of K is also contributed by this source. With a total 62% of S explained, Factor 7 is attributed to secondary aerosol. The presence of Pb (46%) explained in this factor suggests a contribution from the sinter plant emissions. Long range transport of Pb rather than local emissions is an alternative, but unlikely explanation.

The PMF solution for LW fine particles also produced six factors (Figure 7.3 (c)). The first factor is a major contributor to Mg (63%), Na (62%), Al (41%), Se (42%), K (28%) and Pb (10%). This factor could be represented as mixed steel (coking) and marine sources. A large fraction of FDMS PM_{10} occurred in this factor representing 42% of the modelled PM. Despite the fact that Cl does not contribute to this factor, the polar plot (which will be discussed later) showed marine. The second factor is another combined source characterized by contributions to 72% S, 43% Pb, 23% Se, 18% Al and 15% Mn. This factor may represent secondary and steelworks emissions from the sinter plant. The third factor is another steelworks emission from BOS having loading for Zn (89%) and moderate contributions to Pb (30%), K (25%) and Mn (25%). Factor 4 shows abundance of crustal components of Ca (74%) and Al (35%). The fifth factor has associated steelworks signatures of Fe (77%) and Mn (48%) along with contributions from Se (31%), Ca (22%) and K (21%). This source may probably be linked to the BF steelworks unit. Factor 6 has the presence of abundant Cl (91%) and moderate amounts of Na (30%) and Mg (21%) indicating marine aerosol.

The PMF profile for PM_{10} at LW is shown in Figure 7.3 (d). PMF analysis revealed six factors as observed for $PM_{2.5}$. Factor 1 is a steelworks source (BOS) characterized mostly

by Zn (98%) with additional contributions to Mn (22%), K (20%) and Pb (10%). A secondary aerosol origin is apparent for Factor 2 which contributes highly to S (95%). About 45% of total predicted PM_{10} mass is apportioned to this source. The possibility of this factor mixing with crustal matter aerosol is apparent from co-existence of considerable amount of Ti (17%) and Al (16%). Greater abundance of Al (64%), Ti (55%), Ca (35%), Mg (26%) and K (24%) are features of Factor 3 indicating crustal aerosol. In Factor 4 there is a dominant lone steelworks signature of Pb (72%) from the sinter section. Fe (81%), Mn (56%) and Ca (39%) are dominant species in Factor 5. This factor is attributed to emissions from the BF plant. However, the impacts from other steelworks units such as the BOS, sinter plant and perhaps, desulphurization slag processing section may be present (Hleis *et al.*, 2013). Factor 6 is a marine source with significant contributions to 93% Cl, 72% Na, 60% Mg and 24% K.

Appendix XXV shows the hourly contributions to $PM_{2.5}$ and PM_{10} as explained by the PMF model. Whereas the Partisol PMF profiles for $PM_{2.5}$ showed the highest daily peak on May 4 at the FS site, the PIXE PMF depicts major pollution peaks on May 8, 10 and 14 due to the higher resolution information provided by the Streaker. Also at the LW site, pollution events were observed in the PIXE data on May 3, 7, 9 and 14 similar to those seen in the Partisol data for fine PM. The agreement between the Partisol and Streaker PMF data on these episode days may reflect secondary, steelworks (BF/BOS) and/or marine particles as the paramount contributors at the two sites. An elevated pollution event was also seen at LW on May 9 for Streaker PM with large contributions from marine, steelworks BOS and sinter plant emissions. The PMF hourly profiles of PM_{10} showed pollution peaks similar to those for $PM_{2.5}$ at FS dominated by steelworks (BF) and

marine sources. Hourly variations of PMF profiles of PM_{10} data at LW showed several episodic events that are largely driven by marine aerosol.

Average diurnal variations of $PM_{2.5}$ and PM_{10} PMF profiles are depicted in Appendix XXVI. At FS, two significant peaks are shown for $PM_{2.5}$ at 7-8 am and 4 pm. These peaks appear to be the result of contributions from multiple emission sources. Four distinctive diurnal peaks at 5-6 am, 9 am, 4-5 pm and 9-10 pm are shown for the PMF profile of PM_{10} at FS. Previous work at Port Talbot has reported the highest peaks of PM_{10} at 4 pm (AQEG, 2011). The temporal trend of the PMF profile at LW also revealed two peaks between 8am and 2 pm and 4-10 pm, with the marine and steel (BF) sources the major contributors.

Source contributions to Streaker $PM_{2.5}$ and PM_{10} at FS and LW are plotted in Figure 7.4. The PIXE PMF results show domination of steelworks sources at FS and LW. A clear deviation was observed between the $PM_{2.5}$ PMF profiles for Partisol and Streaker data. Abundance of secondary aerosols (sulphate and nitrate) and marine aerosol characterised the Partisol $PM_{2.5}$ profiles. Both the secondary aerosol and steelworks factors impact upon the Streaker $PM_{2.5}$. The crustal source is a prominent factor identified by PMF that was not observed in the Partisol result. The discrepancies observed for the PMF solutions for the two PM measuring instruments might be linked to the chemical species included in the PMF model. Both Partisol and Streaker PMF solutions identified marine aerosol as the largest contributor to PM_{10} at FS and LW. Due to the missing of traffic signature elements, especially Cu in LW $PM_{2.5}$ and PM_{10}, a traffic factor was not identified.

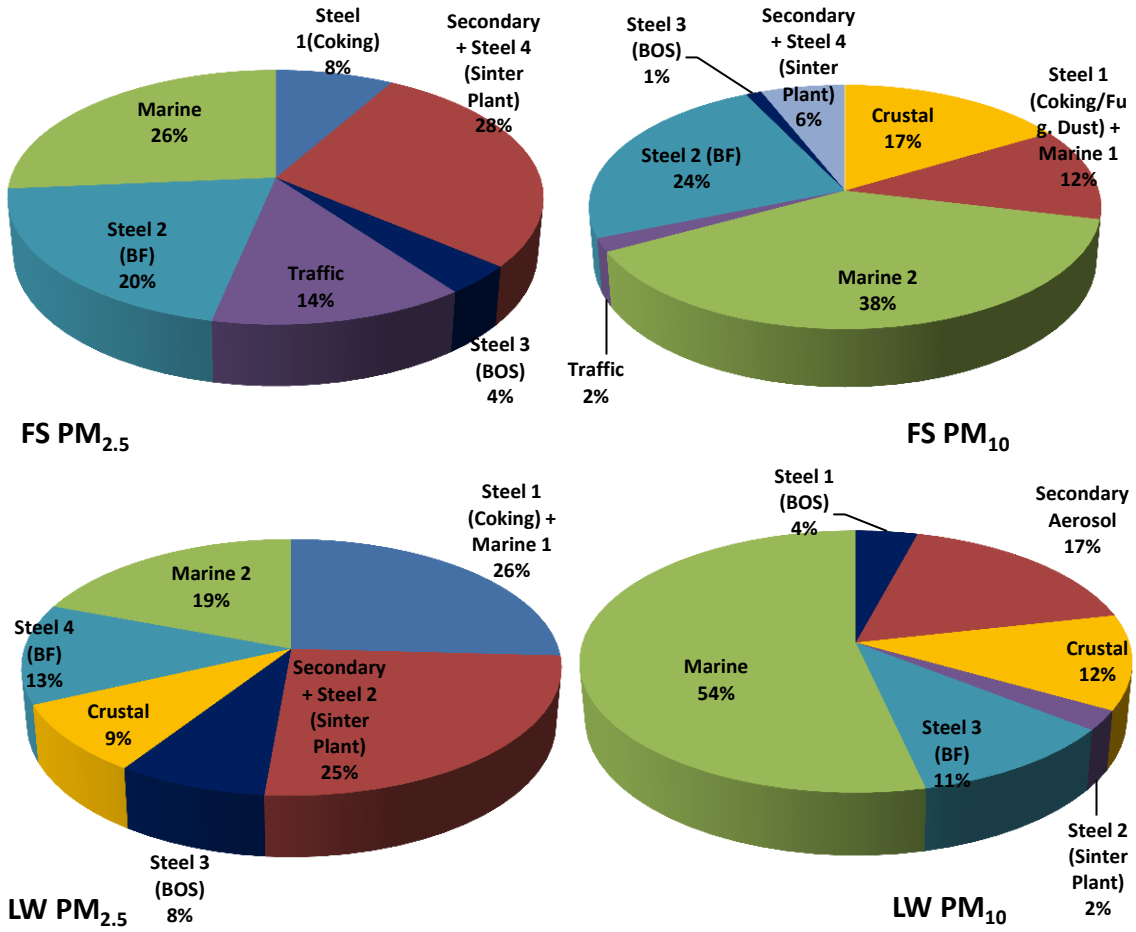

Figure 7.4: Source contributions by PMF at the two monitoring sites for $PM_{2.5}$ and PM_{10} (Streaker samplers)

Figure 7.5 shows polar plots for factors identified by PMF for $PM_{2.5}$ and PM_{10} at the two monitoring stations. The steelworks (BF, sinter plant, BOS, coking, ore stockyards) were located between the southern and western section from the FS (210-270^{o}) site at Port Talbot. This is thus reflected in the directional concentration of steelworks factors for $PM_{2.5}$ observed in the polar plots. Secondary aerosol polar plots for the $PM_{2.5}$ fraction depict elevated concentrations at both the centre and the easterly axis from FS, indicating both local and regional emissions. This agrees with the previous study at Port Talbot, which concluded regional pollutants to be a major contributor to fine PM (AQEG, 2005).

The traffic factor in $PM_{2.5}$ shows a possible contribution from the M4 road to the north of the sampling sites, and also from the A48 road closer to the FS site (DfT, 2012). The polar plots for PM_{10} at the FS site show the sources positioned along the direction of the steelworks complex. Elevated concentration of the Steel 1/Marine 1 factor towards the south-easterly wind sector could be traced to an additional influence from the rolling mills (150-170^{o}). The traffic source shown by PM_{10} polar plots for FS in the direction of the steelworks may be due to fugitive emissions from vehicular movements on paved and unpaved roads (Landeg, 2010). From the LW site, the steel industry is located between the south and south-east sector (100-180^{o}). Most of the polar plots for steel process factors in $PM_{2.5}$ and PM_{10} displayed higher concentrations towards the steel industry. In the southerly direction (180^{o}) the steel factor observed could be traced to fugitive dust from ore stockyards.

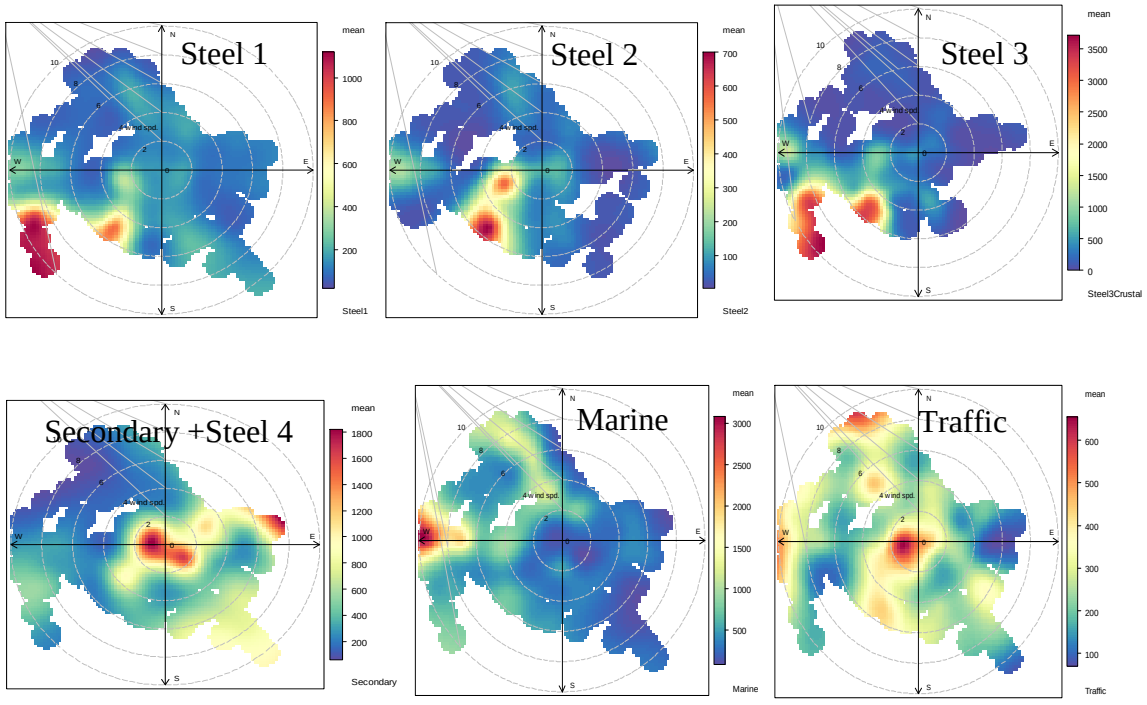

(a) FS $PM_{2.5}$

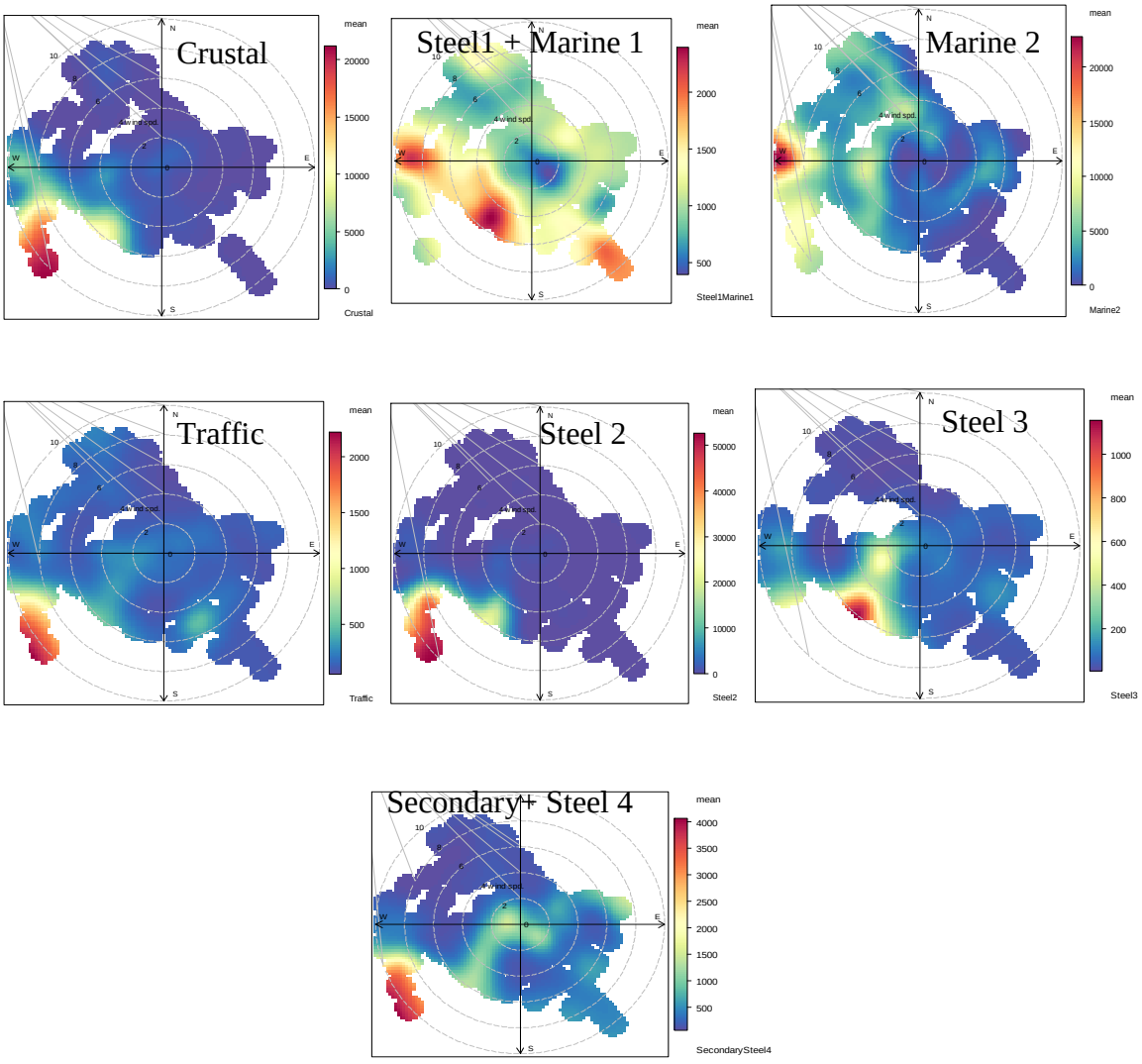
Crustal
Steel1 + Marine 1
Marine 2
Traffic
Steel 2
Steel 3
Secondary+ Steel 4
mean
4 W wind spd
N
S
E
W
Crustal
Steel1Marine1
Marine2
Steel2
Steel3
SecondarySteel4

(b) FS PM_{10}

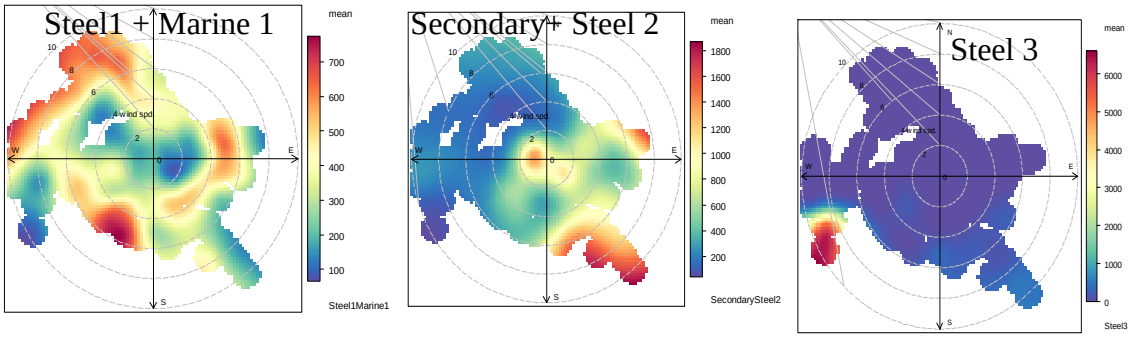
Steel1 + Marine 1
Secondary+ Steel 2
Steel 3
mean
4 W wind spd
N
S
E
W
Steel1Marine1
SecondarySteel2
Steel3

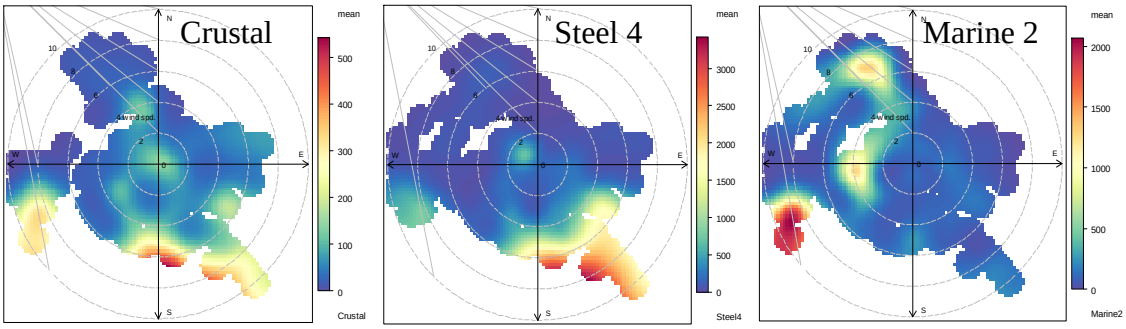

(c) LW $PM_{2.5}$

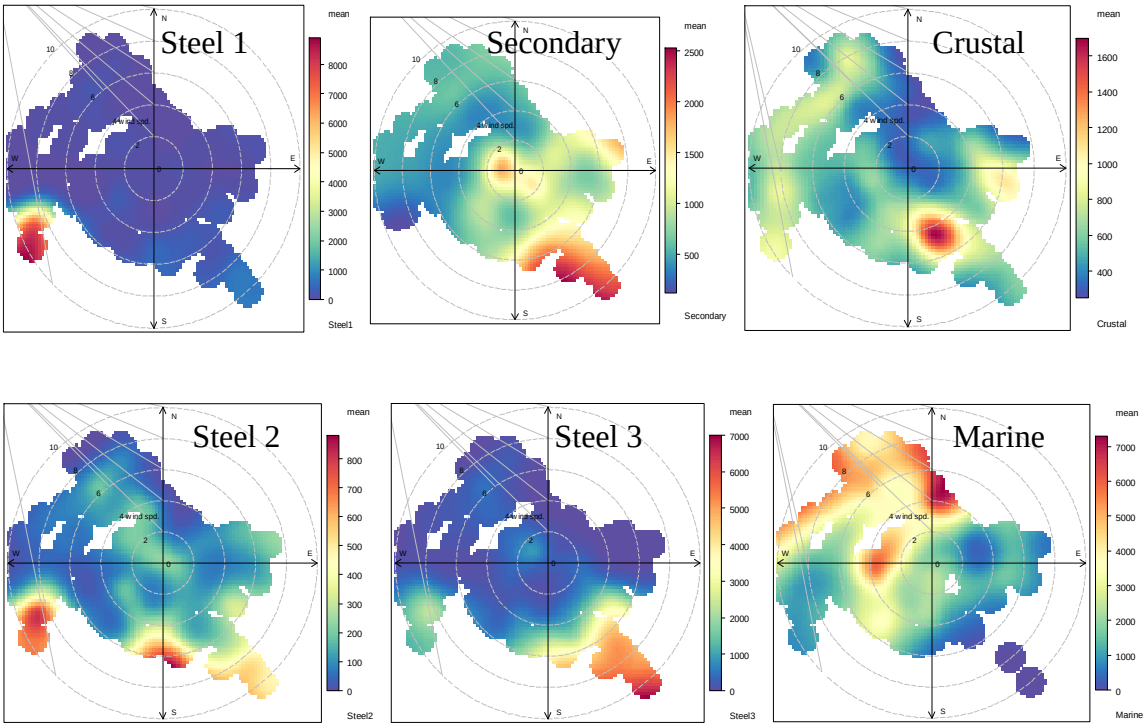

(d) LW PM_{10}

Figure 7.5: Polar Plots for Streaker PMF profiles at FS and LW

7.4.2 Principal component analysis (PCA)

7.4.2.1 PCA for Partisol fine and coarse data

Table 7.2(a) shows the rotated component matrix for fine PM of the pooled data from the four monitoring sites. Rotated PCA produced six factors with 78.8% of data variance explained. Factor 1 with the highest % variance (20.6) is highly loaded for Mn, Fe, Zn, Cd

and Pb indicating steel 1 source from the sinter/blast furnace (BF)/basic oxygen steelmaking (BOS) plants. $PM_{2.5}$ mass, nitrate, nss-sulphates, ammonium and potassium are all significantly elevated in factor 2 with 16.7% variance thereby representing a combined secondary aerosol and woodsmoke source. Factor 3 is positively loaded for Cl^-, Na^+, Mg^{2+} and Ca^{2+}. This factor is a marine source. In the factor 4, Cu and Sb and Ba are strongly associated explaining about one-sixth of the total dataset. This factor represents a traffic source. Factor 5 has a strong affinity for Ca^{2+}, Al and Fe. This factor could be assigned to a steel source from the blast furnace. This factor may also represent crustal matter source. The sixth factor is significant for V and Ni indicating oil/fuel combustion or shipping emission (Pandolfi *et al.*, 2011). This source was not prominent in the PMF model because Ni could not meet the requirement of PMF and was therefore removed.

Table 7.2 (b) represents the PCA for $PM_{2.5-10}$. A total 77.7% variance was explained with 5 factors identified. Factor 1, which has high loading for $PM_{2.5-10}$ mass, Ca^{2+}, Al, V, Mn, Fe, Ni, Ba, Sb and Pb. Factor 1 represents around 40% of the explained total variance, which was a mixed emission source comprising steelworks, crustal matter and oil combustion; Factor 2 is significantly loaded for Cl^-, Na^+ and Mg^{2+}. This factor indicates a marine source. The steel markers of Zn and Cd were abundant in factor 3. This steel source could represent BOS/sinter plant emissions. Cu and Sb are significant for factor 4 and attributable to traffic source. The last factor is highly variable for sulphate and nitrate representing secondary aerosol.

Table 7.2: Rotated Component Matrix for Partisol (a) $PM_{2.5}$

	Component						
	1	2	3	4	5	6	Communalities
$PM_{2.5}$	0.332	**0.748**	-0.068	0.327	0.246	-0.024	**0.842**
Cl^-	0.37	-0.146	**0.779**	-0.197	0.099	-0.144	**0.835**
NO_3^-	-0.195	**0.875**	-0.091	-0.04	-0.214	0.026	**0.861**
nss-SO_4^{2-}	0	**0.817**	-0.229	-0.25	-0.136	-0.008	**0.802**
Na^+	-0.003	-0.284	**0.845**	-0.098	-0.077	-0.219	**0.859**
NH_4^+	-0.209	**0.834**	-0.38	-0.019	-0.106	-0.027	**0.897**
K^+	0.267	**0.711**	0.147	0.161	0.137	0.169	**0.671**
Mg^{2+}	0.325	-0.12	**0.81**	-0.069	0	0.188	**0.816**
Ca^{2+}	-0.2	0.147	**0.546**	-0.126	**0.631**	-0.077	**0.779**
Al	-0.089	-0.204	-0.228	-0.223	**0.648**	0.18	**0.603**
V	-0.264	0.034	-0.191	-0.023	0.124	**0.631**	**0.521**
Cr	-0.285	-0.203	0.226	0.262	0.162	-0.464	**0.484**
Mn	**0.831**	-0.003	0.179	0.224	0.359	-0.081	**0.908**
Fe	0.545	-0.039	0.213	0.328	**0.631**	-0.112	**0.863**
Ni	-0.197	-0.023	0.131	0.182	0.002	**0.757**	**0.662**
Cu	0.326	0.057	-0.07	**0.842**	-0.162	0.098	**0.86**
Zn	**0.897**	-0.078	0.153	0.026	-0.025	-0.118	**0.849**
Cd	**0.91**	-0.072	0.148	0.034	-0.145	-0.1	**0.887**
Sb	-0.146	0.112	-0.172	**0.798**	-0.329	-0.03	**0.81**
Ba	0.116	-0.115	-0.133	**0.843**	0.285	0.028	**0.837**
Pb	**0.907**	0.236	0.036	0.049	-0.081	-0.121	**0.902**
% Variance	20.6	16.7	13.5	12.6	8.6	6.8	-78.8
	Steel 1	Secondary + Woodsmoke	Marine	Traffic	Steel 2	Oil combustion	

(b) $PM_{2.5\text{-}10}$

	Component					
	1	2	3	4	5	Communalities
$PM_{2.5\text{-}10}$	**0.881**	0.407	0.086	0.063	0.006	**0.954**
Cl^-	0.146	**0.967**	0.065	-0.015	0.012	**0.962**
NO_3^-	-0.199	-0.175	0.045	0.107	**0.861**	**0.826**
nss-SO_4^{2-}	0.134	0.232	-0.057	-0.122	**0.799**	**0.729**
Na^+	0.14	**0.965**	0.053	-0.034	0.018	**0.956**
NH_4^+	-0.055	-0.203	-0.048	-0.154	0.248	**0.131**
K^+	0.292	0.349	0.197	-0.088	0.382	**0.4**
Mg^{2+}	0.44	**0.827**	0.269	-0.052	-0.032	**0.955**
Ca^{2+}	**0.885**	0.203	0.244	0.135	-0.07	**0.907**
Al	**0.742**	0.29	-0.067	0.06	-0.004	**0.642**
V	**0.825**	0.239	0.345	0.165	0.02	**0.885**
Cr	-0.326	0.067	0.207	0.438	-0.162	**0.372**
Mn	**0.947**	0.158	0.175	0.027	0.015	**0.953**
Fe	**0.949**	0.157	0.034	-0.009	-0.012	**0.926**
Ni	0.423	0.314	0.021	0.47	-0.039	**0.5**
Cu	0.237	-0.122	-0.009	**0.875**	-0.011	**0.836**
Zn	0.121	0.072	**0.935**	0.068	-0.02	**0.899**
Cd	0.313	0.196	**0.87**	0.012	0.026	**0.894**
Sb	**0.539**	-0.148	-0.028	**0.704**	-0.044	**0.811**
Ba	**0.899**	0.015	0.054	0.388	-0.034	**0.963**
Pb	**0.862**	0.001	0.203	0.163	0.058	**0.813**
% Variance	42.3	13.5	8.1	7.7	6.1	-77.7
	Crustal Matter + Steel 1	Marine	Steel 2	Traffic	Secondary	

Figure 7.6 shows the summary of source contribution to Partisol fine and coarse PM. The combined secondary and woodsmoke factor (43%) remained the leading contributor to $PM_{2.5}$ in Port Talbot. All the steelworks sources formed a total of 36% while traffic formed 19% of $PM_{2.5}$ emission. In the coarse category, the mixed source of crustal and steel emission constituted two-third of total $PM_{2.5-10}$. Marine is the second contributor to $PM_{2.5-10}$ emission. Studies along the coastal areas have allocated an appreciable percentage of coarse particles to sea spray source (Visser *et al.*, 2001; Querol *et al.*, 2004).

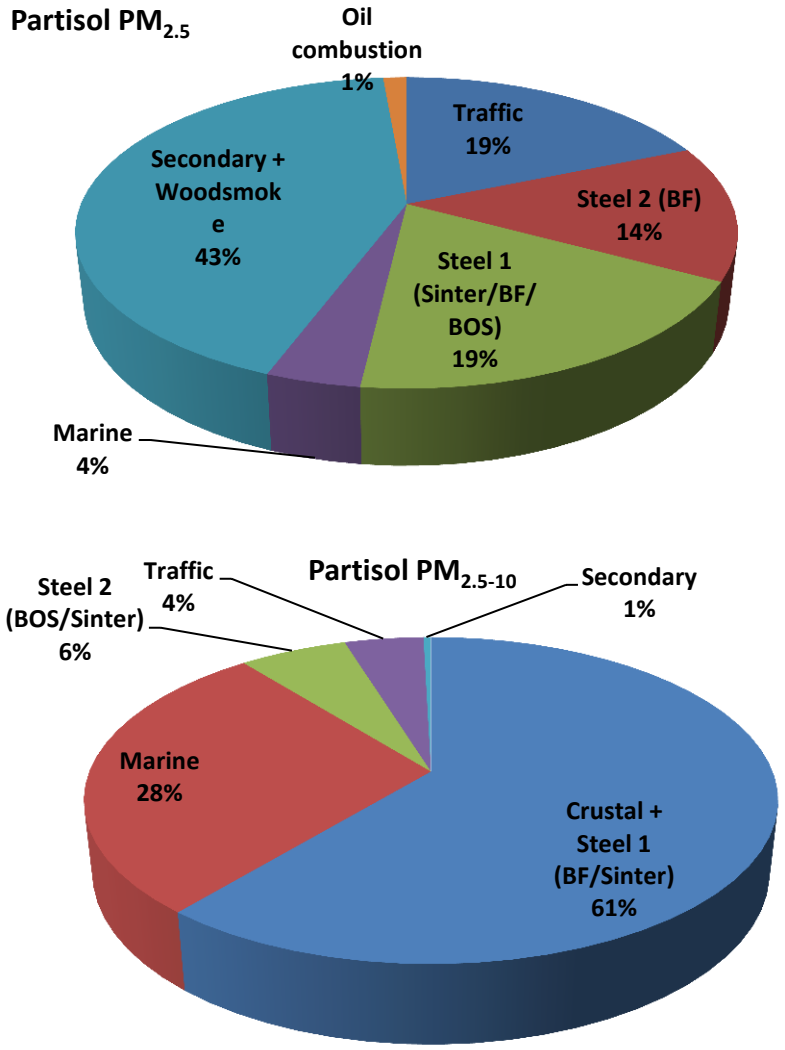

Figure 7.6: PCA source contributions for $PM_{2.5}$ and $PM_{2.5-10}$

7.3.2.2 Rotated PCA for Streaker data

The rotated PCA for fine and coarse particles at FS is shown in Table 7.3 (a, b). In both PM fractions, four components were resolved by the rotated PCA. In the fine PM, 81.6% of the total dataset was explained with factor 1 constituting 38.5% of the explained variance (Table 7.3a). The most abundant elements in factor 1 are Mg, Al, K, Ca, Mn, Fe, Ti and Se. This may indicate a mixed source factor showing markers for steel and crustal matter. Factor 2 shows significance for Na, Mg and Cl, representing a marine source. Component 3 also represents a mixed source with significant contributions from K, Cu and Zn. Fine K is a good tracer for woodsmoke emission while Cu and Zn are markers for brake wear and lining (Harrison *et al.*, 2012b). This factor is therefore a traffic and woodsmoke (Harrison *et al.*, 2012b, c). Component 4 has only Ni as the significant tracer. This source could either represent oil combustion or shipping emission.

The rotated PCA was able to account for 82.6% of coarse PM data at FS (Table 7.3b). Al, Si, Ca, Ti, Mn and Cu are highly loaded in factor 1 with 25.8% variance. This factor is a mixed source from crustal matter and traffic. The second component is significant for Na, Mg, S, Cl and K explaining almost equal variance with factor 1. Factor 2 could be best described as marine (Na, Mg, Cl) and steel source (K, Cl, S). KCl in coarse PM fraction is a notable emission from the sinter plant (Dall'Osto *et al.*, 2008a; Hleis *et al.*, 2013). Factor 3 has high loading in S, Cr, Ni and Zn. This factor could be described as a combined source from the steelworks (BOS/stainless steel welding and oil/coal combustion). Cr is also a notable emission from electroplating industries. It has been also been reportedly emitted through welding of stainless steel (Heung *et al.*, 2007; Querol *et al.*, 2007). The presence of S in this factor could signify steelworks emissions. The fourth factor of coarse

PM is significantly associated with Mn, Fe, Rb and Pb. This is also a steel source from the blast furnace section.

The rotated PCA at the LW monitoring station is shown in Table 7.4 (a, b) for fine and coarse PM. These two PM categories explained 79.8 and 91.6% of their total dataset with four components identified accordingly. Fine PM factor 1 has high loading for K, Ca, Mn, Fe, Ni, Zn and Pb. This is a combined steel (BF/Sinter/BOS) and oil combustion/woodsmoke source. Factor 2 is associated with Na, Mg and Cl representing a marine source. Factor 3 has high loadings of Al, Ca with moderate loading of Ti. This indicates a crustal source. Factor 4 is highly loaded with S and Cr. This source is attributed to steelworks from cokemaking (US EPA, 1995). S has been observed in elevated amounts at a steel smelting plant (Prati *et al.*, 2000), coal-fired plants and refineries (Barret, 2004).

The coarse PM factor 1 is dominated by Na, Mg, Al, Cl, K, Ca, Br and Sr where a total variance of 40% was explained. This factor is a mixed source associated steel and marine emissions. Factor 2 has high loading of Al, Si, K, Ca, Mn, Fe, Ti, Zn and Sr indicating a combination of crustal and steelworks sources. The steel factor in component 1 and 2 could be linked to steelworks production units including the sinter, BF and BOS plants. Factor 3 has significant affinity for Cr but is anti-correlated with Cu. This factor is attributed to stainless steel welding. Lastly, Cr and Ni are highly loaded for factor 4 and thus represents oil/coal combustion source.

Table 7.3: Rotated components for FS Streaker (a) $PM_{2.5}$

	Component				
	1	2	3	4	Communalities
Na	.331	**.914**	.044	-.002	**.946**
Mg	**.626**	**.719**	-.097	-.119	**.932**
Al	**.725**	.242	.035	-.373	**.725**
S	.247	-.405	.246	-.454	**.492**
Cl	-.049	**.924**	.016	-.114	**.869**
K	**.753**	.023	**.529**	.173	**.878**
Ca	**.823**	.391	-.203	-.114	**.884**
Cr	.415	.484	-.268	.443	**.675**
Mn	**.969**	.042	.143	-.033	**.961**
Fe	**.957**	.040	.015	-.007	**.919**
Ni	-.071	-.183	.137	**.818**	**.726**
Cu	.022	-.021	**.872**	-.156	**.785**
Zn	-.006	-.036	**.932**	.170	**.900**
Ti	**.722**	.268	-.077	-.214	**.645**
Se	**.940**	-.024	.036	.108	**.897**
% Variance	**38.5**	**19.5**	**14.3**	**9.3**	**(81.6 %)**
	Steel (BF) + Crustal	**Marine**	**Traffic + Woodsmoke**	**Oil Combustion**	

(b) $PM_{2.5-10}$

	Component				
	1	2	3	4	Communalities
Na	.109	**.934**	.200	.087	**.931**
Mg	.249	**.906**	.260	.122	**.966**
Al	**.867**	.228	.030	.390	**.957**
Si	**.858**	.237	.055	.361	**.926**
S	.029	**.646**	**.695**	.162	**.928**
Cl	.180	**.941**	.108	.075	**.936**
K	.065	**.685**	-.136	.095	**.501**
Ca	**.746**	.363	.168	.451	**.919**
Ti	**.823**	.335	.162	.372	**.954**
Cr	.360	.069	**.813**	-.022	**.796**
Mn	**.693**	.241	.280	**.525**	**.891**
Fe	.366	.487	.451	**.584**	**.916**
Ni	.340	.040	**.677**	.233	**.629**
Cu	**.746**	-.147	.118	-.237	**.648**
Zn	-.133	.068	**.758**	-.027	**.597**
Rb	.279	.376	.310	**.711**	**.821**
Pb	.211	-.041	-.105	**.834**	**.753**
% Variance	**25.8**	**25.2**	**16.3**	**15.4**	**(82.7%)**
	Crustal + Traffic	**Marine + Steel 1(Sinter Plant)**	**Steel 2 (BOS) + Oil/Coal Combustion)**	**Steel 3 (BF)**	

Table 7.4: Rotated Component Matrix of LW Streaker (a) $PM_{2.5}$

	Component				
	1	2	3	4	Communalities
Na	.489	**.828**	-.022	-.208	**.968**
Mg	.123	**.841**	.332	-.239	**.890**
Al	.005	.294	**.899**	.110	**.906**
S	-.041	-.262	-.086	**.760**	**.655**
Cl	.212	**.899**	.230	.014	**.906**
K	**.902**	.350	-.085	-.058	**.946**
Ca	**.625**	.106	**.664**	-.135	**.862**
Ti	-.139	.060	.417	.094	**.206**
Cr	-.069	.122	.379	**.764**	**.747**
Mn	**.959**	.156	.028	-.023	**.946**
Fe	**.854**	-.103	.373	-.103	**.890**
Ni	**.699**	.289	-.430	.324	**.862**
Cu	.345	-.317	.041	.478	**.450**
Zn	**.813**	.408	-.308	-.043	**.924**
Pb	**.868**	.124	-.127	.168	**.813**
% Variance	**34.7**	**19.4**	**14.5**	**11.2**	**(79.8%)**
	Steel 1 (BF/BOS) + Woodsmoke	**Marine**	**Crustal**	**Steel 2 (Cokemaking)**	

(b) $PM_{2.5-10}$

	Component				Communalities
	1	2	3	4	
Na	**0.926**	0.287	0.139	-0.116	**0.972**
Mg	**0.922**	0.337	0.083	-0.075	**0.976**
Al	**0.554**	**0.811**	0.137	0.036	**0.985**
Si	0.489	**0.843**	0.159	0.054	**0.978**
S	**0.779**	0.44	0.097	-0.33	**0.92**
Cl	**0.938**	0.295	0.088	-0.068	**0.979**
K	**0.738**	**0.651**	0.132	-0.017	**0.985**
Ca	**0.689**	**0.673**	0.095	0.053	**0.939**
Cr	-0.008	0.055	**0.576**	**0.652**	**0.759**
Mn	0.474	**0.838**	0.13	-0.002	**0.944**
Fe	0.455	**0.863**	0.121	0.045	**0.969**
Ni	-0.191	0.029	-0.222	**0.821**	**0.76**
Cu	-0.058	-0.158	**-0.83**	0.139	**0.737**
Ti	0.418	**0.848**	0.139	0.144	**0.934**
Zn	0.028	**0.913**	-0.072	-0.139	**0.859**
Br	**0.866**	0.202	-0.307	-0.08	**0.892**
Sr	**0.829**	0.534	0.093	-0.009	**0.981**
% Variance	**40.3**	**35.7**	**7.9**	**7.7**	**-91.60%**
	Marine + Steel 1 (Sinter Plant)	**Crustal + Steel 2 (BF/BOS)**	**Steel 3 (Stainless welding**	**Oil/coal combustion**	

The PCA rotations for Streaker data were able to explain 79.8-81.6% of the total PIXE dataset for $PM_{2.5}$ similar to Prati *et al.* (2000) work at a steelworks site in Italy where 81.7-83.8% variance was explained. In the coarse fraction, Prati *et al.* (2000) study defined 85.1-85.6% of data variance relative to 82.8-91.6% obtained in this study. Related study by D'Alessandro *et al.* (2003) with PCA at four towns in Italy including Genoa, revealed 3-4 components that explained the variance range of 71-84% and 73-87% for $PM_{2.5}$ and $PM_{2.5-10}$ PIXE data, respectively

7.4 Conclusions

The PMF analysis of daily and hourly data collected at Port Talbot has allowed identification of between 6-7 factors for $PM_{2.5}$ and PM_{10} while PCA has identified 4-6 emission components. The hourly data has been found to more effective in resolving sources that the daily data could not detect. Also, diurnal profiles of pollution events were highlighted by the PIXE PMF data. The polar plots for the PMF profiles of PIXE data were helpful to resolve sources with similar signatures. Additionally, the polar plots were able to identify the directional locations of different steel processing units resolved by PMF. By and large, both daily and hourly PMF profiles are complementary and effective in identifying and apportioning pollution sources. The PMF and PCA solutions for both Partisol and PIXE data have been able to separate contributions from different steelworks units.

CHAPTER 8 - SINGLE PARTICLE ANALYSIS DURING THE PORT TALBOT CAMPAIGN

8.1 Abstract

This chapter summarizes the results of the single particle analysis using Aerosol-Time-of-Flight Mass Spectrometry (ATOFMS) during the Port Talbot campaign. During the four week sampling periods (April 18 to May 16, 2012), a total of 5,162,018 particles were sized. Of these, 580, 798 were successfully ionized. ENCHILADA software employed for analysing ATOFMS data utilized 96% of the hit particles to generate 20 clusters. Similar clusters were merged together and 18 clusters were generated from which 8 main particle classes were identified. The particle classes include: K-rich particles (K-CN, K-NO_3, K-EC and K-Cl-PO_3), sea salt (Na-NO_3), Silica dust (Na-$HSiO_2$), sulphate rich particles (K-HSO_4), nitrate rich particles (AlO-NO_3), Ca particles (Ca-NO_3), carbon particles (Mn-OC, Metallic-EC, EC, OC and OC-EC), and aromatic hydrocarbon (Arom) - PAH particles (Arom-CN, Fe-PAH-NO_3 and PAH-CN). With the aid of the wind sector plots, particle clusters of K-Cl-PO_3 and Na-$HSiO_2$ were related to the steelworks blast furnace/sinter plant while Ca-rich particles represented blast furnace emissions. K-CN, K-EC, Na-$HSiO_2$, K-HSO_4, Mn-OC, Arom-CN, Fe-PAH-NO_3, and PAH –CN particles were closely linked with emissions from the cokemaking and mills (hot and cold) steelworks sections. Na-$HSiO_2$ particles were also associated with blast furnace and crustal matter. Altogether, the steelworks showed a significant contribution to emitted single particles in Port Talbot.

8.2 Introduction

Aerosol time of flight mass spectrometry (ATOFMS) is a high time resolution online measuring instrument that provides a better and reliable approach for identification and apportionment of single particles. This method of particles measurement complements filter-based techniques in that it provides abundant information on the chemical mixing states and size of particles and helps to identify episodic pollution events (Dall'Osto *et al.*, 2008a).

The deployment of ATOFMS for both outdoor and indoor pollution studies has been widely reported in published works (Held *et al.*, 2002; Dall'Osto and Harrison, 2012; Ferge *et al.*, 2006; Dall'Osto *et al.*, 2007; Dall'Osto *et al.*, 2008a, b; Gross *et al.*, 2010; Healy *et al.*, 2013; Smyth *et al.*, 2013). Despite the numerous studies conducted around the world on single particle measurement, only a few have been done around the area of steel industries (Dall'Osto *et al.*, 2008a, b). This study aims to identify and apportion individual particles with steelworks fingerprint.

8.3 Materials and Methods

Single particle sampling using ATOFMS instrument has been discussed in chapter two. During the four week campaign, 5,162,018 particles were sized of which 580, 798 successfully ionized (hit particles). Successfully ionized particles were imported to ENCHILADA software for analysis (see details in chapter two). With ENCHILADA, 96% of the hit particles were analysed.

8.4 Results and Discussion

8.4.1 ATOFMS chemical composition

The chemically analysed (hit particles) represented 11.2% of the total sampled particles. Out of the total ionized particles, ENCHILADA utilised 96% (555,525 particles) to generate 20 clusters which are reduced to 18 clusters (by merging similar clusters with related spectral peaks and diurnal or temporal variations). The unscaled mean diameters as well as percentages represented by these particle clusters are also displayed in the Table 8.1. Most of the particle class exhibited mean particle diameter (Da) less than 1.0 µm, except Na-NO_3, which occurred at Da >1.0 µm.

These clusters could be categorized as:

1. K-rich particles and comprises of **K-CN, K-NO_3, K-EC and K-Cl-PO_3**
2. Sea Salt **- Na-NO_3**
3. Silica Dust **-Na-$HSiO_2$**
4. Sulphate-rich particles- **K-HSO_4**
5. Nitrate-rich particles-**AlO-NO_3**
6. Ca-rich particles –**Ca-NO_3**
7. Carbon particles **Mn-OC**, **Metallic-EC, EC, OC and OC-EC**
8. Aromatic Hydrocarbon (Arom) and PAH particles-**Arom-CN, Fe-PAH-NO_3 and PAH-CN**

Table 8.1 Summary ATOFMS particle cluster information

	Particle Classes	Clusters	Notable Peaks	Unscaled Mean Diameter (μm)	Number of Particles	% of Particles
1		K-CN	***m/z* +23, +39, -26, -46, -62, -97**	0.50	28408	5.1%
2		K-NO_3	***m/z* +39, -26, -46 , -62, -97**	0.50	92318	16.6%
3	K-rich	K-EC	***m/z* +23, +39, +60, -24, -26, -46, -48, -60, -62, -72, -84, -96, -108**	0.54	39931	7.2%
4		K-Cl-PO_3	***m/z* +23, +39, -35, -46, -60, -62, -79, -96**	0.67	61513	11.1%
5	Sea Salt	Na-NO_3	***m/z* +23, +39, -62, -46, -120, -147**	1.34	29394	5.3%
6	Silica Dust	Na-$HSiO_2$	***m/z* +23, +39, -16, -26, -36, -46, -48, -61, -72, -79, -97, -142, -144**	0.94	29137	5.2%
7	Sulphate	K-HSO_4	***m/z* +23, +39, +43, -26, -46, -62, -80, -97**	0.51	29845	5.4%
8	Nitrate	AlO-NO_3	***m/z* +43, +137, -46, -62, 97**	0.51	27358	4.9%
9	Ca-rich	Ca	***m/z* +23, +40, -26, -36, -46, -47, -60, -62, -72, -79, -84, -97, -108**	0.58	15303	2.8%
10		Mn-OC	***m/z* +39, +55, -25**	0.56	1742	0.3%
11		OC	***m/z* +38, -26, -46, -48, -62, -79, -97**	0.56	35051	6.3%
12		Metallic-EC	***m/z* +23, +27, +41, +48, +56, +59, -24, -36, -48, -60, -72, -84, -96, -108**	0.57	20339	3.7%
13	Carbonaceous	OC-EC	***m/z* ±36, ±60, +48, -24, -47, -72, -94, -97**	0.56	14619	2.6%
14		EC	***m/z* ±36, ±48, ±60, ±72, ±84, ±96, ±108, ±120, +132, +144, -24**	0.52	50657	9.1%
15		EC-NO_3	***m/z* ±36, ±48, ±60, +39, -24, -46, -62, 97**	0.64	10953	2.0%
16		Aromatic-CN	***m/z* +39, +51, +63, +74, +87, +98, -26, -35, - 46, -49, -62, -73, - 97 (for *m/z*>100, strong peaks were + 188 +200, +202, +224, +250)**	0.40	25242	4.5%
17	Arom-PAH	Fe-PAH-NO_3	***m/z* +56, -46, -62, -97, (for *m/z* >100, strong peaks were +226, +250, +202, +250)**	0.49	24980	4.5%
18		PAH-CN	***m/z* +39, +43, +63, +152, +165, +189, +202, +215, +226, +239, +252, +276, -26, -35, -46, -48, -62, -73, -80, -97**	0.52	18460	3.3%
Total					555,250	

Table 8.2: Locations of the steelwork sectors from the Fire Station sampling site

Sector/plant	Fire Station
Ironmaking	*190–270◦*
Sinter plant	
Blast furnace	
Raw materials	
	170–190◦
Steelmaking/cokemaking	
BOS plant	
Cokemaking	
Mills	*150–170◦*
Hot mill	
Cold mill	

8.4.1.1 K-rich particle class

This category includes **K-CN, K-NO_3, K-EC and K-Cl-PO_3** and formed 40% of the total ionized particles. The high abundance of the K-rich particles could be explained by the extreme sensitivity of ATOFMS instrument to K (Healy *et al.*, 2013). The spectra and polar plots of this particle class are shown in Figures 8.1-8.2.

8.4.1.1.1 K-CN particle

This particle type is characterized by elevated positive ion strength at *m/z* +23 $[Na]^+$ and intense negative signal at *m/z* -26 $[CN]^-$, Other little peaks (weak) are found at *m/z* +39 $[K]^+$, *m/z* -46 $[NO_2]^-$, *m/z* -62 $[NO_3]^-$, *m/z* -97 $[HSO_4]^-$, *m/z* -35 $[Cl]^-$, *m/z* -42 $[CNO]^-$, *m/z* -48 $[C_4]^-$, *m/z* -60 $[C_5]^-$ and *m/z* -72 $[C_6]^-$. The polar plot shows multi-dimensional emissions of this particle with much influence from local emissions (Figure 8.2). The evidence of steelworks contribution could be seen in the elevated concentration of the cluster towards the south-easterly and southerly wind-direction. The mills (hot and cold) and cokemaking units of Port Talbot steelworks are located between 150-190^o wind

sector. Table 8.2 shows the locations of the wind sectors of the steelworks from the Fire Station monitoring site where the ATOFMS instrument was placed. Contributions from the steelmaking section were apparent for this particle type.

K is a notable biomass burning/woodsmoke marker but has also been reported from the steelworks sinter plant (Hleis *et al.*, 2013). ATOFMS K-CN particle sampled at Athens, Greece by Dall'Osto and Harrison (2006) has been attributed to vegetative debris. $[CN]^-$ as suggested by Tao *et al.* (2011) might not necessarily be cyanide but carbon and nitrogen containing organic particle. In this study the identified cyanide with notable peak at *m/z* -26 might be related more to cokemaking emissions. Wastewater from cokemaking at the steelworks has been reported to contain significant amount of cyanide and thiocyanate (http://www1.eere.energy.gov/ manufacturing/ resources /steel /pdfs/roadmap_chap4.pdf).

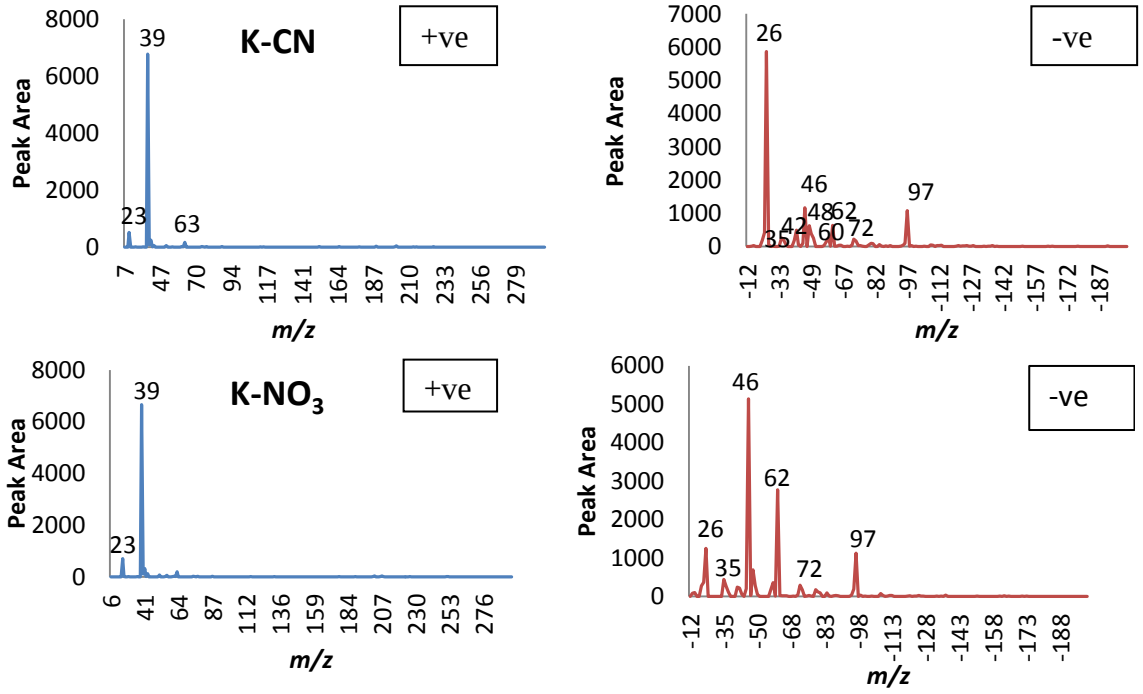

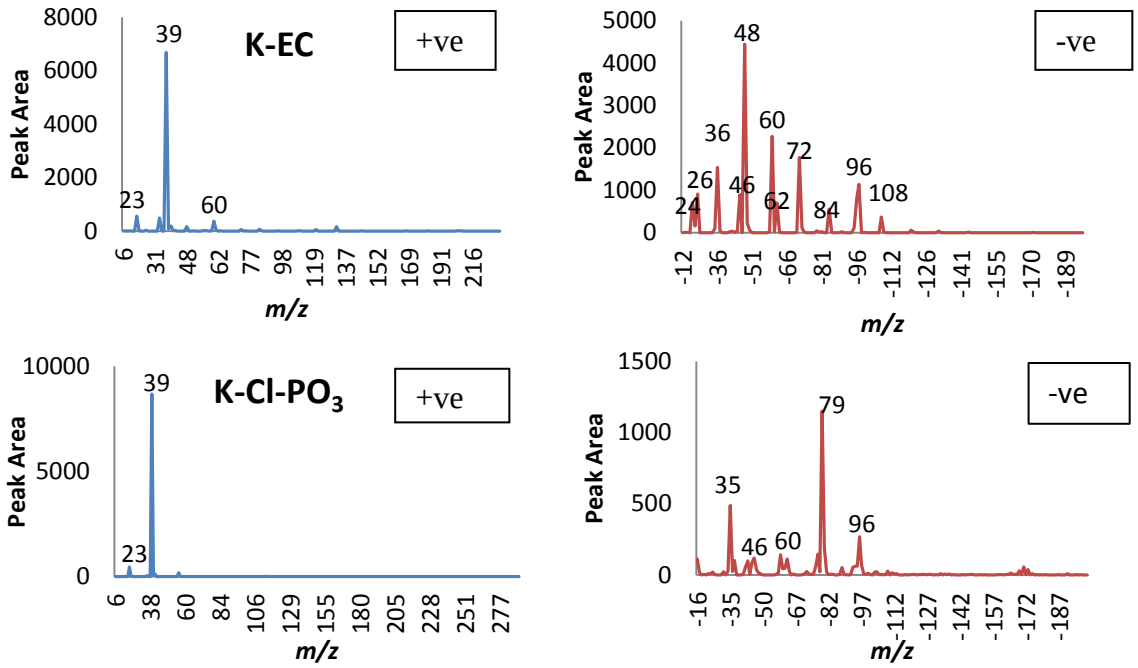

Figure 8.1: Mass spectra plots of K particle class

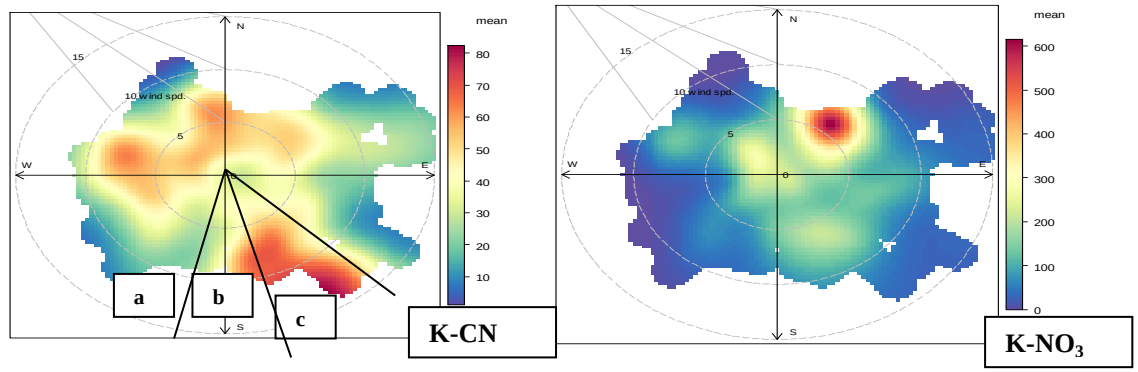

a-Ironmaking, b-Steelmaking/cokemaking, c-Mills

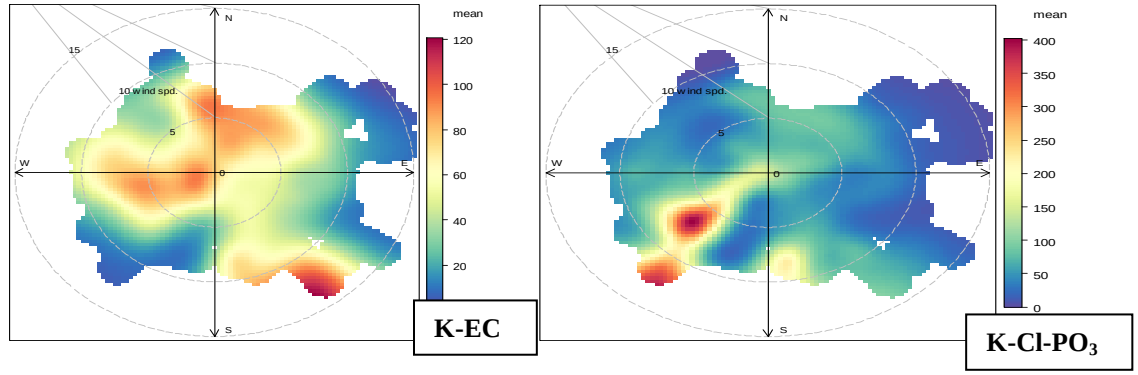

Figure 8.2: Polar plots of K-rich particle class

8.4.1.1.2 K-NO_3 particle

This particle class shows strong peaks for potassium (*m/z* +39) and NO_x (*m/z* -46 and -62) Low peaks are also displayed for $[CN]^-$ (*m/z* -26), $[Cl]^-$ (*m/z* -35), and $[HSO_4]^-$ (*m/z* -97). The polar plot reveals that K-NO_3 particle is concentrated towards the northern axis of the sampling site. This might be related to traffic emissions from the M4 motorway as well as residential woodsmoke (see Port Talbot map in chapter 4). A mild concentration shown at centre of the plot might suggest additional traffic contribution from A48 road.

8.4.1.1.3 K-EC particle type

K-EC particle shows strong peaks for potassium (*m/z* +39) and elemental carbon, EC (*m/z* $[C_n]^-$, n=2-9). Insignificant peaks of nitrite and nitrate (*m/z* -46 and -62), sodium (*m/z* +23) and $[C_5]^+$ (*m/z* +60) are also observed in this class. The evidence of internal mixing of K with EC is obvious in this particle type (Held *et al.*, 2002). The polar plots of K-EC cluster and K-CN appeared similar suggesting a related emission source. However, the temporal correlation between the two clusters is weak (r^2 = 0.13). K is a good marker for woodsmoke while EC could be emitted through traffic and coal combustion (Dan *et al.*, 2004; Harrison *et al.*, 2012c). The wind sector plot (Figure 8.2) showed the mills (cold and hot) as the highest emitter of K-EC particle. Moderate emissions from cokemaking ovens and residential combustions were also revealed by the polar plot. The previous work at Port Talbot has not identified K-EC particle (Dall'Osto *et al.*, 2008b). K-EC particle has been reported by Healy *et al.* (2013) at an urban background in Paris. The particle was attributed to local biomass combustion. The study of Bi *et al.* (2011) at the Pearl River Delta urban area has allocated 10.5% of biomass particle classes identified to K-EC.

8.4.1.1.4 K-Cl-PO_3 particle type

This particle type is characterized by strong peaks observed at *m/z* 39 $[K]^+$, *m/z* -35 $[Cl]^-$, *m/z* -79 $[PO_3]^-$ and *m/z* -96 $[HPO_3]^-$. The evidence of internal mixing of potassium and chloride showed that KCl might be related to an emission from the sinter plant and biomass burning (Li *et al.*, 2003; Dall'Osto *et al.*, 2008a, Hleis *et al.*, 2013). The recent work of Hleis *et al.* (2013) has reported KCl as a good indicator of sinter plant emission. The polar plot also established the sinter plant (located between 190-270^o of the sampling site, Table 8.2) as the major emission route of KCl. But the source of phosphate is unknown. In the filter-based measurement, phosphate was not observed. But the study by Dall'Osto *et al.* (2008a) has linked phosphate emission to the rolling mills contrary to depicted wind sector polar plot.

8.4.1.2 Sea salt class

The cluster found in this particle class is Na-NO_3. This class represents 5.3% of the total ENCHILADA particles. The evidence of coarse domination for Na-NO_3 cluster is clearly oberved by the mean aerodynamic diameter greater than 1.0 µm. Details of mass spectra and polar trends are shown respectively in Figure 8.3.

8.4.1.2.1 Na-NO_3 particle

This cluster is dominated by sodium (*m/z* +23) in the positive spectrum and nitrates in the negative spectrum (*m/z* -46 and -62). Smaller peaks are also found at *m/z* +39 $[K]^+$, +62 $[Na_2O]^+$, +81 $[Na_2Cl]^+$, -16 $[O]^-$, -35 $[Cl]^-$, -93 $[NaCl_2]^-$, -120 $[NaClNO_3]^-$ and -147 $[Na(NO_3)_2]^-$. The negative spectra of *m/z* -46 and -62 might also be suggesting the presence of $[Na_2]^-$ and $[Na_2O]^-$ instead of the conventional nitrate signatures. But the peaks of *m/z* -120

and -147 shows the evidence of internal mixing of sea salt with nitrate. Strong *m/z* -35 $[Cl]^-$ was expected to be high in this cluster but this was not the case. This might be linked to chloride depletion due to reaction between sea salt and nitrate or mineral dust aerosols (Zhao and Gao, 2008). The chloride depletion calculated for MOUDI's samples was 70 % supporting the low intensity of *m/z* -35 found in this cluster. The spectral characteristics displayed by this cluster are related to features of pure and aged salts described by Dall'Osto *et al.* (2004). However, the polar plot suggests that the particle might be mainly of aged sea salt. Tao *et al.* (2011) has adopted *m/z* -147 $[Na(NO_3)_2]^-$ as a marker for aged sea salt which agreed well with this particle cluster.

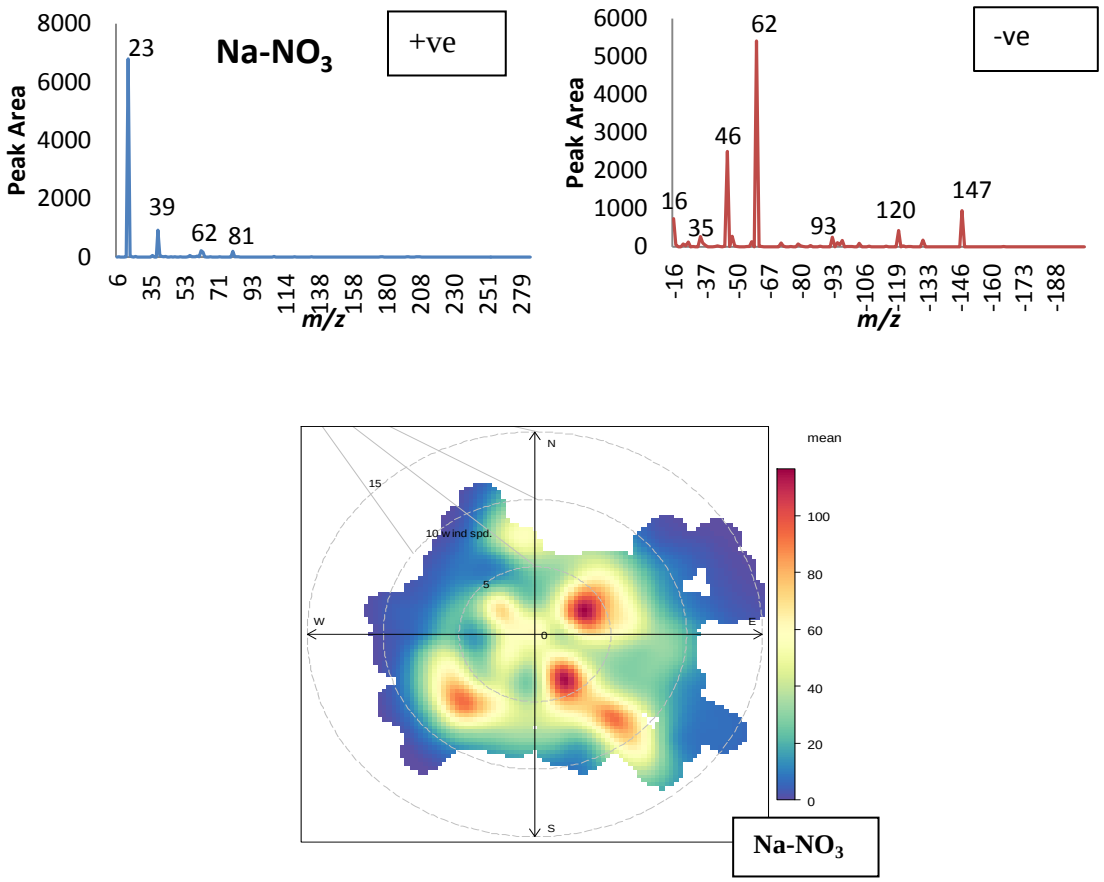

Figure 8.3: Sea salt particle spectra and polar plots

8.4.1.3. Silica dust particle

8.4.1.3. 1 Na-$HSiO_2$ particle

This particle cluster is characterized by intense signals of *m/z* +23 $[Na]^+$ in the positive spectrum and *m/z* -61 $[HSiO_2]^-$ in the negative spectrum (Figure 8.4). Evidence of internal mixing of this particle with EC was found with smaller peaks occuring at *m/z* -36, -48, -72 and -144. Nitrate peaks (*m/z* -46 $[NO_3]^-$ and -142 $[NH_4(NO_3)_2]^-$), *m/z* -16 $[O]^-$, -79 $[PO_3]^-$, and -97 $[HSO_4]^-$ are also identified in this peak. Multi-directional emissions of this particle class from sources such as blast furnace plant, mills and crustal matter was revealed by the polar plot. Silica is a raw material used at a relatively small proportion (0.3-0.9%) at a blast furnace during steel production (Ricketts, 2013). Silicate particles could originate from erosion and abrasion of local geological materials as well as construction activities (Moreno *et al.*, 2004a). The previous work at Port Talbot by Moreno *et al.* (2004a) using scanning electron microscopy revealed silicate particles to constitute 2 and 12% of the total mass of $PM_{2.5}$ and $PM_{2.5\text{-}10}$, respectively. A significant temporal correlation (r^2=0.52) was established between Na-$HSiO_2$ and Na-NO_3 particles indicating possible marine influence (Andreae *et al.*, 1986). The polar plot of Na-$HSiO_2$ particle (Figure 8.4) shows that the formation of this type of particles is favored at higher windspeed, relative to Na-NO_3 particle.

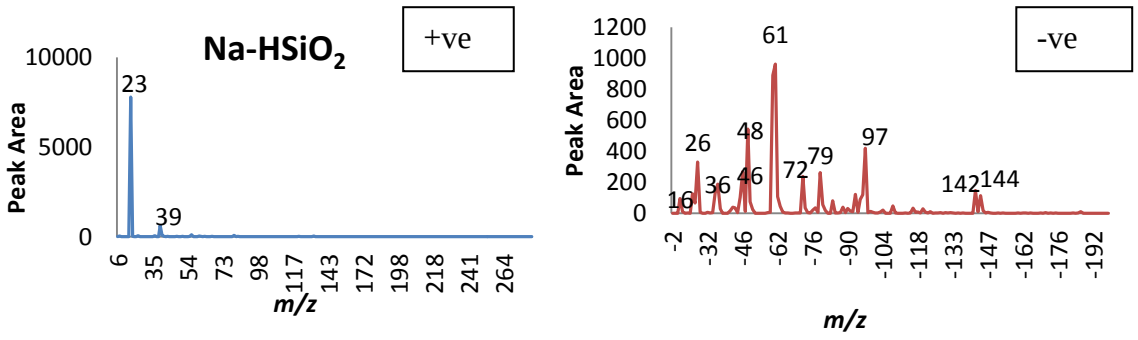

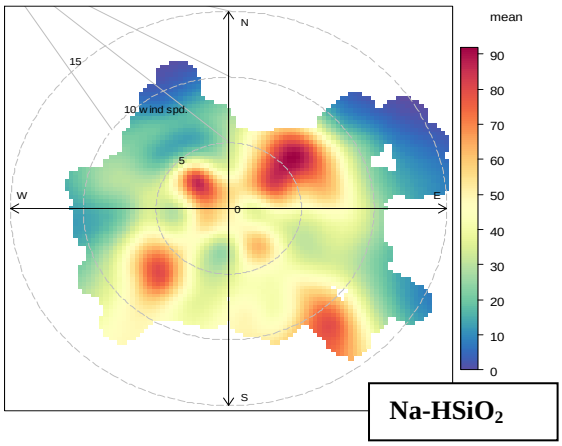

Figure 8.4 Silica particle mass spectra and polar plots

8.4.1.4 Sulphate (K-HSO_4) particle class

Sulphate rich particle is characterized by elevated negative peak of *m/z* -97 $[HSO_4]^-$ plus other weak peaks at *m/z* -26 $[CN]^-$, -46 $[NO_2]^-$, -62 $[NO_3]^-$ and -80 $[SO_3]^-$. The positive spectrum is dominated by the presence of *m/z* +39 [K]+ and other smaller peaks at *m/z* +23 $[Na]^+$, +43 $[AlO]^+$ and +59 $[AlO_2]^+$. $[HSO_4]^-$ particle constituted 5.4% of the total analysed particles. The polar plot depicts the steelworks cokemaking section as the major emitter of this particle. Significant contributions from the sinter and blast furnace plants are also evident in the polar plot. Elevated concentration of this particle observed at the northerly wind sector might suggest a long range transport. The spectra and polar plots of the particle class is shown in Figure 8.5.

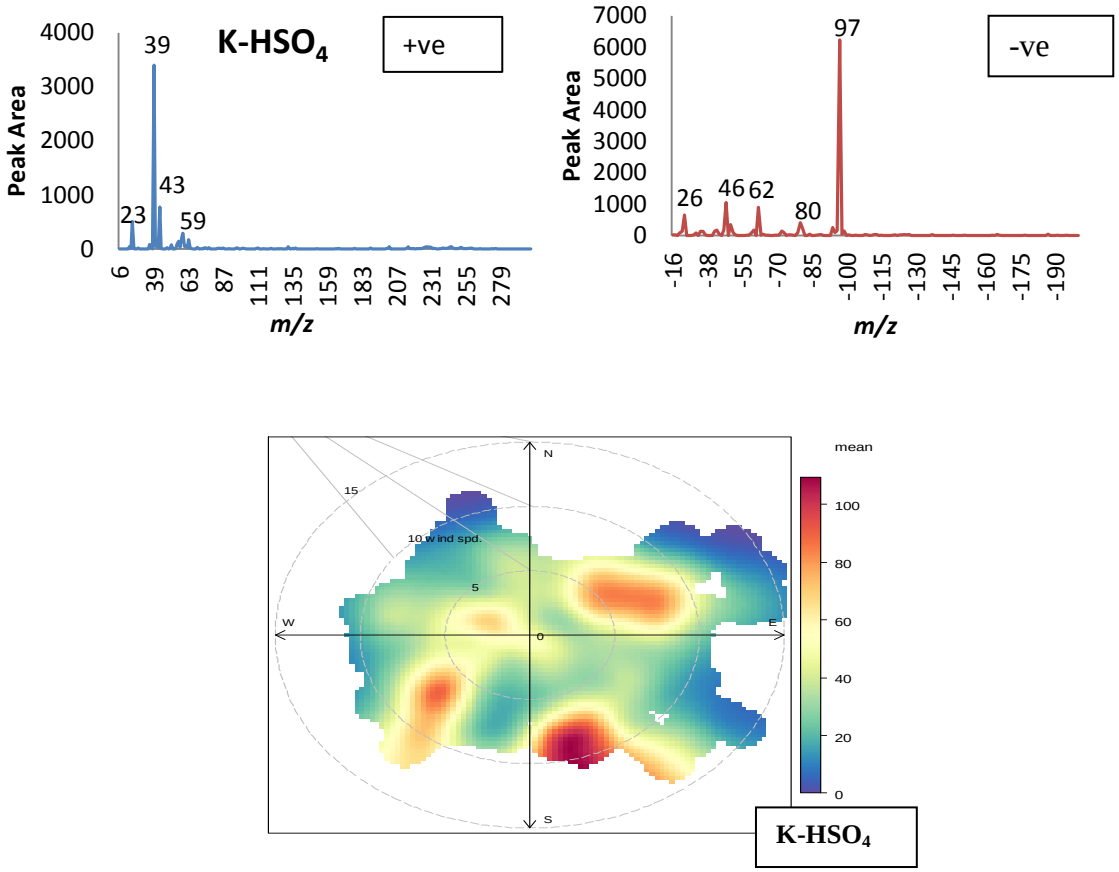

Figure 8.5: Mass spectra and polar plots of $K\text{-}HSO_4$ particle

8.4.1.5 Nitrate (AlO-NO_3) particle class

Abundance of nitrate spectral peaks at *m/z* -46 $[NO_2]^-$ and -62 $[NO_3]^-$ as well as *m/z* +43 $[AlO]^+$ are features of this particle class (Figure 8.6). Smaller peaks are also observed at *m/z* -97 $[HSO_4]^-$ and *m/z* +137 $[Ba]^+$. This particle formed 4.9% of the total ENCHILADA analysed particles. The evidence of a mixed source of secondary nitrate and crustal matter is peculiar with this source. Some published works have interpreted *m/z* +43 as oxidized organic compounds $[C_2H_3O]^+$ or nitrogen- containing organics $[CHNO]^+$ (Dall'Osto *et al.*, 2007; Dall'Osto and Harrison, 2012; Smyth *et al.*, 2013) but the unique *m/z* +137 $[Ba]^+$ occuring in this cluster could also suggest a crustal or soil source.

Barium and aluminium could be associated with traffic emissions from road resuspension and brake wear (Gietl *et al.*, 2010; Harrison *et al.*, 2012b). The directional plot of nitrate particle is also highlighted in Figure 8.6. The mild concentration of this cluster counts at the centre of the plot indicates traffic emissions from vehicular exhaust and road dust. Higher concentration of these particles at the northerly wind direction suggests traffic emissions from the M4 (South Wales to London) motorway. AlO-NO_3 particles show a strong temporal relationship (r^2=0.70) with K-NO_3 particles depicting a related emission source.

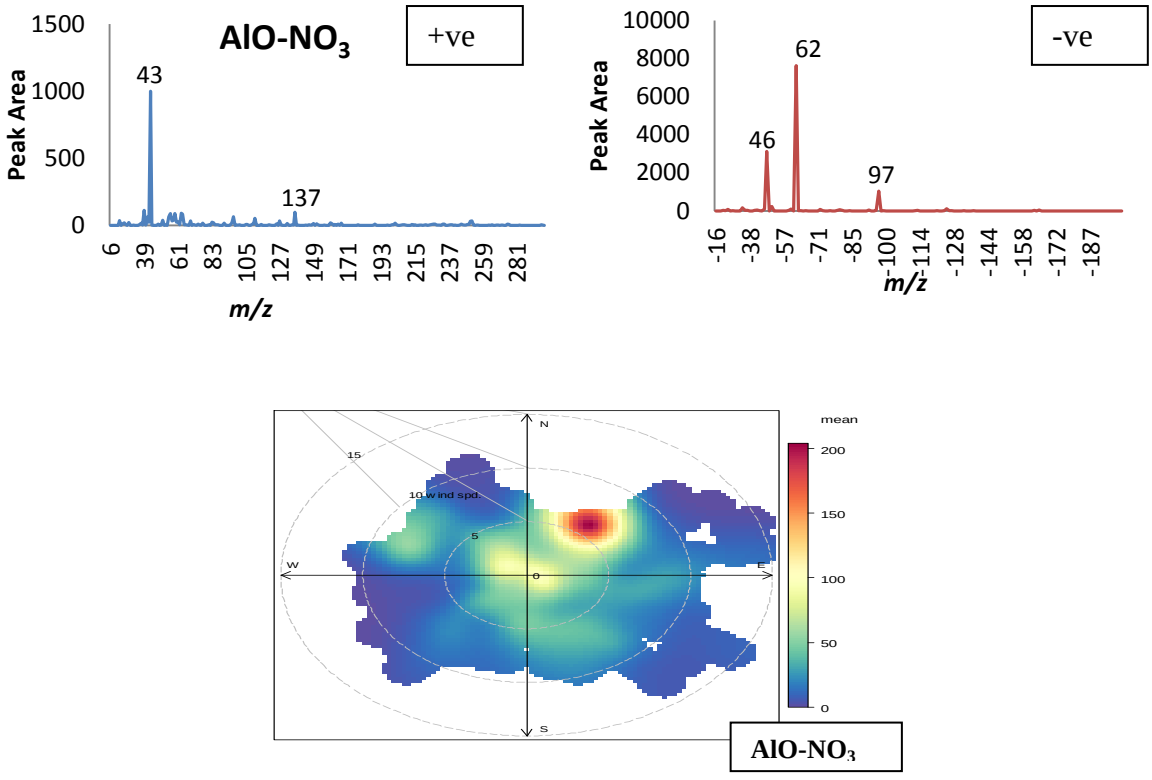

Figure 8.6: Mass spectra, polar and diurnal plots of AlO-NO_3 particle

8.4.1.6 Ca-rich particle class

Calcium-rich particle class constitutes 2.8% of the total ENHILADA analysed particles. The mass spectra, polar and diurnal plots of this particle are displayed in Figure 8.7. The

particle type typically shows high spectra peaks at *m/z* +40 $[Ca]^+$, -46 $[NO_2]^-$ and -62 $[NO_3]^-$. Calcium particle is internally mixed with elemental carbon *m/z* -24 $[C_2]^-$, -36 $[C_3]^-$, -48 $[C_4]^-$, -60 $[C_5]^-$, -72 $[C_6]^-$, -84 $[C_7]^-$, -108 $[C_9]^-$, organic carbon -*m/z* -43 $[C_2H_3O]^-$, phosphate *m/z* -79 $[PO_3]^-$ and sulphate *m/z* -97 $[HSO_4]^-$. A relatively smaller sodium peak *m/z* +23 $[Na]^+$ occurs in this cluster. This particle type might be related to anthropogenic emissions especially from the steelworks. This could be further established with the cluster aerodynamic diameter that is less than 1.0 µm (Table 8.1).

The polar plot shows the blast furnace steel production unit as the main contributor to this particle class. Limestone ($CaCO_3$) and dolomite ($CaMg(CO_3)_2$) are key raw materials in basic furnace unit of steel industry (Machemer, 2004).

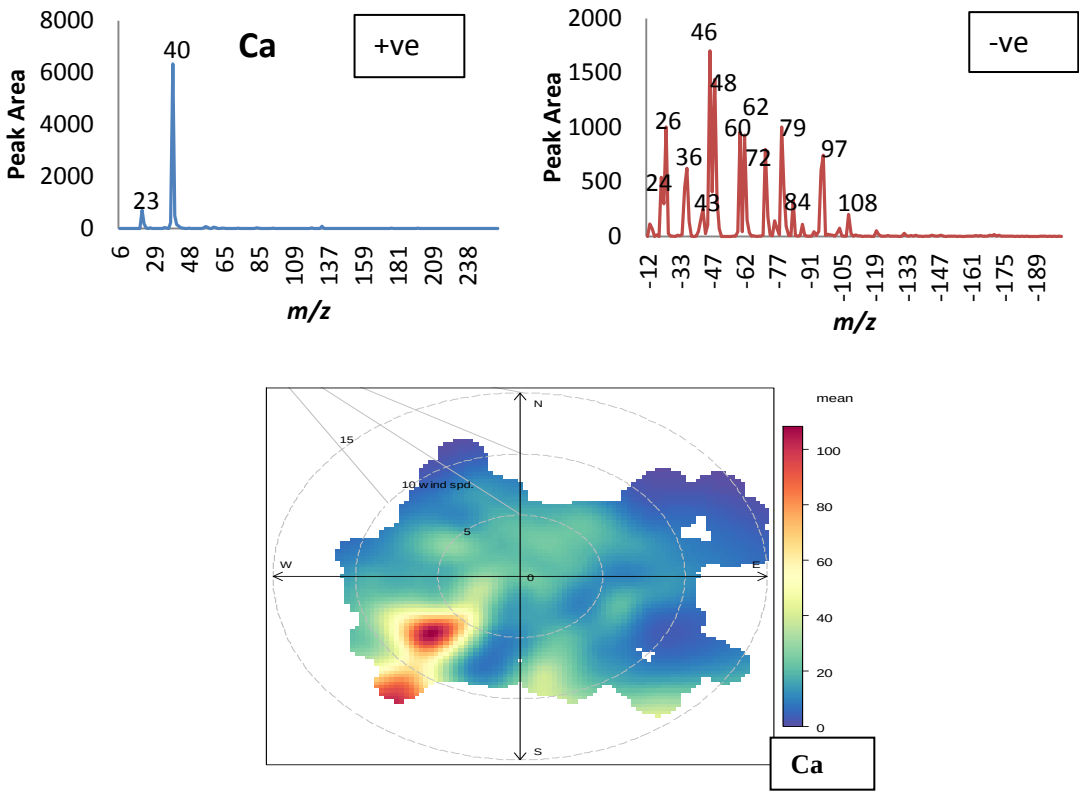

Figure 8:7: Mass spectra, polar and diurnal plots of Ca particle

8.4.1.7 Carbon class particles

The carbon particles comprise the following particle types: Mn-OC, OC, Al, OC-EC, OC-EC, EC and EC-NO_3. Carbon particle class makes a total of 24% of ENCHILADA analysed particles. The mean aerodynamic diameter of carbon class particles are less than 1.0 µm (Table 8.1). Figures 8.8-8.9 show the mass spectra and polar plots of carbon class particles.

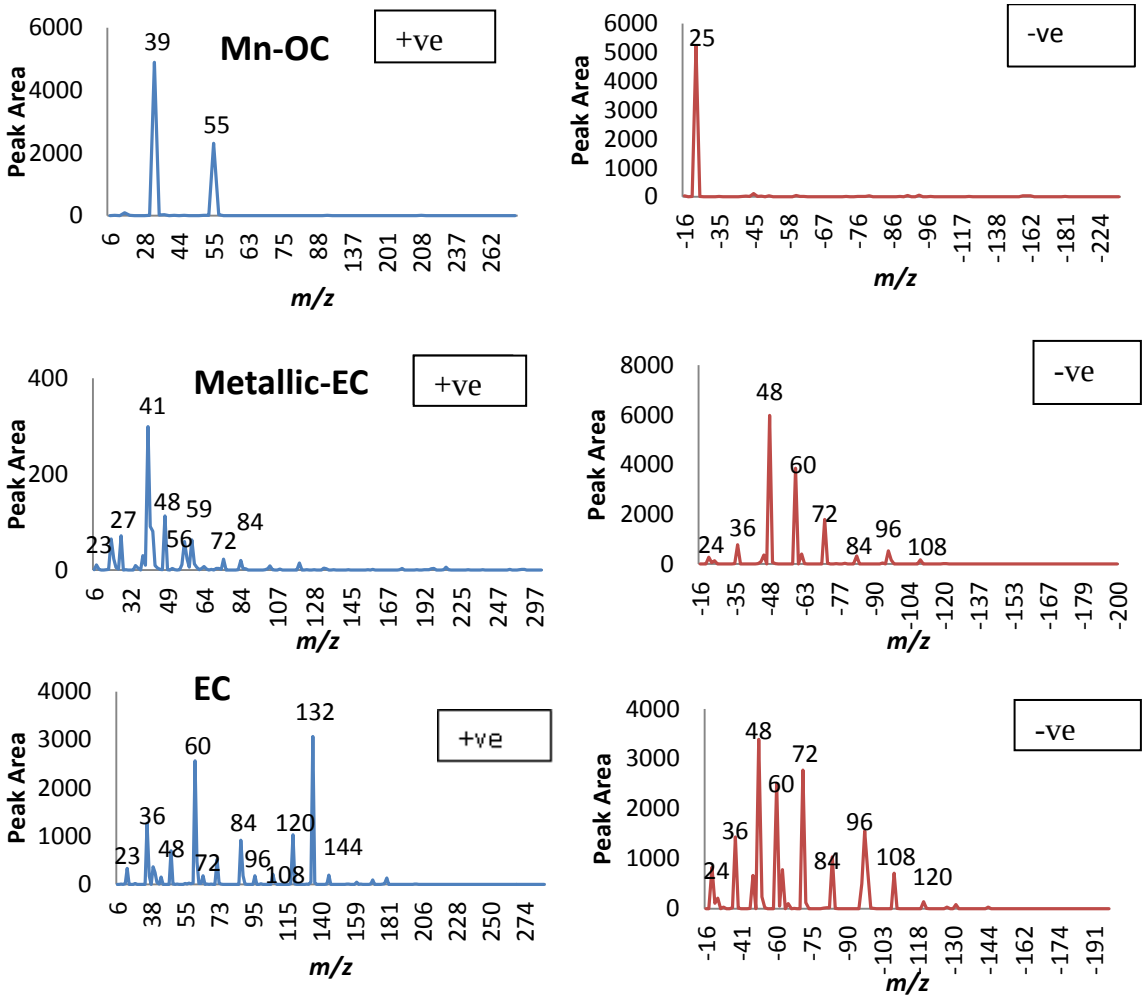

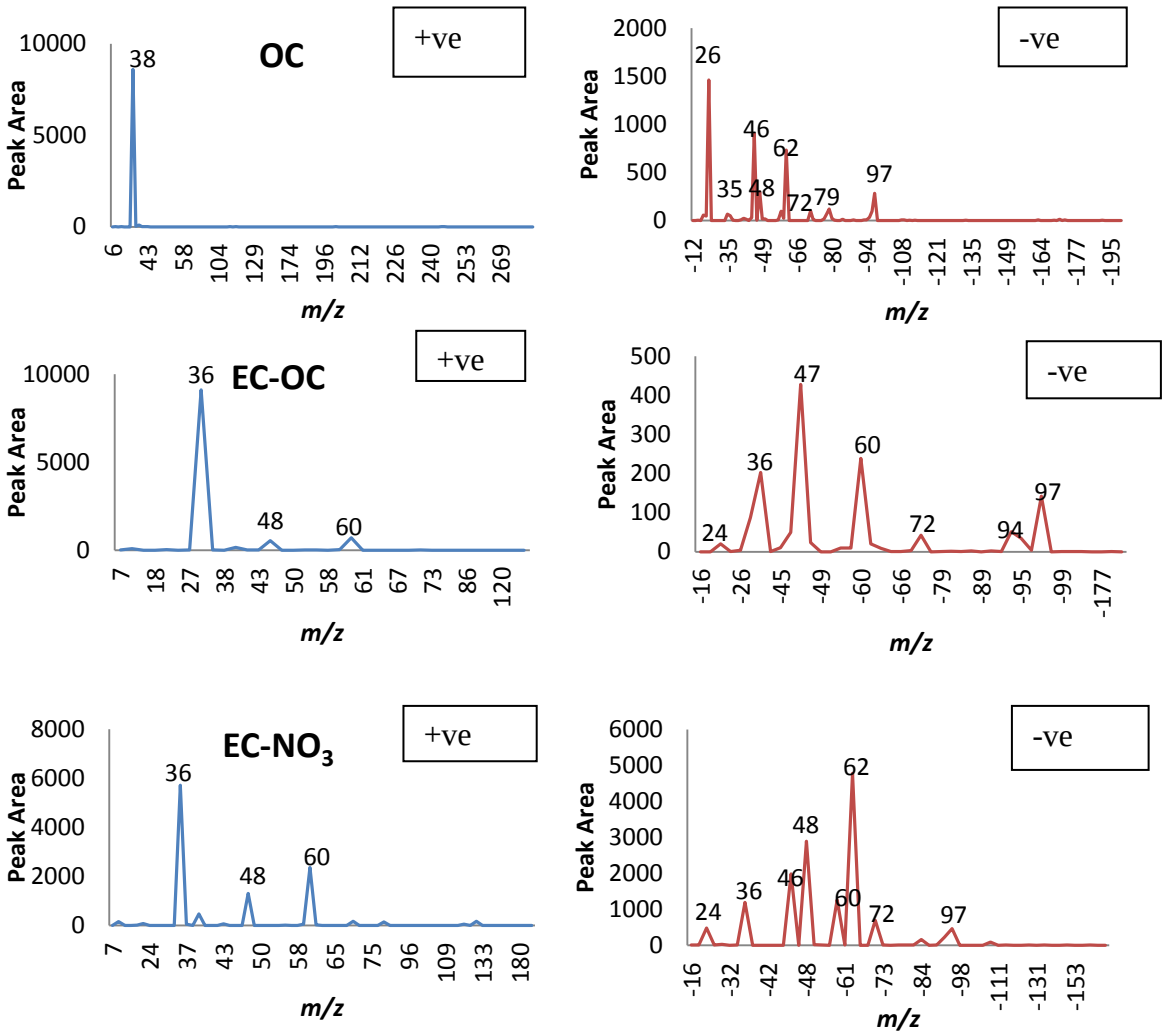

Figure 8:8: Mass spectra trends of carbonaceous particles

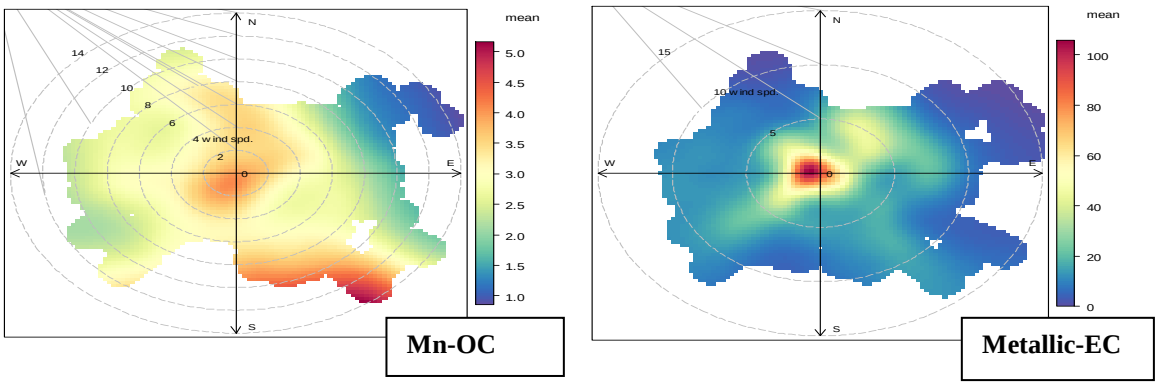

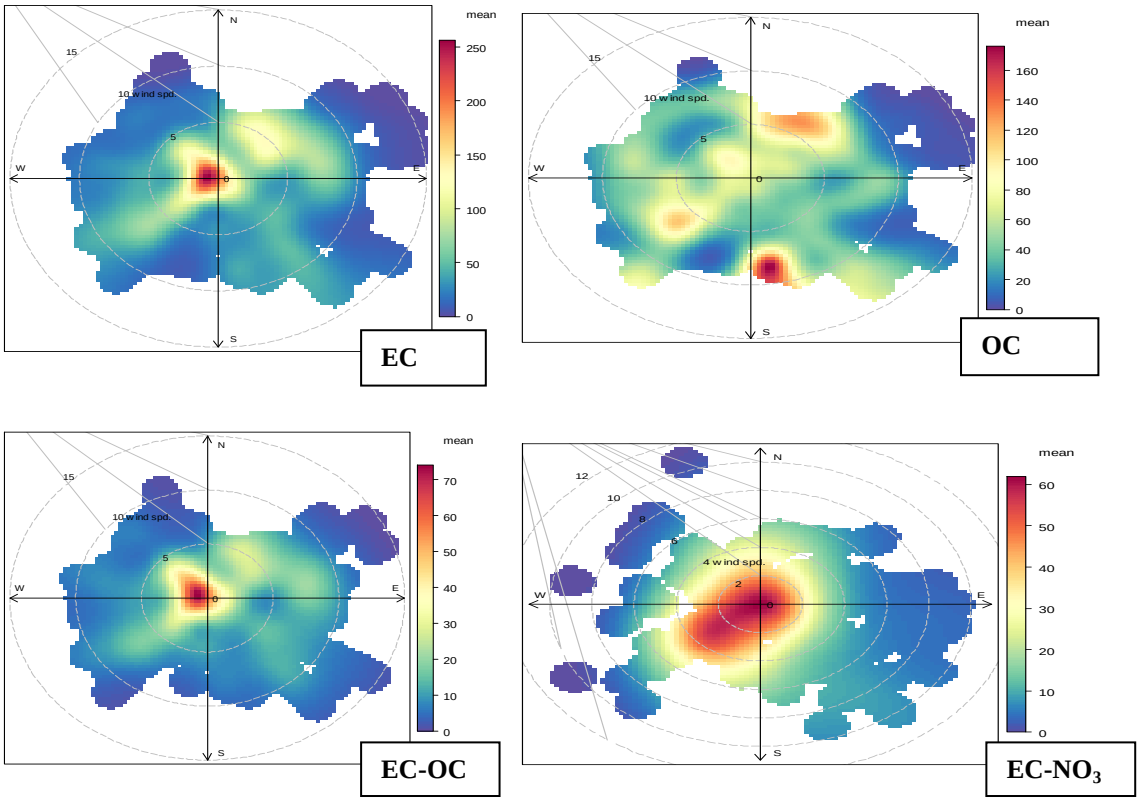

Figure 8:9: Polar plots of carbonaceous particles

8.4.1.7.1 Mn-OC particle type

This particle type is characterized by strong positive peaks at *m/z* +39 $[K]^+$ and +55 $[Mn]^+$. A lone strong negative peak was observed at *m/z* -25 $[C_2H]^-$ (Figure 8.10). Manganese is a notable emission from the steel industry from the ironmaking production unit (Dall'Osto *et al.*, 2008a; Mazzei *et al.*, 2008). The spectra *m/z* +39 and +55 could possibly be due hydrocarbon fragments of $[C_3H_3]^+$ and $[C_4H_7]^+$. The *m/z* +55 might be better attributed to manganese being a standalone signature. Published works have reported *m/z* +55 as organic signatures co-existing with peaks such as *m/z* +27 $[C_2H_3]^+$, +43 $[C_3H_7]^+$, +63 $[C_5H_3]^+$ and +77 $[C_6H_5]^+$ (Bi *et al.*, 2011; Dall'Osto and Harrison, 2012). Organic carbon due to $[C_2H]^+$, is rarely reported in the literature. Occurrences of *m/z* +39 $[K]^+$ and +55 $[Mn]^+$ signatures in particles sampled at Shanghai, China was attributed to biomass

burning (Tao *et al.*, 2011). The directional plot indicates multi-emission pattern of Mn-OC particle which does not support the exclusive emission from the steelworks.

8.4.1.7.2 Metallic-EC particle type

Metallic-EC particle shows positive spectral signal at *m/z* +23 $[Na]^+$, +27 $[Al]^+$, +48 $[Ti]^+$, +56 $[Fe]^+$, +59 $[AlO_2]$, +72 $[FeO]^+$ and +84 $[ZnO]^+$. Elevated *m/z* peak observed at +41 might be related to organic carbon $[C_3H_6]^+$. The negative spectrum is characterized mainly by elemental carbon $[C_n]^-$ where n=2-9. This particle-type may be related to local emissions from the traffic as indicated by polar plot. The review by Thorpe and Harrison (2008) has shown that Al, Fe, Zn, Ti and K can be emitted from brake lining or wear as well as road dust.

8.4.1.7.3 EC particle type

EC particle shows notable peaks at *m/z* $[C_n]^{\pm}$ (n = ±2-10). Other peaks occur at $[C_n]^+$ (n=11 and 12) and *m/z* +23 $[Na]^+$. Among the carbonaceous species, EC particle is the most abundant. Excluding K-EC particle type categorized under K-rich class, EC-particle represented 38% of all carbon-rich particles. As usual, this particle has a signature from local traffic emissions. This is supported by the polar plot which also depicts reasonable contributions from the sinter and blast furnace plants.

8.4.1.7.4 OC particle type

OC particle is mainly characterized by *m/z* spectra showing positive peak at *m/z* +38 $[C_3H_2]^+$ and negative peaks at *m/z* -26 $[CN]^-$, -46 $[NO_2]^-$, -48 $[C_4]^-$, -62 $[NO_3]^-$, -79 $[PO_3]^-$

and -97 $[HSO_4]^-$. Smaller peaks are shown at *m/z* -35 $[Cl]^-$ and -72 $[C_6]^-$. Polar plot suggested the cokemaking plant as the main source of this type of particles.

8.4.1.7.5 OC-EC particle type

The characteristic peaks of this particle class include: *m/z* ±36 $[C_3]^{\pm}$, +48 $[C_4]^+$, ±60 $[C_5]^{\pm}$, -47 $[C_3H_{11}]^-$, -72 $[C_6]^-$, -94 $[C_8H_{10}]^-$ and -97 $[HSO_4]^-$. The presence of *m/z* -47 and -94 could also suggest signatures of carbon-containing-halogen particles which are $[CCl]^-$ and $[(CCl)_2]^-$. Halogenated carbon has been proved very difficult to observe in negative spectrum and has been rarely observed in positive spectrum (Silva and Prather, 2000).

OC-EC exhibits better temporal relationship with metallic-EC (r^2=0.80) than any other carbonaceous particles suggesting common emission sources. OC-EC particle shows a relatively weak association with OC particle class (r^2 = 0.22) and a moderate relationship with EC-NO_3 (r^2 = 0.33). This particle type shows a trend similar to metallic-EC particle polar plot re-establishing related emission sources.

8.4.1.7.6 EC-NO_3 particle type

EC-NO_3 particle is another sub-particle class observed for carbonaceous species. The peaks of this particle type occur at *m/z* ±36 $[C_3]^{\pm}$, ±48 $[C_4]^{\pm}$, ±60 $[C_4]^{\pm}$, -24 $[C_2]^-$, -46 $[NO_2]^-$, -62 $[NO_3]^-$, -72 $[C_6]^-$ and -97 $[HSO_4]^-$. This particle type is moderately correlated with EC particle with coefficient of 0.45. The wind direction plot indicates the traffic and ironmaking sections of the steelworks as a major contributor to this particle type.

8.4.1.8. Aromatic hydrocarbon (Arom) and PAH particle class

Three particle types are found for Arom-PAH particle class (Aromatic-PAH-CN-HSO_4, Fe-PAH-NO_3 and PAH-NO_3) which constitutes 12.3% of ENCHILADA analysed particles. The spectra and polar information of Arom/PAH class particles is shown in Figures 8.10 and 8.11.

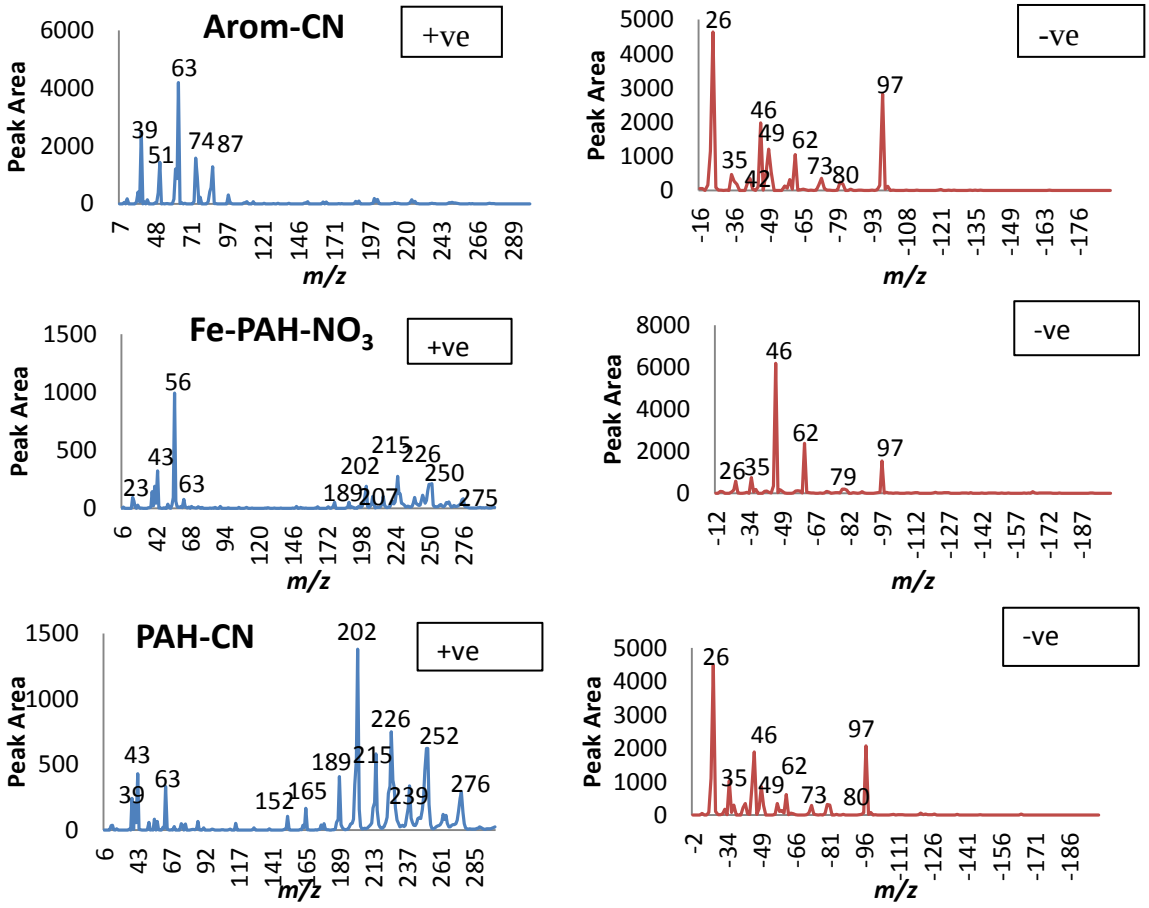

Figure 8.10:Mass spectra plots of Arom-PAH particles

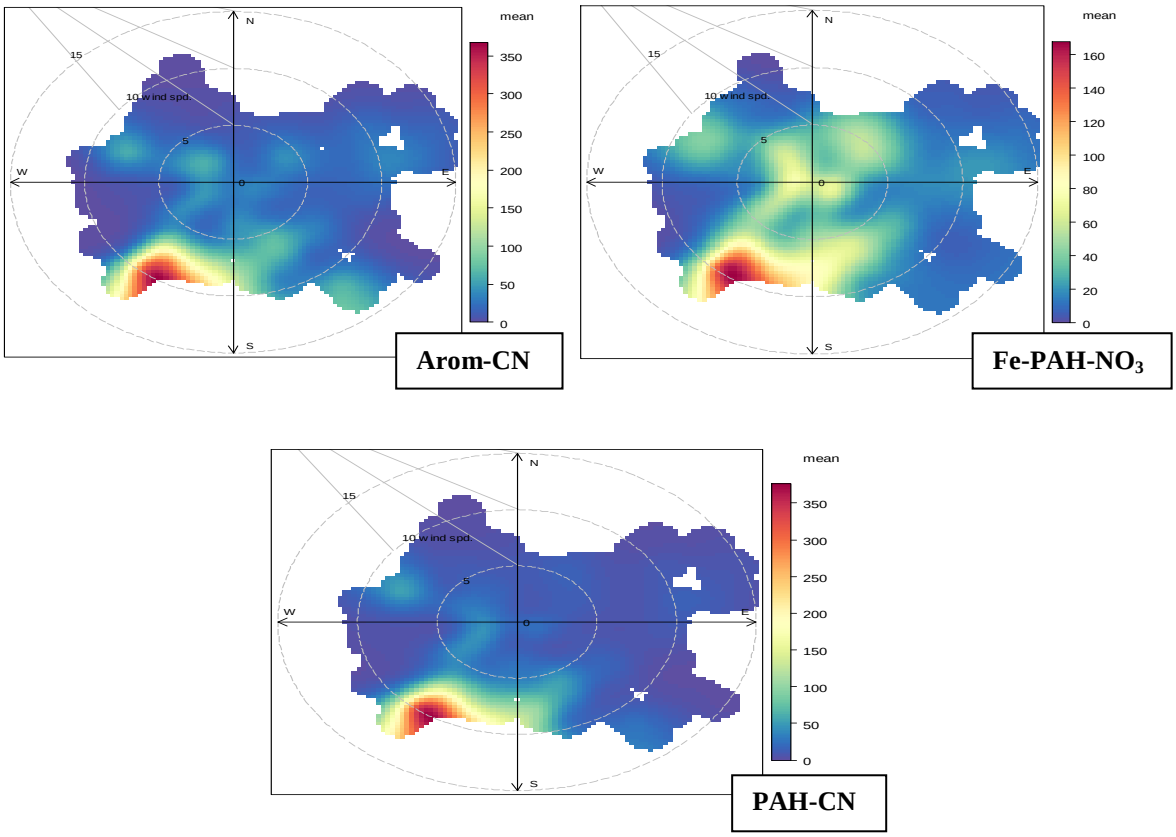

Figure 8.11: Polar plots of Arom-PAH particles

8.4.1.8.1 Aromatic-CN particle type

Arom-CN particles are defined at these significant spectral signals; namely *m/z* +39 $[C_3H_3]^+$, +51 $[C_4H_3]^+$, +63 $[C_5H_3]^+$, +74 $[C_4H_{12}N]^+$, +87 $[C_5H_{13}N]^+$, -26 $[CN]^-$, -35 $[Cl]^-$, -42 $[CNO]^-$, -46 $[NO_2]^-$, -49 $[C_4H]^-$, -62 $[NO_3]^-$, -73 $[C_6H]^-$ and -97 $[HSO_4]^-$. This particle class shows uniqueness for amide functional group at *m/z* +74, +87, -26 and -42. The occurrence of *m/z* -49 and -73 in this particle class also indicates fragmentation of PAH and unsaturated organic carbon (Silva and Prather, 2000; Dall'Osto and Harrison, 2012). Traces of PAH could be seen in this cluster at *m/z* > 100. The *m/z* +39, +51 and +63 might also suggest interference of $[K]^+$, $[V]^+$ and $[Cu]^+$. The polar plot of this particle shows a convincing steelworks emission from the basic furnace (BF) plant (190-270^o) and

moderate contributions from the cokemaking and basic oxygen furnace steelmaking (BOS) sections (170-190^{o}).

8.4.1.8.2 Fe-PAH-NO_3 particle type

Elevated peaks of *m/z* +23, +43, +56, +63, +188, +202, +224 and +250 are found in the positive spectrum of this cluster while the negative spectrum occurs at *m/z* -35, -46, -62, -79 and -97. This particle class shows low intensity for PAH (*m/z*>100) but strong peak for Fe (*m/z* +56), nitrate (*m/z* -46 and -62) and sulphate (*m/z* -97). The previous study at Port Talbot has reported strong *m/z* peak for Fe and PO_3 (FeP particle) which has been attributable to emissions from the rolling mill section (Dall'Osto *et al.*, 2008a). In this study, there is also a convincing evidence of internal mixing of Fe with PO_3 (*m/z* -79); though the phosphate peak is weak. A relatively weak *m/z* +207 appearing in this particle cluster might suggest Pb which has been reported in Dall'Osto *et al.* (2008a) work. With directional plot, emission of this particle is similar to that of Arom-CN particle from the steelworks. Temporal correlation shows a strong association between Fe-PAH-NO_3 and Arom-CN (r^2 = 0.64). PAH emissions have been linked with steelworks emissions in published works (Tsai *et al.*, 2007; Baraniecka *et al.*, 2010; Brown *et al.*, 2013). Fe is a notable BF emission (Oravisjarvi *et al.*, 2003; Machemer, 2004; Moreno *et al.*, 2004a).

8.4.1.8.3 PAH-CN particle particle type

This particle class has a resemblance of both Arom-CN and Fe-PAH (temporal correlation coefficients of 0.57 and 0.87, respectively) but with a unique strong *m/z* signal at +202, +226, +252, -26, -46 and -97. Peaks are also distinctively observed at *m/z* +43, +63, +189, +215, +276, -35, -49, -62 and -73. This particle is a typical PAH cluster

internally mixed with inorganic constituents. The PAH species represented by *m/z* +202, 226 and 252 are most likely to be pyrene (mass=202), chrysene (226), benzo[a]pyrene (252), benzo[k] fluoranthene (252) and benzo[b]fluoranthene (252). Some of these PAH constituents have also been reportedly to be associated with emissions from diesel engine, wood and coal combustion (Lakhani, 2012). PAH is a known human carcinogen (Bostrom *et al.*, 2002; Delgado-Saborit *et al.*, 2011). The polar plot of PAH-CN particle shows more of the steelworks (BF and BOS) emission and no evidence of traffic which distinguishes the particle type from Fe-PAH and Arom-CN. These similarities among the Arom-CN, Fe-PAH-NO_3 and PAH-CN suggest common emission source with probable emission from the BF, sinter, BOS and cokemaking steeworks sections.

8.4.2 Source Contributions by ATOFMS Particles

A summary of ATOFMS identified particle classes is presented in Table 8.3. The K-particle class shows the highest contribution which could be linked to emission sources like biomass burning, wood combustion, vegetation, steelworks and traffic. Next to K-particle class in the ATOFMS source contribution data is the carbon class which constitutes 24% of the total ENCHILADA particles. The least contribution is shown by the calcium particle class which represents 2.8% of the total analysed particles.

Table 8.3: Summary of the particle cluster emission sources

	Particle Classes	Cluster s	All Emissions Sources	Strong Emissions Sources	% of Particle s
1	K-rich	K-CN	Cokemaking/Mills	Cokemaking/Mills	5.1%
2		K-NO_3	Traffic/Biomass	Traffic	16.6%
3		K-EC	Cokemaking/Mills/Biomass	Cokemaking/Mills	7.2%
4		K-Cl-PO_3	BF/Sinter/Mills	BF/Sinter	11.1%
5	Sea Salt	Na-NO_3	Marine	Marine	5.3%
6	Silica Dust	Na-$HSiO_2$	Traffic/BF/Cokemaking/Mills	Cokemaking/Mills	5.2%
7	Sulphate	K-HSO_4	Cokemaking/Mills/Secondary	Cokemaking/Mills	5.4%
8	Nitrate	AlO-NO_3	Traffic/Secondary	Traffic	4.9%
9	Ca-rich	Ca	BF/sinter	BF/sinter	2.8%
10	Carbonaceous	Mn-OC	Cokemaking/Mills	Cokemaking/Mills	0.3%
11		OC	Cokemaking/Mills	Cokemaking/Mills	6.3%
12		Metallic-EC	Traffic	Traffic	3.7%
13		OC-EC	Cokemaking/Mills	Cokemaking/Mills	2.6%
14		EC	Traffic	Traffic	9.1%
15		EC-NO_3	Traffic	Traffic	2.0%
16	Arom-PAH	Aromatic-CN	BF/Sinter/BOS/Cokemaking	BF/Sinter	4.5%
17		Fe-PAH-NO_3	BF/Sinter/BOS/Cokemaking	BF/Sinter	4.5%
18		PAH-CN	BF/Sinter/BOS/Cokemaking	BF/Sinter	3.3%

BF-blast furnace, BOS-basic oxygen furnace steelmaking

From Table 8.3, the source emissions of the ATOFMS particle types could be broadly categorised into steelworks, traffic, marine and secondary aerosols. Source contributions of these particle clusters were calculated from their scaled mass concentrations. Results are shown in Figure 8.12. The combined steelworks (BF/Sinter+/Mills/Cokemaking) show the highest contribution (50%) of the total fine (ATOFMS) particles followed by traffic and marine. The secondary aerosols explain a total contribution of 10%. As depicted in their polar plots (see Figures 8.5 and 8.5) sulphate particles have a close link with the

steelworks emissions from cokemaking and mills while nitrate particles are related with traffic emissions.

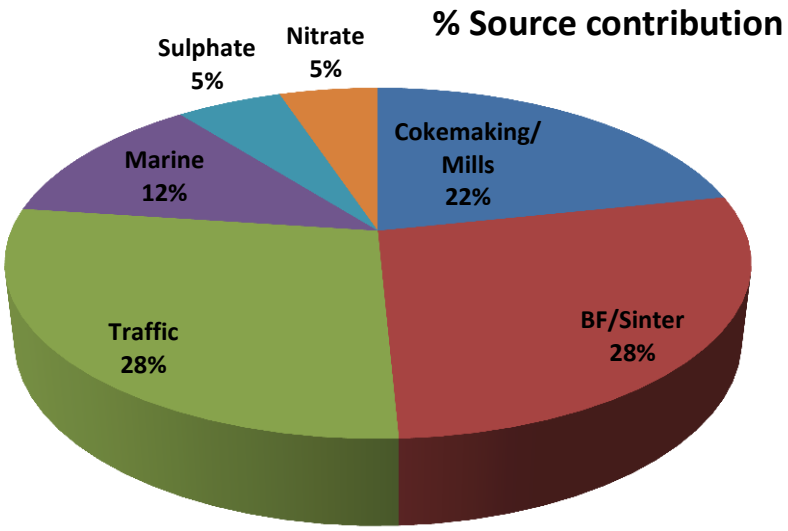

Figure 8.12: Source contribution of particle classes

8.4.3 Size Distribution of Particle Classes

The data collected with the ATOFMS instrument was scaled for particle size distribution and number concentrations with particles' information obtained from the Grimm optical particle counter (OPC). The Grimm OPC was operated simultaneously with the ATOFMS at the Fire Station sampling site. The purpose of this, is to scale and quantify the data generated by the ATOFMS system. The inlet efficiency (inverse transmission efficiency, E) of the ATOFMS instrument was therefore calculated.

The inverse transmission efficiency, E is calculated therefore as:

$$E = N_{Grimm}/N_{ATOFMS} \qquad (8.1)$$

where,

N_{Grimm} is the Grimm particle number concentration

N_{ATOFMS} is ATOFMS particle number concentration

ATOFMS particles are defined by number counts of total hit and missed particles that correspond to same size range of Grimm particle counter. Hit particles are completely sized and ionized particles while missed particles are sized but un-ionized particles in the ATOFMS instrument. The size range of ATOFMS particles during the campaign is 0.2-1.9 µm while the size range for Grimm was 0.3-20 µm. The particle sizes where E was calculated to merge with Grimm size range are in the interval 0.3-0.4, 0.4-0.5, 0.5-0.65, 0.65-0.8, 0.8, 1.0, 1.0-1.6 and 1.6-2.0 µm.

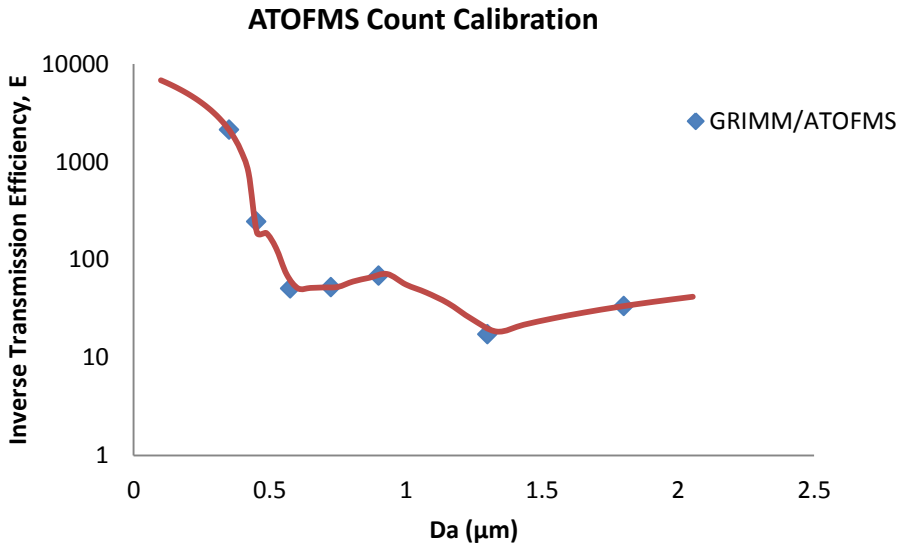

Figure 8.13: Inverse transmission Efficiency versus D_a

By applying the equation 8.1, the resulting curve generated for correcting the ATOFMS counts is displayed in Figure 8.13. The inverse transmission efficiency shows a minimal value at particle diameter, D_a =1.3 µm which therefore represents the maximum inlet

efficiency of the ATOFMS instrument during the campaign. Further details of inverse transmission efficiency has been discussed in Dall'Osto *et al.* (2006).

The hit rate calculated for ATOFMS particles in the size range that corresponds to the Grimm size range is shown in Table 8.4. The hit rate, H is calculated using equation 8.2:

H= Hit/(Hit+Missed) * 100 ***(8.2)***

The hit rate of particle are generally higher for the particle range 0.3-0.4 µm while particles between 0.4-2.0 µm have closely related values of H.

Table 8.4: The hit rate of particle diameters

Size range	Hit	Missed	H (%)
0.3-0.4	120149	389536	31
0.4-0.5	122092	1077979	11
0.5-0.65	172133	1784027	10
0.65-0.8	58978	630383	9
0.8-1.0	30239	367278	8
1.0-1.6	48760	681845	7
1.6-2.0	21166	257752	8

The corrected ATOFMS size distributions of particle number concentrations for the particle clusters identified is presented in Figure 8.14. The scaled ATOFMS particles show higher number concentrations at diameters of 0.3-0.4 µm. K-Cl-PO_3 and some carbon particle clusters also exhibit elevated number concentrations at 0.5 µm.

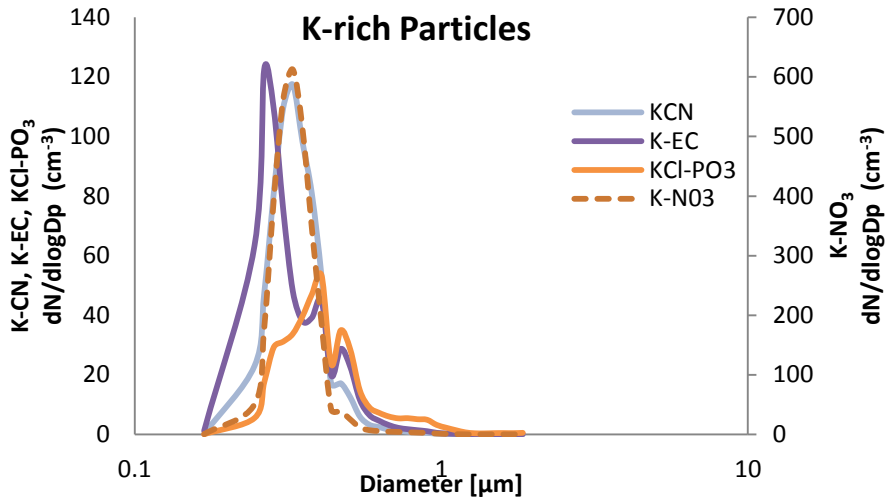
K-rich Particles
K-CN, K-EC, KCl-PO3 dN/dlogDp (cm-3)
K-NO3 dN/dlogDp (cm-3)
KCN
K-EC
KCl-PO3
K-N03
Diameter [µm]

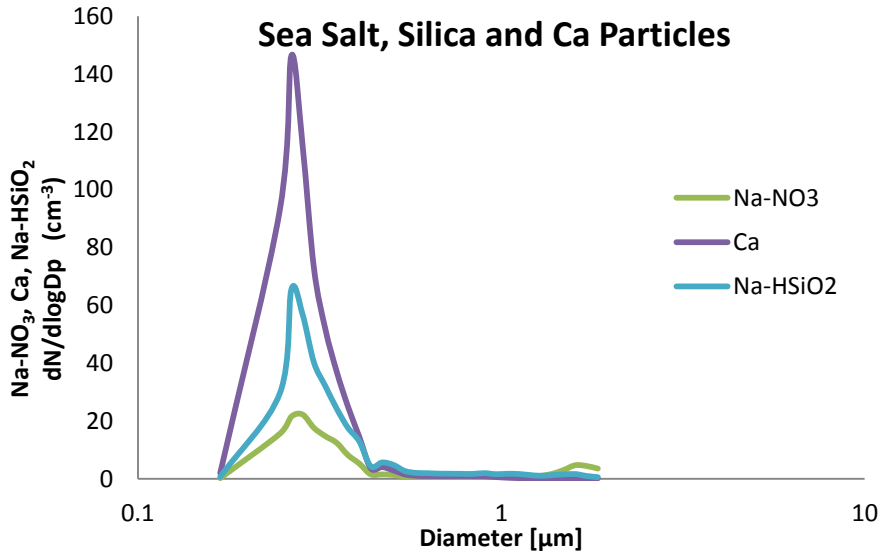
Sea Salt, Silica and Ca Particles
Na-NO3, Ca, Na-HSiO2 dN/dlogDp (cm-3)
Na-NO3
Ca
Na-HSiO2
Diameter [µm]

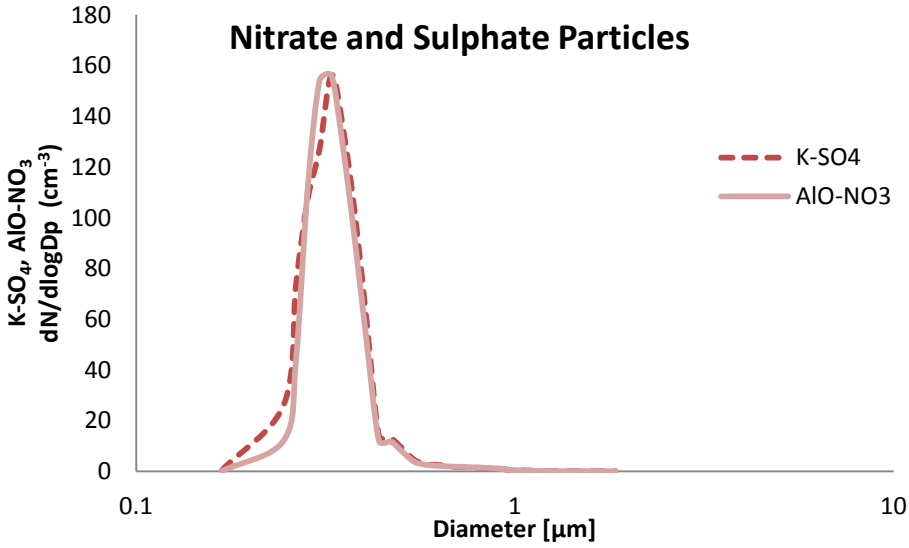
Nitrate and Sulphate Particles
K-SO4, AlO-NO3 dN/dlogDp (cm-3)
K-SO4
AlO-NO3
Diameter [µm]

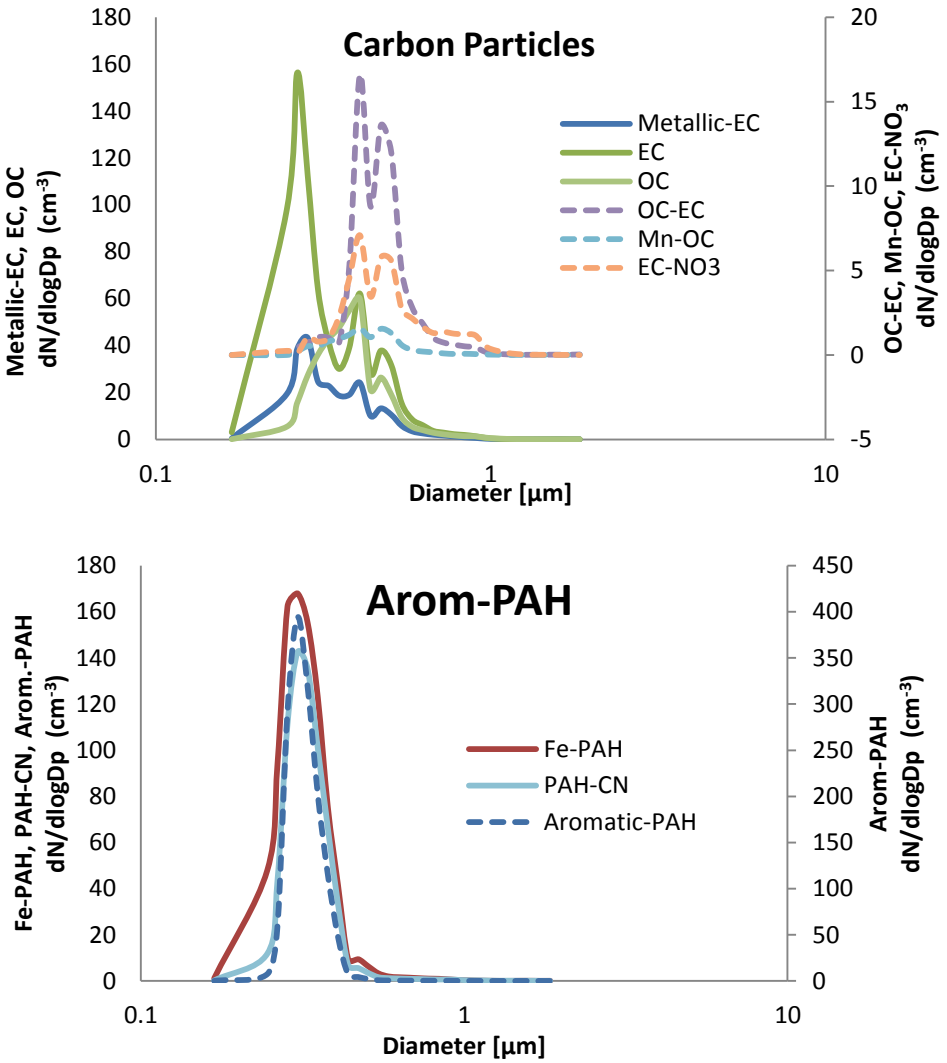

Figure 8.14: Size distribution of scaled particle class counts

The size distributions for mass concentrations of the particle classes are highlighted in Figure 8.15. Mass concentrations for the particle cluster were calculated on the scaled ATOFMS particle counts. The formula adopted was:

$$\mathbf{M = V^{*}\ \rho} \qquad \textit{(8.3)}$$

where,

M= mass,

V=volume of particle,

ρ = particle density (assumed to be 1.7g cm^{-3})

Volume is calculated as:

$$\mathbf{V = 4/3 * \pi *(d/2)^3} \qquad \textit{(8.4)}$$

where,

d=particle diameter

$\boldsymbol{\pi}$ =3.142

Equations 8.3 and 8.4 can be combined as:

$$\mathbf{M= 1/6 * \pi *d^3 *} \rho \qquad \textit{(8.5)}$$

The scaled size distribution for corrected mass concentrations of clusters highlighted in Figure 8.15 shows bimodal peaks for K-rich particles of K-EC and K-Cl-PO_3. The remaining two types of K-containing particles (K-CN and K-NO_3) showed only one peak in the fine mode. The fine modes occur between 0.3 and 1.0 µm while the coarse peak shows at around 1.8 µm. K-Cl-PO_3 exhibits a stronger peak in the coarse mode relative to K-EC particles. As earlier discussed, K-Cl is a typical emission from the sinter plant at a larger particle mode (Hleis *et al.*, 2013). The sea salt particle shows a unique elevated coarse mode at 1.8 µm. Calcium and silica particles are bimodal with peaks at around 0.3 and 1.7 µm indicating both anthropogenic and natural emissions. Sulphate and nitrate particles show peaks at fine modes of 0.4 and 0.9 µm. Most of the carbonaceous species exhibit unimodal peaks at diameter less than 1.0 µm except for OC-EC which shows another insignificant peak around 1.8 µm. The aromatic-PAH class shows a unimodal peak centred at 0.3 µm.

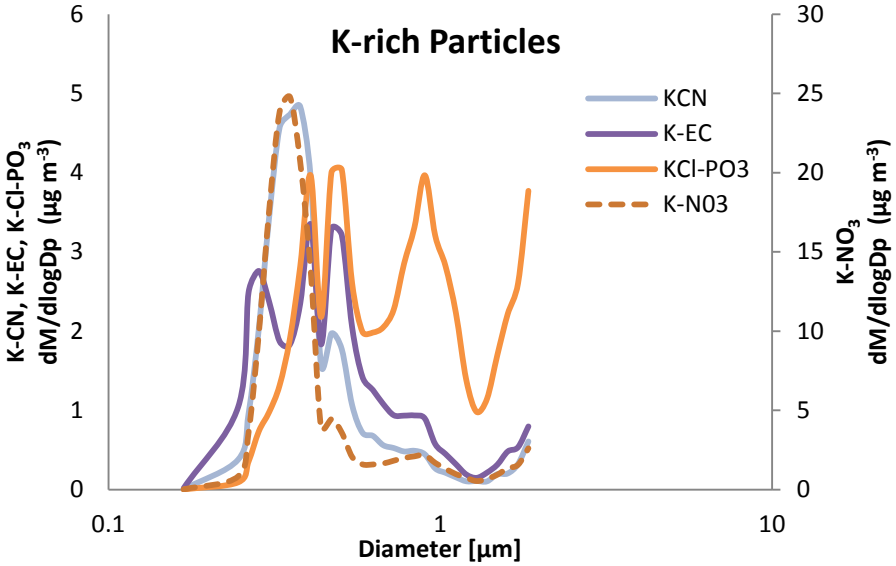
K-rich Particles
KCN
K-EC
KCl-PO3
K-N03
K-CN, K-EC, K-Cl-PO3 dM/dlogDp (µg m-3)
K-NO3 dM/dlogDp (µg m-3)
Diameter [µm]

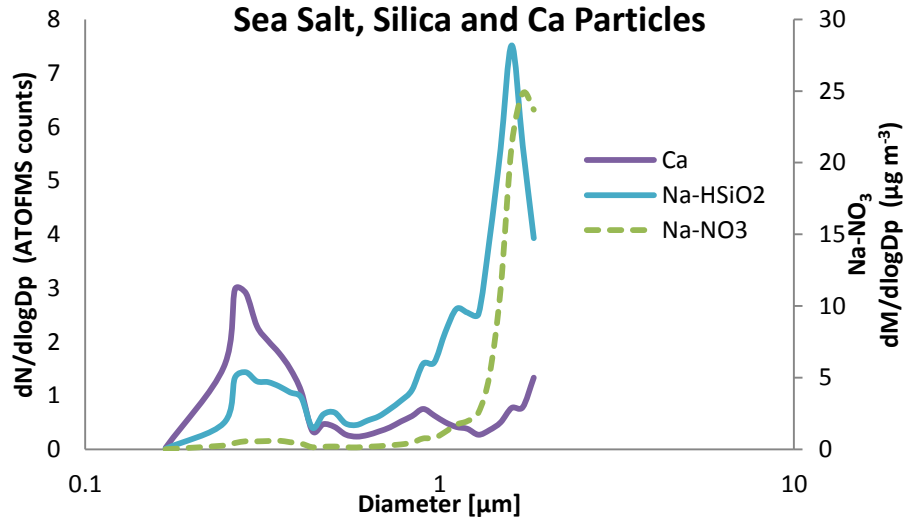
Sea Salt, Silica and Ca Particles
Ca
Na-HSiO2
Na-NO3
dN/dlogDp (ATOFMS counts)
Na-NO3 dM/dlogDp (µg m-3)
Diameter [µm]

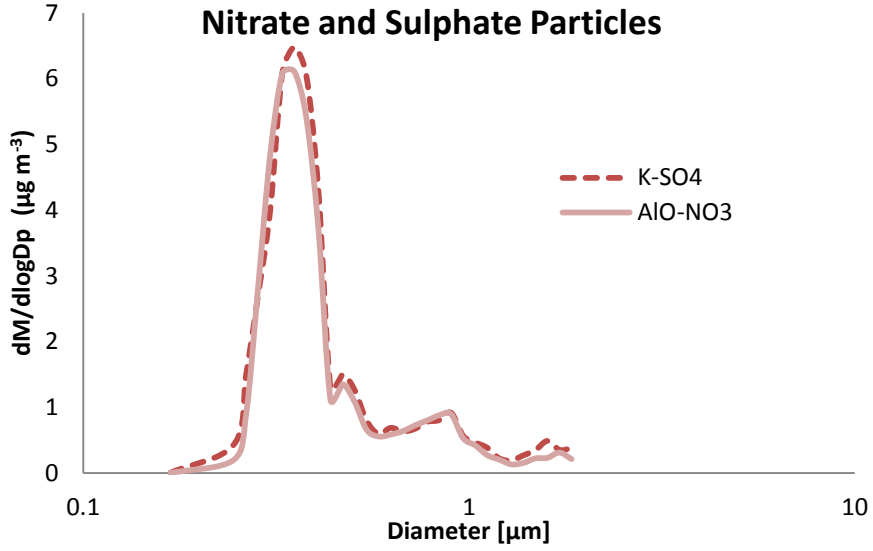
Nitrate and Sulphate Particles
K-SO4
AlO-NO3
dM/dlogDp (µg m-3)
Diameter [µm]

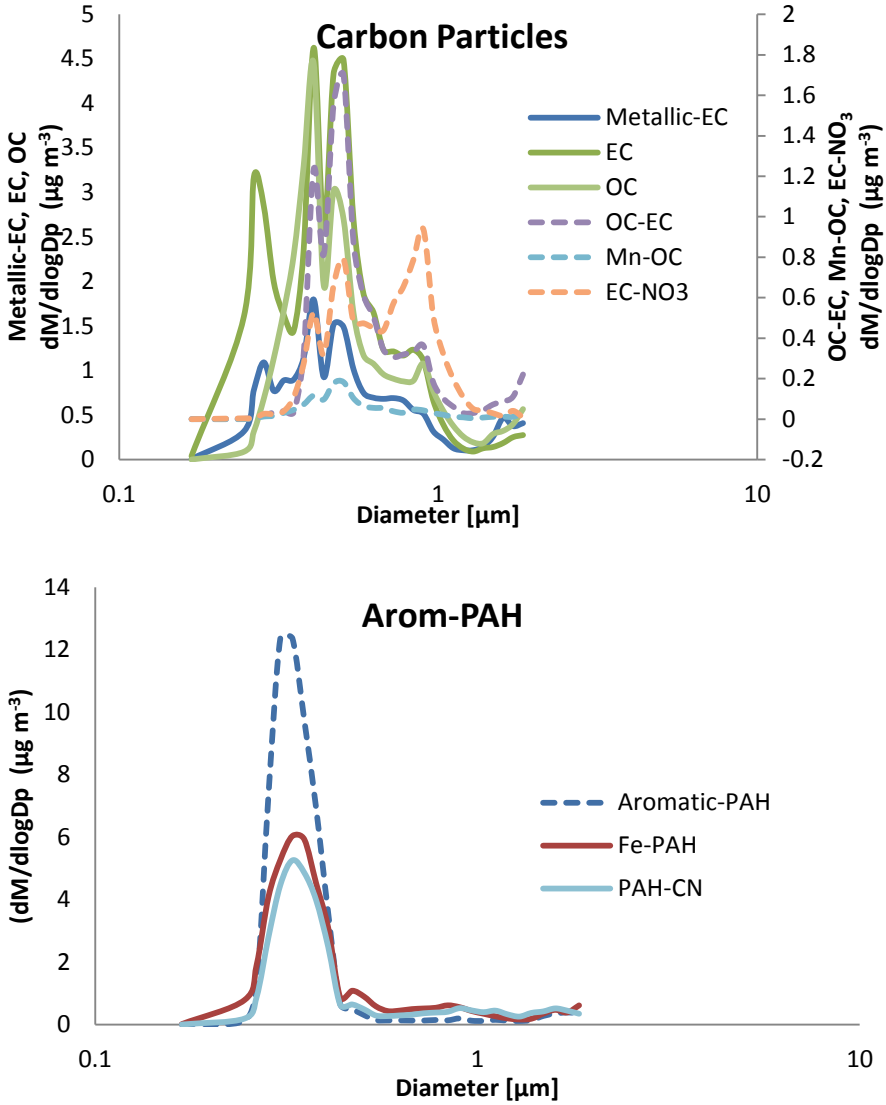

Figure 8.15: Mass distribution of particle classes

8.4.4 Temporal variations and polar plot of total particle number concentration

Figure 8.16 shows temporal variation of total particle number concentration of the 4 week ATOFMS analysed particles. Peaks of elevated counts where particle numbers are greater than 2000 per hour (highlighted with the red cycles in Figure 8.16) were observed on April 19-20, 23-24, 25-26, May 1-2, 6-7 and 9-10. The hourly trend of unscaled ATOFMS total particle numbers shows similar variations with that of Grimm optical particle counter (Appendix XXVII). For individual clusters, the time series plots of the particle number

concentrations are plotted in Appendix XXVIII. Common episodes of particle pollution at May 1-2 and 7-8 were observed for K-rich particles (K-EC, K-NO_3 and KCl-PO_3). Pollution peaks for the sea salt and silica dust classes are similar while metallic-EC and EC particle sub-classes in carbonaceous species exhibited related pollution events. Two common peaks of elevated particle number concentrations were observed for arom-PAH particle class. Occurrences of particle pollution events are most frequently observed for the sea salt particle type.

The polar plot of the total particle counts from the ATOFMS shown in Figure 8.17 has highlighted multiple emission sources of particles in Port Talbot. Elevated concentrations observed at the northerly wind sector suggest traffic and residential emissions. At the centre, the high number concentration of total particles indicates local traffic emissions. The south-easterly high particle number concentrations suggest steelworks emissions from hot and cold mills. Finally, elevated particle concentrations in the south-westerly wind sector signify emission from the steelworks ironmaking section as well as marine sources.

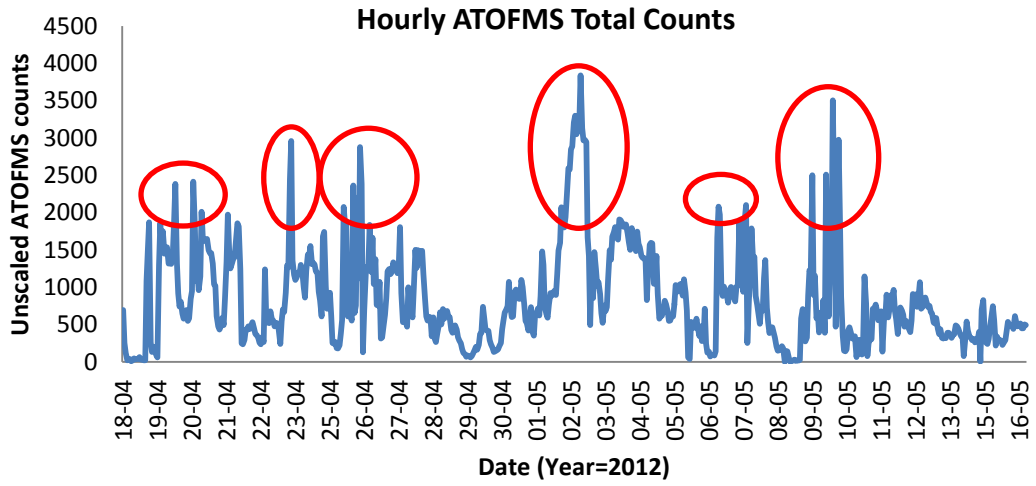

Figure 8.16: ATOFMS total particle number concentration

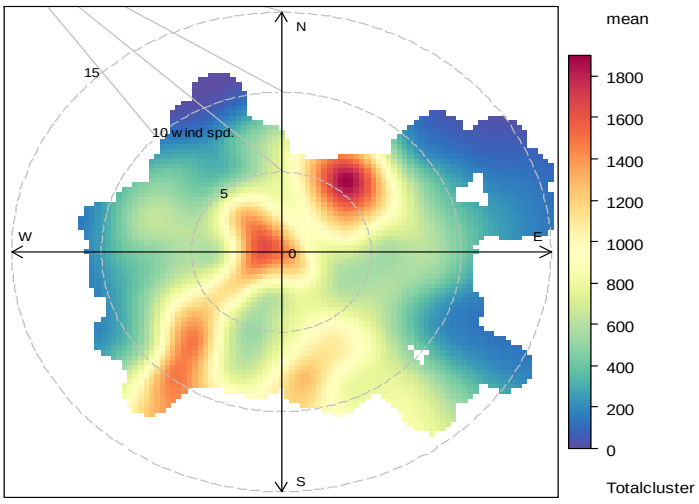

Figure 8.17: Polar plot of ATOFMS total particle counts

8.4.5 Comparison of the Daily ATOFMS Mass and other PM Measuring Instruments

The daily trends of ATOFMS mass concentration with other PM measuring instruments is shown in Figure 8.18. The daily variation plot shows good agreement among the different instruments with common episode of fine particle ($PM_{2.5}$) observed on April 26 and May 08. However, there were occasions where slight differences are observed in peaks shown between ATOFMS and other instruments.

Figure 8.19 shows the wind direction plots of major peaks exhibited by the mass measuring instruments. Prevailing winds during these periods were mostly south-westerly; and occasionally moderate winds from southerly, westerly, north-westerly and northerly axis. The activities of the steelworks were more prominent during these periods of pollution peaks.

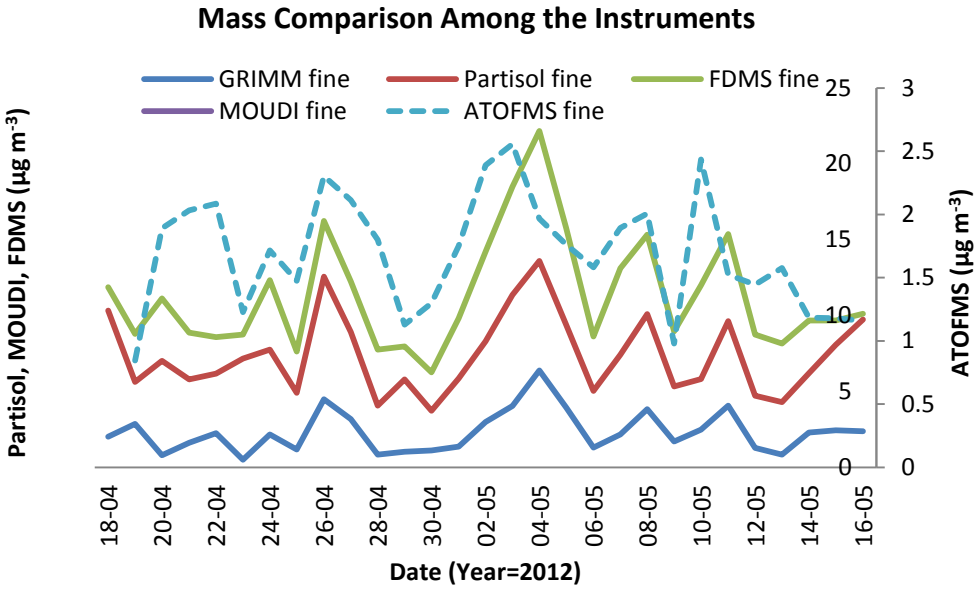

Figure 8.18: Daily mass distribution of ATOFMS and other mass-measuring instruments

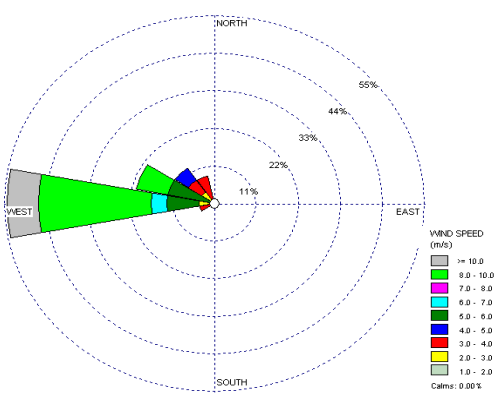

April 22

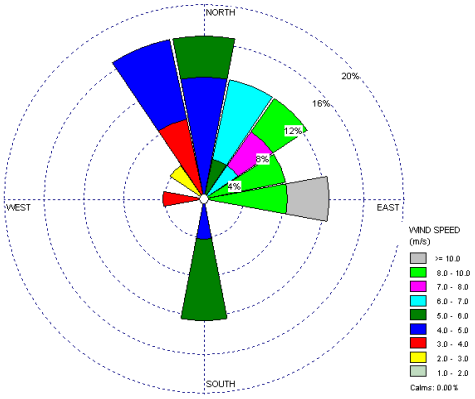

April 24

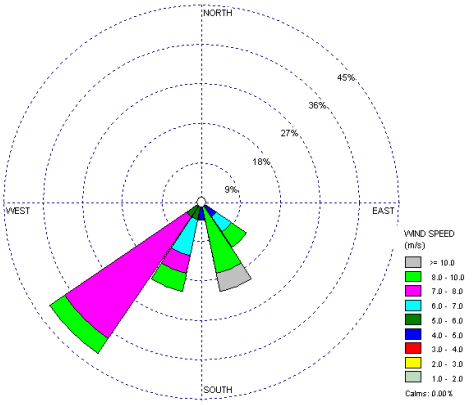

April 26

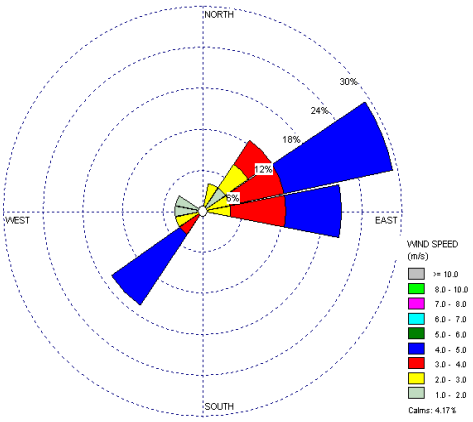

May 3

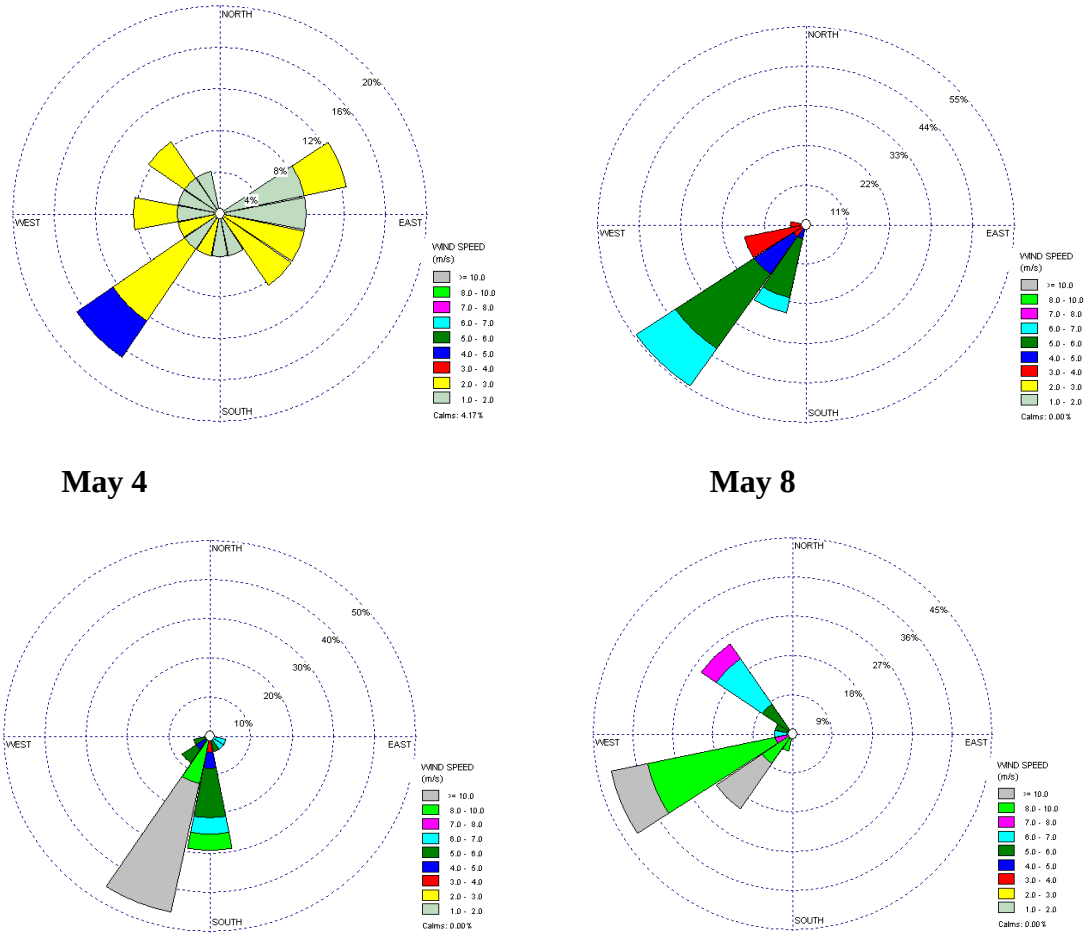

May 4 **May 8**

May 10 **May 11**

Figure 8.19: Wind direction plots during elevated ATOFMS mass concentrations

8.5 Conclusion

The single particle analysis using ATOFMS is useful for source identification and apportionment of particulate matter. With the assistance of ENHILADA software, 20 clusters, which were subsequently grouped into 18 clusters, were identified. These clusters were classified into 8 particle classes viz: K-rich, sea salt, silica dust, sulphate, nitrate, Ca-rich, carbonaceous and Arom/PAH. ENCHILADA software analysed 96% of successfully ionized particles. Among the identified species by ATOFMS, K-rich particles represented the highest percent (40%), followed by carbon-rich particles (24%). Arom/PAH, sea salt,

silica dust, sulphate, nitrate and Ca particles constituted 12, 5, 5, 5, 5 and 3%, respectively. The polar plots of individual cluster indicate that Port Talbot PM is mainly from marine, industrial steelworks, traffic and mineral dust sources. The steelworks showed the greatest contributor to ATOFMS particles representing 50% of the apportioned particles. Out of the 18 particle clusters, 11 were associated with signatures from the steelworks; these include: K-CN, K-NO_3, K-Cl-PO_3, K-HSO_4, Ca, Mn-OC, EC-OC, Arom-CN, Fe-PAH-NO_3 and PAH-CN. The scaled ATOFMS mass concentration for temporal variations is also comparable with other PM measuring instruments indicating the reliability of the ATOFMS for particle analysis.

CHAPTER 9 – SUMMARY AND FURTHER WORKS

In this chapter, the offline and online data during the one month field campaign in Port Talbot were summarized and synthesized. The average increments in daily and hourly average concentration of PM and its components associated with particular wind sectors linking the emission sources to the receptor sites were also calculated.

9.1 Offline Partisol, MOUDI and Streaker Data

9.1.1 Mass and chemical composition

Prior to the Port Talbot campaign, two-week PM sampling has taken place at the EROS-urban background and BROS-roadside sites. The details of the EROS and BROS campaign and the collected physical and chemical data were presented in Chapter 3. The purpose of the EROS and BROS campaign was to compare the PM data of these two sites with that of the industrially polluted site of Port Talbot (PT) (Appendix XXIX).

Port Talbot Partisol PM was dominated by coarse particles (Appendix XXIX) while EROS and BROS PM by fine particles (Appendix XXIX). Partisol $PM_{2.5}/PM_{10}$ ratio at PT is 0.43±0.05, which is similar to the value (0.43) reported by Chung *et al.* (2006) at an industrial site in Daejon, Korea. Studies around the steel industries have reported higher $PM_{2.5}/PM_{10}$ ratios. At Rahee, Finland, the study of Oravisjarvi *et al.* (2003) at the vicinity of a steel industry demonstrated fine particles to constitute 61% of PM_{10}. At Izmir, Turkey, the study of Yatkin and Bayram (2008) at an industrial zone (including steelworks) showed higher ratio of $PM_{2.5}/PM_{10}$ (0.80). An earlier study by Yatkin and Bayram (2007) at an industrial site also reported a high percentage of fine particles (70%).

Elevated levels of Na^+, Cl^-, Ca^{2+}, Fe and Mn were observed for $PM_{2.5}$ and $PM_{2.5-10}$ at PT compared to values obtained at EROS and BROS. The $PM_{2.5}$ constituents of SO_4^{2-}, K^+, Ca^{2+}, Cr and Zn were also higher at PT than at BROS or EROS. This suggests that particle pollution in Port Talbot was influenced by marine aerosols (Na^+, Cl^-) and the steelworks (Ca^{2+}, Fe, Mn, Cr and Zn). Higher concentrations of Ba, Sb, Cu, Al, Pb and NO_3^- at BROS than PT and EROS revealed a higher contribution from vehicular emissions (Sternbeck *et al.*, 2002; Hjortenkrans *et al.*, 2007; Thorpe and Harrison, 2008).

The MOUDI size distributions of particulate matter mass concentration at Port Talbot also supported the dominance of PM_{10} by coarse particles. The size-segregated distribution for chemical species showed significant peaks of Cl^-, Na^+, Mg^{2+} and Ca^{2+} at particle diameter 3-5 μm and of Mn and Fe at 4-6 μm. These results suggested a significant contribution from the sea salt aerosol, crustal and steelworks emissions to the PM_{10} mass. These might be responsible for the low ratio of $PM_{2.5}/PM_{10}$ observed at Port Talbot. Fe and Mn are notable signatures for steelworks especially at the blast furnace and basic oxygen furnace steelmaking (Machemer, 2004; Mazzei *et al.*, 2008; Hleis *et al.*, 2013). These two elements have also been used as crustal matter fingerprints (Hien *et al.*, 2001; Chung *et al.*, 2006; Alleman *et al.*, 2010). In the fine modes, levels of Cr, K^+ and Zn measured by both MOUDI and Partisol instruments at PT were significantly higher than those at EROS and BROS. These PM constituents may be related to the steelworks from cokemaking, sinter and steelmaking (Heung *et al.*, 2007; Hleis *et al.*, 2013). Fine K^+ is also associated with woodsmoke emissions (Harrison *et al.*, 2012c).

Aside from the emission of marine aerosol and the steelworks, meteorological conditions may be another factor leading to the elevated concentrations of coarse PM at PT through soil and dust resuspension (Charron and Harrison, 2005). The average windspeed during the whole sampling period was 6.3±2.3 m s^{-1}. This favoured higher concentration of coarse particles (Charron and Harrison, 2005). Formation of sea spray is also favoured by elevated windspeed (O'Dowd and Leeuw, 2007).

The Streaker samples complement Partisol and MOUDI data with an advantage of providing diurnal variations of elemental concentrations. Comparison of Streaker with Partisol data revealed good agreement for most observed chemical species (Appendices XXI-XXIII). Similar emissions patterns and concentrations were observed for fine Na, Mg, S, Ca, Cr, Cu and Pb; while Al, Ca, Cr, Cu, Mg and Zn showed similar trends for coarse PM concentrations. The Streaker data made it possible to plot the wind sector plots (Figures 6.6-6.9), allowing an identification of particle emissions from specific processes at the steelworks. The polar plots of FS Streaker data showed evidence of steelworks emissions with elevated concentrations of elements (Al, S, Ca, Fe, Cr, Ni, Mn, Pb and Zn) towards the south-westerly wind sector (Figures 6.6 and 6.7). At the LW station, high concentration of elements Ca, Cr, Cu, Fe, Mn, Ni, Zn and S between the southerly and easterly wind directions confirms emissions from the steelworks (Figures 6.8 and 6.9).

At the two sites (FS, LW), the Streaker $PM_{2.5}$ fraction was dominated by S; while Fe (FS) and Na (LW) were the most abundant components of $PM_{2.5-10}$. High concentration of sulphur and Fe could be associated with the local steelworks (Prati *et al.*, 2000). The regional contributions to sulphur levels in PT may also be of significance (AQEG, 2012).

The relative abundance of Na at LW is not surprising, being in the proximity of Swansea Bay. The hourly sum of the measured constituents of Streaker data showed two days where PM_{10} mass concentrations were greater than 50 µg m^{-3} on May 7 and 10 at FS (Figure 6.3a). The daily Partisol and FDMS mass data have shown similar trends at all the stations (Figure 5.2) indicating their comparability with the Streaker hourly data (when calculated as 24-hour averages). General observations during the periods of 24- hour PM_{10} episodes have been summaried in Table 9.1.

Table 9.1: General observation at the FS site during the period when high PM_{10} concentrations were recorded

Sampling date	Partisol PM_{10} (µg m^{-3})	FDMS PM_{10} (µg m^{-3})	Observations
18/04/12	41.4	37.9	Cloudy and raining. Mild plume emissions from the steelworks
26/04/12	64.5	64.5	Sulphur-like odours, calm weather, high plume emissions from the south-western regions where the BF and Sinter plants located
08/05/12	40.2	41.6	Calm weather and high plume emissions from the steelworks
11/05/12	47.8	51.0	Sunny. Mild emissions from the steelworks

The diurnal variations of the Streaker data further revealed the pollution patterns in Port Talbot. The most significant peaks were found at 7-9 am, 1-3 and 5-11 pm. The morning peak indicated by Streaker data at 7-9 am corresponds to peaks shown by gaseous pollutants NO, NO_2, NO_x, SO_2 and CO. Additionally, FDMS $PM_{2.5}$, black carbon and Grimm particle counts (diameter 0.3-1.6 μm) have shown a significant morning peak, indicating traffic contributions (Rattigan *et al.*, 2010). However, the steelworks emissions during this morning peak may not be ignored.

The major aim of this thesis is to identify and apportion different emission sources of air pollutants in Port Talbot using receptor models. Two receptor models, principal component analysis (PCA) and positive matrix factorization (PMF) were used for PM source identification and apportionment. These models have been applied to both daily Partisol and hourly Streaker data. The PCA for fine and coarse PM was able to identify prominent emission sources. Apart from the identified steelworks factors, other notable components were crustal, traffic, oil combustion, secondary and woodsmoke. It should be noted that K^+ has been adopted as a marker for a woodsmoke for fine $PM_{2.5}$ and a sinter plant for coarse PM. The PCA model was able to identify specific steelworks units contributing to particulate pollution in PT. The notable steelworks processes identified were sinter, BF, cokemaking and BOS. The multiple linear regression (MLR) analysis of factors successfully apportioned components identified for Partisol data only. In the case of Streaker, the MLR analysis could not resolve the source contributions due to problems arising from negative factors.

The PMF model has identified some components similar to that of the PCA (BF/Sinter/BOS, secondary aerosol, marine aerosol and traffic). With the PMF model, source contributions of factors for Partisol and Streaker samples were clearly explained. Gaseous pollutants and black carbon data were successfully incorporated into Streaker hourly data. Diurnal trends and wind sector patterns of identified factors were plotted from the hourly data. Not much difference was observed between PMF and PCA factors, except the additional steelworks sinter fugitive dust. Another significant observation for PMF was the traffic factor characterized by significant loadings for BC, NO_x and CO. This study showed a strong accord with the recent published research work of Pancras and co-workers (2013) who applied the PMF model to hourly data collected at Dearbon, Michigan, USA. The study included the gaseous pollutants and identified different steelworks sections including cokemaking, sinter, slag, and iron and steel production (Pacreas *et al.*, 2013).

PCA and PMF models for Partisol data identified secondary aerosol as the leading contributor to $PM_{2.5}$ supporting the report of AQEG (2005). The combination of all the steelworks factors of PCA and PMF represented 31 and 16% for Partisol, and 28 and 38% for Streaker, respectively. The steelworks therefore formed the second largest contributor to $PM_{2.5}$ in PT. For coarse particles, PCA and PMF revealed the combined steelworks constituting 67 and 41% of the apportioned $PM_{2.5-10}$. The summary of sources identified and apportioned by PCA and PMF for Partisol and Streaker fine and coarse PM are displayed in Appendix XXX. In this study, PMF showed a better performance than PCA for source apportionment.

As highlighted in Figure 5.1 and Table 7.3, there are different steelworks sections in Port Talbot. The receptor models used in this study could not identify cold and hot mills, probably due to non-inclusion of their corresponding marker elements in the models. The study of Tsai *et al.* (2007) has reported higher values of OC and total PAHs in cold mill particles collected at the integrated steelworks complex in Taiwan. The daily OC/EC measured with a high-volume sampler could not be included in the receptor models because too few data were collected. OC/EC results are available at the FS site only and thus do not satisfy the requirement for PCA and PMF analysis.

The pragmatic mass closure model described by Harrison *et al.* (2003) was adopted to reconstruct the fine PM mass at FS due to available OC/EC data at the site. The regression plot in Appendix XXXI showed a good correlation between the measured and reconstructed fine PM mass indicating mass closure of measured components.

9.1.2 Average steelworks increments associated with wind sectors

The purpose of this section is to calculate the steelworks increments for PM mass and chemical composition of Partisol and Streaker data. This will provide another method for apportioning source contributions to specific steelworks sections using wind sector analysis. This was achieved by finding the differences between the downwind and upwind PM data that were associated with the steelworks production units. It should be noted that LW represents the upwind site when the prevailing wind blows from westerly and south-westerly (from the Swansea Bay) across to FS site (downwind). In a condition when prevailing wind is blowing from the south-east and south, LW represents the downwind

sector. The wind sectors of different steelworks production units in Port Talbot are shown in Table 9.2.

Table 9.2: The wind sector locations of the steelworks facilities

Steelworks	Wind sectors from FS	Wind sectors from LW
Ore stockyards	W, WSW	S, ESE
Sinter	SW	SE
BF	SSW	SE
BOS/Cokemaking	S	SSE
Mills	SE, SSE	SSE

The average daily Partisol wind sector linking the steelworks location to the receptor site was calculated for the periods where prevailing winds were between the southerly and westerly areas where the steelworks units are located. Figure 9.1 shows the periods when prevailing winds were blowing from the ore stockyards and BF/sinter plants of the steelworks.

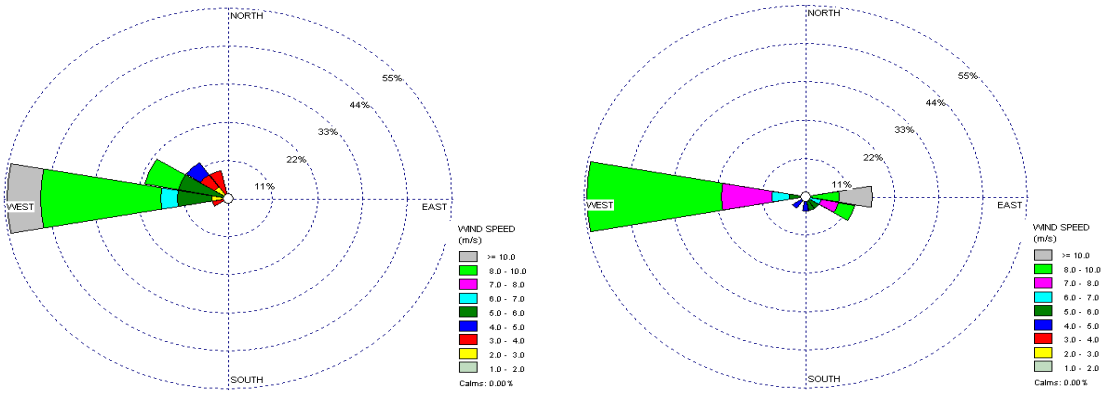

April 22 **April 23**

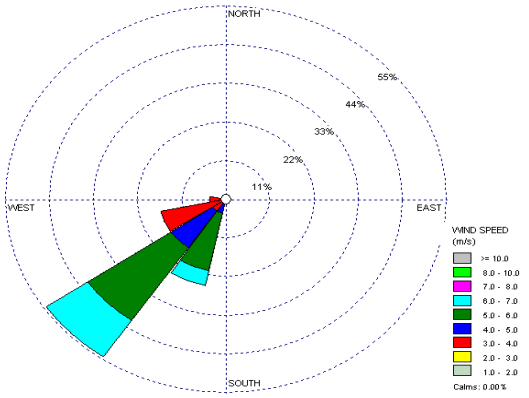

May 8

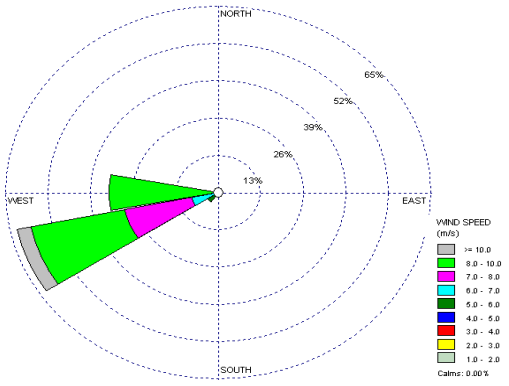

May 14

Figure 9.1: Wind rose plots showing days where prevailing winds blow across the steelworks to the receptor location at FS for which the steelworks increments for Partisol data are calculated

Appendix XXXII (a,b) shows the average increments of daily Partisol PM concentrations associated with a wind sector linking the source to the receptor locations at FS and LW. At the FS (Appendix XXXII a), the wind-determined data showed blast furnace (BF)/Sinter plant to contribute significantly to PM in Port Talbot. Steelworks increments were also observed for PM mass concentrations at the ore stockyard. Coarse Ca and Fe were the major particulate elements from the ore stockyard at FS while Cu, Sb and Ba were observed at relatively low concentrations in $PM_{2.5}$, $PM_{2.5\text{-}10}$ and PM_{10}. PM from the BF/Sinter plant was abundant in Fe, Mn, Ca, nss-SO_4, Al and Zn (Machemer, 2004). Steelworks increments were observed for Pb, Cd, Ni, Sb and Ba at the BF/Sinter plants.

The steelworks elemental increments from BF/Sinter plant at FS could account for about 25% of the PM mass increment with excess mass of 5.2, 17.3 and 22.5 µg m^{-3} for $PM_{2.5}$,

$PM_{2.5-10}$ and PM_{10}, respectively. The excess mass may be attributed to many factors including unmeasured components such as OC/EC, mass-associated oxygen, particle-bound water and other chemical constituents. Additionally, the Streaker PM on the specific day (May 8) when the steelworks increment was calculated (for daily Partsiol BF/Sinter) revealed an elevated value of coarse Fe (10.3 µg m^{-3}) compared to Partisol Fe value of 3.5 µg m^{-3}. Higher amounts of Na, Cl and Ca were observed for Streaker's coarse PM than those of Partisol. A clear underestimation of chemical components of Partisol may therefore provide a reasonable explanation for the unaccounted PM mass.

At LW, most of the measured components demonstrated high elemental increments from the ore stockyard steelworks (Appendix XXXII b). The measured components for ore stockyard steelworks showed over-estimation of $PM_{2.5}$ and PM_{10}. The LW site was more influenced by the ore-stockyard than FS.

The hourly Streaker PM data at FS were grouped into 16 wind sectors (Figure 9.2) from which the sectors relating to the steelworks sections representing the downwind data were calculated. At LW, the Streaker elemental data not affected by the steelworks emissions were used as upwind data.

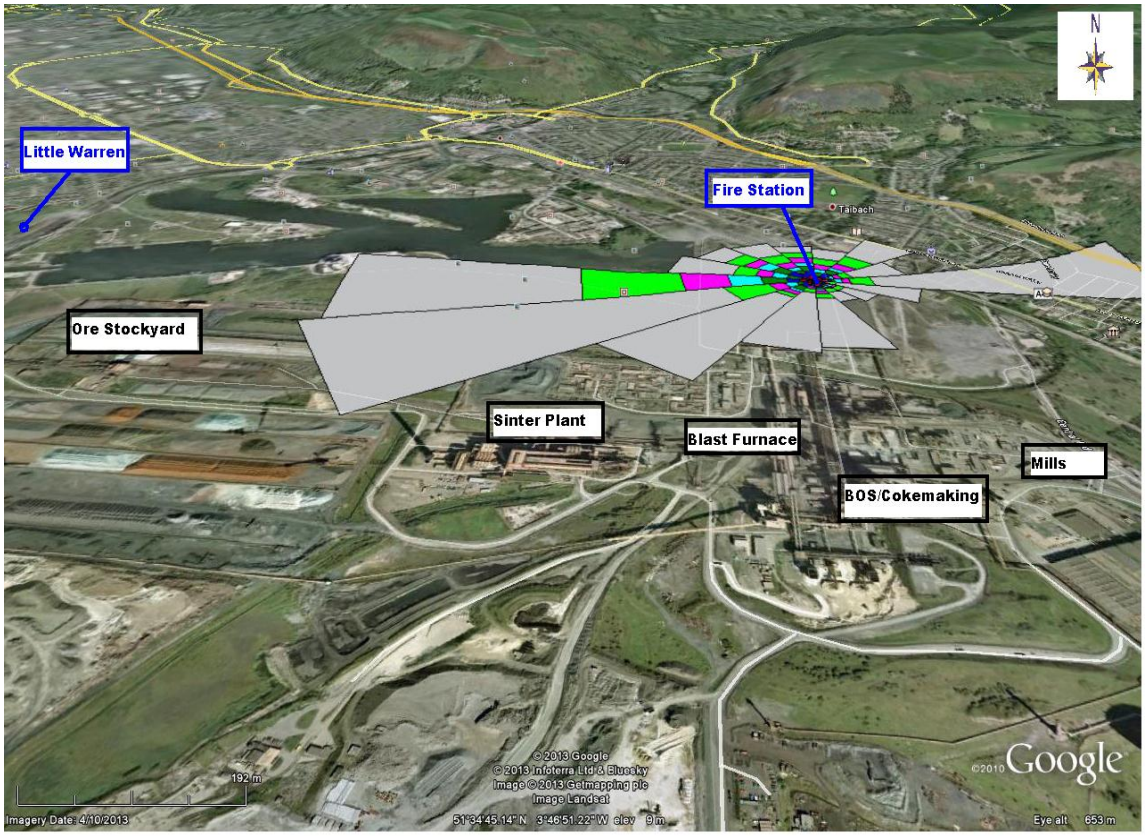

Figure 9.2: Map of Port Talbot showing the 16 wind sectors linking the steelworks productions units to the receptor site at FS

The average steelworks increments for Streaker hourly elemental concentrations associated with wind sectors linking the emission source to the receptor location at FS and LW are presented in Appendices XXXIII and XXXIV, respectively. The wind sector associated data was better defined with Streaker compared to Partisol data. Five steelworks sections {ore stockyard, basic oxygen furnace steelmaking (BOS)/Cokemaking, Sinter, BF and Mills (hot and cold)} were identified by the wind sector linking data at FS (Appendix XXXIII). At LW, two steelworks components were revealed (Appendix XXXIV). These increments provide additional source apportionment information and chemical profiles of the PM collected during this study.

As explained in the previous chapters; Fe, Mn and Ca were better markers for BF; the wind sector associated data showed BF plant as the major contributors to these elements in all the PM fractions. In the coarse PM fraction, a high concentration of Si was also observed at the BF plant. The sinter section was dominated by S, Zn and Pb for fine PM and Na, Mg, Zn, Se and Cu for $PM_{2.5-10}$. At FS, the ore-stockyard demonstrated the highest level of fine K, but at LW, the sinter plant was the largest emitter of K. In the PM_{10}, K has shown elevated concentration at BF while Cl at the sinter plant. The wind-determined data has revealed K and Cl as good makers for sinter plant emissions.

Zn has been adopted as a good tracer element for steelworks for BOS due to the addition of galvanized scraps to the hot molten iron during steelmaking (Hleis *et al.*, 2013). The work published by Dall'Osto *et al.* (2008) has included Zn as one of the major metal emissions from the BOS plant. During the receptor modelling of PMF and PCA, Zn was adopted as a tracer element for BOS. The wind-determined data linking the BOS to FS receptor site has revealed sinter plant as the major emission source of Zn. However, at LW, the wind sector data has shown BOS/Mills/Ore stockyard as major sources of Zn for $PM_{2.5}$ and PM_{10} (Appendix XXXIV).

S, Se and As were also expected to show the highest concentrations at the BOS/Coking plants but were observed at elevated values at the Sinter/BF at FS and LW. The ore stockyard demonstrated highest amounts for fine Mg and Cl and coarse Cl. The mills sector revealed the highest concentration of fine Cu at FS. Generally, BF and sinter sections of the steelworks have displayed elevated components of PM, followed by ore

stockyard while BOS/Coking and Mills showed the lowest incremental values. The high values of elemental concentrations from the ore stockyard suggest additional contributions from the docks.

The wind sector data has revealed the blast furnace and sinter plants as major steelworks contributors to PM at FS while the BOS/Coking/Mill/Ore stockyard sections represented the largest steelworks emissions of PM at LW (Appendix XXXIV). This is consistent with PMF source apportionment results where BF and sinter plants were the dominating steelworks emissions at FS. The ATOFMS also revealed the BF and sinter plants as the largest emission sources of PM. This information is therefore useful for the Steelworks management to put in place particle-control measures at the BF and sinter plants for protection of public health. Recently, the Natural Resources Wales (NRW), upon the complaints by the residents of Port Talbot, issued an enforcement notice to the management of Port Talbot Steelworks to curb pollution around the steelworks (Air Quality News, 2013). The NRW identified the sinter plant section as one of the root causes of particle pollution in Port Talbot.

The wind data analysis of both Partisol and Streaker revealed dominance of Fe, Mn, Pb, SO_4^{2-} / S and Ca at the BF/Sinter plant while significant amounts of Fe and Cu were observed at the ore stockyard. The ore stockyard has also shown a significant increment for fine K while the sinter and BF plants revealed elevated coarse K.

The wind-determined (Appendices XXXII a and XXXIII) and PMF (Appendices XXXV a and XXXVI a) mass and chemical profiles of steelworks factors for Partisol and Streaker PM data at FS are compared in Figures 9.3-9.5.

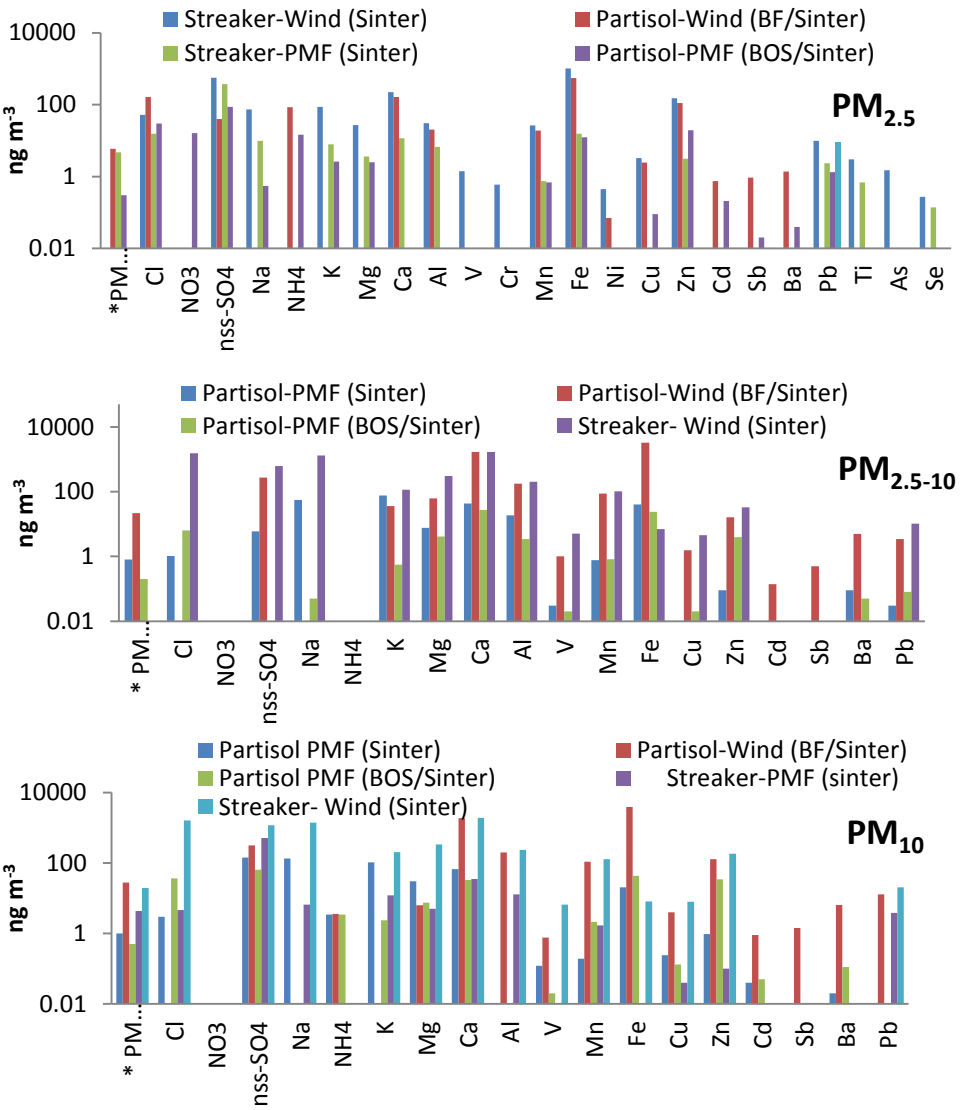

Figure 9.3: Wind-determined and PMF mass and chemical profiles for steelworks sinter plant at FS (Note: *PM =µg m^{-3})

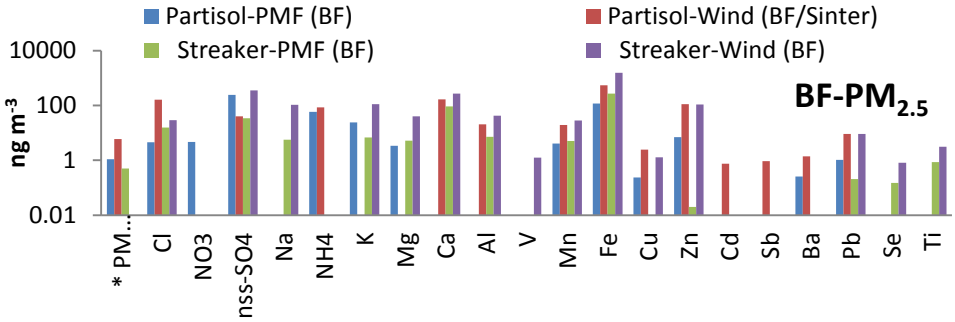

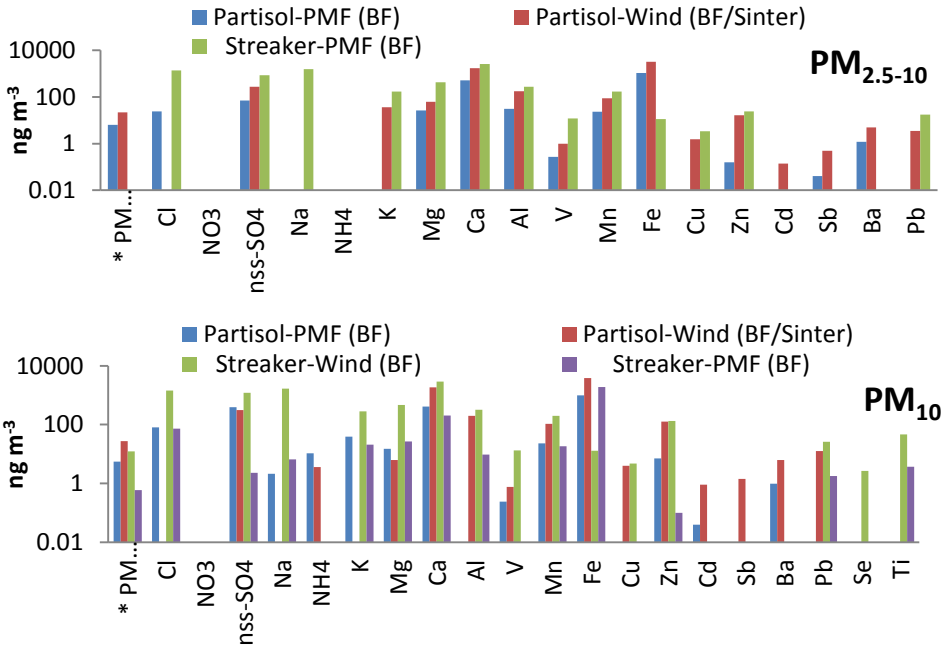

Figure 9.4: Wind-determined and PMF mass and chemical profiles for BF steelworks at FS (Note: *PM =µg m^{-3})

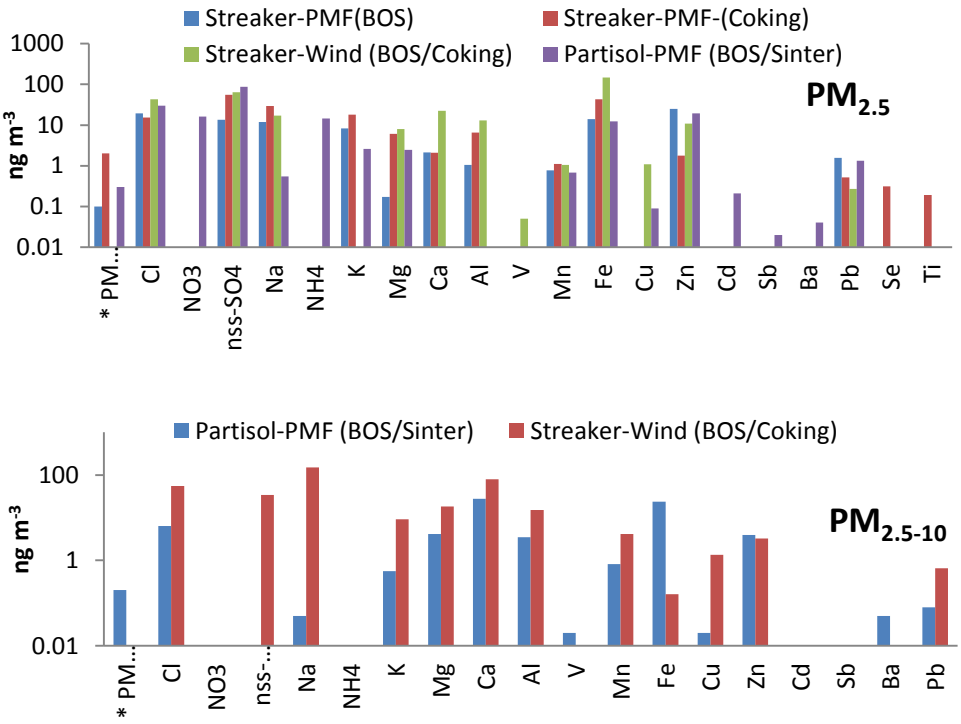

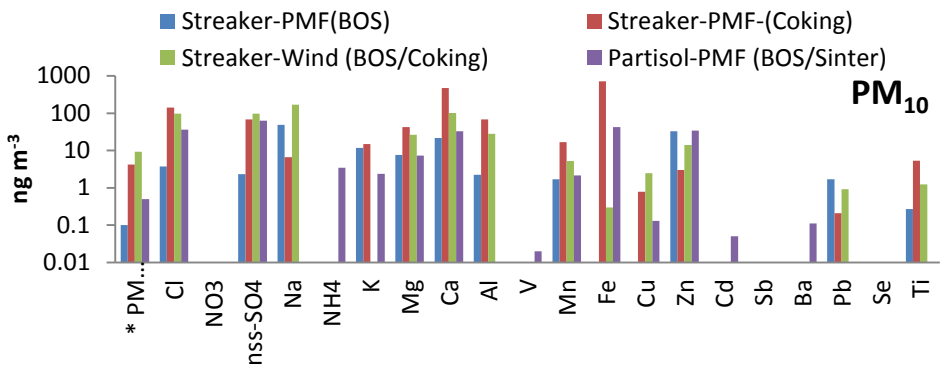

Figure 9.5: Wind-determined and PMF mass and chemical profiles for steelworks BOS/Coking at FS (Note: *PM =µg m^{-3})

Generally, abundance of Fe, Mn, sulphate (Partisol) or sulphur (Streaker), Al, Ca and Pb were observed for all the steelworks factors. For the sinter plant steelworks factor (Figure 9.3), a well-defined relationship was observed for most observed PM components for wind-determined and PMF profiles. The wind-calculated sinter profile appeared to show higher elemental values of PM than for PMF. Elevated levels of Cd and Pb were revealed at the sinter plant for both profiles for $PM_{2.5}$ and PM_{10} compared to other steelworks sections. The coarse K was also relatively higher at the sinter compared to BF and BOS/Coking steelworks units.

The profiles by wind sectors and PMF revealed higher concentrations of Fe, Mn, Ca, V, nss-sulphate /sulphur, Ti, NH_4^+ and Mg at BF (Figure 9.4) than at the other steelworks components. Ba and Al also showed slightly elevated values for PM_{10} fraction for BF. There is no distinctive element that defined the BOS/Coking component in terms of abundance. However, the Partisol PMF (BOS/Sinter) revealed a unique incremental value for nitrate which may represent BOS/Coking signature (Figure 9.5). The mass concentration of PM was slightly higher at the sinter plant than at BF while BOS/Coking

recorded the lowest mass concentration. It should be noted that the FDMS mass concentrations were used in place of the Streaker PM_{10} mass.

The steelworks increments by wind sector (Appendices XXXII b and XXXIV) and PMF (Appendices XXXV b and XXXVI b) analyses at LW are compared in Figure 9.6. The sinter plant also revealed elevated $PM_{2.5-10}$ mass concentration while BF/Sinter represented the highest concentration of PM_{10} mass. At LW, the profiles of BF/sinter steelworks is characterised with elevated concentrations of Fe, Pb, Zn while sinter has high loadings of V, Cu and K. BOS/Sinter revealed higher levels of ammonium and Cd.

The Partisol PMF (BOS/Sinter) and the Streaker wind-determined (BOS/Coking) PM profiles at LW are presented also in Figure 9.6. The Streaker wind-determined profile showed a slightly higher PM mass and elemental increment than the Partisol PMF (BOS/Sinter) component.

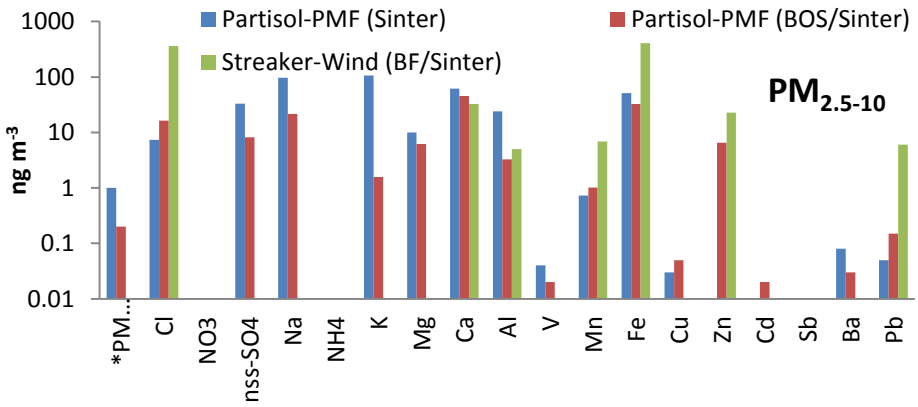

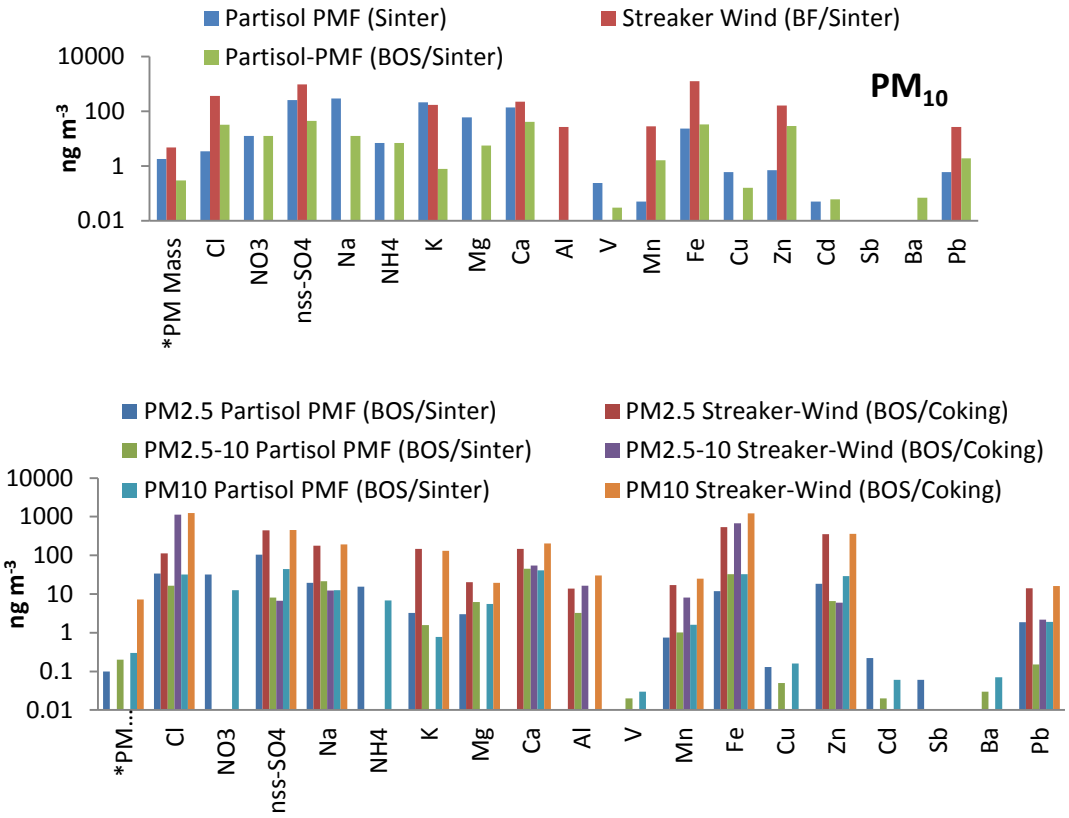

Figure 9.6: Wind-determined and PMF mass and chemical profiles of steelworks factors at LW

The differences between the wind-determined and PMF profiles presented above may be explained by the fact that:

- the wind direction analysis for the Partisol is restricted to a small number of days (Figure 9.1) and therefore, since the work's emissions are not necessarily constant from day-to-day, this may attribute a different influence to that obtained from the larger dataset from the Streaker. The PMF analysis takes account of all days and hence represents a larger dataset than the Partisol wind direction analysis.
- mass increments determined from the Streaker do not contain all of the associated mass because of missing components such as oxygen associated particles.

At the FS site, the total PM mass increments of Partisol wind sector analysis for $PM_{2.5}$, $PM_{2.5-10}$ and PM_{10} are 6.4, 23.6 and 30 μg m^{-3} respectively, while the corresponding values in PM fractions for Partisol PMF are 1.4, 7.4 and 7.0 μg m^{-3}. The Streaker wind sector analysis revealed an elevated value of 55.8 μg m^{-3} for PM_{10} while the Streaker PMF gave incremental values of 7.3 μg m^{-3} for $PM_{2.5}$ and 9.2 μg m^{-3} for PM_{10}.

At the LW site, the steeelworks' increments by wind-determined and PMF PM mass were relatively lower than those at FS. The wind sector data for Partisol showed PM increments of 0.2, 2.3 and 2.5 μg m^{-3} for $PM_{2.5}$, $PM_{2.5-10}$ and PM_{10} respectively. The Streaker PM_{10} showed a steelworks increment of 12.1 μg m^{-3} by the wind-determined analysis and 3.1 μg m^{-3} by PMF analysis.

9.1.3 The annual PM steelworks increments

The chemical profiles calculated from the wind sector and PMF profiles have revealed significant increments for most observed elements by Partisol and Streaker. Increased PM mass concentrations have been observed at the different steelworks production units during the one-month campaign at Port Talbot.

The annual steelworks increments of PM mass from the steelworks units were calculated from the one-month steelworks increment data. Consequently, the one-year windrose showing the wind frequency that corresponds to each steelworks section was plotted. The windrose between January 1 and December 31, 2012 is presented in Figure 9.7. The annual wind frequency was multiplied by the one-month PM mass incremental values to obtain the annual steelworks increments presented in Table 9.3 (a, b). The annual

increment showed the combined BF/Sinter factor as the dominating source emission of $PM_{2.5}$ (0.41µg m^{-3}) while the sinter plant as a single source contributed to (0.38 µg m^{-3}). The sinter plant may therefore represent the highest contributor to $PM_{2.5}$ concentration among other steelworks processing units at FS. However, the PMF model reveals the BF plant as the major emission of observed PM chemical components.

In the $PM_{2.5-10}$ and PM_{10} category wind-determined and PMF steelworks increments of Partisol and Streaker instruments also apportioned the highest mass concentration to the sinter plant. The ore stockyard also contributed significantly to the annual PM_{10} mass at FS. At LW, the PMF steelworks profiles showed equal PM_{10} mass annual increments by the sinter and BF plants while the wind-determined profiles assigned a slightly higher mass to the BF plant. The fine and coarse PM emissions were largely from the BF plant.

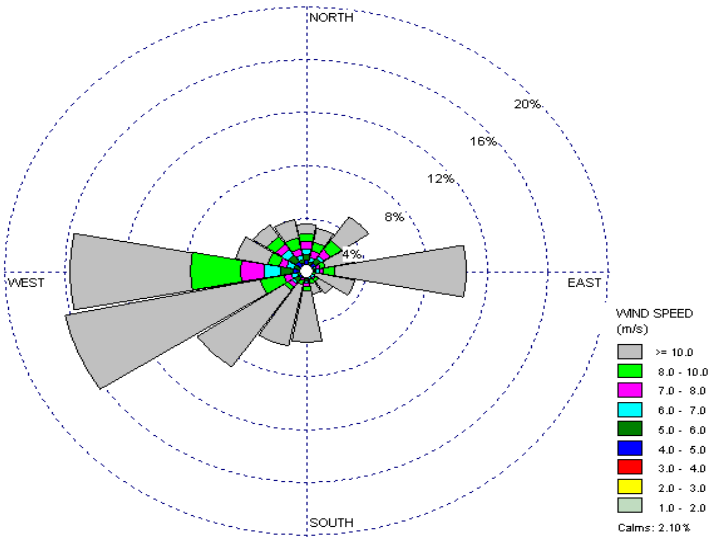

Figure 9.7: The annual wind rose plot at Port Talbot from January 1 to December 31, 2012

Table 9.3: Annual PM steelworks increment calculated from the wind-determined and PMF analyses at (a) FS

Steelworks increments from		$PM_{2.5}$ ($\mu g\ m^{-3}$)	$PM_{2.5-10}$ ($\mu g\ m^{-3}$)	PM_{10} ($\mu g\ m^{-3}$)
Wind-determined (Partisol)	BF/Sinter	0.41	1.52	1.93
	Ore stockyard	0.08	0.30	0.94
Wind-determined (Streaker)	Sinter			1.56
	BF			0.74
	BOS/Coking			0.56
	Mills			0.07
	Ore stockyard			1.81
PMF (Partisol)	Sinter		0.64	0.80
	BF	0.07	0.38	0.33
	BOS/Sinter	0.02	0.01	0.04
PMF (Streaker)	Sinter	0.38		0.34
	BF	0.03		0.04
	BOS	0.01		0.01
	Coking	0.12		0.25

(b) LW

Steelworks increments from ($\mu g\ m^{-3}$)		$PM_{2.5}$ ($\mu g\ m^{-3}$)	$PM_{2.5-10}$ ($\mu g\ m^{-3}$)	PM_{10} ($\mu g\ m^{-3}$)
Wind-determined (Partisol)	Ore stockyard	0.004	0.05	0.05
Wind-determined-Streaker	BF/Sinter			0.10
	BOS/Coking/Mills			0.15
PMF-Partisol	Sinter		0.80	0.04
	BF	0.40	1.60	0.04
	BOS/Sinter	0.08	0.16	0.01
PMF-Streaker	Sinter			0.03
	BF			0.03
	BOS			0.004

9.2 Online Instruments Data

FDMS, Grimm optical particle counter, Aethalometer and ATOFMS system were employed to measure the physical and chemical properties of particulate matter in real time. A good correlation was found between FDMS and Partisol indicating a good agreement between the online and offline mass measuring instruments (Appendix VIII).

The Grimm data for size distributions and particle count numbers revealed emission patterns of particle sizes in Port Talbot. The two distinctive emission types identified by Grimm optical counter (for polar plots) are ground-level with elevated peak concentrations at lower windspeeds and a resuspension source that is associated with the highest windspeeds. Particles with diameter less than 0.5μm have a clear signal of traffic emission while higher concentrations of particles greater than diameter 2.0 μm could be traced to sea salt and resuspension from the steelworks (Figure 4.4). The evidence of steelworks contributions to coarse PM was further established by the wind sector associated data shown in Appendices XXXII and XXXIII. The Grimm calculated mass revealed the coarse PM fraction representing 64% of PM_{10} in agreement with the Partisol $PM_{2.5}/PM_{10}$ ratio.

Aethalometer black carbon (BC) concentration revealed by the polar plot (Figure 5.8) was related to both traffic and steelworks emissions. In the PMF model at FS site, BC co-existed with NO_x in the component assigned to a traffic source. Diurnal variation of BC (Figure 5.7) showed a prominent peak at 7 am which may establish vehicular contributions. Contributions from the steelworks may also be responsible for the elevated BC observed at 7 am morning peak. The PMF profile of Streaker PM revealed the sinter

plant as one of the major contributors to BC (Appendix XXXVI). The polar plot of BC has also revealed a significant contribution by the steelworks from both sinter and cokemaking production units.

The polar plots of the gaseous pollutants have also indicated the steelworks industry as the major emission source of NO, NO_2, NO_x, CO and SO_2. High SO_2/NO_x ratio observed in this study shows the impact of stationary emissions by the steelworks (Aneja *et al.*, 2001). The single particle analysis with the ATOFMS instrument has identified 8 classes of particles in Port Talbot. The particle classes were K-rich (K-CN, K-NO_3, K-EC and K-Cl-PO_3), sea salt (Na-NO_3), silica dust (Na-$HSiO_2$), sulphate rich particles (K-HSO_4), nitrate rich particles (AlO-NO_3), Ca particles (Ca-NO_3), carbon particles (Mn-OC, Metallic-EC, EC, OC and OC-EC), and aromatic hydrocarbon (Arom) - PAH particles (Arom-CN, Fe-PAH-NO_3 and PAH-CN). It should be noted that the ATOFMS data was available only at the FS site.

The emission sources of ATOFMS particle classes were apportioned (Table 8.3) into 6 components, which were BF/Sinter, Cokemaking/Mills, traffic, marine, sulphate and nitrate (Figure 8.12). Most of these emission sources have also been identified by other source apportionment models adopted in this study. The PMF for Partisol at FS has identified BF, BOS/Sinter, traffic, marine, woodsmoke and secondary aerosol as the main emission sources of fine PM. (Figure 7.2). The Streaker PMF revealed $PM_{2.5}$ sources as: BF, sinter (plus secondary), BOS, coking, marine and traffic (Figure 7.4). The PCA model was able to indicate sources including BF, BF/Sinter/BOS, secondary/woodsmoke, oil combustion, traffic and marine for Partsiol $PM_{2.5}$; and BF/crustal, marine,

traffic/woodsmoke and oil combustion for Streaker $PM_{2.5}$. A clear agreement was therefore established between the ATOFMS and other receptor models, establishing the source apportionment ability of ATOFMS.

The polar plots of the ATOFMS K-rich particle showed K-CN and K-EC emissions from the cokemaking/mills/BOS facilities while K-Cl-PO_3 has been strongly linked with the sinter plant. In the PMF solution for Streaker data at FS site, K has 30% of its total concentration in the cokemaking factor. BC (34%) and K (13%) also occurred in the fine PMF profile for sinter factor. Steel emissions from the sinter and cokemaking plants were also established by both PMF and PCA models. In the Partisol PMF, fine K has been allocated to woodsmoke while coarse K allotted to the sinter plant. The ATOFMS mass size distribution for K-Cl-PO_3 showed a dual peak in fine and coarse fractions (Figure 8.15). The polar plot has established emissions of K-Cl-PO_3 particles from the BF/Sinter plants. The source contribution from the BF/Sinter plant revealed by the ATOFMS (28%) may be comparable with the Streaker PMF apportioned $PM_{2.5}$ (28% Sinter and Secondary, and 20% for BF). The Partisol PMF revealed BF contributing 11%, and BOS/Sinter 5% for fine particles. With PCA, the Partisol fine fraction has shown BF constituted 14% while Sinter/BF/BOS was assigned 19%. Cokemaking/Mills was another significant steelworks factor identified by the ATOFMS instrument representing 22% of apportioned single particles. In the PMF profile for Partisol, the cokemaking factor was unidentified, while the Streaker PMF was able to allocate 8% of fine PM to coking. Different percentages might be apportioned to the steelworks factors by the ATOFMS and other offline instruments; however, both online and offline instruments have identified the BF/Sinter plants as the largest steelworks contributor to PM in Port Talbot. For protection

of public health, there is a necessity to install dust suppressant equipment on the BF/Sinter plant sections.

The sulphate and nitrate particle classes formed 10% of the ATOFMS apportioned particles and are related to secondary aerosol. The figure was relatively lower than the Partisol PMF secondary factor (52%, Figure 7.2) for fine PM. For Streaker PMF, secondary aerosol co-existed with the sinter component representing 28% of $PM_{2.5}$. The wind sector plot showed sulphate particulate relating to cokemaking/mills sections. The fine PMF profile for coking at FS revealed significant loading for SO_2 (65% of its modelled concentration). The sulphate particle class identified by ATOFMS may therefore be linked to cokemaking emission (Konieczynski *et al.*, 2012; Pancras *et al.*, 2013).

The nitrate particle class revealed by ATOFMS showed no links with the steelworks emissions. The polar plot of this particle class showed evidence of traffic emissions. The ATOFMS showed traffic as one of the major emission sources of particles in Port Talbot with 28% (Figure 8.12), which is close to the $PM_{2.5}$ PCA resolved factor assigned to traffic at 19% (Figure 7.6). The PMF analysis reported apportioned values of 5% and 14% for Partisol and Streaker data, respectively.

The marine source of ATOFMS particles showed a percent contribution of 12% while the Streaker and Partisol PMF $PM_{2.5}$ marine factors were allotted 16% and 26%, respectively. A relatively lower value of 4% was given by PCA.

The ATOFMS instrument has effectively identified important steelworks marker elements which have been used for sources apportionment by filter-based measurement. Fe, Mn and Ca are important steelworks emissions from the BF plant (Machemer, 2004; Mazzei *et al.*, 2008; Hleis *et al.*, 2013). Ca-rich particles were identified by the ATOFMS instrument with the polar plot revealing the blast furnace unit as the source. Ca-rich particle represented approximately 3% of the total analysed ATOFMS particle (Table 8.3), and therefore was comparable with blast furnace factor of the Streaker PMF for $PM_{2.5}$ at FS site. Ca is the second most abundant element (71% of PMF modelled concentration) apportioned to blast furnace factor after Fe (74%). The scaled ATOFMS dM/dlogD concentrations of Ca showing two peaks at both fine and coarse mode indicate emissions from the steelworks and crustal sources (Figure 8.15). However, the elevated fine peak of Ca demonstrates dominance of steelworks emissions (from the blast furnace). This trend was observed for silica particles but with a relatively small peak at the fine mode probably due to the low quantity input in steel production (Ricketts, 2013). Fe-PAH-NO_3 was also identified by the ATOFMS and indicated BF/Sinter emissions.

The carbon and aromatic/polycyclic aromatic hydrocarbon particle class formed 24% of all the classified particles (Table 8.3). Most of the carbon type particles showed local traffic emissions at a relatively low windspeed. The value of OC/EC ratio (1.6±0.6) of the Digitel $PM_{2.5}$ also confirms the local traffic contribution to carbonaceous species in agreement with reported studies (Hildermann *et al.*, 1991; Watson *et al.*, 1994). This shows consistency between the ATOFMS and the Digitel measured OC/EC. However, the ATOFMS OC and Mn-OC particles showed higher concentration levels around the

cokemaking and mills (Figure 8.9). The study of Tsai *et al.* (2007) has reported elevated value of OC around the cold forming mill in Taiwan.

The aromatic/PAH particle class has revealed cokemaking and BOS sections of the steelworks as the major emitters. These organic constituents were not included in the PMF/PCA model and hence do not allow for their comparison with ATOFMS apportioned particles. However, the evidence of steelworks emission of organics such as hydrocarbons, aromatic and polycyclic aromatic hydrocarbons was established by the ATOFMS instrument. A number of studies based on filter and single particle measurements have reported elevated concentrations of organics around steelworks sites (Yang *et al.*, 2002; Manoli *et al.*, 2004; Liberti *et al.*, 2006; Choi *et al.*, 2007; Tsai *et al.*, 2007; Dall'Osto *et al.*, 2008).

As discussed above, the chemical profiles revealed by both PMF and wind determined analyses have demonstrated significant steelworks increments for Fe, Mn, sulphate, Al, Ca and Pb. In the ATOFMS single particle analysis, these elements were identified as Fe-PAH-NO_3, Mn-OC, HSO_4, AlO and Ca particles. A weak signal of ATOFMS spectra at *m/z* 207, which also occurred with Fe in Fe-PAH-NO_3 particles, may indicate the presence of Pb (Figure 8.10). Assignment of Fe-PAH, Mn-OC, HSO_4, AlO and Ca particles to different steelworks sections can be seen in Table 8.3. A good relationship may therefore be established for ATOFMS, wind-determined and PMF source apportionment methods.

Scaling of the ATOFMS instrument was successfully done with the Grimm particle counting instrument. The scaled ATOFMS counts showed highest dN/dlogDp value for K-

NO_3 and aromatic/PAH particle classes with all the sub-class particles peaking around 0.3 µm. ATOFMS calculated-mass showed sea salt particles peaking at 1.8 µm. These peaks could represent the coarse particles for the ATOFMS instrument. The MOUDI instrument has shown elevated coarse peaks of marine aerosols of Na and Cl. K-Cl-PO_3 which has been attributed to sinter plant emission showed two modal peaks at fine (D_a<1.0 µm) and coarse diameter around 1.8 µm. The MOUDI size distribution of K (Figure 4.2) showed a similar bimodal peak indicating good agreement between the two instruments.

The scaled arom/PAH particles size-distribution in this study peaked at 0.3 µm and agreed well with the work of Dall'Osto *et al.* (2008) and Baraniecka *et al.* (2010). The abundance of *m/z* +202 (pyrene) displayed by PAH-CN particle class (Figure 8.10) is also consistent with the study of Baraniecka *et al.* (2010) at a steel industry in Poland. A related study at Taranto, southern Italy, has observed elevated amounts of Fe and PAH (benzo[a]pyrene (*m/z* +252) (Amodio *et al.*, 2013). Benzo[a]pyrene measured at rolling mills by Baraniecka *et al.* (2010) constituted around 50% of the total PAH determined with size peak at 0.25 µm.

The polar plot of the total particle counts of ATOFMS (Figure 8.17) has highlighted multiple emission sources of particles in Port Talbot which may be related to emissions from the local traffic, residential houses, the steelworks, marine, and regional pollutants. As explained above, the receptor models adopted for apportioning emission sources have also identified these sources indicating the complementary nature of the ATOFMS instrument.

The comparison plot (Fig. 8.18) of PM mass concentrations by all the PM measuring instruments with ATOFMS has shown good agreements in terms of daily variations. The ATOFMS instrument is therefore, a useful tool for identification and apportionment of urban aerosol sources.

9.3 Conclusion

The present study was designed using receptor models to identify and apportion air pollutants sampled at an industrial site. Different offline and online particulate matter (PM) measuring instruments were deployed to the industrial town of Port Talbot during a one-month sampling campaign. Two week sampling of PM was also carried at EROS (an urban background site). The mass distribution patterns of particles showed elevated bimodal peaks for Fe, Zn, Cr, Ca^{2+}, K^{+}, Na^{+} and Cl^{-} at Port Talbot compared to EROS. $PM_{2.5\text{-}10}$ mass concentration and Mn were also found at higher values at Port Talbot relative to EROS. This study also found the PM in Port Talbot to be dominated by the coarse fraction.

The polar plots of particle number size spectra revealed much source-related information including local emissions, probably from road traffic, which dominated the smaller size bins (0.3-0.5 µm), while steelworks emissions dominated the range 0.5-15 µm, and for particles greater than 15 µm marine aerosol appeared dominant. Although there appeared to be contributions from more than a single source within the steelworks, the wind direction-dependence suggested the sinter plant and/or blast furnace plant to be the major contributors.

The receptor models (PCA and PMF), ATOFMS and wind sector associated data were able to resolve different production components of the steelworks. The PMF analysis of daily and hourly data collected at Port Talbot has allowed identification of 6-7 factors for $PM_{2.5,}$ $PM_{2.5\text{ -}10}$ and PM_{10}, while PCA identified 5-6 emission components for Partisol data only. The hourly data has been found to be more effective in resolving sources that the daily data could not detect. PMF and PCA revealed secondary aerosol as the dominating component of $PM_{2.5}$ while the combined steelworks dominated the coarse fraction. The apportionment of PM from the offline measuring instruments revealed the blast furnace and sinter plants to be the major contributors to particle pollution in Port Talbot.

The average increments of Partsol and Streaker by wind sector linking source to receptor locations at FS and LW have revealed steelworks sections including ore stockyard, blast furnace, sinter, BOS/Cokemaking and mills as major sources of PM in Port Talbot. This study has identified the blast furnace and sinter plants as the major emission sources. Urgent action is therefore required from the Local Environmental Agency to enforce a particle control system as part of the management of the steelworks especially at the sinter and blast furnace sections. The wind sector data has also provided steelworks fingerprints from different sections of the integrated steelworks, which can be used for source apportionment studies.

The single particle analysis using ATOFMS has provided further information on the contribution of the steelworks to PM pollution in Port Talbot with BF/Sinter representing the major emission source. Emissions from the steelworks cold and hot mills section, which had not been identified with PCA and PMF were clearly revealed by ATOFMS.

The ATOFMS instrument was able to identify major emission sources highlighted by the PMF and PCA which are marine (12%), traffic (28%), secondary (10%), Cokemaking/Mills (BOS, 22%) and BF/Sinter (28%). PMF and PCA showed the total steelworks PM contributions as 31% and 16% for Partisol, 28% and 38% for Streaker and 50% for ATOFMS.

This study has revealed the significant contributions by the steelworks complex activities in Port Talbot to particulate and gaseous pollutants. Furthermore, secondary aerosol, marine sources and traffic are significant emission sources of PM. During this study, days of PM exceedances where the WHO/EU 24-hour mean limit of 50 μg m^{-3} was breached were observed. This can be damaging to the public health. The ATOFMS result also showed the PAH particle types contributing to *ca* 8% of the total analysed particles. Chronic exposure to PAH may initiate carcinogenic health effects in the exposed population.

The results obtained and presented in this thesis have provided useful information of the steelworks emission sources and their ground-level concentrations at Port Talbot. This will be useful for different environmental and research groups on air quality management as well as the local authority policymakers. Control and abatement measures for reducing particulate emissions at the steelworks (most especially at the BF and sinter plants) are recommended to the management of the steelworks industry at Port Talbot.

9.4 Further Work

The results presented in this study have been based on the offline and online source apportionment methods around the integrated steelworks at Port Talbot. Most of the analysed portions of particulate matter were inorganic chemical species. But with ATOFMS, organic constituents were identified. Since ATOFMS is more of a qualitative measurement, future studies should focus more on the filter-based determination of organic constituents of particulate matter around the steelworks in Port Talbot. An Aerosol Mass Spectrometer (AMS) could also be placed alongside the ATOFMS instrument for quantification of organics in future studies.

As this study was designed, four sampling sites were selected to evaluate the overall impacts of the steelworks activities across Port Talbot town. However, only Partisol samplers were present at each of the sampling sites. It will be worthwhile adding the Streaker samplers at all the monitoring sites instead of the present two sites where these samplers were placed. It was obvious that mass and chemical concentrations of particulate matter measured were the highest at Prince Street. Unfortunately, only 12-day Partisol data was available at this site due to instrumental breakdown. This is one of the limitations of this study. It would be more appropriate to place the mobile laboratory at the Prince Street site rather than at the present Automatic Urban Rural Network (AURN) Fire Station site.

It will be necessary to run two ATOFMS instruments simultaneously at the upwind (Little Warren) and downwind (Fire Station or Prince Street) sites. This will give room for ATOFMS data comparison as well as wind sector analysis. Even though this was done for

Partisol and Streaker instruments in this study, more instruments should be included in future work. If it is possible to place both offline and online particle measuring instruments within the steelworks facilities (sinter, blast furnace, basic oxygen furnace and mills plants) for at least one-week sampling of particulate matter, gaseous pollutants and black carbon, this may provide more distinctive steelworks fingerprint data.

Finally, the health aspects of Port Talbot steelworks should be investigated. The scope of the study should cover the impacts of the steelworks emissions on the health of workers and the residents. The study should also integrate hospital admissions with particulate and gaseous pollutant emissions.

Collaborative work with other research groups might be necessary to investigate different atmospheric pollution issues in Port Talbot. A receptor modelling study with offline and online instruments should be extended to other steelworks industries within the UK.

REFERENCES

Abdalmogith, S.A., Harrison, R.M., Derwen. R.G. (2006). Particulate sulphate and nitrate in Southern England and Northern Ireland during 2002/3 and its formation in a photochemical trajectory model. *Science of the Total Environment* **368** (2-3), 769–780.

Adachi, K, Tainosho, Y. (2004). Characterization of heavy metal particles embedded in tire dust. *Environmental International* **30** (8), 1009-17.

Ahn, Y.C., Lee, J.K. (2006). Physical, chemical, and electrical analysis of aerosol particles generated from industrial plants. *Aerosol Science* **37**, 187–202.

Air Quality News (2013). Welsh steelworks served notice over dust pollution. http://www.airqualitynews.com/2013/07/31/welsh-steelworks-served-notice-over-dust-pollution/). *Accessed 01/09/13*.

Aldabe, J., Elustondo, D., Santamaría, C., Lasheras, E., Pandolfi, M., Alastuey, A., Querol, X., Santamaría, J.M. (2011). Chemical Characterisation and Source Apportionment of $PM_{2.5}$ and PM_{10} at Rural, Urban and Traffic Sites in Navarra (North of Spain). *Atmospheric Research* **102**, 191–205.

Ali, M., Chahouki, Z. (2011). Multivariate Analysis Technique. *In: Environmental Science, Earth and Environmental Sciences*, Dar, I.A. and Dar, A.M. (Ed.), ISBN: 978-953-307-468-9, InTech Publisher. http://www.intechopen.com/books/earth-and-environmental-sciences/multivariate-analysis-techniques-in-environmental-science. Pg. 539-564.

Alleman, L.Y., Lamaison, L., Perdrix, E., Robache, A., Galloo, J.C. (2010). PM_{10} metal concentrations and source identification using positive matrix factorization and wind sectoring in a French industrial zone. *Atmospheric Research* **96**, 612–625.

Allen, A.G., Nemitz, E., Shi, J.P., Harrison, R.M., Greenwood, J.C. (2001). Size distributions of trace metals in atmospheric aerosols in the United Kingdom. *Atmospheric Environment* **35**, 4581-4591.

Almeida, S.M., Pio, C.A., Freitas, M.C., Reis, M.A., Trancoso, M.A. (2005). Source apportionment of fine and coarse particulate matter in a sub-urban area at the Western European Coast. *Atmospheric Environment* **39**, 3127-3138.

Amato, F., Pandolfi, M., Escrig, A., Querol, X, Alastuey, A., Pey, J., Prez, N., Hopke, P.K. (2009). Quantifying road dust resuspension in urban environment by Multilnear Engine: A comparison with PMF2. *Atmospheric Environment* **43**, 2770-2780.

Amato, F., Viana, M., Richard, A., Furger, M., Prevot, A.S.H., Nava, S., Lucarelli, F., Bukowiecki, N., Alastuey, A., Reche, C., Moreno, T., Pandolfi, M., Pey, J., Querol, X. (2011). Size and time-resolved roadside enrichment of atmospheric particulate pollutants.

Atmospheric Chemistry and Physics **11**, 2917–2931, 2011.www.atmos-chem-phys.net /11/2917/2011/.

Amodio, M., Andriani, E., de Gennaro, G., Di Gilio, A., Ielpo, P., Placentino, C.M., Tutino, M. (2013). How a steel plant affects air quality of a nearby urban area: a study on metals and PAH concentrations. *Aerosol and Air Quality Research* **13**, 497–508.

Andreae, M. O., Charlson, R.J., Bruynseels, F., Storms, H., VAN Grieken, R., Maenhaut, W. (1986). Internal mixture of sea salt, silicates, and excess sulfate in marine aerosols. *Science* **232** (4758), 1620-1623.

Anderson, H. R., Bremner, S. A., Atkinson, R. W., Harrison, R. M., Walters, S. (2001). Particulate matter and daily mortality and hospital admissions in the west midlands conurbation of the United Kingdom: associations with fine and coarse particles, black smoke and sulphate. *Occupational and Environmental Medicine* **58**, 504-510.

Anderson, D. R., Fisher, R. (2002). Sources of dioxins in the United Kingdom: the steel industry and other sources. *Chemosphere* **46**, 371-381.

Anderson, M. J., Miller, S. L., Milfor, J. B. (2001). Source apportionment of exposure to toxic volatile organic compounds using positive matrix factorization. *Journal of Exposure Analysis and Environmental Epidemiology* **11**, 295–307.

Aneja, V. P., Agarwal, A., Roelle, P. A., Phillips, S. B., Tong, Q., Watkins, N., Yablonsky, R. (2001). Measurements and Analysis of Criteria Pollutants in New Delhi, India. *Environmental International* **27**, 35-42.

Anenberg, S. C., Horowitz, L. W., Tong, D. Q., West, J. J. (2010). An Estimate of the Global Burden of Anthropogenic Ozone and Fine Particulate Matter on Premature Human Mortality Using Atmospheric Modeling. *Environmental Health Perspective* **118** (9), 1189-1195.

Anttila, P., Paatero, P., Tapper, U., Jarvinen, O. (1995). Application of positive matrix factorization to source apportionment: Results of a study of bulk deposition chemistry in Finland. *Atmospheric Environment* **29**, 1705-1718.

AQEG (2005). Particulate Matter in the United Kingdom: Summary. Defra, London, available at http://www.defra.gov.uk/environment/quality/air/airquality/publications /particulate-matter. Air Quality Expert Group (2005). Accessed *12/02/12*.

AQEG (2011). Understanding PM_{10} in Port Talbot. Advise note prepared for Department of Environment, Food and Rural Affairs: Scottish, Welsh Assembly Government, and Department of the Environment, Northern Ireland. *uk-air.defra.gov.uk /.../110322_AQEG_Port_Talbot_Advice_Note.pd. Accessed on 04/01/13.*

AQEG. (2012). Fine Particulate Matter ($PM_{2.5}$) in the United Kingdom. Air Quality Expert Group, Department for Environment, Food and Rural Affairs, London. http://uk-

air.defra.gov.uk/reports/cat11/1212141150_AQEG_Fine_Particulate_Matter_in_the_UK.pdf. *Accessed:03/06/13.*

Arditsoglou, A. S. C., Samara, C. (2005). Levels of total suspended particulate matter and major trace elements in Kosovo: a source identification and apportionment study. *Chemosphere* **59**, 669–678

Athanasopoulou, E., Tombrou, M., Pandis, S. N., Russell, A. G. (2008). The role of sea-salt emissions and heterogeneous chemistry in the air quality of polluted coastal areas, *Atmospheric Chemistry and Physics* **8**, 5755–5769.

Ayrault, S., Sehou, A., Moskura, M., Gaudry, A. (2010). Atmospheric trace element concentrations in total suspended particles near Paris, France. *Atmospheric Environment* **44**, 3700-3707.

Baltensperger, U., Kalberer, M., Dommen, J., Paulsen, D., Alfarra, M. R., Coe, H., Fisseha, R., Gascho, A., Gysel, M., Nyeki, S., Sax, M., Steinbacher, M., Prevot, A. S. H., Sjogren, S., Weingartner, E., Zenobi, R. (2005). Secondary organic aerosols from anthropogenic and biogenic precursors, *Faraday Discussion*, **130**, 265–278.

Baraniecka, J., Pyrzynska, K., Szewczynska, M., Posniak, M., Dobrzynska, E. (2010). Emission of polycyclic aromatic hydrocarbons from selected processes in steelworks. *Journal of Hazardous Materials* **183** (1-3), 111-115.

Barrett, M. (2004). Atmospheric emission from large point sources in Europe. Swedish NGO Secretariat on Acid Rain, Air Pollution and Climate, 17: 60 p.

Bi, X. H., Zhang, G. H., Li, L., Wang, X. M., Li, M., Sheng, G. Y., Fu, J. M., Zhou, Z. (2011). Mixing state of biomass burning particles by single particle aerosol mass spectrometer in the urban area of PRD, China. *Atmospheric Environment* **45**, 3447–3453.

Bigi, A., Harrison, R. M. (2010). Analysis of the air pollution climate at a central urban background site. *Atmospheric Environment* **44**, 2004-2012.

Bjorseth, A., Ramdahl, T. (1985). Sources and emissions of PAH. In: Emission sources and Recent Progress in Analytical Chemistry Handbook of Polycyclic Aromatic Hydrocarbons. Vol. 2. Marcel Dekker, New York and Barcel.

Bostrom, C-E. Gerde, P., Hanberg, A., Jernstrom, B., Johansson, B. C., Kyrklund, T., Rannug, A., Tornqvist, M., Victorin, K., Westerholm, R. (2002). Cancer risk assessment, indicators, and guidelines for polycyclic aromatic hydrocarbons in the ambient air, *Environmental Health Perspective* **110**, 451–489.

Borderieux, S., Wu, C-Y., Bonzongo, J-C., Powers, K. (2004). Control of Elemental Mercury Vapor in Combustion Systems Using Fe_2O_3. *Nanoparticles, Aerosol and Air Quality Research*, **4** (1), 74–90.

Bourotte, C., Curi-Amarante, A-P., Forti, M. C., Pereira, L. A. A., Braga, A. L., Lotufo, P. A. (2007). Association between ionic composition of fine and coarse aerosol soluble fraction and peak expiratory flow of asthmatic patients in Sao Paulo city (Brazil). *Atmospheric Environment* **41**, 2036–2048.

Braga, C. F., Alves, R. C. M., Teixeira, E. C., Pires, M. (2002). Aerosols concentration in the Candiota area applying different gravimetric methods of sampling and numeric modeling. *Journal of Environment Monitoring* **4**, 897–902.

Braga, C. F., Teixeira, E. C., Meira, L., Wiegand, F., Yoneama, M. L., Dias, J. F. (2005). Elemental composition of PM_{10} and $PM_{2.5}$ in urban environment in South Brazil. *Atmospheric Environment* **39**, 1801-1815.

Brigden, K., Labunska, I., Stringer, R. (2000). Identification of organic pollutants and heavy metal contaminants in filter ash collected from the Siderca primary and secondary steel smelter, Campana, Argentina. Technical note 20/00. http://www z.greenpeace.to/ publications/Siderca%20report.pdf. *Accessed 08/03/13.*

Brown, A. S., Brown, R. J., Coleman, P., Conolly, C., Sweetman, A., Jones, K. C., Butterfield, D. M., Sarantaridis, D., Donovan, B. J., Roberts, I. (2013). Twenty years of measurement of polycyclic aromatic hydrocarbons (PAHs) in UK ambient air by nationwide air quality networks. *Environmental Science: Processes Impacts* **15**, 1199-1215.

Buzea, C., Blandiho, P. I. I., Robbie, K. (2007). Nanomaterials and nanoparticles: sources and toxicity. *Biointerphases* **2**, MR17–71.

Cabada, J. C., Rees, S., Takahama, S., Khlystov, A., Pandis, S. N., Davidson, C. I., Robinson, A. L. (2004). Mass size distributions and size resolved chemical composition offline particulate matter at the Pittsburgh supersite. *Atmospheric Environment* **38**, 3127-3141.

Calzolai, G., Chiari, M., Orellana, I. G, Lucarelli, F., Migliori, A., Nava, S., Taccetti, F. (2006). The new external beam facility for environmental studies at the Tandetron accelerator of LABEC. *Nuclear Instruments and Methods in Physics Research Section B* **249**, 928-931.

Carslaw, D. C. (2013). The openair manual - open-source tools for analysing air pollution data. Manual for version 0.8-0, King's College London.

Celis, J. E., Morales, J. R., Zaror, C. A., Inzunza, J. C. (2004). A study of the particulate matter PM_{10} composition in the atmosphere of Chile. *Chemosphere* **54** (5), 541–550.

Cetin, B., Yatkin, S., Bayram, A., Odabasi, M. (2007). Ambient concentrations and source apportionment of PCBs and trace elements around an industrialized area in Izmir, Turkey. Chemosphere 69, 1267-1277.

Chan, K. C., Yao, X. (2008). Air pollution in mega cities in China. *Atmospheric Environment* **42** (1), 1-42.

Chang, L-P., Tsai, J-H., Chang, K-L., Lin, J.J. (2008). Water soluble inorganic ions in airborne particulates from the nano to coarse mode: a case study of aerosol episodes in southern region of Taiwan. *Environmental Geochemistry and Health* **30**, 291–303.

Charron, A., Harrison, R. M. (2005). Fine ($PM_{2.5}$) and coarse ($PM_{2.5–10}$) particulate matter on a heavily trafficked London highway: sources and processes. *Environmental Science and Technology* **39**, 7768–7776.

Charron, A., Harrison, R. M., Moorcroft, S. and Booker, J. (2004). Quantitative interpretation of divergence between PM_{10} and $PM_{2.5}$ mass measurement by TEOM and gravimetric (Partisol) instruments. *Atmospheric Environment* **38**, 415-423.

Chiari, M., Lucarelli, F., Mazzei, F., Nava, S., Paperetti, L., Prati, P., Valli, G., Vecchi, R. (2005). Airborne particulate matter characterization in an industrial district near Florence, by PIXE and PESA. *X-Ray Spectrometry* **34** (4), 323–329.

Chio, C-P., Cheng, M-T., Wang, C-F. (2004). Source apportionment to PM_{10} in different air quality conditions for Taichung urban and coastal areas, Taiwan. *Atmospheric Environment* **38**, 6893-6905.

Choi, J. C., Lee, M., Chun, Y., Kim, J., Oh, S. (2001). Chemical composition and source signature of spring aerosol in Seoul, Korea. *Journal of Geophysical Research* **106** (D16), 18067–18074.

Choi, S-D., Baek, S-Y., Chang, Y-S. (2007). Influence of a large steel complex on the spatial distribution of volatile polycyclic aromatic hydrocarbons (PAHs) determined by passive air sampling using membrane-enclosed copolymer (MECOP). *Atmospheric Environment* **41**, 6255-6264.

Choi, S-D., Baek, S-Y., Chang, Y-S. (2008). Atmospheric levels and distribution of dioxin-like polychlorinated biphenyls (PCBs) and polybrominated diphenyl ethers (PBDEs) in the vicinity of an iron and steel making plant. *Atmospheric Environment* **42**, 2479-2488.

Chung, Y-S, Kim, S-H., Moon, J-H., Kim, Y-J, Lim, J-M, Lee, J-H. (2006). Source identification and long-term monitoring of airborne particulate matter ($PM_{2.5}$ /PM_{10}) in an urban region of Korea. *Journal of Radioanalytical and Nuclear Chemistry* **267** (1), 35-48.

Connell, D. P., Winter, S. E., Conrad, V. B., Kim, M., Crist, K. C. (2006). The Steubenville Comprehensive Air Monitoring Program (SCAMP): Concentrations and solubilities of $PM_{2.5}$ trace elements and their implications for source apportionment and health research. *Journal of the Air and Waste Management Association* **56**, 1750–1766.

Connell, D. P., Withum, J. A., Winter, S. E., Statnick, R. M. (2005). The Steubenville Comprehensive Air Monitoring Program (SCAMP): Analysis of short-term and episodic

variations in $PM_{2.5}$ concentrations using hourly air monitoring data. *Journal of the Air and Waste Management Association* **55**, 559–573.

Crespo, J., Yubero, E., Nicolás, J. F., Lucarelli, F., Nava, S., Chiari, M., Calzola, G. (2012). High-time resolution and size-segregated elemental composition in high-intensity pyrotechnic exposures. *Journal of Hazardous Materials* **241**, 242, 82– 91.

D'Alessandro, A., Lucarelli, F., Mando, P. A., Marcazzan, G., Nava, S., Prati, P., Valli, G., Vecchi, R., Zucchiatti, A. J. (2003). Hourly elemental composition and sources identification of fine and coarse PM_{10} particulate matter in four Italian towns. *Journal of Aerosol Science* **34**, 243-259.

Dall'Osto, M., Booth, M. J., Smith, W., Fisher, R., Harrison, R. M. (2008a). Study of the size distributions and the chemical characterization of airborne particles in the vicinity of a large integrated steelworks. *Aerosol Science Technology* **42**, 981–991.

Dall'Osto, M., Drewnick, F., Fisher, R., Harrison, R. M. (2008b). Real-time measurements of non-metallic fine particulate matter adjacent to a major integrated steelworks. *Aerosol Science and Technology* **46** (6), 639-653.

Dall'Osto, M., Harrison, R. M. (2006). Chemical characterization of single airborne particles in Athens (Greece) by ATOFMS. *Atmospheric Environment* **40**, 7614-7631.

Dall'Osto, M., Harrison, R. M. (2012). Urban organic aerosols measured by single particle mass spectrometry in the megacity of London. *Atmospheric Chemistry and Physics* **12**, 4127–4142.

Dall'Osto, M., Harrison, R. M., Charpantodou, E., Loupa, G., Rapsomanikis, S. (2007). Characterisation of indoor airborne particles by using real-time aerosol mass spectrometry. *Science of the Total Environment* **384**, *120-123.*

Dall'Osto, M., Beddows, D.C.S. Kinnersley, R. P., Harrison, R. M., Donovan, R. J., Heal, M. R. (2004). Characterization of individual airborne particles by using aerosol time-of-flight mass spectrometry at Mace Head, Ireland. *Journal of Geophysical Research: Atmospheres* **109** (D21), D21302.

Dan, M., Zhuang, G., Li, X., Tao, H., Zhuang, L. (2004). The characteristics of carbonaceous species and their sources in $PM_{2.5}$ in Beijing. *Atmospheric Environment* **38**, 3443–3452.

Daniels, M. J., Dominici, F., Zeger, S. L., Samet, J. M. (2004). The National Morbidity, Mortality, and Air Pollution Study, Part III: PM_{10} Concentration–Response Curves and Threshold for the 20 Largest US Cities. Research Report 94. Boston, MA: Health Effects Institute.

Davidson, C. I., Phalen, R. F., Solomon, P. A. (2005). Airborne particulate matter and human health: A Review. *Aerosol Science and Technology* **39**(8), 737-749.

Debry, E., Fahey, K., Sartelet, K., Sportisse, B., Tombette, M. (2006). Technical Note: A new SIze REsolved Aerosol Model (SIREAM). *Atmospheric Chemistry and Physics Discussions* **6** (6), 11845-11875.

Delgado-Saborit, J. M., Stark, C., Harrison, R. M. (2011). Carcinogenic potential, levels and sources of polycyclic aromatic hydrocarbon mixtures in indoor and outdoor environments and their implications for air quality standards. *Environmental International* **37**, 383–392.

DfT. (2012). Neath Port Talbot: Total traffic on major roads (thousand vehicle miles), 2000 to 2011. www.dft.gov.uk/traffic-counts/area.php?region=Wales&la=Neath+Port+Talbot. *Accessed:27/10/12.*

DiBattista, C., Brown, D. R. (2003). Editorial: quality of life and attainment of National Ambient Air Quality Standards (NAAQS). Are they compatible? More questions than answers. The challenge for risk assessment. *Human Ecological Risk Assessment* **9**, 637–640.

Digitel Elektronik (2010). DIGITEL High Volume Aerosol Sampler Manual. 61p. http://www.digitel-ag.com/Downloads/Dokumentation/Operation%20instructions%20DHA-80%20DMCU%20HT001.pdf. *Accessed 08/08/13*.

Dore, C. J., Murrels, T. P., Passant, N. R., Hobson, M. M., Thistlethwaite, G., Wagner, A., Li, Y., Bush, T., King, K. R., Norris, J., Coleman, P. J., Walker, C., Stewart, R. A., Tsagatakis, I., Conolly, C., Brophy, N., Hann, M. R. (2008). UK Emissions of Air Pollutants 1970 to 2006. Didcot, Oxon, UK.

Dos Santos, M., Dawidowski, L., Smichowski, P., Ulke, A.G., Gomez, D. (2012). Factors controlling sea salt abundances in the urban atmosphere of a coastal South American megacity. *Atmospheric Environment* **59**, 483-491

DoT (2002). Sources of particulate matter in urban areas: Department of Transport. (UK TRAMAQ Project UG 250.

Duan, J., Tan, J., Wang, S., Hao, J., Chai, F. (2012). Size distributions and sources of elements in particulate matter at curbside, urban and rural sites in Beijing. *Journal of Environmental Sciences* **24**(1) 87-94.

Ebert, M., Muller-Ebert, D., Benker, N., Weinbruch, S. (2012). Source apportionment of aerosol particles near a steel plant by electron microscopy. *Journal of Environmental Monitoring* **14**, 3257-3266.

EC (European Commission). (2006). Environment-Air quality standard. http://ec.europa.eu/environment/air/quality/standards.htm. *Accessed: 12/02/12.*

Figueroa D. A., Rodrıguez-Sierra C. J., Jimenez-Velez B. D. (2006). Concentrations of Ni and V, other heavy metals, arsenic, elemental and organic carbon in atmospheric fine particles (PM2.5) from Puerto Rico. *Toxicology and Industrial Health* **22**, 87- 99.

Gard, E. E., Kleeman, M. J., Gross, D. S., Hughes, L. S., Allen, J. O., Morrical, B. D., Fergenson, D. P., Dienes, T., GRalli, M. E., Johnson, R. J., Call, G. R., Prather, K. A. (1998). Direct observation of the heterogeneous chemistry in the atmosphere. *Science*, **279**, 1184–1187.

Gard, E. E., Mayer, J. E., Morrical, B. D., David, T. D., Fergenson, P., Prather, K. A. (1997). Real-Time Analysis of Individual Atmospheric Aerosol Particles: Design and Performance of a Portable ATOFMS. *Analytical Chemistry* **69**, 4083-4091.

Gan, W. Q., Man, S. F., Senthilselvan, A., Sin, D. D. (2004). Association between chronic obstructive pulmonary disease and systemic inflammation: a systemic review and a meta-analysis. *Thorax* **59**:574–580.

Garcia, J.H., Li, W.-W., Cardenas, N., Arimoto, R., Walton, J., Trujillo, D. (2006). Determination of $PM_{2.5}$ sources using time-resolved integrated source and receptor. *Chemosphere* **65**, 2018–2027.

Gauderman, W. J., Avol, E., Gilliland, F., Vora, H., Duncan, T., Berhane, K., McConnell, R., Kuenzli, N., Lurmann, F., Rappaport, E., Margolis, H., Bates, D., Peters, J. (2004). The effect of air pollution on lung development from 10 to 18 years of age. *The NewEngland Journal of Medicine* **351**:1057–1067.

Gavett, S. H., Haykal-Coates, N., Copeland, L. B., Heinrich, J., Gilmour, M.I. (2003). Metal Composition of Ambient PM2.5 influences severity of allergic airways disease in mice. *Environmental Health Perspectives* **111**, 1471-1478.

Ghedini, N., Sabbioni, C., Bonazza, A., Gobbi, G. (2006). Chemical-thermal quantitative methodology for carbon speciation in damage layers on building surfaces. *Environmental Science and Technology* **40** (3), 949-944.

Giorio, C., Tapparo, A., Dall'Osto, M., Harrison, R. M., Beddows, D. C. S., DiMarco , C., Nemitz, E. (2012). Comparison of three techniques for analysis of data from an Aerosol Time-of-Flight Mass Spectrometer. *Atmospheric Environment* **61**, 316-326.

Gietl, J. K., Lawrence, R., Thorpe, A. J., Harrison, R. M. (2010). Identification of brake wear particles and derivation of a quantitative tracer for brake dust at a major road. *Atmospheric Environment* **44**,141-146.

Green, D. (2004). Measurements of Particulate Matter Volatility, London. Prepared for the Department for Environment, Food and Rural Affairs (DEFRA), the Scottish Executive, the Welsh Assembly Government and the DoE in Northern Ireland. KCLERG\MT\DEFRA\PMV2005.

Gross, D. S., Atlas, R., Rzeszotarski, J., Turetsky, E., Christensen, J., Benzaid, S., Olsen, J., Smith, T., Steinberg, L., Sulman, J., Ritz, A., Anderson, B., Nelson, C., Musicant, D. R., Chen, L., Snyder, D. C., Schauer, J. J. (2010). Environmental chemistry through intelligent atmospheric data analysis. *Environmental Modelling and Software* **25**, 760–769

Gross, D. S., Galli, M. E., Silva, P. J., Prather, K. A. (2000). Relative sensitivity factors for alkali metal and ammonium cations in single particle aerosol time-of-flight mass spectra. *Analytical Chemistry* **72** (2):416-22.

Gong, H. Jr, Sioutas, C., Linn, W. S. (2003). Controlled exposures of healthy and asthmatic volunteers to concentrated ambient particles in metropolitan Los Angeles. Research Report Health Effect Institute 118:1–36.

Guo, H., Wang, T., Simpson, I. J., Blake, D. R., Yu, X. M., Kwok , Y. H., Li, Y. S. (2004). Source contributions to ambient VOCs and CO at a rural site in eastern China. *Atmospheric Environment* **38**, 4551–4560.

Gupta, A. K., Karar, K. Srivastava, A. (2007). Chemical mass balance source apportionment of PM_{10} and TSP in residential and industrial sites of an urban region of Kolkata, India. *Journal of Hazardous Materials* **142**, 279–287.

Gupta, I., Salunkhe, A., Kumar, R. (2012). Source apportionment of PM_{10} by positive matrix factorization in urban area of Mumbai, India. *The Scientific World Journal* **2012**, 585791, 1-13. Doi:10.1100/2012/585791.

Guttikunda, S. (2009). *Urban Particulate Pollution Source Apportionment (Part 1) Definition, Methodology, and Resources.* URBANEMISSION. Info, SIM-air Working Paper Series: 16-2009, 1-14. http://www.urbanemissions.info/images/UEI/simseries/SIM-16-2009-PMSA-Part1.pdf.

Hallquist, M., Jerksj, M., Fallgren, H., Westerlund, J. Sjodin, A. (2012). Particle and gaseous emissions from individual diesel and CNG buses. *Atmospheric Chemistry and Physics Discussion* **12**, 27737-27773.

Han, Y-J., Kim, T-S., Kim, H. (2008). Ionic constituents and source analysis of $PM_{2.5}$ in three Korea Cities. *Atmospheric Environment* **42**, 4735–4746.

Hansen, A. D. A. (2005). The Aethalometer, Magee Scientific Company, Berkeley, California, USA, 209 p.

Hara, K., Osada, K., Yabuki, M., Yamanouchi, T. (2012). Seasonal variation of fractionated sea-salt particles on the Antarctic coast. *Geophysical Research Letter* **39**, L18801, doi:10.1029/ 2012GL052761.

Harrison, R. M., Beddows, D. C. S., Dall'Osto, M. (2011). PMF analysis of wide-range particle size spectra collected on a major highway. *Environmental Science and Technology* **45**, 5522-5528.

Harrison, R. M., Beddows, D. C. S., Hu, L., Yin, J. (2012c). Comparison of methods for evaluation of wood smoke and estimation of UK ambient concentrations. *Atmospheric Chemistry and Physics* **12** (17), 8271-8283.

Harrison, R. M., Deacon, A. R., Jones, M. R. (1997). Sources and processes affecting concentrations of PM_{10} and $PM_{2.5}$ particulate matter in Birmingham (U.K.). *Atmospheric Environment* **31**, 4103–4117.

Harrison, R. M., Jones, A. M. (2005). Multisite study of particle number concentrations in urban air. *Environmental Science and Technology* **39** (16), 6063-70.

Harrison, R. M., Jones, A., Gietl, J., Yin, J., Green D. (2012b). Estimation of the contribution of brake dust, tire wear and resuspension to nonexhaust traffic particles derived from atmospheric measurements. *Environmental Science and Technology* **46**, 6523-6529.

Harrison, R. M., Jones, A. M., Lawrence, R.G. (2004). Major component composition of PM_{10} and $PM_{2.5}$ from roadside and urban background sites. *Atmospheric Environment* **38**, 4531-4538.

Harrison, R. M., Jones, A. M., Lawrence, R. G. (2003). A pragmatic mass closure model for airborne particulate matter at urban background and roadside sites. *Atmospheric Environment* **37** (35), 4927–4933.

Harrison, R. M., Laxen, D., Moorcroft, S., Laxen, K. (2012a). Processes affecting concentrations of fine particulate matter ($PM_{2.5}$) in the UK atmosphere. *Atmospheric Environment* **46**, 115-124.

Harrison, R. M., Yin, J. (2000). Particulate matter in the atmosphere: which particle properties are important for its effects on health? *Science of the Total Environment* **249** (1-3), 85-101.

Harrison, R. M., Yin, J., Mark, D., Stedman, J., Appleby, R. S., Booker, J., Moorcroft, S. (2001). Studies of the coarse particle (2.5-10 μm) component in UK urban atmospheres. *Atmospheric Environment* **35**, 3667-3679.

Hayes, E., Chatterton, T. (2009). An independent review of monitoring measures undertaken in Neath Port Talbot in respect of particulate matter (PM_{10}), Report prepared for the Welsh Assembly Government by the University of the West of England, Bristol, October 2009.

Healy, R. M., Sciare, J., Poulain, L., Crippa, M., Wiedensohler, A., Prevot, A. S. H., Baltensperger, U., Sarda-Esteve, R., McGuire, M. L., Jeong, C-H., McGillicuddy, E., O'Connor, I.P., Sodeau, J. R., Evana, G. J., Wenger, J. C. (2013). Quantitative determination of carbonaceous particle mixing state in Paris using single particle mass spectrometer and aerosol mass spectrometer measurements. *Atmospheric Chemistry and Physics Discussion* **13**, 10345-10393.

Held, A., Hinz, K-P., Trimborn, A., Spengler, B., Klemm, O. (2002). Chemical classes of atmospheric aerosol particles at a rural site in Central Europe during Winter. *Journal of Aerosol Scienc*e **33**, 581-594.

Held, T., Ying, Qi, Kleeman, M.J., Schauer, J.J., Fraser, M.P. (2005). A comparison of the UCD/CIT air quality model and the CMB source-receptor model for primary airborne particulate matter. *Atmospheric Environment* **39**, 2281-2297.

Henry, R.C. (1997). History and Fundamentals of Multivariate Air Quality Receptor Models. *Chemometrics and Intelligent Laboratory Systems* **37**, 525–530.

Henry R.C. (2002). Multivariate receptor models- current practices and future trends. *Chemometrics and Intelligent Laboratory Systems* **60**, 43- 48.

Heung, W., Yun, M-J., Chang, D. P., Green, P. G., Halm, C. (2007). Emissions of chromium (VI) from arc welding. *Journal of the Air and Waste Management Association* **57**, 252-60.

Hien, P. D., Binh, N. T., Truong, Y., Ngo, N. T., Sieu, L. N. (2001). Comparative receptor modelling study of TSP, PM2 and PM2-10 in Ho Chi Minh City. *Atmospheric Environment* **35**, 669-2678.

Hildemann, L. M., Markowski, G. R., Cass, G. R. (1991). Chemical composition of emissions from urban sources of fine organic aerosol. *Environmental Science and Technology* **25** (4), 744-759.

Hjortenkrans, D. S. T., Bergback, B. G., Haggerud, A. V. (2007). Metal emissions from brake linings and tires: Case studies of Stockholm, Sweden 1995/1998 and 2005. *Environmental Science and Technology* **41**, 5224-5230.

Hleis, D., Fernandez-Olmo, I., Ledoux, F., Kfoury, K, Courcot, L., Desmonts, T., Courcot, D. (2013). Chemical profile identification of fugitive and confined particle emissions from an integrated iron and steelmaking plant. *Journal of Hazardous Materials* **250-251**, 246–255.

Hong, Y. M., Lee, B. K., Park, K. J., Kang, M. H., Jung, Y. R., Lee, D. S., Kim, M. G. (2002). Atmospheric nitrogen and sulphur containing compounds for three sites of South Korea. *Atmospheric Environment* **36**, 3485–3494.

Hopke, P. K. (2000). A Guide to Positive Matrix Factorization, EPA Workshop Proceedings, materials from the workshop on UNMIX and PMF as applied to $PM_{2.5,}$ 14-16 February, 2000.

Hopke, P. K., Ramadan, Z., Paatero, P., Norris, G. A., Landis, M. S., Williams, R. W., Lewis, C.W. (2003). Receptor modelling of ambient and personal exposure samples: 1998 Baltimore particulate matter epidemiology-exposure study. *Atmospheric Environment* **41**, 6276-6288.

Huang, Y. C., Ghio, A. J., Stonehuerner, J., McGee, J., Carter, J. D., Grambow, S. C., Devlin, R. B. (2003). The role of soluble components in ambient fine particles-induced changes in human lungs and blood. *Inhalation Toxicology* **15**, 327–342.

Huang, M., Wang, Z., Hao, L., Zhou, L., Gu, X., Fang, L., Zhang, W. (2006). Laser aerosol time-of-flight mass spectrometry analysis of individual aerosol particles from photooxidation of toluene. *Optica Applicata* **36** (1), 5.

Huang, H., Zou, C., Cao, J., Tsang, P., Zhu, F., Yu, C., Xue, S. (2012). Water soluble ions in $PM_{2.5}$ on the Qianhu Campus of Nanchang University, Nanchang City: Indoor-outdoor distribution and source implications. *Aerosol and Air Quality Research* **12**, 435–443.

Hueglin, C., Gehriga, R., Baltensperger, U., Gysel, M., Monn, C., Vonmont, H. (2005). Chemical characterisation of $PM_{2.5}$, PM_{10} and coarse particles at urban, near-city and rural sites in Switzerland. *Atmospheric Environment* **39**, 637–651.

Ibald-Mulli, A., Stieber, J., Wichmann, H. E., Koenig, W., Peters, A. (2001). Effects of air pollution on blood pressure: a population-based approach. *American Journal of Public Health* **91,** 571–577.

IPCC. (2001). *Climate change 2001: the scientific basis. Contribution of working group I to the third assessment report of the Inter-governmental Panel on Climate Change*. Cambridge, United Kingdom: Cambridge University Press.

Jacobson, M. Z. (2002). Control of fossil-fuel particulate black carbon and organic matter, possibly the most effective method of slowing global warming. *Journal of Geophysical Research* **107** (D19), 4410.

Jeon, S. J., Meuzelaar, H. L. C., Sheya, S. A. N., Lighty, J. S., Jarman, W. M., Kasteler, C., Sarofim, A. F., Simoneit, B. R. T. (2001). Exploratory studies of PM_{10} receptor and source profiling by GC/MS and principal component analysis of temporally and spatially resolved ambient samples. *Journal of the Air and Waste Management Association* **51**, 766–784.

Johansson, M.T., Soderstrom, M. (2011). Options for the Swedish steel industry- Energy efficiency measures and fuel conversion. *Energy* **36**, 191-198.

Johnson, K. S., de Foy, B., Zuberi, B., Molina, L. T., Molina, M. J., Xie, Y., Laskin, A. Shutthanandan, V. (2006)**.** Aerosol composition and source apportionment in the Mexico City Metropolitan Area with PIXE/PESA/STIM and multivariate analysis. *Atmospheric Chemistry and Physics* **6**, 4591-4600.

Johnson, K. S., Laskin, A., Jimenez, J. L., Shutthanandan, V., Molina, L. T., Salcedo, D., Dzepina, K., Molina, M. J. (2008). Comparative analysis of urban atmospheric aerosol by Proton-Induced X-ray Emission (PIXE), Proton Elastic Scattering Analysis (PESA), and Aerosol Mass Spectrometry (AMS). *Environmental Science and Technology* **42**, 6619–6624.

Johnson, K. S., Zuberi, B., Molina, L. T., Molina, M. J., Iedema, M. J., Cowin, J. P., Gaspar, D. J., Wang, C., Laskin, A. (2005). Processing of soot in an urban environment: Case study from the Mexico City Metropolitan Area. *Atmospheric Chemistry and Physics* **5**, 3033-3043.

Jones, A. M., Harrison, R. M., Baker, J. (2010). The wind speed dependence of the concentrations of airborne particulate matter and NO_x. *Atmospheric Environment* **44**, 1682-1690.

Karthikeyan, S., Balasubramanian, R., Iouri, K. (2006). Particulate air pollution from bushfires: Human exposure and possible health effects. *Journal of Toxicology and Environmental Health Part A* **69** (21), 1895-1908.

Kaufman, Y. J., Tanre, D., Boucher, O. (2002). A satellite view of aerosols in the climate system. *Nature* **419**, 215-223.

Kelly, K. E., Sarofim, A. F., Lighty, J. S., Arnott, W. P., Rogers, C. F., Zielinska, B., Prather, K. A. (2003). User guide for characterizing particulate matter: Evaluation of several real-time methods. http://ds.heavyoil.utah.edu/dspace/handle/123456789/10315. *Accessed 15/07/13.*

Khoder, M. I. (2002). Atmospheric conversion of sulphur dioxide to particulate sulphate and nitrogen dioxide to particulate nitrate and gaseous nitric acid in an urban area. *Chemosphere* 49:675–684.

Kim, E., Hopke, P. K., Edgerton, E. S. (2004). Improving source identification of Atlanta aerosol using temperature resolved carbon fractions in positive matrix factorization. *Atmospheric Environment* **38** (20), 3349-3362.

Kim, E., Hopke, P. K., Kenski, D. M., Koerber, M. (2005). Sources of fine particles in a rural Midwestern U.S. area. *Environmental Science and Technology* **39**, 4953-4960.

Kleeman, M.J., Schauer J.J., Cass, G. R. (2000). Size and composition distribution of fine particulate matter emitted from motor vehicles. *Environmental Science Technology* **34**, 1132-1142.

Konieczynski, J., Zajusz-Zubek, E., Jabłonska, M. (2012). The release of trace elements in the process of coal coking. *The ScientificWorld Journal* **2012**, 294927, 8p. doi:10.1100/2012/294927.

Kothai, P., Saradhi, I. V., Pandit, G. G., Markwitz, A., Puranik, V. D. (2011). Chemical characterization and source identification of particulate matter at an urban site of Navi Mumbai, India. *Aerosol and Air Quality Research* **11**, 560–569.

Laden, F., Neas, L. M., Dockery, D. W. Schwartz, J. (2000). Association of fine particulate matter from different sources with daily mortality in six US cities. *Environmental Health Perspectives* **108**, 941-947.

Lakhani, A. (2012). Source apportionment of particle bound polycyclic aromatic hydrocarbons at an industrial location in Agra, India. *ScientificWorldJournal* **2012**, 781291.

Landeg, G. (2010). Summary of investigative work undertaken to identify the source or sources of PM_{10} from within the steelworks site, Version 1, November 2009, Tata Steel Strip Products UK, Port Talbot.

Laongsri, B., Harrison, R. M. (2013). Atmospheric behaviour of particulate oxalate at UK urban background and rural sites. *Atmospheric Environment* **71**, 319–326.

Ledoux, F., Courcot, L., Courcot, D., Aboukaïs, A., Puskaric, E. (2006). A summer and winter apportionment of particulate matter at urban and rural areas in northern France. *Atmospheric Research* **82**, 633-642.

Lewtas, J. (2007). Air pollution combustion emissions: Characterization of causative agents and mechanisms associated with cancer, reproductive, and cardiovascular effects. *Mutation Research* **636**, 95–133.

Lonati, G., Giugliano, M. Butteli, P., Romele, L., Tardivo, R. (2005). Major chemical components of $PM_{2.5}$ in Milan (Italy). *Atmospheric Environment* **39** (10), 1925-1934.

Levy, J. I., Bennett, D. H., Melly, S. J., Spengler, J. D. (2003). Influence of traffic patterns on particulate matter and polycyclic aromatic hydrocarbon concentrations in Roxbury, Massachusetts. *Journal of Exposure Analysis Environmental Epidemiology* **13** (5), 364-71.

Li, J., Posfai, M., Hobbs, P. V., Buseck, P. R. (2003). Individual aerosol particles from biomass burning in southern Africa: 2, Compositions and aging of inorganic particles. *Journal of Geophysical Research* **108** (D13), 8484. doi:10.1029/2002JD002310.

Liberti, L., Notarnicola, M., Primerano, R., Zanneti, P. (2006). Air pollution from a large steel factory: polycyclic aromatic hydrocarbon emissions from coke-oven batteries. *Journal of the Air and Waste Management Association* **56**, 255-260.

Lin, J. J., Lee, L. C. (2004). Characterization of the concentration and distribution of urban submicron ($PM_{1.0}$) aerosol particles. *Atmospheric Environment* **38**, 469–475.

Lin, J. J., Tai, H. S. (2001). Concentrations and distributions of carbonaceous species in ambient particles in Kaohsiung City, Taiwan. *Atmospheric Environment* **35** (15), 2627-2636.

Liu, Y., Chen, L., Huang, Q., Li, W., Tang, W., Zhao, J. (2009). Source apportionment of polycyclic aromatic hydrocarbons (PAHs) in surface sediments of the Huangpu River, Shanghai, China. *Science of the Total Environment* **407**, 2931-2933.

Liu, J-Y., Harrison, R .M. (2011). Properties of coarse particles in the atmosphere of the United Kingdom. *Atmospheric Environment* **45**, 3267-3276.

Liu, S., Hua, M., Slaninaa, S., Heb, L-Y., Niub, Y-W., Bruegemann, E., Gnauk, T., Herrmann, H. (2008). Size distribution and source analysis of ionic compositions of aerosols in polluted periods at Xinken in Pearl River Delta (PRD) of China. *Atmospheric Environment* **42**, 6284–6295.

Lim, J-M, Lee, J-H., Moon, J-H., Chung, Y-S., Kim, K-H. (2010). Source apportionment of PM_{10} at a small industrial area using positive matrix factorization. *Atmospheric Research* **95**, 88-100.

Lucarelli, F., Nava, S., Calzolai, G., Chiari, M., Udisti, R., Marino, F. (2011). Is PIXE still a useful technique for the analysis of at-mospheric aerosols? The LABEC experience. *X-Ray Spectrom* **40**, 162–167.

Machemer, S. D. (2004). Characterization of airborne and bulk particulate from iron and steel manufacturing facilities. *Environmental Science and Technology* **38** (2), 381–389.

Malm, W. C. (1999). Introduction to visibility. Cooperative Institute for Research in the Atmosphere (CIRA) NPS Visibility Program. 70p.

Manoli, E., Kouras, A., Samara, C. (2004). Profile analysis of ambient and source emitted particle-bound polycyclic aromatic hydrocarbons from three sites in northern Greece. *Chemosphere* **56**, 867-878.

Marcazzan, G. M., Ceriani, M., Valli, G., Vecchi, R. (2003). Source apportionment of PM_{10} and PM2.5 in Milan (Italy) using receptor modelling. *Science of the Total Environment* **317**: 137–147

Marple, V. A., Rubow, K. L., Behm, S. M. (1991). A Microorifice Uniform Deposit Impactor (MOUDI): Description, Calibration, and Use. *Aerosol Science and Technology* **14** (4), 434-446

Mazzei, F., D'Alessandro, A., Lucarelli, Nava, S., Prati, P., Valli, G, Vecchi, R. (2008). Characterization of particulate matter sources in an urban environment. *Science of the Total Environment* **401**, 81-89.

Mazzei, F., Lucarelli, F., Nava, S., Prati, P., Valli, G., Vecchi, R. (2007). A new methodological approach: The combined use of two-stage Streaker samplers and optical particle counters for the characterization of airborne particulate matter. *Atmospheric Environment* **41**, 5525- 5535.

Ming, J., Zhang, D., Kang, S., Tian, W. (2007). Aerosol and fresh snow chemistry in the East Rongbuk Glacier on the northern slope of Mt. Qomolangma (Everest). *Journal of Geophysics and Research* **112**, D15307, doi:10.1029/2007JD008618.

Mysliwiec, M. J., Kleeman, M. J. (2002). Source apportionment of secondary airborne particulate matter in a polluted atmosphere. *Environmental Science and Technology* **36**, 5376-5384.

Moffet, R. C., de Foy, B., Molina, L. T., Molina, M. J., Prather, K. A. (2008). Measurement of ambient aerosols in northern Mexico City by single particle mass spectrometry. *Atmospheric Chemistry and Physics* **8**, 4499–4516.

Morawska, L., Zhang, J. F. (2002). Combustion sources of particles. 1. Health relevance and source signatures. *Chemosphere* **49**, 1045-1058.

Moreno, T., Jones, T. P., Richards, R. J. (2004a). Characterisation of aerosol particulate matter from urban and industrial environments: examples from Cardiff and Port Talbot, South Wales, UK. *Science of the Total Environment* **334-335**, 337-346.

Moreno, T., Kojima, T., Amato, F., Lucarelli, F., de la Rosa, J., Calzolai, G., Nava, S., Chiari, M., Alastuey, A., Querol, X., Gibbons. W. (2013). Daily and hourly chemical impact of springtime transboundary aerosols on Japanese air quality. *Atmospheric Chemistry and Physics* **13**, 1411-1424.

Moreno, T., Merolla, L., Gibbons, W., Greenwell, L., Jones, T., Richards, R. (2004b).Variations in the source, metal content and bioreactivity of technogenic aerosols: a case study from Port Talbot, Wales, UK. *Science of the Total Environment* 334, 59-73.

MSP Corporation (1998). Micro-orifice uniform deposit impactor instruction manual. Pg. 2-8.

Mukherjee, A. B., Zevenhoven, R., Bhattacharya, P., Sajwan, K. S., Kikuchi, R. (2008). Mercury flow via coal and coal utilization by-products: A global perspective, *Resource Conservation Recyclying* **52**, 571–591.

Naeher, L. P., Brauer, M., Lipsett, M., Zelikoff, J. T., Simpson, C. D., Koenig, J. Q., Smith, K. R. (2007). Woodsmoke health effects: a review. *Inhalation Toxicology* **19** (1), 67-106.

Namdeo, A., Bell, M. C. (2005). Characteristics and health implications of fine and coarse particulates at roadside, urban background and rural sites in UK. *Environment International* **31**, 565–573.

Nava, S. (2003). Aerosol characteristic by ion beam analysis technique. Sede Amministrativa: Universita degli Studi di Genova Dipartimento di Fisica. PhD Thesis. 121p.

Nava, S., Becherini, F., Bernardi, A., Bonazza, A., Chiari, M., García-Orellana, I., ... & Vecchi, R. (2010). An integrated approach to assess air pollution threats to cultural heritage in a semi-confined environment: The case study of Michelozzo's Courtyard in Florence (Italy). *Science of the Total Environment* **408** (6), 1403-1413.

Nava, S., Prati, P., Lucarelli, F., Mando, P. A., Zucchiatti, A. (2002). Source apportionment in the town of Spezia (Italy) by continuous aerosol sampling and PIXE analysis. *Water, Air and Soil Pollution Focus* **2**, 247–260.

Noble, C. A., Prather, K. A. (2000). Real-time single particle mass spectrometry: A historical review of a quarter century of the chemical analysis of aerosols. *Mass Spectrometry Reviews* **19**, 248-274.

NTP (2003). National Toxicology Program, *10th Report on Carcinogens*, U.S. Department of Health and Human Services. http://ehis.niehs.nih.gov/roc.

Ny, M.T., Lee, B.K. (2011). Size distribution of airborne particulate matter and associated metallic elements in an urban area of an industrial city in Korea. *Aerosol Air Quality Research* **11**, 643–653.

Oberdorster, G, Oberdorster, E, Oberdorster, J. (2005). Nanotoxicology: An emerging discipline evolving from studies of ultrafine particles. *Environmental Health Perspective* **113**, 823-839.

O'Dowd, C. D., de Leeuw, G. (2007). Marine aerosol production: a review of the current knowledge. *Philosophical Transaction of the Royal Society* **365**, 1753-1774.

Ogulei, D., Hopke P. K., Zhou, L. M., Pancras, J. P., Nair, N., Ondov, J. M. (2006). Source apportionment of Baltimore aerosol from combined size distribution and chemical composition data. *Atmospheric Environment* **40**, S396-S410.

Ooki, A., Uematsu, M., Miura, K., Nakae, S. (2002). Sources of sodium in atmospheric fine particles. *Atmospheric Environment* **36**, 4367–4374.

Oravisjarvi, K., Timonen, K. L., Wiikinkoski, T., Ruuskanen, A. R. Heinanen, K., Ruuskanene, J. (2003). Source contributions to $PM_{2.5}$ particles in the urban air of a town situated close to a steel works. *Atmospheric Environment* **37**, 1013-1022.

Ottley, C. J., Harrison, R. M. (1992). The spatial distribution and particle size of some inorganic nitrogen, sulphur and chlorine species over the North Sea. *Atmospheric Environment* **26**A, 1689-1699.

Paatero, P. (2000). User's guide for positive matrix factorization programs PMF2 and PMF3, *Part 1: Tutorial*. Finland: University of Helsinki.

Paatero, P., Hopke, P. K., Hoppenstock, J., Eberly, S. I. (2003). Advanced factor analysis of spatial distributions of $PM_{2.5}$ in the Eastern United States. *Environmental Science and Technology* **37** (11), 2460-2476.

Paatero, P., Tapper, U. (1994). Positive matrix factorization; A non-negative factor model with optimal utilization of error estimates of data values. *Environmentrics* **5**, 111-126.

Pacyna, E. G., Pacyna, J. M. (2002). Global emission of mercury from anthropogenic sources in 1995. *Atmospheric Environment* **137**, 149–165.

Pacyna, E. G., Pacyna, J. M., Steenhuisen, F., Wilson S. (2006). Global anthropogenic mercury emission inventory for 2000. *Atmospheric Environment* **40**, 4048–4063.

Pan, X. L. Kanaya, Y., Wang, Z. F., Liu, Y., Pochanart, P., Akimoto, H., Dong, H. B., Li, J. (2011). Correlation of black carbon aerosol and carbon monoxide concentrations

measured in the high-altitude environment of Mt. Huangshan, Eastern China. *Atmospheric Chemistry and Physics Discussions* **11**, 4447-4485.

Pancras, J. P., Landis, M. S., Norris, G. A., Vedantham, R., Dvonch, J. T. (2013). Source apportionment of ambient fine particulate matter in Dearborn, Michigan, using hourly resolved PM chemical composition data. *Science of the Total Environment* **448**, 2-13.

Pandolfi, M., Gonzalez-Castanedo, Y., Alastuey, A., de la Rosa, J., Mantilla, E., Sanchez de la Campa, A., Querol, X., Pey, J., Amato, F., Moreno, T. (2011). Source apportionment of PM_{10} and $PM_{2.5}$ at multiple sites in the strait of Gibraltar by PMF: impact of shipping emissions. *Environmental Science Pollution Research* **18**, 260–269.

Parmar, R. S., Satsangi, G.S., Kumari, M., Lakhani, A., Srivastava, S. S., Prakash, S. (2001). Study of size distribution of atmospheric aerosol at Agra. *Atmospheric Environment* **35**, 693–702.

Passant, N. R., Peirce, M., Rudd, H. J., Scott, D. W., Marlowe, I., Watterson, J. D. (2002). UK Particulate and Heavy Metal Emissions from Industrial Processes. A report produced for the Department for Environment, Food & Rural Affairs, the National Assembly for Wales, the Scottish Executive and the Department of the Environment in Northern Ireland. AEAT-6270 Issue 2.

Pastor, S. H., Allen, J. O., Hughes, L. S., Bhave, P., Cass, G. R., Prather, K. A. (2003). Ambient single particle analysis in Riverside, California by aerosol time-of-flight mass spectrometry during SCOS97-NARSTO. *Atmospheric Environment* **37**, Suppl. No. 2, S239-S258.

Penner, J. E., Dong, X., Chen, Y. (2004). Observational evidence of a change in a radiative forcing due to the indirect aerosol effect. *Nature* **427**, 231-234.

Pirrone, N., Costa, P., Pacyna, J. M., Ferrara, R. (2001). Mercury emissions to the atmosphere from natural and anthropogenic sources in the Mediterranean region. *Atmospheric Environment* **35**, 2997–3006. doi: 10.1016/S1352-2310(01)00103-0.

PIXE International Corporation (2003-2008). The Streaker™ Air-Particulate Sampler Instruction Manual. PIXE International Corporation, Tallahassee, USA. 10p. www: http://pixeintl.com. *Accessed: 06/05/12.*

Pitz, M., Cyrys, J., Karg, E., Wiedensohler, A., Wichmann, H. E., Heinrich, J. (2003). Variability of apparent particle density of an urban aerosol. *Environmental Science and Technology*, **37** (19), 4336-4342.

Polissar, A. V., Hopke, P. K., Paatero, P., Malm, W. C., Sisler, J. F. (1998). Atmospheric aerosol over Alaska 2. Elemental composition and sources. *Journal of Geophysical Research* **103**, 19045-19057.

Pope, C. A., Burnett, R. T., Thun, M. J., Calle, E. E., Krewski, D., Ito, K., Thurston, G. D. (2002). Lung cancer, cardiopulmonary mortality, and long-term exposure to fine particulate air pollution. *Journal of American Medical Association* **287** (9), 1132–41.

Pope, C. A. III, Dockery, D. W. (2006). Health effects of fine particulate air pollution: Lines that connect. *Journal of the Air and Waste Management Association* **56,** 709–742.

Prather, K. A. (1998). Aerosol Time-of-Flight Mass Spectrometry (ATOFMS) as a Real-Time Monitor of Individual Aerosol Particles in Field Studies. Contract 95-305. http://www.arb.ca.gov/research/apr/past/95-305.pdf. *Accessed: 29/08/13.*

Prather, K. A., Nordmeyer, T., Salt, K. (1994). Real-time characterization of individual aerosol particles using time-of-flight mass spectrometry. *Analytical Chemistry* **66** (9), 1403–1407.

Prati, P., Zucchiatti, A., Lucarelli, F., Mando, P. A. (2000). Source apportionment near a steel plant in Genoa (Italy) by continuous aerosol sampling and PIXE analysis. *Atmospheric Environment* **34**, 3149–3157.

Pryor, S. C., Barthelmie, R. J., Schoof, J. T., Binkowski, F. S., Delle Monache, L., Stull, R. (2007). Modeling the impact of sea-spray on particle concentrations in a coastal city, *Science of the Total Environment* **391**, 132–142.

Qin, Y., Xie, S. D. (2012). Spatial and temporal variation of anthropogenic black carbon emissions in China for the period 1980–2009. *Atmospheric Chemistry and Physics* **12**, 4825-4841. doi:10.5194/acp-12-4825-2012.

Querol, X., Alastuey, A., de la Rosa, J., Sánchez-de-la-Campa, A., Plana, F., Ruiz, C.R. (2002). Source apportionment analysis of atmospheric particulates in an industrialised urban site in south-western Spain. *Atmospheric Environment* **36** (19), 3113-3125.

Querol, X., Alastuey, A., Ruiz, C. R., Artinano, B., Hasson, H. C., Harrison, R. M., Buringh, E., ten Brink, H. M., Lutz, M., Bruckmann, P., Straehl, P., Schneider, J. (2004). Speciation and origin of PM_{10} and $PM_{2.5}$ in selected European cities. *Atmospheric Environment* **38**, 6547–6565.

Querol, X., Viana, M., Alastuey, A., Amato, F., Moreno, T., Castillo, S., Pey, J., de la Rosa, J., Sanchez de la Campa, A., Artínano, B., Salvador, P., Garcia Dos Santos, S., Fernández-Patier, R., Moreno-Grau, S., Negral, L., Minguillon, M. C., Monfort, E., Gil, J. I., Inza, A. Ortega, L.A., Santamaria, J. M., Zabalza, J. (2007). Source origin of trace elements in PM from regional background, urban and industrial sites of Spain. *Atmospheric Environment* **41** (34), 7219-7231.

Rajkumar, W. S., Chang, A. S. (2000). Suspended particulate matter concentrations along the East–West Corridor, Trinidad, West Indies. *Atmospheric Environment* **34**, 1181–1187.

Ramadan, Z., Song, X. H., Hopke, P. K. (2000). Identification of sources of Phoenix aerosol by positive matrix factorization. *Journal of the Waste Management Association* **50** (8), 1308-1320.

Reddington, C. L., McMeeking, G., Mann, G. W., Coe, H., Frontoso, M. G. Liu, D., Flynn, M., Spracklen, D. V. and Carslaw, K. S. (2012). The size distribution and mixing state of black carbon aerosol over Europe. *Atmospheric Chemistry and Physics Discussion* **12**, 26503–26560.

Reff, A., Eberly, S. I., Bhave, P. V. (2007). Receptor modelling of ambient particulate matter data using positive matrix factorization: review of existing methods. *Journal of the Air and Waste Management Association* **57** (2), 146-154.

Rehwagen, M., Muller, A., Massolo, L. Herbath, O. Ronco, A. (2005). Polycyclic aromatic hydrocarbons associated with particles in ambient air from urban and industrial areas. *Science of the Total Environment* **348** (1-3), 199-210.

Reimann, C., de Caritat, P. (2000). Intrinsic flaws of element enrichment factors (EFs) in environmental geochemistry. *Environmental Science and Technology* **34** (24), 5084–5091.

Reimann, C., de Caritat, P. (2005). Distinguishing between natural and anthropogenic sources for elements in the environment: Regional geochemical surveys versus enrichment factors. *Science of the Total Environment* **337**, 91–107.

Remus, R., Monsonet, M. A. A., Roudier, S., Sancho, L. D. (2013). Best Available Techniques (BAT) Reference Document for Iron and Steel Production. Industrial Emissions Directive 2010/75/EU (Integrated Pollution Prevention and Control). EUR 25521EN.http://eippcb.jrc.ec.europa.eu/reference/BREF/IS_Adopted_03_2012.pdf. *Accessed: 30/01/13.*

Riediker, M., Cascio, W. E., Griggs, T. R., Herbst, M.C., Bromberg, P. A., Neas, L., Williams, R. W., Devlin, R. B. (2004). Particulate matter exposure in cars is associated with cardiovascular effects in healthy young men. *American Journal of Respiratiory and Critical Care Medicine* **169**(8), 934–940.

Ricketts, J. A. (2013). How a blast furnace works. American Iron and Steel Institutes. http://www.steel.org/Making%20Steel/How%20Its%20Made/Processes/How%20A%20Blast%20Furnace%20Works%20larry%20says%20to%20delete.aspx. *Accessed: 26/06/13.*

Rizzo, M. J., Scheff, P. A. (2007). Fine particulate source apportionment using data from the USEPA speciation trends network in Chicago, Illinois: Comparison of two source apportionment models. *Atmospheric Environment* **41**, 6276-6288.

Rodriguez, S., Alastuey, A., Querol, X. (2012). A review of methods for long term in situ characterization of aerosol dust. *Aeolian Research* **6**, 55–74.

Rupprecht & Patashnick Inc. (2001). Operating Manual. Dichotomous Partisol-Plus Model 2025 Sequential Air Sampler.Revision A. R & P Part Number 42-006007.

Rupprecht & Patashnick Co. I. (2003). Series 8500 FDMS Filter Dynamic Measurement System Operating Manual.

Samara, C., Kouimtzis, Th., Tsitouridou, R., Kanias, G., Simeonov, V. (2003). Chemical mass balance source apportionment of PM_{10} in an industrialized urban area of Northern Greece. *Atmospheric Environment* **37**, 41-54.

Samet, J.M. Dominici, F., Curriero, F.C., Coursac, I., Zeger, S.L. (2000). Fine particulate air pollution and mortality in 20 U.S. cities, 1987-1994. *New England Journal of Medicine,* **343**, 1742.1749.

Samsonov, Y.N., Koutsenogii, K.P., Makarov, V.I., Ivanov, A.V., Ivanov, V.A., McRae, D.G., Conard, S.G., Baker, S.P., Ivanova, G.A. (2005). Particulate emissions from fires in central Siberian Scots pine forests. Canadian Journal of Forest Research **35**, 2207–2217.

Schwartz, J. (2000). Assessing confounding, effect modification, and thresholds in the association between ambient particles and daily deaths. *Environmental Health Perspective* **108** (6), 563–568.

Schwartz, J., Dockery, D. W., Neas, L. M. (1996). Is daily mortality associated specifically with fine particles? *Journal of the Air and Waste Management Association* **46** (10), 927-939.

Schwartz, J., Laden, F., Zanobetti, A. (2002). The concentration–response relation between $PM_{2.5}$ and daily deaths. *Environmental Health Perspectives* **110** (10), 1025-1029.

Schwarze, P. E., Ovrevik, J., Lag, M., Refsnes, M., Nafstad, P., Hetland, R. B., Dybing, E. (2006). Particulate matter properties and health effects: consistency of epidemiological and toxicological studies. *Human Exposure Toxicology* **25** (10), 559-579.

Singh, K.P., Malik, A., Kumar, R., Saxena, P., Sinha, S. (2008). Receptor modeling for source apportionment of polycyclic aromatic hydrocarbons in urban atmosphere. *Environmental Monitoring and Assessment* **136** (1-3), 183-196

Silva, P. J., Prather, K. A. (2000). Interpretation of mass spectra from organic compounds in aerosol time-of-flight mass spectrometry. *Analytical Chemistry* **72**, 3553–3562.

Smith, W. (2007). High time resolution chemical fingerprinting and source apportionment of atmospheric particulate emissions from the steel industry. PhD Thesis. School of Geography, Earth and Environmental Sciences. The University of Birmingham, UK. 434p.

Smyth, A. M., Thompson, S. L., de Foy, B., Olson, M. R., Sager, N., McGinnis, J., Schauer, J. J., Gross, D. S. (2013). Sources of metals and bromine-containing particles in Milwaukee. *Atmospheric Environment* **73**, 124 – 130.

Song, F., Gao, Y. (2011). Size distributions of trace elements associated with ambient particular matter in the affinity of a major highway in the New Jersey, New York metropolitan area. *Atmospheric Environment* **45**, 6714-6723.

Soutar, C. A., Robertson, A., Miller, B. G., Searl, A., Bignon, J. (2000). Epidemiological evidence on the carcinogenicity of silica: Factors in scientific judgement. *Annals of Occupational Hygiene*, **44** (1), 3-14.

Stanhill, G., Cohen, S. (2001). Global dimming: a review of the evidence for a widespread and significant reduction in global radiation with discussion of its probable causes and possible agricultural consequences. *Agricultural Forestry. Meteorology* **107,** 255-278.

Sternbeck, J., Sjodin, A., Andreasson, K. (2002). Metal emissions from road traffic and the influence of resuspension - results from two tunnel studies. *Atmospheric Environment* **36**, 4735-44.

Sullivan, R. C., Prather, K. A. (2005). Recent advances in our understanding of atmospheric chemistry and climate made possible by online aerosol analysis instrumentation. *Analytical Chemistry* **77**(12), 3861-85.

Sullivan, R. C., Guazzotti, S. A., Sodeman, D. A., Tang, S., Carmichael, G. R., Prather, K. A. (2007). Mineral dust is a sink for chlorine in the marine boundary layer. *Atmospheric Environment* **41,** 7166-7179.

Sunset Laboratory Inc. (2000). Thermal/Optical Carbon Analyser: A Guide to running and maintaining the Sunset Laboratory OCEC Analyser. Ed 6.2. May 2, 2000.

Tao, S., Wang, X., Chen, H., Yang, X., Li, M., Zhou, Z. (2011). Single particle analysis of ambient aerosols in Shanghai during the World Exposition, 2010: two cases studies. *Frontier of Environmental Science and Engineering in China* **5** (3), 391-401.

Themelis, N. J., Gregory, A. F. (2002). Mercury emissions from high-temperature sources in the NY/NJ Hudson-Raritan basin. *Proceeding of NAWTEC, 10*, 205-215.

Thermo Fischer Scientific Inc. (2012). Dionex ICS-2100 Ion Chromatography System Operator's Manual. Document No. 065291. http://www.dionex.com/en-us/webdocs/73382-Man-IC-ICS2100-Operators-Oct2012-DOC065291-03.pdf. *Accessed 08/08/13.*

Thorpe, A., Harrison, R. M. (2008). Sources and properties of non-exhaust particulate matter form road traffic: a review. *Science of the Total Environment* **400**, 270-282.

Tolbert, P. E., Klein, M., Metzger, K. B., Peel, J., Flanders, W. D., Todd, K., Mulholland, J. A., Ryan, P. B., Frumin, H. (2000). Interim results of the study of particulates and health in Atlanta (SOPHIA). *Journal of Exposure Analytical and Environmental Epidemiology* **10**, 446-460.

Toner, S. M., Shields, L. G., Sodeman, D. A., Prather, K. A. (2008). Using mass spectral source signatures to apportion exhaust particles from gasoline and diesel powered vehicles in a freeway study using UF-ATOFMS. *Atmospheric Environment* **42,** 568–581.

Tsai, J-H., Lin, K-H., Chen, C-Y., Ding, J-Y., Choa, C-G., Chiang, H-L. (2007). Chemical constituents in particulate emissions from integrated iron and steel facility. *Journal of Hazardous Materials* **147**, 111-119.

Tsai, J-H., Lin, K.H., Chen, C-Y., Lai, N., Ma, S.-Y., Chiang, H-L. (2008). Volatile organic compound constituents from an integrated iron and steel facility. *Journal of Hazardous Materials* **157**, 569–578.

Tsai, J-H, Lin, J-H., Yao. Y-C., Chiang, H. L. (2012). Size distribution and water soluble ions of ambient particulate matter on episode and non-episode days in Southern Taiwan. *Aerosol and Air Quality Research* **12**, 263–274.

TSI Inc. (2004). Series 3800 Aerosol Time-of-Flight Mass Spectrometers with Aerodynamic Focusing Lens Technology. http://www.tsi.com/uploadedFiles/Product_ Information/Literature/Spec_Sheets/3800SeriesPN1933798RevD.pdf. *Accessed 08/08/13.*

US EPA (1995). Profile of the Iron and Steel Industry. EPA office of compliance sector notebook project: Profile of the Iron and Steel industry. U.S. Environmental Protection Agency. Washington, D.C. EPA/310-R-95-005. *Accessed 13/08/13.*

US EPA (2004). Air Quality Criteria for Particulate Matter. Volume I. U.S. Environmental Protection Agency, Research Triangle Park, NC.

US EPA (2005). Review of the nation ambient air quality standards for particulate matter: Policy assessment of scientific and technical information. OAQPS Staff Paper. EPA-452/R-05-005. December 2005.

US EPA (2008). National Ambient Air Quality Standards (NAAQS). http://www.epa.gov/oar/criteria.html. *Accessed:19/01/2011*.

Vega, E., Mugica, V., Carmona, R., Valencia, E. (2000). Hydrocarbon source apportionment in Mexico City using the chemical mass balance receptor model. *Atmospheric Environment* **34**, 4121-4129.

Venkataraman, C., Reddy, C. K., Josson, S., Reddy, M. S. (2002). Aerosol size and chemical characteristics at Mumbai, Indian, during the INDOEX-IFP (1999). *Atmospheric Environment* **36**, 1979-1991.

Viana, M., Kuhlbusch, T. A. J., Querol, X., Alastuey, A., Harrison, R. M., Hopke, P. K., Winiwarter, W., Vallius, M., Szidat, S., Prevot, A.S.H., Hueglin, C., Bloemen, H., Wahlin, P., Vecchi, R., Miranda, A. I. , Kasper-Giebl, A., Maenhaut, W., Hitzenberger, R. (2008a). Source apportionment of particulate matter in Europe: A review of methods and results. *Aerosol Science* **39**, 827–849.

Viana, M., Pandolfi, M, Minguillo, M. C., Querol, X., Alastuey, A., Monfort, E., Celades, I. (2008b). Inter-comparison of receptor models for PM source apportionment: Case study in an industrial area. *Atmospheric Environment* **42**, 320-3832.

Visser, H., Buring, E., Breugel, P. B. V. (2001). Composition and origin of airborne particulate matter in the Netherlands. *RIVM Rapport 650010029*.

Wang, T., Anderson, D. R., Thompson, D., Clench, M., Fisher, R. (2003). Studies into the formation of dioxins in the sintering process used in the iron and steel industry. 1. Characterisation of isomer profiles in profiles in particulate and gaseous emissions. *Chemosphere* **51**(7), 585-94.

Wang, Y., Zhuang, G., Tang, A., Yuan, H., Sun, Y., Chen, S., Zheng, A. (2005). The ion chemistry and the source of $PM_{2.5}$ aerosol in Beijing. *Atmospheric Environment* **39**, 3771-3784.

Wallington, T. J., Sullivan, J. L, Hurley, M. D. (2008). Emissions of CO_2, CO, NO_x, HC, PM, HFC-134a, N_2O and CH_4 from the global light duty vehicle fleet. *Meteorologische Zeitschrift* **17** (2), 109-116.

Watkiss, P., Pye, S., Holland, M. (2005). Baseline scenarios for service contract for carrying out cost-benefit analysis of air quality related issues, in particular in the Clean Air for Europe (CAFE) programme. AEAT/ED51014/ Baseline Issue 5. Didcot, United Kingdom.

Watson, J. G., Chow, C. (2007). Receptor models for particle source apportionment of suspended particles. *In: Introduction to Environmental Forensics*, 2nd edn. Murphy, B. and Morrison, R. (Eds), Academic Press: New York, p. 273-310.

Watson, J. G., Chow, J. C., Houck, J. E. (2001). $PM_{2.5}$ chemical source profiles for vehicle exhaust, vegetative burning, geological material, and coal burning in northwestern Colorado during 1995. *Chemosphere* **43** (8), 1141–1151.

Watson, J. G., Chow, J. C., Lu, Z., Fujita, E. M., Lowenthal, D. H., Lawson, D. R., Ashbaugh, L. L. (1994). Chemical mass balance source apportionment of PM_{10} during the Southern California Air Quality Study. *Aerosol Science and Technology* **21**(1), 1-36.

Watson, J. G., Judith, T. Z., Chow, C., Eric, J. E., Fujita, M., Wilson, W. E. (2002). Receptor modeling application framework for particle source apportionment. *Chemosphere* **49** 1093–1136.

Wedepohl, K. H. (1995). The composition of the continental crust. *Geochimica et Cosmochimica Acta* **59**, 1217-1232.

Weitkamp, E. A., Lipsky, E. M., Pancras, P. J., Ondov, J. M., Polidori, A., Turpin, B. J., Robinson, A. L. (2005). Fine particle emission profile for a large coke production facility based on highly time-resolved fence line measurements. *Atmospheric Environment* **39**, 6719-6733.

Widory, D., Liu, X., Dong, S. (2010). Isotopes as tracers of sources of lead and strontium in aerosols (TSP & $PM_{2.5}$) in Beijing. *Atmospheric Environment* **44** (30), 3679-3687.

Wood Protection Association (2010). *Use of CCA-treated timber. A wood Protection Association Guidance note, 2010.* www.ttf.co.uk/Document/Default.aspx? DocumentUid...A063 *Accessed 29/12/12.*

World Bank Group (1998). Airborne Particulate Matter. Pollution Prevention and Abatement Handbook, 201-207.

World Coal Association (2013). Coal and Steel. http://www.worldcoal.org/coal/uses-of-coal/coal-steel/. *Accessed: 01/09/13*.

WHO (2000). Air quality guideline for Europe. WHO Regional publications, European series No. 91, WHO Regional Office for Europe, Copenhagen. Denmark

WHO (2003). Health Aspects of Air Pollution with Particulate Matter, Ozone and Nitrogen Dioxide. Report on a WHO Working Group, Bonn, Germany. EUR/03/504268.

WHO (2006). WHO Air quality guidelines: Global update 2005. World Health Organization, Copenhagen. Denmark.

WHO (2007). Health risks of heavy metals from long-range transboundary air pollution. Joint WHO/Convention Task Force on the Health Aspects of Air Pollution. http://www.euro.who.int/__data/assets/pdf_file/0007/78649/E91044.pdf. *Accessed 17/07/12*.

WHO (2009). Global Health Risks: Mortality and Burden of Disease Attributable to Selected Major Risks.World Health Organization, Geneva. http://whqlibdoc.who.int/ publications/2009/9789241563871_eng.pdf. *Accessed 17/07/13.*

Xia, L., Gao, Y. (2010). Chemical composition and size distributions of coastal aerosols observed on the US East Coast. *Marine Chemistry* **119**, 77–90.

Xie, Y. and Berkowitz, C. M. (2006). The use of positive matrix factorization with conditional probability functions in air quality studies: An application to hydrocarbon emissions in Houston, Texas. *Atmospheric Environment* **40** (17): 3070-3091.

Yang, H-H., Lai, S-O., Hsieh, L-T., Hsueh, H-J., Chi, T-W. (2002). Profiles of PAH emission from steel and iron industries. *Chemosphere* **48**, 1061–1074.

Yang, B., Zhou, L., Xue, N., Li, F., Li, Y., Vogt, R.D., Cong, X., Yan, Y., Liu, B. (2013). Source apportionment of polycyclic aromatic hydrocarbons in soils of Huanghuai Plain, China: Comparison of three receptor models. *Science of the Total Environment* **443**, 31–39.

Yao, X., Chan, C. K., Fang, M., Cadle, S., Chan, T., Mulawa, P., He, K., Ye, B. (2002). The water soluble ionic composition of $PM_{2.5}$ in Shanghai and Beijing, China. *Atmospheric Environment* **36**, 4223-4234

Yatkin S., Bayram, A. (2007). Elemental composition and sources of particulate matter in the ambient air of a Metropolitan City. *Atmospheric Research* **85**, 126-139.

Yatkin, S., Bayram, A. (2008). Source apportionment of PM_{10} and $PM_{2.5}$ using positive matrix factorization and chemical mass balance in Izmir, Turkey. *Science of the Total Environment*, **390**, 109-123.

Yin, J., Harrison, R. M. (2008). Pragmatic mass closure study for $PM_{1.0}$, $PM_{2.5}$ and PM_{10} at roadside, urban background and rural sites. *Atmospheric Environment* **40,** 980–988.

Yin, J., Harrison, R. M., Chen, Q., Rutter, A., Scauer, J. J. (2010). Source apportionment of fine particles at urban background and rural sites in the UK atmosphere. *Atmospheric Environment* **44**, 841-851.

Yvon-Lewis, S. A., Saltzman, E. S., Montzka, S. A. (2009). Recent trends in atmospheric methyl bromide: analysis of post-Montreal Protocol variability. *Atmospheric Chemistry and Physics* **9**, 5963–5974.

Zanobetti, A., Franklin, M., Koutrakis, P., Schwartz, J. (2009). Fine particulate air pollution and its components in association with cause-specific emergency admissions. *Environmental Health* **8**, 58. doi:10.1186/1476-069X-8-58.

Zhang, N., Qin, Y., Xie, S. (2013). Spatial distribution of black carbon emissions in China. *Chinese Science Bulletin*, 1-10.

Zhao, Y., Gao, Y. (2008). Acidic species and chloride depletion in coarse aerosol particles in the US east coast. *Science of the Total Environment* **407**, 541-507.

Zhao, S., Li, Z., Zhou, P. (2011). Ion chemistry and individual particle analysis of atmospheric aerosols over Mt. Bogda of eastern Tianshan Mountains, Central Asia. *Journal of Environmental Monitoring and Assessment* **180**, 409–426.

LIST OF APPENDICES

Appendix I

Chemical concentrations of $PM_{2.5}$ and $PM_{2.5-10}$ at EROS and BROS

	EROS				BROS			
	$PM_{2.5}$ (ng m^{-3})	SD	$PM2_{.5-10}$ (ng m^{-3})	SD	$PM_{2.5}$ (ng m^{-3})	SD	$PM_{2.5-10}$ (ng m^{-3})	
*Mass	12.5	9.3	8.1	5.4	14.4	8.8	9.7	6.2
Cl	105.86	70.59	461.27	417.29	171.40	131.79	718.47	743.45
NO_3	1561.58	1771.39	1221.34	1207.94	2436.32	2207.89	2330.21	3283.17
SO_4	2049.16	1499.62	1868.65	1362.30	1790.23	1347.42	1003.23	870.20
Na	85.76	70.79	329.69	265.24	151.25	146.69	437.52	435.31
NH4	1544.70	1238.89	363.15	618.58	1842.69	1284.17	100.67	45.18
K	50.67	24.93	20.99	10.65	62.46	41.63	365.03	399.16
Mg	19.12	11.14	54.71	35.26	25.94	20.99	65.83	51.13
Ca	40.30	29.85	371.00	300.80	53.47	26.60	391.78	313.30
Al	768.84	879.98	621.85	1085.67	993.91	1228.42	496.66	445.26
Fe	1.37	0.65	0.79	0.33	1.08	0.48	1.01	0.51
V	2.48	1.91	2.44	1.39	2.71	1.84	3.39	2.69
Cr	4.42	5.04	5.89	4.61	5.09	5.12	7.61	5.01
Mn	89.23	61.24	312.95	250.05	153.67	99.29	468.08	307.55
Cu	4.98	4.50	8.03	7.51	6.38	4.88	13.76	10.81
Zn	25.41	23.92	13.39	10.04	26.45	20.17	20.21	12.68
Sb	2.48	1.98	1.74	1.26	2.14	1.50	2.05	1.67
Ba	2.29	1.91	7.73	6.45	3.59	2.79	11.47	8.40
Pb	10.26	7.64	2.87	2.06	11.35	8.89	3.03	2.56

Note: * μg m^{-3}

Appendix II

MOUDI mass and chemical concentrations for $PM_{2.5}$, $PM_{2.5-10}$ and PM_{10} at EROS and Port Talbot sampling sites (SD- standard deviation)

Parameters	EROS			Port Talbot		
	Mean ±SD			Mean ±SD		
	$PM_{2.5}$	$PM_{2.5-10}$	PM_{10}	$PM_{2.5}$	$PM_{2.5-10}$	PM_{10}
PM Mass (µg m^{-3})	7.0±2.5	4.7±2.6	11.8±5.1	8.0±3.6	10.8±4.6	18.8±8.2
Cl^- (µg m^{-3})	0.06 ±0.05	0.58±0.46	0.64±0.51	0.28±0.23	1.09±0.50	1.37±0.73
NO_3^- (µg m^{-3})	0.34±0.18	0.50±0.33	0.84±0.51	0.34±0.15	0.35±0.21	0.69±0.36
SO_4^{2-} (µg m^{-3})	1.71±1.15	0.32±0.22	2.03±1.37	1.04±0.36	0.35±0.23	1.39±0.59
Na^+ (µg m^{-3})	0.11±0.09	0.45±0.31	0.56±0.41	0.37±0.14	0.86±0.36	1.23±0.50
NH_4^+ (µg m^{-3})	0.67±0.42	0.03±0.02	0.70±0.44	0.55±0.40	0.05±0.03	0.60±0.43
K^+ (µg m^{-3})	0.03±0.02	0.02±0.01	0.05±0.03	0.09±0.07	0.07±0.04	0.16±0.11
Mg^{2+} (µg m^{-3})	0.02±0.01	0.07±0.04	0.09±0.05	0.05±0.03	0.13±0.06	0.18±0.08
Ca^{2+} (µg m^{-3})	0.04±0.03	0.19±0.12	0.23±0.15	0.19±0.18	0.74±0.66	0.93±0.84
Al (µg m^{-3})	0.94±0.81	0.82±0.93	1.76±1.74	0.10±0.24	0.06±0.06	0.16±0.30
V (ng m^{-3})	0.93±0.33	0.61±0.22	1.54±0.55	0.55±0.29	0.40±0.22	0.95±0.51
Cr (ng m^{-3})	1.58±1.02	1.75±1.19	3.33±2.21	3.87±2.90	3.01±1.68	6.88±5.58
Mn (ng m^{-3})	3.11±2.74	2.01±1.32	5.12±4.06	5.44±5.26	19.68±18.35	25.12±23.61
Fe (µg m^{-3})	0.06±0.03	0.12±0.06	0.18±0.09	0.19±0.20	1.02±0.11	1.21±1.30
Cu (ng m^{-3})	2.76±0.78	3.39±1.09	6.15±1.86	2.38±2.64	2.09±1.12	4.47±3.76
Zn (ng m^{-3})	24.77±25.57	5.46±3.42	30.23±29.0	38.50±41.82	7.23±6.90	45.73±48.72
Sb (ng m^{-3})	1.19±0.52	0.47±0.12	1.66±0.64	0.55±0.31	0.36±0.12	0.91±0.43
Ba (ng m^{-3})	1.20±0.44	2.50±1.0	3.70±1.44	0.93±0.54	1.96±0.96	2.89±1.51
Pb (ng m^{-3})	6.59±3.58	0.69±0.33	7.28±3.91	4.17±2.92	1.41±1.10	5.58±4.03

Appendix III

Pearson's correlation coefficients of Partisol PM chemical species at EROS and BROS (a) EROS $PM_{2.5}$

	Mass	Cl	NO_3	SO_4	Na	NH_4	K	Mg	Ca	Al	Fe	V	Cr	Mn	Cu	Zn	Sb	Ba	Pb
Mass	**1**	**.216**	**.075**	**-.213**	**-.191**	**.864****	**.860****	**-.351**	**.079**	**-.209**	**.778****	**.342**	**.565***	**.683****	**.558***	**.734****	**.786****	**.668****	**.836****
Cl		**1**	**.029**	**-.255**	**.775****	**.552**	**.354**	**.590**	**.245**	**-.162**	**.586***	**.663***	**.360**	**.363**	**-.258**	**.326**	**-.303**	**-.020**	**.270**
NO_3			**1**	**.622***	**.047**	**-.056**	**.258**	**.463**	**-.024**	**.099**	**.467**	**.302**	**-.139**	**.361**	**.107**	**.289**	**.296**	**.591***	**.163**
SO_4				**1**	**-.191**	**-.303**	**.161**	**.161**	**.054**	**.787****	**.177**	**.187**	**-.329**	**.194**	**-.034**	**.071**	**.075**	**.400**	**-.179**
Na					**1**	**.069**	**-.006**	**.972****	**.083**	**-.207**	**.037**	**.356**	**.018**	**.025**	**-.428**	**-.087**	**-.479**	**-.293**	**-.007**
NH_4						**1**	**.745****	**-.207**	**.193**	**-.265**	**.724****	**.602***	**.839****	**.682****	**.265**	**.769****	**.426**	**.388**	**.806****
K							**1**	**-.064**	**.146**	**.250**	**.791****	**.703***	**.744****	**.877****	**.837****	**.866****	**.683***	**.720***	**.857****
Mg								**1**	**.219**	**-.100**	**-.014**	**.139**	**-.213**	**.006**	**-.336**	**-.324**	**-.486**	**-.087**	**-.167**
Ca									**1**	**.270**	**.147**	**.165**	**.177**	**.569***	**.173**	**.060**	**.344**	**.417**	**.017**
Al									**.**	**1**	**-.123**	**.111**	**-.260**	**.091**	**-.072**	**-.085**	**-.037**	**.155**	**-.273**
Fe											**1**	**.643****	**.534***	**.787****	**.412**	**.860****	**.670***	**.738****	**.761****
V												**1**	**.710****	**.564***	**.235**	**.755****	**.058**	**.281**	**.630***
Cr													**1**	**.608***	**.752****	**.808****	**.268**	**.252**	**.802****
Mn														**1**	**.456**	**.790****	**.795****	**.888****	**.748****
Cu															**1**	**.530***	**.778****	**.774****	**.861****
Zn																**1**	**.598***	**.644***	**.910****
Sb																	**1**	**.895****	**.617***
Ba																		**1**	**.603***
Pb																			**1**

(b) EROS $PM_{2.5\text{-}10}$

	Mass	Cl	NO_3	SO_4	Na	NH_4	K	Mg	Ca	Al	Fe	V	Cr	Mn	Cu	Zn	Sb	Ba	Pb
Mass	**1**	**.246**	**-.378**	**-.373****	**.062**	**.785****	**.726****	**.154**	**.684****	**.060**	**.878****	**.259**	**.797****	**.847****	**.665****	**.837****	**.624**	**.729****	**.864****
Cl		**1**	**-.327**	**-.518**	**.946****	**-.020**	**.599***	**.909****	**-.085**	**.308**	**.059**	**-.276**	**.077**	**-.075**	**-.216**	**-.160**	**-.415**	**-.246**	**.039**
NO_3			**1**	**.721****	**-.229**	**-.088**	**-.147**	**-.219**	**-.365**	**-.222**	**-.529**	**-.074**	**-.513**	**-.364**	**-.238**	**-.313**	**.679***	**-.292**	**-.528**
SO_4				**1**	**.002**	**-.294**	**-.363***	**-.350**	**-.194**	**-.105**	**-.023***	**-.369**	**.196**	**-.328**	**-.181***	**-.235**	**.187***	**-.186***	**-.426**
Na					**1**	**-.207**	**.581***	**.981****	**-.233**	**.388**	**-.124**	**-.273**	**-.066**	**-.265**	**-.409**	**-.183**	**-.462**	**-.326**	**-.009**
NH_4						**1**	**.648***	**-.186**	**.399**	**-.141**	**.578**	**.317**	**.343**	**.703***	**.836****	**.586**	**.872****	**.812****	**.550**
K							**1**	**.619***	**.157**	**.140**	**.424**	**.037**	**.372**	**.364**	**.202**	**.455**	**.313**	**.356**	**.594***
Mg								**1**	**-.082**	**.408**	**-.009**	**-.211**	**.070**	**-.136**	**-.314**	**-.065**	**-.349**	**-.212**	**.106**
Ca									**1**	**-.059**	**.874****	**.324**	**.890****	**.932****	**.842****	**.820****	**.735***	**.856****	**.736****
Al										**1**	**-.099**	**.511**	**-.012**	**-.037**	**-.119**	**-.175**	**-.276**	**-.157**	**.022**
Fe											**1**	**.189**	**.922****	**.926****	**.763****	**.930****	**.687***	**.827****	**.886****
V												**1**	**.245**	**.454**	**.566***	**.199**	**.544**	**.519**	**.383**
Cr													**1**	**.891****	**.690****	**.884****	**.561**	**.747****	**.936****
Mn														**1**	**.926****	**.909****	**.896****	**.951****	**.871****
Cu															**1**	**.748****	**.985****	**.988****	**.694***
Zn																**1**	**.672***	**.815****	**.905****
Sb																	**1**	**.983****	**.617**
Ba																		**1**	**.770****
Pb																			**1**

(a) BROS $PM_{2.5}$

	Mass	Cl	NO_3	SO_4	Na	NH_4	K	Mg	Ca	Al	Fe	V	Cr	Mn	Cu	Zn	Sb	Ba	Pb
Mass	**1**	**.006**	**.222**	**.485**	**-.015**	**.891****	**.791****	**-.068**	**.039**	**-.292**	**.900****	**.085**	**.558***	**.476**	**.495**	**.754****	**.562***	**.466**	**.760****
Cl		**1**	**-.195**	**-.046**	**.290**	**-.001**	**-.186**	**.204**	**.370**	**-.117**	**.052**	**-.373**	**.106**	**-.200**	**-.288**	**-.086**	**-.313**	**-.335**	**-.159**
NO_3			**1**	**.709****	**-.211**	**.198**	**.378**	**-.111**	**-.252**	**.373**	**.095**	**-.332**	**-.200**	**.038**	**.024**	**-.084**	**.100**	**.158**	**.073**
SO_4				**1**	**-.322**	**.355**	**.761****	**-.276**	**-.208**	**-.130**	**.441**	**-.213**	**-.061**	**.398**	**.334**	**.196**	**.382**	**.470**	**.372**
Na					**1**	**-.239**	**-.258**	**.988****	**.443**	**.238**	**-.143**	**.009**	**-.240**	**-.267**	**-.390**	**-.253**	**-.260**	**-.245**	**-.244**
NH_4						**1**	**.686****	**-.302**	**-.003**	**-.351**	**.802****	**.025**	**.658****	**.402**	**.448**	**.643****	**.478**	**.330**	**.583***
K							**1**	**-.337**	**-.264**	**-.384**	**.696****	**-.035**	**.308**	**.610***	**.586***	**.519**	**.610***	**.668****	**.641***
Mg								**1**	**.704***	**.522**	**-.076**	**.234**	**-.266**	**-.054**	**-.354**	**-.240**	**-.123**	**-.014**	**-.250**
Ca									**1**	**-.014**	**.313**	**.324**	**.270**	**.276**	**.152**	**.220**	**.184**	**.149**	**.111**
Al										**1**	**-.392**	**-.104**	**-.375**	**-.380**	**-.407**	**-.405**	**-.314**	**-.377**	**-.397**
Fe											**1**	**.204**	**.665****	**.637***	**.632***	**.855****	**.659****	**.573***	**.809****
V												**1**	**.207**	**.389**	**.451**	**.380**	**.425**	**.354**	**.280**
Cr													**1**	**.512**	**.641****	**.804****	**.636***	**.345**	**.594***
Mn														**1**	**.957****	**.673****	**.935****	**.953****	**.725****
Cu															**1**	**.778****	**.975****	**.911****	**.786****
Zn																**1**	**.794****	**.622***	**.933****
Sb																	**1**	**.900****	**.814****
Ba																		**1**	**.756****
Pb																			**1**

(b) BROS $PM_{2.5-10}$

	Mass	Cl	NO_3	SO_4	Na	NH_4	K	Mg	Ca	Al	Fe	V	Cr	Mn	Cu	Zn	Sb	Ba	Pb
Mass	**1**	**-.459**	**.365**	**.286**	**-.083**	**-.287**	**-.121**	**-.184**	**-.591***	**.000**	**-.478**	**-.202**	**-.481**	**-.454**	**-.447**	**-.397**	**-.422**	**-.492**	**-.429**
Cl		**1**	**-.364**	**-.331**	**.281**	**.202**	**.273**	**.287**	**-.127**	**.186**	**.017**	**-.200**	**-.116**	**-.376**	**-.446**	**.234**	**-.471**	**-.411**	**-.175**
NO_3			**1**	**.889****	**-.056**	**-.354**	**-.035**	**-.076**	**-.526***	**-.138**	**-.430**	**-.292**	**-.347**	**-.226**	**-.159**	**-.413**	**-.163**	**-.198**	**-.305**
SO_4				**1**	**-.151**	**-.059**	**-.053**	**-.058**	**-.442**	**-.322**	**-.305**	**-.236**	**-.145**	**-.041**	**-.017**	**-.267**	**-.009**	**-.028**	**-.150**
Na					**1**	**.451**	**.989****	**.979****	**-.236**	**.440**	**-.224**	**-.554***	**-.206**	**-.318**	**-.267**	**.199**	**-.281**	**-.231**	**-.261**
NH_4						**1**	**.373**	**.444**	**.021**	**.168**	**-.107**	**-.107**	**-.133**	**.005**	**.156**	**-.055**	**.086**	**.078**	**-.064**
K							**1**	**.975****	**-.267**	**.424**	**-.293**	**-.505**	**-.232**	**-.309**	**-.237**	**.193**	**-.255**	**-.203**	**-.256**
Mg								**1**	**-.085**	**.478**	**-.075**	**-.492**	**-.049**	**-.189**	**-.175**	**.268**	**-.188**	**-.127**	**-.126**
Ca									**1**	**.039**	**.862****	**.519***	**.887****	**.855****	**.737****	**.485**	**.752****	**.800****	**.786****
Al										**1**	**-.181**	**-.219**	**-.183**	**-.206**	**-.179**	**-.163**	**-.190**	**-.211**	**-.180**
Fe											**1**	**.411**	**.949****	**.752****	**.523***	**.626***	**.542***	**.638***	**.771****
V												**1**	**.423**	**.580***	**.584***	**.431**	**.562***	**.559***	**.766****
Cr													**1**	**.849****	**.647****	**.601***	**.673****	**.760****	**.805****
Mn														**1**	**.942****	**.481**	**.952****	**.972****	**.814****
Cu															**1**	**.402**	**.997****	**.982****	**.694****
Zn																**1**	**.392**	**.484**	**.601***
Sb																	**1**	**.986****	**.694****
Ba																		**1**	**.750****
Pb																			**1**

Appendix IV

MOUDI mass and water soluble ion size distributions measured at the Port Talbot (PT)

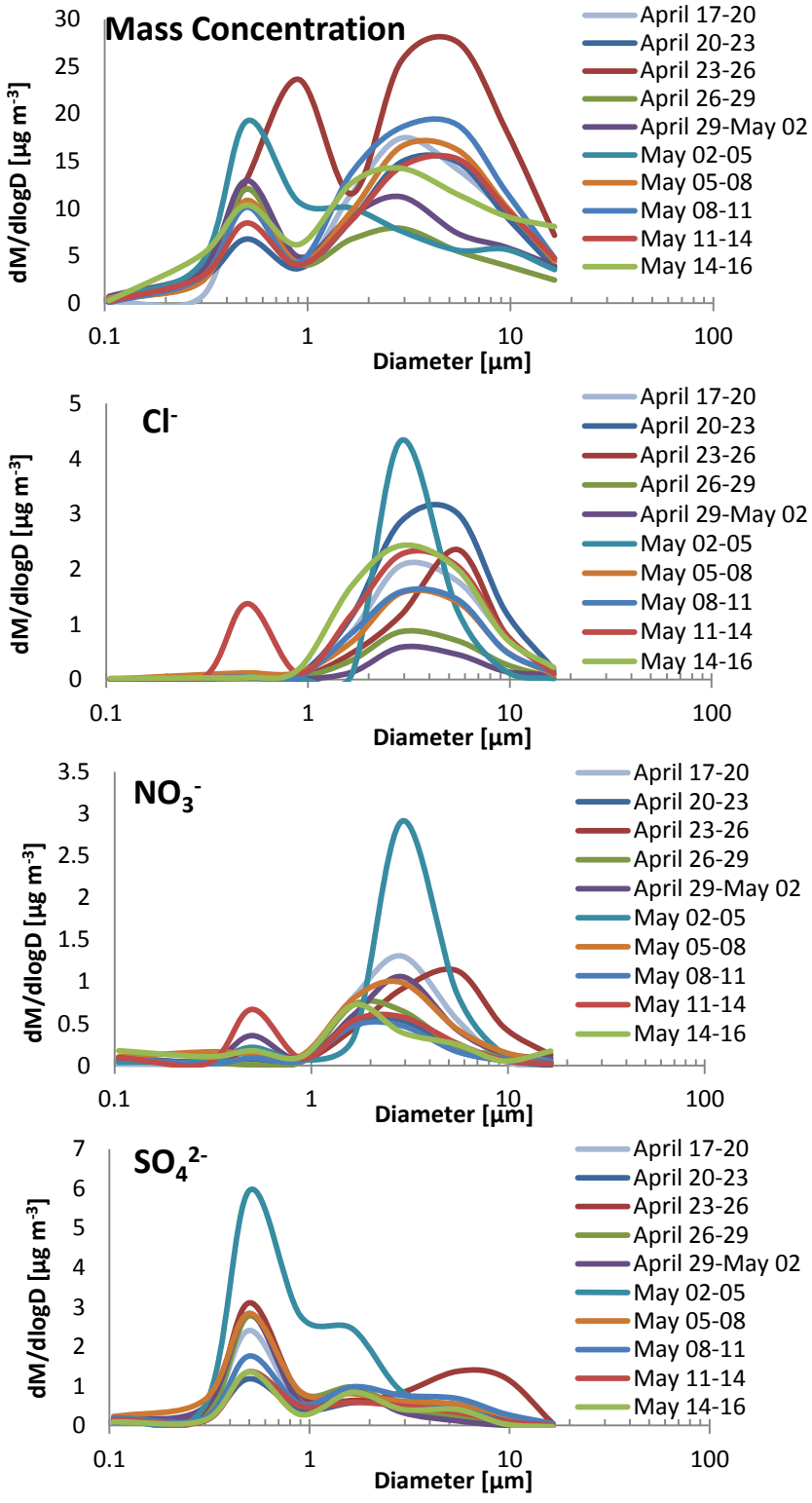

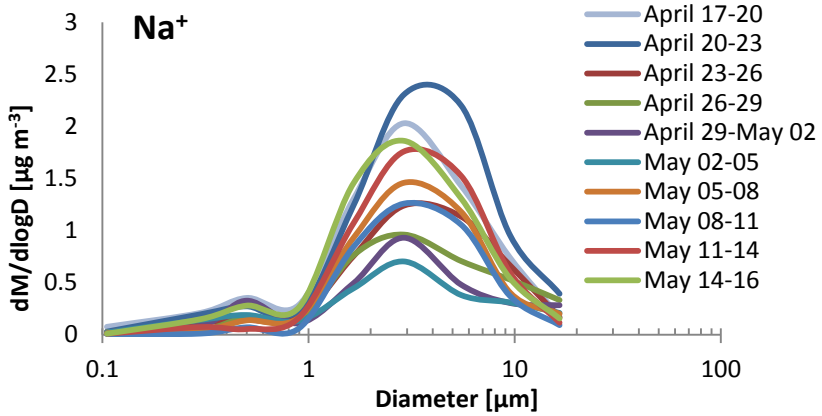
Na+
dM/dlogD [µg m-3]
Diameter [µm]
April 17-20
April 20-23
April 23-26
April 26-29
April 29-May 02
May 02-05
May 05-08
May 08-11
May 11-14
May 14-16

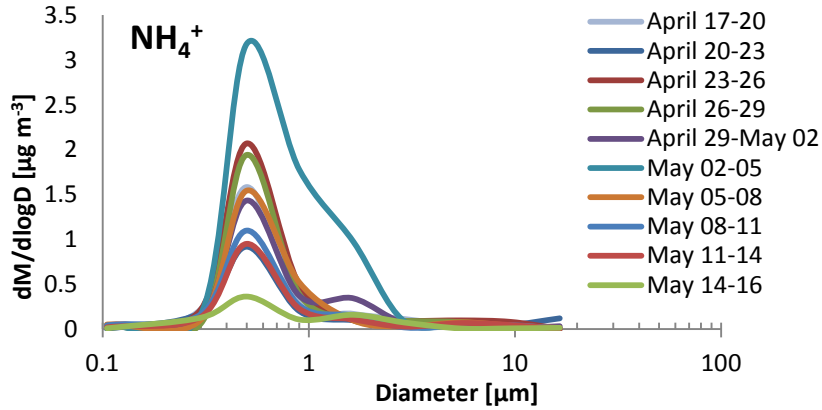
NH4+
dM/dlogD [µg m-3]
Diameter [µm]
April 17-20
April 20-23
April 23-26
April 26-29
April 29-May 02
May 02-05
May 05-08
May 08-11
May 11-14
May 14-16

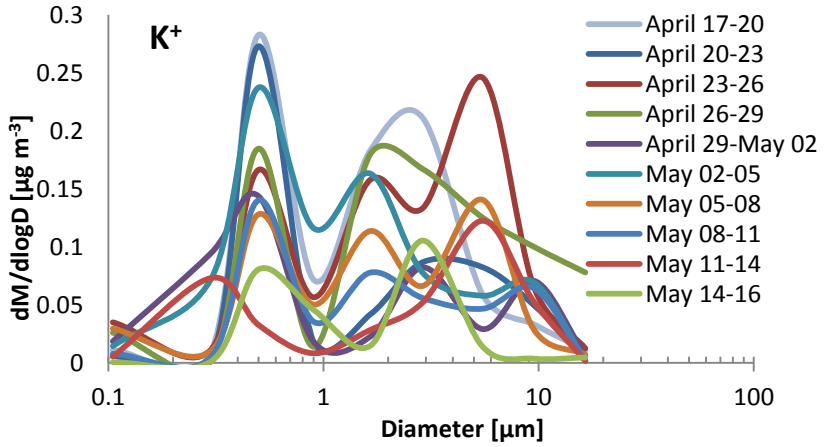
K+
dM/dlogD [µg m-3]
Diameter [µm]
April 17-20
April 20-23
April 23-26
April 26-29
April 29-May 02
May 02-05
May 05-08
May 08-11
May 11-14
May 14-16

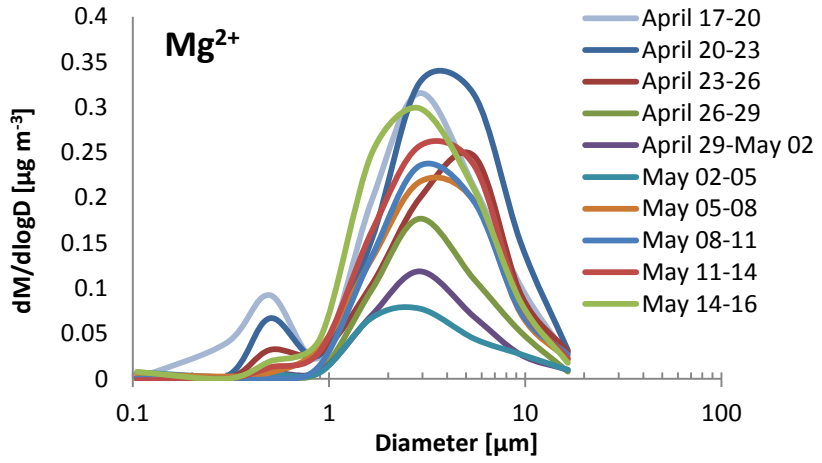
Mg2+
dM/dlogD [µg m-3]
Diameter [µm]
April 17-20
April 20-23
April 23-26
April 26-29
April 29-May 02
May 02-05
May 05-08
May 08-11
May 11-14
May 14-16

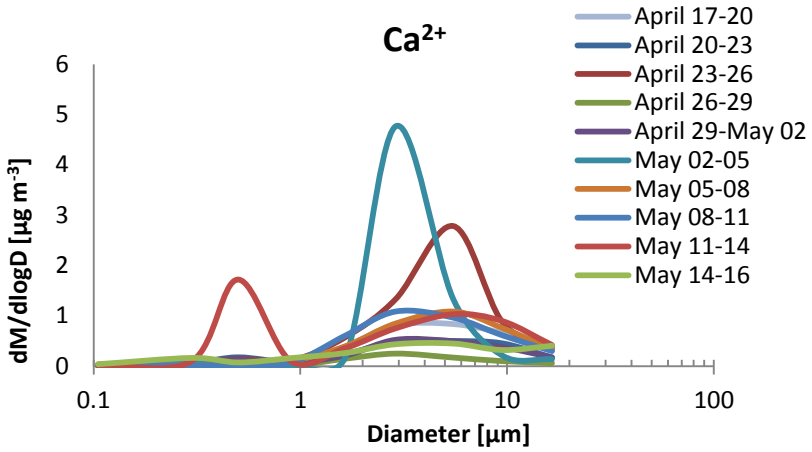
Ca2+
April 17-20
April 20-23
April 23-26
April 26-29
April 29-May 02
May 02-05
May 05-08
May 08-11
May 11-14
May 14-16
dM/dlogD [µg m-3]
0
1
2
3
4
5
6
0.1
1
10
100
Diameter [µm]

Appendix V

Trace metal size distributions measured at the Port Talbot (PT) site

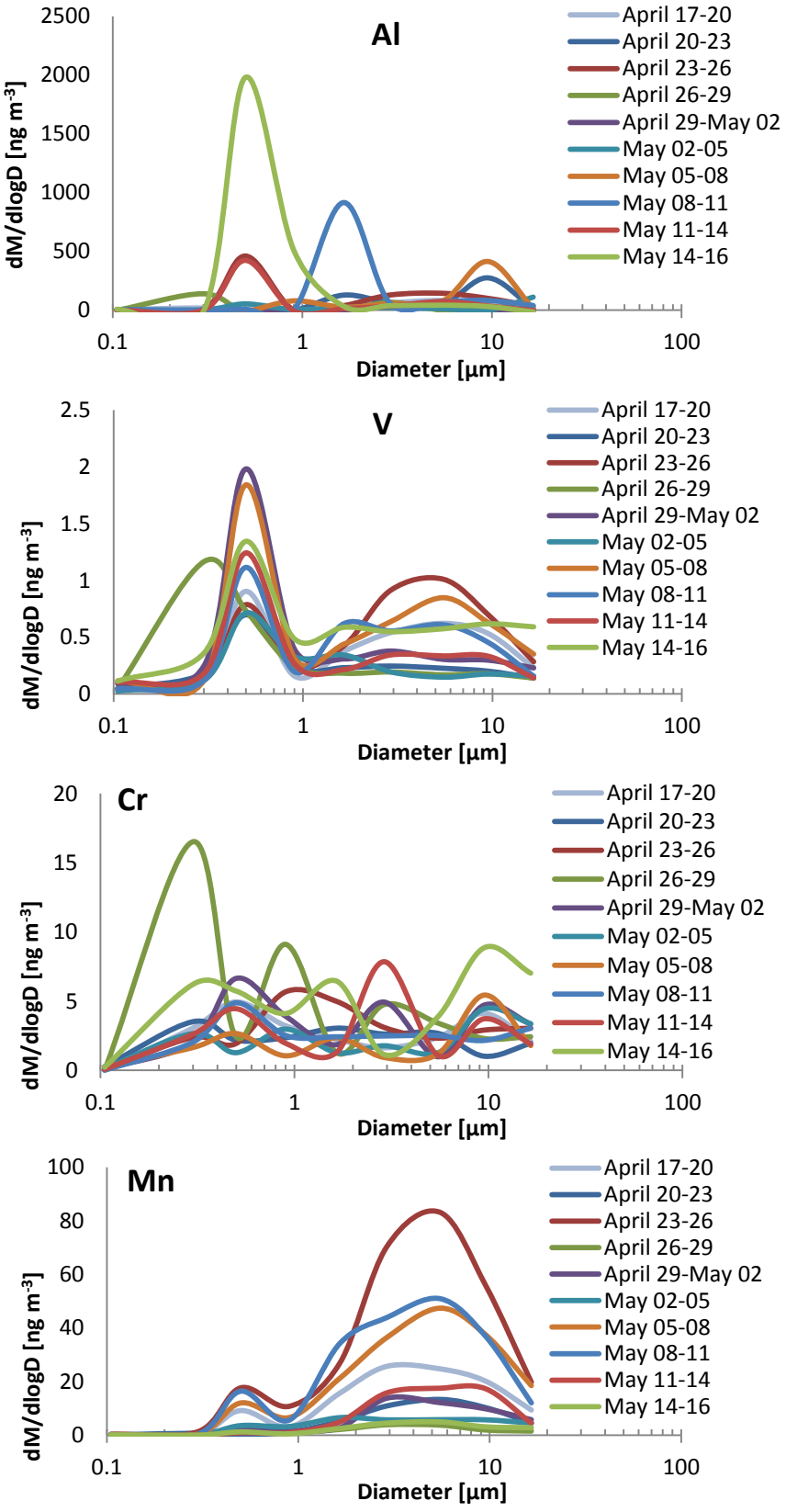

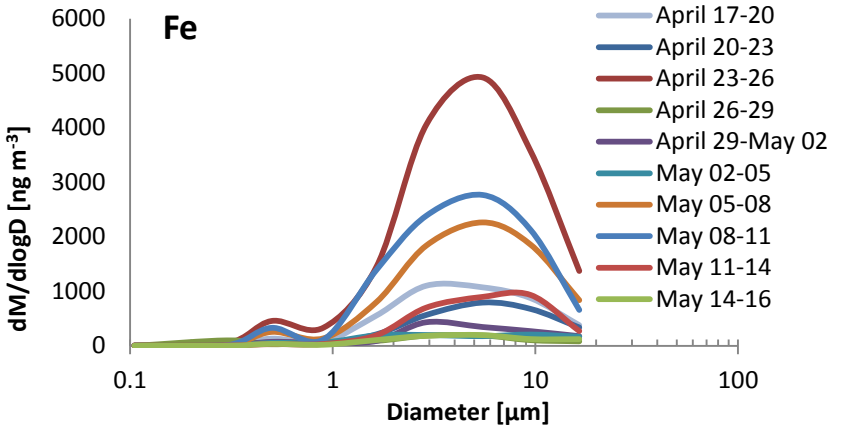
Fe
6000
5000
4000
3000
2000
1000
0
dM/dlogD [ng m-3]
0.1
1
10
100
Diameter [µm]
April 17-20
April 20-23
April 23-26
April 26-29
April 29-May 02
May 02-05
May 05-08
May 08-11
May 11-14
May 14-16

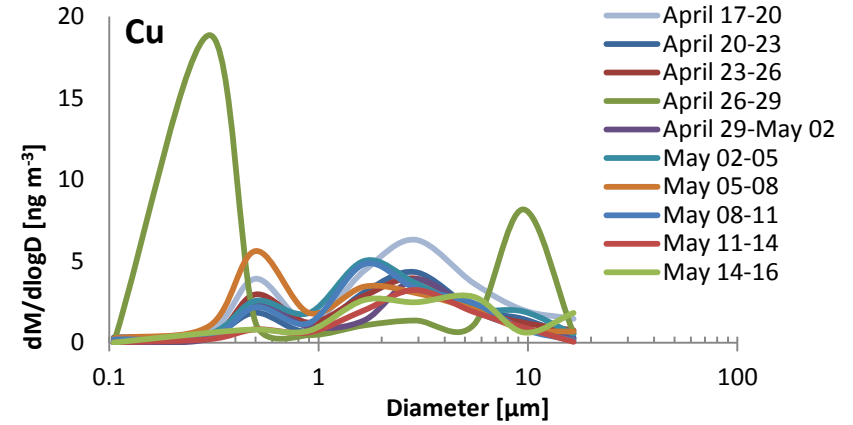
Cu
20
15
10
5
0
dM/dlogD [ng m-3]
0.1
1
10
100
Diameter [µm]
April 17-20
April 20-23
April 23-26
April 26-29
April 29-May 02
May 02-05
May 05-08
May 08-11
May 11-14
May 14-16

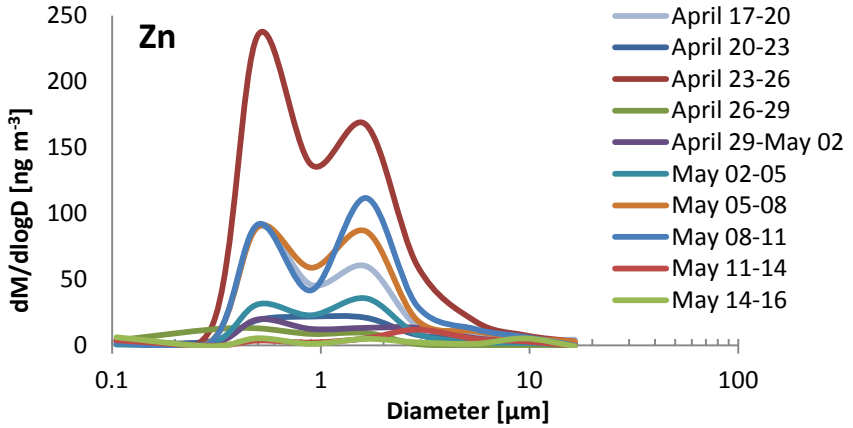
Zn
250
200
150
100
50
0
dM/dlogD [ng m-3]
0.1
1
10
100
Diameter [µm]
April 17-20
April 20-23
April 23-26
April 26-29
April 29-May 02
May 02-05
May 05-08
May 08-11
May 11-14
May 14-16

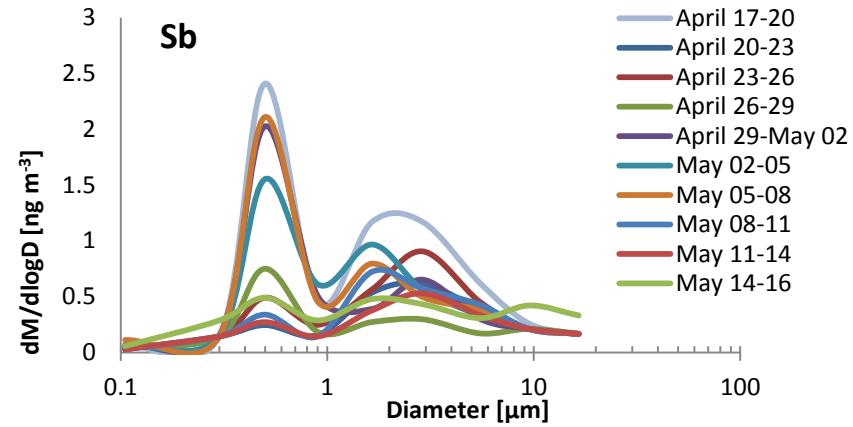
Sb
3
2.5
2
1.5
1
0.5
0
dM/dlogD [ng m-3]
0.1
1
10
100
Diameter [µm]
April 17-20
April 20-23
April 23-26
April 26-29
April 29-May 02
May 02-05
May 05-08
May 08-11
May 11-14
May 14-16

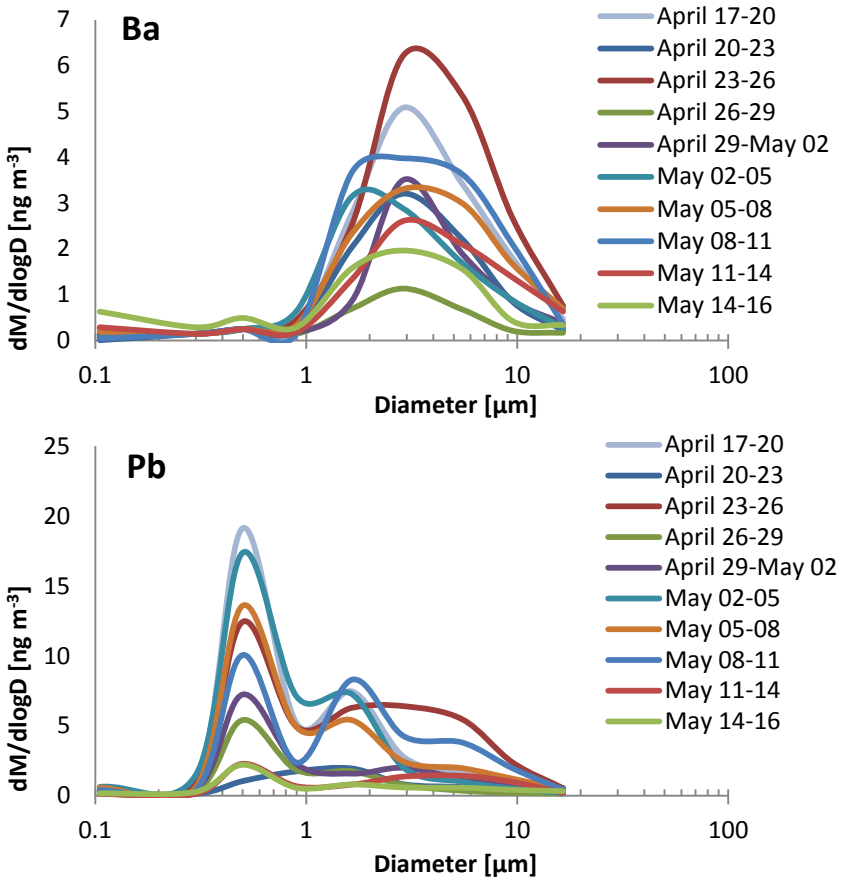
Ba
dM/dlogD [ng m-3]
Diameter [µm]
0.1
1
10
100
0
1
2
3
4
5
6
7
April 17-20
April 20-23
April 23-26
April 26-29
April 29-May 02
May 02-05
May 05-08
May 08-11
May 11-14
May 14-16
Pb
dM/dlogD [ng m-3]
Diameter [µm]
0
5
10
15
20
25
April 17-20
April 20-23
April 23-26
April 26-29
April 29-May 02
May 02-05
May 05-08
May 08-11
May 11-14
May 14-16

Appendix VI

Particle size distribution PM mass and water-soluble ions at the EROS site

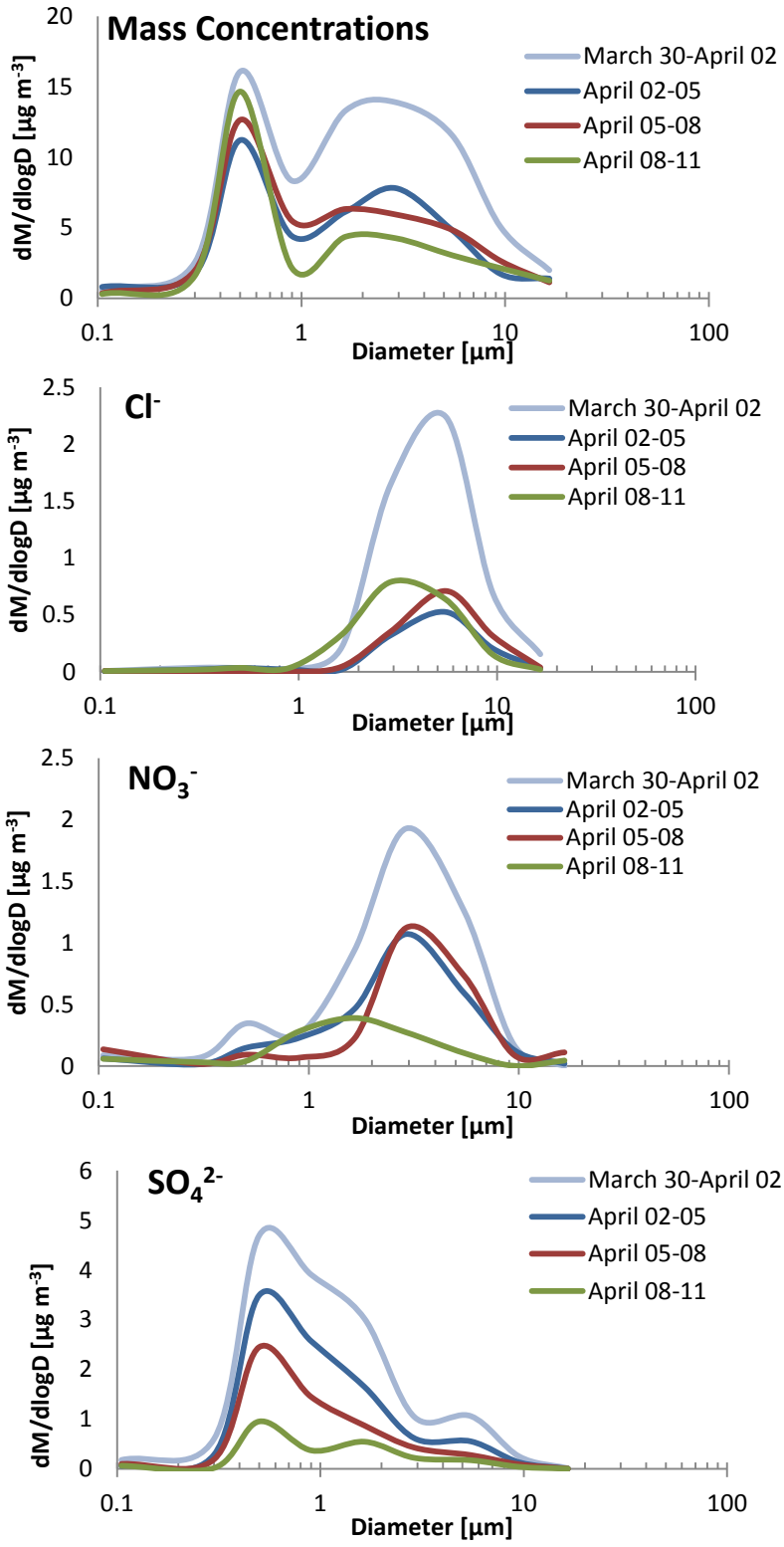

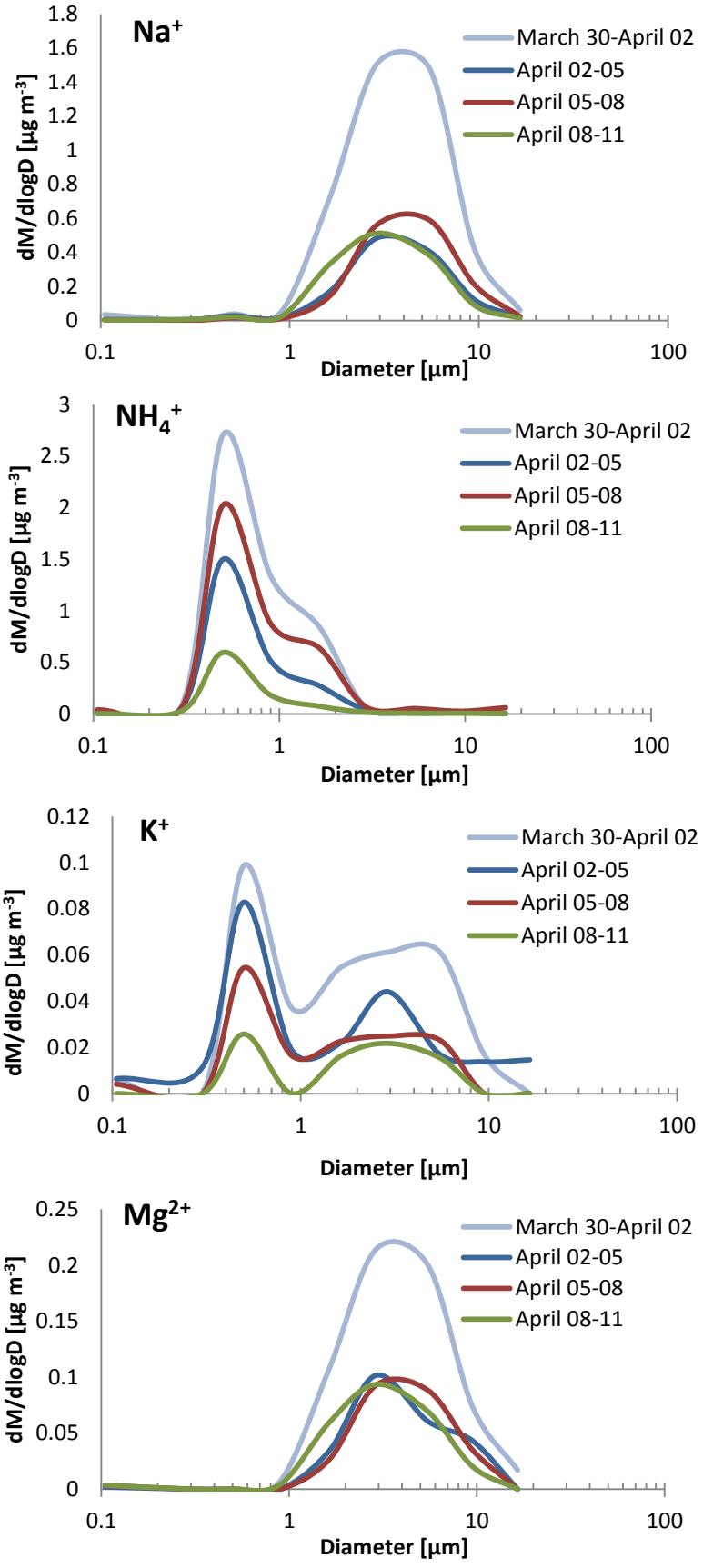
Na+
March 30-April 02
April 02-05
April 05-08
April 08-11
dM/dlogD [µg m-3]
Diameter [µm]
NH4+
K+
Mg2+

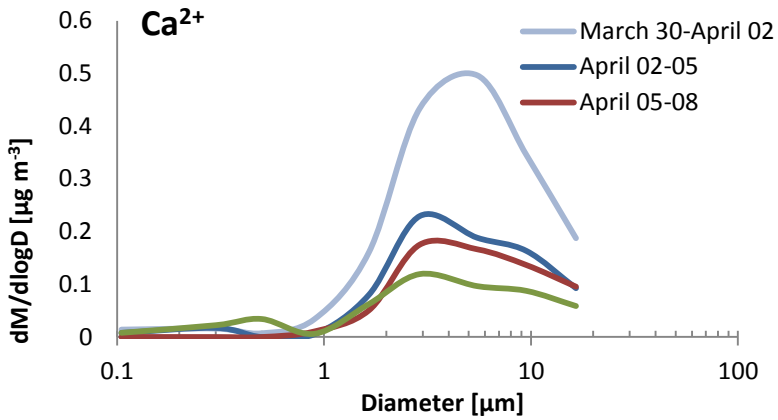
Ca2+
March 30-April 02
April 02-05
April 05-08
dM/dlogD [µg m-3]
0.6
0.5
0.4
0.3
0.2
0.1
0
0.1
1
10
100
Diameter [µm]

Appendix VII

MOUDI trace metal size distributions at the EROS site

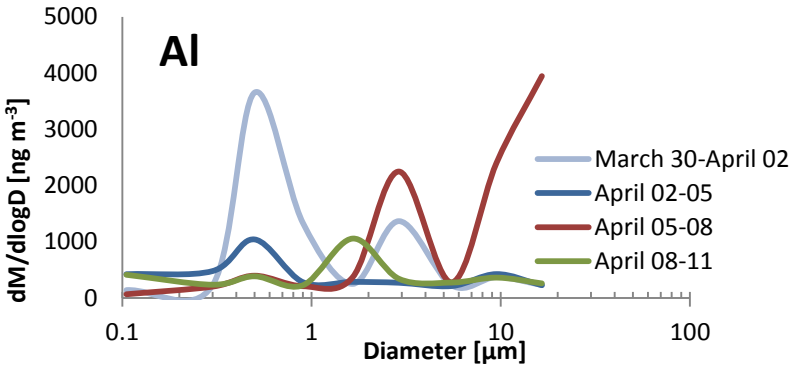

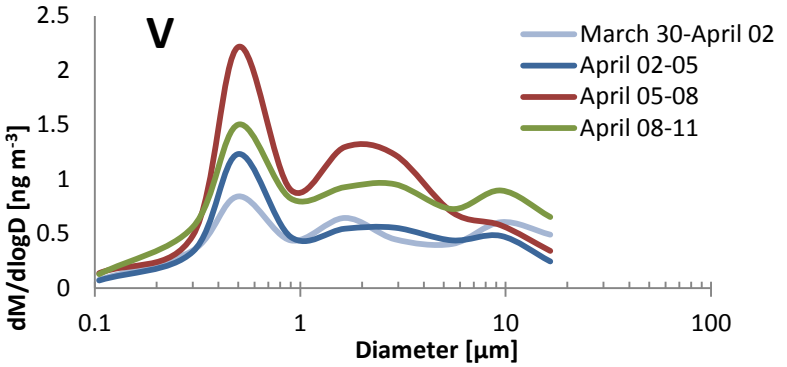

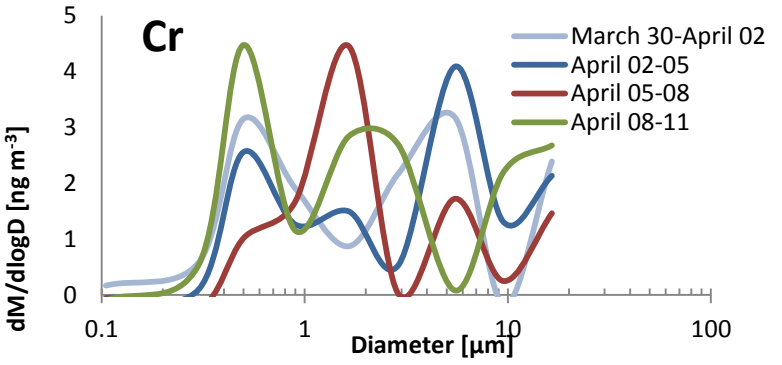

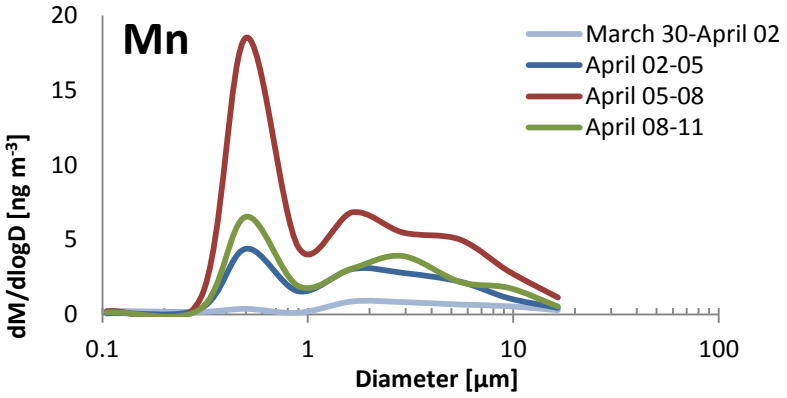

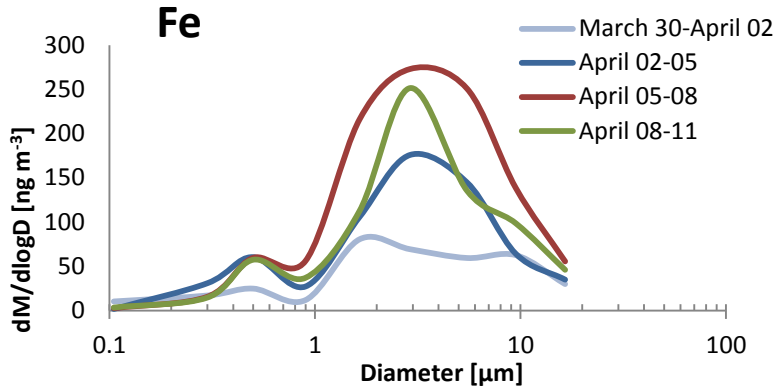
Fe
March 30-April 02
April 02-05
April 05-08
April 08-11
dM/dlogD [ng m-3]
300
250
200
150
100
50
0
0.1
1
10
100
Diameter [µm]

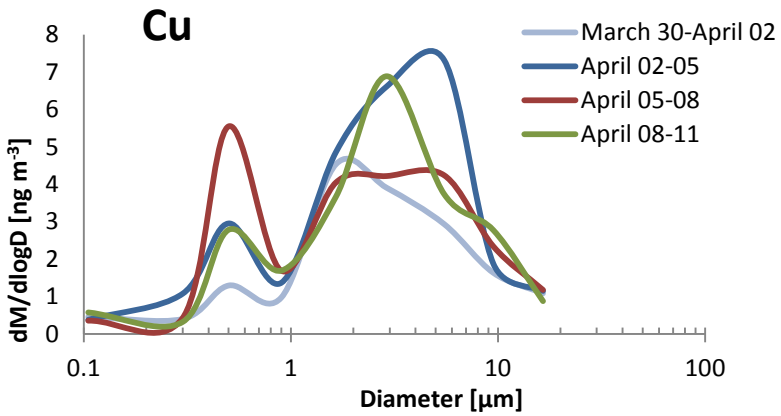
Cu
March 30-April 02
April 02-05
April 05-08
April 08-11
dM/dlogD [ng m-3]
8
7
6
5
4
3
2
1
0
0.1
1
10
100
Diameter [µm]

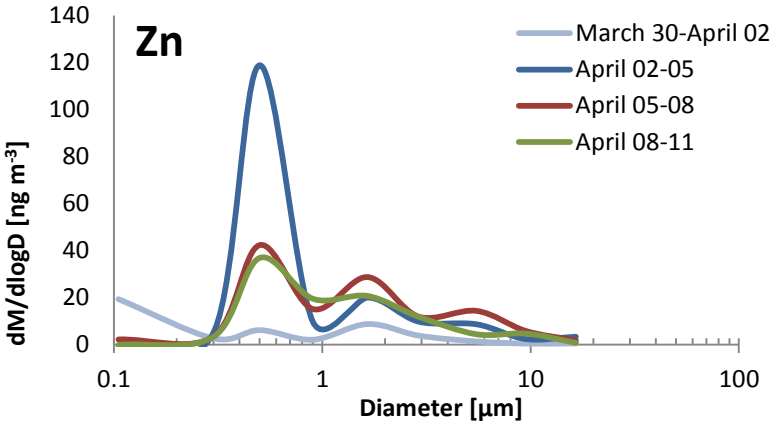
Zn
March 30-April 02
April 02-05
April 05-08
April 08-11
dM/dlogD [ng m-3]
140
120
100
80
60
40
20
0
0.1
1
10
100
Diameter [µm]

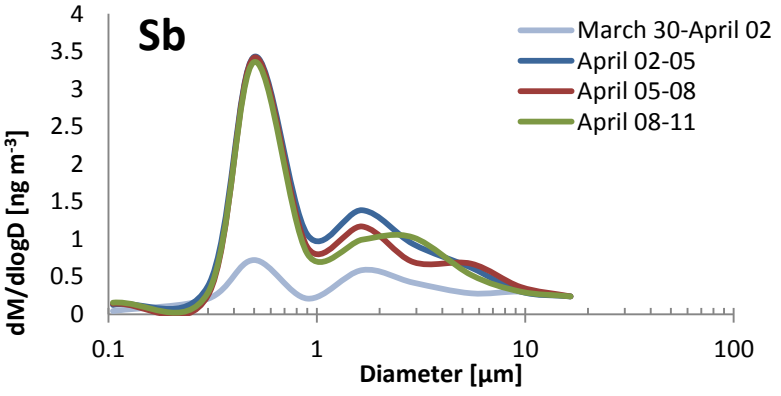
Sb
March 30-April 02
April 02-05
April 05-08
April 08-11
dM/dlogD [ng m-3]
4
3.5
3
2.5
2
1.5
1
0.5
0
0.1
1
10
100
Diameter [µm]

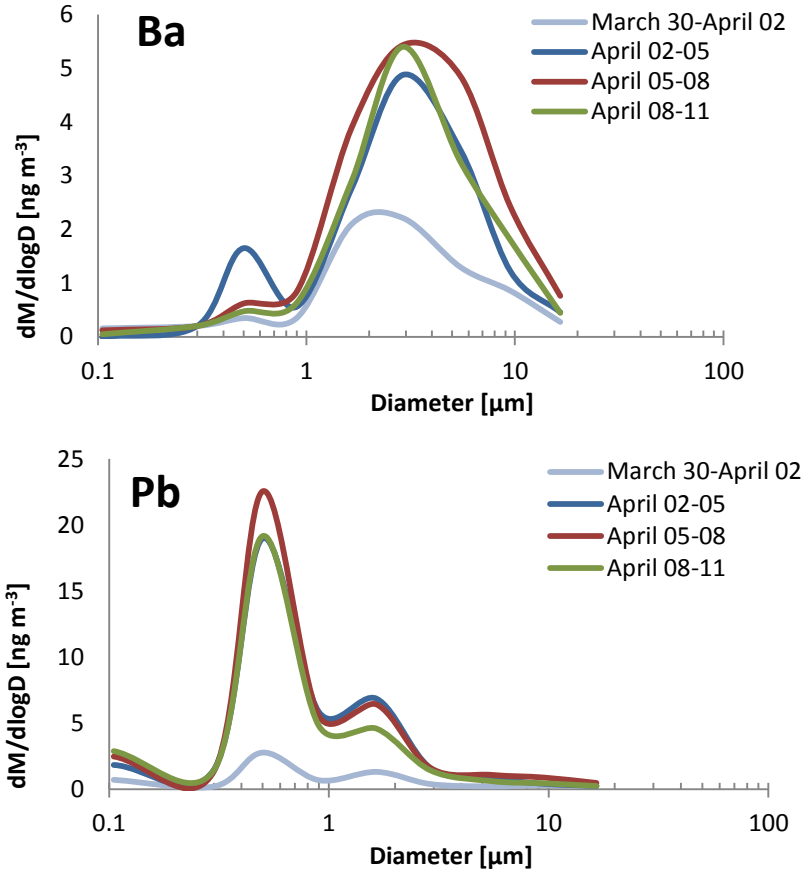
Ba
March 30-April 02
April 02-05
April 05-08
April 08-11
dM/dlogD [ng m-3]
0
1
2
3
4
5
6
0.1
1
10
100
Diameter [µm]

Pb
March 30-April 02
April 02-05
April 05-08
April 08-11
dM/dlogD [ng m-3]
0
5
10
15
20
25
0.1
1
10
100
Diameter [µm]

Appendix VIII

RMA plots between FDMS and Partisol PM in all the four monitoring sites

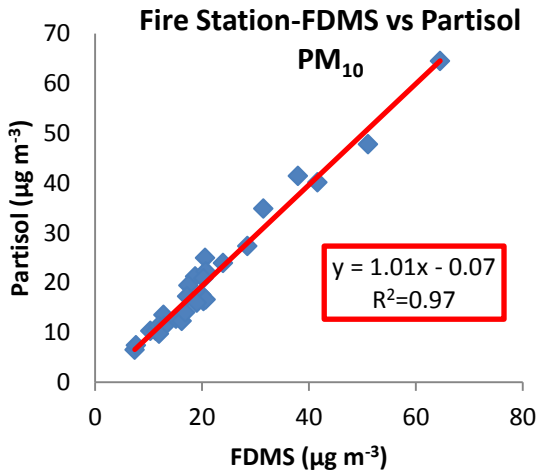

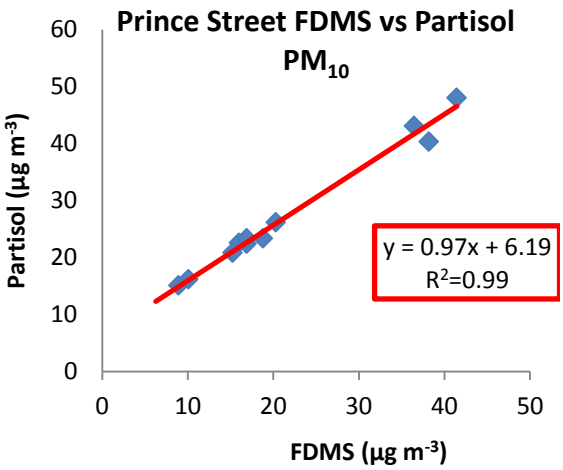

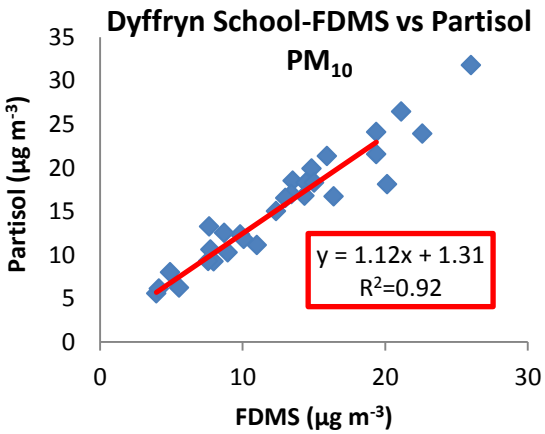

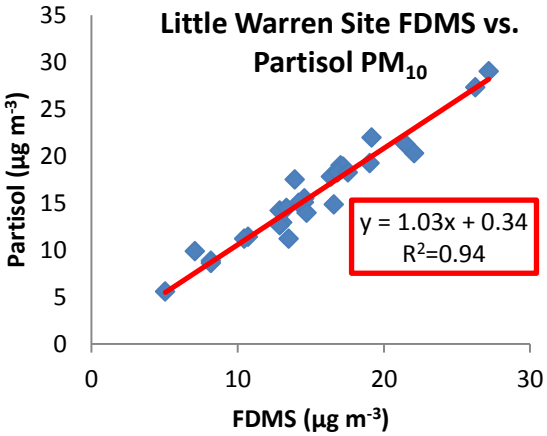

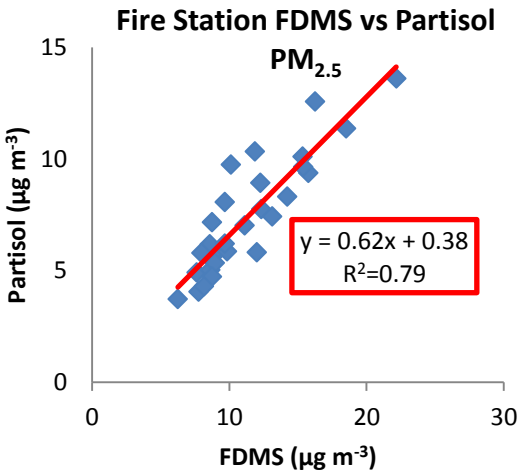

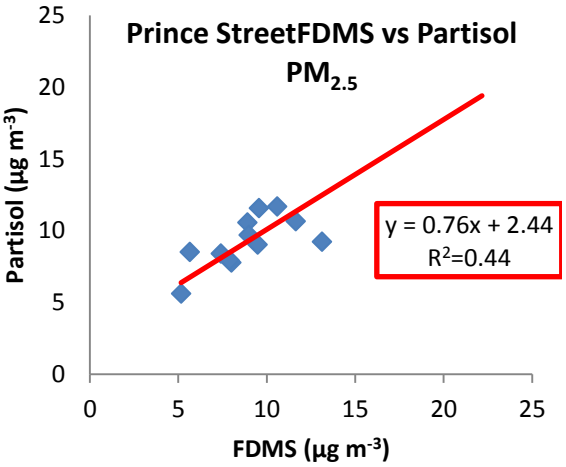

Appendix IX

FDMS and Partisol PM mean values during the days of the week

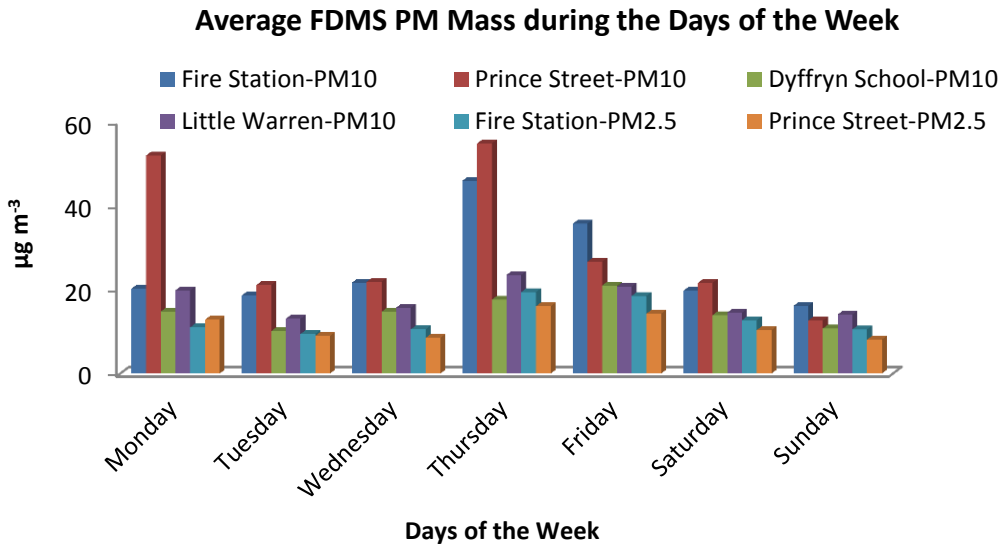

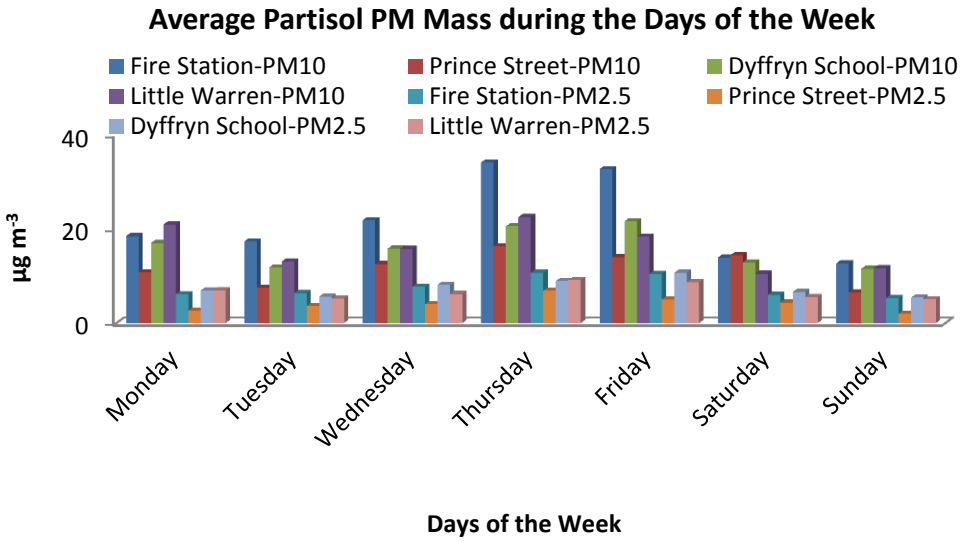

Appendix X

Reduced Major Analysis regression equations for PM_{10} vs. $PM_{2.5}$ and $PM_{2.5-10}$

(a) FDMS

Monitoring sites	$PM_{2.5-10}$	$PM_{2.5}$
Fire Station	$PM_{2.5-10} = 0.88 (PM_{10}) - 8.83$ $r^2=0.92$	$PM_{2.5} = 0.29 (PM_{10}) + 5.07$ $r^2=0.28$
Prince Street	$PM_{2.5-10} = 0.88(PM_{10}) - 6.62$ $r^2=0.99$	$PM_{2.5} = 0.11(PM_{10}) + 6.62$ $r^2=0.76$

(b) Partisol

Monitoring sites	$PM_{2.5-10}$	$PM_{2.5}$
Fire Station	$PM_{2.5-10} = 0.88 (PM_{10}) - 4.94$ $r^2=0.97$	$PM_{2.5} = 0.20 (PM_{10}) + 3.29$ $r^2=0.45$
Prince Street	$PM_{2.5-10} = 0.89 (PM_{10}) - 6.28$ $r^2=0.99$	$PM_{2.5} = 0.15 (PM_{10}) - 5.38$ $r^2=0.64$
Dyffryn School	$PM_{2.5-10} = 0.76 (PM_{10}) - 3.59$ $r^2=0.81$	$PM_{2.5} = 0.46 (PM_{10}) + 0.15$ $r^2=0.48$
Little Warren	$PM_{2.5-10} = 0.58 (PM_{10}) - 1.38$ $r^2=0.85$	$PM_{2.5} = 0.52 (PM_{10}) - 0.08$ $r^2=0.81$

Appendix XI

Linear relationship between PM and NO_x, CO and SO_2

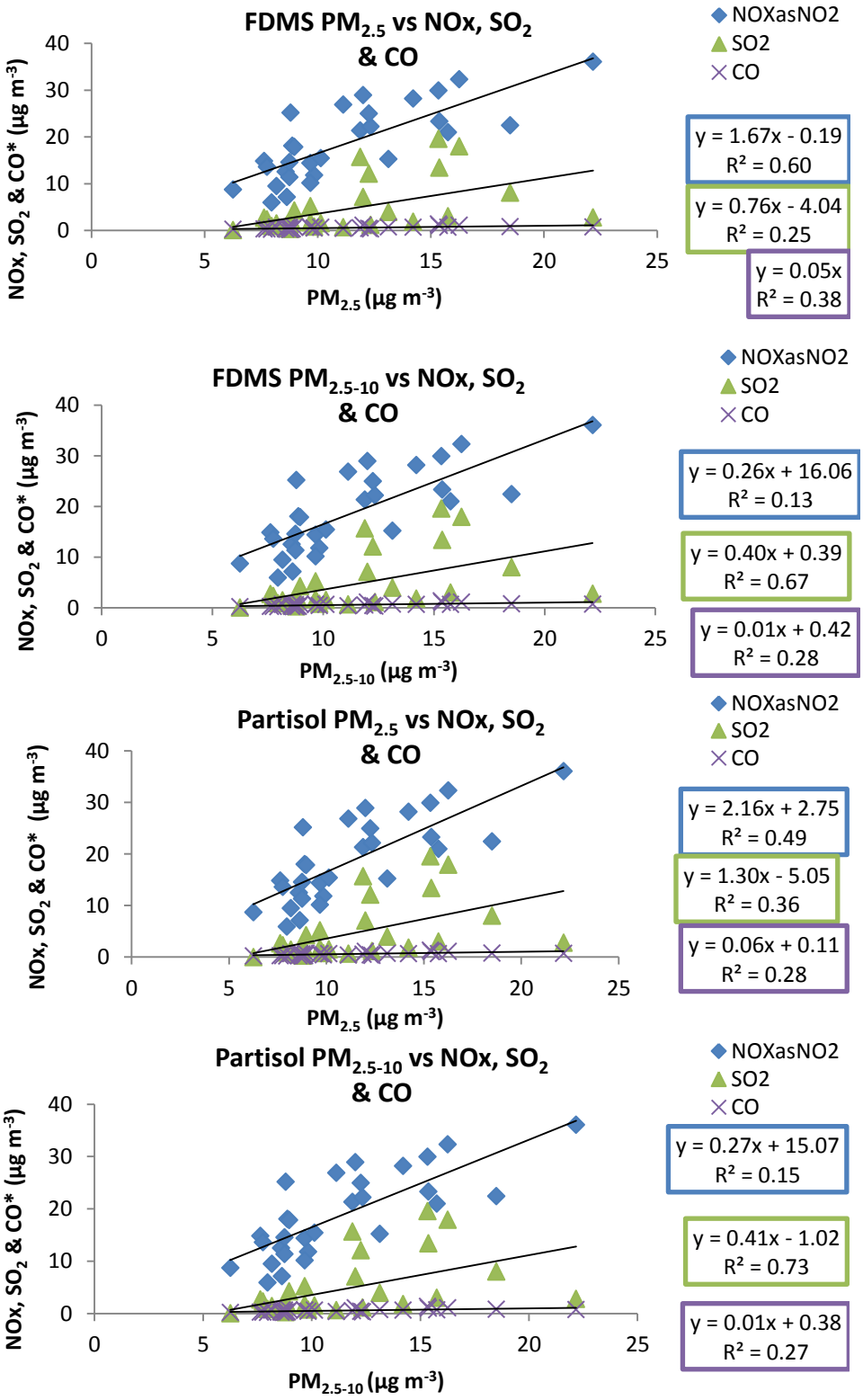

*CO unit in mg m^{-3}

Appendix XII

Reduced Major Axis correlation plots between Grimm, FDMS and Partisol PM size fraction concentrations

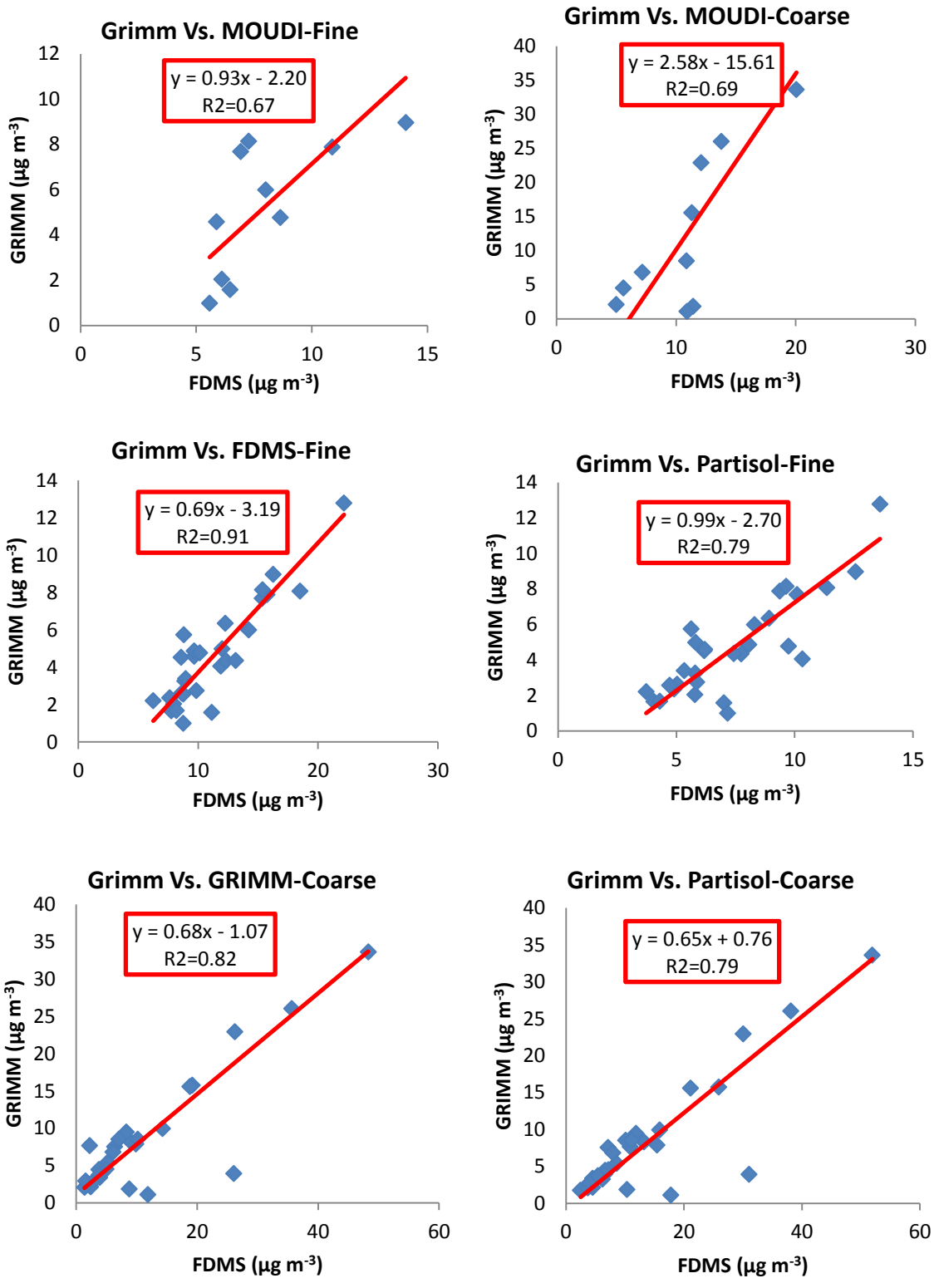

Appendix XIII

Time series plot of $PM_{2.5}$ and $PM_{2.5-10}$ water soluble ion concentrations at the four monitoring sites

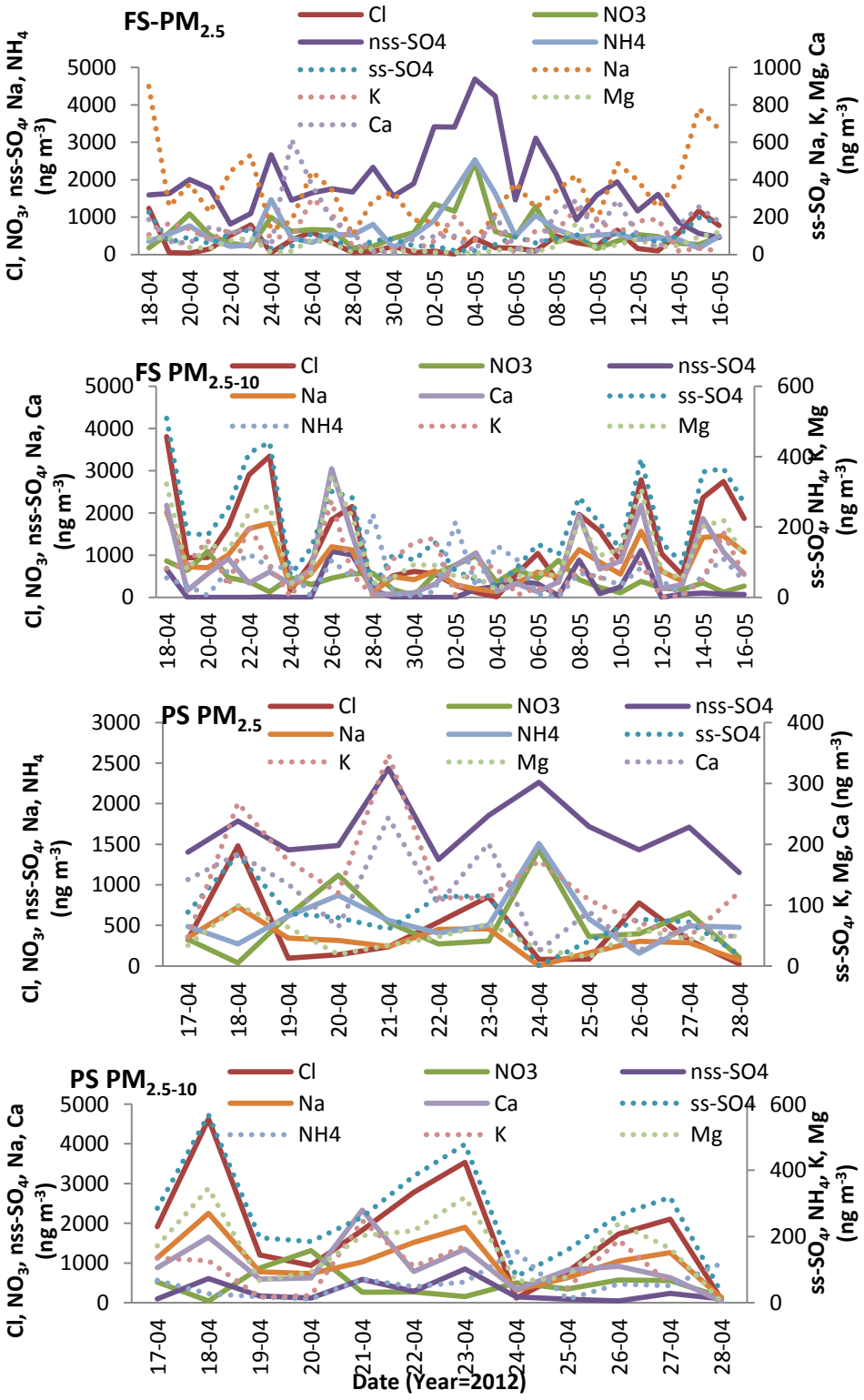

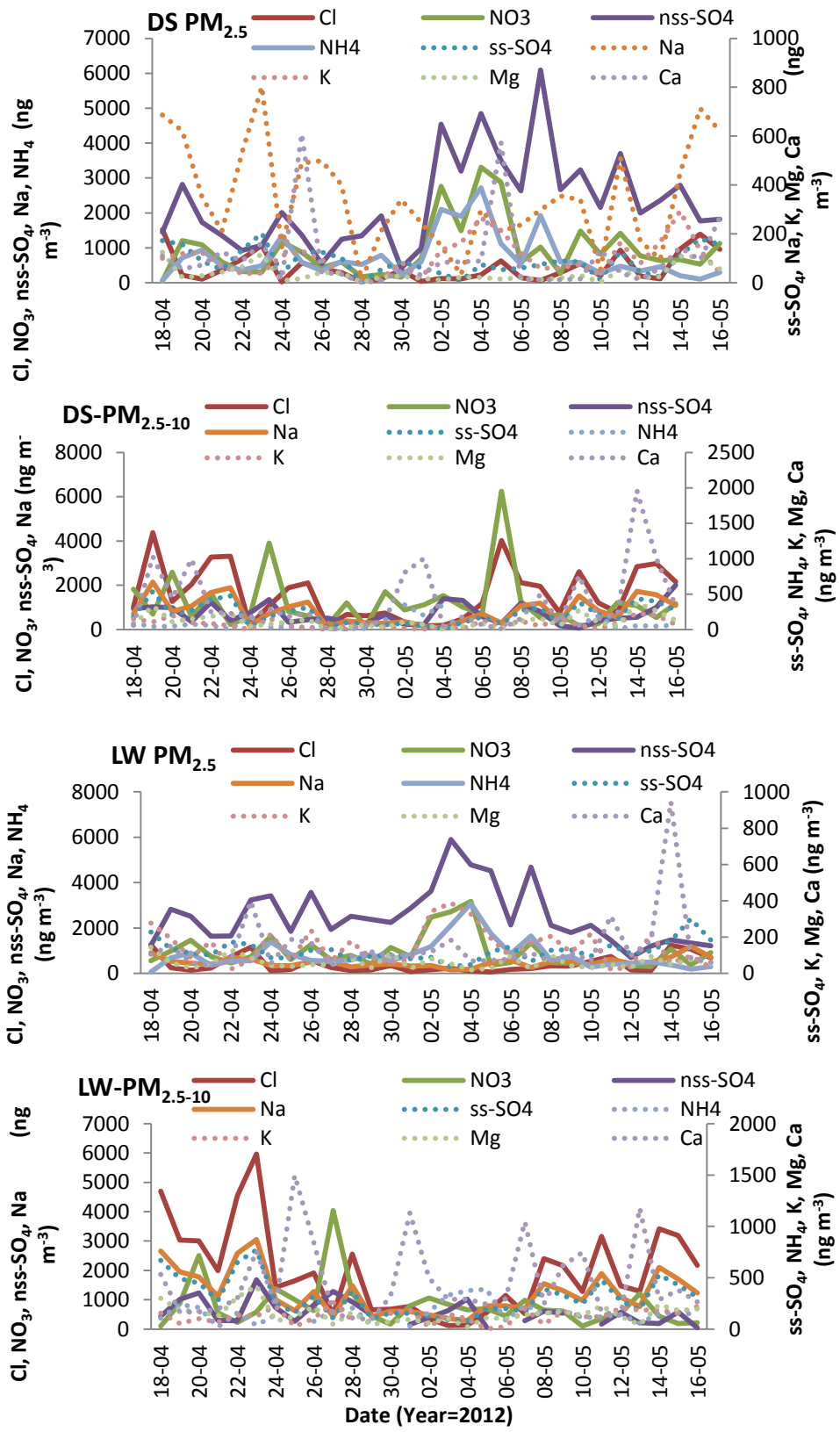
DS PM2.5
Cl
NO3
nss-SO4
NH4
ss-SO4
Na
K
Mg
Ca
Cl, NO3, nss-SO4, Na, NH4 (ng m-3)
ss-SO4, Na, K, Mg, Ca (ng m-3)
DS-PM2.5-10
Cl
NO3
nss-SO4
Na
ss-SO4
NH4
K
Mg
Ca
Cl, NO3, nss-SO4, Na (ng m-3)
ss-SO4, NH4, K, Mg, Ca (ng m-3)
LW PM2.5
Cl
NO3
nss-SO4
Na
NH4
ss-SO4
K
Mg
Ca
Cl, NO3, nss-SO4, Na, NH4 (ng m-3)
ss-SO4, K, Mg, Ca (ng m-3)
LW-PM2.5-10
Cl
NO3
nss-SO4
Na
ss-SO4
NH4
K
Mg
Ca
Cl, NO3, nss-SO4, Na (ng m-3)
ss-SO4, NH4, K, Mg, Ca (ng m-3)
18-04
20-04
22-04
24-04
26-04
28-04
30-04
02-05
04-05
06-05
08-05
10-05
12-05
14-05
16-05
Date (Year=2012)

Appendix XIV

Time variation plots of metals ($PM_{2.5}$ and $PM_{2.5-10}$) at the sampling sites

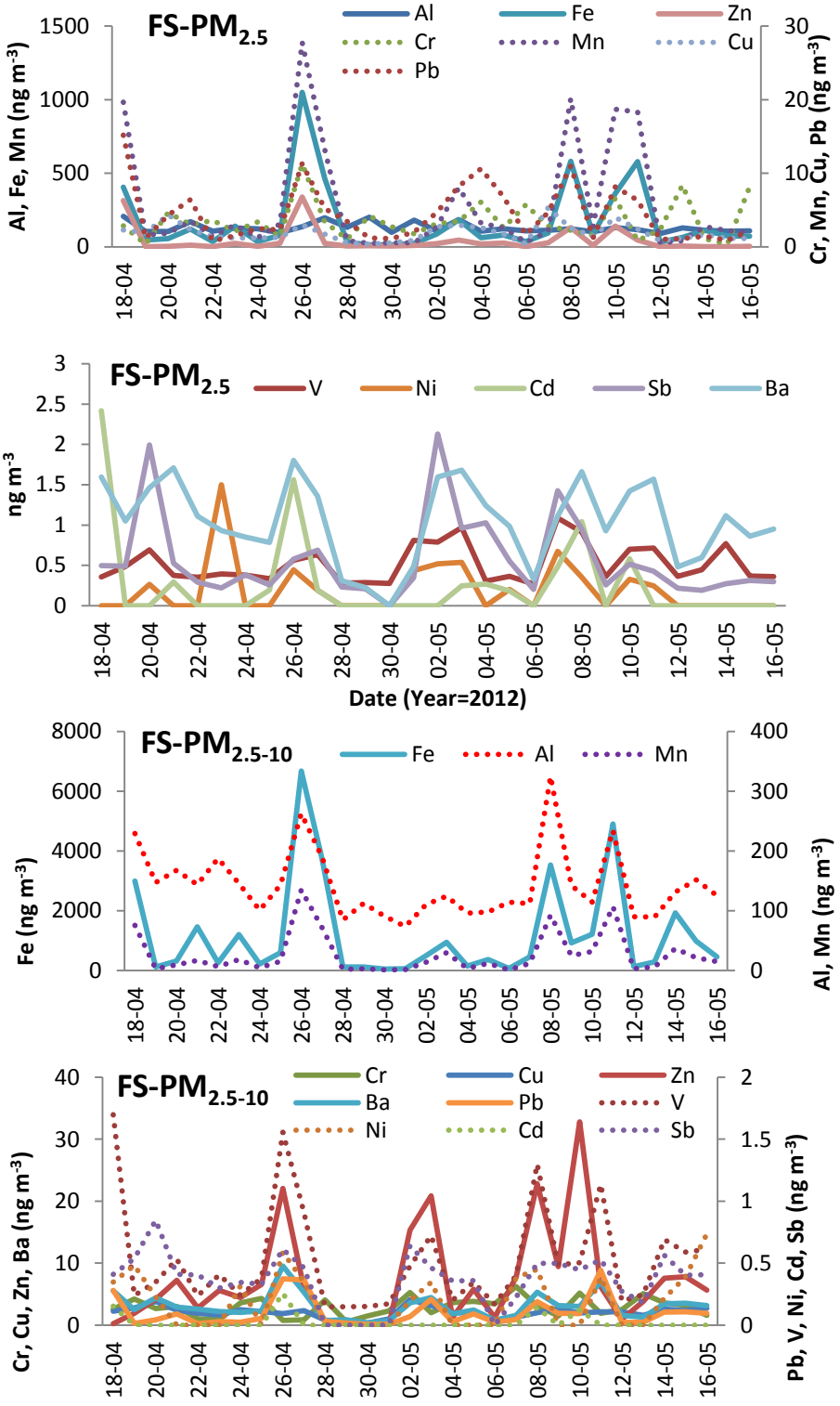

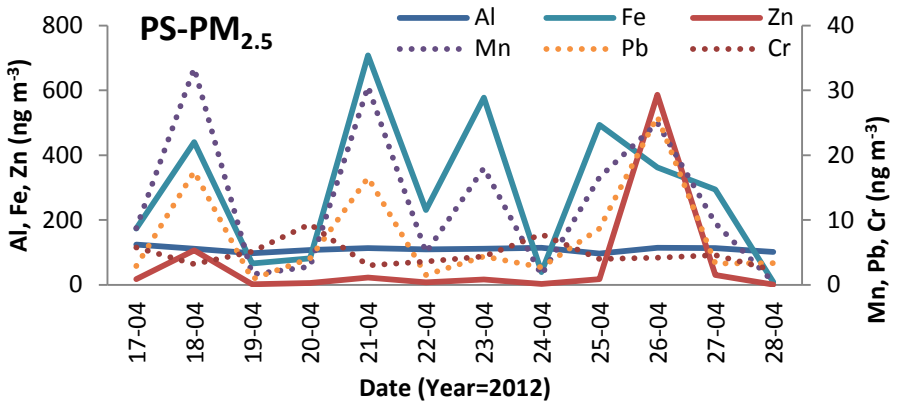
PS-PM2.5
Al
Fe
Zn
Mn
Pb
Cr
Al, Fe, Zn (ng m-3)
Mn, Pb, Cr (ng m-3)
800
600
400
200
0
40
30
20
10
0
17-04
18-04
19-04
20-04
21-04
22-04
23-04
24-04
25-04
26-04
27-04
28-04
Date (Year=2012)

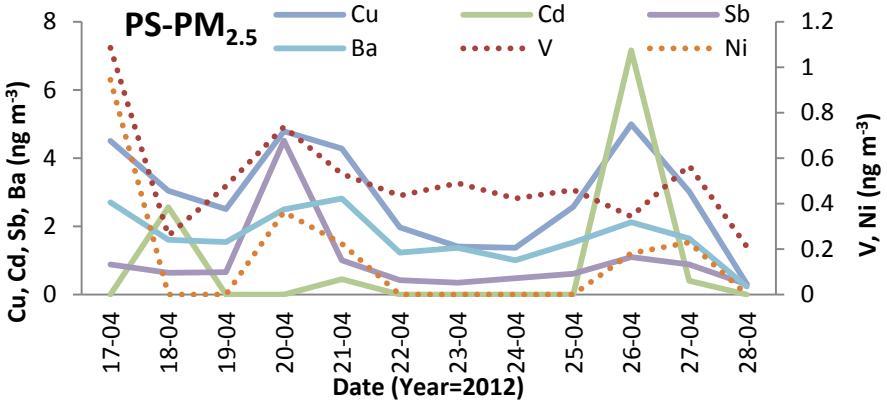
PS-PM2.5
Cu
Cd
Sb
Ba
V
Ni
Cu, Cd, Sb, Ba (ng m-3)
V, Ni (ng m-3)
8
6
4
2
0
1.2
1
0.8
0.6
0.4
0.2
0
17-04
18-04
19-04
20-04
21-04
22-04
23-04
24-04
25-04
26-04
27-04
28-04
Date (Year=2012)

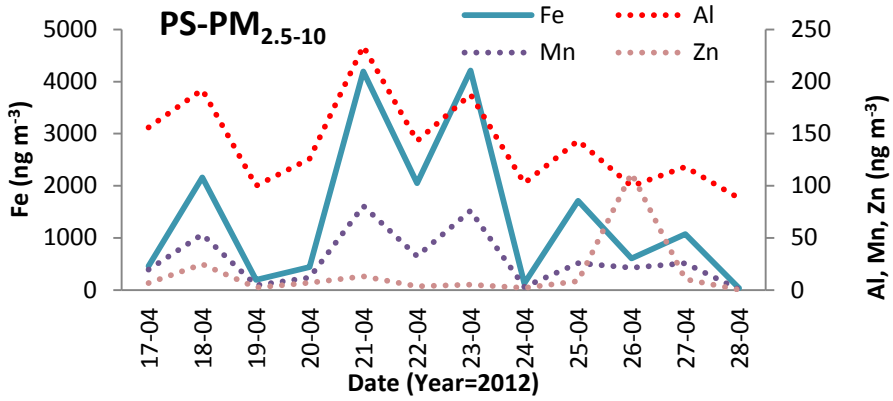
PS-PM2.5-10
Fe
Al
Mn
Zn
Fe (ng m-3)
Al, Mn, Zn (ng m-3)
5000
4000
3000
2000
1000
0
250
200
150
100
50
0
17-04
18-04
19-04
20-04
21-04
22-04
23-04
24-04
25-04
26-04
27-04
28-04
Date (Year=2012)

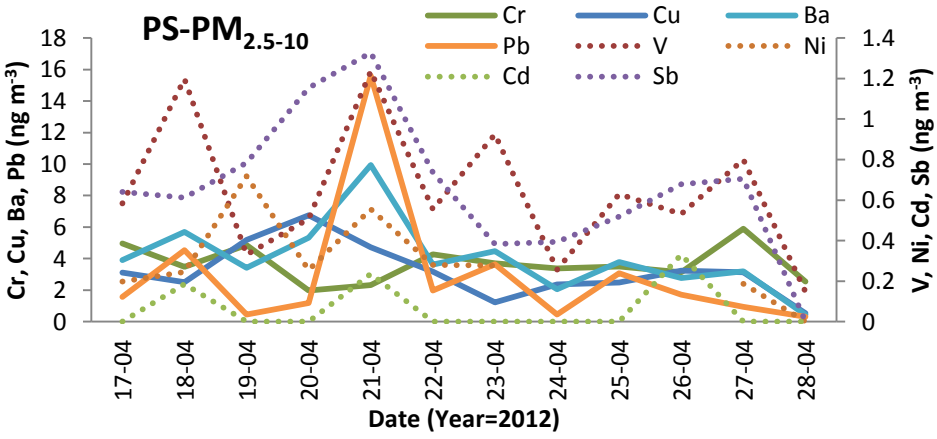
PS-PM2.5-10
Cr
Cu
Ba
Pb
V
Ni
Cd
Sb
Cr, Cu, Ba, Pb (ng m-3)
V, Ni, Cd, Sb (ng m-3)
18
16
14
12
10
8
6
4
2
0
1.4
1.2
1
0.8
0.6
0.4
0.2
0
17-04
18-04
19-04
20-04
21-04
22-04
23-04
24-04
25-04
26-04
27-04
28-04
Date (Year=2012)

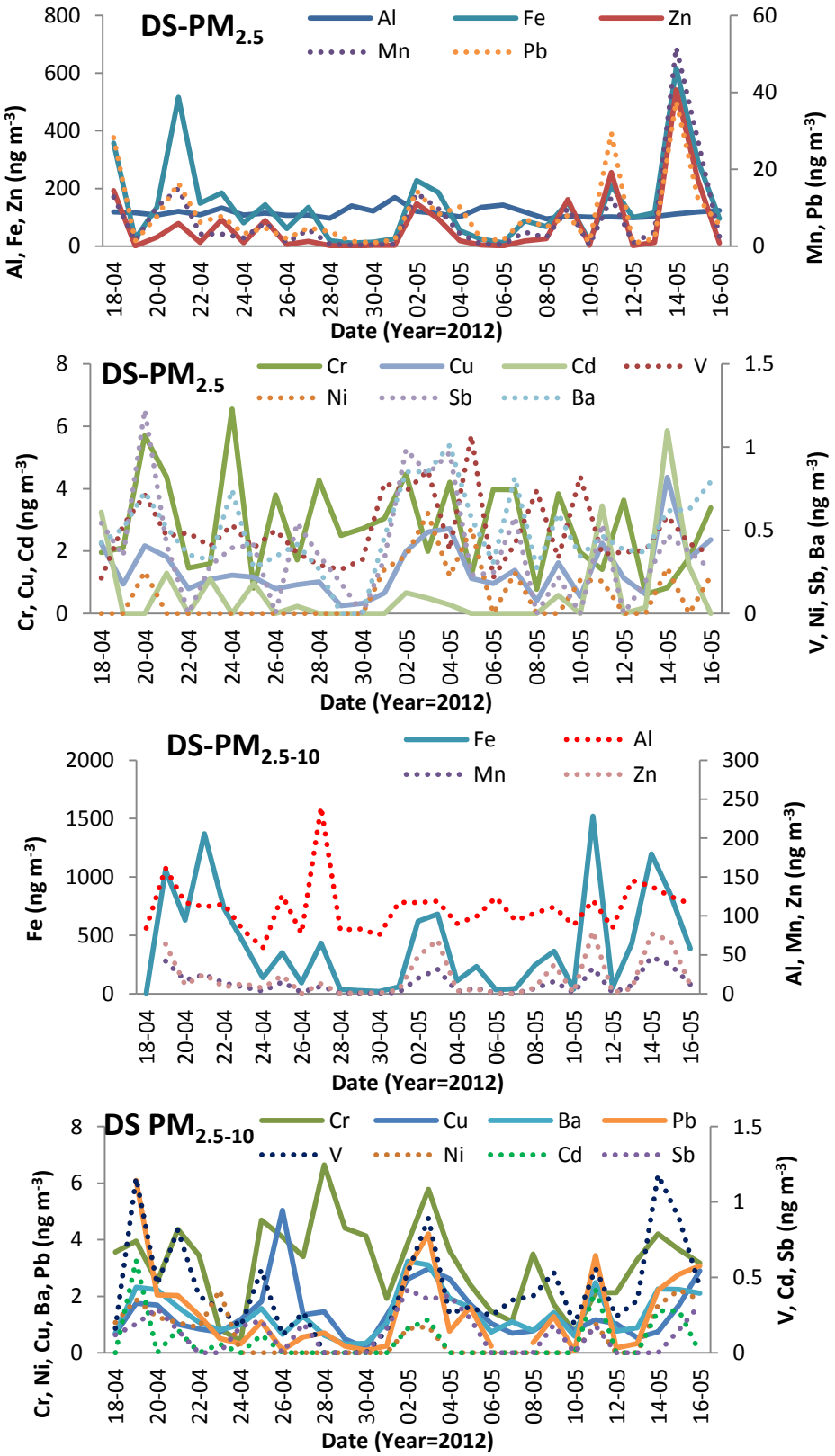
DS-PM2.5
Al
Fe
Zn
Mn
Pb
Al, Fe, Zn (ng m-3)
Mn, Pb (ng m-3)
Date (Year=2012)
DS-PM2.5
Cr
Cu
Cd
V
Ni
Sb
Ba
Cr, Cu, Cd (ng m-3)
V, Ni, Sb, Ba (ng m-3)
Date (Year=2012)
DS-PM2.5-10
Fe
Al
Mn
Zn
Fe (ng m-3)
Al, Mn, Zn (ng m-3)
Date (Year=2012)
DS PM2.5-10
Cr
Cu
Ba
Pb
V
Ni
Cd
Sb
Cr, Ni, Cu, Ba, Pb (ng m-3)
V, Cd, Sb (ng m-3)
Date (Year=2012)

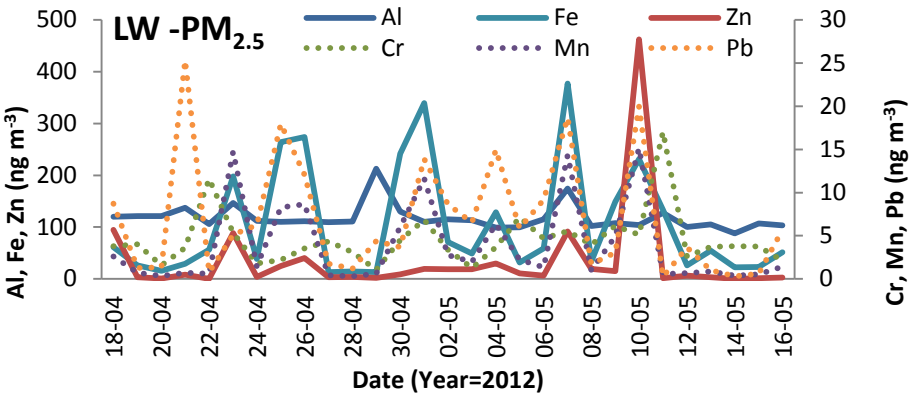
LW -PM2.5
Al
Fe
Zn
Cr
Mn
Pb
Al, Fe, Zn (ng m-3)
Cr, Mn, Pb (ng m-3)
Date (Year=2012)

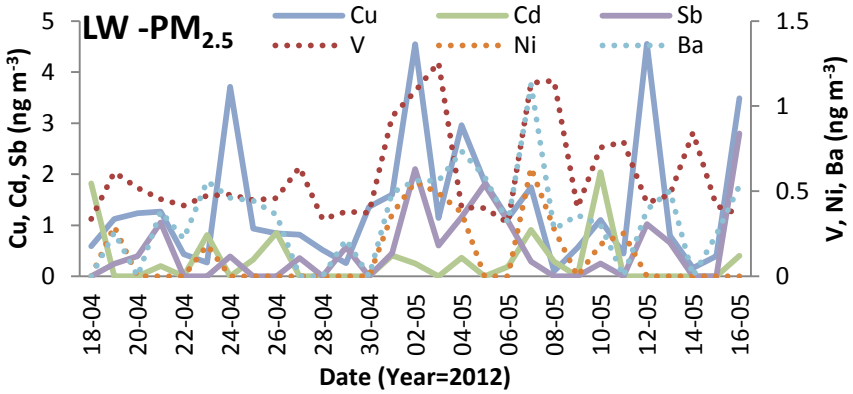
LW -PM2.5
Cu
Cd
Sb
V
Ni
Ba
Cu, Cd, Sb (ng m-3)
V, Ni, Ba (ng m-3)
Date (Year=2012)

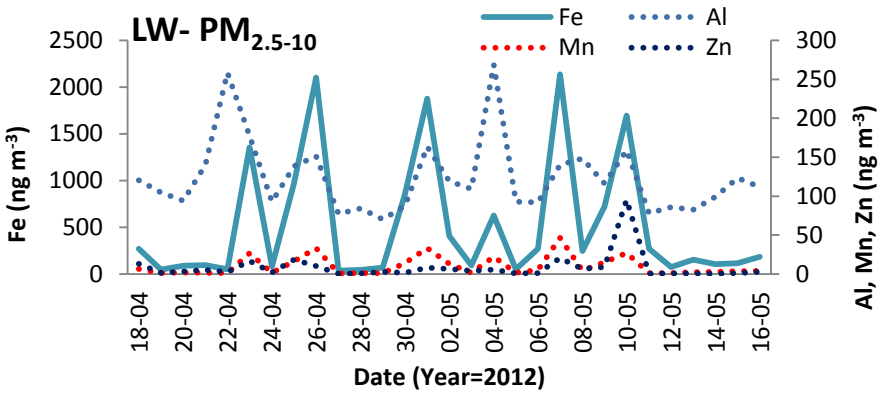
LW- PM2.5-10
Fe
Al
Mn
Zn
Fe (ng m-3)
Al, Mn, Zn (ng m-3)
Date (Year=2012)

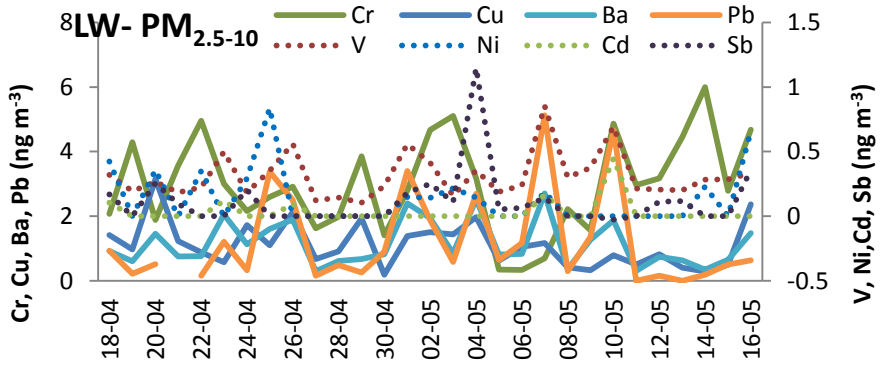
LW- PM2.5-10
Cr
Cu
Ba
Pb
V
Ni
Cd
Sb
Cr, Cu, Ba, Pb (ng m-3)
V, Ni,Cd, Sb (ng m-3)

Appendix XV

Prince Street Pearson's Correlation Coeffients for

(a) $PM_{2.5}$

	PM2.5	Cl	NO3	SO4	Na	NH4	K	Mg	Ca	Al	V	Cr	Mn	Fe	Ni	Cu	Zn	Cd	Sb	Ba
PM2.5	1																			
Cl	.604*	1																		
NO3	.101	-.499	1																	
SO4	.706*	.040	0.413	1																
Na	.425	.847**	-0.51	-0.145	1															
NH4	-.059	-0.536	.875**	0.462	-.591*	1														
K	.505	0.182	0.007	.642*	0.157	0.114	1													
Mg	.289	.816**	-0.552	-0.127	.727**	-0.532	0.236	1												
Ca	.489	0.379	-0.39	0.419	0.546	-0.293	.606*	0.356	1											
Al	.459	0.335	0.087	0.253	0.199	-0.018	-0.084	0.056	0.152	1										
V	-.016	-0.27	0.24	-0.037	0.017	0.136	-0.326	-0.469	0.164	0.497	1									
Cr	.044	-0.318	.841**	0.089	-0.21	.695*	-0.236	-0.472	-0.356	0.175	0.517	1								
Mn	.810**	.690*	-0.435	0.45	0.499	-0.511	0.505	0.438	0.571	0.262	-0.212	-0.467	1							
Fe	.707*	0.451	-0.382	0.544	0.349	-0.414	0.411	0.186	.683*	0.143	-0.093	-0.473	.858**	1						
Ni	-.024	-0.133	0.035	-0.16	0.04	-0.067	-0.319	-0.318	0.088	.643*	.902**	0.331	-0.073	-0.127	1					
Cu	.485	0.135	0.115	0.059	0.253	-0.256	0.019	-0.16	0.122	0.434	0.536	0.295	0.407	0.246	.608*	1				
Zn	.352	0.401	-0.161	-0.156	0.117	-0.45	-0.181	0.284	-0.304	0.224	-0.254	-0.143	0.446	0.171	-0.017	0.465	1			
Cd	.426	0.518	-0.211	-0.114	0.227	-0.481	-0.063	0.402	-0.231	0.232	-0.322	-0.192	0.538	0.205	-0.06	0.46	.982**	1		
Sb	.105	-0.18	0.47	-0.103	0.025	0.195	-0.062	-0.379	-0.178	0.032	0.395	.697*	-0.153	-0.206	0.317	.581*	0.01	-0.005	1	
Ba	.546	.072	0.138	0.259	0.253	-0.148	0.16	-0.223	0.397	0.486	.680*	0.293	0.419	0.384	.666*	.929**	0.203	0.194	0.511	1
Pb	.661*	.053	-0.279	0.236	0.245	-0.469	0.343	0.326	0.128	0.204	-0.333	-0.34	.842**	0.564	-0.089	0.52	.798**	.855**	0.000	0.367

(b) $PM_{2.5-10}$

PS	$PM_{2.5-10}$	Cl	NO_3	nss-SO_4	ss-SO_4	Na	NH_4	K	Mg	Ca	Al	V	Cr	Mn	Fe	Ni	Cu	Zn	Sb	Ba	Pb
$PM_{2.5-10}$	**1**																				
Cl	**.747****	**1**																			
NO_3	**-0.457**	**-0.426**	**1**																		
Nss-SO_4	**.890****	**.738****	**-0.511**	**1**																	
ss-SO_4	**.741****	**.994****	**-0.366**	**.723****	**1**																
Na	**.741****	**.994****	**-0.366**	**.723****	**1.000****	**1**															
NH_4	**-0.246**	**-0.382**	**-0.334**	**-0.062**	**-0.413**	**-0.413**	**1**														
K	**.811****	**.582***	**-0.38**	**0.566**	**.582***	**.582***	**-0.114**	**1**													
Mg	**.794****	**.938****	**-0.419**	**.728****	**.944****	**.944****	**-0.259**	**.762****	**1**												
Ca	**.939****	**.625***	**-0.348**	**.729****	**.615***	**.615***	**-0.27**	**.849****	**.706***	**1**											
Al	**.947****	**.629***	**-0.426**	**.790****	**.620***	**.620***	**-0.212**	**.738****	**.655***	**.931****	**1**										
V	**.933****	**.757****	**-0.385**	**.768****	**.754****	**.754****	**-0.348**	**.734****	**.778****	**.924****	**.901****	**1**									
Cr	**-0.128**	**0.247**	**-0.028**	**-0.075**	**0.283**	**0.283**	**-0.14**	**-0.109**	**0.107**	**-0.191**	**-0.166**	**-0.021**	**1**								
Mn	**.989****	**.697***	**-0.506**	**.895****	**.694***	**.694***	**-0.176**	**.813****	**.767****	**.908****	**.921****	**.902****	**-0.134**	**1**							
Fe	**.945****	**.604***	**-0.515**	**.880****	**.604***	**.604***	**-0.161**	**.727****	**.662***	**.834****	**.878****	**.815****	**-0.154**	**.974****	**1**						
Ni	**0.401**	**0.215**	**0.197**	**0.352**	**0.218**	**0.218**	**-0.503**	**0.201**	**0.084**	**0.464**	**0.414**	**0.343**	**0.16**	**0.343**	**0.366**	**1**					
Cu	**0.006**	**-0.115**	**.809****	**-0.189**	**-0.072**	**-0.072**	**-0.524**	**0.011**	**-0.122**	**0.177**	**0.06**	**0.08**	**-0.117**	**-0.08**	**-0.112**	**0.568**	**1**				
Zn	**0.014**	**0.129**	**0.037**	**-0.178**	**0.137**	**0.137**	**-0.1**	**0.453**	**0.357**	**0.15**	**-0.149**	**0.078**	**-0.152**	**0.022**	**-0.087**	**-0.318**	**0.027**	**1**			
Sb	**0.411**	**0.139**	**0.485**	**0.123**	**0.177**	**0.177**	**-0.482**	**0.413**	**0.19**	**0.57**	**0.453**	**0.472**	**-0.143**	**0.34**	**0.294**	**.602***	**.879****	**0.089**	**1**		
Ba	**.813****	**0.408**	**-0.021**	**0.574**	**0.414**	**0.414**	**-0.357**	**.662***	**0.458**	**.908****	**.871****	**.818****	**-0.275**	**.762****	**.712****	**.600***	**0.503**	**-0.045**	**.808****	**1**	
Pb	**.788****	**0.256**	**-0.329**	**0.564**	**0.233**	**0.233**	**-0.047**	**.721****	**0.356**	**.888****	**.835****	**.747****	**-0.37**	**.785****	**.762****	**0.447**	**0.189**	**0.009**	**.577***	**.887****	

Appendix XVI

Dyffryn School Pearson's Correlation Coeffients for

(a) $PM_{2.5}$

DS	$PM_{2.5}$	Cl	NO_3	nss-SO_4	ss-SO_4	Na	NH_4	K	Mg	Ca	Al	V	Cr	Mn	Fe	Ni	Cu	Zn	Cd	Sb	Ba
$PM_{2.5}$	1																				
Cl	-0.254	1																			
NO3	.725**	-0.225	1																		
nss-SO_4	.828**	-0.362	.713**	1																	
ss-SO_4	-.461*	.778**	-.493**	-.592**	1																
Na	-.461*	.778**	-.493**	-.592**	1.000**	1															
NH_4	.883**	-.505**	.749**	.844**	-.622**	-.622**	1														
K	.516**	-0.225	.628**	.631**	-.381*	-.381*	.540**	1													
Mg	-.476**	.437*	-0.212	-0.334	.478**	.478**	-.420*	0.026	1												
Ca	-0.116	.546**	0.016	-0.102	0.205	0.205	-0.159	-0.199	-0.023	1											
Al	0.034	-0.096	-0.059	0.157	-0.179	-0.179	0.026	-0.107	-0.117	-0.1	1										
V	0.314	-0.09	0.366	.421*	-0.331	-0.331	0.24	0.345	-0.17	0.21	0.014	1									
Cr	-0.109	0.245	-0.272	-0.144	0.212	0.212	-0.136	-0.34	0.125	0.12	-0.059	0.086	1								
Mn	.431*	0.069	0.071	0.337	-0.273	-0.273	0.139	0.073	-0.243	0.023	0.192	0.209	0.066	1							
Fe	0.303	-0.027	0.065	0.261	-0.288	-0.288	0.11	-0.046	-0.222	0.005	0.185	0.229	0.213	.884**	1						
Ni	.629**	-0.196	.585**	.637**	-.442*	-.442*	.527**	.487**	-0.204	-0.014	0.174	.803**	0.118	.403*	.388*	1					
Cu	.375*	-.392*	.446*	0.189	-0.317	-0.317	0.352	0.215	-0.276	-0.296	-0.187	0.035	-0.26	-0.029	-0.04	0.235	1				
Zn	0.151	0.172	-0.105	0.037	-0.094	-0.094	-0.12	0.209	-0.11	-0.066	-0.007	0.154	0.028	.633**	.379*	0.175	-0.067	1			
Cd	0.153	.373*	-0.065	0.024	0.08	0.08	-0.167	0.286	0.111	-0.07	0.064	0.077	-0.022	.648**	.461*	0.178	-0.068	.816**	1		
Sb	0.274	-0.31	0.26	0.149	-0.14	-0.14	0.279	0.166	-0.204	-0.26	-0.11	-0.04	-0.213	-0.193	-0.254	0.118	.703**	-0.132	-0.114	1	
Ba	.710**	-0.326	0.363	.583**	-.401*	-.401*	.604**	0.364	-367*	-0.188	0.15	0.293	-0.132	.496**	.425*	.578**	.444*	0.1	0.145	.416*	1
Pb	.383*	-0.221	0.195	0.271	-.414*	-.414*	0.24	0.299	-0.339	-0.235	0.167	0.11	-0.149	.588**	.549**	0.287	0.199	.464*	.538**	0.169	.514*

(b) $PM_{2.5-10}$

	$PM_{2.5-10}$	Cl	NO_3	nss-SO_4	ss-SO_4	Na	NH_4	K	Mg	Ca	Al	V	Cr	Mn	Fe	Ni	Cu	Zn	Sb	Ba	Pb
$PM_{2.5-10}$	1																				
Cl	.689**	1																			
NO_3	-0.174	0.21	1																		
nss-SO_4	0.049	0.083	0.182	1																	
ss-SO_4	.838**	.826**	-0.228	0.147	1																
Na	.838**	.826**	-0.228	0.147	1.000**	1															
NH_4	-0.145	0.29	.747**	-0.169	-0.253	-0.253	1														
K	.401*	0.326	0.186	0.212	.397*	.397*	-0.158	1													
Mg	.950**	.717**	-0.292	0.023	.913**	.913**	-0.239	.455*	1												
Ca	.850**	0.356	-0.176	-0.093	.506**	.506**	-0.116	.398*	.777**	1											
Al	.467*	0.319	-0.004	0.059	.408*	.408*	-0.124	0.152	.408*	0.362	1										
V	.850**	.498**	0.011	0.108	.562**	.562**	-0.001	.420*	.751**	.913**	.448*	1									
Cr	0.092	-0.183	-0.101	0.06	-0.059	-0.059	-0.23	0.027	0.019	0.282	0.162	0.221	1								
Mn	.908**	.462*	-0.14	0.015	.604**	.604**	-0.132	.395*	.823**	.942**	.456*	.947**	0.279	1							
Fe	.895**	.487**	-0.185	-0.073	.635**	.635**	-0.148	0.294	.783**	.826**	.428*	.809**	0.191	.895**	1						
Ni	.764**	.556**	-0.156	0.201	.680**	.680**	-0.137	.415*	.738**	.632**	0.171	.645**	0.08	.690**	.643**	1					
Cu	0.051	-0.119	-0.036	0.186	-0.064	-0.064	-0.045	-0.234	-0.032	0.106	-0.001	0.113	0.292	0.103	0.012	0.074	1				
Zn	.813**	0.348	-0.191	-0.132	.486**	.486**	-0.093	0.245	.747**	.884**	.375*	.853**	0.235	.941**	.813**	.588**	0.135	1	0.353		
Sb	0.15	-0.257	0.042	0.346	-0.17	-0.17	-0.014	-0.188	-0.031	0.246	0.235	0.319	0.141	0.31	0.251	0.219	.502**	0.353	1		
Ba	.620**	0.127	0.027	0.139	0.198	0.198	0.062	0.08	.438*	.715**	.375*	.750**	0.224	.770**	.674**	.533**	.414*	.786**	.784**	1	
Pb	0.333	0.486	-0.04	0.408	0.449	0.449	0.19	-0.067	0.373	0.045	0.034	0.122	-0.128	0.16	0.249	0.15	-0.059	0.057	-0.309	0.01	1

Appendix XVII

Little Warren Pearson's Correlation Coeffients for

(a) $PM_{2.5}$

LW	$PM_{2.5}$	Cl	NO_3	nss-SO_4	ss-SO_4	Na	NH_4	K	Mg	Ca	Al	V	Cr	Mn	Fe	Ni	Cu	Zn	Cd	Sb	Ba	Pb
PM2.5	1																					
Cl	0.132	1																				
NO3	.719**	-0.169	1																			
nss-SO_4	.568**	-0.188	.695**	1																		
ss-SO_4	-0.023	.788**	-0.235	-0.241	1																	
Na	-0.023	.788**	-0.235	-0.241	1.00**	1																
NH_4	.681**	-.468*	.758**	.728**	-.385*	-.385*	1															
K	.664**	0.175	.580**	.458*	0.007	0.007	0.348	1														
Mg	0.141	.887**	-0.334	-0.273	.770**	.770**	-.438*	0.146	1													
Ca	0.148	0.315	0.31	-0.029	0.177	0.177	-0.025	0.294	0.045	1												
Al	-0.038	0.032	-0.039	-0.141	0.111	0.111	-0.032	-0.165	0.099	0.169	1											
V	0.349	-0.231	.425*	0.187	-0.317	-0.317	0.29	0.218	-0.286	0.311	0.103	1										
Cr	0.067	-.448*	0.214	0.106	-0.327	-0.327	.383*	-0.154	-.367*	-0.367	0.012	-0.096	1									
Mn	.412*	.491**	-0.006	0.123	0.247	0.247	-0.141	.542**	.586**	0.041	-0.092	0.039	-0.205	1								
Fe	.379*	.533**	-0.102	-0.005	0.277	0.277	-0.187	0.367	.656**	0.071	-0.086	-0.052	-0.164	.871**	1							
Ni	.682**	-0.113	.637**	.513**	-0.31	-0.31	.546**	.436*	-0.173	0.297	0.184	.714**	-0.014	0.181	0.055	1						
Cu	.727**	.393*	0.366	0.367	0.177	0.177	0.235	.657**	.438*	0.112	-0.149	0.052	0.064	.771**	.706**	.474**	1					
Zn	.412*	.594**	0.005	0.16	0.324	0.324	-0.178	.529**	.631**	0.061	-0.1	-0.034	-0.304	.940**	.819**	0.163	.753**	1				
Cd	0.349	.637**	-0.087	0.075	0.366	0.366	-0.258	.500**	.683**	0.088	-0.075	-0.128	-0.353	.853**	.821**	0.091	.716**	.943**	1			
Sb	.704**	-0.087	.522**	.452*	-0.059	-0.059	.644**	.414*	0.006	0.001	-0.021	0.154	0.35	0.304	0.27	.503**	.613**	0.238	0.195	1		
Ba	.765**	-0.007	.704**	.631**	-0.047	-0.047	.669**	.472**	-0.016	0.044	-0.115	0.318	.382*	0.29	0.241	.600**	.672**	0.207	0.093	.697**	1	
Pb	.506**	.599**	0.046	0.213	0.333	0.333	-0.079	.480**	.641**	-0.002	-0.133	-0.108	-0.192	.818**	.840**	0.176	.793**	.893**	.944**	.381*	0.279	1

(b) $PM_{2.5-10}$

LW	$PM_{2.5-10}$	Cl	NO_3	nss-SO_4	ss-SO_4	Na	NH4	K	Mg	Ca	Al	V	Cr	Mn	Fe	Ni	Cu	Zn	Sb	Ba	Pb
$PM_{2.5-10}$	1																				
Cl	.580**	1																			
NO_3	-0.117	-0.238	1																		
nss-SO_4	0.272	0.306	.528**	1																	
ss-SO_4	.590**	.982**	-0.253	0.284	1																
Na	.590**	.982**	-0.253	0.284	1.000**	1															
NH_4	-0.17	-0.235	0.182	0.219	-0.131	-0.131	1														
K	0.205	0.059	0.244	0.076	0.072	0.072	-0.043	1													
Mg	.703**	.925**	-0.321	0.233	.932**	.932**	-0.154	0.087	1												
Ca	.384*	-0.06	-0.08	-0.192	-0.131	-0.131	-.385*	0.082	0.03	1											
Al	.397*	0.191	-0.271	0.125	0.182	0.182	0.129	-0.054	0.264	0.245	1										
V	.643**	-0.022	-0.208	-0.103	0.002	0.002	-0.1	0.142	0.202	.643**	.420*	1									
Cr	0.05	0.159	-0.247	-0.078	0.147	0.147	-0.064	0.081	0.136	-0.02	0.212	-0.056	1								
Mn	.567**	-0.148	-0.147	-0.003	-0.145	-0.145	-0.139	0.107	0.077	.679**	.453*	.929**	-0.169	1							
Fe	.577**	-0.112	-0.164	-0.059	-0.112	-0.112	-0.269	0.108	0.12	.704**	0.366	.902**	-0.148	.969**	1						
Ni	0.075	0.132	0.002	-0.154	0.065	0.065	-0.067	0.106	0.15	0.301	0.176	0.081	0.164	0.001	-0.02	1					
Cu	-0.049	-0.144	0.191	0.228	-0.159	-0.159	0.135	-0.099	-0.12	-0.087	0.113	0.084	0.062	0.086	0.05	.438*	1				
Zn	0.258	-0.036	-0.197	-0.173	-0.031	-0.031	-0.132	-0.022	0.07	.368*	0.256	.623**	0.166	.490**	.543**	-0.003	-0.049	1			
Sb	-0.172	-0.291	0.018	0.154	-0.29	-0.29	.430*	0.05	-0.318	-0.069	.477**	0.095	0.054	0.166	-0.004	0.215	.495**	-0.08	1		
Ba	.418*	-0.197	-0.076	0.091	-0.209	-0.209	0.035	0.04	-0.014	.570**	.539**	.813**	-0.073	.863**	.774**	0.239	.429*	.406*	.496**	1	
Pb	0.339	-0.318	-0.14	-0.263	-0.332	-0.332	-0.118	-0.009	-0.142	.796**	.387*	.872**	-0.098	.883**	.855**	0.126	0.089	.664**	0.198	.818**	1

Appendix XVIII

Analysis of Variance (ANOVA) for fine and coarse PM chemical compositions

	$PM_{2.5}$		$PM_{2.5-10}$	
	F values	**Significance**	**F values**	**Significance**
PM Mass	3.010	0.034*	4.514	0.005*
Cl	0.293	0.830	1.255	0.294
NO_3	2.461	0.067	4.807	0.004*
nss-SO_4	2.249	0.088	4.445	0.006*
Na	3.837	0.012*	2.696	0.050
NH_4	0.550	0.649	1.161	0.329*
K	1.834	0.146	2.080	0.108
Mg	2.031	0.115	0.851	0.470
Ca	0.642	0.642	4.383	0.006*
Al	2.267	0.086	2.563	0.059
V	0.875	0.457	3.831	0.012
Cr	3.176	0.028*	0.879	0.455
Mn	3.181	0.027	3.857	0.012
Fe	3.130	0.029	4.285	0.007
Ni	0.647	0.587	1.581	0.199
Cu	5.576	0.001	14.053	0.000
Zn	0.743	0.529	2.518	0.063
Cd	1.501	0.219	1.560	0.204
Sb	2.608	0.056	23.764	0.000
Ba	37.707	0.000	16.758	0.000
Pb	1.454	0.232	1.745	0.163

*Significance at $p<0.05$

Appendix XIX

Hourly elemental concentrations of Streaker PM at Fire Station (FS) site

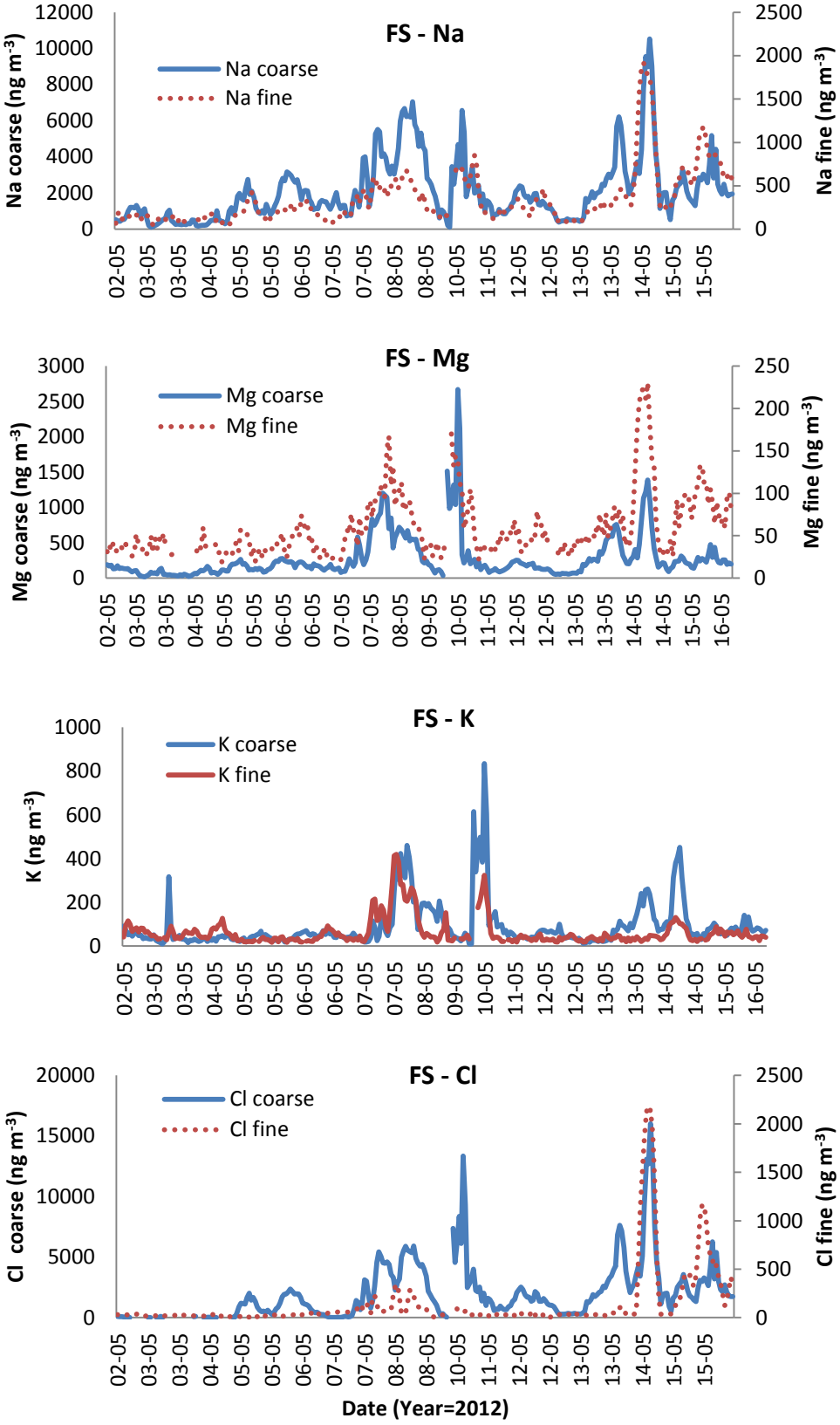

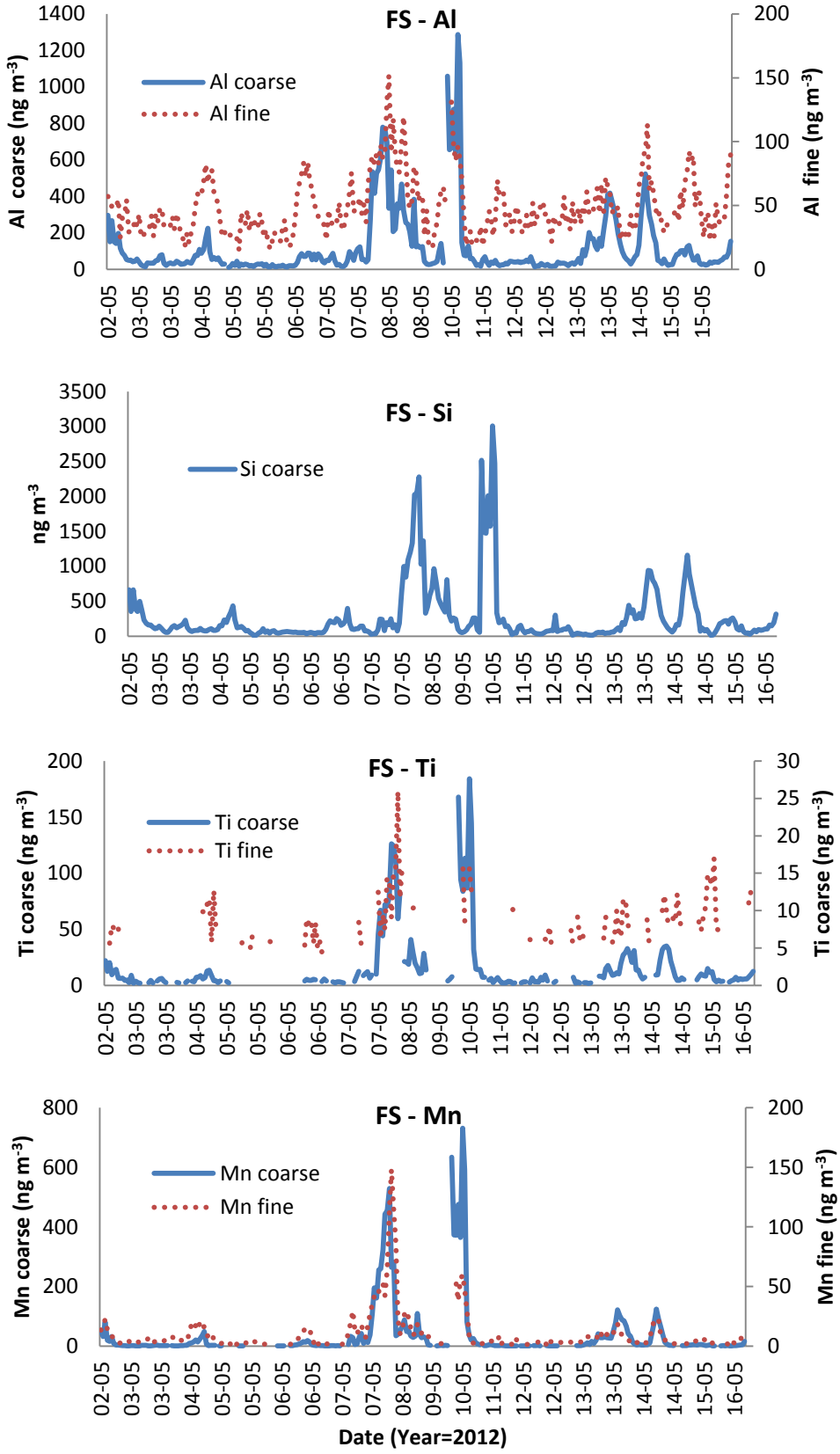
FS - Al
Al coarse
Al fine
Al coarse (ng m-3)
Al fine (ng m-3)
FS - Si
Si coarse
ng m-3
FS - Ti
Ti coarse
Ti fine
Ti coarse (ng m-3)
FS - Mn
Mn coarse
Mn fine
Mn coarse (ng m-3)
Mn fine (ng m-3)
Date (Year=2012)

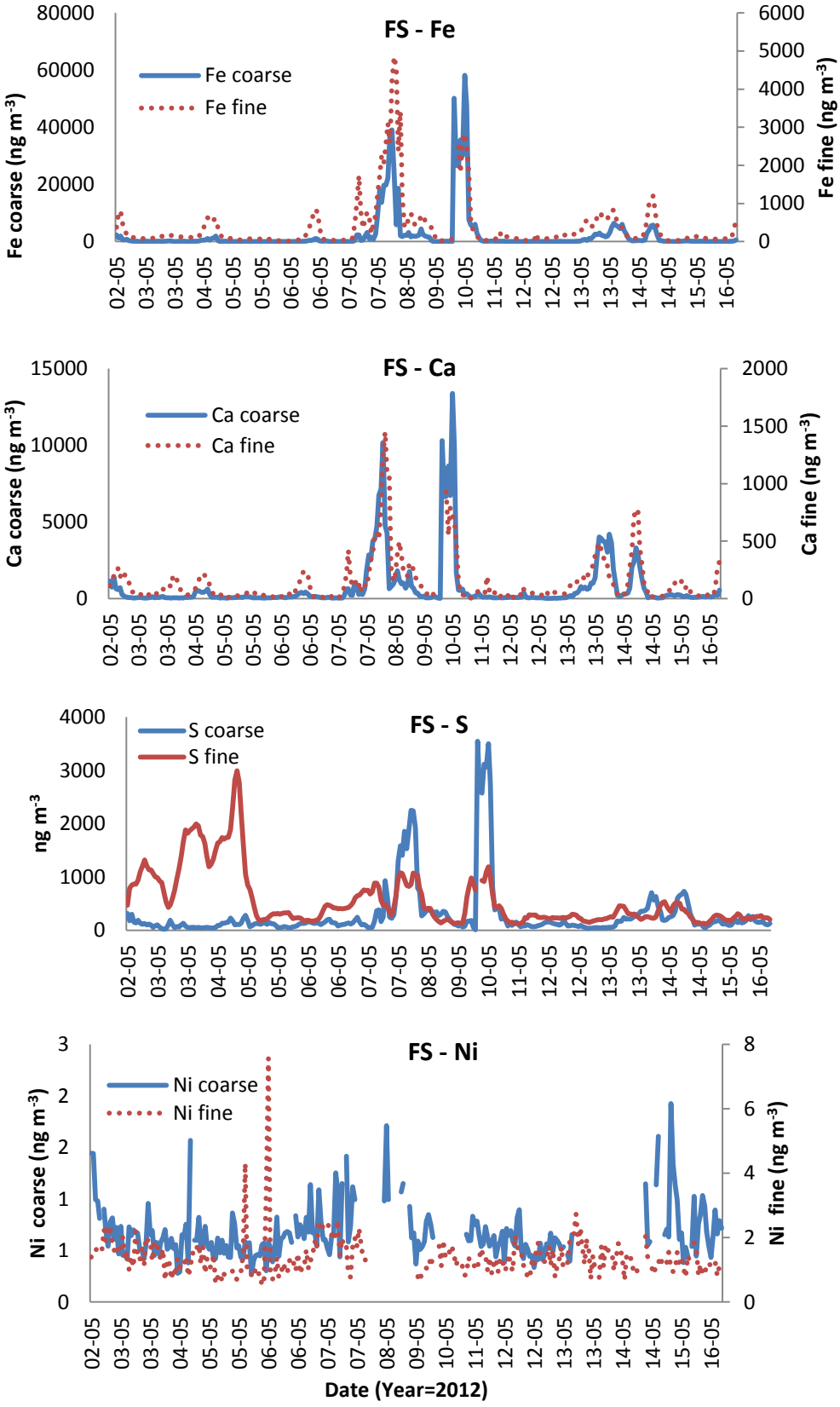
FS - Fe
Fe coarse
Fe fine
Fe coarse (ng m-3)
Fe fine (ng m-3)
FS - Ca
Ca coarse
Ca fine
Ca coarse (ng m-3)
Ca fine (ng m-3)
FS - S
S coarse
S fine
ng m-3
FS - Ni
Ni coarse
Ni fine
Ni coarse (ng m-3)
Ni fine (ng m-3)
Date (Year=2012)

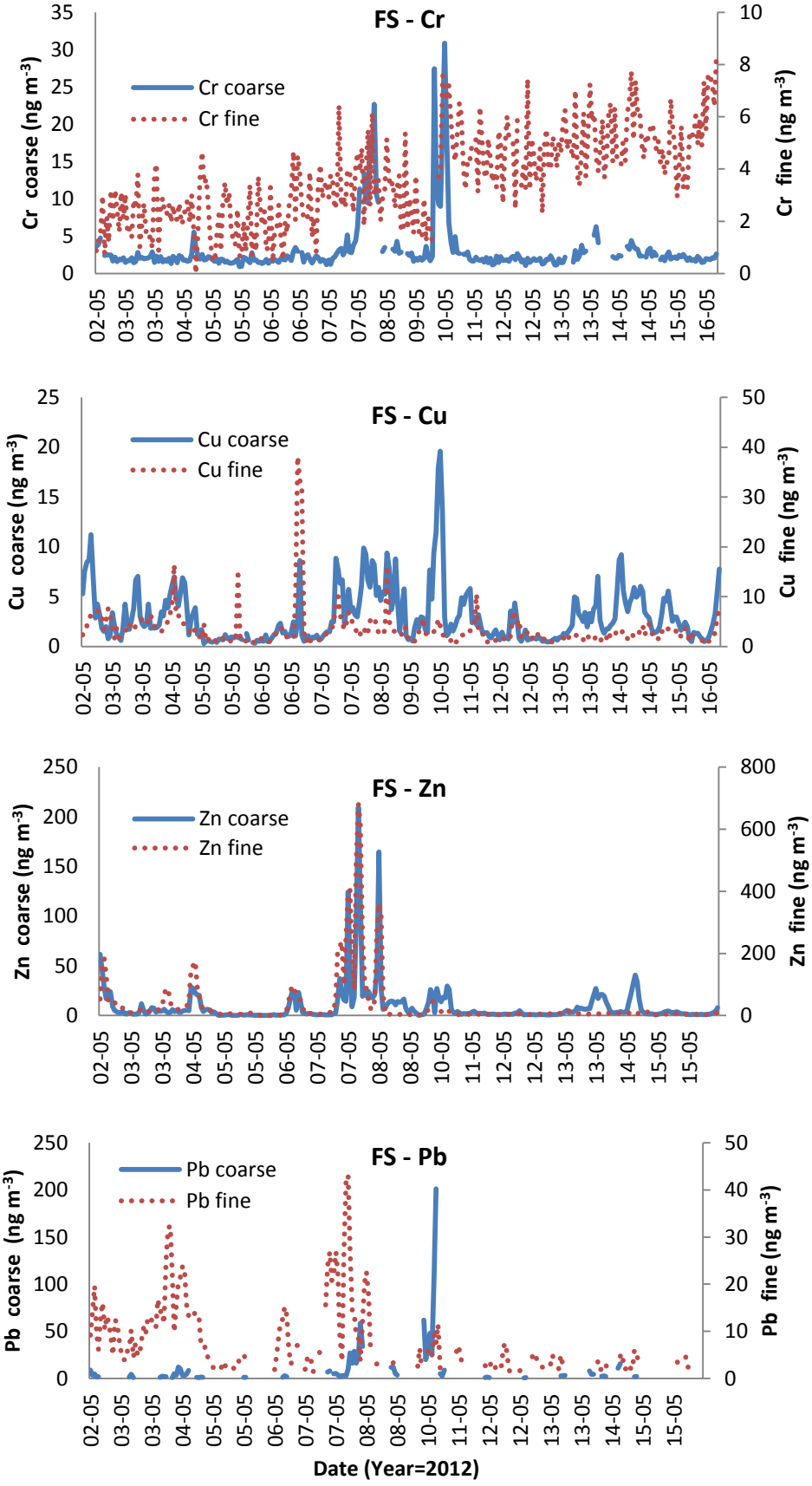
FS - Cr
Cr coarse
Cr fine
Cr coarse (ng m-3)
Cr fine (ng m-3)
FS - Cu
Cu coarse
Cu fine
Cu coarse (ng m-3)
Cu fine (ng m-3)
FS - Zn
Zn coarse
Zn fine
Zn coarse (ng m-3)
Zn fine (ng m-3)
FS - Pb
Pb coarse
Pb fine
Pb coarse (ng m-3)
Pb fine (ng m-3)
Date (Year=2012)

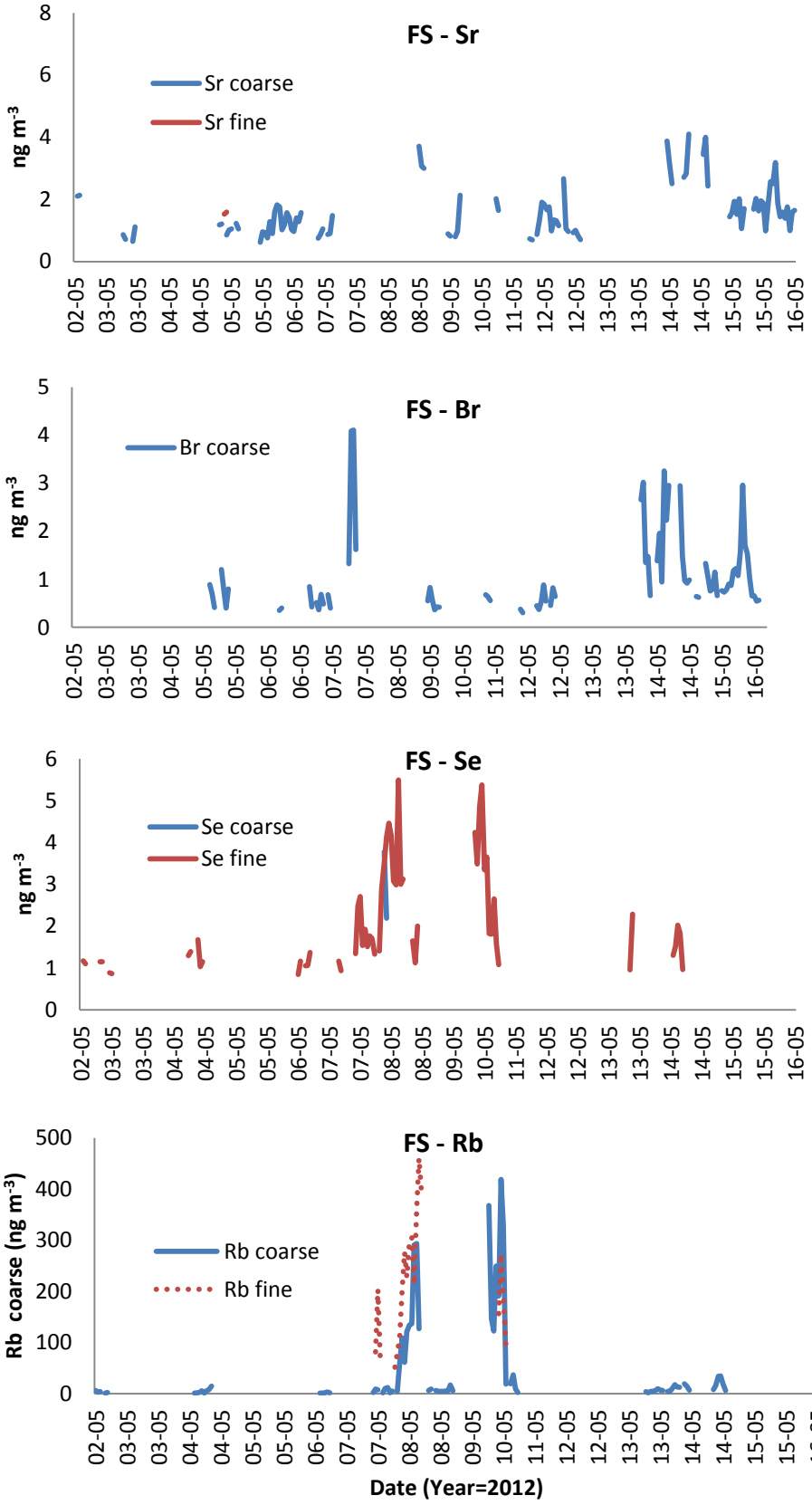
FS - Sr
Sr coarse
Sr fine
ng m-3
FS - Br
Br coarse
FS - Se
Se coarse
Se fine
FS - Rb
Rb coarse
Rb fine
Rb coarse (ng m-3)
Rb fine (ng m-3)
Date (Year=2012)

Appendix XX

Hourly elemental concentrations of Streaker PM at Little Warren (LW) site

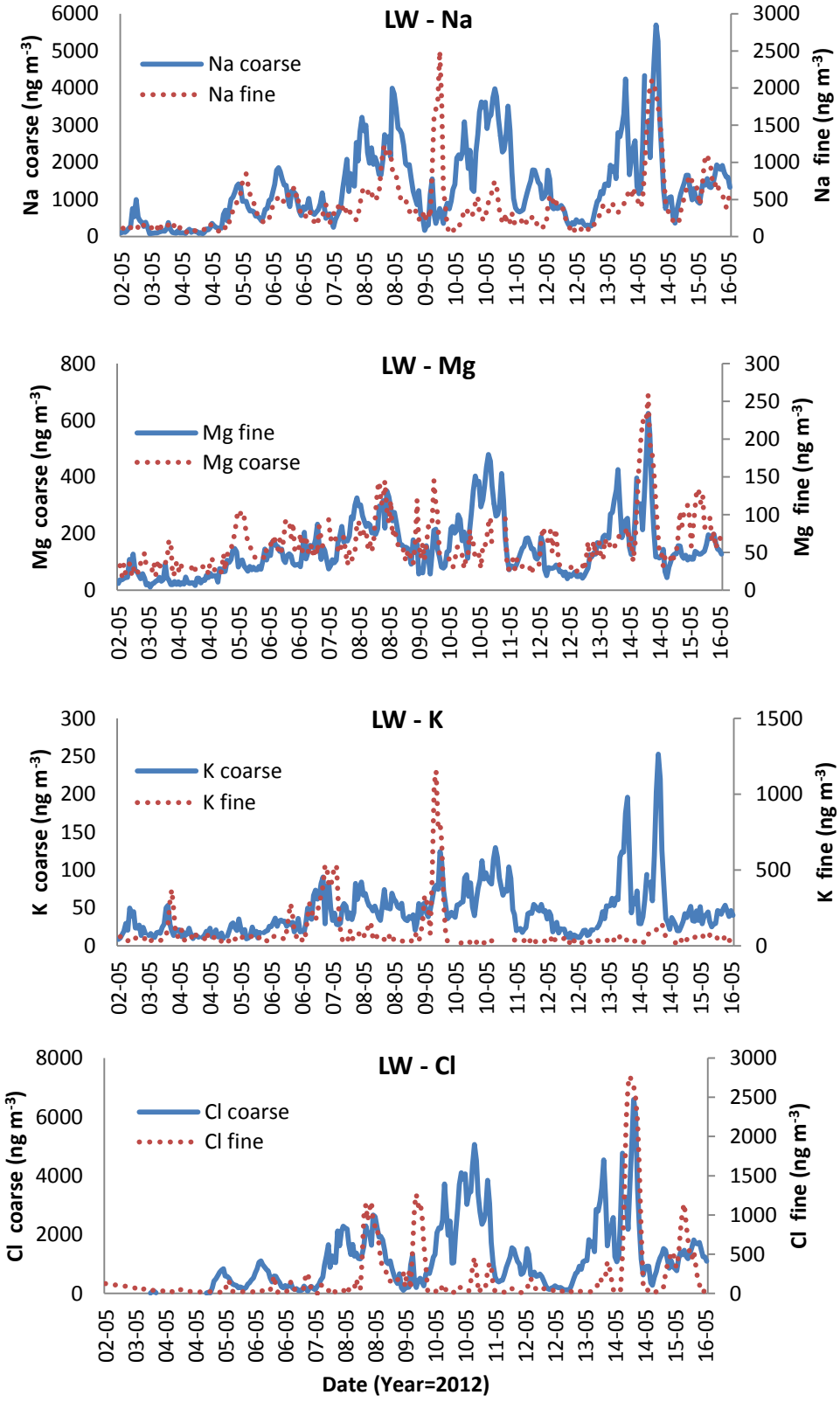

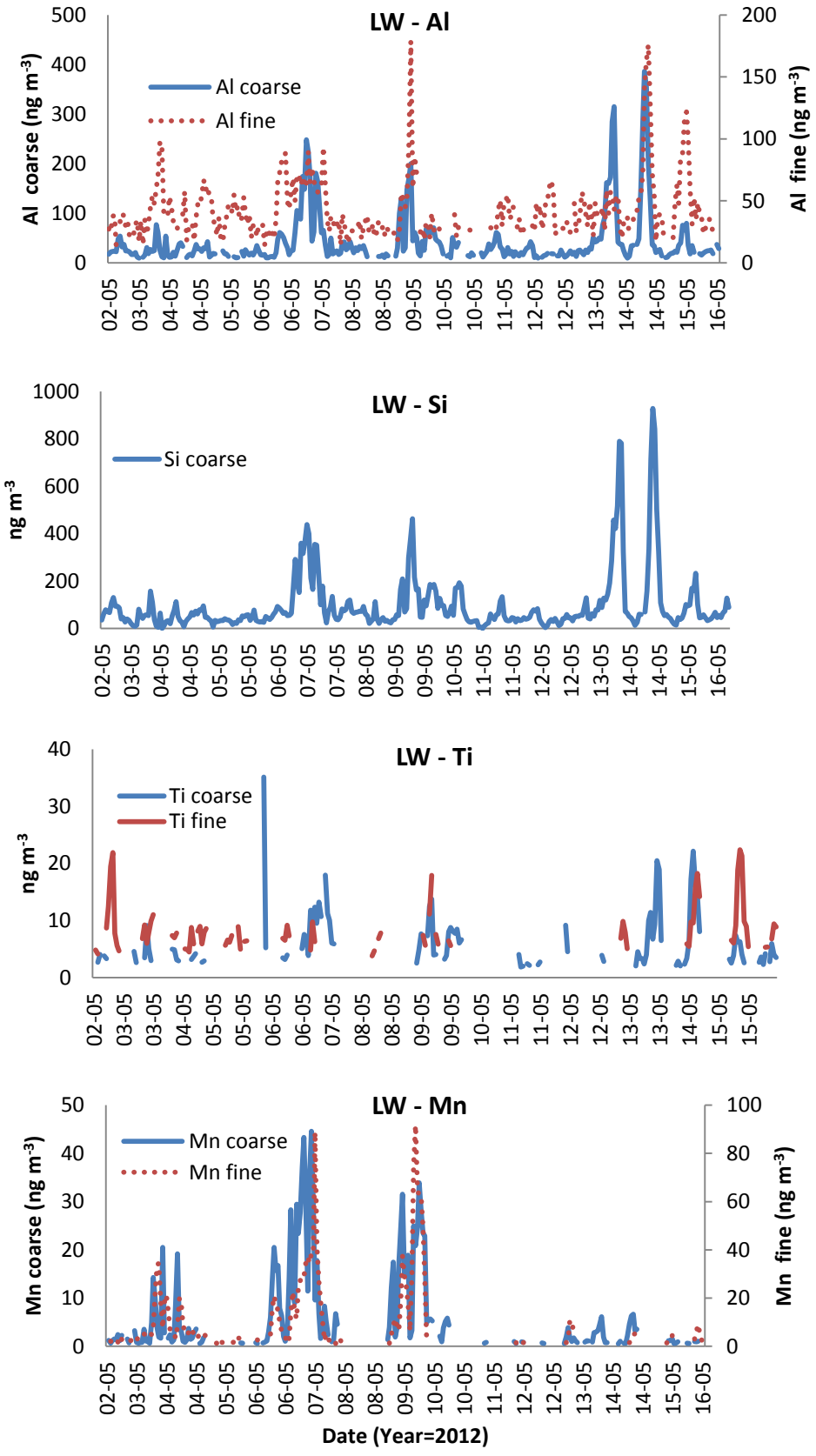
LW - Al
Al coarse
Al fine
Al coarse (ng m-3)
Al fine (ng m-3)
LW - Si
Si coarse
ng m-3
LW - Ti
Ti coarse
Ti fine
ng m-3
LW - Mn
Mn coarse
Mn fine
Mn coarse (ng m-3)
Mn fine (ng m-3)
Date (Year=2012)

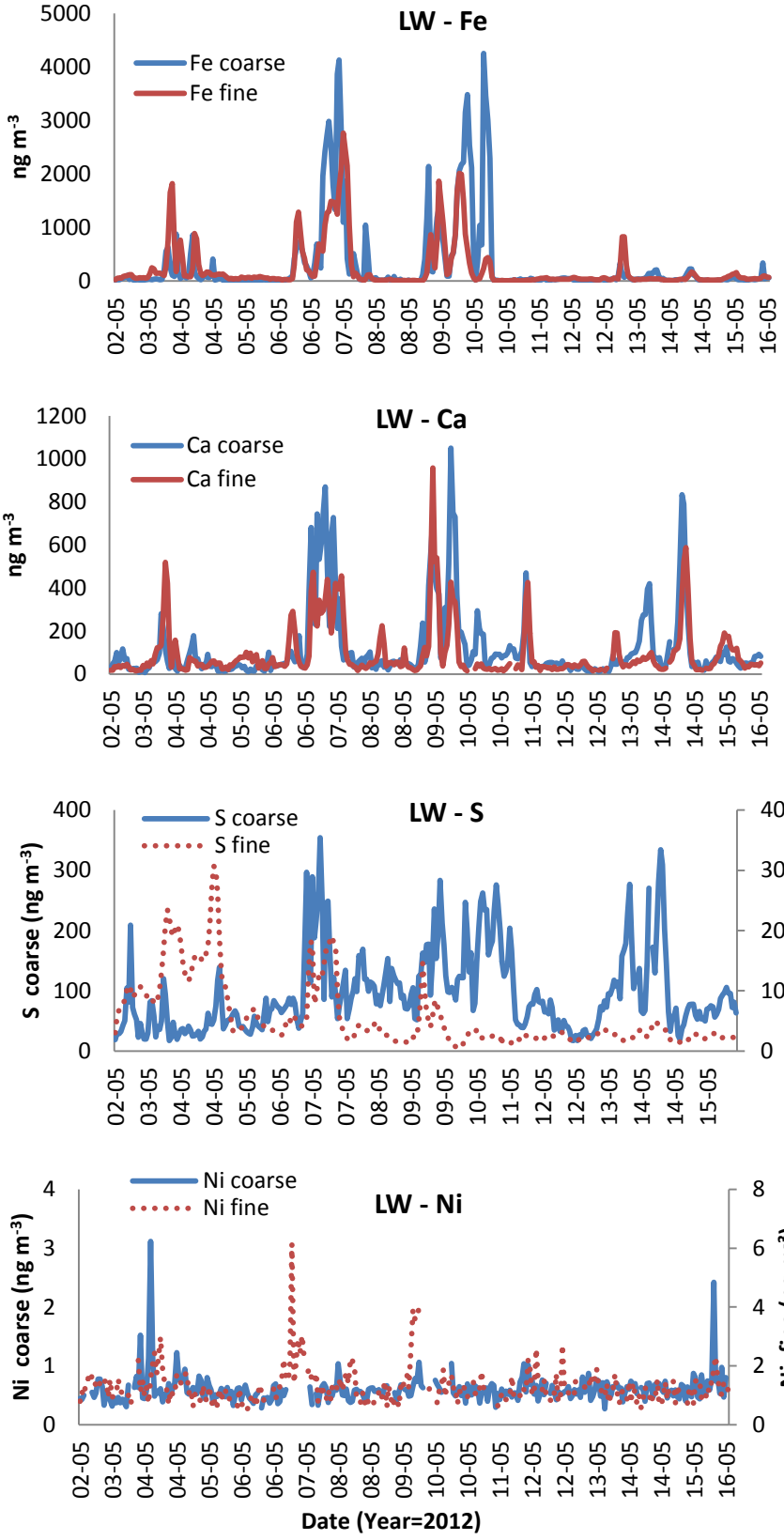
LW - Fe
Fe coarse
Fe fine
ng m-3
LW - Ca
Ca coarse
Ca fine
ng m-3
LW - S
S coarse
S fine
S coarse (ng m-3)
S fine (ng m-3)
LW - Ni
Ni coarse
Ni fine
Ni coarse (ng m-3)
Ni fine (ng m-3)
Date (Year=2012)

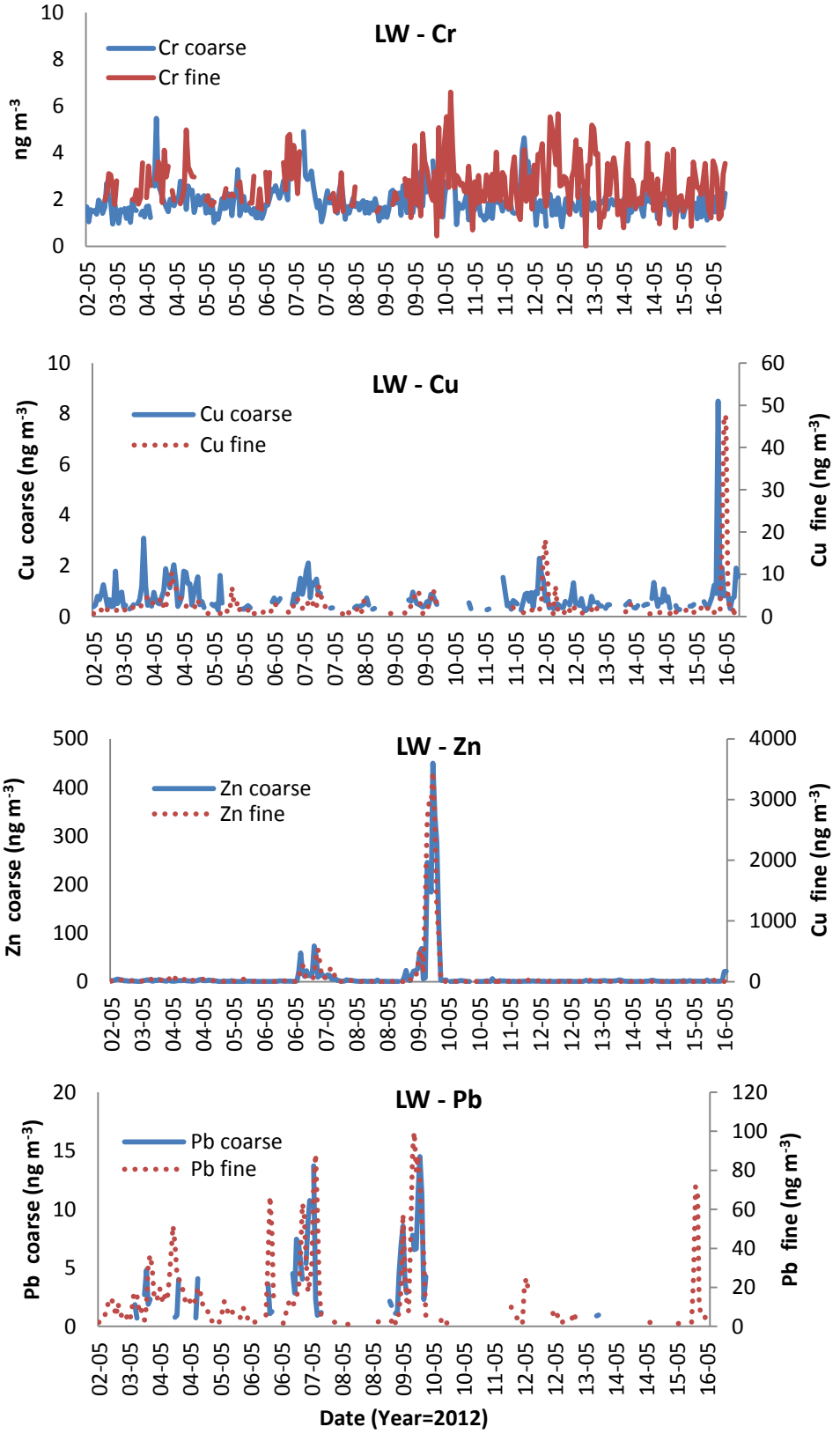
LW - Cr
Cr coarse
Cr fine
ng m-3
LW - Cu
Cu coarse
Cu fine
Cu coarse (ng m-3)
Cu fine (ng m-3)
LW - Zn
Zn coarse
Zn fine
Zn coarse (ng m-3)
Cu fine (ng m-3)
LW - Pb
Pb coarse
Pb fine
Pb coarse (ng m-3)
Pb fine (ng m-3)
Date (Year=2012)

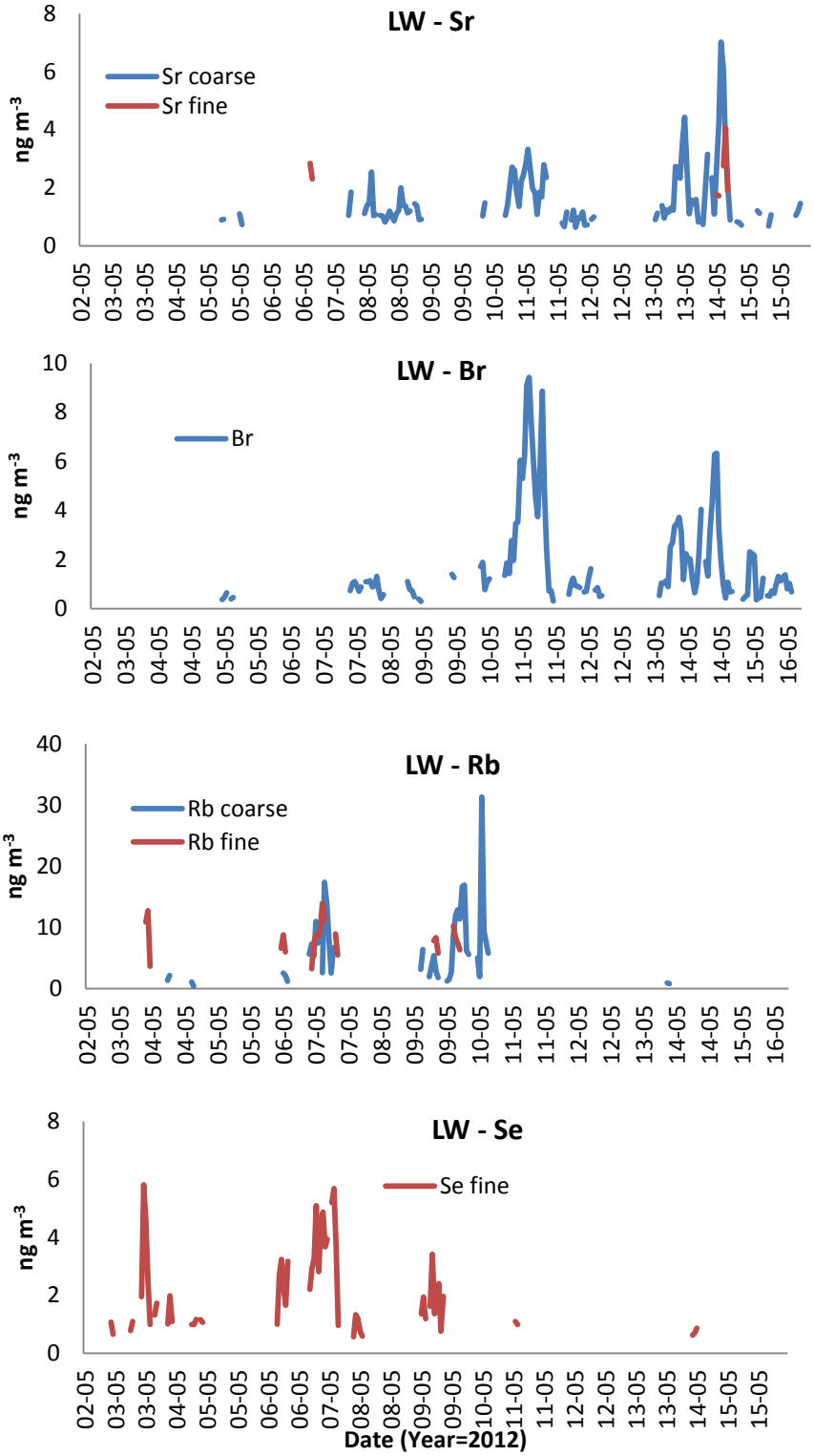
LW - Sr
Sr coarse
Sr fine
ng m-3
LW - Br
Br
LW - Rb
Rb coarse
Rb fine
LW - Se
Se fine
Date (Year=2012)

Appendix XXI

Daily comparison of Partisol and Streaker $PM_{2.5}$ and $PM_{2.5-10}$ data at FS and LW

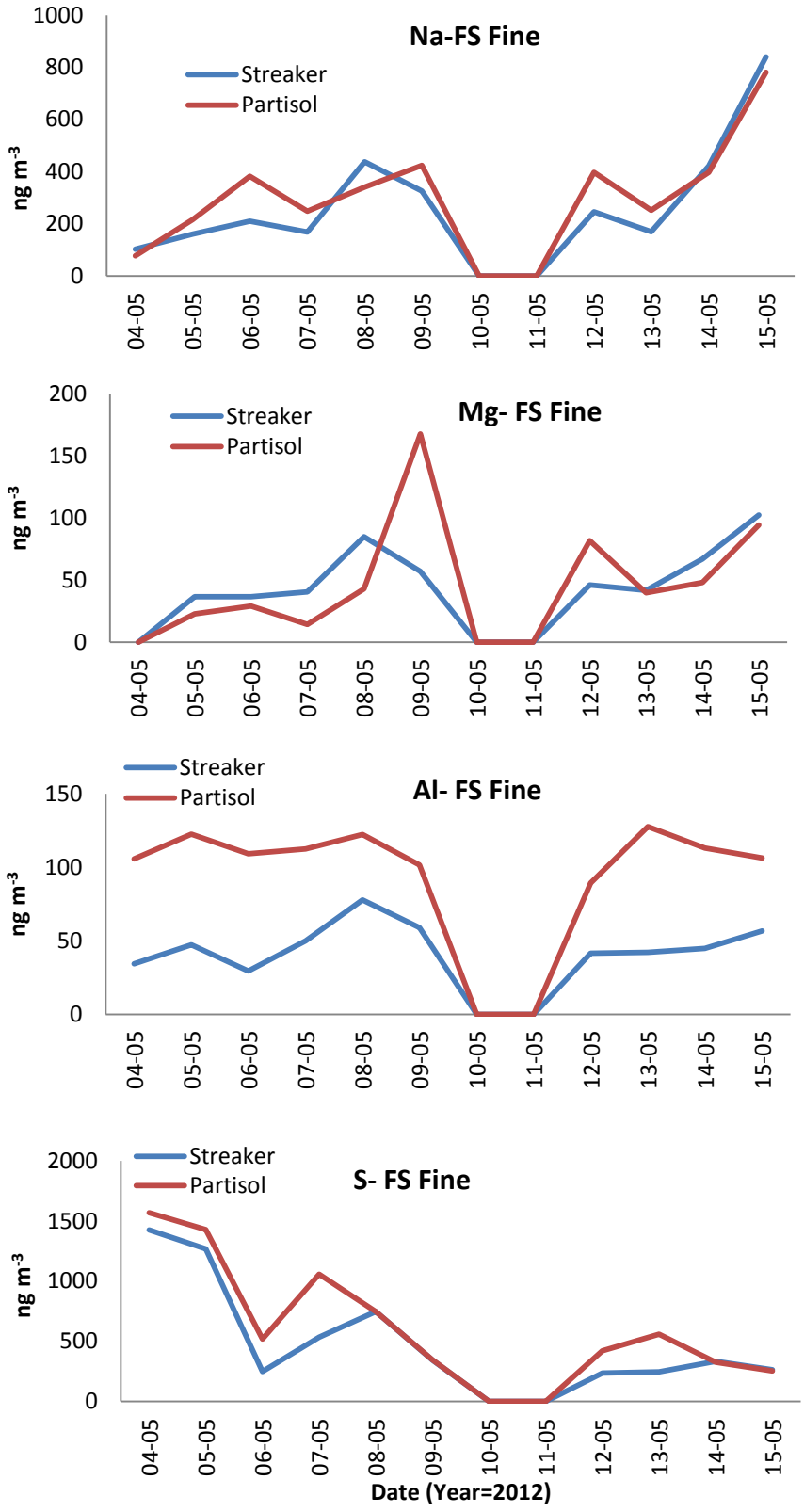

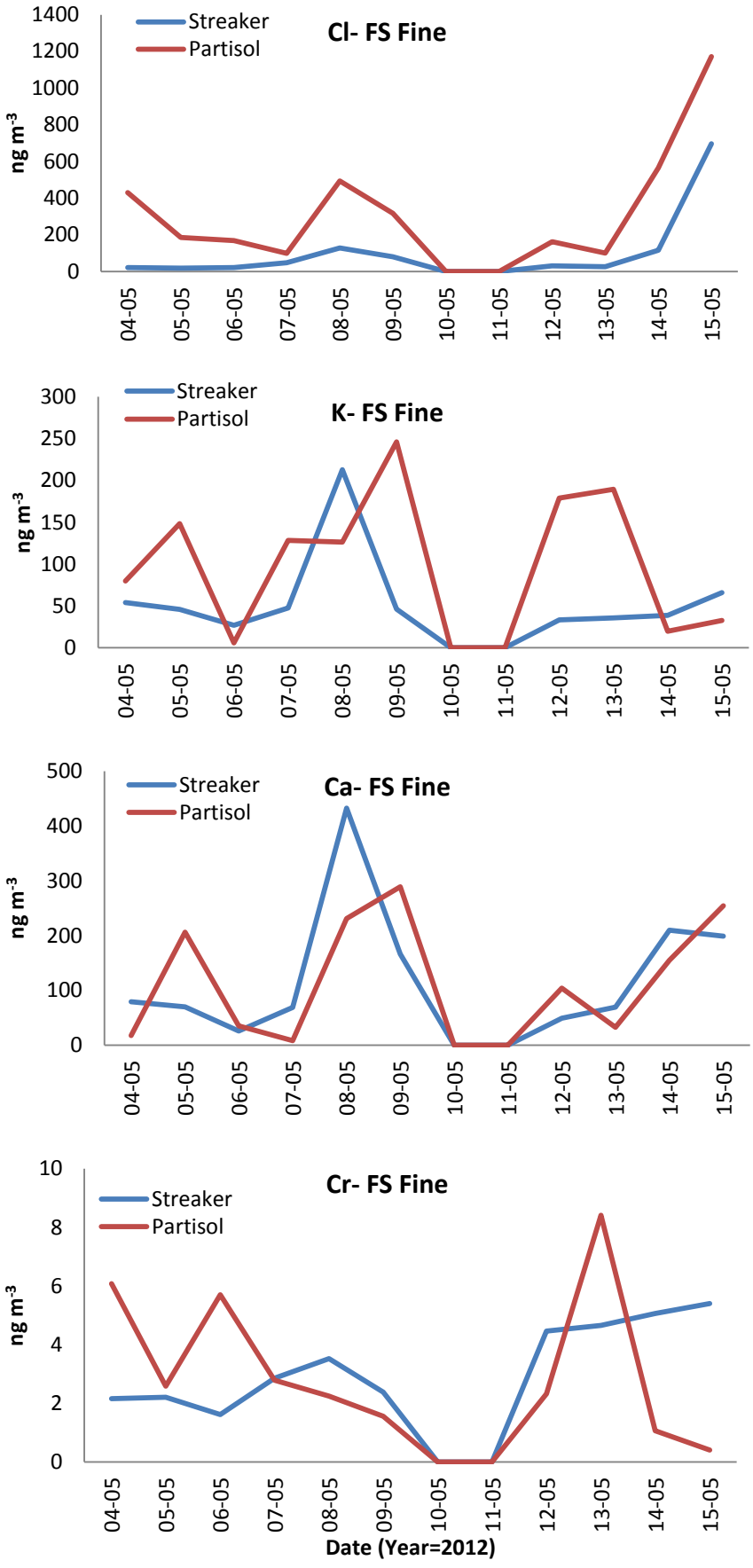
Cl- FS Fine
Streaker
Partisol
ng m-3
1400
1200
1000
800
600
400
200
0
04-05
05-05
06-05
07-05
08-05
09-05
10-05
11-05
12-05
13-05
14-05
15-05
K- FS Fine
Streaker
Partisol
ng m-3
300
250
200
150
100
50
0
Ca- FS Fine
Streaker
Partisol
ng m-3
500
400
300
200
100
0
Cr- FS Fine
Streaker
Partisol
ng m-3
10
8
6
4
2
0
Date (Year=2012)

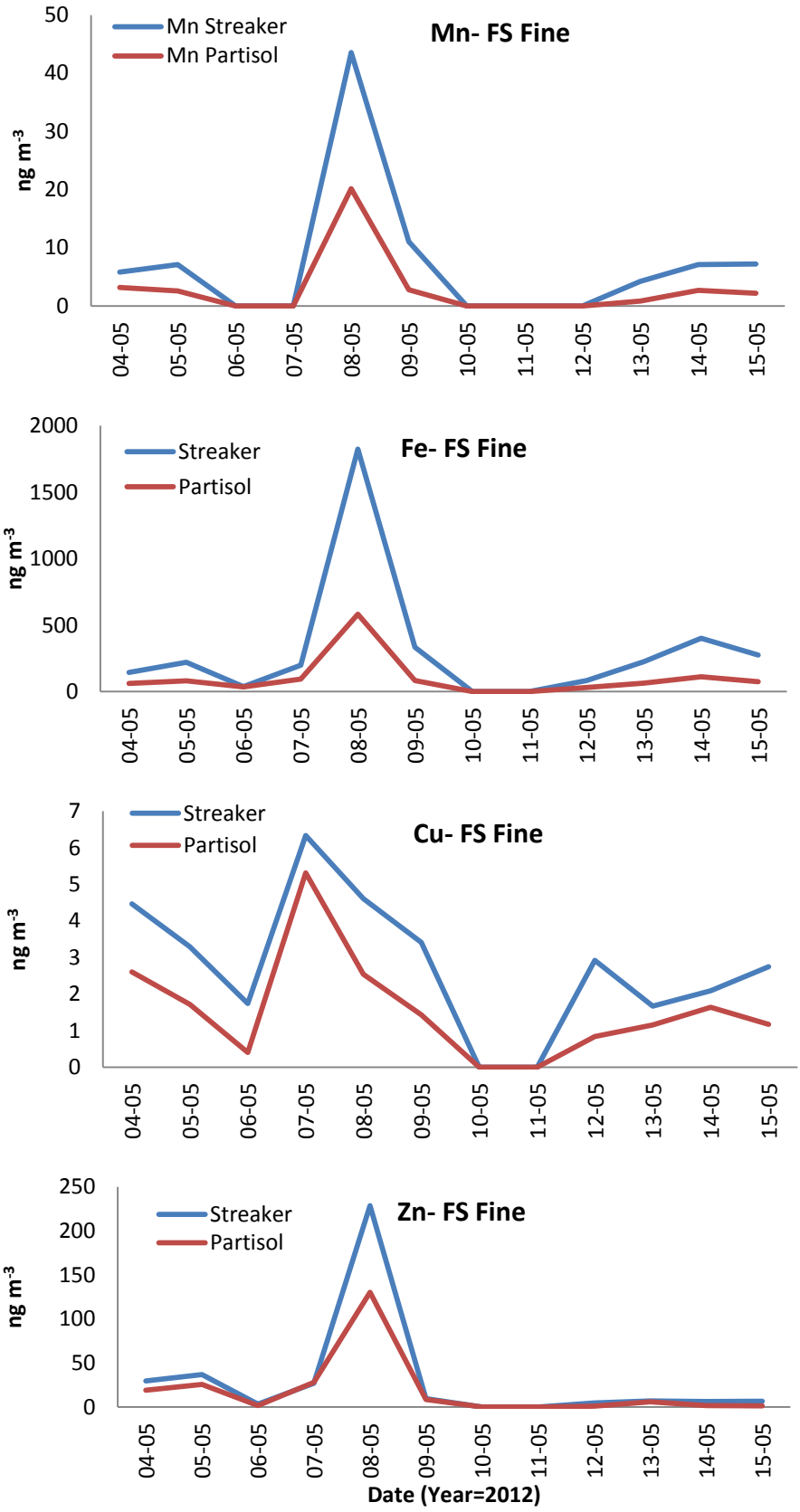
Mn- FS Fine
Mn Streaker
Mn Partisol
ng m-3
50
40
30
20
10
0
Fe- FS Fine
Streaker
Partisol
2000
1500
1000
500
0
Cu- FS Fine
7
6
5
4
3
2
1
0
Zn- FS Fine
250
200
150
100
50
0
04-05
05-05
06-05
07-05
08-05
09-05
10-05
11-05
12-05
13-05
14-05
15-05
Date (Year=2012)

(a) FS Fine

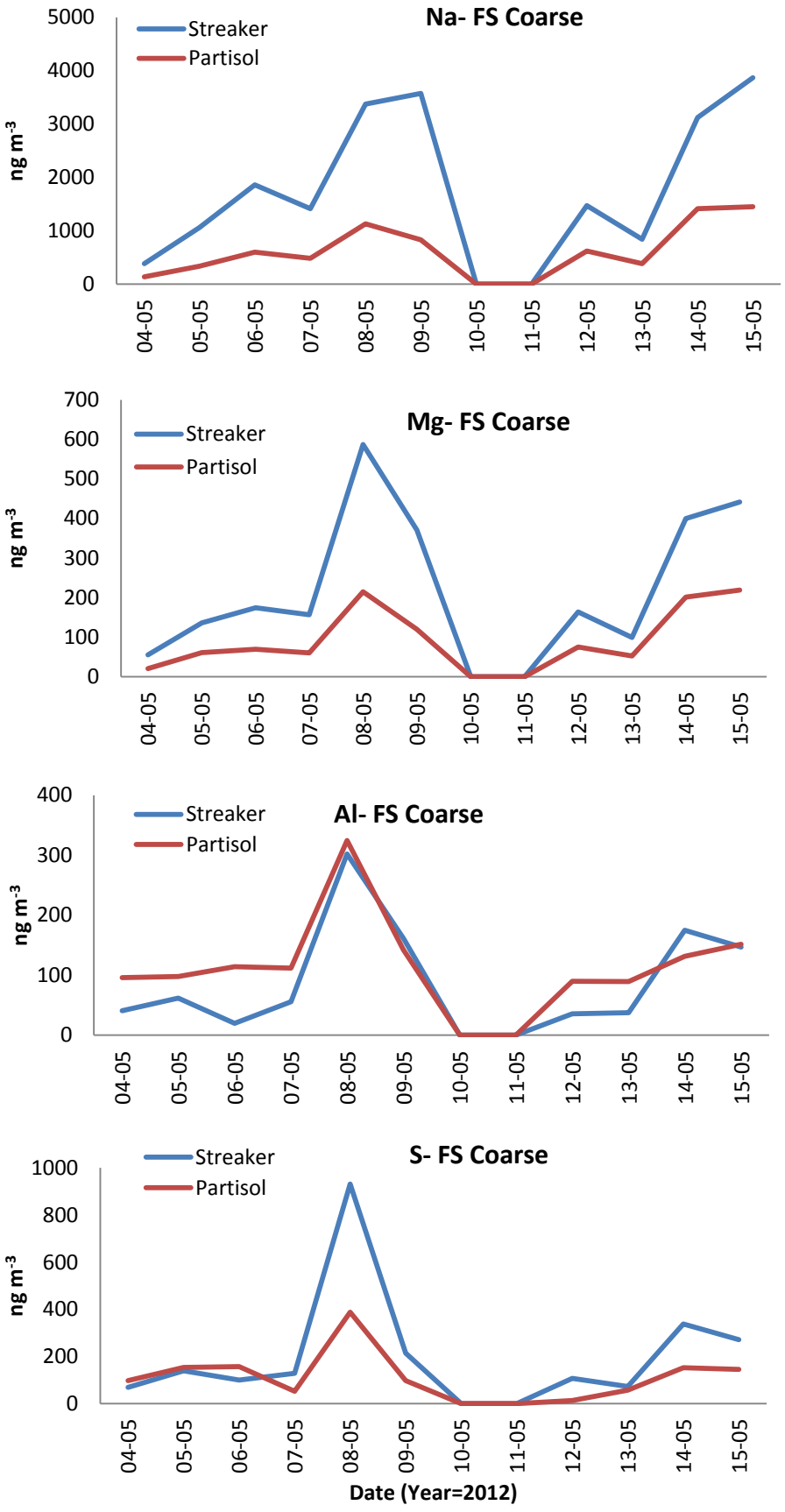
Na- FS Coarse
Streaker
Partisol
ng m-3
5000
4000
3000
2000
1000
0
04-05
05-05
06-05
07-05
08-05
09-05
10-05
11-05
12-05
13-05
14-05
15-05
Mg- FS Coarse
Streaker
Partisol
ng m-3
700
600
500
400
300
200
100
0
04-05
05-05
06-05
07-05
08-05
09-05
10-05
11-05
12-05
13-05
14-05
15-05
Al- FS Coarse
Streaker
Partisol
ng m-3
400
300
200
100
0
04-05
05-05
06-05
07-05
08-05
09-05
10-05
11-05
12-05
13-05
14-05
15-05
S- FS Coarse
Streaker
Partisol
ng m-3
1000
800
600
400
200
0
04-05
05-05
06-05
07-05
08-05
09-05
10-05
11-05
12-05
13-05
14-05
15-05
Date (Year=2012)

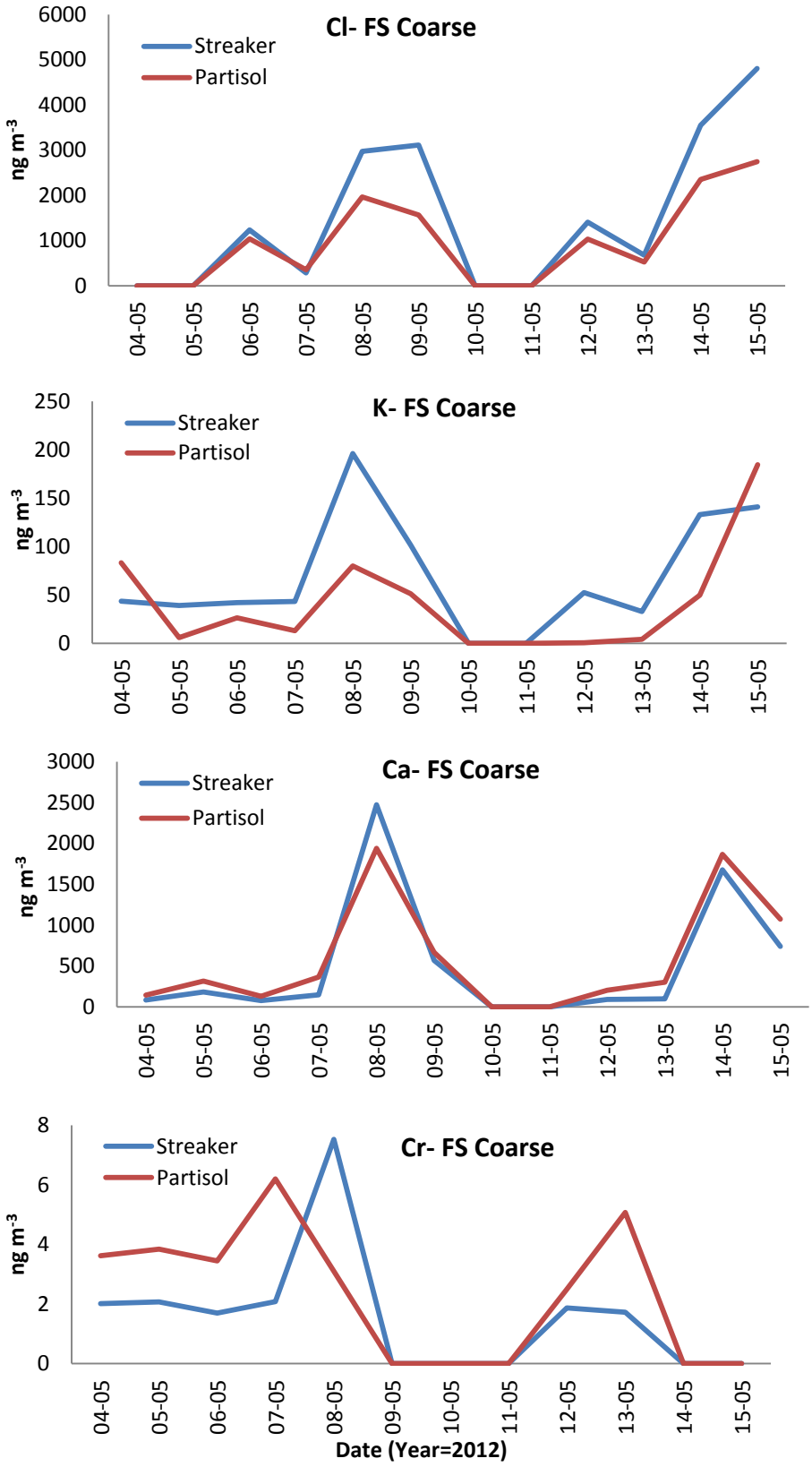
Cl- FS Coarse
Streaker
Partisol
ng m-3
6000
5000
4000
3000
2000
1000
0
04-05
05-05
06-05
07-05
08-05
09-05
10-05
11-05
12-05
13-05
14-05
15-05
K- FS Coarse
Streaker
Partisol
ng m-3
250
200
150
100
50
0
04-05
05-05
06-05
07-05
08-05
09-05
10-05
11-05
12-05
13-05
14-05
15-05
Ca- FS Coarse
Streaker
Partisol
ng m-3
3000
2500
2000
1500
1000
500
0
04-05
05-05
06-05
07-05
08-05
09-05
10-05
11-05
12-05
13-05
14-05
15-05
Cr- FS Coarse
Streaker
Partisol
ng m-3
8
6
4
2
0
04-05
05-05
06-05
07-05
08-05
09-05
10-05
11-05
12-05
13-05
14-05
15-05
Date (Year=2012)

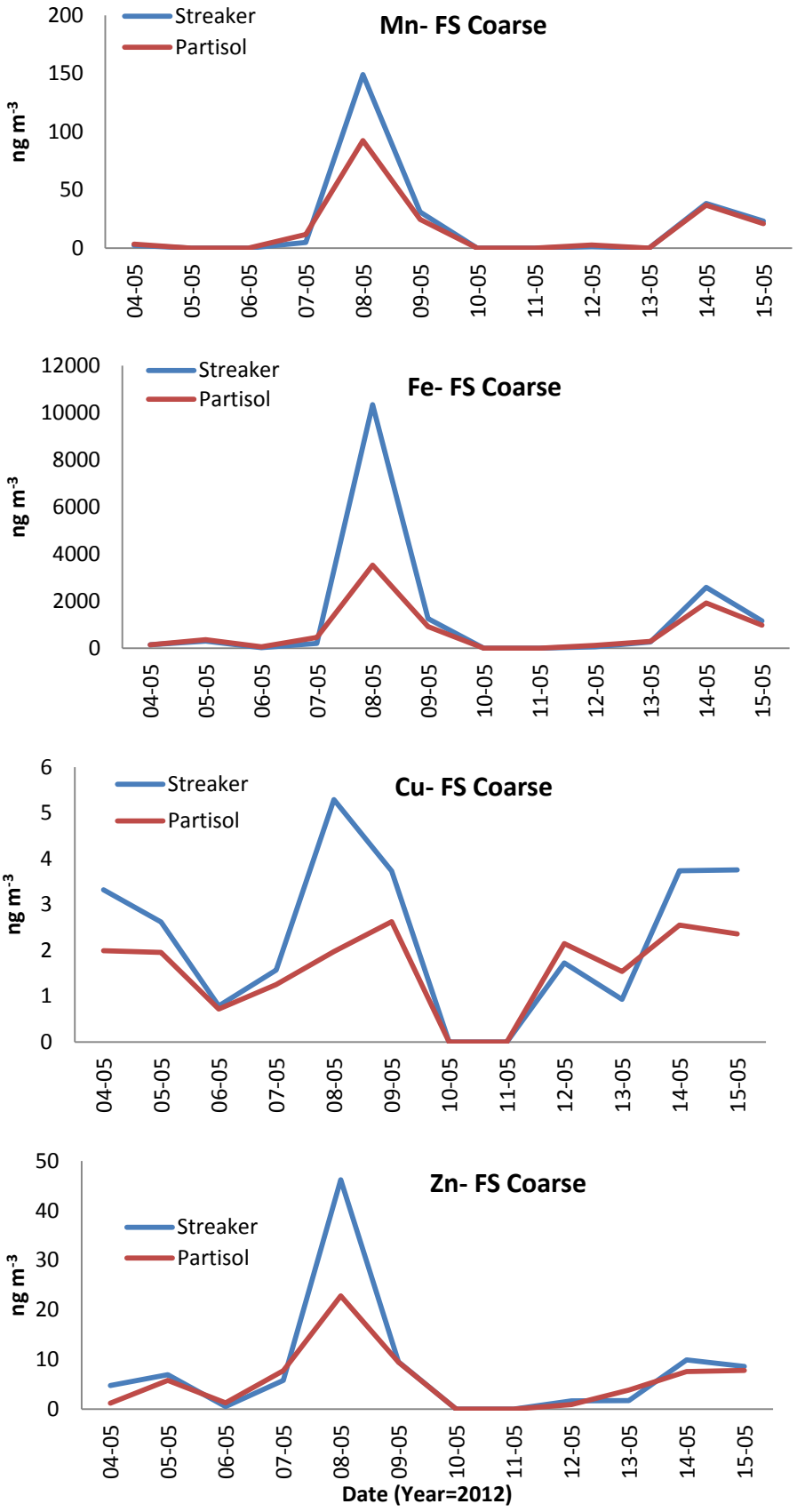
Mn- FS Coarse
Streaker
Partisol
ng m-3
200
150
100
50
0
04-05
05-05
06-05
07-05
08-05
09-05
10-05
11-05
12-05
13-05
14-05
15-05
Fe- FS Coarse
Streaker
Partisol
ng m-3
12000
10000
8000
6000
4000
2000
0
Cu- FS Coarse
Streaker
Partisol
ng m-3
6
5
4
3
2
1
0
Zn- FS Coarse
Streaker
Partisol
ng m-3
50
40
30
20
10
0
Date (Year=2012)

(b) FS Coarse

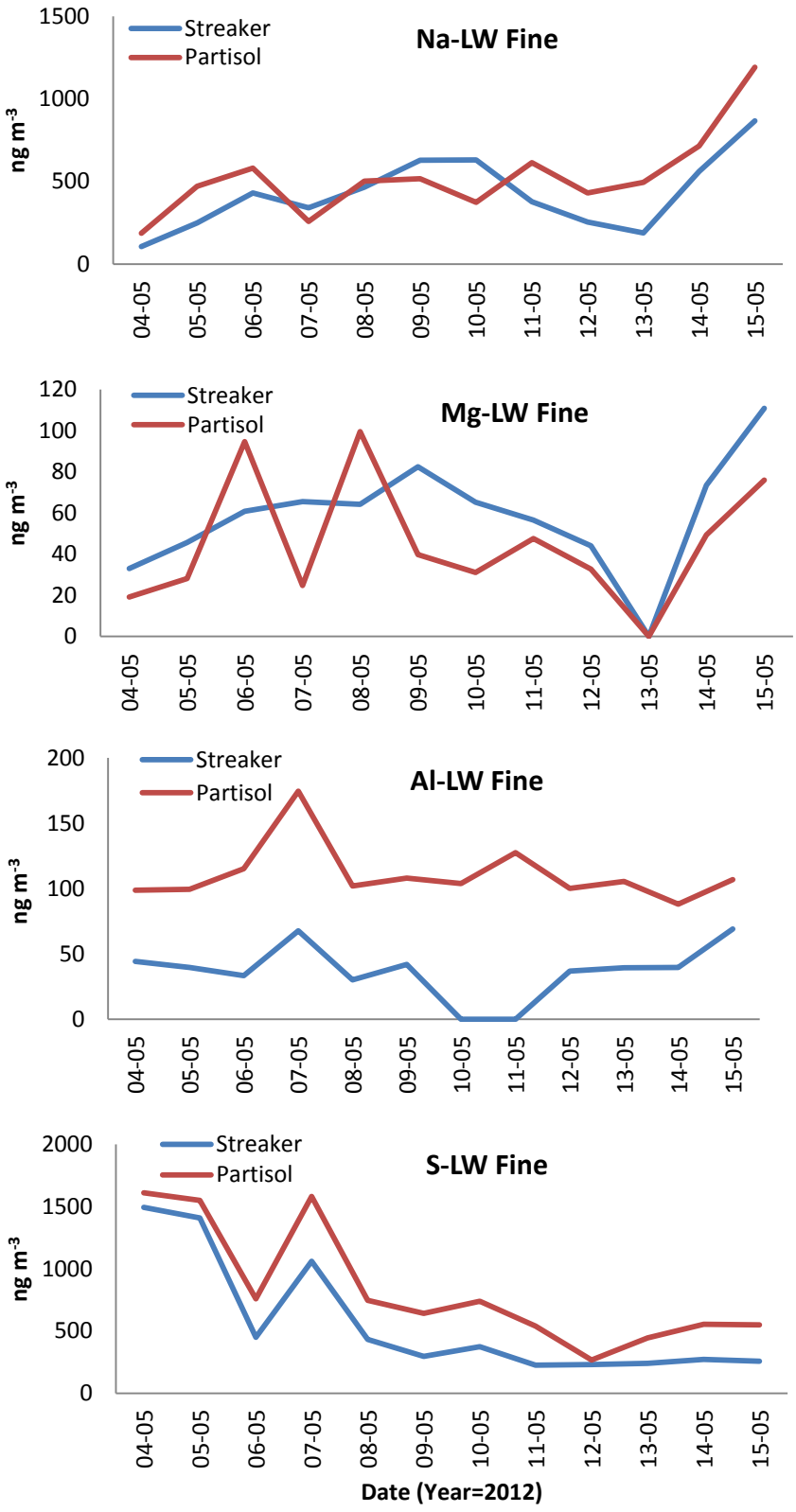
Na-LW Fine
Streaker
Partisol
ng m-3
1500
1000
500
0
Mg-LW Fine
120
100
80
60
40
20
Al-LW Fine
200
150
50
S-LW Fine
2000
04-05
05-05
06-05
07-05
08-05
09-05
10-05
11-05
12-05
13-05
14-05
15-05
Date (Year=2012)

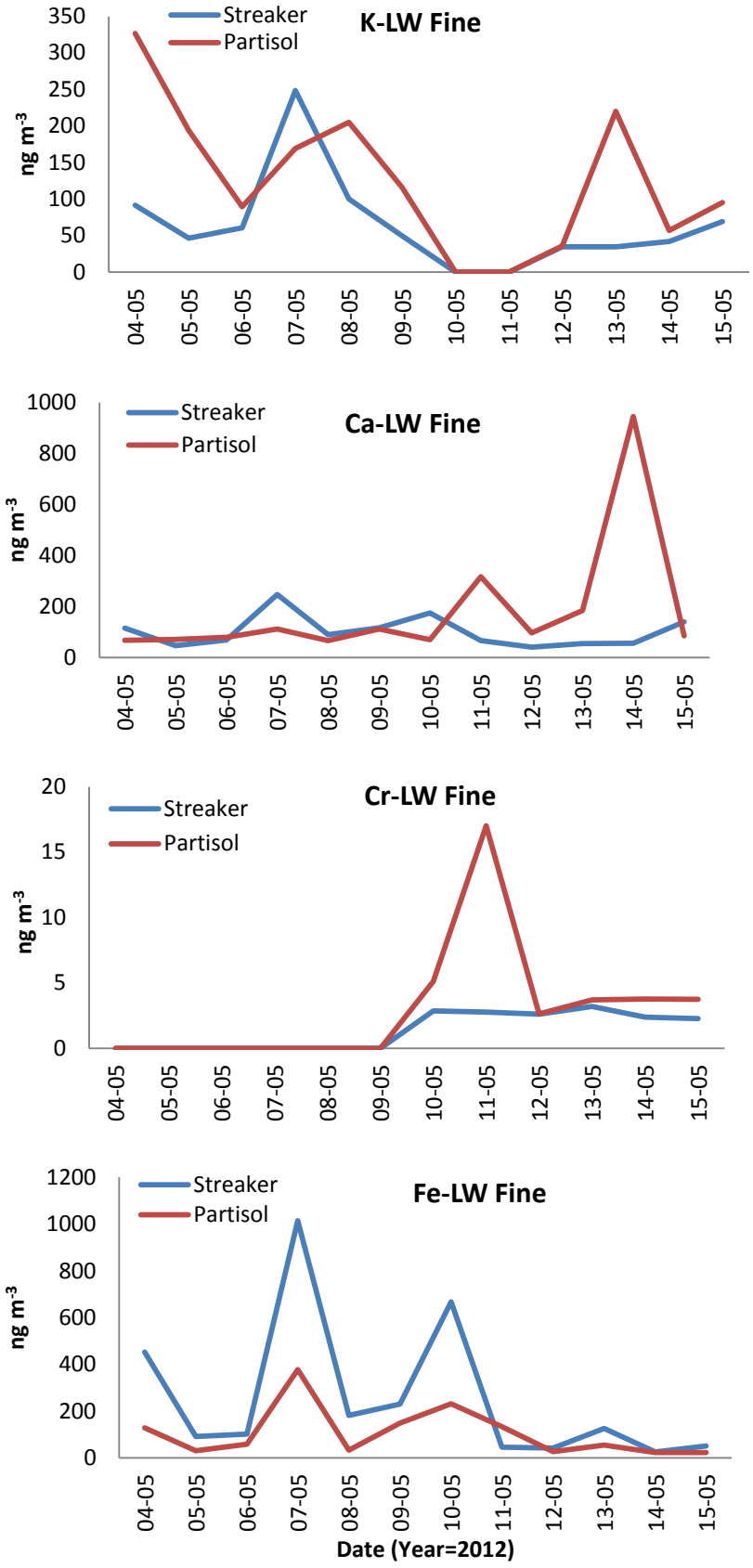
K-LW Fine
Streaker
Partisol
ng m-3
350
300
250
200
150
100
50
0
04-05
05-05
06-05
07-05
08-05
09-05
10-05
11-05
12-05
13-05
14-05
15-05
Ca-LW Fine
Streaker
Partisol
ng m-3
1000
800
600
400
200
0
04-05
05-05
06-05
07-05
08-05
09-05
10-05
11-05
12-05
13-05
14-05
15-05
Cr-LW Fine
Streaker
Partisol
ng m-3
20
15
10
5
0
04-05
05-05
06-05
07-05
08-05
09-05
10-05
11-05
12-05
13-05
14-05
15-05
Fe-LW Fine
Streaker
Partisol
ng m-3
1200
1000
800
600
400
200
0
04-05
05-05
06-05
07-05
08-05
09-05
10-05
11-05
12-05
13-05
14-05
15-05
Date (Year=2012)

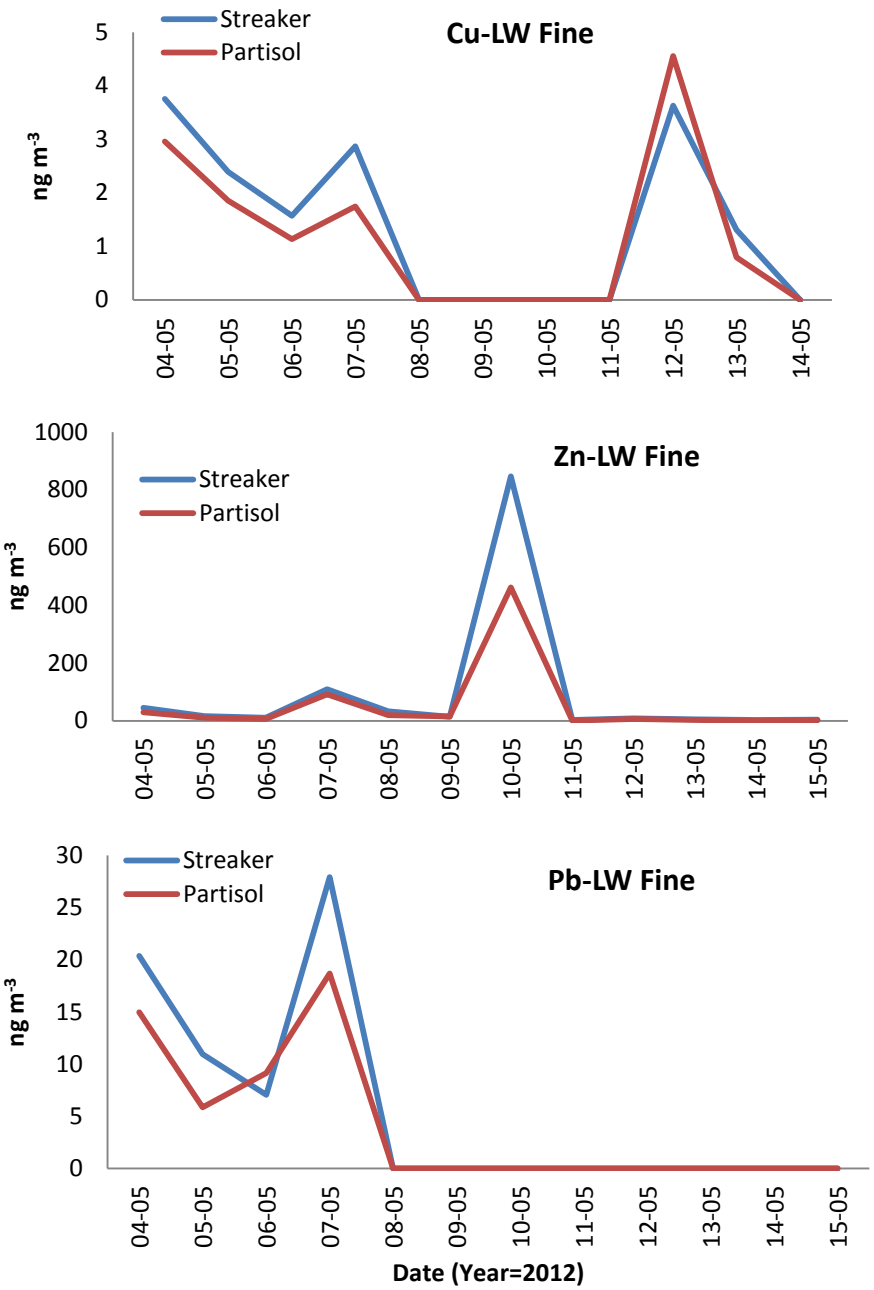
Cu-LW Fine
Streaker
Partisol
ng m-3
0
1
2
3
4
5
04-05
05-05
06-05
07-05
08-05
09-05
10-05
11-05
12-05
13-05
14-05
Zn-LW Fine
Streaker
Partisol
ng m-3
0
200
400
600
800
1000
04-05
05-05
06-05
07-05
08-05
09-05
10-05
11-05
12-05
13-05
14-05
15-05
Pb-LW Fine
Streaker
Partisol
ng m-3
0
5
10
15
20
25
30
04-05
05-05
06-05
07-05
08-05
09-05
10-05
11-05
12-05
13-05
14-05
15-05
Date (Year=2012)

(c) LW Fine

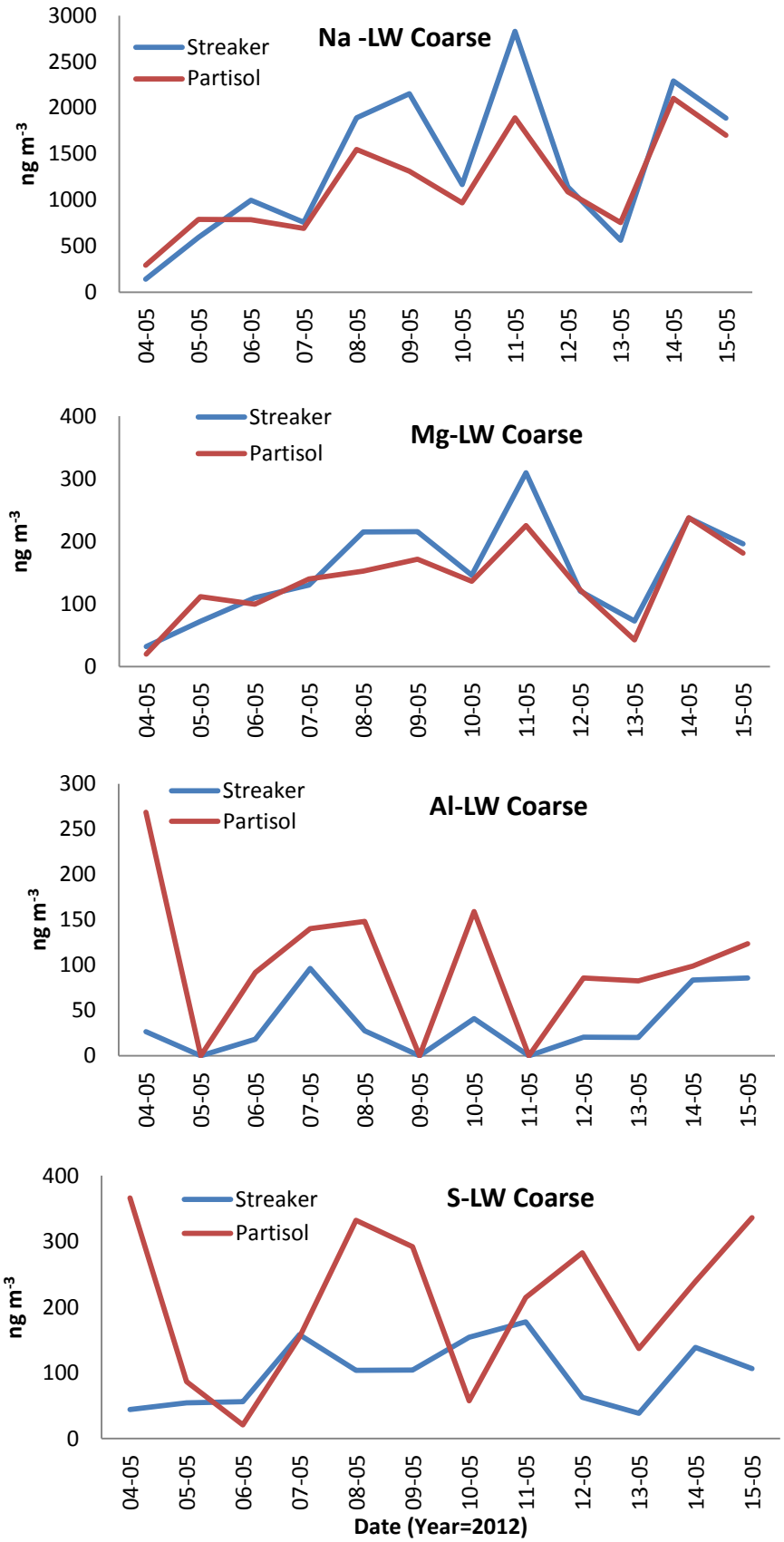
Na -LW Coarse
Streaker
Partisol
ng m-3
3000
2500
2000
1500
1000
500
0
Mg-LW Coarse
400
300
200
100
Al-LW Coarse
250
150
50
S-LW Coarse
04-05
05-05
06-05
07-05
08-05
09-05
10-05
11-05
12-05
13-05
14-05
15-05
Date (Year=2012)

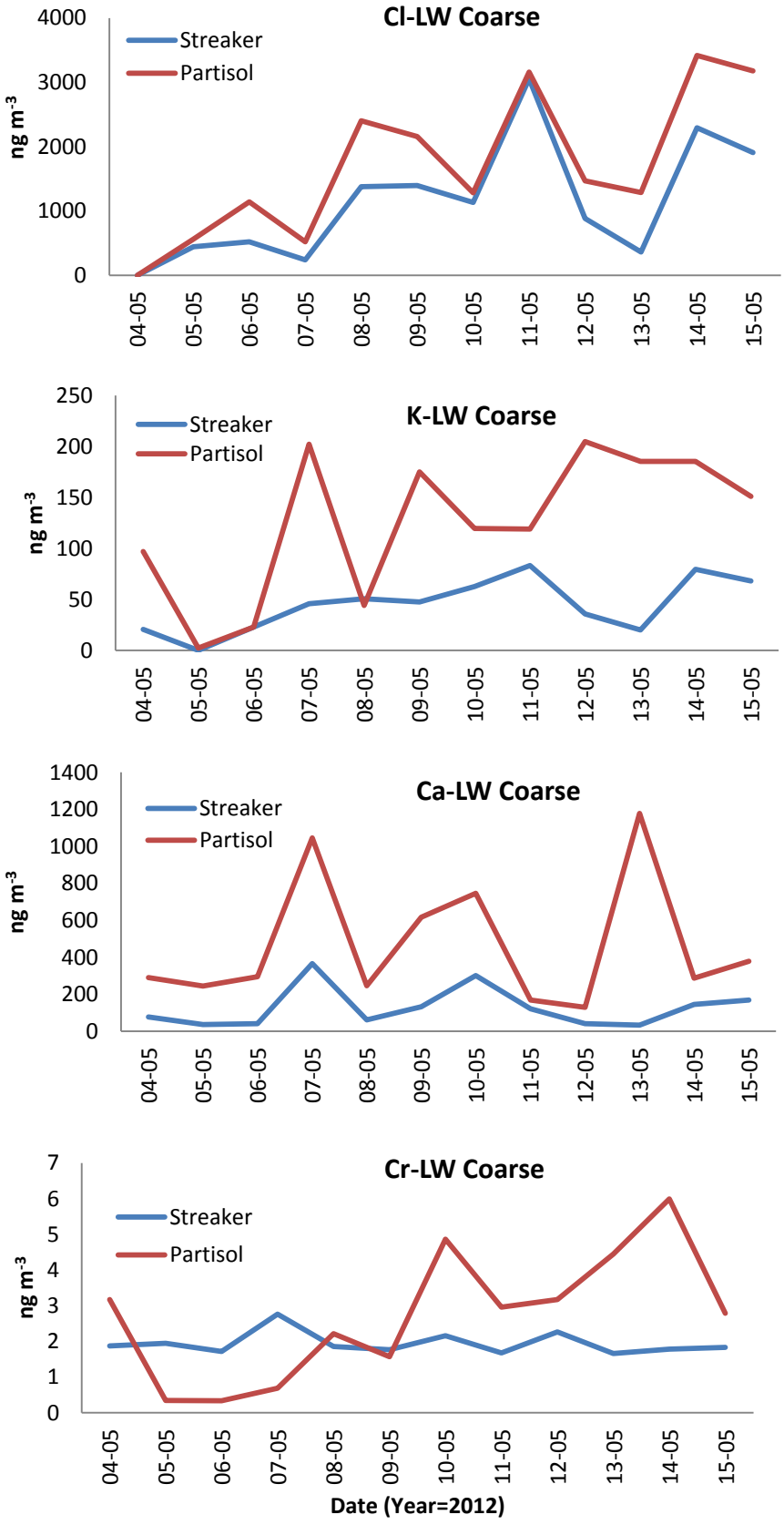
Cl-LW Coarse
Streaker
Partisol
ng m-3
4000
3000
2000
1000
0
K-LW Coarse
250
200
150
100
50
0
Ca-LW Coarse
1400
1200
1000
800
600
400
200
0
Cr-LW Coarse
7
6
5
4
3
2
1
0
04-05
05-05
06-05
07-05
08-05
09-05
10-05
11-05
12-05
13-05
14-05
15-05
Date (Year=2012)

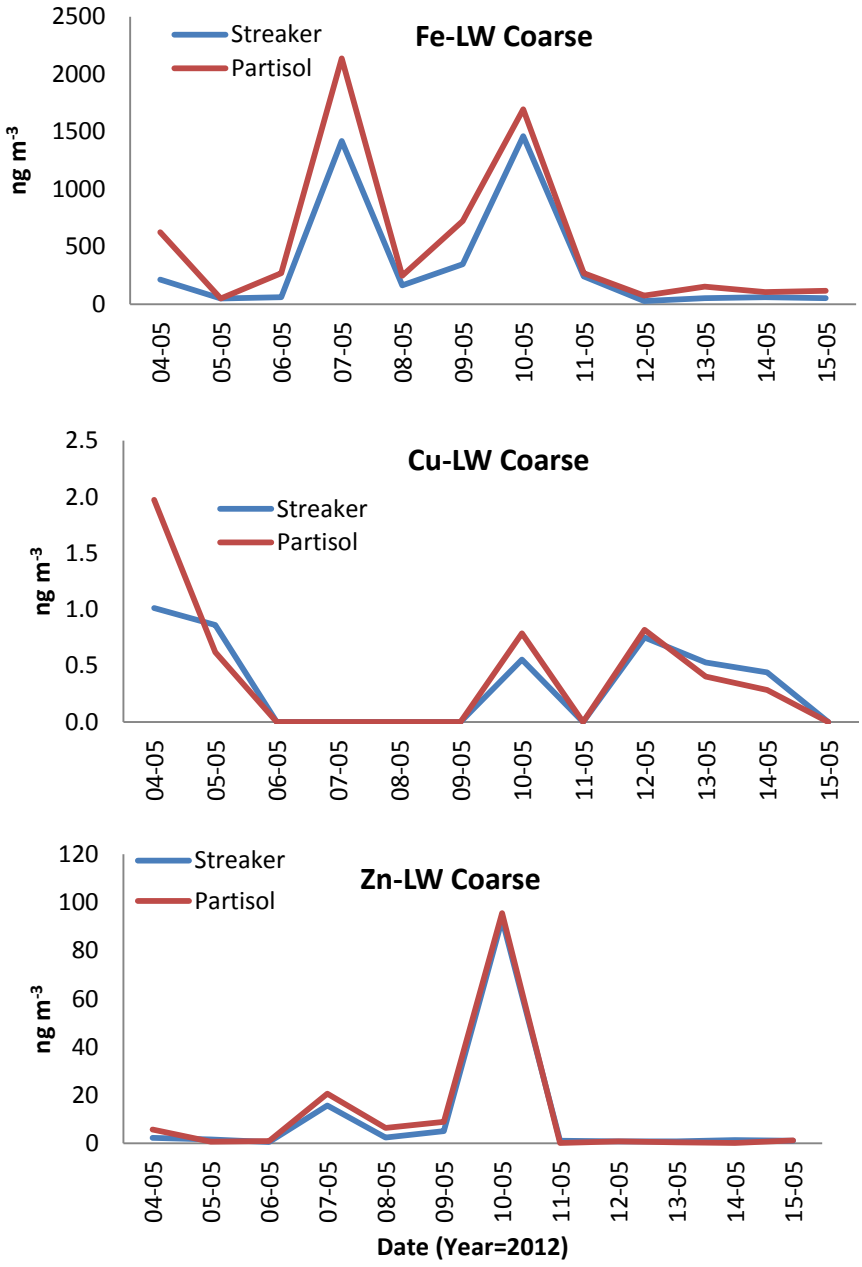
Fe-LW Coarse
Streaker
Partisol
ng m-3
2500
2000
1500
1000
500
0
Cu-LW Coarse
2.5
2.0
1.5
1.0
0.5
0.0
Zn-LW Coarse
120
100
80
60
40
20
0
04-05
05-05
06-05
07-05
08-05
09-05
10-05
11-05
12-05
13-05
14-05
15-05
Date (Year=2012)

(d) LW coarse

Appendix XXII

Bar chart depicting relative average PM data of Partisol and Streaker data

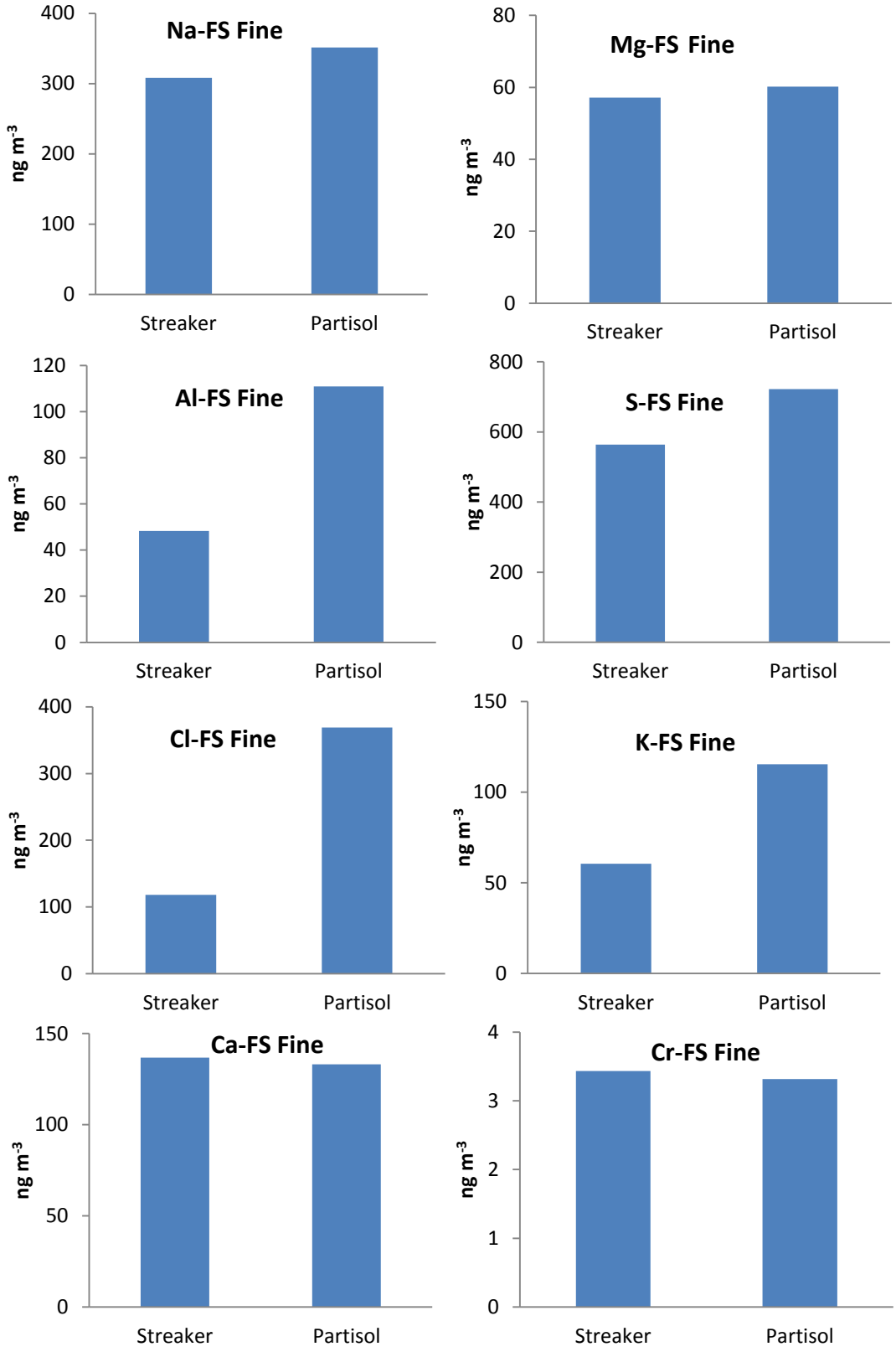

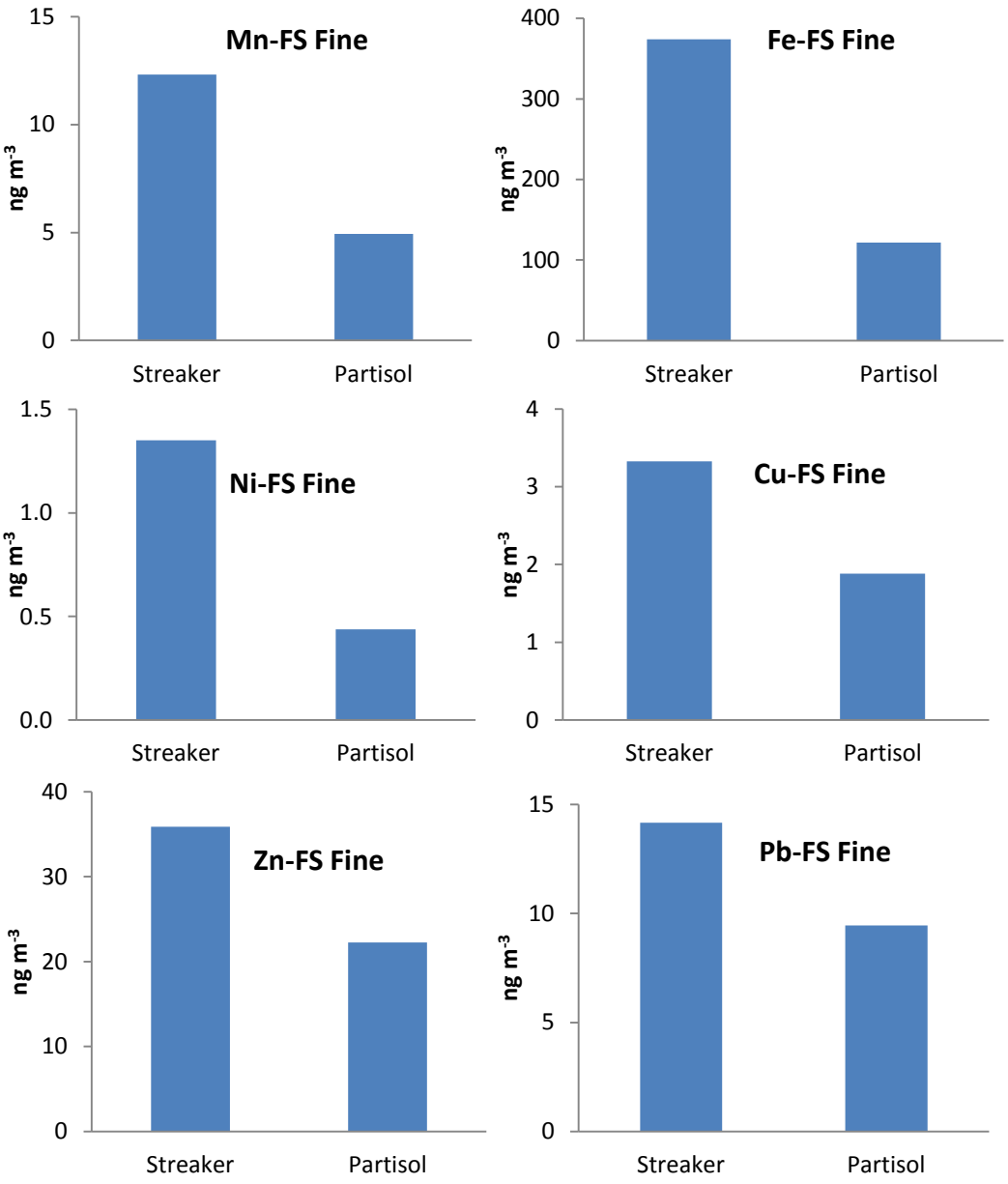
Mn-FS Fine
Fe-FS Fine
Ni-FS Fine
Cu-FS Fine
Zn-FS Fine
Pb-FS Fine
ng m-3
Streaker
Partisol
15
10
5
0
400
300
200
100
1.5
1.0
0.5
0.0
4
3
2
1
40
30
20
10

(a) FS Fine PM

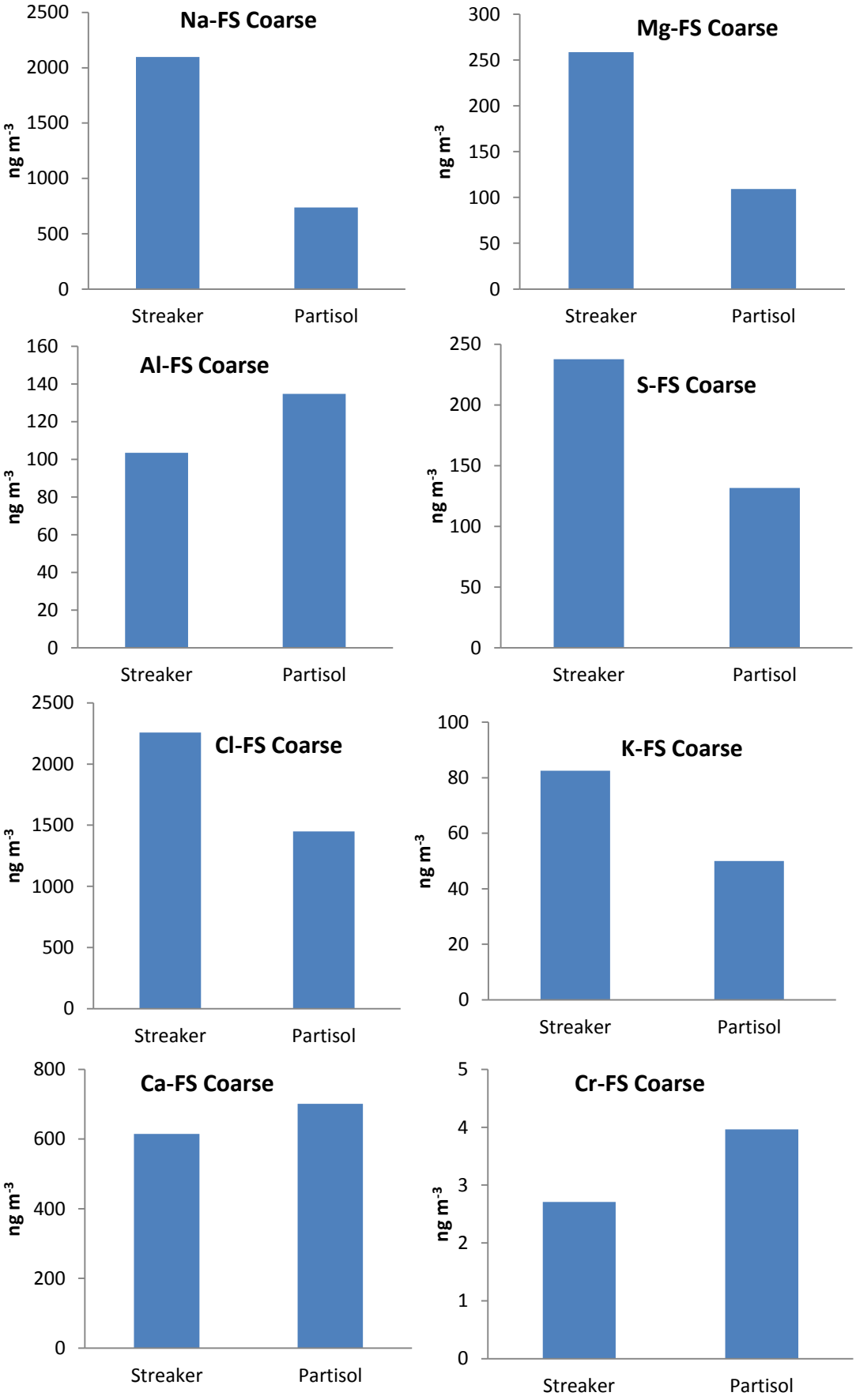
Na-FS Coarse
ng m-3
2500
2000
1500
1000
500
0
Streaker
Partisol
Mg-FS Coarse
ng m-3
300
250
200
150
100
50
0
Streaker
Partisol
Al-FS Coarse
ng m-3
160
140
120
100
80
60
40
20
0
Streaker
Partisol
S-FS Coarse
ng m-3
250
200
150
100
50
0
Streaker
Partisol
Cl-FS Coarse
ng m-3
2500
2000
1500
1000
500
0
Streaker
Partisol
K-FS Coarse
ng m-3
100
80
60
40
20
0
Streaker
Partisol
Ca-FS Coarse
ng m-3
800
600
400
200
0
Streaker
Partisol
Cr-FS Coarse
ng m-3
5
4
3
2
1
0
Streaker
Partisol

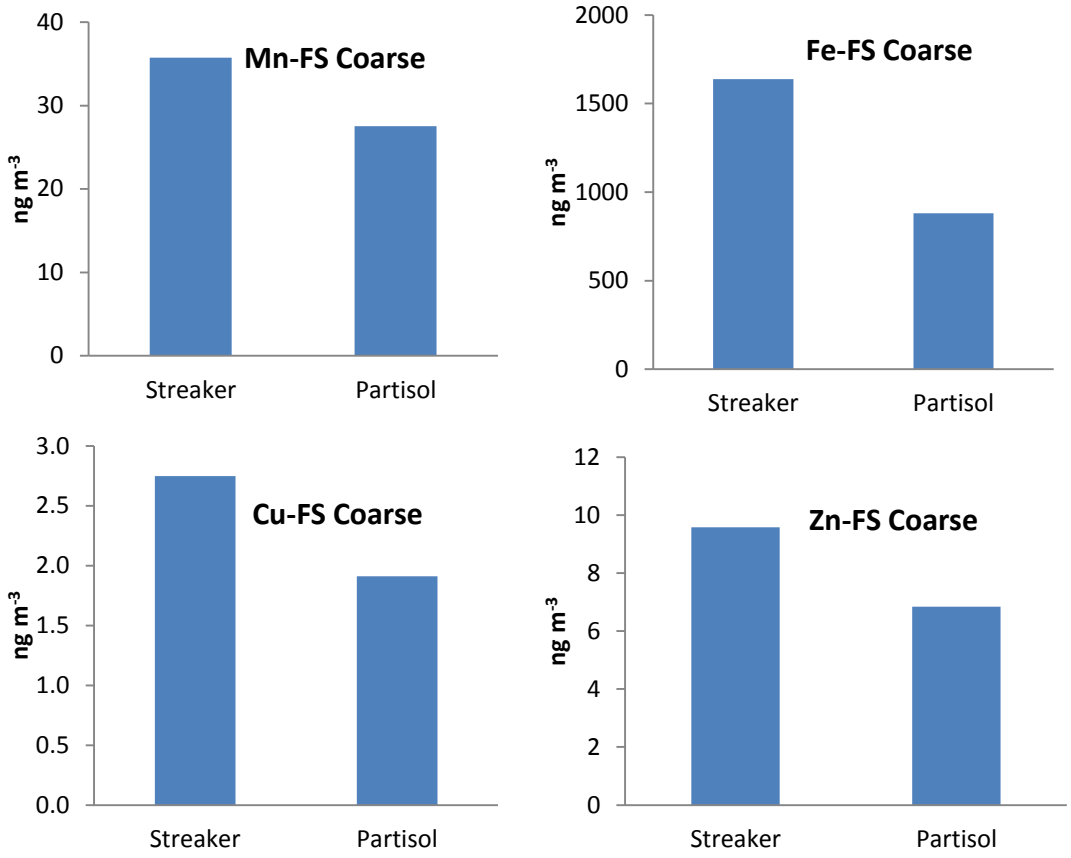
Mn-FS Coarse
ng m-3
40
30
20
10
0
Streaker
Partisol
Fe-FS Coarse
2000
1500
1000
500
0
Cu-FS Coarse
3.0
2.5
2.0
1.5
1.0
0.5
0.0
Zn-FS Coarse
12
10
8
6
4
2

(b) FS Coarse

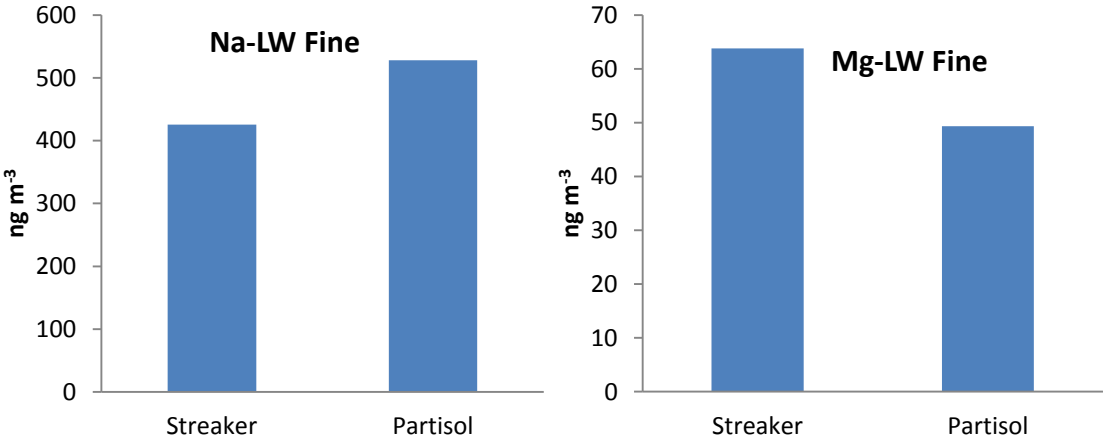
Na-LW Fine
ng m-3
600
500
400
300
200
100
0
Streaker
Partisol
Mg-LW Fine
70
60
50
40
30
20
10

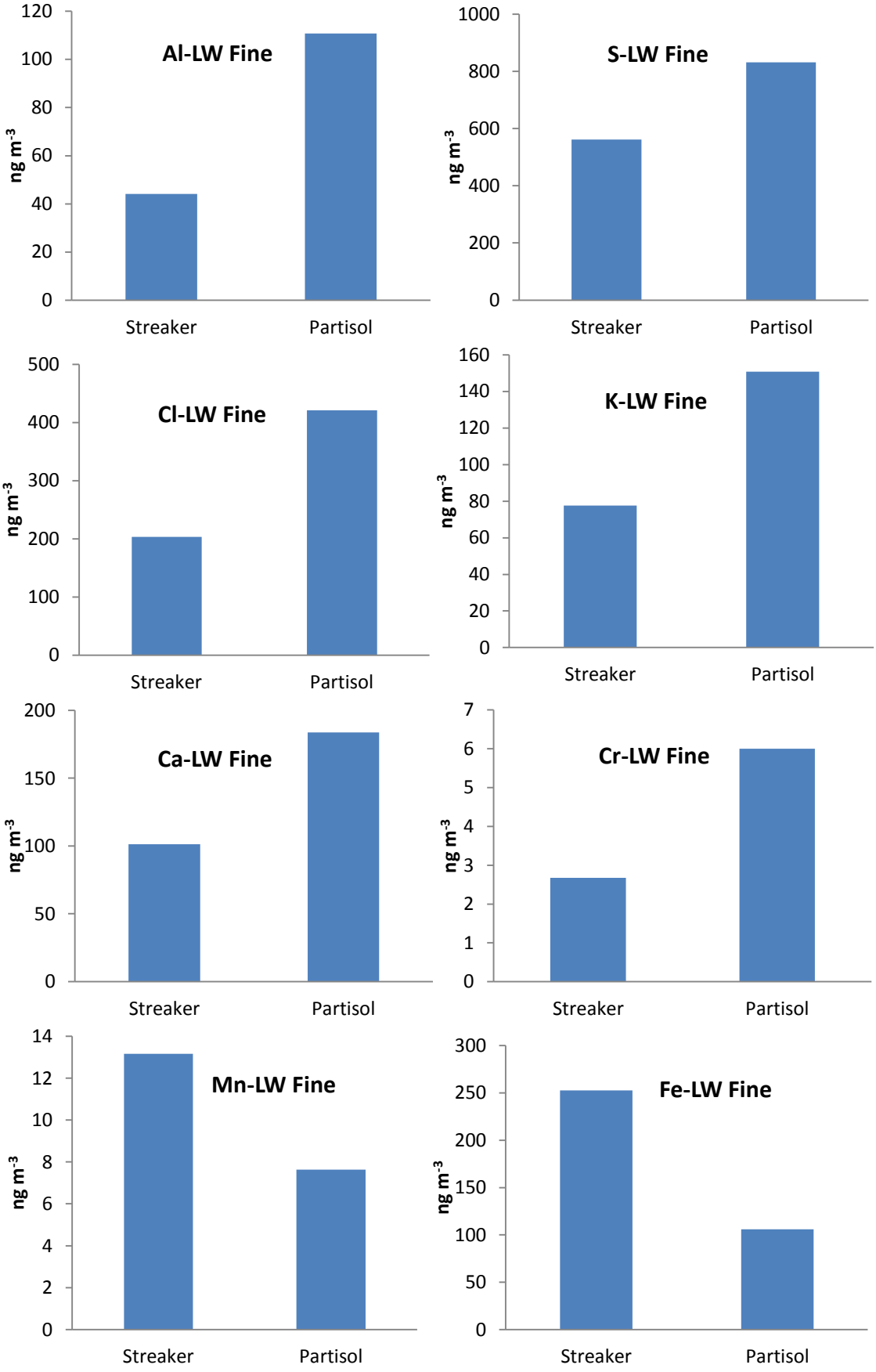
Al-LW Fine
ng m-3
120
100
80
60
40
20
0
Streaker
Partisol
S-LW Fine
ng m-3
1000
800
600
400
200
0
Streaker
Partisol
Cl-LW Fine
ng m-3
500
400
300
200
100
0
Streaker
Partisol
K-LW Fine
ng m-3
160
140
120
100
80
60
40
20
0
Streaker
Partisol
Ca-LW Fine
ng m-3
200
150
100
50
0
Streaker
Partisol
Cr-LW Fine
ng m-3
7
6
5
4
3
2
1
0
Streaker
Partisol
Mn-LW Fine
ng m-3
14
12
10
8
6
4
2
0
Streaker
Partisol
Fe-LW Fine
ng m-3
300
250
200
150
100
50
0
Streaker
Partisol

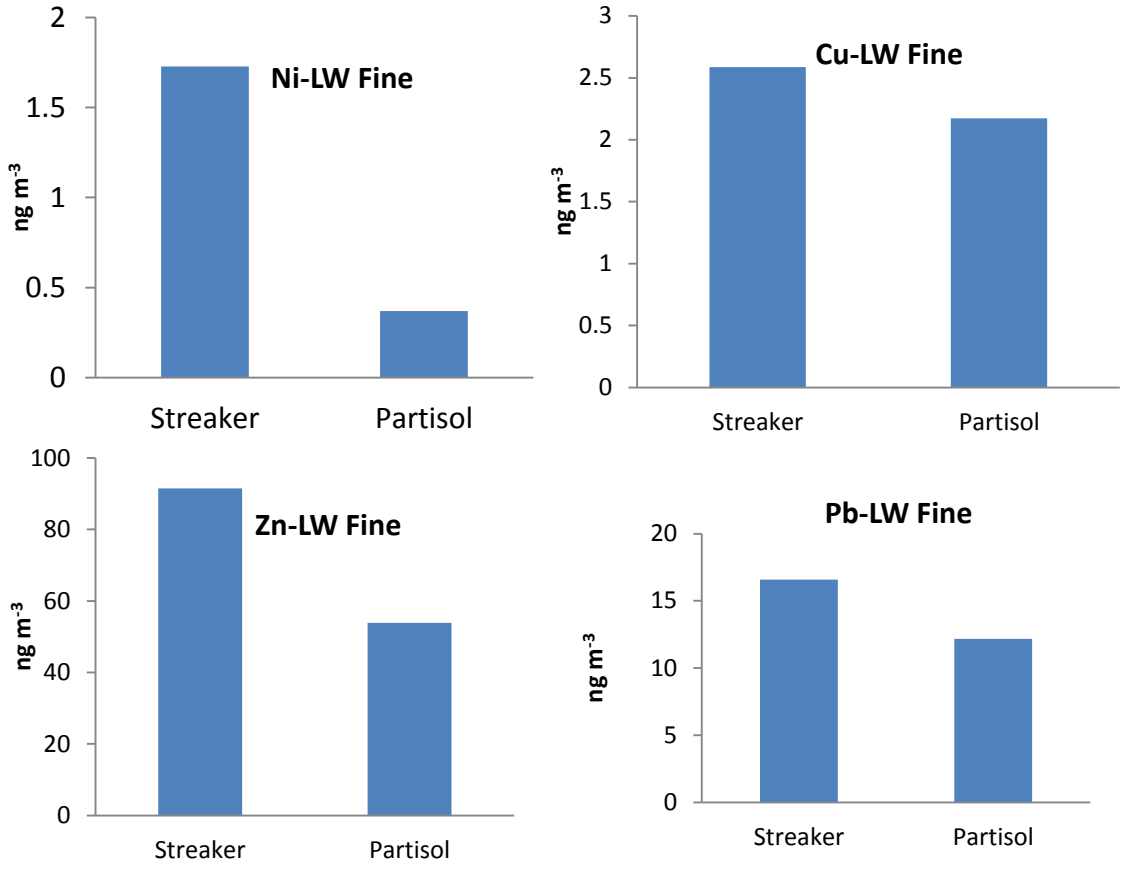
Ni-LW Fine
Cu-LW Fine
Zn-LW Fine
Pb-LW Fine
ng m-3
Streaker
Partisol
2
1.5
1
0.5
0
3
2.5
100
80
60
40
20
20
15
10
5

(c) LW Fine

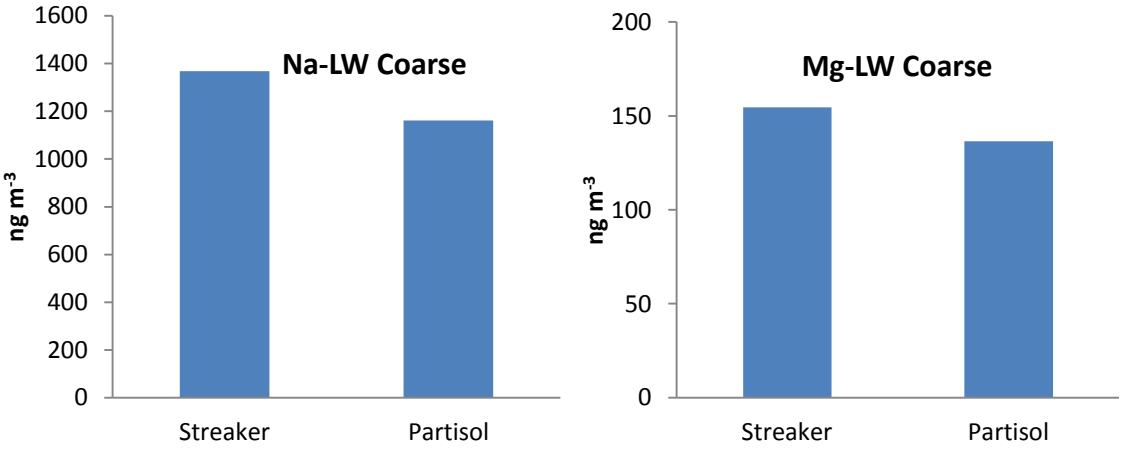
Na-LW Coarse
Mg-LW Coarse
ng m-3
Streaker
Partisol
1600
1400
1200
1000
800
600
400
200
0
150
100
50

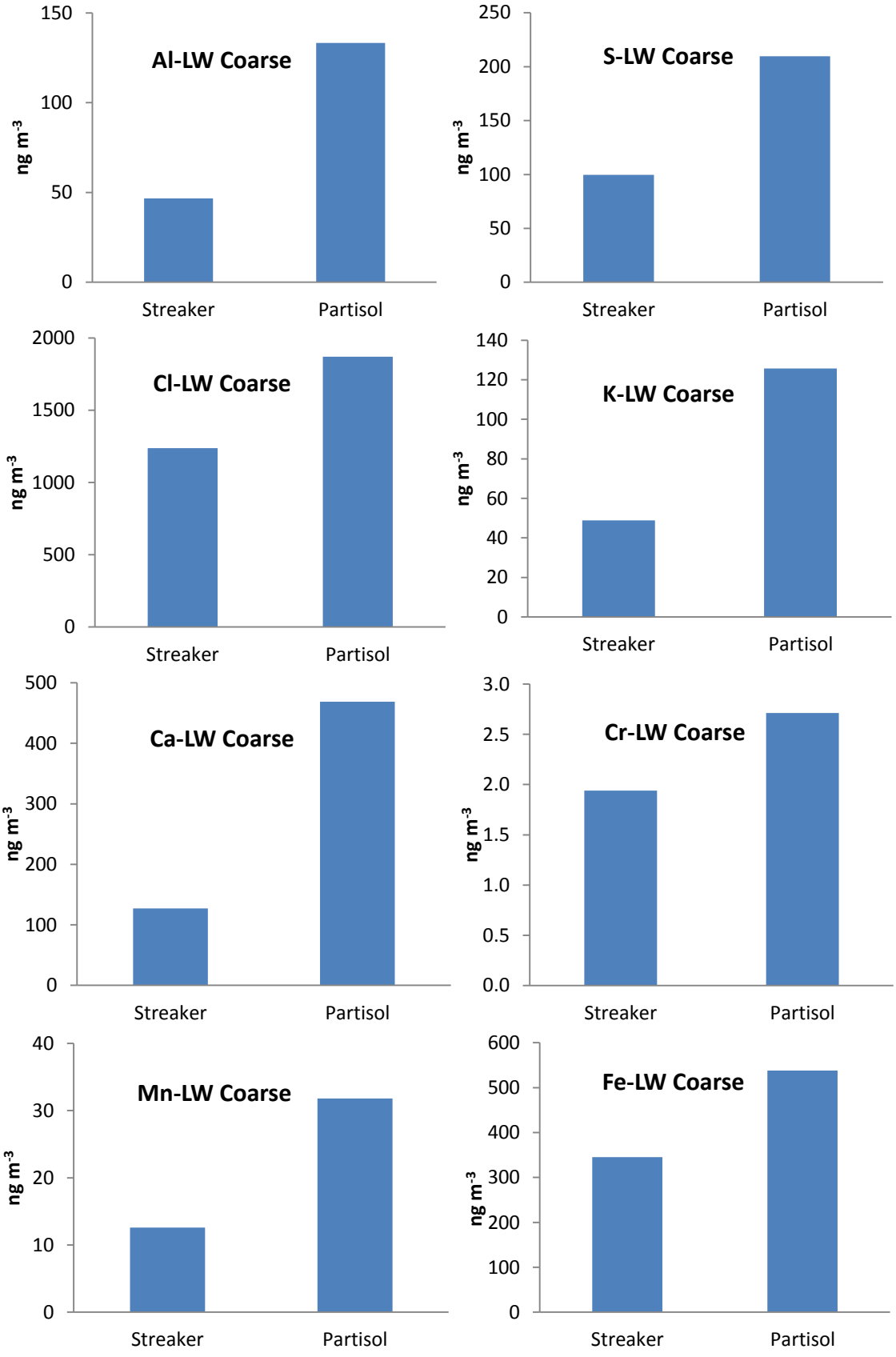
Al-LW Coarse
ng m-3
150
100
50
0
Streaker
Partisol
S-LW Coarse
ng m-3
250
200
150
100
50
0
Streaker
Partisol
Cl-LW Coarse
ng m-3
2000
1500
1000
500
0
Streaker
Partisol
K-LW Coarse
ng m-3
140
120
100
80
60
40
20
0
Streaker
Partisol
Ca-LW Coarse
ng m-3
500
400
300
200
100
0
Streaker
Partisol
Cr-LW Coarse
ng m-3
3.0
2.5
2.0
1.5
1.0
0.5
0.0
Streaker
Partisol
Mn-LW Coarse
ng m-3
40
30
20
10
0
Streaker
Partisol
Fe-LW Coarse
ng m-3
600
500
400
300
200
100
0
Streaker
Partisol

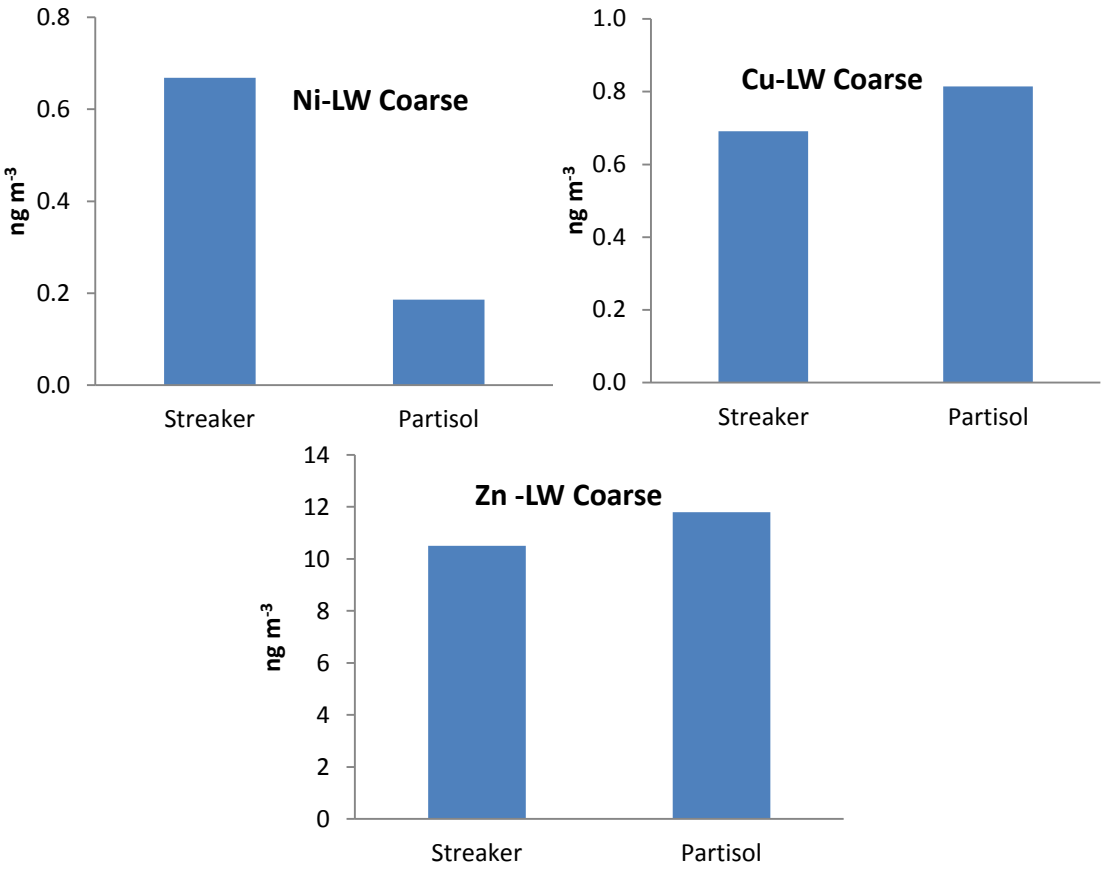
Ni-LW Coarse
ng m-3
0.8
0.6
0.4
0.2
0.0
Streaker
Partisol
Cu-LW Coarse
ng m-3
1.0
0.8
0.6
0.4
0.2
0.0
Streaker
Partisol
Zn -LW Coarse
ng m-3
14
12
10
8
6
4
2
0
Streaker
Partisol

(d) LW Coarse

Appendix XXIII

Least regression analysis of Partisol and Streaker daily data

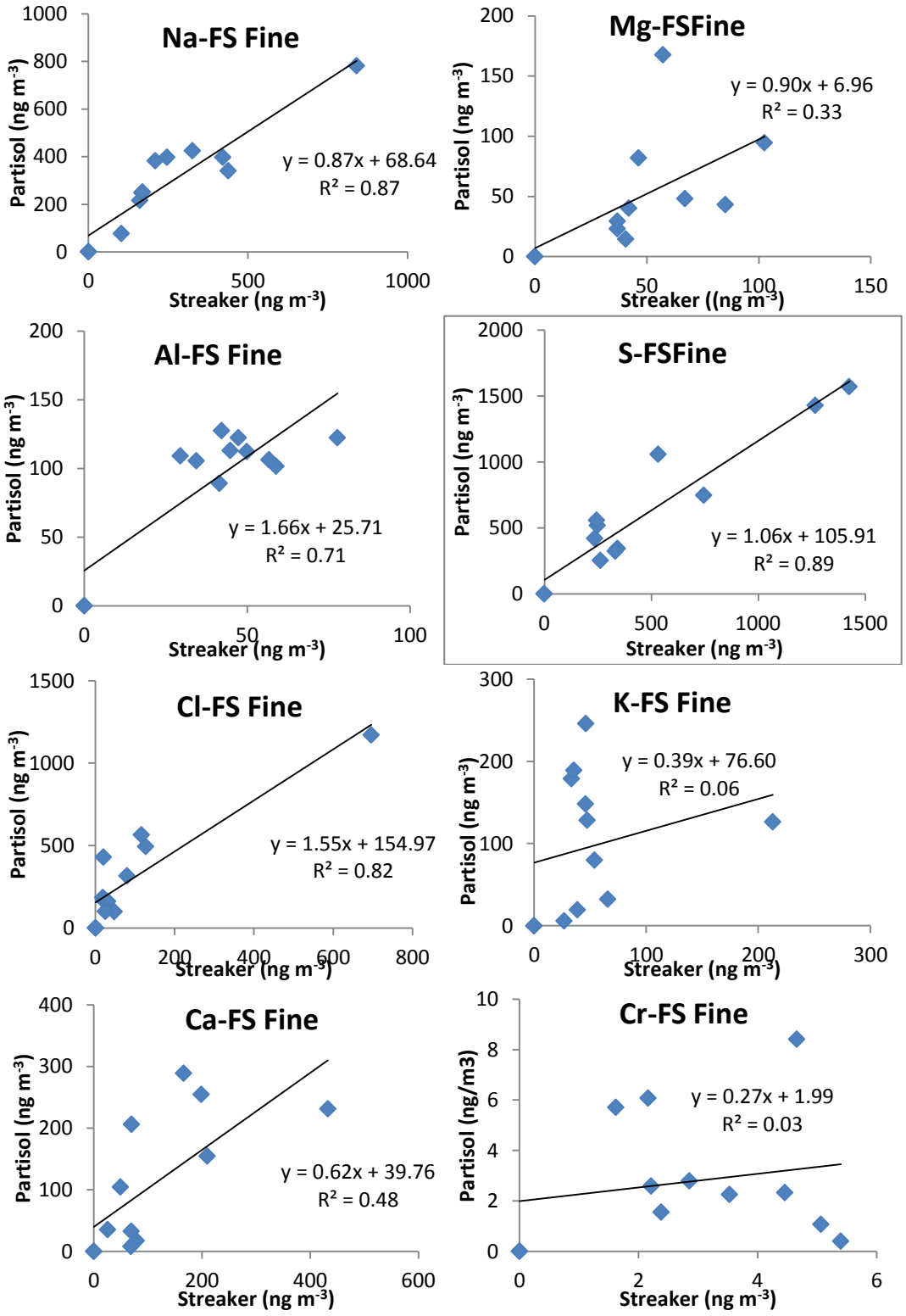

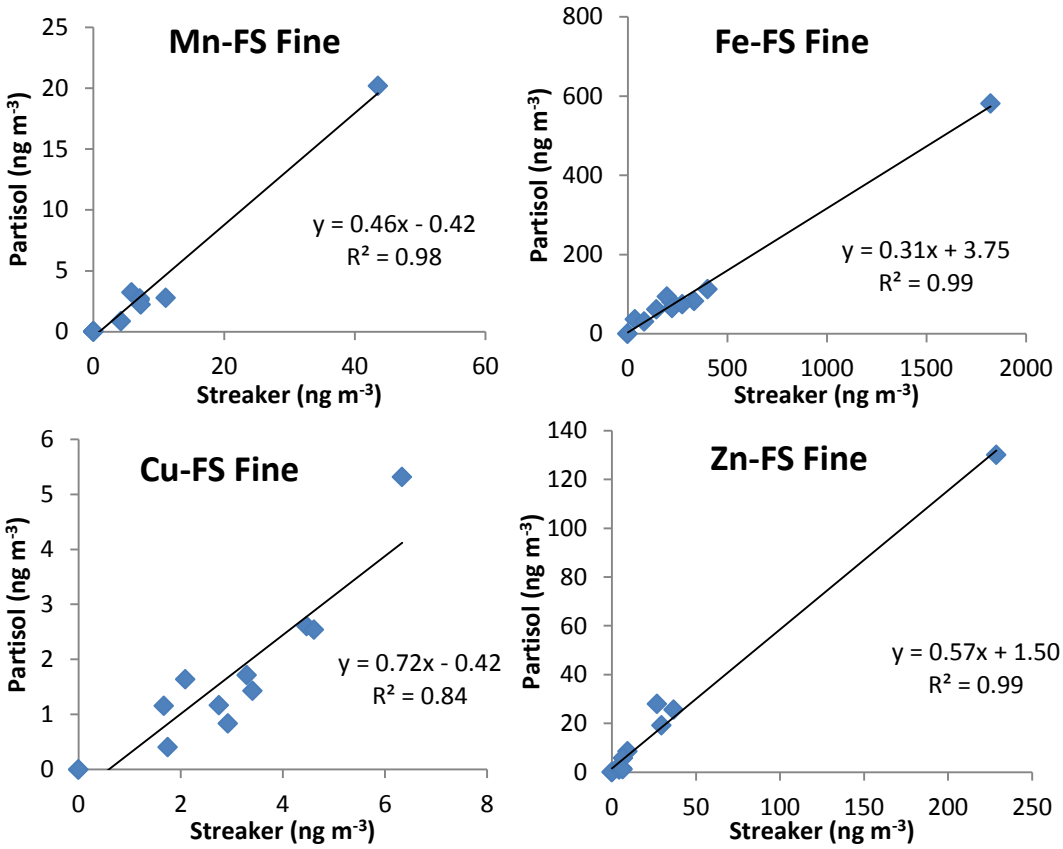
Mn-FS Fine
y = 0.46x - 0.42
R² = 0.98
Partisol (ng m-3)
Streaker (ng m-3)
Fe-FS Fine
y = 0.31x + 3.75
R² = 0.99
Cu-FS Fine
y = 0.72x - 0.42
R² = 0.84
Zn-FS Fine
y = 0.57x + 1.50
R² = 0.99

(a) FS Fine

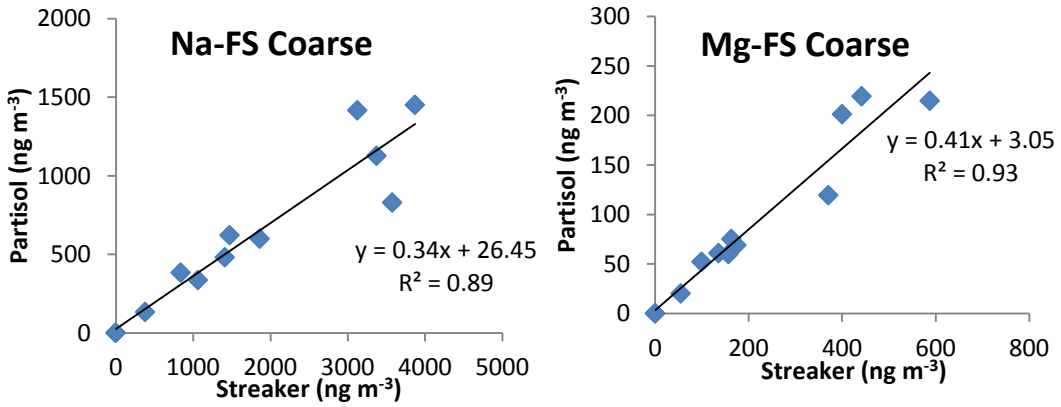
Na-FS Coarse
y = 0.34x + 26.45
R² = 0.89
Partisol (ng m-3)
Streaker (ng m-3)
Mg-FS Coarse
y = 0.41x + 3.05
R² = 0.93

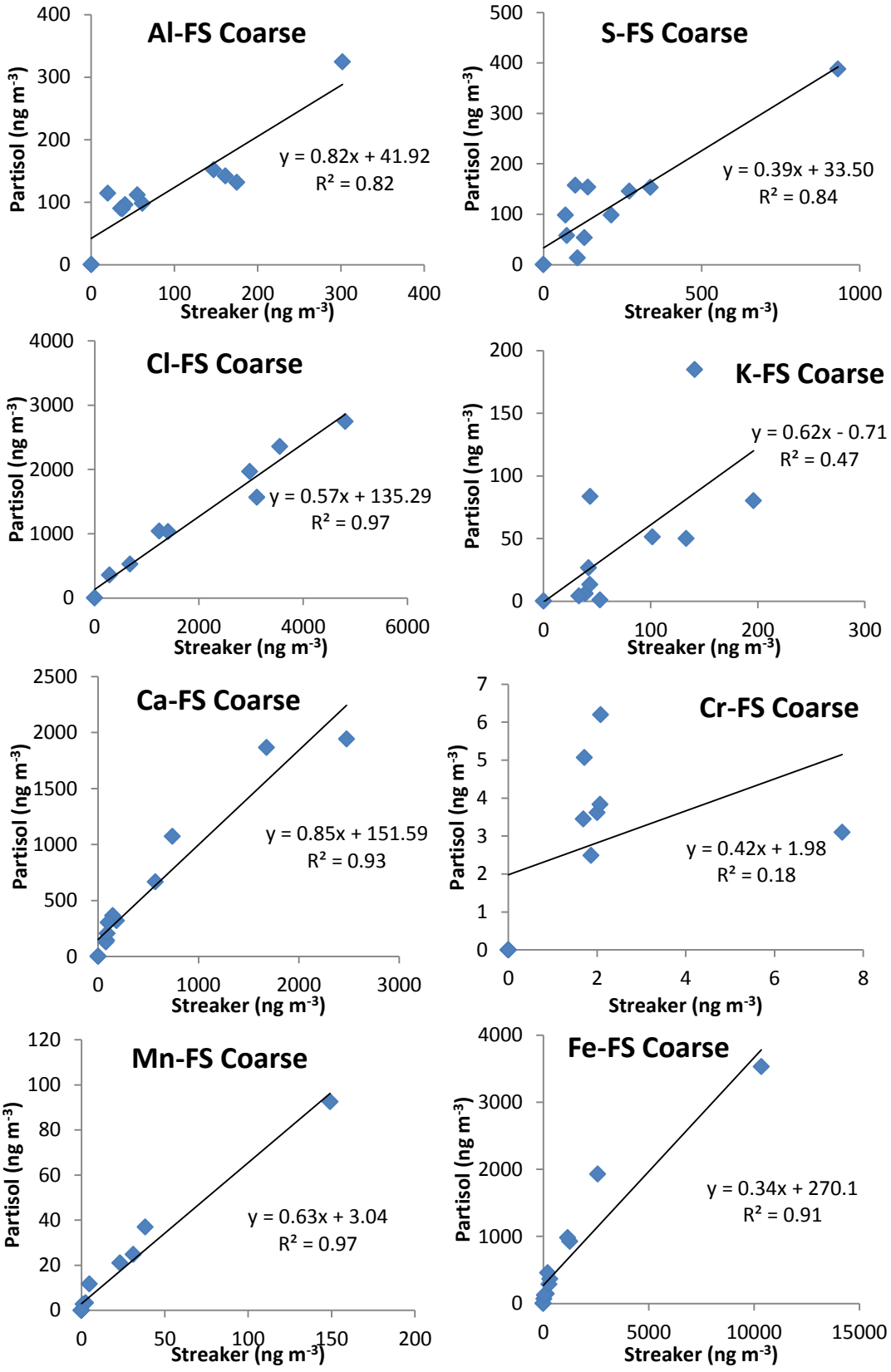
Al-FS Coarse
y = 0.82x + 41.92
R² = 0.82
S-FS Coarse
y = 0.39x + 33.50
R² = 0.84
Cl-FS Coarse
y = 0.57x + 135.29
R² = 0.97
K-FS Coarse
y = 0.62x - 0.71
R² = 0.47
Ca-FS Coarse
y = 0.85x + 151.59
R² = 0.93
Cr-FS Coarse
y = 0.42x + 1.98
R² = 0.18
Mn-FS Coarse
y = 0.63x + 3.04
R² = 0.97
Fe-FS Coarse
y = 0.34x + 270.1
R² = 0.91
Partisol (ng m-3)
Streaker (ng m-3)

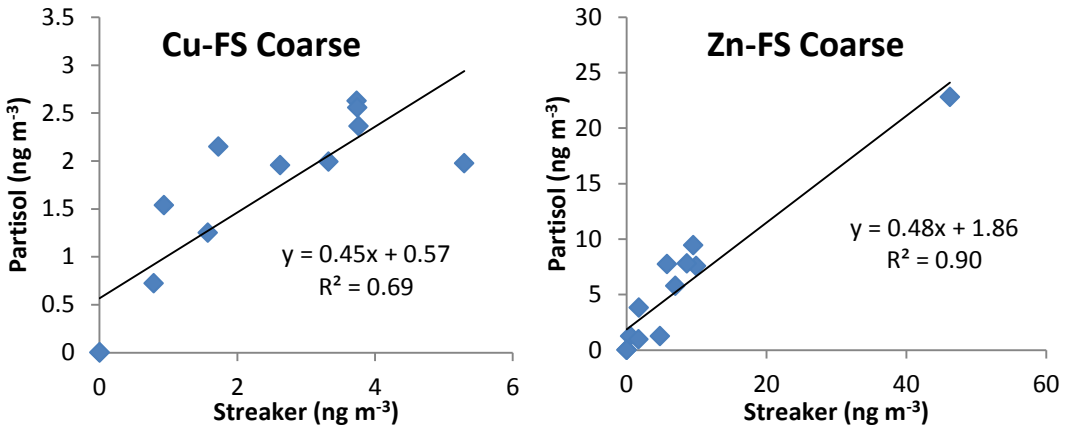
Cu-FS Coarse
y = 0.45x + 0.57
R² = 0.69
Partisol (ng m-3)
Streaker (ng m-3)
Zn-FS Coarse
y = 0.48x + 1.86
R² = 0.90
Partisol (ng m-3)
Streaker (ng m-3)

(b) FS Coarse

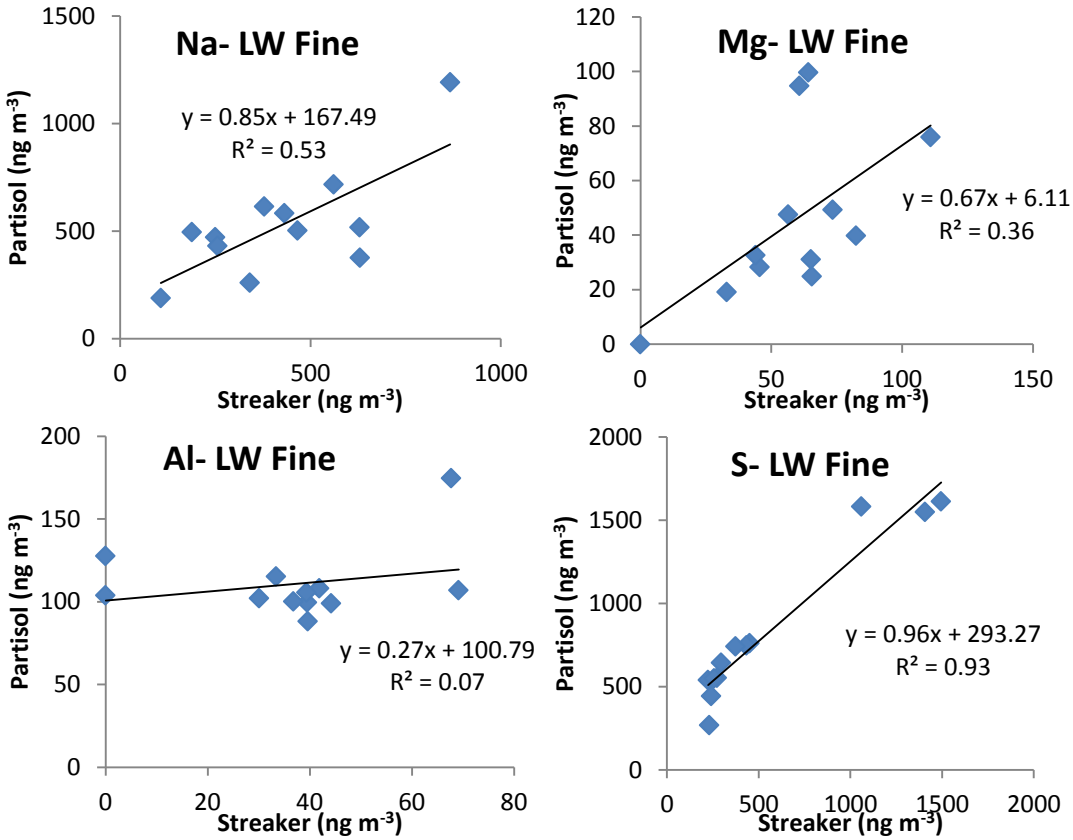
Na- LW Fine
y = 0.85x + 167.49
R² = 0.53
Partisol (ng m-3)
Streaker (ng m-3)
Mg- LW Fine
y = 0.67x + 6.11
R² = 0.36
Partisol (ng m-3)
Streaker (ng m-3)
Al- LW Fine
y = 0.27x + 100.79
R² = 0.07
Partisol (ng m-3)
Streaker (ng m-3)
S- LW Fine
y = 0.96x + 293.27
R² = 0.93
Partisol (ng m-3)
Streaker (ng m-3)

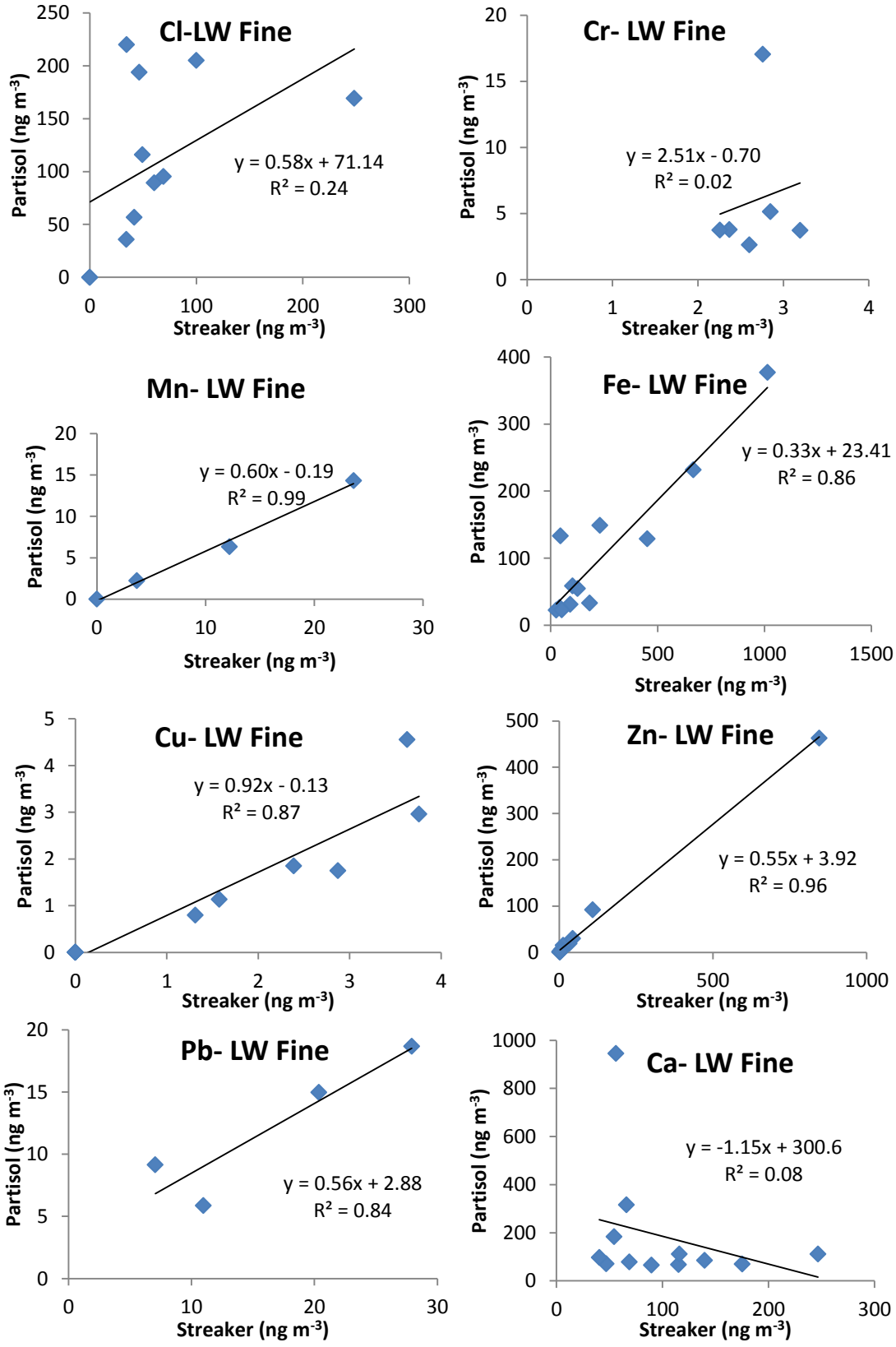
Cl-LW Fine
y = 0.58x + 71.14
R² = 0.24
Partisol (ng m-3)
Streaker (ng m-3)
Cr- LW Fine
y = 2.51x - 0.70
R² = 0.02
Mn- LW Fine
y = 0.60x - 0.19
R² = 0.99
Fe- LW Fine
y = 0.33x + 23.41
R² = 0.86
Cu- LW Fine
y = 0.92x - 0.13
R² = 0.87
Zn- LW Fine
y = 0.55x + 3.92
R² = 0.96
Pb- LW Fine
y = 0.56x + 2.88
R² = 0.84
Ca- LW Fine
y = -1.15x + 300.6
R² = 0.08

(c) LW Fine

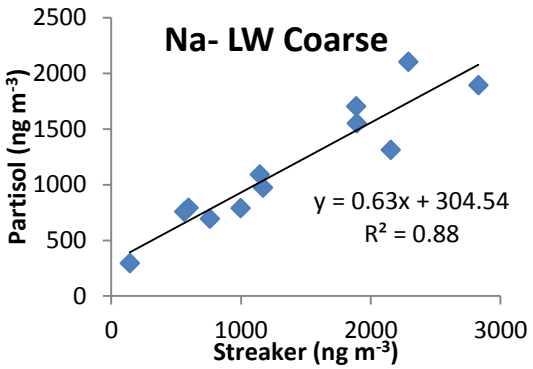
Na- LW Coarse
Partisol (ng m-3)
Streaker (ng m-3)
y = 0.63x + 304.54
R² = 0.88

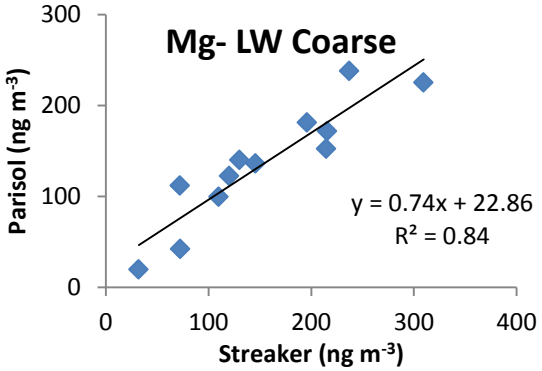
Mg- LW Coarse
Parisol (ng m-3)
Streaker (ng m-3)
y = 0.74x + 22.86
R² = 0.84

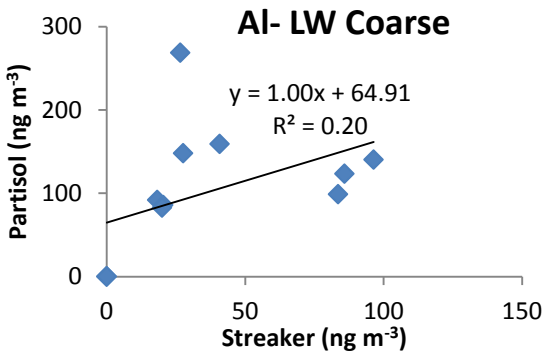
Al- LW Coarse
Partisol (ng m-3)
Streaker (ng m-3)
y = 1.00x + 64.91
R² = 0.20

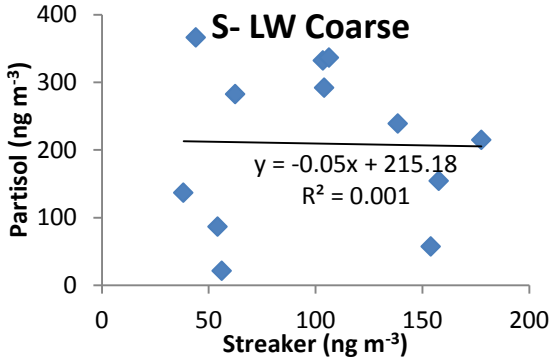
S- LW Coarse
Partisol (ng m-3)
Streaker (ng m-3)
y = -0.05x + 215.18
R² = 0.001

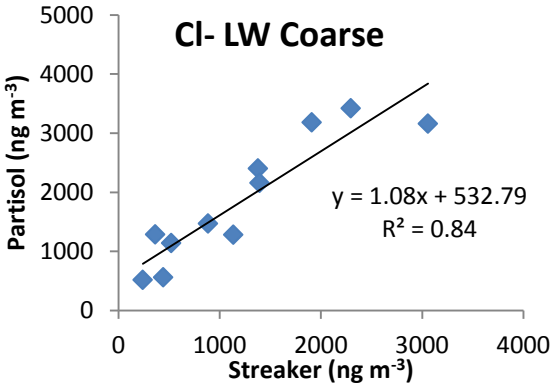
Cl- LW Coarse
Partisol (ng m-3)
Streaker (ng m-3)
y = 1.08x + 532.79
R² = 0.84

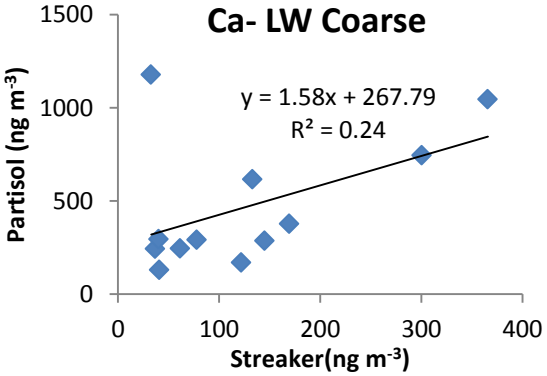
Ca- LW Coarse
Partisol (ng m-3)
Streaker(ng m-3)
y = 1.58x + 267.79
R² = 0.24

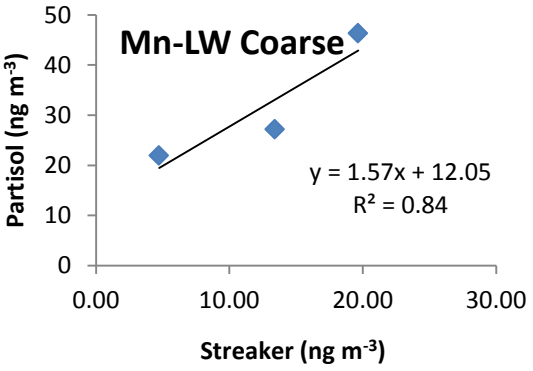
Mn-LW Coarse
Partisol (ng m-3)
Streaker (ng m-3)
y = 1.57x + 12.05
R² = 0.84

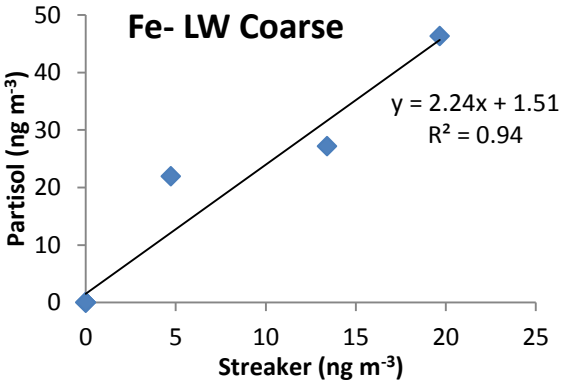
Fe- LW Coarse
Partisol (ng m-3)
Streaker (ng m-3)
y = 2.24x + 1.51
R² = 0.94

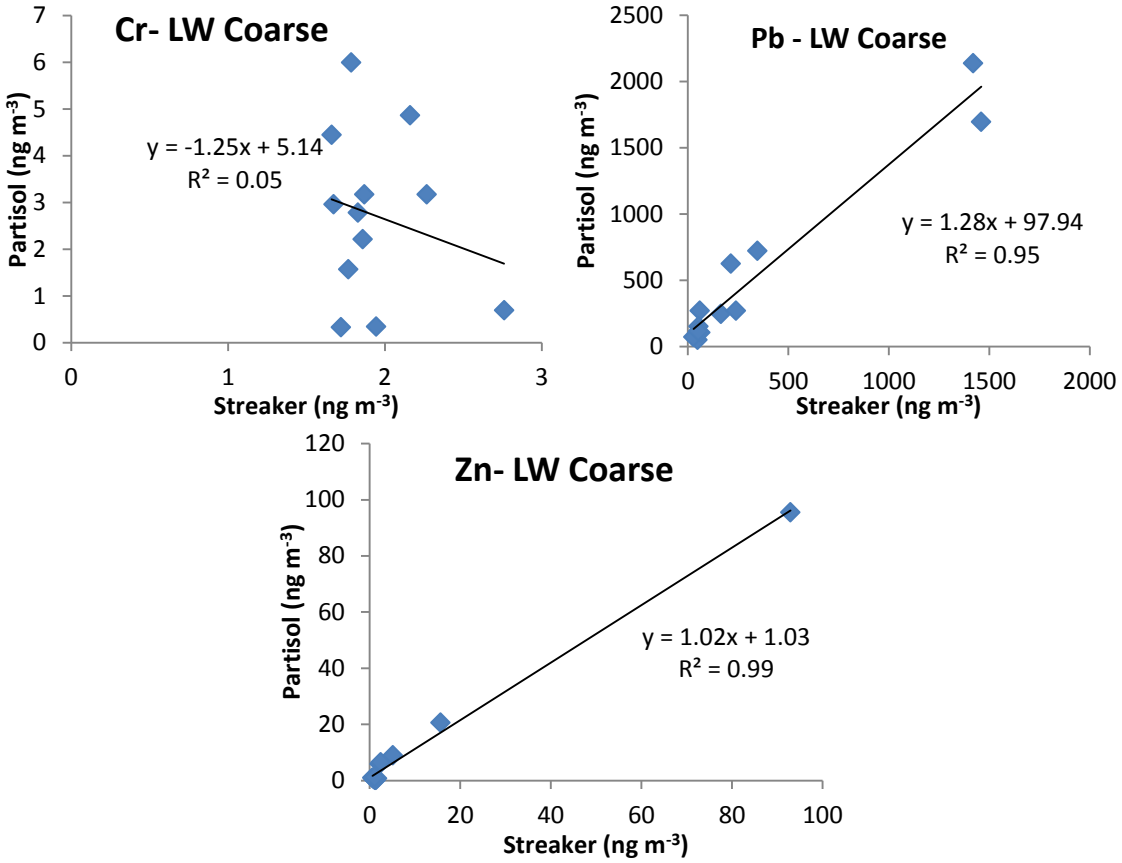
Cr- LW Coarse
y = -1.25x + 5.14
R² = 0.05
Partisol (ng m-3)
Streaker (ng m-3)
Pb - LW Coarse
y = 1.28x + 97.94
R² = 0.95
Partisol (ng m-3)
Streaker (ng m-3)
Zn- LW Coarse
y = 1.02x + 1.03
R² = 0.99
Partisol (ng m-3)
Streaker (ng m-3)

(d) LW coarse

Appendix XXIV

Daily variations in PMF source contributions for Partisol PM

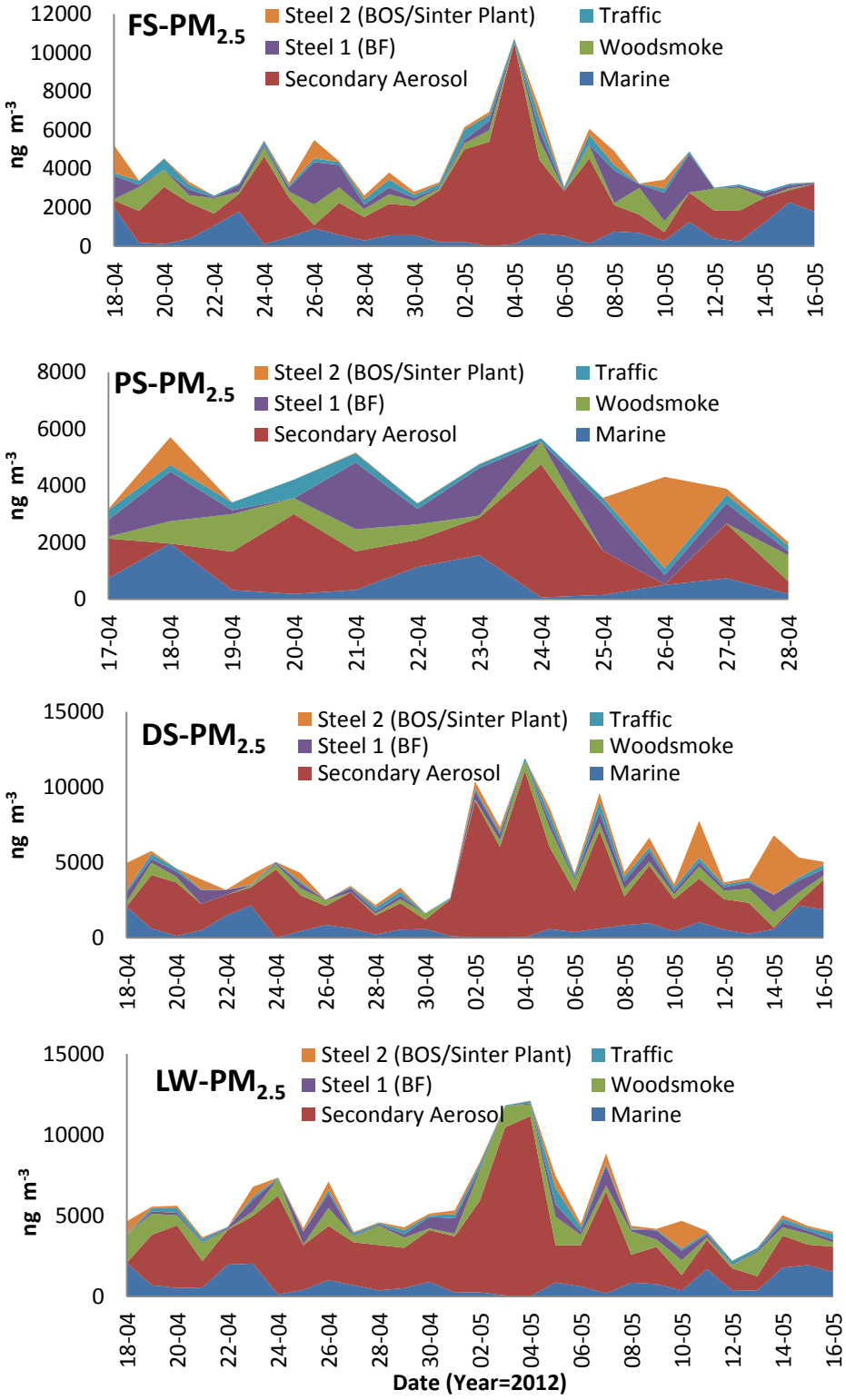

(a) Partisol $PM_{2.5}$

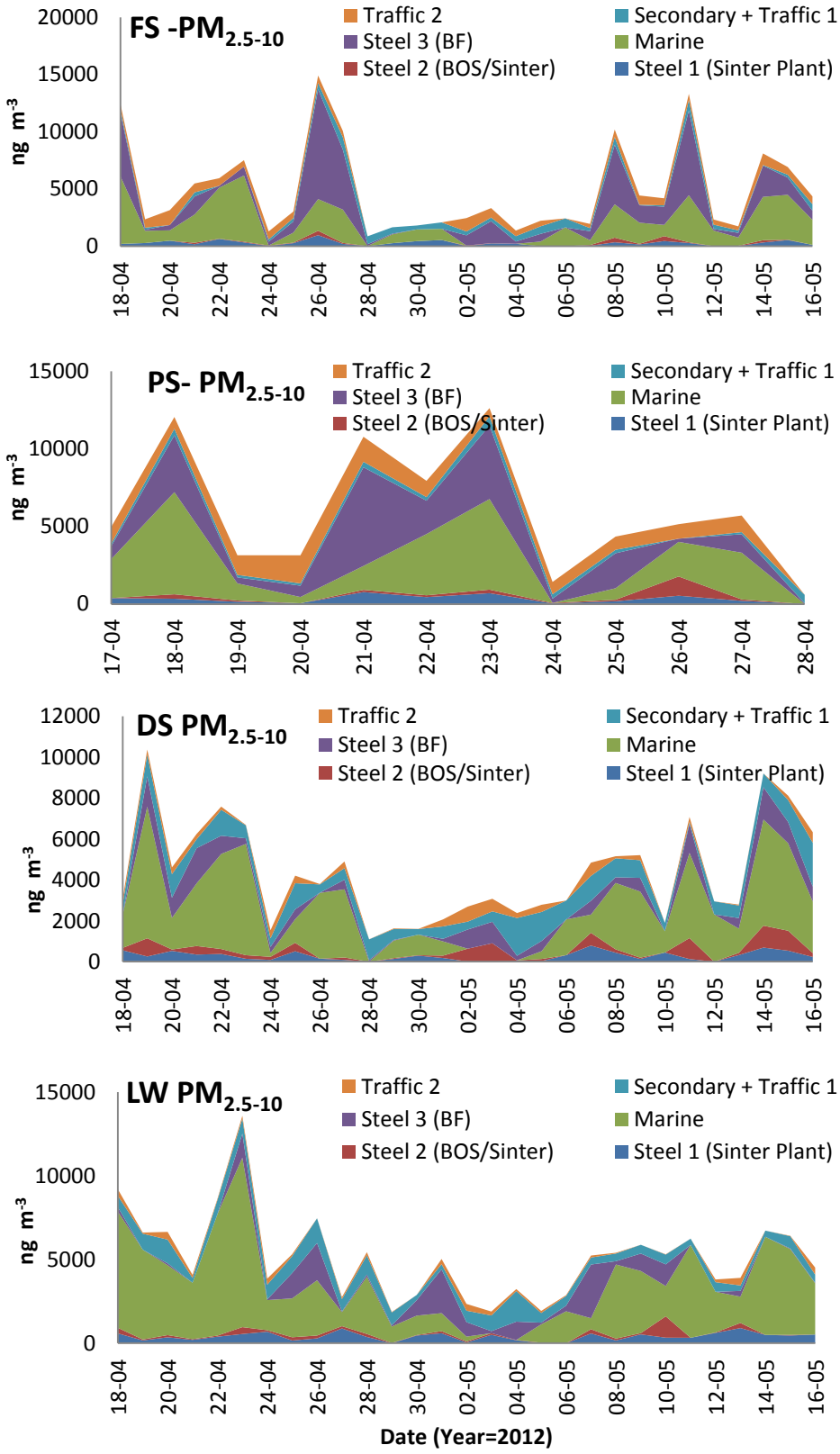

(b) Partisol $PM_{2.5\text{-}10}$

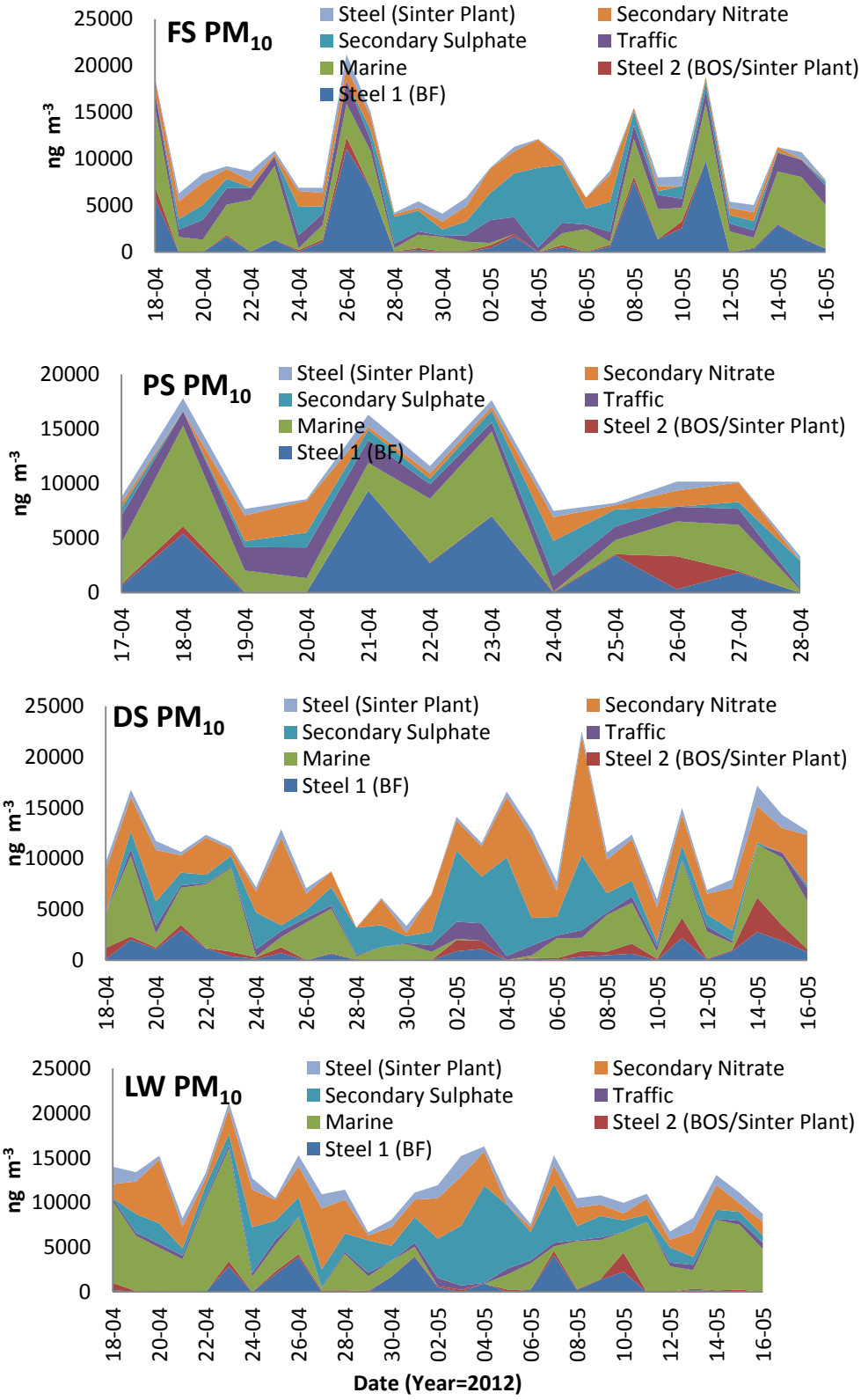

(c) Partisol PM_{10}

Appendix XXV

Time series plots of Streaker hourly variations in PMF source contributions

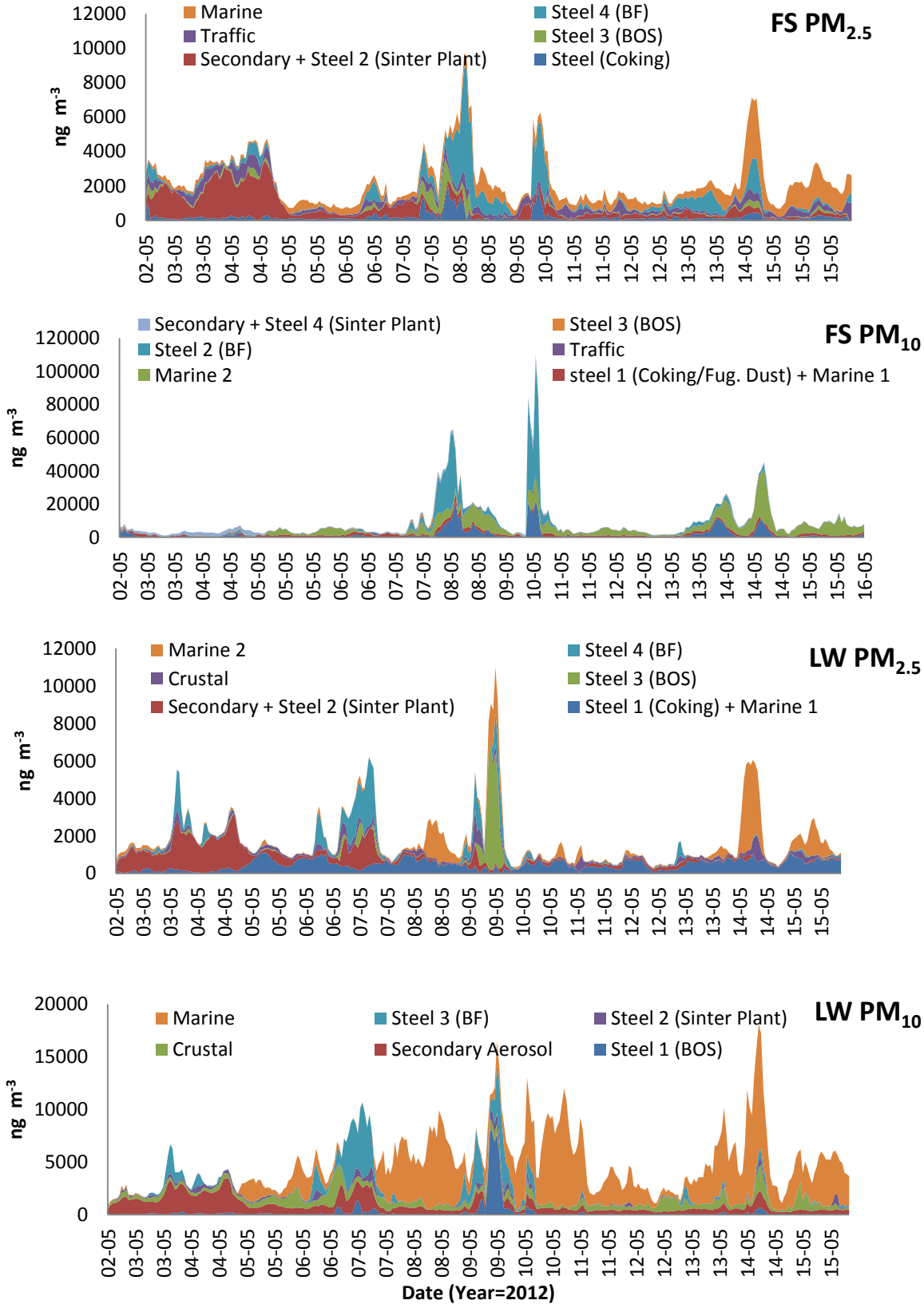

Appendix XXVI

Diurnal Variations of PMF source conributions

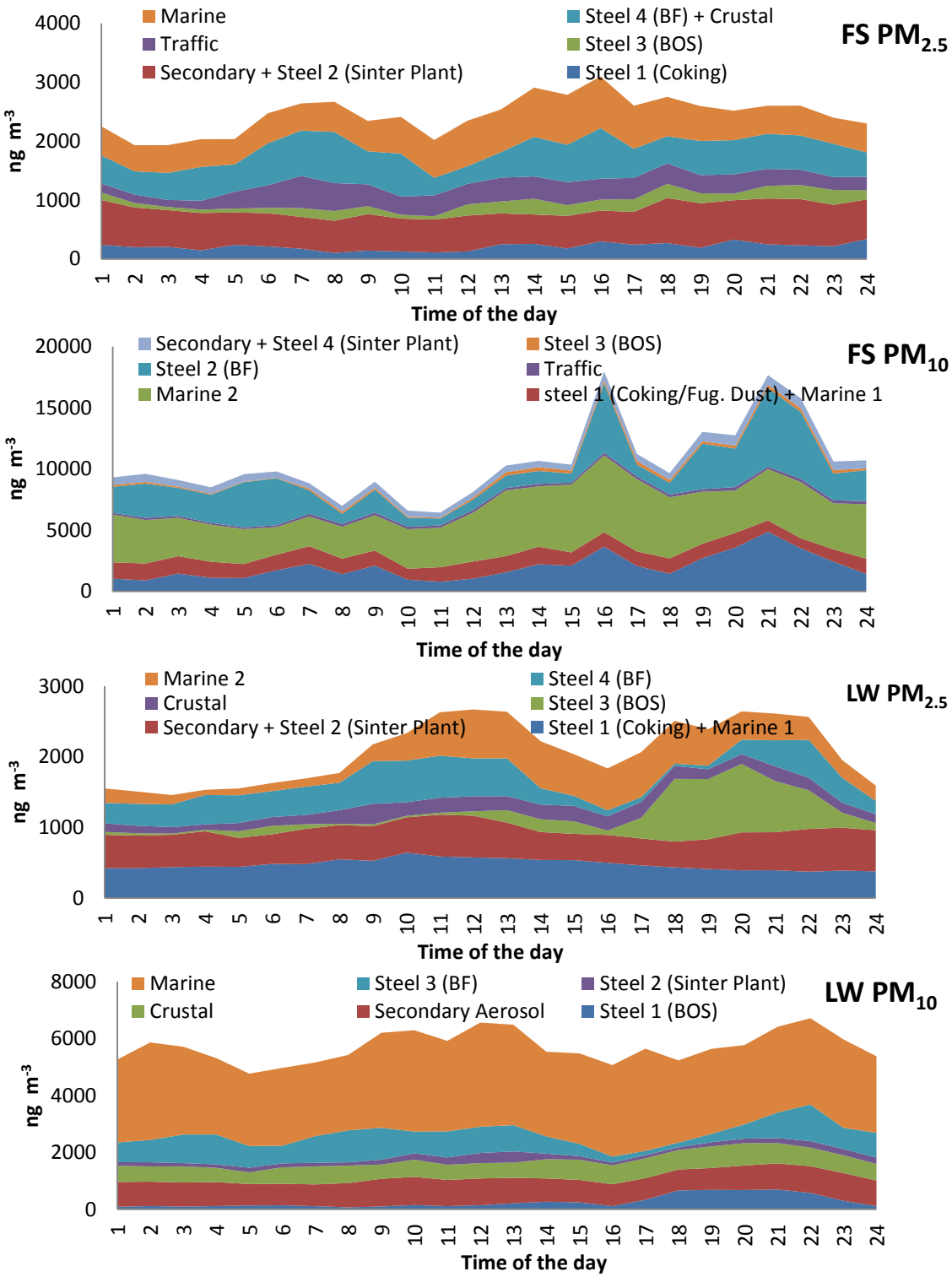

Appendix XXVII

Hourly trends of unscaled ATOFMS counts and Grimm OPC

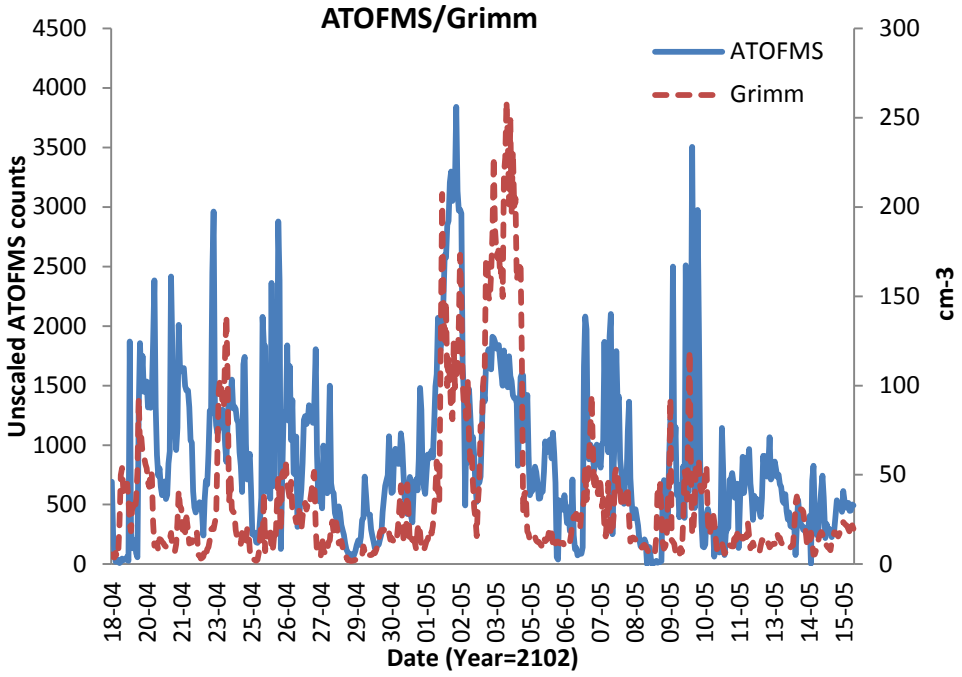

Appendix XXVIII

Daily variations of particle class counts

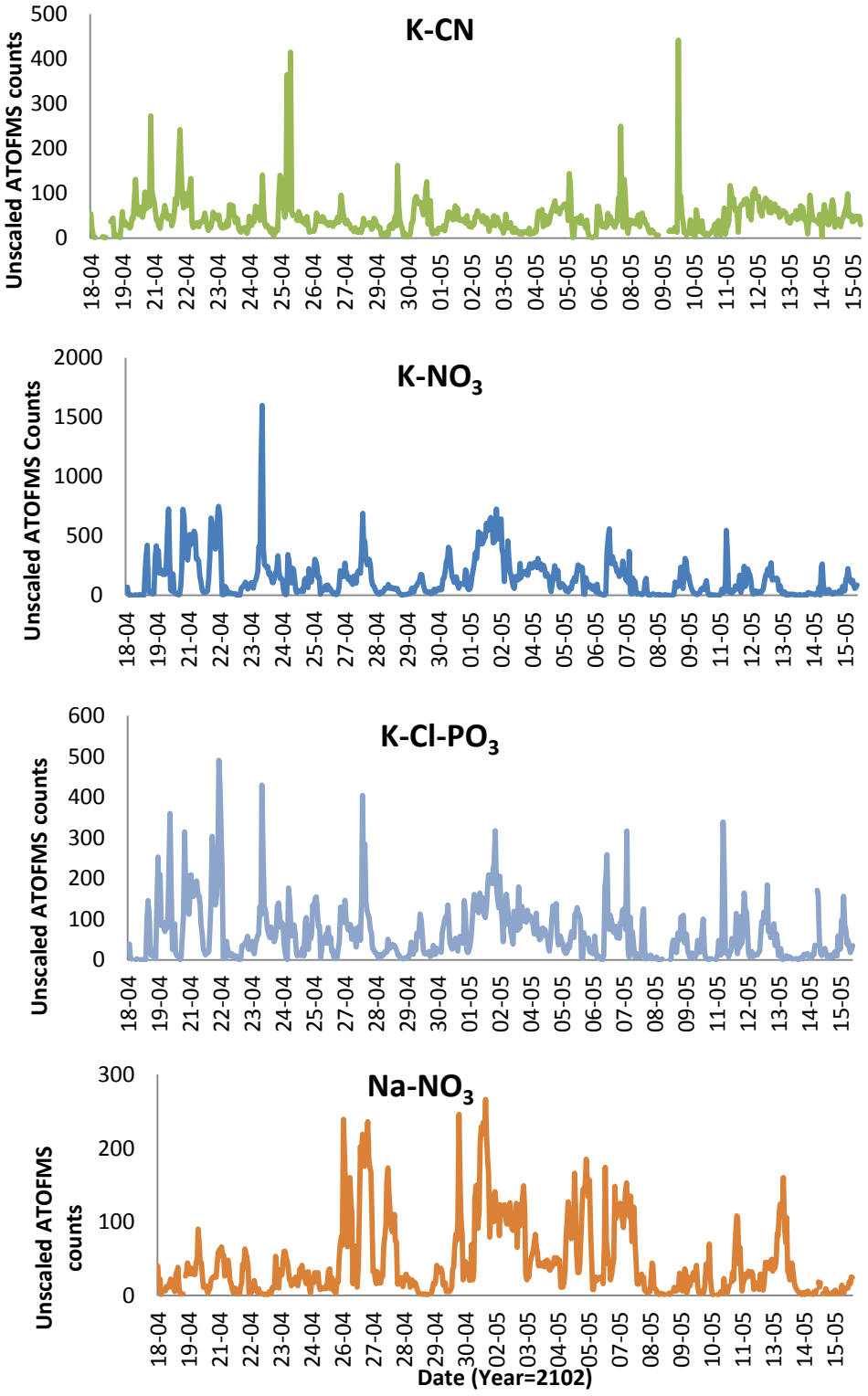

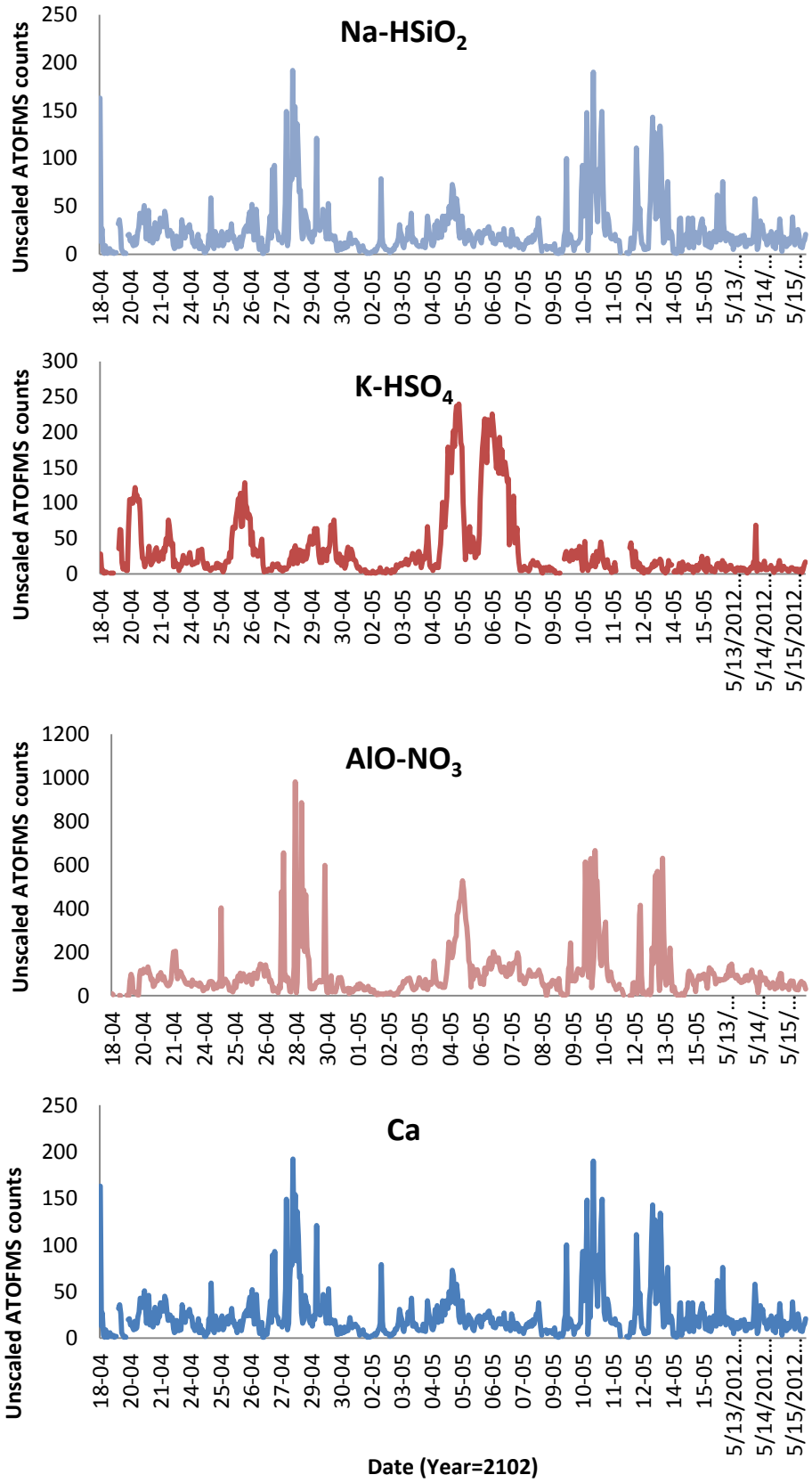
Na-HSiO2
Unscaled ATOFMS counts
K-HSO4
AlO-NO3
Ca
Date (Year=2102)

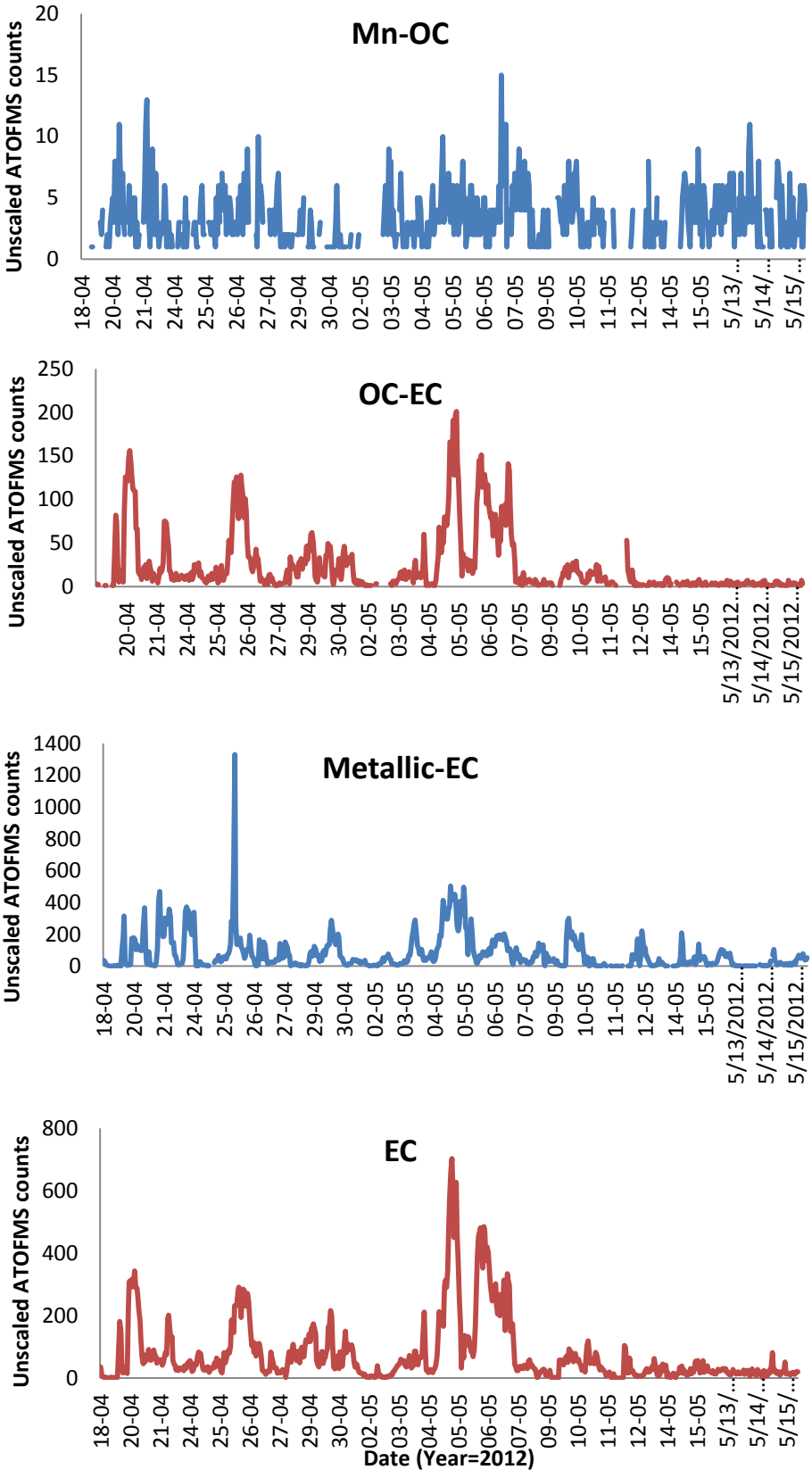
Mn-OC
Unscaled ATOFMS counts
0
5
10
15
20
OC-EC
0
50
100
150
200
250
Metallic-EC
0
200
400
600
800
1000
1200
1400
EC
0
200
400
600
800
18-04
20-04
21-04
24-04
25-04
26-04
27-04
29-04
30-04
02-05
03-05
04-05
05-05
06-05
07-05
09-05
10-05
11-05
12-05
14-05
15-05
5/13/2012...
5/14/2012...
5/15/2012...
Date (Year=2012)

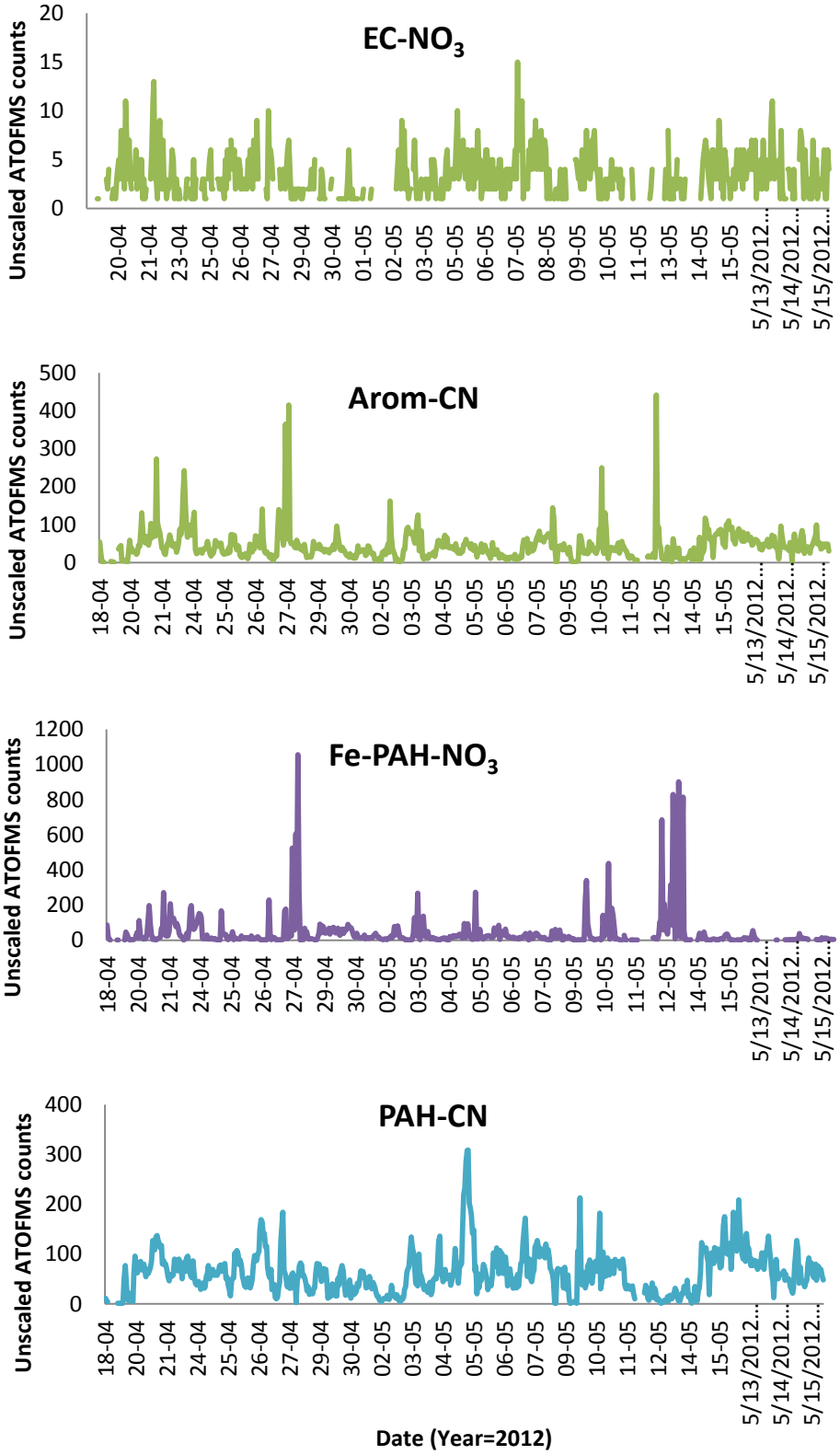
EC-NO3
Arom-CN
Fe-PAH-NO3
PAH-CN
Unscaled ATOFMS counts
Date (Year=2012)

Appendix XXIX

Partisol PM data comparing urban background (EROS), traffic (BROS) and industrial (PT) sites

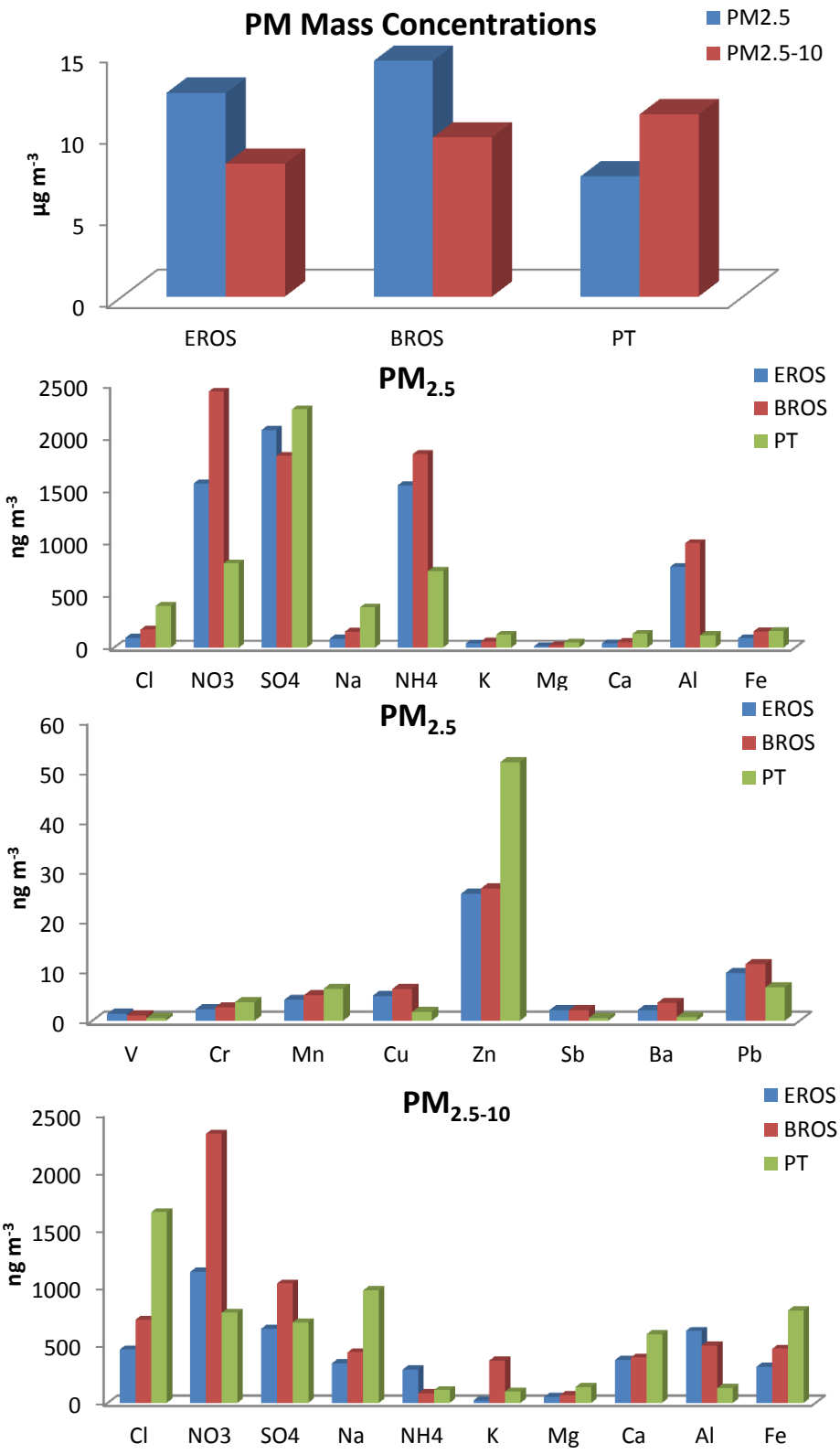

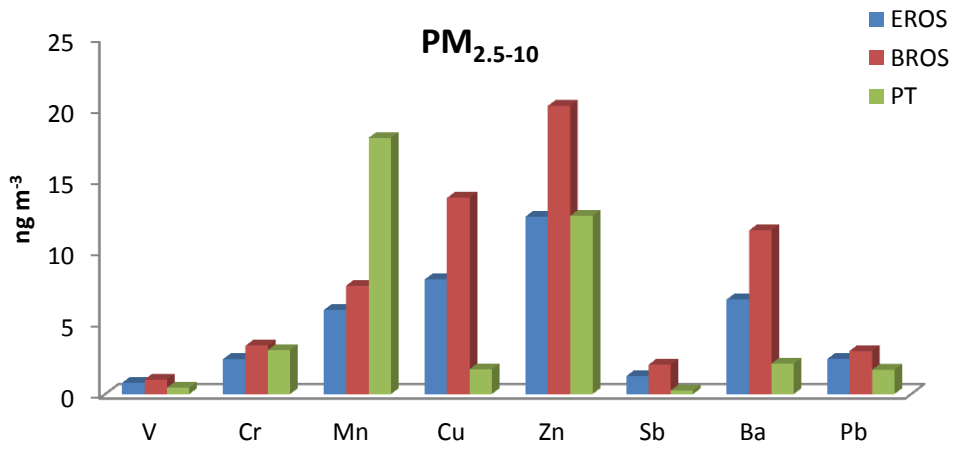
PM2.5-10
EROS
BROS
PT
ng m-3
25
20
15
10
5
0
V
Cr
Mn
Cu
Zn
Sb
Ba
Pb

Appendix XXX

Summary of Source Apportionment

(a) $PM_{2.5}$

Source Contributions (%)	Partisol			Streaker		ATOFMS
	FS		LW	FS	LW	FS
	PMF	PCA	PMF	PMF	PMF	
BF	11	14	6	20	11	28
BOS/Sinter	5	19	4			
Coking/Mills				8	26	22
Woodsmoke	11		14			
Secondary	52	43	58	28	25	20
Traffic	5	19	3	14		28
Marine	16	4	15	26	19	12
Oil combustion		1				

(b) $PM_{2.5-10}$

Source Contributions (%)		Partisol	
	FS	LW	
	PMF		PCA
Sinter	5	8	
BF	36	12	61
BOS/Sinter	2	3	6
Coking+Marine			
Woodsmoke			
Secondary	8	14	1
Traffic	11	3	4
Marine	38	60	28

(c) PM_{10}

		Partisol		Streaker	
	PMF	PCA			
	FS		LW	FS	LW
Sinter	5		9	6	2
BF	21		7	24	11
BOS/Sinter	2		2	1	4
Coking+Marine				12	
Woodsmoke					
Secondary Sulphate	18		24		17
Secondary Nitrate	12		22		
Traffic	13		3	2	
Marine	29		33	38	54
Crustal				17	12

Appendix XXXI

Relationship between measured and reconstructed $PM_{2.5}$ at FS, during Port Talbot sampling campaign (April 23-May 16, 2012)

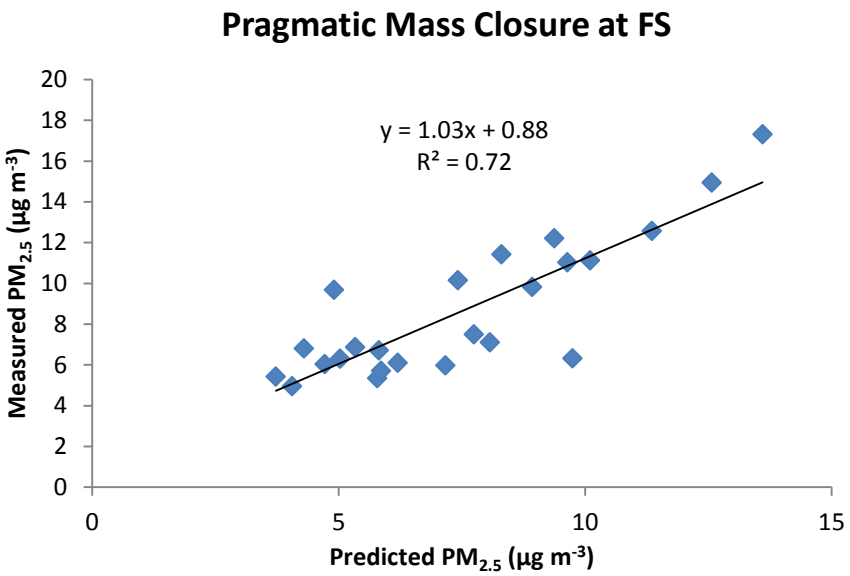

Appendix XXXII

Average increment in 24-hour Partisol PM concentrations associated with a wind sector linking the source to the receptor locations (a) Fire Station

ng m^{-3}	Ore stockyard			BF/Sinter		
	$PM_{2.5}$	$PM_{2.5-10}$	PM_{10}	$PM_{2.5}$	$PM_{2.5-10}$	PM_{10}
*PM Mass	0.5	1.9	2.4	5.9	21.7	27.6
Cl^-	-418.6	-1777.1	-2195.7	163.1	-437.8	-274.8
NO_3^-	-480.6	-135.8	-616.4	-133.7	-225.6	-359.3
nss-SO_4^{2-}	-1193.7	-655.3	-1849.0	39.66	274.9	314.5
ss-SO_4^{2-}	-55.35	-247.8	-303.1	-40.71	-106.4	-147.1
Na^+	-219.7	-983.2	-1202.8	-161.5	-422.1	-583.6
NH_4^+	-194.1	-25.71	-219.8	85.63	-82.05	3.58
K^+	14.77	-32.04	-17.27	-78.89	35.89	-43.00
Mg^{2+}	-16.41	-90.19	-106.6	-56.53	62.77	6.25
Ca^{2+}	-336.1	488.5	152.4	165.1	1696.6	1861.7
Al	1.60	-23.39	-21.79	20.28	176.4	196.7
V	-0.07	0.11	0.04	-0.24	1.00	0.76
Cr	-4.64	-2.82	-7.46	-1.71	0.88	-0.83
Mn	-2.88	10.22	7.34	19.17	87.96	107.1
Fe	3.35	623.5	626.8	547.7	3283.8	3831.5
Ni	0.44	-0.12	0.34	0.07	0.45	0.52
Cu	1.10	1.45	2.55	2.44	1.56	3.99
Zn	-20.43	-1.05	-21.48	111.0	16.37	127.4
Cd	-0.27	-0.04	-0.31	0.75	0.14	0.90
Sb	0.24	0.42	0.66	0.93	0.50	1.43
Ba	0.78	1.68	2.48	1.39	4.96	6.34
Pb	-0.79	0.44	-0.36	9.25	3.45	12.70

Note: * (μg m^{-3})

(b) LW site

ng m^{-3}	Ore stockyard		
	$PM_{2.5}$	$PM_{2.5-10}$	PM_{10}
*PM mass	0.2	2.3	2.5
Cl^-	116.7	64.35	181.0
NO_3^-	707.2	127.8	835.0
nss-SO_4^{2-}	674.2	0.0	674.2
ss-SO_4^{2-}	19.95	48.16	68.11
Na^+	79.17	191.1	270.3
NH_4^+	361.5	23.76	310.5
K^+	27.29	-4.78	22.51
Mg^{2+}	95.14	-19.68	75.46
Ca^{2+}	92.5	215.4	307.9
Al	32.04	-3.68	28.36
V	0.1	0.08	0.18
Cr	1.77	-0.04	1.73
Mn	5.47	13.09	18.56
Fe	228.9	799.2	1028.1
Ni	0.0	0.0	0.0
Cu	0.83	-0.13	0.7
Zn	4.58	1.52	6.1
Cd	0.0	0.0	0.0
Sb	0.0	0.0	0.0
Ba	0.0	0.46	0.46
Pb	2.58	0.8	3.38

Note: * (μg m^{-3})

Appendix XXXIII

Average increment in Streaker hourly PM concentrations associated with a wind sector linking the source to the receptor location at FS

(a) FS $PM_{2.5}$

ng m^{-3}	Ore-stockyard	Sinter	BF	BOS/Coking	Mills
Na	355.9	74.05	104.3	16.95	-88.16
Mg	50.12	27.21	40.3	8.04	-4.38
Al	23.19	30.69	41.88	13.04	7.40
S	154.9	562.3	356.7	64.07	300.2
Cl	265.5	52.53	28.86	42.95	-0.47
K	21.70	86.03	111.1	-13.58	-7.85
Ca	188.5	223.1	270.5	22.31	-3.47
Ti	1.26	2.98	3.16	-0.42	-0.46
V	1.28	1.41	1.27	0.05	-0.04
Cr	2.07	0.59	1.26	1.48	0.55
Mn	9.27	26.22	28.43	1.05	1.68
Fe	553.4	1009.2	1542	148.0	138.7
Ni	0.31	0.45	0.42	0.31	0.42
Cu	0.99	3.28	1.28	1.09	4.68
Zn	20.66	150.7	109.1	10.80	12.90
As	-0.72	1.51	0.66	-0.72	0.26
Se	-0.06	0.27	0.81	-0.85	-0.97
Rb	1.11	5.74	10.76	-3.63	-2.04
Sr	-0.05	-1.98	-1.98	0.23	-1.01
Pb	3.17	9.96	9.14	0.27	2.64

(b) FS $PM_{2.5\text{-}10}$

ng m^{-3}	Ore-stockyard	Sinter	BF	BOS/Coking	Mills
Na	2644.9	1309.8	1575.1	151.3	259.8
Mg	389.3	307.1	422.7	18.22	28.00
Al	190.3	204.3	275.4	15.06	26.64
S	446.3	618.2	866.8	34.23	67.54
Cl	3482.2	1552.2	1395.8	55.34	-450.3
K	130.9	114.9	172.9	9.21	8.98
Ca	1631.9	1685.9	2634.3	79.66	111.4
Ti	19.49	29.65	43.19	1.67	0.80
V	5.87	5.08	11.94	-1.46	-0.77
Cr	2.41	4.15	5.54	0.24	0.48
Mn	64.83	101.4	172.3	4.13	5.25
*Fe	4.68	7.03	11.39	0.16	0.25
Ni	0.24	0.11	0.05	0.01	0.08
Cu	4.33	4.55	3.44	1.36	1.59
Zn	11.65	33.18	23.84	3.28	2.45
As	1.48	0.29	-0.28	0.04	0.06
Se	1.22	3.60	1.87	0.25	-0.32
Rb	31.87	50.20	88.15	1.79	2.15
Sr	1.11	-0.42	-0.57	-0.46	-0.48
Pb	14.59	10.31	17.35	0.65	2.01
Si	446.6	481.7	743.7	55.79	102.0

Note: * (μg m^{-3})

(c) FS PM_{10}

ng m^{-3}	Ore-stockyard	Sinter	BF	BOS/Coking	Mills
*PM Mass	11.3	19.5	12.4	9.3	3.3
Na	3000.8	1383.9	1679.4	168.2	171.7
Mg	439.4	334.3	463.0	26.26	23.62
Al	213.5	235.0	317.3	28.10	34.03
S	601.3	1180.5	1223.5	98.30	367.7
Cl	3747.7	1604.7	1424.6	98.28	-450.7
K	152.6	200.9	284.0	-4.37	1.14
Ca	1820.4	1909.0	2904.8	102.0	107.9
Ti	20.8	32.62	46.35	1.24	0.33
V	7.15	6.49	13.21	-1.41	-0.81
Cr	4.47	4.73	6.80	1.72	1.03
Mn	74.11	127.6	200.7	5.18	6.93
*Fe	5.24	8.04	12.93	0.30	0.39
Ni	0.55	0.56	0.47	0.32	0.50
Cu	5.32	7.83	4.72	2.45	6.27
Zn	32.31	183.9	133.0	14.08	15.35
As	0.75	1.80	0.38	-0.69	0.32
Se	1.16	3.87	2.67	-0.60	-1.30
Rb	32.98	55.94	98.91	-1.84	-1.44
Sr	1.06	-2.40	-2.54	-0.23	-0.37
Pb	17.76	20.27	26.49	0.92	4.22

Note: * (μg m^{-3})

Appendix XXXIV

Average increment in Streaker hourly PM concentrations associated with a wind sector linking the source to the receptor location at LW

ng m^{-3}	BF/Sinter			BOS/Coking/Mill/Ore Stockyard		
	$PM_{2.5}$	$PM_{2.5-10}$	PM_{10}	$PM_{2.5}$	$PM_{2.5-10}$	PM_{10}
*PM Mass			4.8			7.3
Na	-50.39	-429.4	-479.8	178.5	12.34	190.8
Mg	7.84	-36.45	-28.61	20.32	-0.75	19.57
Al	21.44	5.02	26.46	13.82	16.38	30.19
S	958.2	-13.13	945.1	444.5	6.74	451.3
Cl	-0.66	363.6	363.0	112.8	1141.2	1254.0
K	199.6	-30.14	169.5	147.6	-17.30	130.27
Ca	187.6	32.59	220.2	148.0	54.55	202.51
Ti	-2.11	-0.09	-2.2	-0.91	0.47	-0.43
V	0.61	-2.3	-1.7	-1.03	-1.30	-2.33
Cr	-1.43	0.14	-1.29	-1.98	0.02	-1.96
Mn	21.22	6.9	28.12	17.10	8.07	25.17
Fe	858.6	405.3	1263.9	535.5	673.5	1209.0
Ni	0.74	-0.14	0.6	0.38	-0.11	0.27
Cu	0.20	-1.56	-1.36	-0.53	-1.35	-1.89
Zn	137.1	22.67	159.7	352.2	6.00	358.2
As	0.36	-0.05	0.31	-0.07	-0.15	-0.23
Se	1.88	-0.44	1.43	1.12	-0.44	0.68
Rb	5.85	6.09	11.93	4.07	5.40	9.48
Sr	1.33	-0.09	1.25	-0.84	0.06	-0.78
Pb	20.87	6.01	26.88	14.02	2.18	16.20
Si		129.8			35.83	

Note: * (μg m^{-3})

Appendix XXXV
Steelworks PMF Profiles for Partisol data at (a) FS

ng m^{-3}	Sinter			**BF**			BOS/Sinter	
	$PM_{2.5-10}$	PM_{10}	$PM_{2.5}$	$PM_{2.5-10}$	PM_{10}	$PM_{2.5}$	$PM_{2.5-10}$	PM_{10}
* PM Mass	0.8	1.0	1.1	6.4	5.5	0.3	0.2	0.5
Cl^-	1.04	2.96	4.58	24.25	81.65	29.95	6.33	36.21
NO_3^-		-1.73	4.65		-1.73	16.25		-1.73
nss-SO_4^{2-}	5.9	141.6	239.7	70.92	387	86.55	-12.26	63.64
Na^+	55.36	134.1	-2.31	-3.26	2.16	0.55	0.05	-2.76
NH_4^+		3.43	59.11		10.58	14.46		3.43
K^+	76.72	104.6	23.91	-0.15	39.09	2.58	0.56	2.37
Mg^{2+}	7.59	30.1	3.38	26.63	14.96	2.48	4.16	7.35
Ca^{2+}	43.12	66.3		510.3	407.8		27.59	32.51
Al	18.64			30.97			3.48	
V	0.03	0.12		0.27	0.24		0.02	0.02
Mn	0.76	0.19	4.11	23.31	23.02	0.68	0.82	2.13
Fe	39.94	20.04	118.35	1060.7	988.2	12.44	23.73	42.76
Cu	0.01	0.24	0.24	0.01	-0.03	0.09	0.02	0.13
Zn	0.09	0.96	6.95	0.16	7.12	19.46	3.96	34.35
Cd	0.0	0.04	0.0	0	0.04	0.21	0.01	0.05
Sb	0.0		0.0	0.04		0.02	0.0	
Ba	0.09	0.02	0.26	1.2	0.98	0.04	0.05	0.11
Pb	0.03		1.04	1.61		1.32	0.08	

Note: * (μg m^{-3})

(b) LW

ng m^{-3}	Sinter			BF			BOS/Sinter	
	$PM_{2.5-10}$	PM_{10}	$PM_{2.5}$	$PM_{2.5-10}$	PM_{10}	$PM_{2.5}$	$PM_{2.5-10}$	PM_{10}
*PM Mass	1.0	1.8	0.5	2.0	2.0	0.1	0.2	0.3
Cl^-	7.40	3.40	6.36	14.61	33.52	33.84	16.33	31.75
NO_3^-		12.59	19.85		12.59	31.76		12.59
nss-SO_4^{2-}	33.11	258.3	153.6	33.98	147.6	103.9	8.16	44.30
Na^+	96.46	295.3	16.50	15.91	14.52	19.43	21.50	12.63
NH_4^+		6.88	38.57		9.61	15.52		6.88
K^+	106	213.6	12.91	0.38	14.21	3.24	1.58	0.78
Mg^{2+}	10.03	59.40	3.01	9.44	5.82	3.04	6.16	5.56
Ca^{2+}	61.42	135.4		172.6	175.2		45.22	41.06
Al	24.02			11.39			3.28	
V	0.04	0.24		0.08	0.10		0.02	0.03
Mn	0.73	0.05	2.18	7.11	8.67	0.75	1.02	1.61
Fe	51.14	23.21	61.38	338.3	380.3	11.97	32.52	32.84
Cu	0.03	0.59	0.17	0.03	0.03	0.13	0.05	0.16
Zn	0.00	0.70	3.51	0.02	3.05	18.47	6.53	29.17
Cd	0.00	0.05	0.01	0.00	0.05	0.22	0.02	0.06
Sb	0.01		0.04	0.02		0.06	0.01	
Ba	0.08	-0.01	0.09	0.36	0.36	-0.02	0.03	0.07
Pb	0.05	0.59	1.06	0.54	1.28	1.87	0.15	1.92

Note: * (μg m^{-3})

Appendix XXXVI
Steelworks PMF Profiles for Streaker data at (a) FS

ng m^{-3}	Sinter (Secondary)		BF		BOS		Coking	
	$PM_{2.5}$	PM_{10}	$PM_{2.5}$	PM_{10}	$PM_{2.5}$	PM_{10}	$PM_{2.5}$	PM_{10}
*PM Mass	4.7	4.3	0.5	0.6	0.1	0.1	2.0	4.2
Na	9.93	6.58	5.59	6.58	11.93	48.44	29.69	6.58
Mg	3.6	5	5.23	26.94	0.17	7.59	6.1	42.65
Al	6.68	12.78	7.17	9.59	1.04	2.22	6.51	67.7
S	369.4	509.3	34.56	2.33	13.56	2.33	55.93	68.06
Cl	15.61	4.6	15.54	72.95	19.51	3.74	15.35	140.4
K	7.95	12.08	6.79	21.14	8.33	11.74	17.96	15.02
Ca	11.58	34.6	92.81	202.6	2.13	21.71	2.08	471.9
Ti	0.68	1.12	0.86	3.75	-0.05	0.27	0.19	5.33
Mn	0.75	1.68	5.01	18.34	0.77	1.7	1.1	16.86
Fe	15.36	-8.58	267.8	1898.3	14.05		42.8	721.2
Cu		0.04		0.01		0.01		0.78
Zn	3.12	0.1	0.02	0.1	24.86	33.07	1.76	3.03
Se	0.14		0.15		-0.01		0.31	
Pb	2.33	3.81	0.21	1.79	1.55	1.68	0.52	0.21
BC	155.0		11.85		18.02		26.19	
NO_x	2.01		1.16		0.57		0.7	
SO_2	0.1		0.74		0.07		3.14	
CO	0.01		0.01		0.01		0.13	

Note: * (μg m^{-3})

(b) LW

ng m^{-3}	Sinter Plant (Secondary)		BF		BOS		Coking
	$PM_{2.5}$	PM_{10}	$PM_{2.5}$	PM_{10}	$PM_{2.5}$	PM_{10}	$PM_{2.5}$
*PM Mass		1.5		1.4		0.2	
Na	1.47	63.63	4.64	1.79	23.94	29.91	262.6
Mg	3.1	8.21	1.55	4.95	0.46	2.87	36.11
Al	7.09	1.34	1.52	11.53	0.65	0.77	15.09
S	400.6	2	1.62	10.34	15.38	26.36	107.7
Cl	0.37	35.52	0.19	29.57	0.21	43.33	1.73
K	10.82	7.75	17.66	17.14	19.74	25.18	21.93
Ca	0.23	5.81	19.51	74.62	2.34	12.81	0.72
Ti		0.43		0.81		0.33	
Mn	0.94	0.36	2.81	5.04	1.47	2.14	0.33
Fe	21.11	24.5	174.0	392.2	9.1	13.03	12.25
Zn	5.28	1.41	3.24	2.56	68.84	82.64	0.41
Se	0.17		0.23		-0.01		0.32
Pb	3.39	7.42	1.48	0.7	2.49	1.07	1.12

Note: * (μg m^{-3})